7th Hellenic Polymer Conference

Ioannina, September 28th - October 1st 2008

Program

UNIVERSITY OF IOANNINA

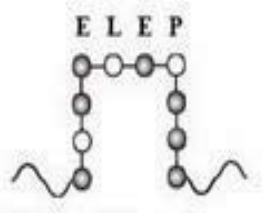

HELLENIC POLYMER SOCIETY

Acknowledgements

The 7th Hellenic Polymer Conference could not be accomplished without the financial support of the following sponsors:

Hellenic Ministry for the Environment, Physical Planning & Public Works
Ministry of National Education & Religious Affairs
University of Ioannina
Department of Materials Science & Engineering, University of Ioannina
Hellenic Petroleum
Rigas Labs S.A.
Chrotex
Help S.A.
Megaplast
Biochem
ChemiC.S.
N. Asteriadis S.A.

7th Hellenic Polymer Conference
Ioannina, September 28th - October 1st 2008
Science and Technology Park of Epirus

Organizing Committee

George Floudas
Chairman
Department of Physics
University of Ioannina

Marios Kosmas
Vice Chairman
Department of Chemistry
University of Ioannina

Apostolos Avgeropoulos
Vice Chairman
Dept. of Materials Science & Engineering
University of Ioannina

Konstantinos Beltsios
Dept. of Materials Science & Engineering
University of Ioannina

Costas Vlachos
Department of Chemistry
University of Ioannina

Nikolaos E. Zafeiropoulos
Dept. of Materials Science & Engineering
University of Ioannina

Nektaria M. Barkoula
Dept. of Materials Science & Engineering
University of Ioannina

Efthymios Bokaris
Department of Chemistry
University of Ioannina

Michael Siskos
Department of Chemistry
University of Ioannina

Ioannis Kallitsis
Department of Chemistry
University of Patras & FO.R.T.H./I.C.E.-H.T.

Scientific Committee

Spyros Anastasiadis
Department of Chemical Engineering
Aristotle University of Thessaloniki & FO.R.T.H./I.E.S.L

Andreas Andreopoulos
School of Chemical Engineering
National Technical University of Athens

Dimitris Vlassopoulos
Dept. of Materials Science & Technology
University of Crete & FO.R.T.H./I.E.S.L.

Costas Galiotis
Department of Materials Science
University of Patras & FO.R.T.H./I.C.E.-H.T.

Doros Theodorou
School of Chemical Engineering
National Technical University of Athens

Ioannis Kallitsis
Department of Chemistry
University of Patras & FO.R.T.H./I.C.E.-H.T.

Constantinos Kiparissides
Department of Chemical Engineering
Aristotle University of Thessaloniki & CE.R.T.H.

Constantinos Panayiotou
Department of Chemical Engineering
Aristotle University of Thessaloniki

Constantinos Papaspyrides
School of Chemical Engineering
National Technical University of Athens

Polycarpos Pissis
Department of Physics
National Technical University of Athens

Johannis Simitzis
School of Chemical Engineering
National Technical University of Athens

Constantinos Tsitsilianis
Department of Chemical Engineering
University of Patras & FO.R.T.H./I.C.E.-H.T.

George Fytas
Dept. of Materials Science & Technology
University of Crete & FO.R.T.H./I.E.S.L.

Georges Hadziioannou
University Louis Paster, France

Nikos Hadjichristidis
Department of Chemistry
University of Athens

Sunday Sept. 28
17:00 - 20:00 Registration – Welcome Party

Monday Sept. 29	Tuesday Sept. 30	Wednesday Oct. 1
08:15 - 09:15 Registration	Session 5: BIOPOLYMERS Presiding: M. Kosmas, A. Andreopoulos	Session 9: POLYMER DYNAMICS Presiding: D. Vlassopoulos, V. Mavrantzas
09:15 – 09:30 Opening Remarks	**09:00 – 09:40 IL6 M. Muthukumar** *"Packaging biological macromolecules and delivery"*	**09:00 – 09:40 IL10 D.N. Theodorou** *"From chemical structure to physical properties of polymers via hierarchical modeling"*
Session 1**:** NANOTECHNOLOGY Presiding: N. Hadjichristidis, G. Floudas	**09:40 – 10:00 O12 A. Gitsas** *"Self-assembly and dynamics of poly(γ-benzyl-L-glutamate) embedded into nanoporous alumina templates"*	**09:40 – 10:00 O27 V. Raptis** *"A poly(dimethylsiloxane) quantum mechanical force-field: Molecular dynamics calculations for the prediction of physical properties"*
09:30 – 10:10 IL1 E.L. Thomas *"Periodic polymers for photonics, phononics and mechanics"*	**10:00 – 10:20 O13 H. Iatrou** *"Vesicles from well-defined block copolypeptides"*	**10:00 –10:20 O28 V. Harmandaris** *"Structure and dynamics of entangled polystyrene melts through hierarchical multi-scale dynamic simulations"*
10:10 – 10:30 O1 M. Pitsikalis *"Synthesis and characterization of amphiphilic block copolymers. Association behavior in aqueous solutions. Potential use of the micellar structure as drug carriers"*	**10:20 – 10:40 O14 P. Papadopoulos** *"Hierarchies in the structural organization of spider silk – a quantitative model"*	**10:20 – 10:40 O29 G. Tsolou "***Topological and dynamical mapping of atomistic simulation data onto the tube model for entangled polymer melts"*
10:30 – 10:50 O2 E. Pefkianakis *"Synthesis and characterization of polymeric [Ru^{2+}] complexes and their application as dyes in solar cells"*	**10:40 – 11:00 O15 S. Chaitidou** *"Synthesis of molecularly imprinted polymers via precipitation polymerization from the selective separation of peptides"*	**10:40 – 11:00 O30 A. Rissanou** *"Molecular dynamics simulations of diblock-arm star copolymers"*
10:50 - 11:10 Coffee Break – (Conference Photo)	**11:00 – 11:20 Coffee Break**	**11:00 – 11:20 O31 I.G. Economou** *"Atomistic simulations of poly(dimethylsiloxane) permeability properties to gases and n-alkanes"*
Session 2: POLYMER SYNTHESIS Presiding: J. Kallitsis, C. Tsitsilianis	Session 6: SURFACES AND INTERFACES Presiding: G. Floudas, C. Panayiotou	**11:20 – 11:40 Coffee Break**
11:10 – 11:50 IL2 N. Hadjichristidis *"Well-defined complex macromolecular architectures by anionic polymerization high vacuum techniques"*	**11:20 – 12:00 IL7 H.-J. Butt** *"Single polymer binding: Towards a universal adhesive"*	Session 10: POLYMER TECHNOLOGY Presiding: C. Papaspyrides, I. Simitzis
11:50 – 12:10 O3 G. C. Vougioukalakis *"Vinyl polymerization of norbornene with a novel nickel (II) diphosphinoamine/methylaluminoxane catalytic system"*	**12:00 – 12:20 O16 D. Vlassopoulos** *"Viscoelasticity of semifluorinated alkanes at the air-water interface"*	**11:40 – 12:00 O32 E. Mitsoulis** *" Steady capillary flow of polytetrafluoroethylene (PTFE) paste: Experiments and simulations"*
12:10 – 12:50 IL3 J. Mays *"Novel ion-containing polymers via post-polymerization chemistry"*	**12:20 – 12:40 O17 C. Toprakcioglu** *"Adsorption of oligomers and polymers in nanoporous alumina"*	**12:00 – 12:20 O33 D. S. Achilias** *"Thermal degradation kinetics of light-cured dimethacrylate resins used as biomaterials in dental applications"*
12:50 - 13:10 O4 M. Vamvakaki *"Responsive microgel particles"*	**12:40 – 13:00 O18 B. Loppinet** *"Dynamics of zwitterion terminated polystyrene at a glass-solution interface studied by evanescent wave dynamic light scattering"*	**12:20 – 12:40 O34 P.A. Tarantili** *"Study of polyblends containing plastics used in electrical and electronic applications"*
13:10 – 13:30 O5 N. Zafeiropoulos *"Smart multifunctional hybrid microgels"*	**13:00 - 13:20 O19 G. Kritikos** *"Theoretical study of adsorption of star-polymers by mean-field theory"*	**12:40 - 13:00 O35 C. Tsioptsias** *"Porous materials from polysaccharide gels processed by supercritical CO2"*
	13:20 – 13:40 O20 G. Sakellariou *"A general approach to surface initiation polymerizations from multi-wall carbon nanotubes"*	**13:00 – 13:20 O36 L. Zoumpoulakis** *"Chemical modification of carbon fibers and its evaluation based on their composites with epoxy resin"*

13:30 - 15:00 Lunch Break	**13:40 – 15:00 Lunch Break**	**13:20 – 14:20 Lunch Break**
Session 3: COLLOIDS/GELS Presiding: D.N. Theodorou, C. Kiparissides	Session 7: SURFACES AND NANOCOMPOSITES Presiding: S.H. Anastasiadis, C. Galiotis	**14:20 - 14:40 O37 S.N. Vouyiouka** *"Post-polymerization in the solid state of sulfonated nylon 66 copolymers"*
15:00 – 15:40 IL4 G. Fytas *"Tailoring sound propagation by mesoscopic engineering of soft matter"*	**15:00 – 15:40 IL8 M. Stamm** *"Polymer brushes for functional surfaces"*	**14:40 - 15:00 O38 I. Raptis** *"Evaluation of a polymer based chemocapacitive sensor array for the detection of vapor analytes and their mixtures"*
15:40 – 16:00 O6 I. Bitsanis *"Simulations of temperature induced ageing and crystallization in dense suspensions of ultrasoft colloids"*	**15:40 – 16:00 O21 P. Pissis** *"Dynamics of poly(propylene oxide) amines intercalated in clay"*	**15:00- 15:20 O39 G.C. Psarras** *"Electrical response of polymer matrix-titanium carbide composites*
16:00 - 16:20 O7 G. Petekidis *"Yielding mechanisms and particle rearrangements in colloidal glasses and gels"*	**16:00 – 16:20 O22 K. Chrissopoulou** *"Crystallization behavior in polymer/layered silicate nanocomposites"*	**15:20 -15:40 Best Poster Award - Closing Remarks** (Award Committee: D. N. Theodorou, N. Hadjichristidis, G. Fytas)
16:20 – 16:40 O8 G. Staikos *"Hydrogen-bonded interpolymer complexes soluble at low pH"*	**16:20 – 16:40 O23 K. Triantafyllidis** *"The use of aliphatic di/triamines (Jeffamines) as clay surface modifiers for the preparation of epoxy-clay nanocomposites"*	
16:40 – 17:00 Coffee Break	**16:40 – 17:00 Coffee Break**	
Session 4: SELF-ASSEMBLY Presiding: G. Fytas, C. Toprakcioglu	Session 8: NANOCOMPOSITES Presiding: A. Avgeropoulos, P. Pissis	
17:00 – 17:40 IL5 P. Alexandridis *"Block copolymer-directed nanomaterials synthesis and organization"*	**17:00 – 17:40 IL9 M.R. Bockstaller** *"Tailoring the physical properties of nanocomposite materials- Why structure matters"*	
17:40 – 18:00 O9 S. Pispas *"Self-assembled nanostructures from block copolymers and vesicle-forming surfactant in aqueous solutions"*	**17:40 – 18:00 O24 A. Horechyy** "Synthesis and selective segregation of Fe_3O_4 nanoparticles inside of the poly-2vinylpyridine domain of poly(styrene-b-2vinylpyridine)"	
18:00 – 18:20 O10 E. Ioannou *"Effect of Lithium salt concentration on the self-assembly of PEO-based block copolymer electrolytes"*	**18:00 – 18:20 O25 E. Pavlopoulou** *"Impregnation of pH-responsive polymeric matrices with metal nanoparticles"*	
18:20 – 18:40 O11 D. Tasis *"Fabrication of nanoobjects from star-shaped copolymers"*	**18:20 - 18:40 O26 G. Bokias** *"Complexation of anionic polyelectrolytes with Cu^{2+} ions and/or cationic surfactants: Design of the polymer architecture to control the behavior in aqueous solution"*	
18:40 – 20:00 Poster Session I	**18:40 – 20:00 Poster Session II**	
	21:00 – Conference Dinner	

POSTERS

A. SYNTHESIS / POLYMER TECHNOLOGY

[1] O.-N. Ciocoiu "Contribution to obtain the graft copolymers of alginic acid with pnipam"
[2] I. Manolakis "High-temperature iminisation of crystalline poly(aryl ether ketones) using aromatic/aliphatic amines"
[3] S.G. Nanaki "Synthesis, characterization and enzymatic hydrolysis of poly(propylene adipate)-co-poly(e-caprolactone) block copolymers"
[4] D.N. Bikiaris "Synthesis, solid state and enzymatic degredation of novel poly(propylene-co-ethylene succinate)s"
[5] E. Kaditi "b-Lactam functionalized amphiphilic block copolymers from poly(isoprene-b-ethylene oxide) copolymers"
[6] A. Mateescu "Responsive polymer brushes on flat surfaces by surface-initiated polymerization"
[7] V.A. Kosma "On the formation of apatite aggregates through precipitation from polymer-containing solutions"
[8] D.S. Achilias "A kinetic investigation of the vinyl neo-decanoate bulk free-radical polymerization over the full monomer conversion"
[9] S. Rangou "Synthesis and characterization of 2nd generation dendritic terpolymer"
[10] G. Evangelou "Synthesis of poly(a-methylstyrene-b-4-hydroxystyrene) diblock copolymers via anionic polymerization"
[11] C. Ntaras "Synthesis of graft copolymers with divinyl-terminated poly(dimethelsiloxane) and polystyrene ("grafting to" approach)"
[12] M. Constantinou "Synthesis of block copolymers with poly(methyl methacrylate) and 2-(Trimethylsilyloxy) ethyl methacrylate [PMMA-b-(TMS-HEMA)]"
[13] N. Politakos "Synthesis, molecular and morphological characterization of modified diblock copolymers with organic acid chloride derivatives"
[14] K. Misichronis "Synthesis, molecular and morphological characterization of linear triblock terpolymers where one of the blocks is poly(cyclohexadiene)"
[15] G. Zapsas "Synthesis and characterization of linear tetrablock quaterpolymers consisting of polystyrene, polybutadiene, polyisoprene and poly(methyl methacrylate)"
[16] P. Georgopanos "Nanostructures from well defined diblock copolymers of polystyrene (PS) and poly(dimethylsiloxane) (PDMS)"
[17] E. Grana "Thiophene conducting copolymers"
[18] A. Tomou "Incorporation of Magnetic Nanoparticles in a PI3,4-b-PB1,4 polymeric matrix"
[19] A. Enotiadis "Intercalation of an amphiphilic diblock copolymer in layered materials"
[20] I. Kalamaras "Synthesis and characterization of proton exchange membrane nanocomposites for high temperature fuel cells"
[21] K.P. Koutroumanis "Crosslinked 2-carboxybenzylchitosan: Synthesis, characterization and potential use for transdermal delivery of fluconazole"
[22] S. Papadaki "Synthesis of copolyesters based on adipic acid, glycolic acids and 1,4-butanediol and their hydrolytic degradation"
[23] A.C. Boussia "Low temperature process for the production of long chain aliphatic polyamides"
[24] Th. Vasilakopoulos "Synthesis of symmetric and asymmetric miktoarm star copolymers $(PI)_2(PEO)_2$"
[25] N. Petzetakis "Titanium catalyzed ring opening polymerization of lactides. A route to novel macromolecular architectures"
[26] A. Nikopoulou "Synthesis of well defined graft polymers"
[27] A. Touris "New approach to 'click chemistry' - Combination of 'click chemistry' and anionic polymerization"
[28] E. Driva "Controlled functional nanoparticles"
[29] M. Gkikas "Synthesis of water soluble polypeptides containing (L-) Proline"
[30] L.-F. Arakelian "Synthesis and characterization of triblock copolymers by combination of anionic and atom transfer radical polymerization"
[31] A.K. Andreopoulou "Terpyridine-ruthenium complexes for the decoration of CNTs, semiconducting oligomers and polymers"
[32] D. Triantou "Synthesis of copolymers based on benzene and biphenyl and their characterization by XRD and DSC"
[33] P. Georgiou "Electrochemical surface treatment of laboratorily produced carbon fibers by cyclic votlammetry"
[34] I. Zuburtikudis "Nanofiller effect on the thermal response of poly(3-hydroxybutyrate) nanocomposites and isoconversional kinetic analysis of the thermal degradation"
[35] D. Kontziampasis "Periodic nanodot formation on polymers with plasmas: Towards plasma-directed polymer self-assembly?"
[36] C. Kiparissides "Stochastic prediction of the exact topological characteristics of LDPE produced in Tubular reactors"
[37] C. Kiparissides "Effect of reaction conditions and catalyst design on the rheological properties of polyolefins produced in gas-phase olefin polymerization reactors"
[38] C. Kiparissides "Modeling of industrial catalytic olefin polymerization slurry reactors"

[39] E. Voyiatzis "Viscoelastic tube inflation under constant rate of growth"
[40] D. Papapetros "On-line monitoring of the industrial formaldehyde resin production"
[41] M.M. Karabela "Effect of the concentration of silane-coupling agent on physical properties of dental resin-nanocomposites"
[42] G. Karadimos "Plain and modified phase inversion membranes for gas separation"
[43] N.M. Barkoula "Effect of the environmental degradation on the viscoelastic response of nano modified epoxies and CFRPs"
[44] D.-E. Baciu "Synthesis and characterization of acrylic bone cements reinforced with bioceramics"
[45] I. Raptis "Processing effects on the dissolution properties of thin polymer based chemically amplified photoresist films"
[46] A. Pikasi "Electrical properties of polymeric carbons produced from the precursor system of novolac resin – naphthakene/catalyst – olive stones biomass"
[47] Z. Ioannou "Novolac resin and lignocellulosic materials as precursors for carbonaceous adsorbents"
[48] K. Papadimitriou "New high temperature polymer electrolyte membranes. Influence of the chemical structure on their properties"
[49] A. Tsimpliaraki "The effect of nanoclay content on the electrospun fibrous structure of biodegradable polymer nanocomposites"
[50] M. Siskos "Type II photoinitiator systems based on novel fluorenone and fluorene chromophores. A mechanistic study by Laser flash photolysis"

B. NANOTECHNOLOGY / SELF-ASSEMBLY / COLLOIDS / BIOPOLYMERS / SURFACES AND INTERFACES / NANOCOMPOSITES / POLYMER DYNAMICS

[1] G. Choudalakis "Measurements of free volume in polymer nanocomposite coatings using positron annihilation lifetime spectroscopy"
[2] E. Anyfantakis "Light-induced micro-fiber formation in transparent polymer solutions"
[3] P. Voudouris "Does Brillouin light scattering probe the primary glass transition process?"
[4] K. Raftopoulos "A thermal and dielectric study of molecular dynamics in polyurethane-POSS hybrids"
[5] A. Kanapitsas "Dielectric-mechanical and thermal studies of molecular mobility and phase morphology in epoxy-amine/carbon black nanocomposites"
[6] A. Pamvouxoglou "Dynamics and rheology in suspensions and glasses of soft colloids"
[7] E. Logakis "Thermal and electrical properties of multi-walled carbon nanotube nanocomposites prepared by diluting a masterbatch with various types of modified and non-modified polypropylenes"
[8] A. Stathopoulos "Dielectric studies of molecular dynamics in swollen poly(ethyl acrylate) networks with non-polar colvents"
[9] S. Soulis "Dynamic mechanical and tensile properties of thermally oxidized homopolymer pan fibers"
[10] G. Tsoukleri "Synthesis and mechanical properties of A_nB_n star copolymers and $A_n(B\text{-}b\text{-}C)_n$ star terpolymers"
[11] G. Mitsis "Influence of maleic anhydrite component of cured polyesters on their relaxations determined by dielectric spectroscopy (DS) and dynamic mechanical thermal analysis (SMTA)"
[12] G. Floudas "Self-assembly and dynamics of discotic liquid crystals"
[13] A. Gitsas "Effect of architecture on the self-assembly and dynamics of model diblock and star copolypeptides"
[14] M. Yiannourakou "Modeling the lateral aggregation of membrane proteins"
[15] M. Karayianni "Complexation of hen egg with lysozyme with sodium (sulfamate-carboxylate) isoprene polyelectrolytes"
[16] A. Hasimi "Study of the release kinetics of a drug and an MRI contrast agent from poly(vinyl alcohol) matrices"
[17] K. Tsougeni "Wetting, optical property and protein adsorption control of polymer surfaces by plasma nanotexturing"
[18] A. Panagopoulou "Bulk and interfacial dynamics of PDMS/Titania nanocomposites"
[19] A. Giannakas "Synthesis and properties of unmodified LDPE/organosilicate nanocomposites"
[20] S. Fotiadou "Organic-inorganic nanocomposites: A study of the structure and dynamics in confined geometry"
[21] Th. V. Kosmidou "Glass transition, structural characterization and segmental dynamics in epoxy/carbon fillers nanocomposites"

[22] C.G. Delides "Dynamics of epoxy nanocomposites: The effect of filler's content and the size structure and geometry of the nanoparticles"
[23] A. Voulomenou "Study of silicone rubber nanocomposites reinforced with organophilic montmorillonite"
[24] P. Maroulas "Molecular mobility studies in hybrid PCN clay nanocomposites"
[25] P. Efthymiopoulos "A theoretical study on the size and the shape of linear dendronized polymers in good and selective solvents"
[26] M. Kosmas "On the conformational properties of a DNA chain with loops"
[27] A.N. Rissanou "Collapse transitions in thermosensitive alternating copolymers: A Monte Carlo study"
[28] I. Tanis "Molecular dynamics of PAMAM dendrimers and their complexes with linear polymers in aqueous solutions"
[29] C. Vlahos "Off lattice monte carlo simulations of AB and ABA hybrid star dendritic copolymers"
[30] A. G. Koutsioubas "Neutron reflectivity and computer simulation studies of centrally adsorbed star polymer brushes"
[31] Th. E. Raptis "Detection of diffusive jumps of small penetrants dispersed in polymer systems"
[32] G.S. Dritsas "Investigation of thermodynamic properties of polyethylene glycol by inverse gas chromatography and computer simulations"
[33] G. Tsolou "Atomistic simulations of the sorption of small gas molecules in polyisobutelene"
[34] V. Harmandaris "Studying the Elasticity of Biological Membranes through Theory and Simulations"
[35] M. Iakovidis "Structural and electronic properties of Nb nanowires by tight binding molecular dynamics calculations"
[36] M. Gialambouki "Structural and electronic properties of Ti and TiO_2 on C nanotubes by ab-initio calculations"
[37] E. Ioannou "Lithium ion induced nanophase ordering and ion mobility in ionic block copolymers"
[38] C. Mantzaridis "Reversible self-assembled nanostructures from block polyampholytes"
[39] K. Dimitroulopoulos "Self-assembly in mixed amphiphilic diblock copolymers-zwitterionic surfactants aqueous solutions"
[40] S. Papadimitriou "Self-assembly core-shell PCL-*co*-PSu nanoparticles based on crystalline amorphous moieties for efficient controlled drug release"
[41] A. Meristoudi "Formation of gold nanoparticles in the corona of di- and triblock copolymers"
[42] K. Mpoukouvalas "Charge transport of conjugated polymer coated core-shell nanoparticles"
[43] S.I. Marras "Microcellular nanocomposite polymers prepared with supercritical CO_2: The role of nanoclays on porous structure"
[44] A.A. Vassiliou "Poly(ethylene succinate) nanocomposites with a multifunctional nanofiller: Mechanical properties and biodegradability"
[45] C.A. Stergiou "A new approach of segmental orientation in amorphous epoxy resin/carbon black nanocomposites"
[46] D.S. Achilleos "End-grafted polymer chains onto inorganic nanoparticles"
[47] S. Karagiovanaki "Adsorption of oligomers and polymers in nanoporous alumina"
[48] S.K. Papadopoulou "Fluorinated methacrylic homopolymers: Polymerization, characterization, surface properties and effectiveness for the protection of stone"
[49] A. Kakalis "Fabrication and thermal characterization of a thin poly(L-lactic acid) film with the layer-by layer spin coating process and the use of thickness shear mode resonators"
[50] K.E. Christodoulakis "Colloidal microgel particles carrying acidic or basic moieties"
[51] E. K. Oikonomou "Cu^{2+}-induced gelation in aqueous solutions of maleic acid-containing polyeletrolytes"
[52] Ch. Pandis "Hydration properties of nanostructured hydrogels based on poly(2-hydroxyethyl acrylate) and poly(2-hydroxyethyl-co-ethyl acrylate"
[53] G.Z. Kyzas "Molecularly imprinted polymers (MIPs) as selective sorbents in trichromatic dye mixtures"
[54] Z. Iatridi "pH-controlled quenching of the fluorescence of hydrophobic probes solubilized in ternary poly(acrylic acid) – surfactant-Cu^{+2} complexes in aqueous solution"
[55] A.A. Stefopoulos "Development of new semiconducting polymer functionalized carbon nanotubes"

7th Hellenic Polymer Conference
Science and Technology Park of Epirus

Program

Sunday, September 28th 2008

17:00 - 20:00 ***Registration - Welcome Party***

Monday, September 29th 2008

08:15 - 09:15 ***Registration***

09:15 - 09:30 ***Opening Remarks***

Session 1: NANOTECHNOLOGY
Presiding: N. Hadjichristidis, G. Floudas

09:30 - 10:10 ***I.L.1: "Periodic polymers for photonics, phononics and mechanics"***
E. L. Thomas
Materials Science and Engineering, MIT

10:10 - 10:30 ***O.1: "Synthesis and characterization of amphiphilic block copolymers. Association behavior in aqueous solutions. Potential use of the micellar structure as drug carriers"***
N. Karanikolopoulos, M. Pitsikalis, N. Hadjichristidis
Department of Chemistry, University of Athens

10:30 - 10:50 ***O.2: "Synthesis and characterization of polymeric [Ru^{2+}] complexes and their application as dyes in solar cells"***
E. K. Pefkianakis[1], N. P. Tzanetos[1], T. Stergiopoulos[2], P. Falaras[2] and J. K. Kallitsis[1]
[1]Department of Chemistry, University of Patras
[2]Institute of Physical Chemistry, NCSR Demokritos

10:50 - 11:10 ***Coffee Break - Conference Photo***

Session 2: POLYMER SYNTHESIS
Presiding: J. Kallitsis, C. Tsitsilianis

11:10 - 11:50 ***I.L.2: "Well-defined complex macromolecular architectures by anionic polymerization high vacuum techniques"***
N. Hadjichristidis
Department of Chemistry, University of Athens

11:50 - 12:10 ***O.3: "Vinyl polymerization of norbornene with a novel nickel (II) diphosphinoamine/methylaluminoxane catalytic system"***
G. C. Vougioukalakis[1], N. Petzetakis[1], M. Pitsikalis[1], N. Hadjichristidis[1], I. Stamatopoulos[2], P. Kyritsis[2], A. Terzis[3], C. Raptopoulou[3]
[1]Department of Chemistry, University of Athens
[2]National and Kapodistrian University of Athens, Department of Chemistry, Inorganic Chemistry Laboratory
[3]National Centre of Scientific Research "Demokritos", Institute of Materials Science

12:10 - 12:50 ***I.L.3: "Novel ion-containing polymers via post-polymerization chemistry"***
J. W. Mays
Department of Chemistry, University of Tennessee and Center for Nanophase Materials Sciences and Chemical Sciences Division, Oak Ridge National Laboratory

12:50 - 13:10 ***O.4: "Responsive microgel particles"***
M. Vamvakaki
Institute of Electronic Structure and Laser, FO.R.T.H. and Department of Materials Science and Technology, University of Crete

13:10 - 13:30 ***O.5: "Smart multifunctional hybrid microgels"***
J. Rubio-Retama[1,2], M. Agrawal[1], M. Stamm[1], N. E. Zafeiropoulos[3]
[1]Dept. of Nanostructured Materials, Leibniz-Institut für Polymerforschung, Dresden
[2]Dpto. Físico-Química Farmacéutica, Facultad Farmacia, Universidad Complutense, Madrid
[3]Department of Materials Science & Engineering, University of Ioannina

13:30 - 15:00 ***Lunch Break***

Session 3: COLLOIDS/GELS
Presiding: D. N. Theodorou, C. Kiparissides

15:00 - 15:40 ***I.L.4: "Tailoring sound propagation by mesoscopic engineering of soft matter"***
G. Fytas[1,2]
[1]Max Planck Institute for Polymer Research
[2]Department of Materials Science & Technology and FO.R.T.H

15:40 - 16:00 ***O.6: "Simulations of temperature induced ageing and crystallization in dense suspensions of ultrasoft colloids"***
I. A. Bitsanis[1], A. N. Rissanou[1,2], M. Yannourakou[2], I. G. Economou[2], D. Vlassopoulos[1,3]
[1]Institute of Electronic Structure and Laser, FO.R.T.H.
[2]Molecular Thermodynamics and Modeling of Materials Laboratory, Institute of Physical Chemistry, NSCR "Demokritos"
[3]Department of Materials Science University of Crete

16:00 - 16:20 **O.7 *"Yielding mechanisms and particle rearrangements in colloidal glasses and gels"***
G. Petekidis
Dept. of Materials Science and Technology, University of Crete & IESL-FORTH

16:20 - 16:40 ***O.8: "Hydrogen-bonded interpolymer complexes soluble at low pH"***
G. Staikos[1], M. Sotiropoulou[1], G. Bokias[2], F. Bossard[3], J. Oberdisse[4], E. Balnois[5]
[1]Department of Chemical Engineering, University of Patras
[2]Department of Chemistry, University of Patras
[3]Laboratoire de Rheologie, UMR 5520, Université Joseph Fournier
[4]Laboratoire des Colloides, Verres et Nanomateriaux, UMR CNRS/UM2, Université Montpellier
[5]Laboratoire Polyméres, Propriétés aux Interfaces et Composites (L2PIC), Université de Bretagne Sud

16:40 - 17:00 ***Coffee Break***

Session 4: SELF-ASSEMBLY
Presiding: G. Fytas, C. Toprakcioglu

17:00 - 17:40 ***I.L.5: "Block copolymer-directed nanomaterials synthesis and organization"***
P. Alexandridis
Department of Chemical and Biological Engineering, The State University of New York (SUNY), Buffalo

17:40 - 18:00 ***O.9: "Self-assembled nanostructures from block copolymers and vesicle-forming surfactant in aqueous solutions"***
S. Pispas
Theoretical & Physical Chemistry Institute, National Hellenic Research Foundation

18:00 - 18:20 ***O.10: "Effect of Lithium salt concentration on the self-assembly of PEO-based block copolymer electrolytes"***
E. F. Ioannou[1], K. D. Gatsouli[1], S. Pispas[1], E. I. Kamitsos[1] and G. Floudas[2]
[1]*Theoretical and Physical Chemistry Institute, National Hellenic Research Foundation*
[2]*Department of Physics, University of Ioannina and Foundation for Research and Technology-Hellas, Biomedical Research Institute (FORTH-BRI)*

18:20 - 18:40 ***O.11: "Fabrication of nanoobjects from star-shaped copolymers"***
C. Tsitsilianis[1,2], D. Tasis[3], C. Galiotis[1,3],V. Bocharova[4], A. Kiriy[4], M. Stamm[4]
[1]*Foundation of Research and Technology Hellas, Institute of Chemical Engineering and High Temperature Processes*
[2]*Department of Chemical Engineering, University of Patras*
[3]*Department of Materials Science, University of Patras*
[4]*Leibniz-Institut für Polymerforschung, Dresden*

18:40 - 20:00 ***Poster Session I***

Tuesday, September 30th 2008

Session 5: BIOPOLYMERS
Presiding: M. Kosmas, A. Andreopoulos

09:00 - 09:40 ***I.L.6: "Packaging biological macromolecules and delivery"***
M. Muthukumar
Polymer Science and Engineering Department, University of Massachusetts, Amherst

09:40 - 10:00 ***O.12: "Self-assembly and dynamics of poly(γ-benzyl-L-glutamate) embedded into nanoporous alumina templates"***
A. Gitsas[1], G. Floudas[1], H. Duran[2], W. Knoll[2], M. Mondeshki[2], M. Steinhart[3]
[1]*University of Ioannina, Department of Physics, and Foundation for Research and Technology-Hellas (FORTH), Biomedical Research Institute (BRI).*
[2]*Max Planck Institute for Polymer Research, Mainz*
[3]*Max Planck Institute of Microstructure Physics, Halle*

10:00 - 10:20 ***O.13: "Vesicles from well-defined block copolypeptides"***
H. Iatrou[1], N. Ferderigos[1], N. Hadjichristidis[1], H. Frielinghaus[2], D. Richter[2], S. Nevanpää[3], O. Ikkala[3]
[1]*University of Athens, Department of Chemistry*
[2]*Institut für Festkörperforschung, Forscunszentrum Jülich*
[3]*Optics and Molecular Materials, Helsinki University of Technology*

10:20 - 10:40 ***O.14: "Hierarchies in the structural organization of spider silk - a quantitative model"***
P. Papadopoulos, J. Sölter, R. Ene, I. Weidner, F. Kremer
University of Leipzig, Faculty of Physics and Geosciences, Leipzig

10:40 - 11.00 ***O.15: "Synthesis of molecularly imprinted polymers via precipitation polymerization from the selective separation of peptides"***
S. Chaitidou, O. Kotrotsiou and C. Kiparissides
Department of Chemical Engineering, Aristotle University of Thessaloniki and Chemical Process Engineering Research Institute

11:00 - 11:20 ***Coffee Break***

Session 6: SURFACES AND INTERFACES
Presiding: G. Floudas, C. Panayiotou

11:20 - 12:00 ***I.L.7: "Single polymer binding: Towards a universal adhesive"***
J. Wang[1], M. Kappl[1], H.-J. Butt[1], M. N. Tahir[2], W. Tremel[2]
[1]*Max-Planck Institute for Polymer Research, Mainz*
[2]*Institut für Anorganische Chemie und Analytische Chemie, Mainz*

12:00 - 12:20 ***O.16: "Viscoelasticity of semifluorinated alkanes at the air-water interface"***
C. Christopoulou [1,2], U. Jonas[1,3], C. Clark[3], D. Vlassopoulos[1,2]
[1]*FORTH, Institute of Electronic Structure & Laser*
[2]*University of Crete, Department of Materials Science and Technology*
[3]*Max-Planck Institute for Polymer Research, Mainz*

12:20 - 12:40 ***O.17: "Adsorption of oligomers and polymers in nanoporous alumina"***
S. Karagiovanaki, A. G. Koutsioubas, N. Spiliopoulos, C. Toprakcioglu
Department of Physics, University of Patras

12:40 - 13:00 ***O.18: "Dynamic of zwitterion terminated polystyrene at a glass-solution interface studied by evanescent wave dynamic light scattering"***
A. Tsigkri[1], B. Loppinet[1], S. Pispas[2]
[1]*Institute of Electronic Structure and Laser, FO.R.T.H.*
[2]*Theoretical and Physical Chemistry Institute, N.H.R.F.*

13:00 - 13:20 ***O.19: "Theoretical study of adsorption of star-polymers by mean field theory"***
G. Kritikos and A. F. Terzis
Department of Physics, School of Natural Sciences, University of Patras

13:20 - 13:40 ***O.20: "A general approach to surface initiation polymerizations from multi-wall carbon nanotubes"***
D. Priftis[1], G. Sakellariou[1], D. Baskaran[2], J. W. Mays[2], N. Hadjichristidis[1]
[1]*Department of Chemistry, University of Athens*
[2]*Department of Chemistry, University of Tennessee*

13:40 - 15:00 ***Lunch Break***

Session 7: SURFACES AND NANOCOMPOSITES
Presiding: S.H. Anastasiadis, C. Galiotis

15:00 - 15:40 ***I.L.8: "Polymer brushes for functional surfaces"***
M. Stamm
Leibniz-Institut für Polymerforschung, Dresden

15:40 - 16:00 ***O.21: "Dynamics of poly (propylene oxide) amines intercalated in clay"***
P. Pissis[1], A. Kyritsis[1], S. Kripotou[1], A. Panagopoulou[1], P. I. Xidas[2], K. S. Triantafyllidis[2]
[1]*Department of Physics, National Technical University of Athens*
[2]*Department of Chemistry, Aristotle University of Thessaloniki*

16:00 - 16:20 ***O.22: "Crystallization behavior in polymer / layered silicate nanocomposites"***
K. Chrissopoulou[1], E. Pavlopoulou[1,2], H. Papananou[3], S. Fotiadou[3], G. Portale[4], W. Bras[4], S. H. Anastasiadis[1,3]
[1]*Institute of Electronic Structure and Laser, Foundation for Research & Technology-Hellas*
[2]*Department of Materials Science and Technology, University of Crete*
[3]*Department of Chemical Engineering, Aristotle University of Thessaloniki*
[4]*DUBBLE CRG, European Synchrotron Radiation Facility, Grenoble*

16:20 - 16:40 ***O.23: "The use of aliphatic di/triamines (Jeffamines) as clay surface modifiers for the preparation of epoxy - clay nanocomposites"***
P. I. Xidas[1,2], D. Gournis[2], K. S. Triantafyllidis[1]
[1]*Department of Chemistry, Aristotle University of Thessaloniki*
[2]*Department of Materials Science & Engineering, University of Ioannina*

16:40 - 17:00 ***Coffee Break***

Session 8: NANOCOMPOSITES
Presiding: A. Avgeropoulos, P. Pissis

17:00 - 17:40 ***I.L.9: "Tailoring the physical properties of nanocomposite materials - why structure matters"***
M. R. Bockstaller
Department of Materials Science and Engineering, Carnegie Mellon University, Pittsburgh

17:40 - 18:00 ***O.24: "Synthesis and selective segregation of Fe_3O_4 nanoparticles inside of the poly-2vinylpyridine domain of poly(styrene-b-2vinylpyridine)"***
A. Horechyy[1], N. E. Zafeiropoulos[1,2], C. Tsitsilianis[3], M. Stamm[1]
[1]*Leibniz-Institut für Polymerforschung Dresden*
[2]*Department of Materials Science and Engineering, University of Ioannina*
[3]*Department of Chemistry Engineering, University of Patras*

18:00 - 18:20 ***O.25: "Impregnation of pH-responsive polymeric matrices with metal nanoparticles"***
E. Pavlopoulou[1,2], V. Katsamanis[1,3], K. Christodoulakis[1,2], G. Portale[4], W. Bras[4], M. Vamvakaki[1,2], S.H.Anastasiadis[1,5]
[1]*Foundation for Research and Technology-Hellas, I.E.S.L*
[2]*Department of Materials Science and Technology, University of Crete*
[3]*Department of Physics, University of Crete*
[4]*DUBBLE CRG/European Synchrotron Radiation Facility, Grenoble*
[5]*Department of Chemical Engineering, Aristotle University of Thessaloniki*

18:20 - 18:40 ***O.26: "Complexation of anionic polyelectrolytes with Cu^{2+} ions and/or cationic surfactants: Design of the polymer architecture to control the behavior in aqueous solution"***
Z. Iatridi[1], E. K. Oikonomou[1,2], Ch. Daktyloudis[1], G. Bokias[1]
[1]*Department of Chemistry, University of Patras*
[2]*Foundation of Research and Technology Hellas, Institute of Chemical Engineering and High-Temperature Chemical Processes (ICE/HT)*

18:40 - 20:00 ***Poster Session II***
21:00 ***Conference Dinner***

Wednesday, October 1st 2008

Session 9: POLYMER DYNAMICS
Presiding: D. Vlassopoulos, V. Mavrantzas

09:00 - 09:40 ***I.L.10: "From chemical structure to physical properties of polymers via hierarchical modeling"***
D. N. Theodorou
School of Chemical Engineering, National Technical University of Athens

09:40 - 10:00 ***O.27: "A Poly(dimethylsiloxane) quantum mechanical force-field: Molecular dynamics calculations for the prediction of physical properties"***
K. D. Papavasileiou[1], V. E. Raptis[1,2] and V. S. Melissas[1]
[1]Department of Chemistry, University of Ioannina
[2]Department of Materials Science and Engineering, University of Ioannina

10:00 - 10:20 ***O.28: "Structure and dynamics of entangled polystyrene melts through hierarchical multi-scale dynamic simulations"***
V. Harmandaris[1,2] and K. Kremer[1]
[1]Max-Planck Institute for Polymer Research, Mainz, Germany
[2]Department of Applied Mathematics, University of Crete, Greece

10:20 - 10:40 ***O.29: "Topological and dynamical mapping of atomistic simulation data onto the tube model for entangled polymer melts"***
P. S. Stephanou[1], C. Baig[1], G. Tsolou[1], V. G. Mavrantzas[1], M. Kröger[2]
[1]Department of Chemical Engineering, University of Patras & FORTH-ICE/HT
[2]Polymer Physics, ETH Zürich, Department of Materials

10:40 - 11.00 ***O.30: "Molecular dynamics simulations of diblock-arm star copolymers"***
A. N. Rissanou[1,3], D. Vlassopoulos[1,2], C. N. Likos[3]
[1]FO.R.T.H., Institute of Electronic Structure and Laser
[2]University of Crete, Department of Materials Science and Technology
[3]Institut für Theoretische Physik II Weiche Materie, Heinrich-Heine-Universität, Düsseldorf

11:00 - 11:20 ***O.31: "Atomistic simulation of poly(dimethylsiloxane) permeability properties to gases and n-alkanes"***
Z. A. Makrodimitri and I. G. Economou
Molecular Thermodynamics and Modeling of Materials Laboratory, Institute of Physical Chemistry, National Center of Scientific Research "Demokritos"

11:20 - 11:40 ***Coffee Break***

Session 10: POLYMER TECHNOLOGY
Presiding: C. Papaspyrides, I. Simitzis

11:40 - 12:00 ***O.32: "Steady capillary flow of polytetrafluoroethylene (PTFE) paste: experiments and simulations"***
E. Mitsoulis[1], Th. Zisis[1], S.G. Hatzikiriakos[2]
[1]School of Mining Engineering and Metallurgy, National Technical University of Athens
[2]Department of Chemical and Biological Engineering, The University of British Columbia

12:00 - 12:20 ***O.33: "Thermal degradation kinetics of light-cured dimethacrylate resins used as biomaterials in dental applications"***
D. S. Achilias, M. M. Karabela, I. D. Sideridou
Department of Chemistry, Aristotle University of Thessaloniki

12:20 - 12:40 ***O.34: "Study of polyblends containing plastics used inelectrical and electronic applications"***
P.A. Tarantili, A.N. Mitsakaki, M.A. Petoussi, A.G. Andreopoulos
School of Chemical Engineering, National Technical University of Athens

12:40 - 13:00 ***O.35: "Porous materials from polysaccharide gels processed by supercritical CO_2"***
C. Tsioptsias, C. Panayiotou
Department of Chemical Engineering, Aristotle University of Thessaloniki

13:00 - 13:20 ***O.36: Chemical modification of carbon fibers and its evaluation based on their composites with epoxy resin"***
L. Zoumpoulakis, V. Oikonomopoulou, J. Simitzis
School of Chemical Engineering, National Technical University of Athens

13:20 - 14:20 ***Lunch Break***

14:20 - 14:40 ***O.37: "Post-polymerisation in the solid state of sulfonated nylon 66 copolymers"***
S. N. Vouyiouka, C. D. Papaspyrides
School of Chemical Engineering, National Technical University of Athens

14:40 - 15:00 ***O.38: "Evaluation of a polymer based chemocapacitive sensor array for the detection of vapor analytes and their mixtures"***
K. Manolia[1,2], E. Karonis[1], D. Goustouridis[1], S. Chatzandroulis[1], I. Raptis[1], M. Sanopoulou[2]
[1]Institute of Microelectronics, NCSR "Demokritos"
[2]Institute of Physical Chemistry, NCSR "Demokritos"

15:00 - 15:20 ***O.39: "Electrical response of polymer matrix - titanium carbide composites"***
C. G. Raptis, G. C. Psarras
Department of Materials Science, University of Patras

15:20 - 15:40 ***Best Poster Award***
(Award Committee: D. N. Theodorou, N. Hadjichristidis, G. Fytas)
Closing Remarks

Posters

Monday, September 29th 2008

Poster Session I

Synthesis / Polymer Technology

1 ***"Contribution to obtain the graft copolymers of alginix acid with pnipam"***
N.-O. Ciocoiu, G. Staikos
Department of Chemical Engineering, University of Patras - FORTH/ICEHT

2 ***"High-temperature iminisation of crystalline poly(aryl ether ketones) using aromatic/aliphatic amines"***
I. Manolakis, H. M. Colquhoun
Department of Chemistry, University of Reading

3 ***"Synthesis, characterization and enzymatic hydrolysis of poly(propylene adipate)-copoly(ε-caprolactone) block copolymers"***
S. G. Nanaki, D. N. Bikiaris
Department of Chemistry, Aristotle University of Thessaloniki

4 ***"Synthesis, solid state and enzymatic degradation of novel poly(propylene-co-ethylene succinate)s"***
G. Z. Papageorgiou, I. Palazi, P. Andria, Ch. A. Stergiou, D. N. Bikiaris
Department of Chemistry, Aristotle University of Thessaloniki

5 ***"β-Lactam functionalized amphiphilic block copolymers from poly(isoprene-b-ethylene oxide) copolymers"***
E. Kaditi, S. Pispas
Theoretical and Physical Chemistry Institute, National Hellenic Research Foundation

6 ***"Responsive polymer brushes on flat surfaces by surface - initiated polymerization"***
A. Mateescu[1,2], M. Vamvakaki[2,3]
[1]*Department of Chemistry, University of Crete*
[2]*Institute of Electronic Structure and Laser, FO.R.T.H.*
[3]*Department of Materials Science and Technology, University of Crete*

7 ***"On the formation of apatite aggregates through precipitation from polymer-containing solutions"***
V. A. Kosma, K. G. Beltsios
Department of Materials Science and Engineering, University of Ioannina

8 ***"A kinetic investigation of vinyl neo-decanoate bulk free-radical polymerization over the full monomer conversion"***
D. S. Achilias
Department of Chemistry, Aristotle University of Thessaloniki

9 ***"Synthesis and characterization of 2nd generation dendritic copolymers"***
S. Rangou[1], E.L. Thomas[2], A. Avgeropoulos[1]
[1]*Department of Materials Science & Engineering, University of Ioannina*
[2]*Department of Materials Science & Engineering and Institute of Soldier Nanotechnologies, Massachusetts Institute of Technology*

10 ***"Synthesis of poly(α-methylstyrene-b-4-hydroxystyrene) diblock copolymers via anionic polymerization"***
G. Evangelou, C. Ntaras, S. Rangou, A. Avgeropoulos
Department of Materials Science & Engineering, University of Ioannina

11 ***"Synthesis of graft copolymers with divinyl - terminated poly(dimethylsiloxane) and polystyrene ("grafting to" approach)"***

C. Ntaras[1], G. Evangelou[1], S. Rangou[1], A. Avgeropoulos[1], R.M. Hill[2]
[1]*Department of Materials Science & Engineering, University of Ioannina*
[2]*Dow Corning Corporation, Midland, Michigan, USA*

12 ***"Synthesis of block copolymers with poly(methyl methacrylate) and 2-(trimethylsilyloxy) ethyl methacrylate [PMMA-b-(TMS-HEMA)]"***

M. Constantinou, P. Georgopanos, A. Avgeropoulos
Department of Materials Science & Engineering, University of Ioannina

13 ***"Synthesis, molecular and morphological characterization of modified diblock copolymers with organic acid chloride derivatives"***

N. Politakos[1], C.J. Weinman[2], C.K. Ober[2], A. Avgeropoulos[1]
[1]*Department of Materials Science & Engineering, University of Ioannina,*
[2]*Department of Materials Science & Engineering, Cornell University*

14 ***"Synthesis, molecular and morphological characterization of linear triblock terpolymers where one of the blocks is poly(cyclohexadiene)"***

K. Misichronis[1], S. Rangou[1], E. Aschroft[2], J. W. Mays[2], A. Avgeropoulos[1]
[1]*Department of Materials Science & Engineering, University of Ioannina*
[2]*Department of Chemistry, University of Tennessee at Knoxville*

15 ***"Synthesis and characterization of high molecular weight linear triblock terpolymer consisting of polystyrene, polybutadiene, polyisoprene with different isomerisms"***

G. Zapsas[1], S. Rangou[1], A. Avgeropoulos[1], E. L. Thomas[2]
[1]*Department of Materials Science & Engineering, University of Ioannina*
[2]*Department of Materials Science & Engineering and Institute of Soldier Nanotechnologies, Massachusetts Institute of Technology*

16 ***"Nanostructures from well defined diblock copolymers of polystyrene (PS) and poly(dimethylsiloxane) (PDMS)"***

P. Georgopanos[1], C. C. Chao[2], R. M. Ho[2,3], A. Avgeropoulos[1]
[1]*Department of Materials Science & Engineering, University of Ioannina*
[2]*Institute of Microelectromechanical System, National Tsing Hua University, Taiwan*
[3]*Department of Chemical Engineering, National Tsing Hua University, Taiwan*

17 ***"Thiophene conducting copolymers"***

E. Grana[1], V. Goulas[2], A. Katsoulidis[3], T. Makris[4], D. Katsigiannopoulos[1], E. Skouras[4], P. Pomonis[3], A. Avgeropoulos[1]
[1]*Polymers' Laboratory, Department of Materials Science & Engineering, University of Ioannina*
[2]*Section of Organic Chemistry & Biochemistry, Department of Chemistry, University of Ioannina*
[3]*Section of Industrial Chemistry, Department of Chemistry, University of Ioannina*
[4]*Nanotechnology Laboratory, Department of Materials Science & Engineering, University of Ioannina*

18 ***"Incorporation of magnetic nanoparticles in a $PI_{3,4}$-b-$PB_{1,4}$ polymeric matrix"***

A. Tomou[1], A. Enotiadis[1], S. Rangou[1], M. Kitsas[1], A. P. Douvalis[1,2], A. Avgeropoulos[1], I. Panagiotopoulos[1], D. Gournis[1], T. Bakas[2]
[1]*Department of Materials Science and Engineering, University of Ioannina*
[2]*Department of Physics, University of Ioannina*

19 ***"Intercalation of an amphiphilic diblock copolymer in layered materials"***

Enotiadis A.[1], Sotiriou I.[1], Douli E.[2], Georgopanos P.[2], Avgeropoulos A.[2], Gournis D.[1]
[1]*Ceramics and Composites Laboratory, Department of Materials Science and Engineering, University of Ioannina*
[2]*Polymers' Laboratory, Department of Materials Science & Engineering, University of Ioannina,*

20 *"**Synthesis and characterization of proton exchange membrane nanocomposites for high temperature fuel cells"***
I. Kalamaras[1], J. K. Kallitsis[2,3], V. G. Gregoriou[1,2]
[1]*Foundation for Research and Technology-Hellas, Institute of Chemical Engineering and High Temperature Chemical Processes (FORTH/ICEHT)*
[2]*Advent Technologies S. A., Scientific Park of Patras*
[3]*Department of Chemistry, University of Patras*

21 ***"Crosslinked 2-carboxybenzylchitosan: synthesis, characterization and potential use for transdermal delivery of fluconazole"***
K. P. Koutroumanis, D. N. Bikiaris
Department of Chemistry, Aristotle University of Thessaloniki

22 ***"Synthesis of copolyesters based on adipic acid, glycolic acid and 1,4-butanediol and their hydrolytic degradation"***
S. Papadaki, D. Triantou, J. Simitzis
School of Chemical Engineering, National Technical University of Athens

23 ***"Low temperature process for the production of long chain aliphatic polyamides"***
A. C. Boussia, S. N. Vouyiouka, C. D. Papaspyrides
School of Chemical Engineering, National Technical University of Athens

24 ***"Titanium catalyzed ring opening polymerization of lactides. A route to novel macromolecular architectures"***
N. Petzetakis, D. Let, V. Kotzabasakis, M. Pitsikalis, N. Hadjichristidis
Industrial Chemistry Laboratory, Department. of Chemistry, University of Athens

25 ***"Synthesis of symmetric and asymmetric miktoarm star copolymers $(PI)_2(PEO)_2$"***
Th. Vasilakopoulos, H. Iatrou, N. Hadjichristidis
Industrial Chemistry Laboratory, Department of Chemistry, University of Athens

26 ***"Synthesis of well defined graft polymers"***
A. Nikopoulou, N. Hadjichristidis
Industrial Chemistry Laboratory, Department of Chemistry, University of Athens

27 ***"New approach to 'click chemistry' - combination of 'click chemistry' and anionic polymerization"***
A. Touris, N. Hadjichristidis
Industrial Chemistry Laboratory, Department of Chemistry, University of Athens

28 ***"Controlled functional nanoparticles"***
E. Driva[2], G. Sakellariou[2], D. Baskaran[2], J. W. Mays[1,2]
[1]*Chemical Sciences Division and Center for Nanophase Materials Science, Oak Ridge National Laboratory, Oakridge, TN, USA*
[2]*Industrial Chemistry Laboratory, Department of Chemistry, University of Tennessee*

29 ***"Synthesis of water soluble polypeptides containing (L)-proline"***
Gkikas M., Iatrou H., Hadjichristidis N.
Industrial Chemistry Laboratory, Department of Chemistry, University of Athens

30 ***"Synthesis and characterization of triblock copolymers by combination of anionic and atom transfer radical polymerization"***
L.-F. Arakelian, M. Pitsikalis, N. Hadjichristidis
Industrial Chemistry Laboratory, Department of Chemistry, University of Athens

31 ***"Terpyridine-ruthenium complexes for the decoration of CNTs, semiconducting oligomers and polymers"***

A. K. Andreopoulou[1,2], A. A. Stefopoulos[1,2], E. K. Pefkianakis[1,2], N. P. Tzanetos[1,2], C. Papagellis[3], M. Hammond[4], R. Mezzenga[4], J. K. Kallitsis[1,2]

[1]*Department of Chemistry, University of Patras*

[2]*Foundation of Research and Technology Hellas, Institute of Chemical Engineering and High Temperature Processes*

[3]*Department of Materials Science, University of Patras*

[4]*Department of Physics and Fribourg Center for Nanomaterials, University of Fribourg*

32 ***"Synthesis of copolymers based on benzene and biphenyl and their characterization by XRD and DSC"***

D. Triantou, S. Soulis, J. Simitzis

School of Chemical Engineering, National Technical University of Athens

33 ***"Electrochemical surface treatment of laboratorily produced carbon fibers by cyclic voltammetry"***

P. Georgiou, A. Photiou, S. Soulis, J. Simitzis

School of Chemical Engineering, National Technical University of Athens

34 ***"Nanofiller effect on the thermal response of poly(3-hydroxybutyrate) nanocomposites and isoconversional kinetic analysis of the thermal degradation"***

E. Panayotidou[1,2], S. I. Marras[1], I. Zuburtikudis[1], D. S. Achilias[2]

[1]*Department of Industrial Design Engineering, TEI of Western Macedonia*

[2]*Department of Chemistry, Aristotle University of Thessaloniki*

35 ***"Periodic nanodot formation on polymers with plasmas: Towards plasma-directed polymer self-assembly?"***

D. Kontziampasis, N. Vourdas, G. Boulousis, V. Constantoudis, A. Tserepi, E. Gogolides

Institute of Microelectronics, NCSR Demokritos

36 ***"Stochastic prediction of the exact topological characteristics of LDPE produced in tubular reactors"***

D. Meimaroglou[1,2], P. Pladis[2], A. Baltsas[2], C. Kiparissides[1,2]

[1]*Department of Chemical Engineering, Aristotle University of Thessaloniki*

[2]*Chemical Process Engineering Research Institute, Centre for Research and Technology*

37 ***"Effect of reaction conditions and catalyst design on the rheological properties of polyolefins produced in gas-phase olefin polymerization reactors"***

P. Pladis[2], V. Kanellopoulos[2] C. Chatzidoukas[2], C. Kiparissides[1,2]

[1]*Department of Chemical Engineering, Aristotle University of Thessaloniki*

[2]*Chemical Process Engineering Research Institute, Centre for Research and Technology Hellas*

38 ***"Modeling of industrial catalytic olefin polymerization slurry reactors"***

V. Touloupides[1,2], V. Kanellopoulos[2], P. Pladis[2], A. Krallis[2], C. Kiparissides[1,2]

[1]*Department of Chemical Engineering, Aristotle University of Thessaloniki*

[2]*Chemical Process Engineering Research Institute, Centre for Research and Technology Hellas*

39 ***"Viscoelastic tube inflation under constant rate of growth"***

E. Voyiatzis, C. Tsenoglou

School of Chemical Engineering and School of Applied, National Technical University of Athens

40 ***"On-line monitoring of the industrial formaldehyde resin production"***

D. Papapetros[1,2], I. Katsampas[1], C. Panayiotou[2]

[1]*Chimar Hellas S.A., Thessaloniki*

[2]*Department of Chemical Engineering, Aristotle University of Thessaloniki*

41 ***"Effect of the concentration of silane-coupling agent on physical properties of dental resin-nanocomposites"***
M.M. Karabela, I.D. Sideridou
Department of Chemistry, Aristotle University of Thessaloniki

42 ***"Plain and modified phase inversion membranes for gas separation"***
G. Karadimos, V. Kosma, K. G. Beltsios
Department of Materials Science and Engineering, University of Ioannina

43 ***"Effect of the environmental degradation on the viscoelastic response of nano modified epoxies and CFRPs"***
N. M. Barkoula[1], E. Fiamegou[2], A. Paipetis[1]
[1]Dept. of Materials Science & Engineering, University of Ioannina
[2]Department of Mechanical Engineering and Aeronautics, University of Patras

44 ***"Synthesis and characterization of acrylic bone cements reinforced with bioceramics"***
D.-E. Baciu, D. Giannakopoulos, S. Soulis, J. Simitzis
School of Chemical Engineering, National Technical University of Athens

45 ***"Processing effects on the dissolution properties of thin polymer based chemically amplified photoresist films"***
D. Drygiannakis[1,2], G. P. Patsis[1], K. van Werden[3], A. Boudouvis[2], I. Raptis[1]
[1]Institute of Microelectronics, NCSR "Demokritos"
[2]School of Chemical Eng., National Technical University of Athens
[3]AZ Electronic Materials GmbH, Wiesbaden, Germany

46 ***"Electrical properties of polymeric carbons produced from the precursor system of novolac resin - naphthalene/caralyst - olive stones biomass"***
A. Pikasi, P. Georgiou, J. Simitzis
School of Chemical Engineering, National Technical University of Athens

47 ***"Novolac resin and lignocellulosic materials as precursors for carbonaceous adsorbents"***
Z. Ioannou, J. Simitzis
School of Chemical Engineering, National Technical University of Athens

48 ***"New high temperature polymer electrolyte membranes influence of the chemical structure on their properties"***
N. Gourdoupi[1,3], K. Papadimitriou[1], S. Neophytides[2,3], J.K. Kallitsis[1,2,3]
[1]Department of Chemistry, University of Patras, Patras 26500, Greece
[2]Foundation of Research and FORTH-ICE/HT
[3]Advent Technologies S.A., Patras Science Park

49 ***"The effect of nanoclay content on the electrospun fibrous structure of biodegradable polymer nanocomposites"***
A. Tsimpliaraki, S. Svinterikos, C. Panayiotou
Department of Chemical Engineering, Aristotle University of Thessaloniki

50 ***"Type II photoinitiator systems based on novel fluorenone and fluorene chromophores. A mechanistic study by laser flash photolysis"***
X. Asvos[1], M. G. Siskos[1], A. K. Zarkadis[1], O. Brede[2], R. Hermann[2]
[1]Department of Chemistry, University of Ioannina
[2]Interdisciplinary Group Time-Resolved Spectroscopy, University of Leipzig

Tuesday, 30th September 2008

Poster Session II

Nanotechnology / Self-Assemply / Colloids / Biopolymers / Surfaces and interfaces / Nanocomposites / Polymer Dynamics

1 ***"Measurements of free volume in polymer nanocomposite coatings using positron annihilation lifetime spectroscopy"***
G. Choudalakis, A. D. Gotsis
Department of Sciences, Technical University of Crete

2 ***"Light induced micro-fiber formation in transparent polymer solutions"***
E. Anyfantakis[1,2], B. Loppinet[2], C. Mantzaridis[3,4], S. Pispas[4], G. Fytas[2,3]
[1]*Chemistry Department, University of Crete*
[2]*Institute of Electronic Structure and Laser, FO.R.T.H.*
[3]*Materials Science and Technology Department, University of Crete*
[4]*Theoretical and Physical Chemistry Institute, N.H.R.F*

3 ***"Does Brillouin light scattering probe the primary glass transition process?"***
P. Voudouris[1,2], G. Fytas[1, 3, 4]
[1]*FORTH/ Institute of Electronic Structure and Laser*
[2]*Department of Chemistry, University of Crete*
[3]*Department of Materials Science and Technology, University of Crete*
[4]*Max Planck Institute for Polymer Research*

4 ***"A thermal and dielectric study of molecular dynamics in polyurethane-poss hybrids"***
K. Raftopoulos[1], C. Pandis[1], L. Apekis[1], B. Janowski[2], K. Pielichowski[2], P. Pissis[1]
[1]*National Technical University of Athens, Department of Physics*
[2]*Department of Chemistry and Technology of Polymers, Cracow University of Technology*

5 ***"Dielectric - mechanical and thermal studies of molecular mobility and phase morphology in epoxy-amine / carbon black nanocomposites"***
E. Logakis[1], Th. V. Kosmidou[3], A. Kanapitsas[2], C. Tsonos[2], C. G. Delides[3], P. Pissis[1]
[1]*National Technical University of Athens, Department of Physics*
[2]*Technological Educational Institute of Lamia, Department of Electronics*
[3]*Technological Educational Institute of Western Macedonia*

6 ***"Dynamics and rheology in suspensions and glasses of soft colloids"***
A. Pamvouxoglou[1,2] and G. Petekidis[1,2]
[1]*FORTH/ Institute of Electronic Structure and Laser*
[2]*Department of Materials Science and Technology, University of Crete*

7 ***"Thermal and electrical properties of multi-walled carbon nanotube nanocomposites prepared by diluting a masterbatch with various types of modified and non-modified polypropylenes"***
E. Logakis[1], C. Pandis[1], V. Peoglos[1], P. Pissis[1], M. Mičušík[2], M. Omastová[2], J. Pionteck[3], P. Pötschke[3]
[1]*National Technical University of Athens*
[2]*Polymer Institute, Slovak Academy of Sciences*
[3]*Leibniz Institute of Polymer Research, Dresden*

8 ***"Dielectric studies of molecular dynamics in swollen poly(ethyl acrylate) networks with non-polar solvents"***
A. Stathopoulos[1], A. Kyritsis[1], P. Pissis[1], J.L. Gomez Ribelles[2], M. Monleon Pradas[2]
[1]*Department of Physics, National Technical University of Athens, Greece*
[2]*Department of Applied Thermodynamics, Universidad Politecnica de Valencia, Spain*

9 ***"Dynamic mechanical and tensile properties of thermally oxidized homopolymer PAN fibers"***
S. Soulis, M. Pisania, P. Stergiou, J. Simitzis
School of Chemical Engineering, National Technical University of Athens

10 *"**Synthesis and mechanical properties of A_nB_n star copolymers and $A_n(B\text{-}b\text{-}C)_n$ star terpolymers"***
G. Tsoukleri[1,2], G. Linardatos[1,3], J. Parthenios[1], C. Galiotis[1,2], C. Tsitsilianis[1,3]
[1]*Foundation of Research and Technology Hellas, Institute of Chemical Engineering and High Temperature Processes*
[2]*Department of Materials Science, University of Patras*
[3]*Department of Chemical Engineering, University of Patras*

11 ***"Influence of maleic anhydrite component of cured polyesters on their relaxations determined by dielectric spectroscopy (DS) and dynamic mechanical thermal analysis (DMTA)"***
G. Mitsis, D. Triantou, S. Soulis, J. Simitzis
School of Chemical Engineering, National Technical University of Athens

12 ***"Self-assembly and dynamics of discotic liquid crystals"***
M. M. Elmahdy[1,2], X. Dou[3], M. Mondeshki[3], G. Floudas[1,2], H. -J. Butt[3], H. W. Spiess[3], K. Müllen[3]
[1]D*epartment of Physics, University of Ioannina*
[2]*Foundation for Research and Technology-Hellas (FORTH), Biomedical Research Institute (BRI)*
[3]*Max-Planck Institut für Polymerforschung, Mainz*

13 ***"Effect of architecture on the self-assembly and dynamics of model diblock and star copolypeptides"***
A. Gitsas[1], G. Floudas[1], M. Mondeshki[2], H. -J. Butt[2], H. W. Spiess[2], H. Iatrou[3], N. Hadjichristidis[3]
[1]*University of Ioannina, Department of Physics and Foundation for Research and Technology-Hellas (FORTH), Biomedical Research Institute (BRI)*
[2]*Max Planck Institute for Polymer Research*
[3]*University of Athens, Department of Chemistry, Industrial Chemistry Laboratory*

14 ***"Modeling the lateral aggregation of membrane proteins"***
M. Yiannourakou[1], L. Marsella[2], F. De Meyer[2,3], B. Smit[3]
[1]*NCSR "Demokritos"*
[2]*CECAM - Centre Europeen de Calcul Atomique et Moleculaire, Lyon, France*
[3]*Department of Chemical Engineering, University of California*

15 ***"Complexation of hen egg white lysozyme with sodium (sulfamate-carboxylate) isoprene polyelectrolytes"***
M. Karayianni, G. Mountrichas, S. Pispas, G. D. Chryssikos, V. Gionis
Theoretical & Physical Chemistry Institute, National Hellenic Research Foundation

16 ***"Study of the release kinetics of a drug and an MRI contrast agent from poly (vinyl alcohol) matrices"***
A. Hasimi, K. G. Papadokostaki, M. Sanopoulou
Institute of Physical Chemistry, NCSR "Demokritos

17 ***"Wetting, optical property and protein adsorption control of polymer surfaces by plasma nanotexturing"***
K. Tsougeni[1], M. E. Vlachopoulou[1], K. Kontakis[1], D. Papageorgiou[1], P. S. Petrou[2], S. E. Kakabakos[2], A. Tserepi[1], E. Gogolides[1]
[1]*Institute of Microelectronics, NCSR "Demokritos"*
[2]*Institute of Radioisotopes and Radiodiagnostic Products NCSR "Demokritos"*

18 ***"Bulk and interfacial dynamics of PDMS/Titania nanocomposites"***
A. Panagopoulou[1], A. Spanoudaki[1], P. Pissis[1], L. Bokobza[2]
[1]*National Technical University of Athens, Department of Physics*
[2]*Laboratoire de Physico-Chimie Structurale et Macromoléculaire ESRCI, France*

19 ***"Synthesis and properties of unmodified LDPE/Organosilicates nanocomposites"***
A. Giannakas[1], C. G. Spanos[1], P. Xidas[2], K. S. Triantafyllidis[2], A. Katsoulidis[3], A. Ladavos[1]
[1]*School of Natural Resources and Enterprise Management, University of Ioannina*
[2]*Department of Chemistry, Aristotle University of Thessaloniki*
[3]*Department of Chemistry, University of Ioannina*

20 ***"Organic - Inorganic Nanocomposites: A study of the structure and dynamics in confined geometry"***
S. Fotiadou[1], K. Chrissopoulou[2], B. Frick[3], S. H. Anastasiadis[1,2]
[1]*Chemical Engineering Department, Aristotle University of Thessaloniki*
[2]*Institute of Electronic Structure and Laser, Foundation for Research and Technology-Hellas*
[3]*Institut Laue Langevin, Grenoble, France*

21 ***"Glass transition, structural characterization and segmental dynamics in epoxy/carbon fillers nanocomposites"***
Th. V. Kosmidou[1], C. G Delides[1], C. A. Stergiou[2], A. S. Vatalis[1], P. Pissis[3]
[1]*Technological Education Institute (TEI) of Western Macedonia, Laboratories of Physics and Materials Technology*
[2]*Department of Electrical Engineering and Computers, Aristotle University of Thessaloniki*
[3]*National Technical University of Athens, Department of Physics*

22 ***"Dynamics of epoxy nanocomposites: The effect of filler's content and the size structure and geometry of the nanoparticles"***
C. G. Delides
Technological Education Institute (TEI) of Western Macedonia, Laboratories of Physics and Materials Technology

23 ***"Study of silicone rubber nanocomposites reinforced with organophilic montmorillonite"***
A. Voulomenou, P.A. Tarantili
School of Chemical Engineering, National Technical Univ. of Athens

24 ***"Molecular mobility studies in hybrid PCN clay nanocomposites"***
P. Maroulas[1], S. Kripotou[1], P. Pissis[1], A. Fainleib[2], K. Gusakova[2]
[1]*Department of Physics, National Technical University*
[2]*Institute of Macromolecular Chemistry of National Academy of Sciences*

25 ***"A theoretical study on the size and the shape of linear dendronized polymers in good and selective solvents"***
P. Efthymiopoulos, M. Kosmas, C. Vlahos
Department of Chemistry, University of Ioannina

26 ***"On the conformational properties of a DNA chain with loops"***
M. Kosmas, C. Vlahos
Chemistry Department, University of Ioannina

27 ***"Collapse transitions in thermosensitive alternating copolymers: a monte carlo study"***
A. N. Rissanou[1,2], E. Manias[3] and I. A. Bitsanis[1]
[1]*Institute of Electronic Structure and Laser, FO.R.T.H.*
[2]*Molecular Thermodynamics and Modeling of Materials Laboratory, Institute of Physical Chemistry, National Center for Scientific Research "Demokritos*
[3]*Department of Materials Science & Eng., Pennsylvania State University*

28 ***"Molecular dynamics of PAMAM dendrimers and their complexes with linear polymers in aqueous solutions"***

I. Tanis, K. Karatasos
Department of Chemical Engineering, Aristotle University of Thessaloniki

29 ***"Off lattice monte carlo simulations of AB and ABA Hybrid star dendritic copolymers"***

L. Gergidis[1], O. Moultos[2], C. Georgiadis[2], M. Kosmas[2] and C. Vlahos[2]
[1]Department of Materials Science & Engineering, University of Ioannina,
[2]Department of Chemistry, University of Ioannina

30 ***"Neutron reflectivity and computer simulation studies of centrally adsorbed star polymer brushes"***

I. Hiotelis[1], A. G. Koutsioubas[1], N. Spiliopoulos[1], D. Anastassopoulos[1], A. A. Vradis[1], C. Toprakcioglu[1], A. Menelle[2], G. Sakellariou[3], Nikos Hadjichristidis[3]
[1]Physics Department, University of Patras
[2]Laboratoire Leon Brillouin, CEA SACLAY, France
[3]Chemistry Department , University of Athens

31 ***"Detection of diffusive jumps of small penetrants dispersed in polymer systems"***

Th. E. Raptis[1], V. E. Raptis[2,3], J. Samios[4]
[1]Division of Applied Technology, NCSR "Demokritos"
[2]Department of Chemistry, University of Ioannina.
[3]Department of Materials Science and Engineering, University of Ioannina.
[4]Department of Chemistry, University of Athens

32 ***"Investigation of thermodynamic properties of polyethylene glycol by inverse Gas chromatography and computer simulations"***

G. S. Dritsas, I. Tanis, M. Stournara, K. Karatasos, C. Panayiotou
Department of Chemical Engineering, Aristotle University of Thessaloniki

33 ***"Atomistic simulation of the sorption of small gas molecules in polyisobutylene"***

G. Tsolou[1] ,V. G. Mavrantzas[1], Z. A. Makrodimitri[2], I. G. Economou[2], R. Gani[3]
[1]Department of Chemical Engineering, University of Patras & FORTH-ICE/HT
[2]Molecular Thermodynamics and Modeling of Materials Laboratory, Institute of Physical Chemistry, National Center for Scientific Research "Demokritos"
[3]CAPEC, Department of Chemical Engineering, Technical University of Denmark

34 ***"Studying the elasticity of biological membranes through theory and simulations"***

V.Harmandaris, M. Deserno
Max Planck Institute for Polymer Research, Mainz, Germany

35 ***"Structural and electronic properties of Nb nanowires by tight binding molecular dynamics calculations"***

M. Iakovidis and Ch.E. Lekka
Department of Materials Science and Engineering, University of Ioannina

36 ***"Structural and electronic properties of Ti and TiO2 on C nanotubes by ab-initio calculations"***

M. Gialambouki and Ch.E. Lekka
Department of Materials Science and Engineering, University of Ioannina

37 "***Lithium ion induced nanophase ordering and ion mobility in ionic block copolymers"***

E. F. Ioannou[1], G. Mountrichas[1], S. Pispas[1], E. I. Kamitsos[1] and G. Floudas[2]
[1]Theoretical and Physical Chemistry Institute, National Hellenic Research Foundation [2]Department of Physics and Foundation for Research and Technology-Hellas, Biomedical Research Institute (FORTH-BRI)

38 ***"Reversible self-assembled nanostructures from block polyampholytes"***

C. Mantzaridis, S. Pispas
Theoretical and Physical Chemistry Institute, National Hellenic Research Foundation

39 ***"Self-assembly in mixed amphiphilic diblock copolymers-zwitterionic surfactants aqueous solutions"***

K. Dimitroulopoulos, S. Pispas
Theoretical and Physical Chemistry Institute, National Hellenic Research Foundation

40 ***"Self assembly core-shell PCL-co-PSu nanoparticles based on crystalline amorphous moieties for efficient controlled drug release"***

S. Papadimitriou[1], D. Bikiaris[1], K. Avgoustakis[2]
[1]*Department of Chemistry, Aristotle University of Thessaloniki*
[2]*Department of Pharmacy, University of Patras*

41 ***"Formation of gold nanoparticles in the corona of di- and triblock copolymers"***

A. Meristoudi[1,2], S. Pispas[1], N. Vainos[1,2]
[1]*Theoretical and Physical Chemistry Institute, National Hellenic Research Foundation*
[2]*Materials Science Department, University of Patras*

42 ***"Charge transport of conjugated polymer coated core-Shell nanoparticles"***

K. Mpoukouvalas[1], J. Wang[1], L. Sun[1], C. Wei[1], T. Beierlein[2], A. Muehlebach[3], E. Bonaccurso[1], H. -J. Butt[1], G. Wegner[1]
[1]*Max Planck Institute for Polymer Research*
[2]*CSEM - Centre Suisse d'Electronique et de Microtechnique SA*
[3]*Ciba Specialty Chemicals Inc. Group Research, K-420.3.15, Switzerland*

43 ***"Microcellular nanocomposite polymers prepared with supercritical CO_2: The role of nanoclays on porous structure"***

I. Tsivintzelis[1], S. I. Marras[1,2], I. Zuburtikudis[2], C. Panayiotou[1]
[1]*Department of Chemical Engineering, Aristotle University of Thessaloniki*
[2]*Department of Industrial Design Engineering, TEI of Western Macedonia*

44 ***"Poly(ethylene succinate) nanocomposites with a multifunctional nanofiller: Mechanical properties and biodegradability"***

A. A. Vassiliou, D. N. Bikiaris
Department of Chemistry, Aristotle University of Thessaloniki

45 ***"A new approach of segmental orientation in amorphous epoxy resin/carbon black nanocomposites"***

C. A. Stergiou[1], Th. V. Kosmidou[2], C. G. Delides[2]
[1]*Department of Electrical and Computer Engineering, Aristotle University*
[2]*Technological Education Institute (TEI) of Western Macedonia, Laboratories of Physics and Materials*

46 ***"End-grafted polymer chains onto inorganic nanoparticles"***

D. S. Achilleos, D. Moatsou, M. Vamvakaki
Institute of Electronic Structure and Laser, FO.R.T.H. and Department of Materials Science and Technology, University of Crete

47 ***"Adsorption of oligomers and polymers in nanoporous alumina"***

S. Karagiovanaki, A. G. Koutsioubas, N. Spiliopoulos, C. Toprakcioglu
Department of Physics, University of Patras

48 ***"Fluorinated methacrylic homopolymers: Polymerization, characterization, surface properties and effectiveness for the protection of stone"***

S. K. Papadopoulou[1], C. Michailof[1], I. Karapanagiotis[2], A. Tsakalof [3], I. Zuburtikudis[4], C. Panayiotou[1]
[1]*Department of Chemical Engineering, Aristotle University of Thessaloniki, 54124, Thessaloniki, Greece*
[2]*"Ormylia" Art Diagnosis Centre, Ormylia, Chalkidiki*
[3]*Department of Medicine, University of Thessaly*
[4]*Department of Industrial Design Engineering, TEI of Western Macedonia*

49 ***"Fabrication and thermal characterization of a thin poly(L-lactic acid) film with the layer-by-layer spin coating process and the use of thickness shear mode resonators"***
A. Kakalis, C. Panayiotou
Department of Chemical Engineering, University of Thessaloniki

50 ***"Colloidal microgel particles carrying acidic or basic moieties"***
K. E. Christodoulakis, M. Vamvakaki
Institute of Electronic Structure and Laser, Foundation for Research and Technology
Department of Materials Science and Technology, University of Crete

51 ***"Cu^{2+}-induced gelation in aqueous solutions of maleic acid-containing polyelectrolytes"***
E. K. Oikonomou[1,2], G. Bokias[1], J. K. Kallitsis[1,2]
[1]*Department of Chemistry, University of Patras*
[2]*Foundation of Research and Technology Hellas, Institute of Chemical Engineering and High-Temperature Chemical Processes (ICE/HT FORTH)*

52 ***"Hydration properties of nanostructrured hydrogels based on poly(2-hydroxyethyl acrylate) and poly(2-hydroxyethyl-co-ethyl acrylate)"***
Ch. Pandis[1], A. Stathopoulos[1], P. Klonos[1], A. Spanoudaki[1], A. Kyritsis[1], P. Pissis[1], M. M. Pradas[2], J. C. Rodriguez Hernandez[2], J. L. Gomez Ribelles[2]
[1]*Department of Physics, National Technical University of Athens*
[2]*Center for Biomaterials, Polytechnic University of Valencia*

53 ***"Molecularly imprinted polymers (MIPs) as selective sorbents in trichromatic dye mixtures"***
G. Z. Kyzas, D. N. Bikiaris, N. K. Lazaridis
School of Chemistry, Aristotle University of Thessaloniki

54 ***"pH-controlled quenching of the fluorescence of hydrophobic probes solubilized in ternary poly(acrylic acid)-surfactant-Cu^{2+} complexes in aqueous solution"***
Z. Iatridi, G. Bokias
Department of Chemistry, University of Patras

55 ***"Development of new semiconducting polymer functionalized carbon nanotubes"***
A. A. Stefopoulos[1,2], C. L. Chochos[1], K. Papagelis[3], J. K. Kallitsis[1]
[1]*Department of Chemistry, University of Patras*
[2]*FO.R.T.H., Institute of Chemical Engineering and High Temperature Processes*
[3]*Department of Materials Science, University of Patras*

Route to Conference Location

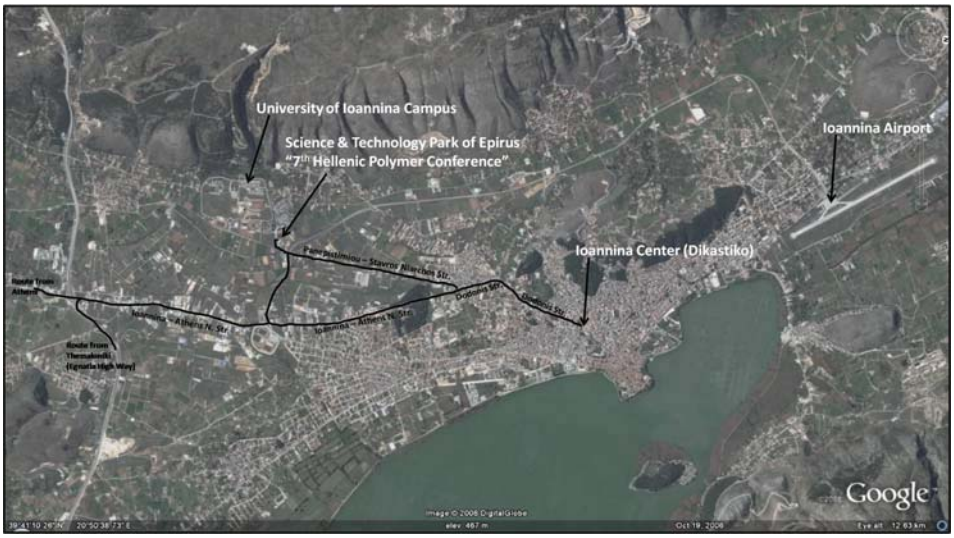

Invited Lecture 1

Periodic Polymers for Photonics, Phononics and Mechanics

Edwin L. (Ned) Thomas
Morris Cohen Professor and Department Head
Materials Science and Engineering
MIT, Cambridge, MA. 02139 USA

Nanotechnology requires control of materials from the atomic scale to the 100 nanometer scale to the macroscopic level. Exploiting the size and shape dependence of material properties and creating a set of functional properties holds great promise for the development of materials that will significantly contribute to future technologies. Polymers are a class of materials that have a very broad range of properties and moreover, can act as hosts or as templates for metallic and dielectric nanoparticles as well as organic molecules, resulting in multi-functional nanocomposites with combinations of properties not otherwise available. *Periodic* structural assemblies are of particular interest, due to their interesting interactions with waves: especially light and mechanical waves. Progress in this exciting area requires excellent control of 2D and 3D structure formation. A top-down approach, involving interference lithography via multiple beam optics or using phase masks is demonstrating good success in fabricating the requisite structures with desirable properties for photonics and phononics and mechanics.

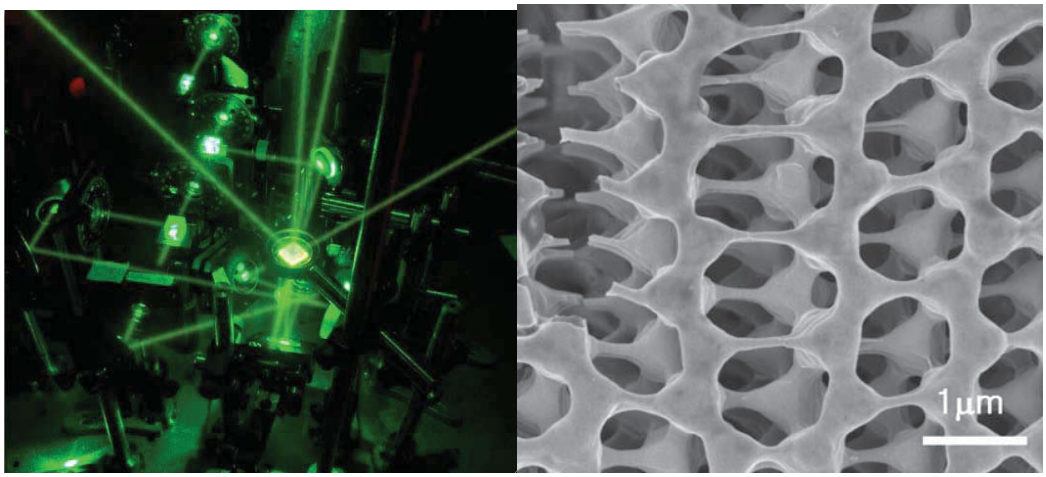

Fig. 1 (left) Multiple beams of coherent light interfere in a photoresist to form periodic structures. (right) An epoxy microframe exhibits large plasticity.

We utilize both negative and positive tone resists for interference lithography and target bicontinuous structures, since these are exemplary when considering expressing the inherent properties of both component materials (e.g. polymer/ceramic) due to the dominant role of the 3D connectivity of a phase on composite properties. To create multicomponent bicontinuous materials, after exposure and development, the initial polymer structure is infiltrated by a sol gel material and a high temperature consolidation is performed to convert to the ceramic while the polymer degrades to form a set of interconnected air channels. Double inversion using the ceramic structure as a template can lead to the formation of periodic metallic structures.

We are interested in phononic, photonic band gaps and particularly, dual band gap materials, so called “deaf and blind” materials. Simultaneous localization of light and sound in purposefully made

imperfections presents a novel means to enhance acousto-optical interactions. 3D polymeric microframes also provide intriguing mechanical behavior, where enhanced plasticity and toughness occurs for features sizes below a critical length scale. The computation of the properties of periodic materials is straightforward since the fabricated structure arises from a Fourier representation from the intensity interference equation.

References

Maldovan, M. and Thomas, E.L., *"Periodic Materials via Interference Lithography: Photonics, Phononics and Mechanics,"* Wiley-VCH, November, 2008.

Jang, J.-H., Dendukuri, D., Hatton, T.A., Thomas, E.L., Doyle, P.S., "A Route to Three Dimensional Structures in a Microfluidic Device: Stop Flow Interference Lithography," *Angewandte Chemie,* 46 (47), 9027-9031 (2007).

Maldovan, M., Ullal, C.K., Jang, J.-H., and Thomas, E.L., "Sub-Micrometer Scale Periodic Porous Cellular Structures: Microframes Prepared by Holographic Interference Lithography," *Advanced Materials,* 19 (22), 3809-3813 (2007).

Jang, J.-H., Ullal, C.K., Maldovan, M., Gorishnyy, T., Kooi, S., Koh, C.Y., Thomas, E.L., "3D Micro- and Nanostructures via Interference Lithography," *Advanced Functional Materials*, 17, 3027-3041, (2007).

Bita, I., Choi, T., Walish, J., Smith, H.I., and Thomas, E.L., "Large Area 3D Nanostructures with Octagonal Quasicrystalline Symmetry via Phase Mask Lithography," *Advanced Materials*, 19 (10), 1403, (2007).

Cheng, W., Gorishnyy, T., Krikorian, V., Fytas, G., Thomas, E.L., "In-plane elastic excitations in 1D polymeric photonic structures," *Macromolecules,* 39 (26): 9614-9620, (2006).

Thomas, E. L., Gorishnyy, T., Maldovan M., "Phononics: colloidal crystals go hypersonic," *Nature Materials*, 5 (10): 773-774, (2006).

Jang, J-H, Ullal, C.K., Choi, T., Lemieux, M.C., Tsukruk, V.V. and Thomas,E.L. "3D Polymer Microframes That Exploit Length-Scale-Dependent Mechanical Behavior," *Advanced Materials*, 18 (16), 2123-2127, (2006).

Choi, T., Jang, J.H., Ullal, C.K., LeMieux, M.C., Tsukruk, V.V., Thomas, E.L., "The Elastic Properties and Plastic Behavior of Two-Dimensional Polymer Structures Fabricated by Laser Interference Lithography," *Advanced Functional Materials*, 16 (10), 1324-1330 (2006).

Oral 1

SYNTHESIS AND CHARACTERIZATION OF AMPHIPHILIC BLOCK COPOLYMERS. ASSOCIATION BEHAVIOR IN AQUEOUS SOLUTIONS. POTENTIAL USE OF THE MICELLAR STRUCTURES AS DRUG CARRIERS.

Nikos Karanikolopoulos, Marinos Pitsikalis, Nikos Hadjichristidis
Department of Chemistry, University of Athens
Panepistimiopolis Zografou, 15771 Athens Greece

Using a combination of ring opening (ROP) and atom transfer radical polymerization (ATRP), amphiphilic linear diblock copolymers of poly(L-lactide), PLA, poly(DL-lactide), PDLLA, poly(dimethylaminoethyl methacrylate), PDMAEMA, poly(oligoethyleneglycol methacrylate), POEGMA, and poly(oligoethyleneglycol acrylate), POEGA, PLA-*b*-PDMAEMA, PDLLA-*b*-POEGMA and PDLLA-*b*-POEGA, where successfully synthesized. The homopolymers of poly(lactid acid), synthesized by the ROP of the corresponding lactide, after purification from the catalyst, bear functional end hydroxyl groups. The esterification reaction with 2-bromoethyl bromoisobutyrate leads to the synthesis of macroinitiators capable of initiating ATRP of DMAEMA, OEGMA and OEGA monomers. All the polymers, were characterized by size exclusion chromatography (SEC) and nuclear magnetic resonance spectroscopy (^{1}H-NMR). The 1,3–dipolar cycloaddition reaction between the terminal azide group of the copolymer PDLLA-*b*-POEGA and the triple bond of the product of reaction between propargylamine and activated carboxyl groups of biotin and folic acid, led to the introduction of functionalized groups at the end of the hydrophilic POEGA block. The percentage of incorporation of folic acid and biotine in diblock copolymers, were determinated with ultraviolet-visible spectroscopy (UV-vis).

The solid state properties of PLA-*b*-PDMAEMA and PDLLA-*b*-POEGMA, were studied with differential scanning calorimetry (DSC). Dynamic light scattering (DLS), atomic force microscopy (AFM) as well as scanning electron microscopy (SEM), were used to study the micellar behaviour of amphiphilic copolymer aqueous solutions. The zeta potential (for specific pH values), was measured for pH responsive polymer micelles made from PDLLA-*b*-PDMAEMA. The afore mentioned characterization techniques indicated the presence of spherical micelles with narrow size distribution and diameter ~100nm for each case of PDLLA-*b*-POEGMA, PDLLA-*b*-POEGA and PDLLA-*b*-POEGA-(folic acid or biotine) copolymers. The pH responsive polymer micelles, made from copolymers PDLLA-*b*-PDMAEMA at pH=7,40, are spherical, with narrow size distribution and diameter in the range of 17-37 nm, depending on the molecular weight and composition of block copolymers. At pH=6,40, the micelles remain spherical, having broad distribution of sizes and diameter ranging between 84 and 162nm, due to the swelling of their corona. The degree of the micellar swelling, increases at pH=5,00, leading to existence of micellar aggregation in aqueous solution.

The study of encapsulation ability, of different pharmaceutical substances and pyrene at polymer micelles, as well as the determination of partition coefficients, *K*, of pharmaceutical substances and pyrene between polymer micelles and aqueous solutions was investigated with the use of fluorescence spectroscopy.

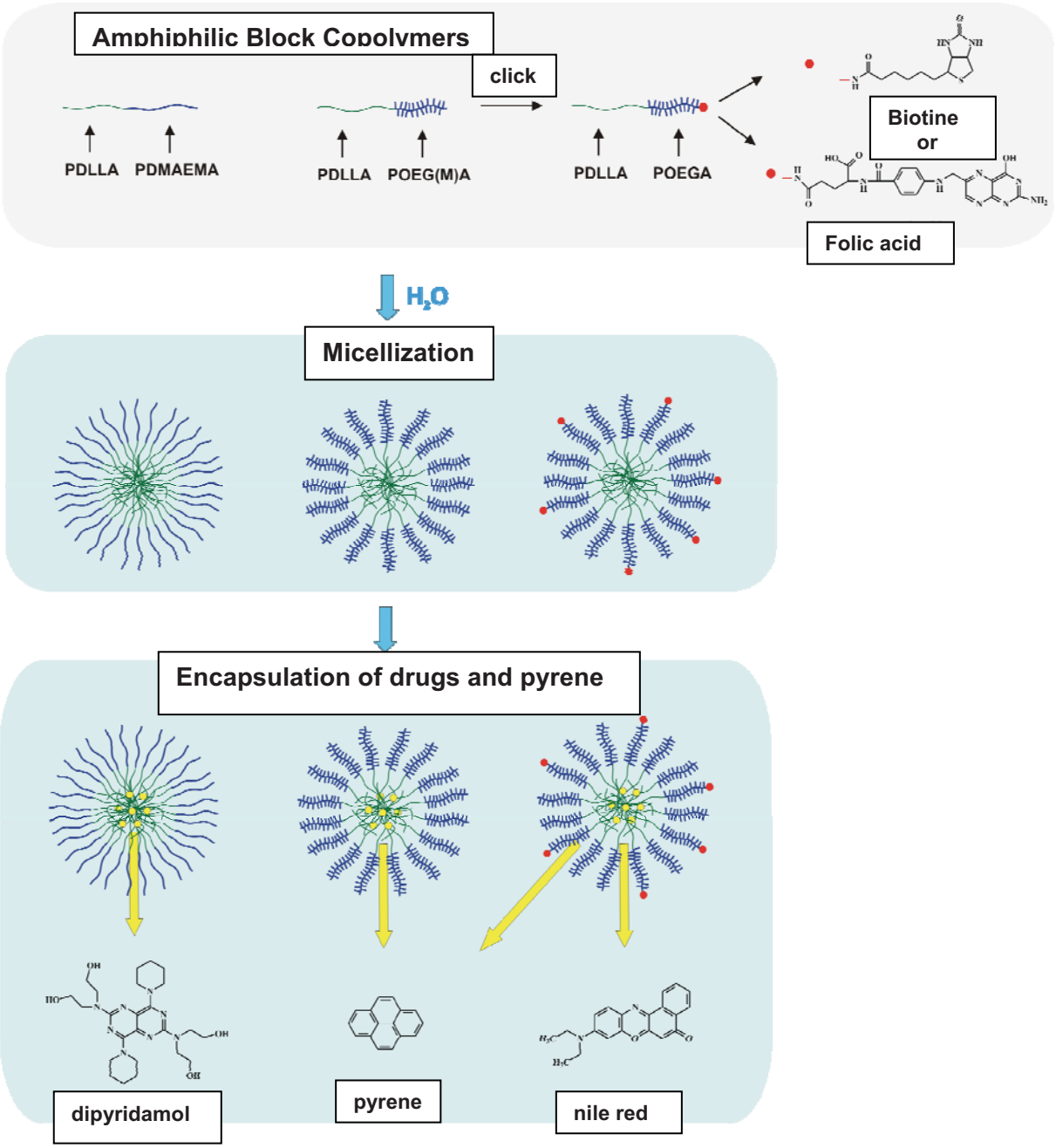

Synthesis of amphiphilic block copolymers and association behavior in aqueous solutions.

Oral 2

Synthesis and Characterization of Polymeric [Ru2+] Complexes and their Application as Dyes in Solar Cells

E.K.Pefkianakis[1], N.P.Tzanetos[1], T.Stergiopoulos[2], P.Falaras[2] and J.K.Kallitsis[1]

1.Department of Chemistry, University of Patras, 26504, Patras, Greece
2. Institute of Physical Chemistry, NCSR Demokritos, Aghia Paraskevi 15310, Athens, Greece

The technology of renewable energies, aims in the long run, to efficiently contribute to the solution of the energy problem both economically and environmentally friendly. In respect to the materials science, the development of energy related materials is of great interest and one of the main achievements focused into Organic Solar Cells. These are categorized to Cells of Organic Molecules, Polymeric/Plastic Cells (OPVs)[1,2] and Dye Sensitized Cells (DSSCs)[3,4]. Our main objective in DSSCs is to replace the commonly used dyes (complexes of transition metal ions with organic molecules) with polymeric dyes, thus utilizing the advantages of the polymers' character in a sensitized Solar Cell. Such materials, consist of polymeric complexes of the Ruthenium (II) ion, with tridentateor bidentate ligands[5-7], like 2,2':6',2''-terpyridine and 2,2'-bipyridine, respectively.

More specifically in this work we prepared terpyridine and bipyridine vinyl monomers and in consequence we performed Atom Transfer Radical Polymerization, using functional initiators (carrying carboxylic groups aiming at the attachment of the dye onto the TiO2) leading to homopolymers of controlled architecture (e.g. homopolymer A and B). After complexation with Ruthenium (II) ions, these materials can be applied as dyes in Hybrid Photovoltaic Cells (PVs). The resulting polymer structures were confirmed via NMR and their optical properties were investigated using UV-Vis and Photoluminescence.

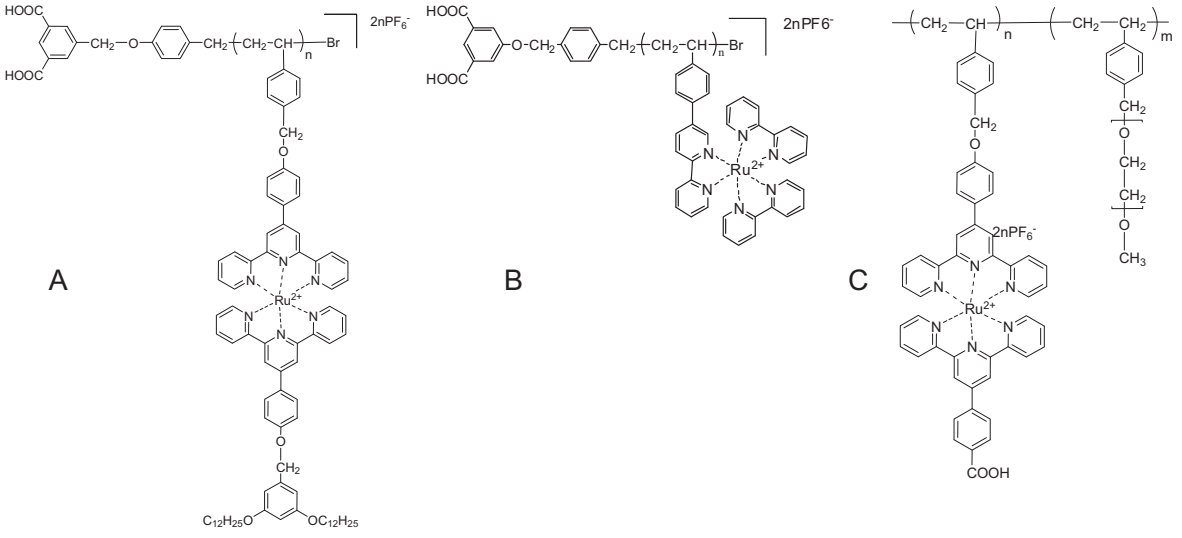

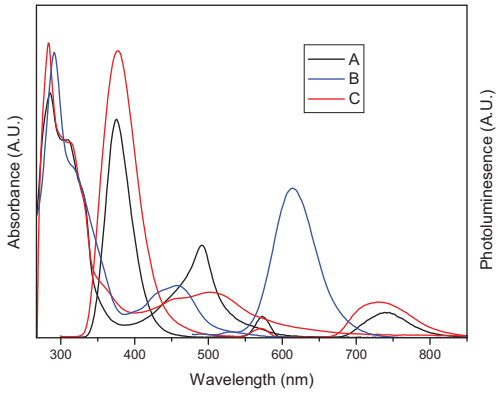

Taking this effort one step further we combined the polymeric dye of Ru(II) complexes with the most commonly used polyelectrolyte in hybrid PVs, like PEO. The random copolymers produced (copolymer C) were examined equally as before with NMR, UV-Vis and Photoluminescence.

The performance of these materials in solar cells was also tested. As an example, homopolymer B gave a short circuit photocurrent density Jsc= 39 μA/cm2, open circuit potential Voc= 350 mV, fill factor ff=0.39 and power conversion efficiency n=0.005%.

Dye	JSC (μA/cm2)	VOC (mV)	ff	n (%)
A	54	248	0.44	0.006
B	39	350	0.39	0.005
N719	9290	583	0.53	2.87

Besides this relatively poor efficiency, the obtained results look promising and justify further investigations in the field. In an attempt to improve the efficiency of these systems we combined the polymeric dyes with poly(ethylene oxide) in copolymers with different architectures. These new copolymers of various structural compositions are now under investigation for their photovoltaic performance.

References:

1. F. Padinger, R.S. Ritberger, N.S. Sariciftci *Adv. Funct. Mater*. **2003**, 13, 85.
2. G. Li, V. Shrotriga, J. Huang, Y. Yao, T. Moriarty, K. Emery, Y. Yang *Nature Mater*. **2005**, 4, 864.
3. B. O'Regan, M. Grätzel, *Nature* **1991**, 355, 737,.
4. M.K. Nazeeruddin, A. Kay, I. Rodicio, R. Humphrey-Baker, E. Müller, P. Liska, N. Vlachopoulos and M. Grätzel, *J. Am. Chem. Soc*., **1993**,115, 6382 .
5. U. S Schubert, C. Eschbaumer *Anew. Chem. Int. Ed*. **2002**, 41 , 2829.
6. N. P. Tzanetos, A. K Andreopoulou, J. K. Kallitsis J.*Polym. Sci. Part A : Polym. Chem.* **2005**, 43, 4838.
7. A. K. Andreopoulou, J. K. Kallitsis *Eur. J. Org. Chem*. **2005**, 2005, 4448.

Aknowledgement: Financial support for this project from the Greek Ministry of Development under the research grant PENED 03ED118 "Organic Solar Cells" is gratefully acknowledged.This research project (PENED) is co-financed by E.U.-European Social Fund (75%) and the Greek Ministry of Development-GSRT (25%)

Invited Lecture 2

Well-Defined Complex Macromolecular Architectures by Anionic Polymerization High Vacuum Techniques

Nikos Hadjichristidis, *Department of Chemistry, University of Athens, Greece*

Abstract

Anionic polymerization high vacuum techniques have proven to be a very powerful tool for the synthesis of well-defined macromolecules with complex architectures. Until now, however, only a relatively limited number of such structures with two or thee different components (star block, miktoarm star, graft, branched, cyclic, hyperbranched) have been created, the potential of anionic polymerization is unlimited. Imagination, nature, and other scientific disciplines (i.e., polymer physics, materials science, molecular biology) will lead polymer scientists to novel structures, with the ultimate goal of designing and synthesizing polymeric materials with predetermined properties.

A short review of the structure/property relationships of selected polymers, synthesized by the Athens group, will be initially presented. Subsequently, recent work on a few novel well-defined complex architectures (dendritic, *Janus* H-shaped, molecular *chimeras*) will be discussed.

Selected References

N. Hadjichristidis, M. Pitsikalis, S. Pispas, H. Iatrou
"Polymers with complex architecture by living anionic polymerization"
Chem. Rev. **101**, 3747 -3792, 2001.

N. Hadjichristidis, S. Pispas, G. Floudas
“Block copolymers. Synthetic strategies, physical properties and applications”
J. Wiley & Sons,1-419(2003)

N. Hadjichristidis, H. Iatrou, M. Pitsikalis, S. Pispas, A. Avgeropoulos
“Linear and non-linear multiblock terpolymers. Synthesis, self-assembly in selective solvents and in Bulk”
*Progr. Polym. Sci. **30**, 725-782 (2005)*

K.Orfanou, E. Iatrou, D.Lohse , N. Hadjichristidis
“Synthesis of well-defined second (G-2) and third (G-3) generation dendritic polybutadienes”
*Macromolecules **39**, 4361-4365 (2006)*

E. Ruymbeke, K. Orfanou, M. Kapnistos, H. Iatrou, M. Pitsikalis, Hadjichristidis, D. Lohse, D.Vlassopoulos
“Entangled dendritic polymers and beyond: rheology of symmetric Cayley-tree polymers and *macromolecular self-assemblies”*
*Macromolecules **40**, 5941-5952 (2007)*

S. Christodoulou, P. Driva, H. Iatrou, N.Hadjichristidis
“Synthesis and micellization behavior of Janus H-shaped A_2BC_2 terpolymers”
*Macromolecules **41**, 2607-2615 (2008)*

P. Driva, D. Lohse, N. Hadjichristidis
“Well-defined complex macromolecular architectures by anionic polymerization of styrenic single and double homo/miktoarm star-tailed macromonomers”
*J. Polym Sci A: Polym Chem **46**, 1826-1842 (2008)*

A. Karatzas, H. Iatrou, N. Hadjichristidis
“Complex Macromolecular *Chimeras*”
*Biomacromolecules, **9**, A-I (ASAP, 2008)*

Oral 3

Vinyl Polymerization of Norbornene with a Novel Nickel(II) Diphosphinoamine / Methylaluminoxane Catalytic System

Georgios C. Vougioukalakis, Nikolaos Petzetakis, Marinos Pitsikalis, and Nikos Hadjichristidis
National and Kapodistrian University of Athens, Department of Chemistry, Industrial Chemistry Laboratory. E-mail: vougiouk@chem.uoa.gr

Ioannis Stamatopoulos, and Panayotis Kyritsis
National and Kapodistrian University of Athens, Department of Chemistry, Inorganic Chemistry Laboratory

Aris Terzis, and Catherine Raptopoulou
National Centre of Scientific Research "Demokritos", Institute of Materials Science

Recent progress in the field of transition metal catalyzed olefin polymerization and copolymerization has led to the development of a wide range of new, high-performance polyolefin materials.[1] In this regard, the unique physical properties of vinyl-type polynorbornene (PNB),[2] such as optical transparency, heat resistivity and good mechanical strength, has rendered this material of considerable interest. To date, the metal catalyzed vinyl polymerization of norbornene has been achieved with a variety of transition metals such as Ni, Pd, Co, Cr, Zr, and Ti.[3] The resulting PNB may be crystalline or amorphous, depending on the catalyst utilized. It also has to be mentioned that, apart from vinyl (or addition) polymerization, norbornene can be polymerized via ring-opening metathesis polymerization,[1a] and cationic or radical polymerization.[4]

The present work focuses on the synthesis of a novel, Ni(II)-based complex (**1**, Figure 1), coordinated with a bidentate diphosphinoamine ligand.[5] This complex was completely characterized via Nuclear Magnetic Resonance (NMR) and Infrared Spectroscopy (IR), Elemental Analysis, and Mass Spectrometry. Single crystals of good quality were also obtained and analyzed via X-rays (Figure 1).

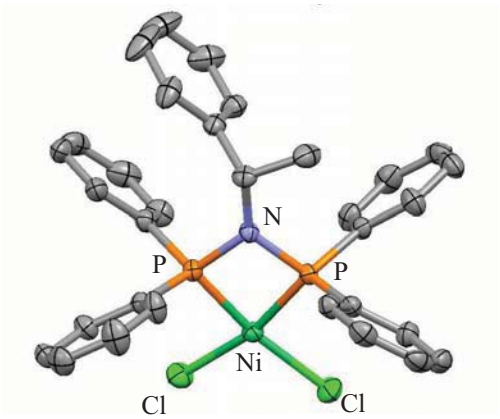

1

Figure 1. X-ray crystal structure of Ni(II) complex **1**.

The catalytic activity of Ni(II)-based complex **1** in the vinyl polymerization of norbornene will be discussed as well. The dependence of the molecular weight of the obtained polymer and the yield of the polymerization reaction on the equivalents of monomer, the equivalents of methylaluminoxane (MAO) used to activate the Ni(II) precatalyst, and the reaction time was also studied. The produced polymers were characterized by NMR and IR spectroscopy, GPC (using the universal calibration curve), and low-angle laser light scattering.

Unlike previous results with other Ni/MAO catalytic systems, regarding the vinyl polymerization of norbornene, in the present work relatively low molecular weight distributions (1.27 to 1.46) were recorded. Moreover, the isolated yields of the PNB obtained were almost quantitative. Finally, an unprecedented correlation between the molecular weight of the obtained polymer and the equivalents of monomer used was observed (Figure 2).

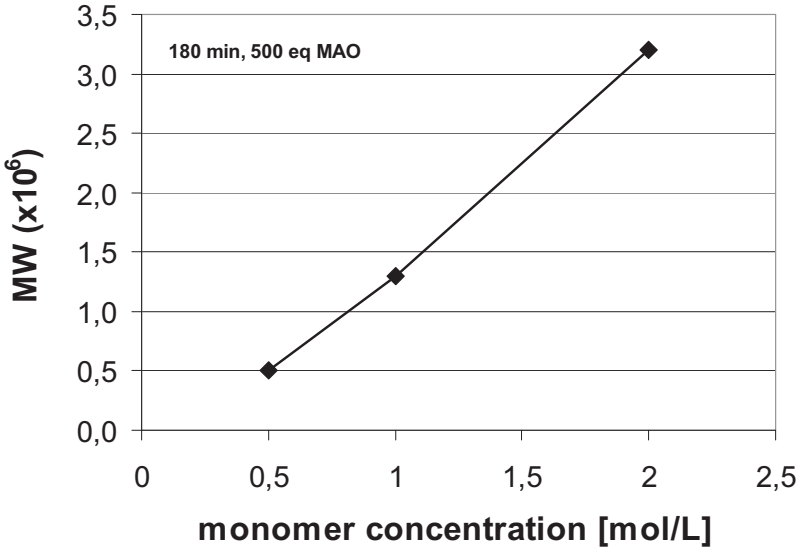

Figure 2. Dependence of the molecular weight of the PNB obtained (in the vinyl polymerization of norbornene with Ni-based complex **1**) on norbornene concentration. The molecular weights were measured by SEC using the universal calibration curve.

References

1. (a) *Handbook of Metathesis* (Ed.: R. H. Grubbs), Wiley-VCH, Weinheim, **2003**. (b) Böhm, L. L. *Angew. Chem. Int. Ed.* **2003**, *42*, 5010. (c) Mülhaupt, R. *Macromol. Chem. Phys.* **2003**, *204*, 289.
2. For a recent review on vinyl polymerization of norbornene, see: Blank, F.; Janiak, C. *Coord. Chem. Rev.* **2008**, doi:10.1016/j.ccr.2008.05.010.
3. For some representative examples, see: (a) Sun, Z.; Zhu, F.; Lin, S. *Appl. Organometal. Chem.* **2006**, *20*, 175. (b) Li, Y.; Gao, M.; Wu, Q. *Appl. Organometal. Chem.* **2007**, *21*, 965. (c) Tang, G.; Lin, Y. J.; Jin, G. X. *J. Polym. Sci. Part A: Polym. Chem.* **2008**, *46*, 489.
4. (a) Kennedy, J. P.; Makowski, H. S. *J. Macromol. Sci. Chem.* **1967**, *A1*, 345. (b) Gaylord, N. G.; Mandal, B. M.; Martan, M. *J. Polym. Sci., Polym. Lett. Edn* **1976**, *14*, 555. (c) Gaylord, N. G.; Deshpande, A. B.; Mandal, B. M.; Martan, M. *J. Macromol. Sci. Chem.* **1977**, A11, 1053. (d) Gaylord, N. G.; Deshpande, A. B. *J. Polym. Sci., Polym. Lett. Edn* **1976**, *14*, 613.
5. For some references related to this family of ligands, see: (a) Babu, R. P. K.; Krishnamurthy, S. S.; Nethaji, M. *Tetrahedron Asymmetry* **1995**, *6*, 427. (b) Simon-Manso, E.; Valderrama, M.; Gantzel, P.; Kubiak, C. P. *J. Organomet. Chem.* **2002**, *651*, 90. (c) Faller, J. W.; Lloret-Fillol, J.; Parr, J. *New. J. Chem.* **2002**, *26*, 883. (d) Simon-Manso, E.; Valderrama, M. *J. Organomet. Chem.* **2006**, *691*, 380.

Invited Lecture 3

Novel Ion-Containing Polymers Via Post-Polymerization Chemistry

Jimmy Mays
Department of Chemistry, University of Tennessee, Knoxville, TN 37996
and
Center for Nanophase Materials Sciences and Chemical Sciences Division, Oak Ridge National Laboratory, Oak Ridge, TN 37831
jimmymays@utk.edu

Abstract
Despite great advances in several controlled/living polymerization strategies over recent years, living anionic polymerization, now more than 50 years old, is still the method that gives the best control over polymer architecture, molecular weight, and polydispersity. However, the range of monomers that can undergo living anionic polymerization is quite limited due to intolerance of this polymerization mechanism toward many common functional groups. Post-polymerization chemical modification of the products of anionic polymerization is therefore an important approach for generating novel well-defined linear and branched polymer and copolymer architectures.

This lecture will describe our recent progress with several different classes of polymeric materials containing sulfonate moieties. These include: novel morphologies formed by diblock copolymer based on fluorinated polyisoprene and sulfonated polystyrene; solution properties and self-assembly of polymers and copolymers containing sulfonated poly(cyclohexadiene); and novel proton conducting membranes based on 1,3-cyclohexadiene.

Oral 4

Responsive Microgel Particles

M. Vamvakaki
Institute of Electronic Structure and Laser, Foundation for Research and Technology - Hellas, P.O. Box 1527, 711 10 Heraklion Crete, Greece and
Department of Materials Science and Technology, University of Crete, 710 03 Heraklion Crete, Greece

Stimuli-responsive microgel particles have attracted great attention due to their potential applications as thickeners, as the stationary phase in liquid chromatography and in waste removal.[1,2] pH-sensitive microgels based on either acidic or basic monomer units are particularly attractive for use in biomedical and biotechnological applications such as protein absorption, drug delivery and immobilization of biomolecules.[3] In the present work, pH-responsive microgels with a diameter between 150 and 500 nm have been synthesized by emulsion polymerization (Figure 1). Basic microgels were prepared by the polymerization of the hydrophobic monomer 2-(diethylamino)ethyl methacrylate (DEAEMA),[4] while *t*-butyl methacrylate (*t*-BuMA) was used as the protected ester to obtain methacrylic acid (MAA)-based microgel particles after the acid hydrolysis of the ester groups. These microgels exhibit reversible swelling properties in water by adjusting the solution pH. Thus, when ionized the microgel particles are swollen due to the hydrophilicity of the charged monomer units. Basic microgels swell at low pH due to the protonation of the tertiary amine units, while MAA-based microgels swell at high pH upon neutralization of the acid groups. A change of the solution pH above or below a critical value (effective pK_α of the protonated monomer units) leads to the formation of collapsed PDEAEMA or PMAA latex particles, respectively.

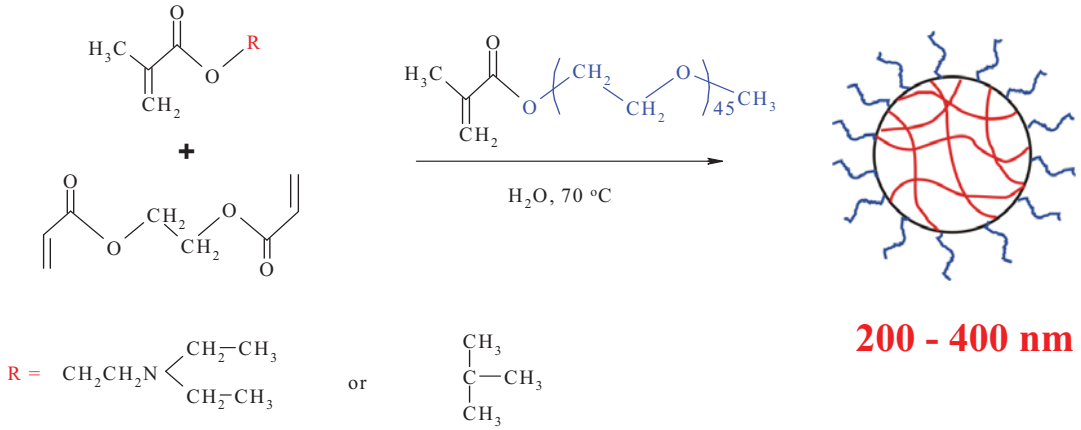

Figure 1: Schematic representation of the synthetic procedure followed for the preparation of the responsive microgel particles.

The microgel particles were prepared by emulsion copolymerization of a suitable hydrophobic monomer with a bifunctional cross-linker in water using a monomethoxy-capped poly(ethylene glycol) methacrylate (M_n = 2000) stabilizer. After the synthesis the microgels were purified by ultrafiltration to remove any unreacted monomers and stabilizer. The *t*-BuMA microgels were deprotected by acid hydrolysis using HF in dichloromethane. The aqueous solution behavior of the microgel particles was investigated as a function of solution pH by potentiometric titrations and by dynamic light scattering using an ALV spectrophotometer and a Nd-YAG laser with λ=532 nm. The hydrodynamic radius R_h of the diffusing moieties was calculated by the Stokes-Einstein equation $R_h = k_B T/(6\pi\eta D)$.

Figure 2 shows the potentiometric titration curves for the PDEAEMA and PMAA-based microgel particles. The effective pK_α of the microgels was calculated from the plateau region plotted as the pH versus the degree of ionization, α_{eff} (in the range 0< α_{eff} <1) as the pH at 50 % ionization. The pK_α for the PDEAEMA particles was found 5.9, while an effective pK_α of 7.2 was calculated for the PMAA microgels.

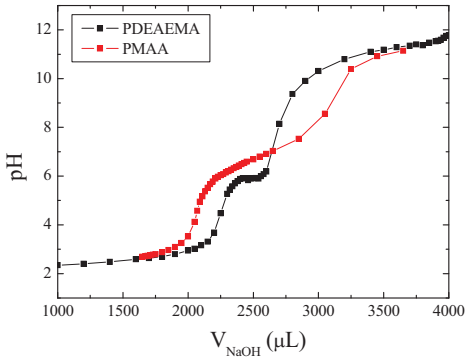

Figure 2: Potentiometric titration curves of the PDEAEMA and PMAA microgel particles.

The change in the hydrodynamic diameter of the microgel particles by altering the solution pH was followed by dynamic light scattering (Figure 3). When ionized the microgels swell due to the increase in the hydrophilicity of the polymer which allows water to enter the microgel particles. Besides, ionization increases the osmotic pressure created within the microgels due to the counterions to the charged monomer units (Figure 4). The swelling process is accompanied by a change in the turbidity of the sample from milky-white in the collapsed state to clear-transparent for the swollen microgel. Furthermore, a change in the pH of the transparent solution above or below the effective pK_α of the charged DEAEMA or MAA units, respectively, induces an increase in turbidity suggesting the reversibility of the swelling-deswelling process.

Mixed microgels based on both DEAEMA and MAA units randomly distributed within the microgel particle have been synthesized. These polyampholytic microgels exhibit a complex swelling behavior being swollen at high and low pH when ionized, while they collapse at the isoelectric point due to charge neutralization, mimicking the behavior of protein molecules.

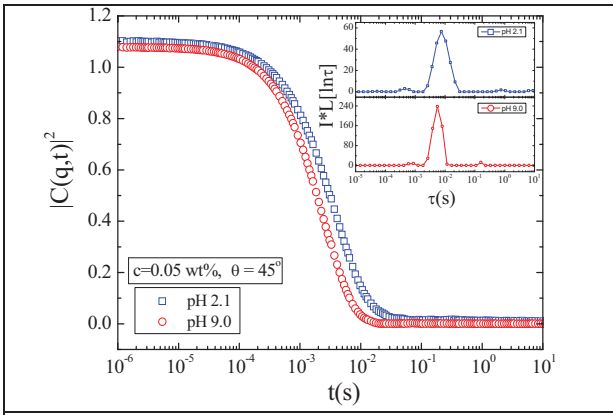

Figure 3. Intensity autocorrelation functions of a 0.05 wt% PDEAEMA microgel solution at 45º scattering angle for pH 2.1 (□) and pH 9.0 (○). Inset: distributions of relaxation times multiplied by the total scattering intensity (normalized to that of toluene).

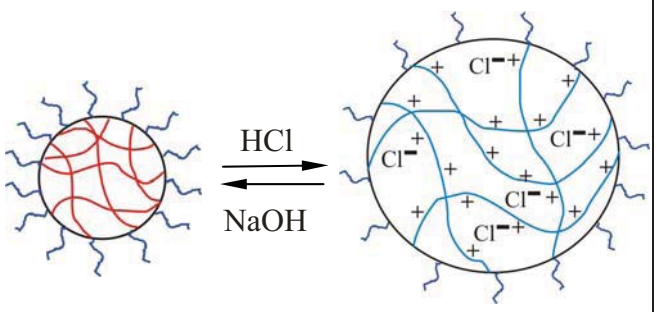

Figure 4: Schematic representation of the acid-induced latex-to-microgel transition observed for the PDEAEMA particles. This transition is reversible on addition of base.

Conclusions

pH-sensitive microgel particles have been synthesized by emulsion polymerization. DLS measurements verified the reversible swelling-deswelling process upon adjustment of the solution pH. Such responsive colloidal particles can find applications in drug delivery, sensor development, membrane filtering and catalysis.

References

1. Kawaguchi, H.; Fujimoto, K.; Mizuhara, Y. *Colloid Polym. Sci.* **1992,** 270, 53.
2. Rodriguez, B.E; Wolfe, M.S.; Fryd, M. *Macromolecules* **1994,** 27, 6642.
3. Murphy, N.; et al. *Proc. Natl. Acad. Sci.* **2003,** 100, 4995.
4. Palioura, D.; Armes, S. P.; Anastasiadis S. H.; Vamvakaki, M. *Langmuir* **2007**, *23,* 5761.

Oral 5

Smart Multifunctional Hybrid Microgels

Jorge Rubio-Retama[1,2], Mukesh Agrawal[1], Manfred Stamm[1], and Nikolaos E. Zafeiropoulos[3]

[1] *Dept. of Nanostructured Materials, Leibniz-Institut für Polymerforschung Dresden e.V., Hohe strasse 6, Dresden, 01069, Germany*
[2] *Dpto. Físico-Química Farmacéutica, Facultad Farmacia, Universidad Complutense, 28040 Madrid, Spain*
[3] *Department of Materials Science & Engineering, University of Ioannina, Ioannina, 45110, Greece*

Hydrogels based on poly(Nisopropylacrylamide), (PNIPAM), are very promising materials for several applications since they exhibit an LCST at around 33 ºC and are biocompatible. For this reason PNIPAM hydrogels have commonly been referred as smart materials for drug delivery or sensor applications, because they are responsive to thermal stimulus. However, the response time in bulk gels is slow, prompting microgels to be considered better systems when shorter response times are required.

The present study reports on a simple pathway to prepare multifunctional smart materials that are multifunctional and could be used either as drug carriers or sensors. With the aim of obtaining such hybrid materials, magnetic nanoparticles (iron oxide) or quantum dots (CdTe) were attached on the surface of P(NIPAM) microgels. As result of the procedure P(NIPAM) microgels were covered with e.g. magnetic nanoparticles of γ-Fe_2O_3 (figure 1a and 1b), rendering magnetic response to the hybrid material (figure 1c and 1b). When a magnet is approached to the aqueous dispersion, the Fe-PNIPAM-AA microgels move due to the magnetic field and form a film on the flash wall close to the magnet, as seen in figure 1D. As a consequence of successive polymer modifications and iron oxide incorporation the LCST of the PNIPAM microgels changes, figure 2. As shown in figure 2 the modified P(NIPAM) microgels exhibit different swelling behaviour, as well as a shift in the temperature at which the LCST occurs. In the case of the magnetic thermosensitive microgels, its LCST is shifted to 40ºC, making the system sensitive for human hyperthermia. Additionally the microgel magnetic response permit a controlled magnetic guidance of such microgels on particular tissues, serving as smart targeted drug delivery system, which could be triggered off by the heat produced

during the "*inflammation"* process, releasing the active medicine in the vicinity of the affected tissue, thus minimizing potential toxic side-effects (for example in some cases of chemotherapy). In contrast the incorporation of CdTe nanoparticles does not affect the LCST of the neat microgels, but different photoluminescent behaviour is detected above and below the LCST.

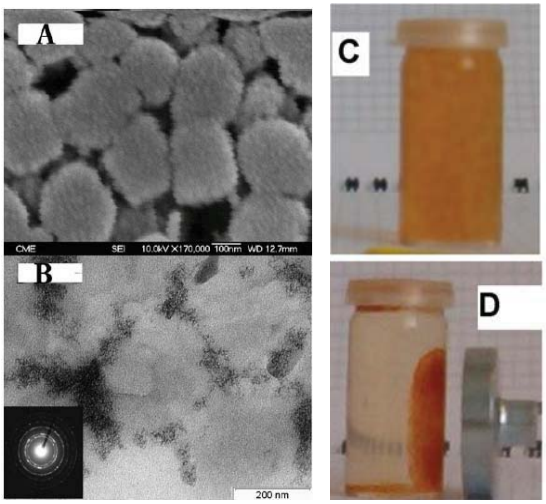

Figure 1 A) Detailed SEM micrograph of Fe-PNIPAM microgels B) TEM micrograph of Fe-PNIPAM microgels, inset ED pattern of the iron oxide nanoparticles that cover the microgels C) Aqueous dispersion of Fe-PNIPAM-AA microgels in absence of magnetic field, C) Response of the microgels after applying a magnetic field

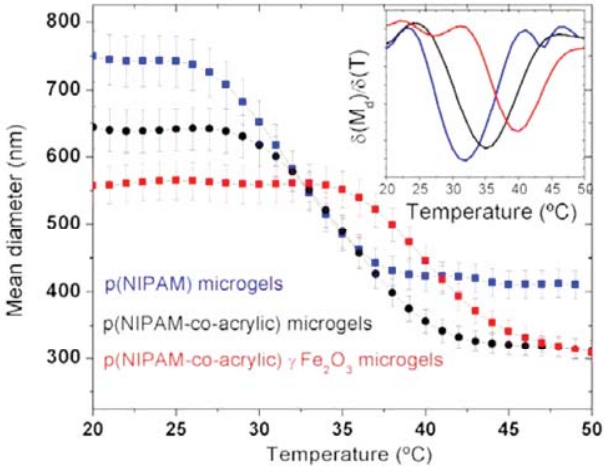

Figure 2. Experimental mean particle diameter *vs.* temperature for different microgels, inset differential Mean particle diameter as a function of the temperature.

References

(1) J. Rubio-Retama, N. E. Zafeiropoulos, C. Serafinelli, R. Rojas-Reynas, B. Voit, E. Lopez Cabarcos, and M. Stamm, Synthesis and Characterization of Thermosensitive PNIPAM Microgels covered with Superparamagnetic γ-Fe_2O_3 Nanoparticles, Langmuir, 23, 2007, 10280-10285

(2) M. Agrawal, S. Gupta, V. Cimrova, V. Lesniak, N. Gaponik, E. López-Cabarcos, S. Tzavalas, R. Rojas-Reyna, J. Rubio-Retama, N. E. Zafeiropoulos, and M. Stamm, Switchable Photoluminescent CdTe Nanocrystals by Temperature Responsive Microgels, Langmuir, accepted (2008)

Invited Lecture 4

Tailoring sound propagation by mesoscopic engineering of soft matter

G. Fytas[1,2]
[1]*Max Planck Institute for Polymer Research, P.O. Box 3148, 55128 Mainz, Germany*
[2]*Department of Materials Science & Technology and FO.R.T.H, P.O. Box 1385, 71110 Heraklion, Greece*

Soon after the birth of the photonic crystals with periodic variations of dielectric constant, theoretical and experimental work embarked on the propagation of acoustic waves in structures with periodic variations of density and/or sound velocities. The experimental realization of phononic crystals was up to now restricted to manually fabricated structures with macroscopic spacing and hence band gaps in the sub MHz frequency range. In contrast to the sonic and ultrasonic crystals, the study of hypersonic crystals at the submicron scale imposes substantial demand on fabrication and characterization techniques, which are currently being developed. Colloid and polymer science offer methods to create novel materials that are characterized by periodic variations of density and elastic properties at mesoscopic length scales commensurate with the wave length of hypersonic phonons. Polymer-and colloid-based phononics is an emerging new field less than 10 years old at the interface of well established fields of soft materials science and condensed matter physics with rich perspectives ahead.

Here, we focus on colloid-based phononics and self-ordered aluminum oxide (AAO) with aligned cylindrical nanopores containing either fluids or solids as a second component for the rational design of hypersonic systems characterized by customized and tunable sound propagation.

The dispersion of high frequency (GHz) acoustic excitations in three-dimensional colloidal crystalline or amorphous assemblies of sub-micron colloidal particles in different matrices was measured by high resolution Brillouin light scattering (BLS) in order to explore the phononic and elastic properties of nanostructured materials. In air, we record eigenmodes of the individual particles, which are shown to be independent from the crystallinity and the composition of the sample but sensitively depend on the particle architecture (e.g core/shell silica/poly(methylmethacrylate), hollow capsules) and their mechanical properties at nanoscale. In fluid matrices, the dispersion relation between the frequency and the wave vector ($k_{||}$ parallel to the fcc (111) plane) of the thermally excited acoustic waves has revealed two hypersonic phononic band gaps of different nature: (i) a Bragg gap occurring at the boundary of the first Brillouin zone and (ii) a hybridization-gap resulting from the interaction of particle eigenmodes with the acoustic mode of the effective medium. The hybridization gap is robust against structural disorder while disorder eliminates the Bragg gap. Depending on the particle size and the speed of sound in the infiltrated fluid, the frequency and the width of the hypersonic phononic gaps can be tuned.

AAO offers unique advantages as a material platform for the engineering of sound propagation in the GHz frequency range; pronounced anisotropic behavior, exceptionally large elastic contrast between their constituents, hybrid systems with tailored phononic properties are accessible by the proper choice of the infiltrated component, AAO is inert, shape-defining scaffold and transparent to UV and visible light allowing for structural transitions in the nanopores .Using Brillouin spectroscopy (BLS), we report the realization of directional elastic energy flow, phonon localization, tunability of the phononic band structure and mode switching via external stimuli.

Since hypersonic crystals can simultaneously exhibit phononic and photonic band gaps in the visible spectral region, the technological applications could range from tunable filters and heat management to acoustic-optical devices.

References
1. T.Gorishnyy, L.U.Ullal, M.Maldovan, G.Fytas, E.L.Thomas, *Phys. Rev. Lett.*, ***94,****115501(2005)*
2. W.Cheng, J.Wang, U.Jonas, G.Fytas, N.Stefanou *Nature Materials* **5**,830 (2006)
3. W. Cheng, N. Gomopoulos, G. Fytas, T. Gorishnyy, J. Walish, E. L. Thomas, A.Hiltner, E. Baer" Nano Lett. 8,1423-1428 (2008).
4. T.Still,W.Cheng,M.Retsch,R.Sainidou,J.Wang,U.Jonas,N.Stefanou G,Fytas, Phys.Rev.Lett.100, 194301 (2008)

Oral 6

Simulations of Temperature Induced Ageing and Crystallization in Dense Suspensions of Ultrasoft Colloids

I.A. Bitsanis[*,1], A.N. Rissanou[*,+], M. Yannourakou[+], I.G. Economou[+], D. Vlassopoulos[*,#]

[*]Institute of Electronic Structure and Laser,
Foundation for Research and Technology Hellas,
GR-711 10 Heraklion, Greece

[+]Molecular Thermodynamics and Modeling of Materials Laboratory, Institute of Physical Chemistry, National Center for Scientific Research "Demokritos"
GR-153 10, Aghia Paraskevi Attikis, Greece

[#]Department of Materials Science
University of Crete
GR-711 10 Heraklion, Greece

Multi-arm star polymers and block-copolymer micelles can be viewed as soft, spherically symmetric colloidal particles. Dense suspensions of these supramolecules were experimentally found to solidify upon *increase* of temperature. We present results from molecular Dynamics simulations of soft colloidal spheres interacting via a theoretically developed potential. Vitrification of the suspensions, caused by soft-sphere swelling upon heating and subsequent free-volume deprivation, was observed at temperatures differing by less than 5K from the experimental solidification T. Features of glassy states in the simulations were consistent with predictions of ideal mode-coupling theory. Further ageing of the amorphous structures produced imperfect FCC crystals, characterized by slow, yet detectable, diffusion and lower degree of crystallinity than their thermodynamically equilibrated counterpart. The first unambiguous experimental evidence for slow (enhanced) ageing and subsequent crystal formation was reported only very recently.

[1] Corresponding author: E-mail: bitsanis@iesl.forth.gr

Oral 7

Yielding mechanisms and particle rearrangements in colloidal glasses and gels

G. Petekidis

Department of Materials Science and Technology, University of Crete and
IESL-FORTH, Heraklion, Crete, Greece

Colloids consist of a wide class of soft matter systems which are ubiquitous both in nature as well as in commercial products (personal care, paints etc.). Their flow properties are thus of great importance both for designing efficient processing and as well as for final applications. On the other hand, due to their experimentally accessible time and length scales and easiness in driving them out of equilibrium by external fields, colloids are often used as model systems for the study of fundamental problems in condensed matter physics such as crystallization and glass transition.

To this end polymer colloids consisting of poly-methylmethacrylate (PMMA) hard cores sterically stabilized by a thin chemically grafted layer of poly-12-hydroxystearic acid chains suspended in organic solvents are used as model hard spheres. Moreover when linear homopolymer chains (poly-styrene) are included in the solution they introduce an effective short range attraction between particles due to depletion effect, that may be easily tuned both in terms of strength and range. At high volume fractions or/and large interparticle attractions such hard sphere or attractive systems may be kinetically frozen either due to entropic or/and enthalpic reasons forming colloidal glasses and gels.

Here we present rheological measurements in a wide range of particle volume fractions and polymer concentrations in order to explore the macroscopic behavior of such frustrated states under shear. At the same time the microscopic particle dynamics under oscillatory shear are probed by simultaneous rheometry and dynamic light scattering (LS echo technique) [1]. While hard sphere glasses yield under shear above a yield strain corresponding to the breakage of the cage formed by neighboring particles (the structural arrest length scale) attractive glasses exhibit a two step yielding mechanism reflecting the particle confinement both by bonding and entropic caging [2]. We also follow the rheological transition from a high volume fraction attractive glass with a two-step yielding process to low colloid volume fractions fractal gel structure (at equal attraction strength) where a simple yielding process, due to bond breakage, is recovered.

[1] G. Petekidis, A. Moussaid and P. N. Pusey, *Phys. Rev. E*, **66**, 051402, (2002).
[2] K. Pham, G. Petekidis, D. Vlassopoulos, S.U. Egelhaaf, W.C.K Poon and P.N. Pusey J. Rheol., 52, 649 (2008)

In collaboration with: N. Koumakis, P. Ballesta, D. Vlassopoulos, M. Laurati, S.U. Egelhaaf, K. Pham, W.C.K Poon and P.N. Pusey

Oral 8

Hydrogen-Bonded Interpolymer Complexes Soluble at Low pH

Georgios Staikos[1], Maria Sotiropoulou[1], Georgios Bokias[2], Frederic Bossard[3], Julian Oberdisse[4], Eric Balnois[5]

[1]*Department of Chemical Engineering, University of Patras, GR-26504 Patras, Greece*

[2]*Department of Chemistry, University of Patras, GR-26504 Patras, Greece*

[3]*Laboratoire de Rheologie, UMR 5520, Université Joseph Fournier, 1301, rue de la piscine, BP 53, 38041 Grenoble Cedex, France*

[4]*Laboratoire des Colloides, Verres et Nanomateriaux, UMR CNRS/UM2, Université Montpellier, France*

[5]*Laboratoire Polyméres, Propriétés aux Interfaces et Composites (L2PIC), Université de Bretagne Sud, Rue de Saint Maudé, BP 92116, 56231 Lorient, France*

The formation of hydrogen-bonded interpolymer complexes (IPCs) between proton donor and proton acceptor polymers in aqueous solution has been widely studied during the past four decades. [1, 2] The proton donors are usually weak polycarboxylic acids, such as poly(acrylic acid) (PAA) and poly(methacrylic acid) (PMAA), whereas the proton acceptors are nonionic polybases, such as poly(ethylene glycole) (PEG) or polyethyleneoxide (PEO), polyacrylamides, poly(vinyl ethers), etc. The research interest in this field has been further stimulated by potential applications of these hydrogen-bonded interpolymer complexes to various fields, such as drug delivery formulations, biomaterials, emulsifiers, and membrane and separation technology.

In general, in aqueous solutions of mixtures of such complementary polymers occurs hydrogen-bonding association between the carboxylic groups of the polyacid and the nonionic polybase, leading to the formation of compact hydrogen-bonded IPCs. An important limitation is that they are usually soluble only within a narrow pH window. At pH values higher than 4-5, dissociation of these hydrogen-bonded IPCs occurs, due to the increase of the ionized sites (carboxylate groups) in the polyacid chain. On the other hand, at pH values lower than 3–3.5, the hydrogen-bonded IPC formed precipitates, because the fraction of the carboxylate anions in the polyacid chain, mainly responsible for the solubility of the complex, decreases considerably. In summary, when pH is higher than 4-5 hydrogen-bonding interpolymer complexation is not possible, while at pH lower than 3-3.5 associative phase separation takes place.

Extension of the solubility of the hydrogen-bonded IPCs in the low pH region is of importance, as this would allow original properties to be observed and could enlarge the spectrum of the potential applications of such complexes. To achieve this aim, the non-ionic polybase poly (*N, N*-dimethylacrylamide) (PDMAM) was grafted onto a highly charged anionic backbone, consisting of 2-acrylamido-2-methyl-1- propanesulphonic acid (AMPSA) and acrylic acid (AA) monomer units, P(AA-*co*-AMPSA). It was shown that, the graft copolymers synthesized, P(AA-*co*-AMPSA)-*g*-PDMAM, could form with PAA soluble hydrogen-bonded IPCs at low pH.[3] Viscometry, small angle neutron scattering, static and dynamic light scattering, and atomic force microscopy studies of aqueous solutions of the above graft copolymers with PAA at low pH,[3, 4, 5] suggest the formation of negatively charged core-shell colloidal particles, comprised by a hydrophobic core of a hydrogen-bonded interpolymer complex formed between the PDMAM side chains of the graft copolymer and PAA, and a hydrophilic shell of the anionic backbone of the graft copolymer, Scheme 1. Rheological studies in semidilute

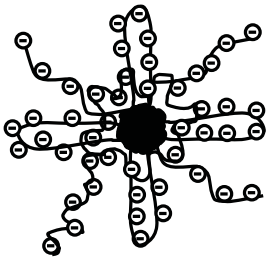

Scheme 1. Negatively charged colloidal particles formed through hydrogen-bonding interpolymer complexation of PAA with the PDMAM side chains of the graft copolymer P(AA-*co*-AMPSA)-*g*-PDMAM (G48), at low pH.

solutions of the mixtures P(AA-*co*-AMPSA)-*g*-PDMAM/PAA have shown the formation of reversible gels at low pH, Scheme 2.[3, 6]

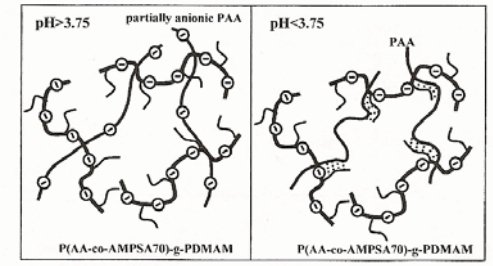

Scheme 2. A Schematic explanation of the pH-controlled thickening behavior of the P(AA-*co*-AMPSA70)-*g*-PDMAM/PAA500 mixtures in semidilute aqueous solution through reversible hydrogen-bonding association.

Alternatively, it has been shown that PEG also forms soluble hydrogen-bonded IPCs with PAA grafted with the negatively charged poly(2-acrylamido-2-methyl-1-propanesulphonic acid) (PAMPSA) chains.[7] These complexes should be comprised by a hydrophobic core of hydrogen-bonded interpolymer complexes formed between PEG chains and the PAA backbone of the graft copolymer, and a hydrophilic shell of the PAMPSA side chains of the graft copolymer, Scheme 3.

Scheme 3: Schematic illustration of the influence of salt and composition in PAMPSA side chains on the structure of the colloidal nanoparticles.

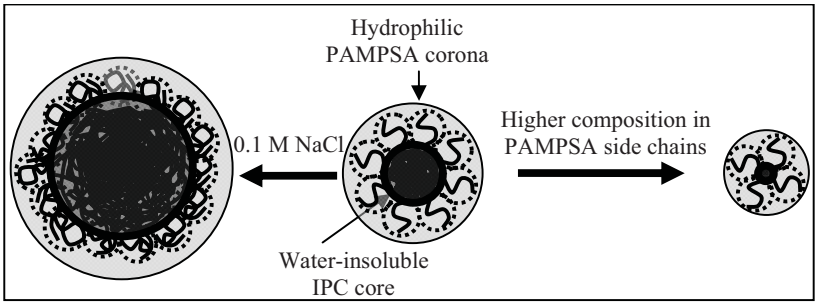

References

1. E.A. Bekturov and L.A. Bimendina, *Adv. Polym. Sci.* **43**, 100 (1980).
2. E. Tsuchida and K. Abe, *Adv. Polym. Sci.* **45**, 1 (1982).
3. M. Sotiropoulou, G. Bokias and G. Staikos, *Macromolecules* **36**, 1349 (2003).
4. M. Sotiropoulou, J. Oberdisse and G. Staikos, *Macromolecules* **39**, 3065 (2006).
5. M. Sotiropoulou, F. Bossard, E. Balnois, J. Oberdisse and G. Staikos, *Langmuir* **23**, 11252 (2007).
6. F. Bossard, M. Sotiropoulou and G. Staikos, *j. Rheol.* **48**, 927 (2004).
7. P. Ivopoulos, M. Sotiropoulou, G. Bokias and G. Staikos, *Langmuir* **22**, 9181 (2006).

Invited Lecture 5

Block copolymer-directed nanomaterials synthesis and organization.

Paschalis Alexandridis
Department of Chemical and Biological Engineering University at Buffalo - The State University of New York (SUNY) Buffalo, NY 14260-4200, USA
http://www.cbe.buffalo.edu/alexandridis.htm

The development of self-assembly as a useful approach to the synthesis and manufacturing of complex systems and materials has been recognized as a "grand challenge" facing scientists and engineers. In our laboratory we utilize the self-assembly afforded by amphiphilic molecules (e.g., surfactants, block copolymers, proteins) and the directed assembly facilitated by external fields (e.g., shear, electric) for the (i) fundamental elucidation of structure and interactions in hierarchically ordered systems[1,2], (ii) formulation of nanostructured dispersions with desired properties[3], (iii) templated synthesis of nanomaterials[4,5], and (iv) surface modification and organization of colloidal particles[6].
This presentation will highlight the interplay between the fundamentals of amphiphilic block copolymer (ABC) self-assembly and ABC applications in the synthesis of nanoparticles (NP) in a size- and shape-controlled manner. In the presence of selective solvent, ABCs can provide nanoscale environments of varying and tunable shape, dimensions, mobility, local polarity, concentration, and reactivity. ABCs can thus seed NP formation, facilitate NP growth, and control NP size and shape. Furthermore, ABCs are useful in modifying NP surfaces for dispersibility in a matrix and in promoting long-range NP organization. Continuous three-dimensional nanostructures can also be synthesized in ABC templates.

References

[1] Gu, Z.; Alexandridis, P. "Osmotic Stress Measurements of Intermolecular Forces in Ordered Assemblies Formed by Solvated Block Copolymers" Macromolecules 2004, 37 (3), 912-924.
[2] Singh, I.; Shankaran, H.; Beauharnois, M. E.; Xiao, Z.; Alexandridis, P.; Neelamegham, S. "Solution Structure of Human vonWillebrand Factor Studied Using Small Angle Neutron Scattering" J. Biol. Chem. 2006, 281 (50), 38266-38275.
[3] Lin, Y.; Smith, T. W.; Alexandridis, P. "Adsorption of a Rake-Type Siloxane Surfactant onto Carbon Black Nanoparticles Dispersed in Aqueous Media" Langmuir 2002, 18 (16), 6147-6158.
[4] Sakai, T.; Alexandridis, P. "Mechanism of Gold Metal Ion Reduction, Nanoparticle Growth and Size Control in Aqueous Amphiphilic Block Copolymer Solutions at Ambient Conditions" J. Phys. Chem. B 2005, 109 (16), 7766-7777.
[5] Karanikolos, G. N.; Law, N.-L.; Mallory, R.; Petrou, A.; Alexandridis, P.; Mountziaris, T. J. "Water-based Synthesis of ZnSe Nanostructures Using Amphiphilic Block Copolymer Stabilized Lyotropic Liquid Crystals as Templates" Nanotechnology 2006, 17, 3121-3128.
[6] Docoslis, A.; Tercero Espinoza, L. A.; Zhang, B.; Cheng, L.-L.; Israel, B. A.; Alexandridis, P.; Abbott, N. L. "Using Nonuniform Electric Fields to Accelerate the Transport of Viruses to Surfaces from Media of Physiological Ionic Strength" Langmuir 2007, 23 (7), 3840-3848.

Oral 9

Self-assembled nanostructures from block copolymers and vesicle-forming surfactant in aqueous solutions

S. Pispas
Theoretical and Physical Chemistry Institute, National Hellenic Research Foundation, 48 Vass. Constantinou Ave., 11635 Athens, Greece, E-mail: pispas@eie.gr

Aqueous systems containing block copolymers and low molecular weight surfactants attract current scientific interest of polymer and colloid chemists due to their ability to form mixed self-assembled nanostructures with tailored properties.[1,2] The academic interest in such complex systems stems from the possibilities for basic understanding of biological behavioural motifs, since nature is extensively using analogous systems (i.e. biomacromolecules and phospholipids) to create functional self-assembled nanostructures. Important technical applications, especially those related to interfacial and rheological properties of complex fluids and colloid formulations, nanomedicine and nanotemplating are also closely connected to behavioural characteristics of solutions of mixed amphiphiles.

In this work we investigate the self-assembly in two different bioinspired macromolecular/surfactant mixed colloidal systems: a) neutral amphiphilic block copolymers and vesicle forming cationic surfactant[3] and b) neutral-anionic double hydrophilic block copolymer[4] and vesicle forming cationic surfactant systems. Self-assembly in the systems of interest is discussed by taking into account the amphiphilicity of the components, hydrophobic and electrostatic interactions between them, as well as redistribution and self-organization of the individual components.

In the first system the self-assembly behaviour of mixed solutions consisted of poly(isoprene-b-ethylene oxide) (IEO) copolymer micelles and vesicle forming didodecyldimethylammonium bromide (DDAB) was investigated. Dynamic light scattering indicated the presence of two populations of nanoassemblies in the solutions.[3] By aid of atomic force microscopy the larger ones were identified as block copolymer modified surfactant vesicles (BCMSVs) and the smaller ones as surfactant modified block copolymer micelles (SMBCMs). This identification is based on the amphiphilic character of the low and high molecular weight molecules and the notion that exchange of unimers of both types can take place between the initial nanoassemblies in aqueous solution. Electrophoretic light scattering experiments showed that the nanostructures carry positive charges originating from the surfactant. The sizes of the nanoassemblies depend on the relative concentrations of both components. The behaviour of the mixed systems was also found to depend on block copolymer composition and temperature. Nanoassemblies of smaller sizes were formed at higher temperatures. BCMSVs and SMBCMs are thermosensitive, in contrast to the temperature stability of pure block copolymer micelles. On the other hand, BCMSVs showed lesser sensitivity to temperature increase compared to the pure DDAB vesicles. This indicates that incorporation of macromolecules into the DDAB bilayer increases the stability of the vesicles.

The second mixed system consists of a poly[(2-sulfamate-3-carboxylate)isoprene-b-ethylene oxide] (SCIEO-3) double hydrophilic block copolymer and DDAB.[5] In these solutions electrostatic interactions exist between the anionic poly[(2-sulfamate-3-carboxylate)isoprene] block and the cationic surfactant. Combined static and dynamic light scattering measurements indicate that at low copolymer concentration vesicles of DDAB with adsorbed block copolymer chains are present in the solutions. As block copolymer concentration increases the structure of the nanoassemblies transforms to a core-shell, micellar-like structure, with a poly(ethylene oxide) corona and a core formed by the complex of poly[(2-sulfamate-3-carboxylate)isoprene] chains and DDAB molecules. This transformation of global aggregate structure should be attributed to a collapse of the DDAB vesicle bilayer as the number of complexed surfactant head groups to anionic polymeric segments increases. This happens in order to satisfy the conformational requirements of the complexing polymeric block and the steric requirements in the PEO corona, which apparently overcome the existing interactions between surfactant

molecules in the ordered bilayer. Block copolymer decorated vesicles show lower stability to an increase in solution temperature compared to micellar-like aggregates. Both nanostructures are found to be highly stable to changes in solution ionic strength, due to the combination of electrostatic and hydrophobic interactions acting within the mixed aggregates.

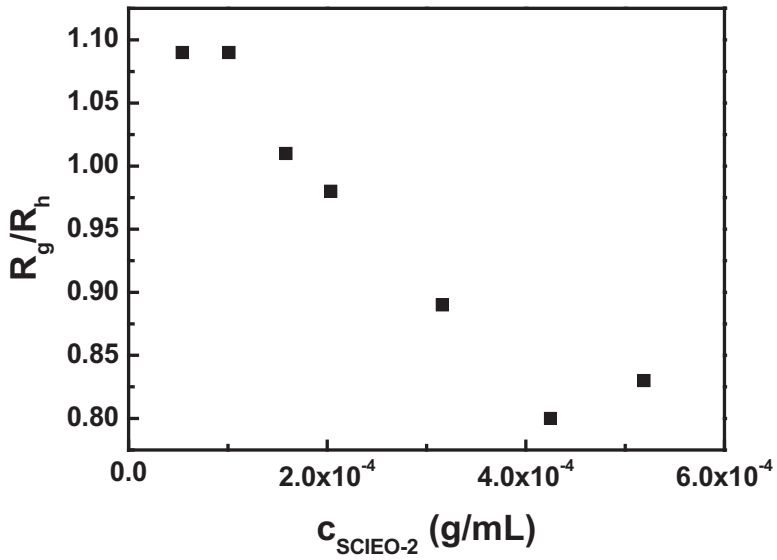

Figure 1. R_g/R_h ratio for SCIEO-3/DDAB mixed solutions, calculated from static and dynamic light scattering measurements (DDAD concentration is constant at $c_{surf} = 3.5 \times 10^{-4}$ g/mL).

The results presented are contributing to a better understanding of principles governing the creation of functional nanoassemblies in solution, in synthetic and biological systems, and have relevance to nano(bio)technological applications.

References

1. B. Jonsson, B. Lindman, K. Holmberg, B. Kronberg “Surfactants and Polymers in Aqueous Solutions”, J. Wiley & Sons, Chichester, UK, 1998.
2. N. V. Sastry, H. Hoffmann Colloids Surf. A 2004, 250, 247.
3. S. Pispas, E. Sarantopoulou Langmuir 2007, 23, 7484.
4. S. Pispas J. Polym. Sci. Part A: Polym. Chem. 2006, 44, 606.
5. S. Pispas, in preparation.

Oral 10

Effect of Lithium Salt Concentration on the Self-assembly of PEO-based Block Copolymer Electrolytes

E. F. Ioannou[1], K. D. Gatsouli[1], S. Pispas[1], E. I. Kamitsos[1] and G. Floudas[2]
[1]*Theoretical and Physical Chemistry Institute, National Hellenic Research Foundation 48 Vass. Constantinou Ave., 116 35 Athens, Greece*
[2]*Department of Physics and Foundation for Research and Technology-Hellas, Biomedical Research Institute (FORTH-BRI), University of Ioannina, P.O. Box 1186, 45110 Ioannina, Greece*

In recent years, interest has been focused on the development of polymer solid electrolytes that exhibit enhanced ion transport properties.[1-2] A class of these materials derives from block copolymers[3], as this was demonstrated previously in a poly(styrene-*b*-methacrylic acid) block copolymer system where incorporation of lithium ions was found to lead to changes in local structure and microdomain morphology, and to enhanced ionic conductivity.[4] When a salt-solvating polymer is chosen as one of the block components, continuous, nanoscopic ion-conducting pathways can form. Poly(ethylene oxide) (PEO) is usually chosen as one of the blocks, due to its solvating ability, its high flexibility and good mechanical stability up to its melting point.[5]

In the present study diblock copolymers of poly(isoprene-*b*-ethylene oxide) (IEO) of various compositions have been prepared by anionic polymerization and were employed as templates for the development of polymer electrolyte systems. Lithium trifluoromethane sulfonate salt (lithium triflate, CF_3SO_3Li) was introduced in the PEO phase with O:CF_3SO_3Li rations varying from 8:1 to 1:1, with respect to the ether groups. The salt is the effective component that alters the phase state of the resulted solid polymer electrolytes. The local structure and the microdomain morphology of the pure block copolymers and of the solid polymer electrolytes were investigated by infrared (IR) and Raman spectroscopy, small and wide -angle X-ray scattering (SAXS, WAXS) and differential scanning calorimetry (DSC).

Structural aspects at the molecular level were studied by IR and Raman. Figure 1 shows infrared spectra of diblock copolymer IEO4 (M_w=16400, 54% wt in PEO) and of the resulted solid polymer electrolytes. Interactions between the polyether matrix and the salt are probed by using characteristic stretching modes of ether group of PEO (ν_a(C-O-C): 1081–1108 cm^{-1})[6], informative of the local bonding in the PEO phase and characteristic stretching modes of the sulfonic group of the triflate anion (ν_s(-SO_3): 1030–1050 cm^{-1} and ν_a(-SO_3): 1228–1290 cm^{-1})[7], as they are sensitive to the nature of the cationic environment. IR spectra reveal progressive ion association of triflate anions with Li cations forming ion pairs and larger aggregates at higher salt concentrations. The local bonding in PEO phase also changes, indicating complexation of PEO oxygens with Li cations, for certain concentrations.

Investigation of the microdomain morphology by DSC, SAXS and WAXS revealed changes in the phase state and morphology of the copolymers. The effect of lithium salt incorporation was to decrease the crystallinity of the PEO block (as observed by DSC and WAXS). In addition, SAXS revealed transitions between different nanophases as observed in Figure 2 for the IEO4 diblock and the resulted solid polymer electrolytes. SAXS curves indicate hexagonal-to-lamellar transitions for IEO4Li2, with O:CF3SO3Li ratios of 2:1, respectively. Also, for low O:CF3SO3Li ratios a new complex phase is formed between PEO and the salt, indicated by a new peak at low *q* values in SAXS curves, for certain salt concentrations. This new complex phase was also manifested by a new melting point above that of PEO in DSC for certain salt concentrations, and is consistent with the evolution of the IR spectra.

The above results reveal strong effects of lithium salt incorporation in a PEO-based block copolymer electrolyte. Different techniques indicate changes in the copolymers' phase state and morphology, deriving from different coordination environments of anions and cations, which can lead to the formation of distinct ionic species and from different local conformation of the PEO backbone, accompanying cation-ether oxygens interactions. These structures persist in the amorphous regions of the polymer-salt system and should play an important role in ion transport. Along these lines, incorporation of other entities has been considered as well, including ionic liquids for the formation of PEO-based block copolymer electrolytes.

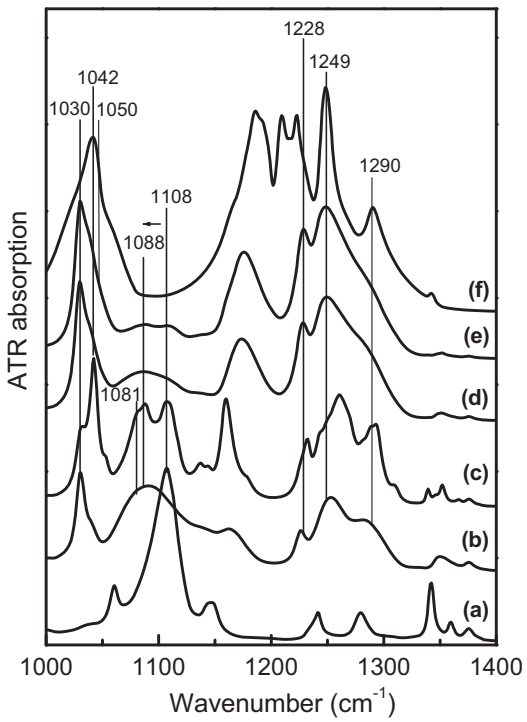

Figure 1

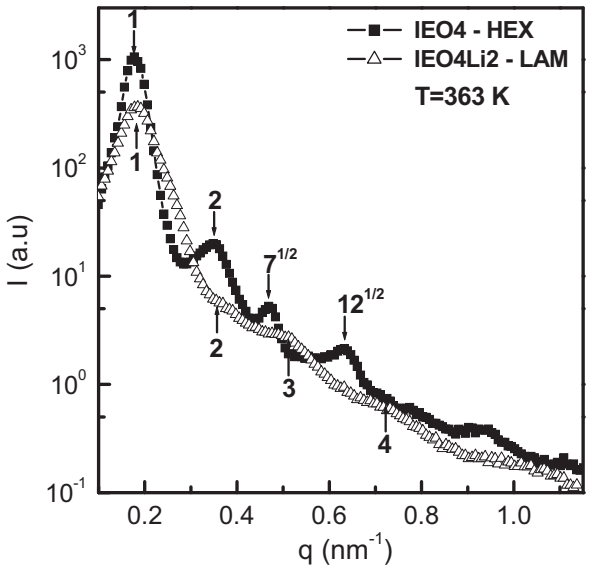

Figure 2

Fig. 1. ATR absorption spectra of the diblock copolymer IEO4 (a) and of the solid polymer electrolytes resulting from the introduction of lithium triflate in the PEO phase: IEO4Li8, with ratio O:CF_3SO_3Li=8:1 (b), IEO4Li4, O:CF_3SO_3Li=4:1 (c), IEO4Li2, O:CF_3SO_3Li=2:1 (d), IEO4Li1, O:CF_3SO_3Li=1:1 (e) and CF_3SO_3Li salt (f). The spectra are offset to facilitate comparison.

Fig. 2. SAXS curves from the diblock copolymer and the resulting polymer electrolytes at T=363 K. IEO4 (squares): arrows indicate peaks at positions $1:2:7^{1/2}:12^{1/2}$ relative to the main peak and IEO4Li2, O:CF_3SO_3Li=2:1 (triangles): arrows indicate peaks at positions 1:2:3:4 relative to the main peak.

References

1. Chandrasekhar, V. *Adv. Polym. Sci.* **1998**, 135, 139-205.
2. Tarascon, J. M.; Armand, M. *Nature* **2001**, 414, 359-367.
3. Trapa, P. E.; Won, Y-Y.; Mui, S. C.; Olivetti, E. A.; Huang, B.; Sadoway, D. R.; Mayes, A. M.; Dallek, S. *J. Electrochem Soc.* **2005**, 152(1), A1-A5.
4. Ioannou, E. F.; Mountrichas, G., Pispas, S.; Kamitsos, E. I.; Floudas, G. *Macromolecules*, submitted.
5. Kim, S. H.; Misner, M. J..; Yang, L.; Gang, O.; Ocko, B. M.; M.; Russell, T. P. *Macromolecules* **2006**, 39, 8473-8479.
6. Dissanayake, M. A. K. L.; Frech, R. *Macromolecules* **1995**, 28, 5312-5319.
7. Bishop, A. G.; MacFarlane, D. R.; McNaughton, D.; Forsyth, M. *J. Phys. Chem.* **1996**, 100, 2237-2243.

Oral 11

Fabrication of nanoobjects from star-shaped copolymers

C. Tsitsilianis[1,2], D. Tasis[3], C. Galiotis[1,3] V. Bocharova[4], A. Kiriy[4], M. Stamm[4]

[1] *Foundation of Research and Technology Hellas, Institute of Chemical Engineering and High Temperature Processes, P.O. Box 1414, Patras GR-265 04, Greece*
[2] *Department of Materials Science, University of Patras, Patras GR-265 04, Greece*
[3] *Department of Chemical Engineering, University of Patras, , GR26500 Patras, Greece*
[4] *Leibniz-Institut für Polymerforschung Dresden, 01069 Dresden, Germany*

Block copolymers have recently received much attention not only thanks to the scale of the microdomains (nanometers) and their various physical properties (hydrophilic, hydrophobic, glassy, elastromers etc) but also due to the tunability of the size and shape of the formed self assemblies afforded simply by the choice of their molecular weights architecture and compositions. Moreover, several hierarchy levels can be distinguished for block copolymers with characteristic lengths ranging from 1 nm to 1 μm i.e. monomer (chemical functionality), block copolymer (macromolecular scale), self assembly (10-100 nm length scale) and superlattice (a three dimensional ordered structure in μm scale). Therefore block copolymers are excellent candidates for “bottom-up” strategy to design and develop composite materials with multifunctional properties. The aim of the present communication is to present synthetic strategies leading to the development of polymeric nanocomposites the matrix of which is constituted of a nanostructured block copolymer (bearing at least two kinds of compartments) while the nanometer-sized fillers are crosslinked polymeric nanoobjects arisen from self-organization of block copolymers of different nature from that of the matrix.
More precisely we report on our attempt to fabricate “hairy” nanocylinders from star-shaped block copolymers of the type A_nB_n after their self-organization either in solution or in the bulk and stabilization by suitable cross-linking reaction of the internal compartment of the self-assembly

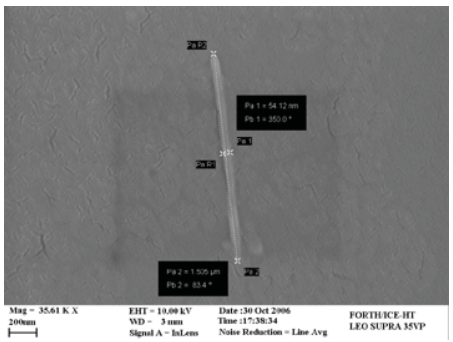

SEM image of an isolated nanorod formed from PS_nPEO_n stars in water stabilized by crooslinking and embedded on mica substrate from THF solution.

Invited Lecture 6

PACKAGING BIOLOGICAL MACROMOLECULES AND DELIVERY

M. Muthukumar
Polymer Science and Engineering Department
University of Massachusetts
Amherst, MA 01003

We will discuss how biological macromolecules are packaged in viruses and how they undergo translocation through pores and protein channels. In the packaging problem, we will consider the menagerie of viruses and address the question of whether the diverse chemical sequences or simple electrostatics control the assembly. The genome packing in hundreds of viruses is investigated by analyzing the chemical sequences of the genomes and the corresponding capsid proteins, in combination with experimental facts on the structures of the packaged genomes. A universal model, based simply on non-specific electrostatic interactions, is able to predict the essential aspects of genome packing in diversely different viruses, such as the genome size and its density distribution. Our result is in contrast to the long-held view that specific interactions between the sequenced amino acid residues and the nucleotides of the genome control the genome packing. Implications of this finding in the evolution and biotechnology will be discussed. In the second problem, we will address how single DNA/RNA molecules navigate through protein channels, by implementing concepts from polymer physics. Implications in designing strategies for sequencing of biopolymers and gene therapy will be presented.

Oral 12

Surface and confinement effects on the self-assembly and dynamics of poly(γ-benzyl-L-glutamate) embedded into nanoporous alumina templates

Gitsas A.[1,*], Floudas G.[1], Duran H.[2], Knoll W.[2], Mondeshki M.[2], Steinhart M.[3]
1. University of Ioannina, Department of Physics, P.O. Box 1186, 451 10 Ioannina, Greece, and Foundation for Research and Technology-Hellas (FORTH), Biomedical Research Institute (BRI).
2. Max Planck Institute for Polymer Research, D-55021 Mainz, Germany.
3. Max Planck Institute of Microstructure Physics, D-06120 Halle, Germany.

Poly(γ-benzyl-L-glutamate) (PBLG) is an electro-optic polypeptide, whose electrical and optical properties are closely related, and thus attractive for the design of optical biosensors.[1,2] In this work,[3] N-carboxy anhydride (NCA) monomer molecules were polymerized on the pore walls of an initiator-coated nanoporous alumina (Al_2O_3) template[4]. Since the polypeptide nanorods formed are replicas of the template pores, their dimensions are arranged by using templates of proper size. The effect of confinement and the interplay with the template on the self-assembly and the liquid-to-glass transition (T_g) is investigated. The structure and the associated dynamics have been investigated for a series of pore sizes in the range 25 – 400 nm using differential scanning calorimetry (DSC), wide-angle X-ray scattering (WAXS), powder diffraction (XRD), Fourier transform infrared spectroscopy (FTIR), nuclear magneric resonance spectroscopy (NMR), and dielectric spectroscopy (DS), respectively. The resulting PBLG nanorods were first investigated as embedded in the templates and then as free-standing nanorods, i.e. following etching of the templates (Figure 1).

The polypeptide secondary structure in both the embedded and the free standing samples is maintained. In both cases, solid state NMR and WAXS detect the formation of hexagonally packed *α*-helices. The XRD structural characterization of the pure PBLG showed a strong peak of the lyotropic liquid crystalline phase at $2\theta = 6.7°$. This reflection corresponds to an intermolecular spacing of *α*-helical chains with a spacing of 13.2 Å. The respective patterns of the PBLG nanorods had only one – albeit very broad – reflection at $2\theta = 6.5°$. The broader reflection and the absence of higher order reflections are in agreement with the DS study revealing “broken” helices.[5]

High molecular weight bulk PBLG exhibits a T_g at about 286 K and a broad endothermic peak at around 333-353 K during the first heating run (DSC). The dynamic investigation of the free standing nanorods by DS revealed two main relaxation processes: (i) the *α*-process, originating from amorphous peptide segments,[6] and (ii) a slower process, associated with the segmental relaxation and with the relaxation of helical defects[5], respectively. The analysis of the dielectric strength ($\Delta\varepsilon$) of the latter process allows an estimation of the helix persistence length, also suggesting "broken" helices.[5]

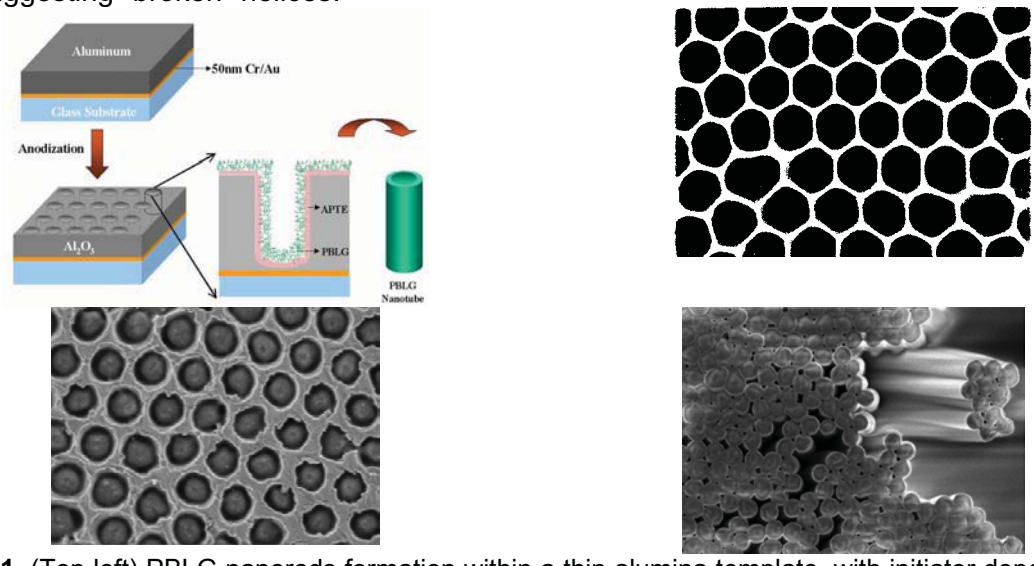

Figure 1. (Top left) PBLG nanorods formation within a thin alumina template, with initiator deposition and polymerization. Scanning electron microscopy (SEM) images of the empty template (top right,

d_{pore}=400nm), the template after the polymerization of PBLG (bottom left), and free standing PBLG nanorods (bottom right).

First the segmental process was investigated in the free-standing PBLG nanorods. It was shown that both the temperature dependence of the relaxation times and the actual glass temperature were unaffected (identical dynamics to bulk PBLG[5]). However, when the same PBLG nanorods were embedded within the Al_2O_3 template the temperature dependence of the relaxation times changed from “fragile” to “strong” and the extrapolated glass temperatures fro the pores smaller than 65 nm was reduced by as much as 55 K (Figure 2, left). The segmental relaxation exhibits again a Vogel-Fulcher-Tammann *T*-dependence, although the local segments follow different dynamics than in the bulk. The observation that the dynamics recover completely on removing the template, leads to the conclusion that they are due to strongly interacting peptide segments with the Al_2O_3 walls; a kind of interfacial relaxation. Based on the experimental findings, we propose a model of the arrangement of the embedded polypeptides within the nanorods (Figure 2, right).

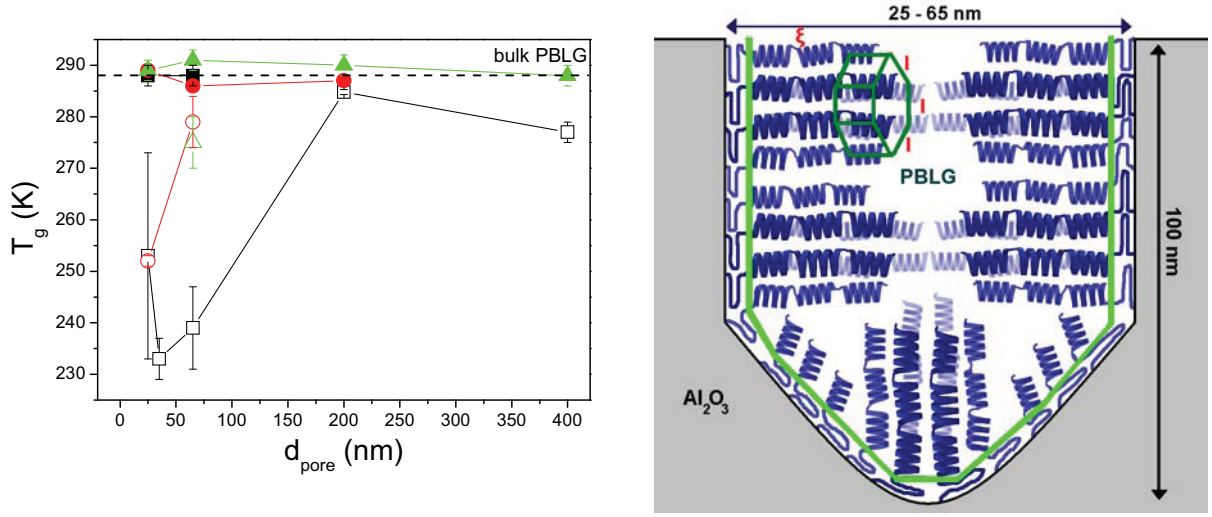

Figure 2. (Left) Variation of the glass temperature with the template pore size for the embedded (open sympols) and the free-standing (filled symbols) PBLG nanorods. The free-standing samples exhibit a T_g similar to the bulk, whereas the T_g is reduced when the pore diameter is ≤65 nm. The different symbols correspond to different NCA solvent: THF (squares), DMF (circles) and NCA from melt (triangles), and the dashed line indicates the bulk PBLG T_g. (Right) A realistic schematic representation of the assembly of the polypeptide chains within the nanopores, based on the experimental findings. The secondary structure is composed of hexagonally packed *α*-helices (WAXS, NMR), protruding from a layer next to the wall (up to the green line), which originate surface effects (DS).

References
1. Duran, H.; Jonas, U.; Steinhart, M.; Knoll, W. *Polym. Mat.: Sci. & Eng.* **2006**, *94*, 291.
2. Hartmann, L.; Kratzmüller, T.; Braun, H.-G.; Kremer, F. *Macrom. Rapid. Com.* **2000**, *21*, 814.
3. Duran, H.; Gitsas, A.; Knoll, W.; Floudas, G.; Mondeshki, M.; Steinhart, M. In preparation.
4. Lee, W.; Ji, R.; Gösele, U.; Nielsch, K. *Nature Materials* **2006**, *5*, 741.
5. Papadopoulos, P.; Floudas, G.; Klok, H.-A.; Schnell, I.; Pakula, T. *Biomacromolecules* **2004**, *5*, 81.
6. Papadopoulos, P.; Floudas, G.; Schnell, I.; Klok, H.-A.; Aliferis, T.; Iatrou, H.; Hadjichristidis, N. *J. Chem. Phys.* **2005**, *122*, 224906.

* e-mail: me01296@cc.uoi.gr

Oral 13

Vesicles from Well-Defined Block Copolypeptides

Hermis Iatrou, Nikos Ferderigos, Nikos Hadjichristidis
University of Athens, Chemistry Department, Greece

Henrich Frielinghaus, Dieter Richter
Institut für Festkörperforschung, Forscunszentrum Jülich GmbH, Germany

Sirkku Nevanpää, Olli Ikkala
Optics and Molecular Materials, Helsinki University of Technology, Finland

For more than fifty years, the synthesis of model block copolypeptides, through the ring-opening polymerization of the N-carboxy anhydrides (NCA) of amino acids by nucleophile/base initiators, was prevented by unwanted termination reactions. Recently, it was found that the use of the High Vacuum Techniques together with very careful purification of the reagents, lead to the formation of well-defined homo- and copolypeptides. By using the difunctional initiator 1,6 hexyl diamine we have synthesized amphiphilic triblock copolypeptides of the ABA- type, where A and B are poly-L-lysine and poly(γ-benzyl-L-glutamate), respectively. The copolypeptides were excessively characterized by Membrane Osmometry, NMR Spectroscopy and Size Exclusion Chromatography. By treatment with trifluoroacetic acid the ε-tert-butyloxy carbonyl groups was selectively removed to produce the corresponding amphiphilic triblock copolypeptides.

The investigation of the micellar behavior of the amphiphilic triblock copolypeptides was performed by Small Angle Neutron Scattering, Dynamic and Static Light Scattering, in pH 7.5 at room temperature. It was found that large vesicles were formed, with single or multiple walls, depending on the composition of the copolypeptide precursor. The vesicles were pH and temperature responsive. These vesicles will be used as vehicles for non-viral gene delivery.

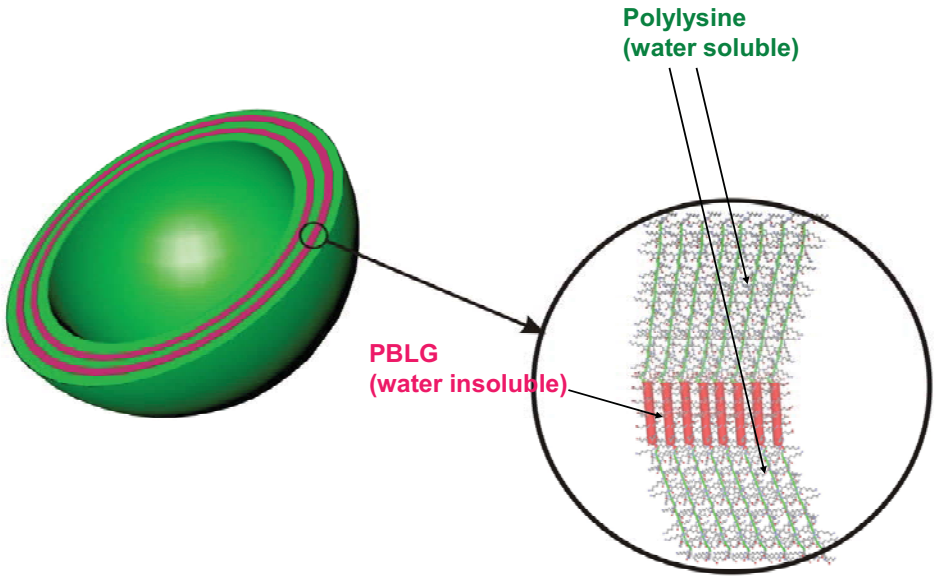

References:

1. Aliferis, Th.; Iatrou, H.; Hadjichristidis, N. *Biomacromolecules* **2004**, *5*, 1653-1656.
2. Iatrou, H.; Frielinghaus, H.; Hanski, S.; Ferderigos, N.; Ruokolainen, J.; Ikkala, O.; Richter, D.; Mays, J.; Hadjichristidis, N. Biomacromolecules **2007**, *8*, 2173-2181.
3. Karatzas, A.; Iatrou, H.; Hadjichristidis, N.; Inoue, K.; Sugiyama, K.; and Hirao, A. ASAP to Biomacromolecules

Oral 14

Hierarchies in the structural organization of spider silk – a quantitative model

P. Papadopoulos, J. Sölter, R. Ene, I. Weidner and F. Kremer
University of Leipzig, Faculty of Physics and Geosciences, Linnéstrasse 5, 04103 Leipzig, Germany

The understanding of the mechanical properties of the various types of spider silk requires a combination of techniques which can trace the effects of external fields on the microscopic level. Fourier-transform infrared (FTIR) spectroscopy is particularly suitable, because it can distinguish between different aminoacid groups as well as different secondary structures. The simultaneous stress-strain measurements unravel the microscopic response under equilibrium and non-equilibrium conditions.

In the case of major ampullate silk, crystalline and amorphous regions are affected in different ways by external strain. The alanine-rich crystals remain always almost perfectly aligned parallel to the fiber axis, whereas the glycine-rich amorphous chains exhibit a very low order parameter. An important effect is the frequency shift of vibrations corresponding to crystalline structures, which depends on stress rather than strain and can be used as a microscopic probe of the force[1]. The linear thresholdless response (Fig. 1) implies that crystals are interconnected by *pre-strained chains*.

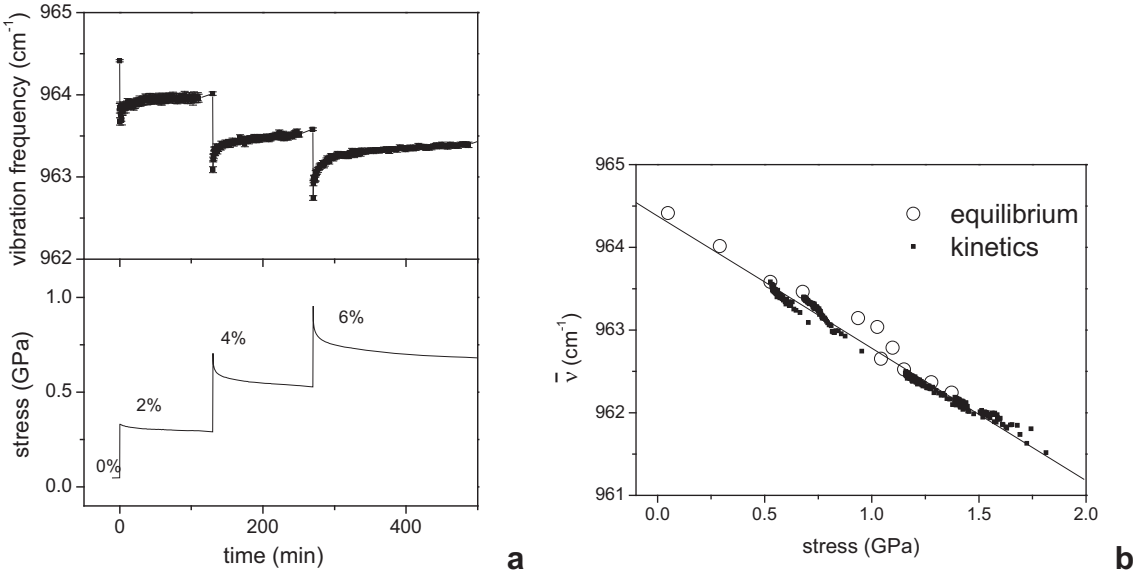

Fig. 1. Effect of stress on the frequency of a polyalanine main chain vibration in the nanocrystals. (a) Kinetic measurements after stepwise strain increase. The frequency follows the stress jump as well as its relaxation. (b) The dependence of the frequency is linearly dependent on stress rather than strain, as indicated by both equilibrium and kinetic measurements. Spectroscopy can be, therefore, used as a force nanosensor.

A model assuming a gaussian distribution of pre-strain and a *worm-like* behavior of the amorphous chains (Fig. 2) can reproduce the mechanical properties of both native and supercontracted silk[2]. The internal pre-stress is counterbalanced by the fiber skin and is released upon hydration. This model applies also to minor ampullate silk, which has different properties, even though its chemical structure is similar. The difference can be explained by a lower degree of pre-strain[3].

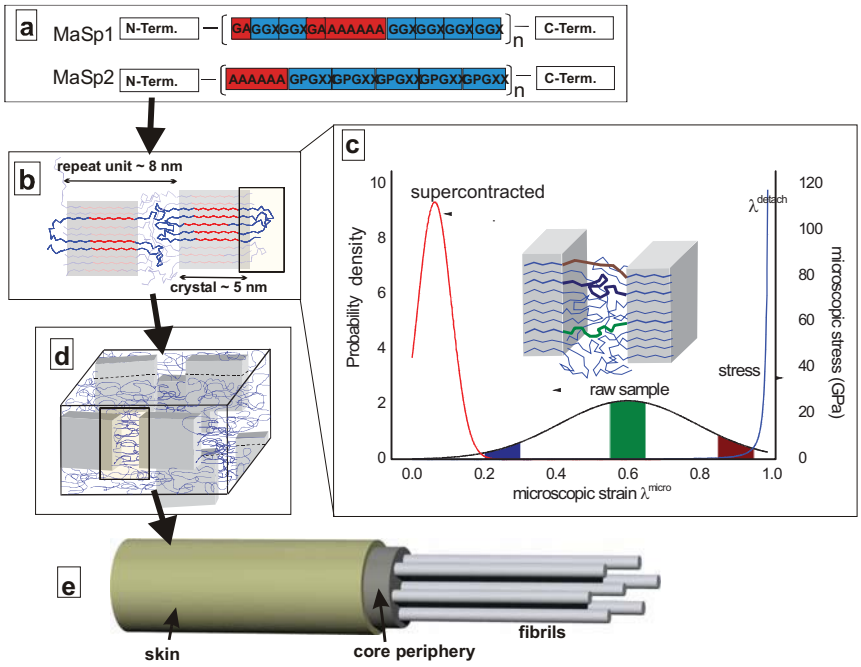

Fig. 1. Proposed structural levels of organization in spider silk. The alanine-rich protein parts (a) form highly oriented crystals (b) which are interconnected by amorphous worm-like chains with a Gaussian pre-strain distribution (c). The so assembled β-sheeted blocks (d) form a core of fibrils inside the silk fiber (e). The skin balances the internal pre-strain.

References

1. P. Papadopoulos, J. Sölter, and F. Kremer; “Structure-property relationships in major ampullate spider silk as deduced from polarized FTIR spectroscopy” *Eur. Phys. J. E: Soft Matter* **2007**, *24*, 193.
2. P. Papadopoulos, J. Sölter and F. Kremer; “Hierarchies in the structural organization of spider silk – a quantitative model” **2008** (submitted to *Phys. Rev. Lett.*)
3. P. Papadopoulos, J. Sölter, R. Ene, I. Weidner and F. Kremer (in preparation)

Oral 15

SYNTHESIS OF MOLECULARLY IMPRINTED POLYMERS VIA PRECIPITATION POLYMERIZATION FOR THE SELECTIVE SEPARATION OF PEPTIDES

S. Chaitidou, O. Kotrotsiou and C. Kiparissides

Department of Chemical Engineering, Aristotle University of Thessaloniki and Chemical Process Engineering Research Institute, P.O. Box 472, 54124 Thessaloniki, Greece

Molecular imprinting is an efficient method for the synthesis of polymers with highly specific recognition site where a functional monomer and a cross-linker are co-polymerized, via a free-radical polymerization mechanism, in the presence of a template molecule (i.e., the imprint molecule) that interact with the functional monomers through covalent or non-covalent interactions. Subsequent removal of the imprint molecules reveals specific binding sites that are complementary in size and shape to the template molecule.

In general, non-covalent imprinting is easy to achieve and applicable to a wide range of template molecules since many of practically important molecules possess polar groups that can interact non-covalently with the functional groups of polymerizable monomer. In particular, hydrogen bonding is the most suitable for precise molecular recognition since this type of bonding is highly dependent on both distance and direction between the monomer and template molecules. Coordination bonds can be also employed for the association between the template and the functional monomer. In this case, the functional monomers (polymerizable ligands) are complexed to the metal ion, generally a transition metal ion which, in turn, coordinates to the template molecule. The most important advantage of this method is that the strong binding interactions between the metal ions and the ligands are not affected by the solvent environment.

In their most common form, molecularly imprinted polymers (MIPs) are prepared, via free-radical bulk polymerization, as macro porous monoliths. Precipitation polymerization has emerged as an alternative to the above technique. This polymerization technique can lead to free of any stabilizer particulate MIPs. In addition, precipitation polymerization can be readily adapted to the synthesis of good imprints both in non polar aprotic solvents using non-covelent interactions to polar protic solvents using strong coordination bonds.

In the present study, precipitation polymerization was employed in order to synthesize molecularly imprinted polymers towards an oligo-peptide of tryptophan (i.e., boc-$\{Trp\}_3$), using methacrylic acid as functional monomer, ethylene glycol dimethacrylate as crosslinker and acetonitrile as porogen. Non-imprinted polymeric nanoparticles (NIPs) were also prepared under the same conditions in order to compare their affinity to the template molecules with that of the MIPs. It was proved that the presence of the template into the reaction medium has a direct impact on the particle morphology. More specifically, it was shown that the uniformity of the particles disappeared when boc-$\{Trp\}_3$ was employed, probably due to the bridging that the specific template causes to the final product. Thus, MIPs towards different boc-$\{Trp\}_3$ concentrations were utilized during the reaction in order to synthesize optimized polymeric particles. Batch-wise guest binding experiments were then performed for the determination of the rebinding capacity and selectivity of the molecularly imprinted particles. By comparing the activity of the imprinted polymer with that of the non-imprinted polymer, the rebinding capacity of the molecularly imprinted polymers was evaluated. Comparative analysis was, also, performed employing the tripeptide of tyrosine (boc-$\{Tyr\}_3$) and the tripeptide of phenylalanine (boc-$\{Phe\}_3$) in order to examine the specificity of Boc-$\{Trp\}_3$ imprinted polymeric receptors towards the template molecule. These results are crucial for the future development of MIPs for larger biomolecules using the epitope approach. In this method instead of the whole proteins, a short peptide sequence, often exposed at the protein surface, is used as template molecule. Once the matrix has been polymerized the resultant imprinted polymer should be able to recognize and bind the whole protein.

Additionally, in the present study is reported the synthesis of metal-complexing polymer microparticles capable of specific binding to z-(Histidine)$_2$-ome, a N- and C- protected histidine dipeptide, by precipitation polymerization in methanol. For the synthesis of these materials, 4-vinylpyridine and 1-vinylimidazole (vinyl monomers with metal chelate properties) were used as functional monomers, cobalt and copper acetate as metal sources, and ethylene glycol dimethacrylate as cross-linker. Initially, the formation of the binary complexes between the metal ions and the ligands (i.e., z-(Histidine)$_2$-ome, 4-VP and 1-VID) was studied by applying the continuous variation method (Job's plot analysis) and the stoichiometry and the formation constant of each complex were derived. The above analysis allowed the assessment of the affinity between the metal ions and the ligands. In a second stage, it was studied the formation of the polymerizable ternary complexes between the functional monomer(s), the template and the metal ions through a complexiметric titration of the functional monomer in a model of the prepolymerization mixtures (in the absence of cross-linker and initiator) followed by scanning UV/Vis spectrophotometry. The results of the above analysis were used to define the (template: metal ion: functional monomer) molar ratio in the polymerization reaction mixture. The binding properties of the MIPs and the corresponding BLANKs, prepared in the absence both of the template and the metal ion, were assessed by batch-wise rebinding experiments. The derived binding isotherms showed that the MIPs had a much higher rebinding capacity towards the template molecule than the BLANKs.

Acknowledgements: EU for supporting this research under the STREP Project, Proposal No. 516981.

Invited Lecture 7

Single polymer binding: Towards a universal adhesive

J. Wang[1], M. Kappl[1], H.-J. Butt[1], M.N. Tahir[2], W. Tremel[2]

[1]*Max-Planck-Institute for Polymer Research, Ackermannweg 10, 55128 Mainz, Germany*
[2]*Institut für Anorganische Chemie und Analytische Chemie, Johannes Gutenberg-Universität, Duesbergweg 10-14, 55099 Mainz, Germany*

A biological model for wet adhesion is the mussel, which is well known for its ability to cling to wet surfaces. Mussels secrete specialized adhesion proteins, which contain a high content of the catecholic amino acid 3,4-dihydroxyphenylalanine (DOPA). Both natural and synthetic adhesives containing DOPA showed strong adhesion. However, the detailed binding mechanisms has never been fully explained. We synthesized the mussel-mimetic polymer poly(dopamine methacrylamide-co-butylamine methacrylamide) (p(DMA-co-BMA)), with free catechol groups. The ratio of catechol groups was varied. Using an atomic force microscope (AFM) we analyse the adhesion of single p(DMA-co-BMA) chains to titanium in aqueous medium. The same adhesion force was measured for catechol contents between 10 and 100%. A model is presented to account for this independence of the desorption force on the degree of funtionalization. That only a minor ratio of active sites is sufficient for strong adhesion opens new strategies to design adhesive polymers.

Oral 16

Viscoelasticity of semifluorinated alkanes at the air-water interface

C.Christopoulou [1,2], U. Jonas, C. Clark, and D.Vlassopoulos[1, 2]

[1]FORTH, Institute of Electronic Structure & Laser, Heraklion, Crete, Greece
[2]University of Crete, Department of Materials Science and Technology, Heraklion, Crete, Greece
[3]Max-Planck Institute for Polymer Research, Mainz, Germany

Abstract

We investigated the viscoelastic properties of semifluorinated alkanes $F(CF_2)_n(CH_2)_mH$ (referred as F_nH_m) spread on the air-water interface. These specially synthesized model 'doubly-hydrophobic' macromolecules of varying architecture reside at the air-water interface in the form of surface micelles that minimize the free energy. Earlier small angle x-ray scattering over studies indicated a typical 'disc' diameter about of 30 nm in diameter. Pressure area isotherms performed on Langmuir monolayers of the micelles appear to exhibit two transitions. In both regimes the film exhibited a solid like viscoelastic response but with different stiffness. As the surface pressure increased in each regime values of the storage and the loss surface moduli increased as well. The film stability was studied by compression-expansion cyclic experiments. These findings are discussed in view of recent theoretical developments and provide opportunities for manipulating surface structure and rheology of such types of macromolecules.

Oral 17

Adsorption of oligomers and polymers in nanoporous alumina

Sotiria Karagiovanaki, Alexandros G. Koutsioubas, Nikolaos Spiliopoulos and Chris Toprakcioglu

Department of Physics, University of Patras, Greece 26500

ABSTRACT

We have studied the adsorption of end-functionalised oligomers and polymers in nanoporous alumina by means of FTIR spectroscopy. Under suitable anodisation conditions using electrolyte solutions of sulphuric or oxalic acid, thin films (ca. 10 μm - 100 μm) of aluminium can be oxidized electrochemically to produce nanoporous Al_2O_3 with nearly monodisperse regular, hexagonally packed arrays of parallel pores with diameters typically in the range ca. 10 nm - 200 nm. The adsorption of oligomers and polymers on the walls of such pores was investigated with FTIR spectroscopy. We have used carboxy-terminated alkane oligomers (carboxylic acids) in the range C6-C24, homopolymers such as polymethylmethacrylate (PMMA) and polyethyleneoxide (PEO), as well as polystyrene-polyethyleneoxide (PS-PEO) block copolymers. Both commercial and in-house prepared porous alumina substrates with pore diameters in the range ca. 20-200 nm were employed. The pore size was measured by electron microscopy. It is found that polymers whose radius of gyration is greater than or comparable to the pore diameter adsorb negligibly, as they are entropically hindered from entering the pores, while smaller chains or oligomers readily adsorb and populate the pore walls. Our results demonstrate the size-related selectivity of such well-defined nanoporous media and point to potential applications in size-exclusion processes and nanofluidics.

Oral 18

Dynamic of zwitterion terminated polystyrene at a glass-solution interface studied by evanescent wave dynamic light scattering

A. Tsigkri[1], B. Loppinet[1], S. Pispas[2]

[1]*Institute of Electronic Structure and Laser, FO.R.T.H., Heraklion, Greece*

[2]*Theoretical and Physical Chemistry Institute, N.H.R.F, Athens, Greece*

Zwitterion terminated polymer chains are expected to end adsorb to a glass surface due to the large interaction (8 kT) between the strong dipole moment of the Zwitterion and the glass surface. This is a commonly used to realize polymer brushes. However for large molecular weight, the chain crowding at the interface may limit the adsorb amount to a lower value than the predicted equilibrium. Here we report on the adsorption of large 10^6 g/mol polystyrene chains onto glass and the dynamic of the steady state layer as investigated by evanescent wave dynamic light scattering. The technique utilizes the short penetration depth of the optical evanescent wave produced at total internal reflection to probe the fluctuation at the glass-liquid interface. A smaller Zw-PS (0.175 10^6 g/mol) is found to show typical brush behavior. In the large Zw-PS, large scattering intensity is measured, and the associated dynamic is found to present a strong wave vector dependence ($\Gamma \sim q^4$) . This is interpreted as an in plane diffusion of large entities. Possibilities for the microscopic origin and nature of the inhomogeneities are discussed

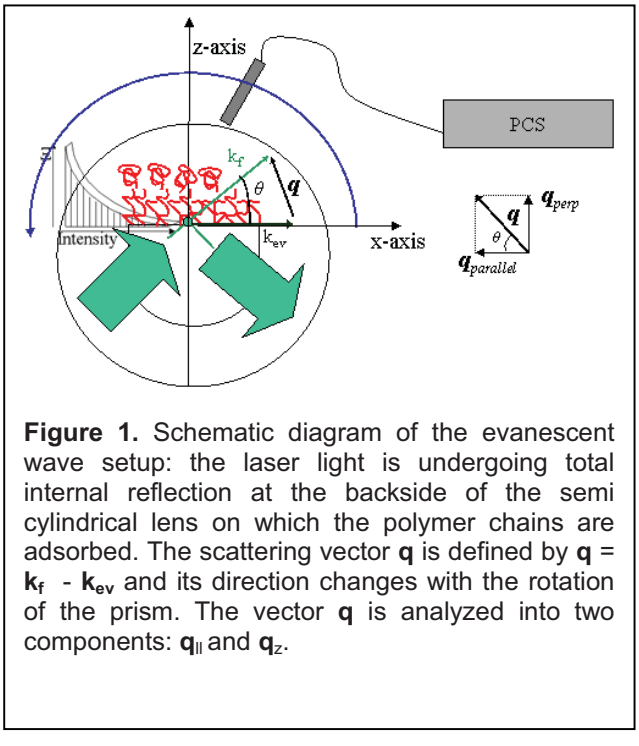

Figure 1. Schematic diagram of the evanescent wave setup: the laser light is undergoing total internal reflection at the backside of the semi cylindrical lens on which the polymer chains are adsorbed. The scattering vector **q** is defined by **q** = $\mathbf{k_f}$ - $\mathbf{k_{ev}}$ and its direction changes with the rotation of the prism. The vector **q** is analyzed into two components: $\mathbf{q_{||}}$ and $\mathbf{q_z}$.

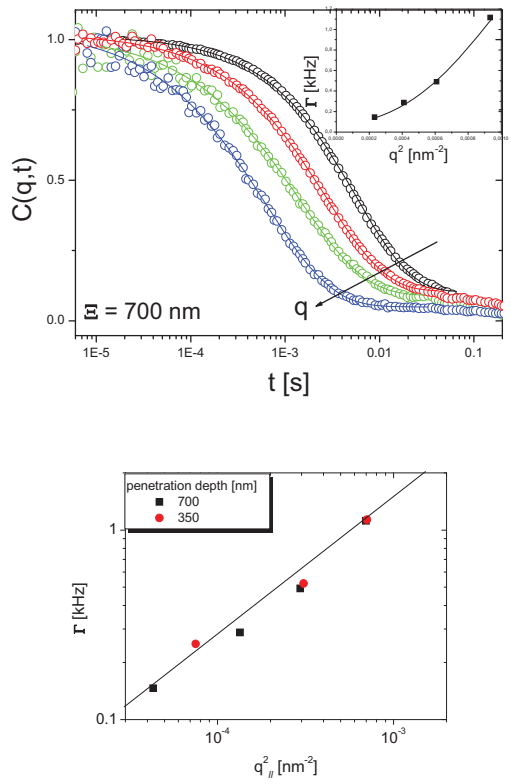

Figure 3. top : Normalized correlation functions and their fits for the case of the adsorbed layer in contact with the dilute solution, at penetration depth Ξ = 700 nm and different q . Insets: the characteristic rates Γ(q) vs q^2. **bottom** : $q_{//}^2$ dependence of the rates at two different penetration depths

Oral 19

Theoretical study of adsorption of star-polymers by mean field theory

Georgios Kritikos and Andreas F. Terzis

Department of Physics
School of Natural Sciences
University of Patras
GR 26504, Patras, GREECE

In this work we theoretically investigate the behavior of star-like polymers when they are adsorb in a solid surface from a solution. Our tool is a recently developed new approach to the numerical self-consistence mean field method (bnSCF)[1]. According to this new version the polymer segments are considered to be contained in a tube filled with solvent, which allow the realization of several configurations of the chain. The conformation of this chain-tube is developed on a lattice using Kuhn segment, such that the volume of the polymer-chain is the same with the one measured experimentally. Each polymeric segment is calculated using the Flory segment introduced in previous nSCF method[1-3]. As in each point of the lattice the total polymer volume fraction is consisted of more realistic polymer configurations than in previous methods, we can extract in a more efficient way the contribution to the volume fraction of each polymer configuration with important statistical weight.

The experimental results, which we have tried to reproduce with the bnSCF method, refer to a solution that contained three copolymers $(nPS_{70K})-X$ (n=1,2,3), functionalized at one end by a zwitterionic group $X=(CH_3)_2N^+(CH_2)_3SO_3^-$ and attached via short polybutadiene spacers[4-6]. Moreover we have investigated mixtures of other various architectures.

In figure 1 we plot the volume fraction profiles for three polymers. The results are in very good agreement with NR results[5] and show the improvement compare to previous nSCF method.

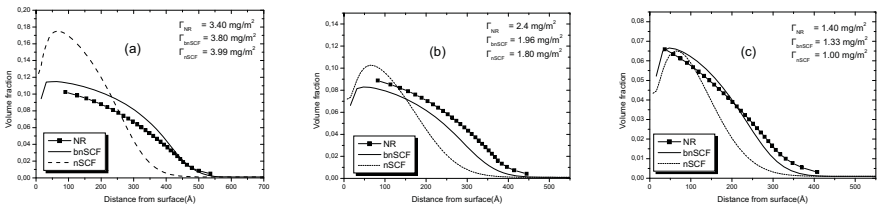

FIGURE 1. The systems studied are: (b) Linear polymers with one PS branch, AI. (c) Star polymers with two PS branches, AII and (d) Star polymers with three PS branches, AIII.

In figure 2 we present the volume fraction of the free ends of the systems presented above. It is found that as the number of branches increase, the free ends are distributed closer to the

surface. The more branched polymers succeed lower adsorption and so the elongation of the brush is less intense compare to linear polymers. So due to entropic reason the more branched polymers need more space to develop and this force the free ends to cover the whole brush area (not just the outer region).

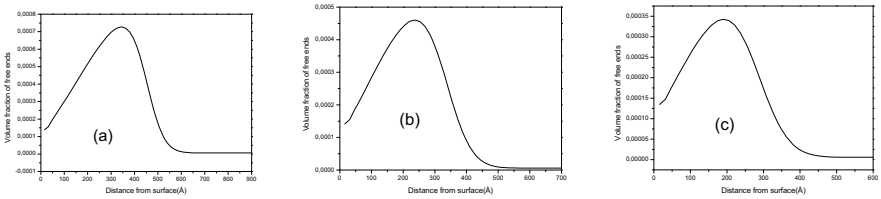

FIGURE 2. Volume fraction profiles of the free ends as a function of the distance from the surface.

Next we show results for the behavior of other star and linear architectures where the anchor is longer. The zwitterionic group is the end of an additional branch (anchor) smaller than the others but we same interacting behaviour. In figure 3 we show results for the volume fraction for a mixture of linear (BI) and two-branch star-polymers (BII). In general the polymers with two branches tend to develop in the outer region of the brush. In case of low percentage (25%) of the BII this tendency is more obvious. As the percentage of the BII polymer increase they need more space to develop and so they are distributed more broadly. The total volume fraction of the mixture doesn't show two regions (not shown) as the bimodal case of linear polymers[7].

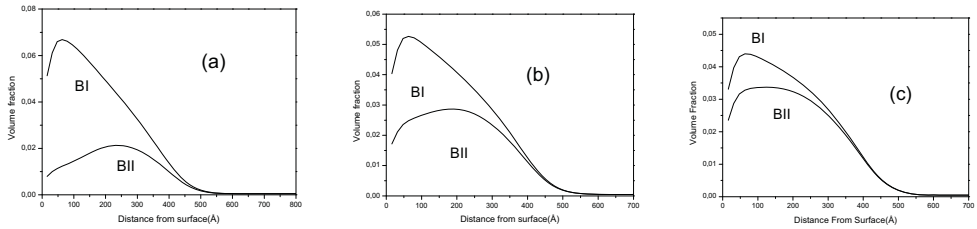

FIGURE 3. We present the volume fraction profiles as a function of the distance from the surface (bnSCF). The systems studied are: (a) 75% BI and 25%BII, (b) 50% BI and 50%BII and (c) 25% BI and 75% BII.

The same conclusion could be generalized for oher mixtures of star polymers with different number of branches (BII-BIII, BI-BIV).

REFERENCES

1. G. Kritikos,A.F. Terzis, *Polymer*, **48**, 638-651 (2007).
2. G.J. Fleer, M.A. Cohen Stuart, J.M. Scheutjens, T. Cosgrove, B. Vincent, *Polymers at Interfaces*, Cambridge, Chapman and Hall, 1993.
3. A.F. Terzis, D.N. Theodorou, A. Stroeks, *Macromolecules*, **31**, 1385-1396 (2000);
4. Taunton HJ, Toprakcioglu C, Fetters LJ, Klein J. *Macromolecules,* **23** 571-580 (1990)
5. G. Sakellariou, S. Pispas, N. Hadjichristidis, *Macromolecular Chemistry and Physics*, **204**, 146-154 (2003).
6. I. Hiotelis, A. Koutsioubas, N. Spiliopoulos, D. Anastasopoulos, A. Vradis, C. Toprakcioglou, Macromolecules, accepted for publication (2008).
7. Kritikos, A.F. Terzis, *Polymer*, **46**, 8355-8365 (2005).

Oral 20

A general approach to surface initiation polymerizations from multi-wall carbon nanotubes

Dimitrios Priftis, George Sakellariou, Durairaj Baskaran, Jimmy W. Mays, N. Hadjichristidis

Department of Chemistry, University of Athens, 15771 Panepistimiopolis Zografou, Athens, Greece

Department of Chemistry, University of Tennessee, 522 Buehler Hall, Knoxville, TN 37996

ABSTRACT: Multi wall carbon nanotubes (MWNT) were functionalized with different substituted benzocyclobutenes through Diels-Alder cycloaddition reactions[1]. Surface functionalized MWNTs were characterized by FT-IR, Raman spectroscopy, and TGA. These MWNTs were used for the surface initiated anionic[2], ring openning, atom transfer, titanium-mediated coordination and dual simultaneous polymerizations. The resulting polymer grafted nanotubes were characterized by GPC, ^{1}H-NMR, DSC, Raman spectroscopy, TEM (figure) and TGA. The kinetics of the Ring Opening Polymerization (ROP) of ε-caprolactone (ε-CL) was monitored with TGA and GPC. The PCL and PEO homopolymers grafted on MWNTs were used as macroinitiators for the synthesis of diblock copolymers. The aggregation behavior of these grafted copolymers was investigated by light scattering and AFM. $CpTiCl_2$ was used for the surface polymerization of n-hexyl isocyanate, L-Lactide and ε-CL, while MWNTs with ATRP and ROP grafted initiators were used for dual simultaneous polymerizations.

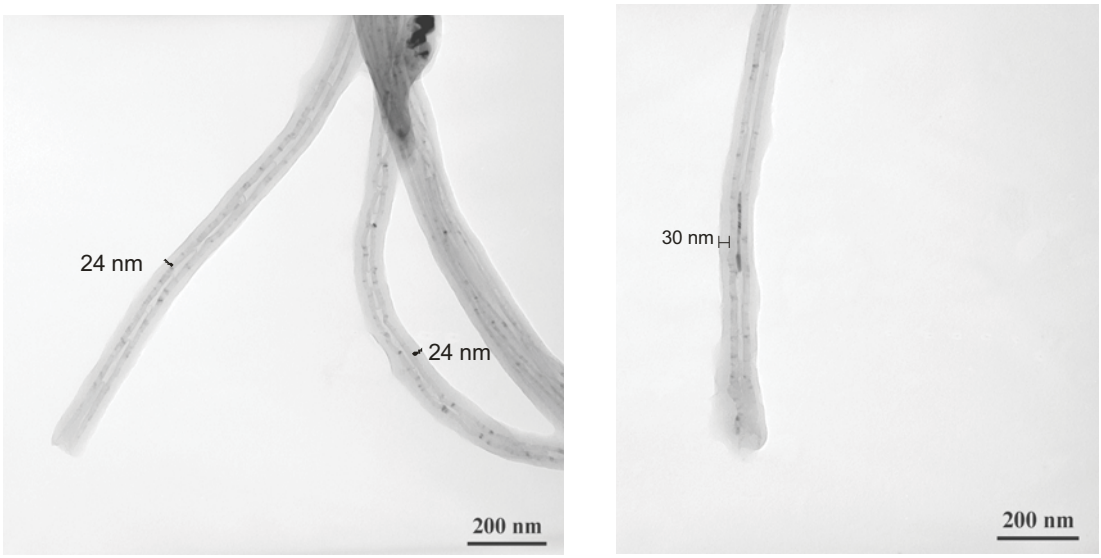

Figure: TEM of surface grown PS from MWNT-g-(BCB-PE)$_n$ exhibiting up to 30 nm PS layer on the surface of MWNTs .

References:

1. Georgios Sakellariou, Haining Ji, Jimmy W. Mays, Nikos Hadjichristidis, Durairaj Baskaran, *Chemistry of Materials*, 19, 6370-6372, **2007**

2. Georgios Sakellariou, Jimmy W. Mays, Durairaj Baskaran, submitted to *Chemistry of Materials*, **2008**

Invited Lecture 8

Polymer Brushes for Functional Surfaces

Manfred Stamm

Leibniz-Institut für Polymerforschung Dresden (IPF),
Hohe Strasse 6, 01069 Dresden, Germany
stamm@ipfdd.de

Functional and adaptive surface properties can be achieved with functional brush surfaces at nanometer scale which are of interest for several possible applications. A fairly robust way for the generation of a functional thin film is the attachment of polymer chains to the surface by covalent bonding. At high grafting density a brush-like layer will be formed, and surface properties can be changed significantly. Utilizing mixed polymer brushes the surface properties can be switched between different states /1/, and it is even possible to switch between ultra-hydrophobic and ultra-hydrophilic behavior by introduction of additional surface roughness, i.e. a combination of physical and chemical modification of the surface /2/. Depending on solvent conditions, one or the other polymer chain occupies the surface layer and thus determines surface properties, which depend on the outermost surface layer. With selective solvents a wide range of surface properties can be achieved. The thin polymer brush films are laterally structured in the dry state, which can be investigated by AFM /1,7,8.10,13/.

The surface properties can in addition be modified by the introduction of nanoparticles, which may be attached to the polymer brush chains (see figure 1) /6,11,12/. Depending on the degree of swelling of the brush layer, the nanoparticles will be close to the surface or further away. If the nanoparticles emit fluorescence light, the different emitted beams will interfere with each other in different ways depending on the distance to the surface. Thus the emitted light intensity will be modulated and can reveal information on the state of swelling, in this way serving as a sensitive optical sensor for the degree of swelling of the brush.

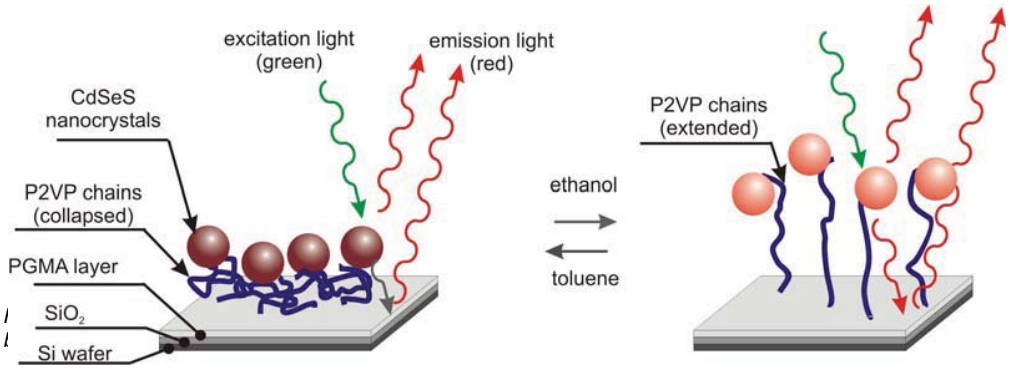

Fig.1 Scheme of polymer brushes functionalized with fluorescent nanoparticles for sensing applications /6/

The adsorption of polyelectrolytes and protein molecules is similarly depending on the state of the brush /5,9/. In particular salt concentration and pH will influence the adsorbed amount. In a fluid cell of an ellipsometric set-up the adsorption can be measured in-situ and as a function of time. We were able to identify a regime where the adsorbing molecules repel the attached counterions in the brush (counterion evaporation effect) and where the adsorption process is favored by the entropic driving force /9/. Investigations of this sort are very much easier, when gradient brush layers are utilized. There the composition of the brush or the grafting density is varied uniformly along the silicon wafer /3,4/. In one adsorption experiment several parameters then can be investigated in a time efficient way.

References

1. S. Minko, M. Müller, D. Usov, A. Scholl, C. Froeck, M. Stamm, Lateral versus perpendicular segregation in mixed polymer brushes, Physical Review Letters 88, 035502-1-035502-4 (2002)
2. M. Motornov, S. Minko, K.-J. Eichhorn, M. Nitschke, F. Simon, M. Stamm, Reversible Tuning of Wetting Behavior of Polymer Surface with Responsive Polymer Brushes, Langmuir, 19, 8077 (2003)
3. L. Ionov, A. Sidorenko, K.-J. Eichhorn, M. Stamm, Stimuli-Responsive Mixed Grafted Polymer Films with Gradually Changing Properties: Direct Determination of Chemical Composition, Langmuir, 21, 8711-8716 (2005)
4. L. Ionov, M. Stamm, S. Diez, Size Sorting of Protein Assemblies Using Polymeric Gradient Surfaces, Nano Letters, 5, 1910-1914 (2005)
5. L. Ionov, M. Stamm, S. Diez, Reversible Switching of Microtubule Motility Using Thermoresponsive Polymer Surfaces, Nano Letters, 6, 1982-1987 (2006)

6. L. Ionov, S. Sapra, A. Synytska, A. L. Rogaci, M. Stamm, S. Diez, Fast and spatially resolved environmental sensing using grafted composite layers of stimuli-responsive polymers and fluorescent semiconductor nanocrystals, Advanced Materials, 18, 1453-1457 (2006)
7. Y. Mikhaylova, L. Ionov, J. Rappich, M. Gensch, N. Esser, S. Minko, K.-J. Eichhorn, M. Stamm, K. Hinrichs, In Situ Infrared Ellipsometric Study of Stimuli-Responsive Mixed Polyelectrolyte Brushes, Anal. Chem., 79, 7676-7682 (2007)
8. A. Synytska, M. Stamm, S. Diez, L. Ionov, Simple and Fast Method for the Fabrication of Switchable Bicomponent Micropatterned Polymer Surfaces, Langmuir, 23, 5205-5209 (2007)
9. P. Uhlmann, N. Houbenov, N. Brenner, K. Grundke, M. Stamm, In-situ Investigation of the Adsorption of Globular Model Proteins on Stimuli Responsive Binary Polyelectrolyte Brushes, Langmuir, 23, 57-64 (2007)
10. D. Usov, V. Gruzdev, M. Nitschke, M. Stamm, O. Hoy, I. Luzinov, I. Tokarev, S. Minko, Three-Dimensional Analysis of Switching Mechanism of Mixed Polymer Brushes, Macromolecules, 40, 8774-8783 (2007)
11. S. Gupta, P. Uhlmann, M. Agrawal, V. Lesnyak, N. Gaponik, F. Simon, M. Stamm, A. Eychmüller, Covalent immobilization of quantum dots on macroscopic surfaces using poly(acrylic acid) brushes, Journal of Materials Chemistry, 18, 214-220 (2008)
12. S. Gupta, P. Uhlmann, M. Agrawal, S. Chapuis, U. Oertel, M. Stamm, Immobilization of Silver Nanoparticles on Responsive Polymer Brushes, Macromolecules, 41, 2874-2879 (2008)
13. K. Roodenko, Y. Mikhailova, L. Ionov, M. Gensch, M. Stamm, S. Minko, U. Schade, K.-J. Eichhorn, N. Esser, K. Hinrichs, Ultra-thin Responsive Polyelectrolyte Brushes studied by Infrared Synchrotron Mapping Ellipsimetry, Applied Physics Letters 92, 103102 (2008)
14. M. Stamm (ed.), Polymer Surfaces and Interfaces: Characterisation, Modification and Applications, Springer Verl., Berlin, ISBN 978-3-540-73846-0, 324p. (2008)

Oral 21

Dynamics of poly (propylene oxide) amines intercalated in clay

P. Pissis[1], A. Kyritsis[1], S. Kripotou[1], A. Panagopoulou[1], P. I. Xidas[2] and K. S. Triantafyllidis[2]

[1] *Department of Physics, National Technical University of Athens, Zografou Campus, 15780, Athens, Greece*
[2] *Department of Chemistry, Aristotle University of Thessaloniki, 54124 Thessaloniki, Greece*

Polymer-layered silicate nanocomposites (PLSN) have, recently, attracted much attention because of significant improvement in several properties in comparison to pristine polymers[1]. For the synthesis of PLSNs the choice of layered materials is often the smectite clays (e.g. montmorillonite, hectorite) due to their highly expansive characteristic and their rich intercalation chemistry which allows them to be chemically modified and to become compatible with the polymer precursors. The organoclay is synthesized by ion-exchange of inorganic cations of the parent clay with hydrophobic organic onium ions. It is well established that macroscopic properties in PLSNs depend on the choice of the clay mineral and the type of organic modifier that greatly affect interfacial interactions and nanoscale morphology of the polymer - layered silicate [1]. Recently, a new method of preparing epoxy-clay nanocomposites has been proposed[2]: the direct incorporation of poly (propylene oxide) amines (also used as epoxy curing agents) in the galleries of montmorillonite clays via ion-exchange. These intercalated diamines have various functions during the formation of the thermoset epoxy-clay nanocomposite: clay surface modifier, intragallery polymerization catalyst and curing agent.

In this work we investigate the dynamics of poly (propylene oxide) amines intercalated in montmorillonite clays by means of Differential Scanning Calorimetry (DSC), Thermally Stimulated Depolarization Currents (TSDC) and broadband Dielectric Relaxation Spectroscopy (DRS) methods. The amines of interest were the commercially available α, ω-diamines known as Jeffamine D-series amines with molecular weights in the range 400 – 4000. Depending on the chain length of the diamine, different orientations of the PPO chains were adopted in the clay galleries: Low molecular weight Jeffamines (MW ~ 400) intercalate as lateral bilayer to inclined monolayer and the gallery heights are restricted to d_{001} basal spacing values of approximately 17 Å. For Jeffamines with MW values of 2000 and 4000 the PPO chains adopted a folded configuration within the galleries resulting in d_{001} values of approximately 20 – 46 Å[2].

The polymeric chain motions are restricted between successive clay nanolayers which define a 3D gallery system where diamines are actually confined in one dimension related to the gallery height. This system is well suited for the investigation of confinement effects on chain mobility and relaxations since we were able to vary gallery height (i.e. the available space for chain motion) by using Jeffamines of different chain length and to affect interfacial properties by interacting protonated diamines with the negatively charged surface of the clay platelets. Jeffamines exhibit the dielectric normal mode due to the fluctuation of the end-to-end vector as well as the segmental mode due to local, segmental fluctuations. Dielectric Spectroscopy, thus, can provide information on the chain dynamics monitoring all the possible motions of the macromolecules, from local chain motions up to global chain translational and rotational motions.

Our results reveal a remarkable dependence of the segmental mobility (α relaxation) of the intercalated diamines on the chain length of the polymeric chains and on the basal spacing of the organoclays which reflects differences in gallery height. Specifically, for the intercalated D400 (the shortest chain, ~ 6 repeating units) the segmental relaxation is suppressed and the molecular mobility exhibits Arrhenius temperature dependence. For the intercalated D2000 the segmental mobility is retarded whereas for the intercalated D4000 (the longest chain) the segmental mobility seems to be unaffected. Exploring the origin of the observed behavior (anchored chain-ends or pure confinement effects) we measured a D2000-intercalated organoclay exhibiting disordered structure and having stronger geometrical restriction (basal spacing of 18.78 Å in comparison to a

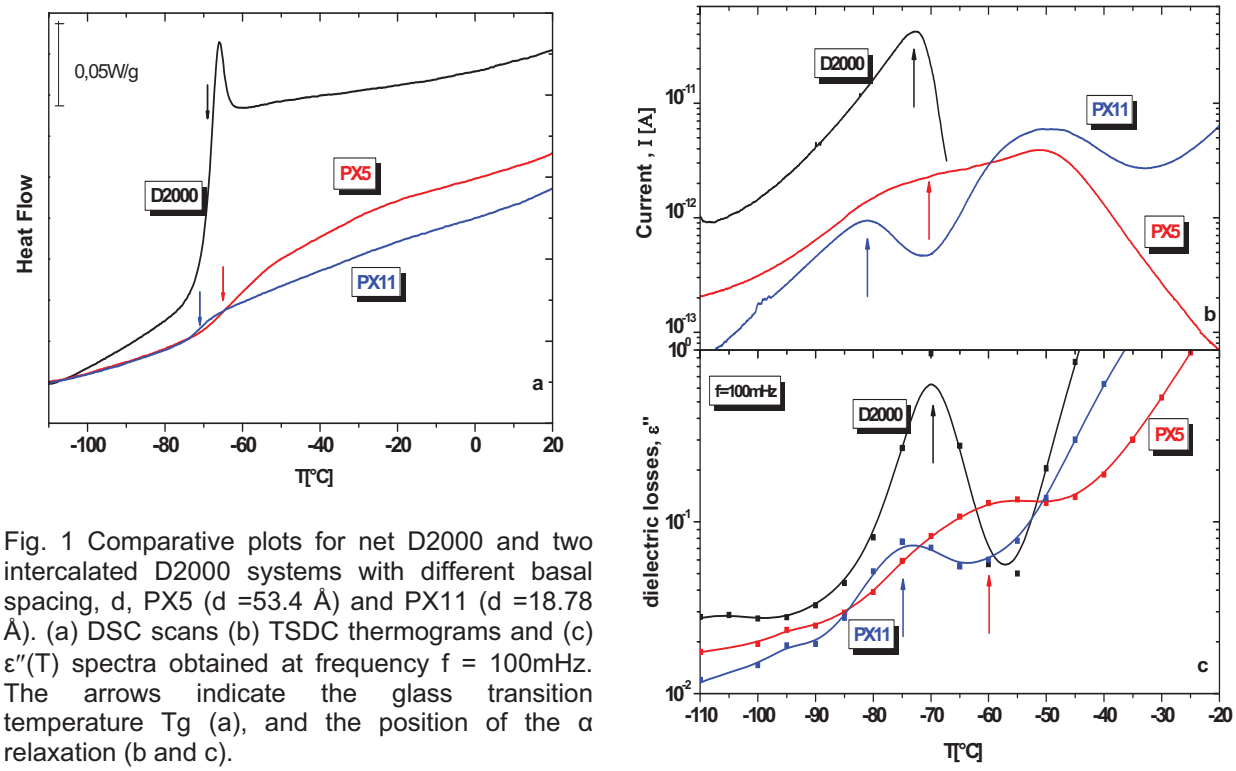

Fig. 1 Comparative plots for net D2000 and two intercalated D2000 systems with different basal spacing, d, PX5 (d =53.4 Å) and PX11 (d =18.78 Å). (a) DSC scans (b) TSDC thermograms and (c) ε″(T) spectra obtained at frequency f = 100mHz. The arrows indicate the glass transition temperature Tg (a), and the position of the α relaxation (b and c).

more ordered structure with basal spacing of 53.4 Å). In Fig. 1 we show the obtained DSC, TSDC and DRS spectra which indicate that for the intercalated chains with stronger confinement the segmental mobility is accelerated.

The comparative study of the secondary relaxation mechanism of the diamines and of the global chain motions (although with higher uncertainty for the intercalated chains) provide additional information with respect to the effects of a restrictive environment on chain dynamics.

Acknowledgements. A.K, S.K. and A.P acknowledge financial support of NTUA via program «PEVE 2007». KST acknowledges partial support of EU and Greek Ministry of Development via program EPAN-PENED2003.

References

1. T.J. Pinnavaia, G.W. Beall (Eds.) “Polymer-Clay Nanocomposites”, John Wiley & Sons (2000)
2. C.S. Triantafillidis, P.C. LeBaron, T.J. Pinnavaia, *Journal of Solid State Chemistry* 167, 354-362 (2002).

Oral 22

Crystallization Behavior in Polymer / Layered Silicate Nanocomposites

K. Chrissopoulou,[1] E. Pavlopoulou,[1,2] H. Papananou,[3] S. Fotiadou,[3] G. Portale,[4] W. Bras,[4] and S. H. Anastasiadis[1,3]

[1] *Institute of Electronic Structure and Laser, Foundation for Research and Technology-Hellas, P. O. Box 1527, 711 10 Heraklion, Crete, Greece*
[2] *Department of Materials Science and Technology, University of Crete, Heraklion, Crete, Greece*
[3] *Department of Chemical Engineering, Aristotle University of Thessaloniki, 54124 Thessaloniki, Greece*
[3] *DUBBLE CRG, European Synchrotron Radiation Facility, Grenoble, France*

Polymer / layered silicate nanocomposites constitute an interesting class of materials which allow the investigation of basic scientific problems and at the same time are utilized in many applications. Mixing polymers with layered silicates leads to three different micro- or nanostructures depending on the interactions between the chains and the inorganic surfaces: the phase separated, where the two materials are immiscible, the intercalated that the polymer chains reside in the interlayer galleries of the silicates forming 0.8-2.5nm films and the exfoliated, in which the structure of the inorganic material is destroyed and the platelets are dispersed in the polymeric matrix.[1] A reason that these materials have attracted the scientific interest is related with their unique properties that render them candidates for numerous technological applications. In the case of crystalline polymers, the improvement in the properties can be attributed further than the reinforcing contribution of the inorganic additives and the formation of different nanostructures, to the alteration of the crystalline behaviour and characteristics of the polymer chains due to the presence of the inorganic material.

In this work we investigate the structure, morphology and crystallization behavior of a hydrophilic, crystalline polymer, poly(ethylene oxide), PEO, (M_n=100000, T_g=-67°C, T_m=65°C) when mixed with natural montmorillonite (Na^+-MMT) in a range of compositions that covers the whole regime from pure polymer to pure clay. The structure of the hybrids was investigated by X-ray diffraction, Polarizing Optical Microscopy (POM), Differential Scanning Calorimetry (DSC) and Small Angle X-ray Scattering (SAXS, performed at ESRF, France).

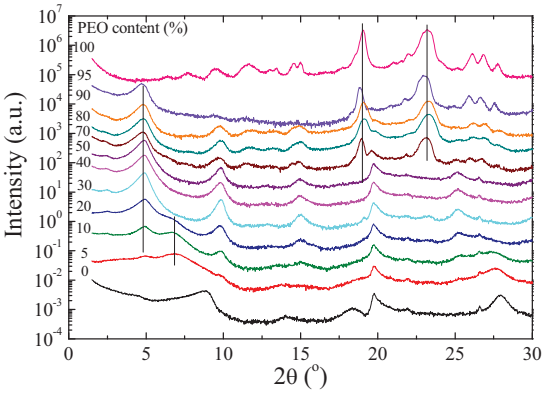

Figure 1: X-ray diffraction spectra of PEO/ Na^+MMT nanocomposites

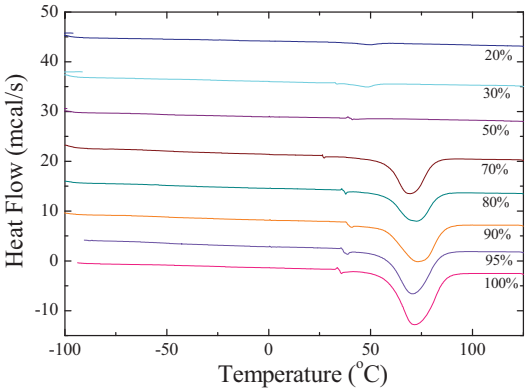

Figure 2: Non-isothermal DSC scan for PEO and for various nanohybrids

Figure 1 shows the X-ray diffraction patterns for the pure components and the nanohybrids.[2] The pure Na^+MMT shows a main (001) diffraction peak at 2θ=8.8°, which corresponds to an interlayer spacing of 1.0 nm. As the PEO concentration increases, the Na^+MMT diffraction peak disappears and two other peaks emerge at 6.8° and 4.8° that correspond to interlayer distances of 1.30 and 1.85 nm and whose relative intensities depend on the PEO content. At concentrations up to 20 wt%, the PEO chains within the galleries form either a single- or a double-layer structure of disordered liquid-like chains. Further increase of the PEO concentration reveals only double-layers of intercalated PEO chains. Moreover, for PEO

content below 70 wt% no peaks are observed that can be assigned to the crystalline structure of PEO.

Indeed DSC measurements (Figure 2) on these hybrids[3] reveal that the PEO chains remain amorphous in agreement with the XRD data. It is only for PEO concentrations higher than 70 wt% that two peaks at 18.9° and 23.2° emerge, which agree with the diffraction peaks of bulk PEO due to its monoclinic crystal structure (with a unit cell parameter of 1.93 nm along the helix axis). This indicates crystallization of the excess polymer outside the completely full galleries.

Polarized Optical Microscopy images were recorded for pure PEO and nanohybrids with low amount of additive (Figures 3 and 4).[4] The samples were placed in a heating stage, melted at 120°C for 5min and then cooled down to room temperature. The images reveal that even the presence of very small amount of the inorganic material causes an important decrease in the spherulite size. Additionally, the behavior at different crystallization temperatures were probed.

Time resolved SAXS and isothermal DSC measurements were performed following quenching from the melt as well as above the melting temperature, T_{melt}, to reveal the crystallization kinetics, illuminate the role of the inorganic material in the nucleation process and to record the lamellar formation and growth in the presence of the inorganic components.[4]

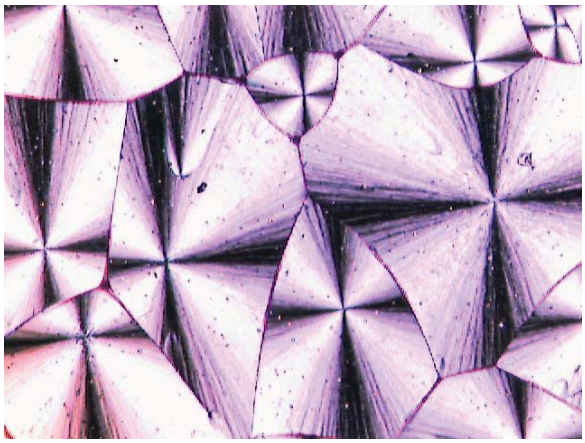

Figure 3: Polarized Optical Microscopy image of pure PEO at 25°C.

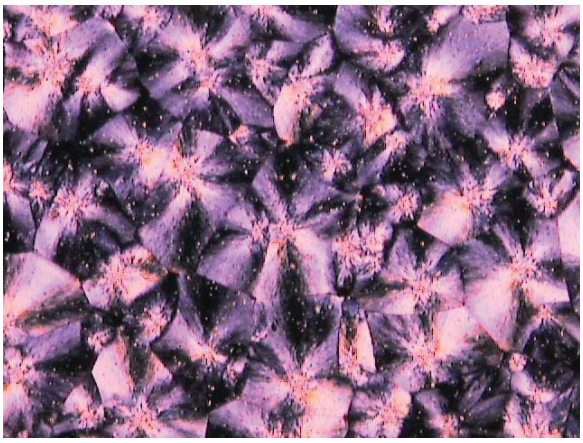

Figure 4: Polarized Optical Microscopy image of a nanohybrid with 96%PEO+4% Na^+MMT at 25°C

References

1. T. J. Pinnavaia and G. W. Beall, *Polymer-Clay Nanocomposites*, John Wiley & Sons, West Sussex, 2000. E. P. Giannelis, R. Krishnamoorti and E. Manias, *Adv. Polym. Sci.* **138**, 107-147 (1999). S. Sinha Ray and M. Okamoto, *Prog. Polym. Sci.* **28**, 1539-1641 (2003). S. C. Tjong, *Mat. Sci. and Eng. R* **53**, 73-197 (2006).
2. M. M. Elmahdy, K. Chrissopoulou, A. Afratis, G. Floudas and S. H. Anastasiadis, *Macromolecules* **39**, 5170-5173 (2006).
3. S. Fotiadou, K. Chrissopoulou, K. Andrikopoulos and S. H. Anastasiadis in preparation (2008).
4. K. Chrissopoulou, E. Pavlopoulou, H. Papananou, S. Fotiadou and S. H. Anastasiadis in preparation (2008)

Acknowledgements

Part of this research was sponsored by the Greek General Secretariat for Research and Technology (Programmes ΠΕΝΕΔ 03ΕΔ581 and ΠΑΒΕΤ 05ΡΑΒ96).

Oral 23

The use of aliphatic di/triamines (Jeffamines) as clay surface modifiers for the preparation of epoxy - clay Nanocomposites

P.I. Xidas[1,2], D. Gournis[2], K.S. Triantafyllidis[1]*

[1]*Department of Chemistry, Aristotle University of Thessaloniki, 54124 Thessaloniki, Greece,*
[2] *Department of Materials Science & Engineering, University of Ioannina, 45110 Ioannina, Greece*

Introduction

Polymer-layered silicate nanocomposites (PLSN) represent a relatively new class of organic - inorganic hybrid materials of interest for fundamental materials research studies, as well as commercial application. The PLSN materials exhibit improved properties in comparison to pristine polymers and conventional composites, due mainly to their unique phase morphology and the interfacial interactions between the polymer matrix and the highly dispersed inorganic silicate nanolayers[1, 2]. Organo-functionalization of the clay surface to render it hydrophobic and compatible with the polymer precursors is of high importance, especially in the case of non-polar polymers, for the effective mixing of the two phases and the preparation of nanocomposites with homogeneously distributed inorganic nanoparticles. However, overloading of the clay interlayer space (gallery) with alkylammoniun ions, which are the most commonly used organo-modifiers, can inhibit the direct interaction between the polymer chains and the silicate surface and induce plasticizing effects in the final polymer nanocomposite. Previous studies[3, 4] have shown that highly intercalated clay – epoxy polymer nanocomposites can be formed by the use of homostructured mixed inorganic/organic cation exchanged forms of montmorillonite or fluorohectorite smectite clays. In these mixed-ion homostructures both the organic onium ions and the inorganic exchange ions co-occupy the gallery surfaces of the clay, thereby dramatically reducing the amount of organic modifier needed to access the galleries for nanocomposite formation. In addition, the clay modifier used were protonated primary α, ω – diamines, which can also be used as curing agents for glassy or rubbery epoxy polymers and nanocomposites. In a more recent study[5], we have further investigated the potential use of triamines (Jeffamines) as clay modifiers for the preparation of epoxy – clay nanocomposites. In this study, we present a comparison between various di/triamines (Jeffamines) with different size and molecular weight as clay modifiers for the preparation of glassy epoxy – clay nanocomposites, emphasizing on relatively small triamines (T-403) and partially-exchanged large triamines (T-5000).

Experimental

The epoxy resin used was a diglycidyl ether of bisphenol A, commercially known as Epon 826 (Hexion Inc.). The curing agent for the preparation of glassy epoxy polymers was a polyoxypropylene diamine D-230 (Jeffamine, Huntsman Inc.) with relatively low MW=230. The inorganic parent clay was a Na^+-PGW (Montmorillonite) kindly provided by Nanocor Inc. The homoionic organic clays and the mixed-ion inorganic/organic clays were prepared by ion exchange of the inorganic clay with the desired amount of protonated diamines (D-400, D-2000) or triamines (T-403, T-5000), also provided by Huntsman Inc. In the case of the mixed-ion clays the concentration of onium ions in the reaction mixture was adjusted to achieve the desired degree of protons exchange on the clay surface, while for the homoionic organic clays a small excess of onium ions to that required for 100% ion-exchange of protons was added in the solution. The pristine glassy epoxy polymer was synthesized by mixing of EPON 826 prepolymer with the curing agent diamine D-230 followed by appropriate outgassing and curing at 75^0C for 3h and 125^0C for another 3h in N_2 atmosphere. The epoxy-clay nanocomposites containing 3 wt.% clay (on silicate basis) were prepared by pre-mixing of the clay with epoxy precursors at 60^oC for 1h followed by the addition of curing agent and subsequent curing under conditions similar to those for the pristine epoxy polymer.

Results and Discussion

Homoionic organic clays exchanged with long chain diamines (D-2000) and triamines (T-5000) resulted in exfoliated/partially intercalated clay – epoxy nanocomposites as indicated from the XRD patterns of the respective nanocomposite samples in Fig. 1. When smaller chain amines were used as clay modifiers the resulting nanocomposite structure depended on the type of Jeffamine used; the diamine D-400 modified clay resulted in intercalated nanocomposite while the triamine T-403 modified clay induced an almost exfoliated structure, as it can be revealed from the respective XRD patterns. The mixed-ion organic/inorganic clay with 35% exchange of protons with D-2000 and T-5000 onium ions resulted in an intercalated nanocomposite structure although long chain modifiers have been used. Apparently, the lower modifier's concentration wasn't sufficient for adequate exfoliation of the clay layers within the polymer matrix. However, the Dynamic Mechanical Analysis tests (Fig. 2) showed a remarkable improvement of storage modulus not only for the exfoliated but for the intercalated nanocomposites as well. The intercalated structures could be also more favourable since they did not induce any significant decrease of the glass transition temperature (T_g) due to plastisizing effects. Thermal stability of the epoxy polymer was not sacrificed with the addition of the clay fillers, irrespective of the degree of nanolayer exfoliation (TGA results, not shown).

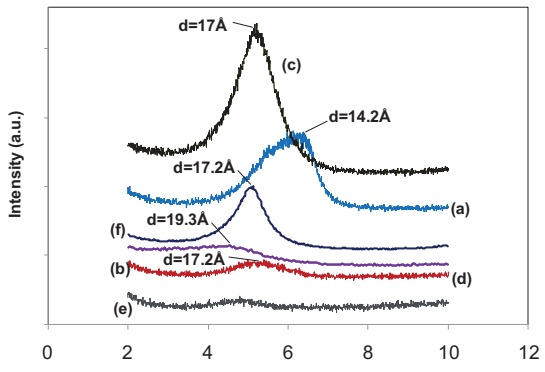

Figure 1. XRD patterns of epoxy–clay nanocomposites with 3 wt.% clay loading (silicate basis). The clay was modified by: (a) D-400 (100% exch.), (b) T-403 (100% exch.), (c) D-2000 (35% exch.), (d) D-2000 (100% exch.), (e) T-5000 (100% exch.), (f) T-5000 (35% exch.)

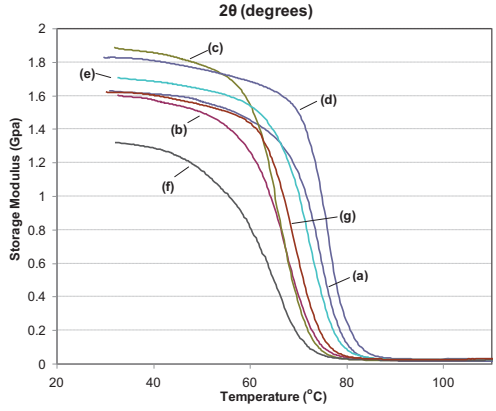

Figure 2. Storage modulus versus temperature curves for (a) the pristine glassy epoxy polymer, and nanocomposites prepared by 3 wt.% clay filler that has been modified with: (a) D-400 (100% exch.), (b) T-403 (100% exch.), (c) D-2000 (35% exch.), (d) D-2000 (100% exch.), (e) T-5000 (100% exch.), (f) T-5000 (35% exch.)

Acknowledgements. *Co-funding of this research by EU and the Greek Ministry of Development-GSRT through the program EPAN/PENED 2003 is gratefully acknowledged.*

References

1. Vaia R.A. & Giannelis E.P. *MRS BULLETIN* (2001).
2. Pinnavaia T.J. & Beall T.W.(eds) Polymer-Clay Nanocomposites. *Wiley Series in Polymer Science* (2000).
3. Triantafillidis, C.S., LeBaron, P.C. & Pinnavaia, T. *Journal of Solid State Chemistry* **167**, 354-362 (2002).
4. Triantafillidis, C.S., LeBaron, P.C. & Pinnavaia, T. *Chem. Mater.* **14**, 4088-4095 (2002).
5. Triantafyllidis, K., Xidas, P. & Pinnavaia, T. *Macromolecular Symposia* (2007) (in print).

Invited Lecture 9

Tailoring the Physical Properties of Nanocomposite Materials – Why Structure Matters

Michael R. Bockstaller

Department of Materials Science and Engineering, Carnegie Mellon University, Pittsburgh, PA 15213

Current interest in polymer/nanoparticle composites is driven by two major motivations: from a fundamental perspective, polymer/particle mixtures represent fascinating model systems to study the structure formation in soft/hard heterogeneous materials in which subtle changes of entropic or enthalpic interactions can result in dramatic changes of material morphologies and properties. From a more application-oriented point-of-view, polymer composites have shown to exhibit intriguing optical and mechanical properties that arise from the combination of the particular properties of inorganic nanomaterials with the processability of the polymer host. New opportunities for controlling the properties of polymer/particle composites arise from emerging synthetic techniques that facilitate precise control of the architecture and composition of polymer-coated particle additives as well as the use of microphase separated polymer templates to control the distribution of filler particles over multiple length scales.
This presentation will review our research efforts in designing the structure and properties of polymer nanocomposites. In a first part, the effect of polymer grafts on the optical properties of nanoparticle additives will be discussed and it will be demonstrated that precise control of the composition of polymer-coated particle fillers that is afforded by the novel ARGET-ATRP technique (ARGET-ATRP = activators re-generated by electron transfer for atom transfer radical polymerization) presents opportunities to reduce the scattering strength of particle fillers by several orders of magnitude as illustrated in Figure 1.

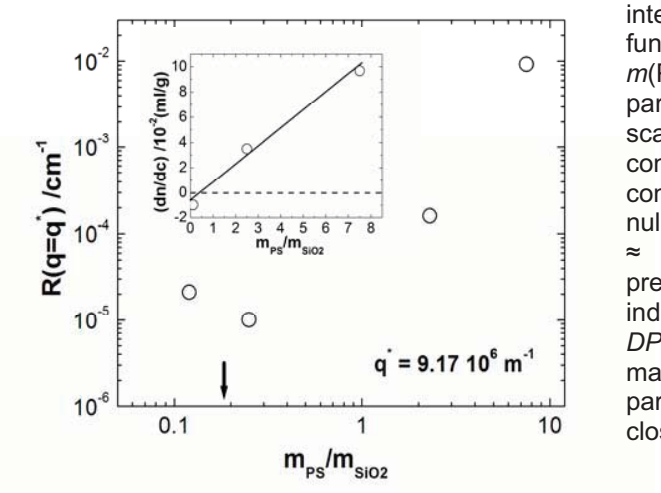

Figure 1. Plot of the total scattering intensity $R(q)$ at q = 9.16 × 10^6 m^{-1} as function of the particle composition m(PS)/m(SiO_2) for a series of PS@SiO_2 particle samples. The reduction of forward scattering at m(PS)/m(SiO_2) = 0.22 confirms the approximate index-matching condition. The arrow indicates theoretical null-scattering composition m(PS)/m(SiO_2) ≈ 0.19 based on effective medium prediction. The insert shows the refractive index increment for particle samples *DP*10, *DP*150 and *DP*760 confirming that index-matching (*i.e.* d*n*/d*c* = 0) is expected for particle compositions m(PS)/m(SiO_2) ≈ 0.2, close to the theoretical value.

In a second part, the structure formation of block copolymer/nanoparticle blends will be discussed with emphasis on the effect of copolymer architecture on the miscibility of particle additives as well as the equilibrium structure formation. By systematic variation

of the block connectivity encompassing linear di- and triblock as well as mikto-arm topologies ‘chain ends’ will be shown to be critical for facilitating the compatibilization of particle additives. Control of the block-selective polydispersity (as afforded by ARGET-ATRP) will be shown to be an efficient means to enhance the compatibility of particle additives. The highly asymmetric morphologies that are characteristic for polydisperse block copolymers will be shown to be ideal candidate systems for the design of novel super-transparent composite materials.
Whereas the study of the equilibrium microstructure formation process contributes important insight into the physics of self-organization of heterogeneous materials, the ultimate macroscopic properties of nanocomposites will be related to the defect and grain boundary formation on the microscopic scale. In a third part the effect of particle fillers on the structure evolution in block copolymer/particle bends on a microscopic level will be discussed with focus on grain size distribution as well as type and frequency of grain boundaries that are formed in quiescent organized block copolymers. The ‘orientation distribution function (ODF)’ – a concept commonly employed to characterize the grain structure in metal or ceramic materials – will be introduced as a powerful tool to capture anisotropy and microstructure evolution in block copolymer materials. It will be shown that particle additives exert a wide range of implications on the ordering of block copolymer materials depending on the compatibility of the particle filler. In particular, compatible filler particles are found to stabilize high-energy grain boundary structures (such as asymmetric tilt grain boundaries, see Figure 2) thus resulting in more disordered morphologies and reduced average grain sizes.

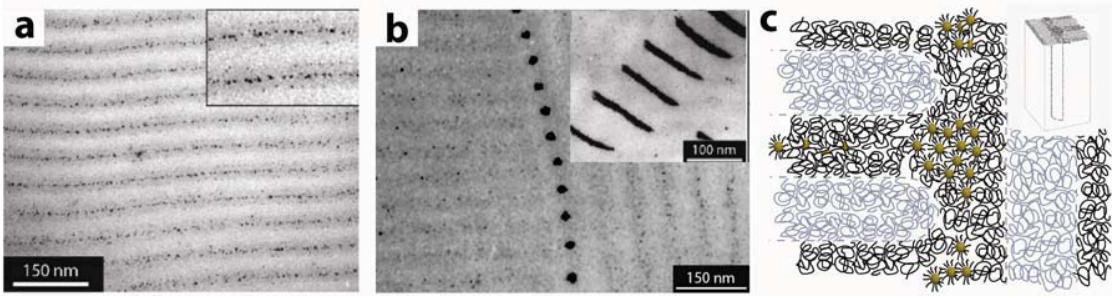

Figure 2. Bright-field electron micrograph of the unstained poly(styrene-b-ethylene propylene)/poly(styrene)-coated gold nanocrystals microstructure. Panel a: lamellar equilibrium microstructure revealing particles located at center of the PS domains. Panel b: Cross-section of an individual T-junction grain boundary structure. Nanocrystals aggregate in the T-junction area that is constituted of the PS domain. Inset shows a cross-sectional view of the aggregate structure after sectioning in off-normal direction to the boundary. Panel c: Schematic of the T-junction GB shown in panel b. Inset shows schematic of string-like particle aggregate.

References

1. Bombalski, L.; Hongchen, D.; Listak, J.; Matyjaszewski, K.; Bockstaller, M. R. *Null-Scattering Hybrid Particles Using Controlled Radical Polymerization.* Advanced Materials, 2007. **19**: p. 4486-4490.
2. Bockstaller, M.R.; Mickievitch, R.; Thomas, E.L. *Block copolymer nanocomposites: Perspectives for tailored functional materials.* Advanced Materials, 2005. **17**(11): p. 1331-1349.
3. Listak, J.; Bockstaller, M.R. Stabilization of grain boundary morphologies in lamellar block copolymer/nanoparticle blends. Macromolecules, 2006. **39**(17): p. 5820-5825.

Oral 24

Synthesis and selective segregation of Fe_3O_4 nanoparticles inside of the poly-2vinylpyridine domain of poly(styrene-b-2vinylpyridine)

Andriy Horechyy[1], Nikolaos Zafeiropoulos[1,2], C. Tsitsilianis[3] and Manfred Stamm[1]

[1] *Leibniz-Institut für Polymerforschung Dresden e.V., Hohe Strasse 6, 01069 Dresden, Germany*
[2] *University of Ioannina, Ioannina 45110, Greece*
[3] *University of Patras, Patras 26504, Greece*

Block copolymers (BCP) acting as a template for spatial arrangement with different types of nanoparticles (NP), such as metal, metal oxides, semiconductors, quantum dots, are an attractive system with potential application in high density data storage, optoelectronic materials, sensor devices.[1] The Self-assembling aspect of BCPs offers a simple and cost effective way to create periodic and well ordered structures in the nanometer scale, whilst the additional selective incorporation of specific NPs into one of the BCP phases leads to the formation of polymer matrix with discrete targeting properties.[2]
Different methods have been applied in order to achieve specific arrangement of NP inside of one of the BCP domains, e.g. “in situ” synthesis via complex decomposition [3,4,5], micelle-mediated NP synthesis and deposition [6], nanoparticles surface modification by specific ligands [7,8] or by polymer brush approach.[9,10]
Nevertheless, it is still a tremendous challenge to generate well ordered nanostructured templates with precise and uniform nanoparticle distribution within one of the co-polymer blocks under reproducible condditions.
In the present work we report a convenient route for Fe_3O_4 magnetic nanoparticles (MNPs) introduction into the poly-2vinylpyridine (P2VP) domain of a linear diblock poly(styrene-b-2vinylpyridine) (PS-*b*-P2VP) matrix. The key advantage of the presented method is that as-synthesized NPs with no further need for any additional processing, e.g. surface treatment,s ligand exchange steps, polymer brush grafting and so on, can be used yielding excellent results. Well ordered nanoparticles arrays are formed inside of the P2VP domain of BCP matrix either with lamellae or cylindrical morphology.
Iron oxide MNPs synthesis was performed by a modified method first described by S.Sun *et al*. [11] This process proceeds with thermal decomposition of iron(III) acetylacetoneate in the presence of polyalcohols as reducing agents and leads to the formation of particles with narrow size distribution. The method also allows in parallel for the possibility to tune the nanoparticle size in the range of 4-15 nm by adjusting the reactants concentration and/or surfactant/precursor ratio. [12] Instead of the commonly used oleic acid and oleyl amine as surfactants [11,12] in the synthesis, tri-n-octylphosphine oxide (TOPO) or a combination of oleyl omine and (TOPO) were applied.

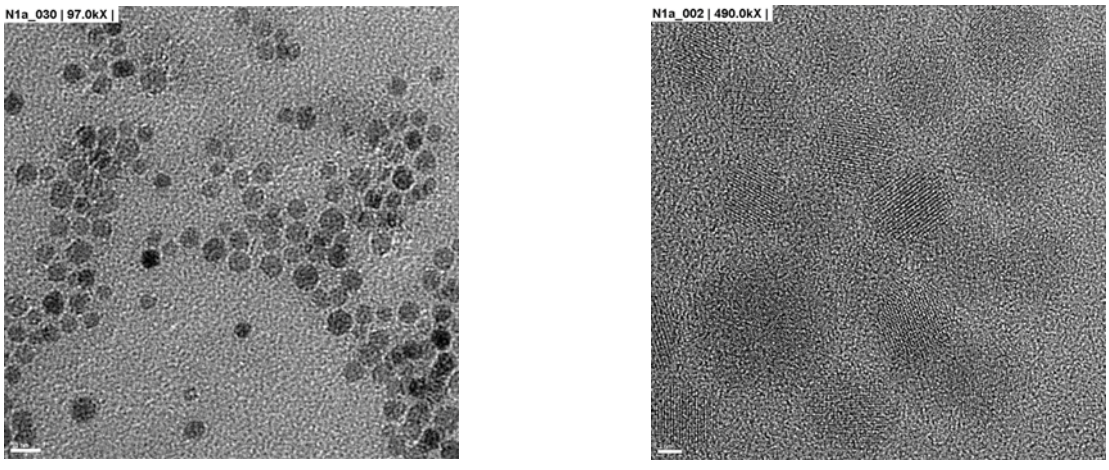

a **b**

Fig.1 TEM (a) and HRTEM (b) images of the MNP prepared in the presence of TOPO and oleyl amine. Scale bar is 10 nm for image **a** and 2 nm for image **b**

The crystal structure of Fe_3O_4 was verified by XRD analysis. The particle diameter and size distribution were estimated by transition electron microscopy giving an average particles diameter of about 6 nm.
Different compositions of PS-b-P2VP (BCP1, Mn=100 000, 50 000-b-50000 PDI=1,03) with MNP were prepared by dissolving / dispersing of certain amounts of polymer and nanoparticles in THF giving the concentration range of polymer 0,5-5,0% (w/w against to the solvent weight) and concentration of nanoparticles 0,1-10% (w/w with respect to the polymer weight). Samples for AFM imaging were prepared by dip-coating on cleaned Si-wafers and exposed to saturated solvent vapour.

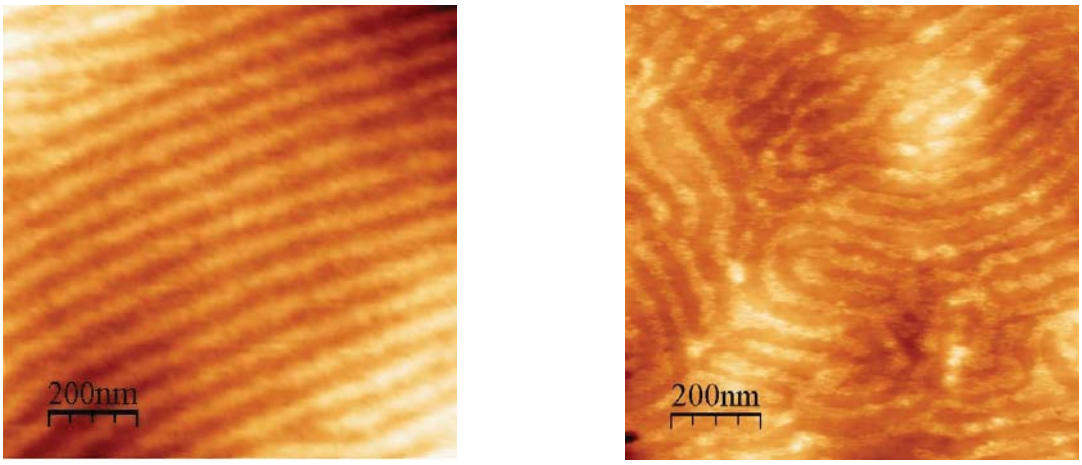

Fig.2 AFM topographical images of pure BCP1 (**a**) and BCP1-MNP (10%) (**b**) thin films with lamellae morphology after vapour annealing. The z-scale is 10 nm with 1μm x 1 μm scan size

As is clearly visible (Fig.2) the nanoparticles are ordered within a single domain of PS-P2VP matrix forming array-like structures. Cross-sectional AFM and TEM investigations of bulk samples are in progress in order to see influence of interfaces on the structure and morphology of composites.
Alternatively, PS-b-P2VP (BCP2, Mn=77 000, 56 000-b-21 000, PDI=1,06, Polymer Source, Inc) was used to prepare BCP2-MNP composites with a purpose to obtain cylindrically structured templates. Preliminary AFM investigation show that MNP occupy P2VP domains (cylinders) providing a possibility of well ordered hexagonally-packed structure formation.

References

1. Hamley, I.W.,*Nanotechnology* **2003**, 14, R39-R54.
2. Förster, S., Antonietti, M. *Adv. Mater.* **1998**, 10, 195-217.
3. Chan, Y. N. C.; Schrock, R. R.; Cohen, R. E. *Chem. Mater.* **1992**, *4*, 24-27.
4. Chan, Y. N. C.; Craig, G. S. W.; Schrock, R. R.; Cohen, R. E. *Chem. Mater.* **1992**, *4*, 885-8945.
5. Abes, J. I.; Cohen, R. E.; Ross, C. A. *Chem. Mater.* **2003**, *15*, 1125-1131.
6. Krishnamoorthy, S., Pugin, R., Brugger, J., Heinzelmann, H., Hinderling, C., *Adv. Funct. Mater.* **2006**, *16*, 1469-1475.
7. Lin, Y.; Boker, A.; He, J. B.; Sill, K.; Xiang, H. Q.; Abetz, C.; Li, X. F.; Wang, J.; Emrick, T.; Long, S.; Wang, Q.; Balazs, A.; Russell, T. P. *Nature* **2005**, *434*, 55-59.
8. Zou, S.; Hong, R.; Emrick, T.; Walker, G. C. *Langmuir* **2007**, *23*, 1612-1614.
9. Julia J. Chiu, Bumjoon J. Kim, Edward J. Kramer, and David J. Pine, *J. Am. Chem. Soc* **2005**, 127, 5036-5037.
10. Garcia, I., Tercjak, A., Zafeiropoulos, N.E., Stamm, M., Mondragon, I. *J. Pol. Sci.,* Part A: Polymer Chemistry **2007**, 45, 4744-4750.
11. S.H. Sun, H. Zeng, *J. Am. Chem. Soc*. **2002**, 124, 8204-8205.
12. J. Xie, S. Peng, N. Brower, N. Pourmand, S. X. Wang and S. H. Sun, *Pure Appl. Chem.* **2006**, 78, 1003–1014.

Oral 25

Impregnation of pH-Responsive Polymeric Matrices with Metal Nanoparticles*

E. Pavlopoulou[1,2], V. Katsamanis[1,3], K. Christodoulakis[1,2], G. Portale[4], W. Bras[4], M. Vamvakaki[1,2] and S.H.Anastasiadis[1,5]

[1] *Foundation for Research and Technology-Hellas, I.E.S.L., Heraklion, Crete, Greece*
[2] *Department of Materials Science and Technology, University of Crete, Heraklion, Crete, Greece*
[3] *Department of Physics, University of Crete, Heraklion, Crete, Greece*
[4] *DUBBLE CRG/European Synchrotron Radiation Facility, Grenoble, France*
[5] *Department of Chemical Engineering, Aristotle University of Thessaloniki, Thessaloniki, Greece*

Metal nanoparticles display unique desirable properties and characteristics in comparison to bulk materials and, consequently, find applications in many areas of modern technology. In particular, the enormous surface-to-volume ratio of nanoscale particles (about 100-3000 m^2/cm^3) is a promising feature for their use as catalysts. In the past decade, the use of nanostructured polymeric matrices for nanoparticle synthesis and stabilization has received considerable attention, and a number of polymeric matrices have been shown to provide stabilization and control of particle growth. Among them, pH-sensitive materials (block copolymer micelles and microgels) is a very promising category of responsive materials, since they can be used as nanoscopic reaction vessels for the in-situ growth of inorganic nanocrystals in water, resulting in hybrid nanocomposite materials.

In our research two types of polymeric matrices have been used for the growth of colloidal Pt nanoparticles: (1) Polymeric micelles formed by the pH-driven self-assembly of amphiphilic poly(hexa(ethylene glycol) methacrylate)-*b*-poly(2-(diethylamino)ethyl methacrylate) diblock copolymers, PHEGMA-*b*-PDEA; at low pH the copolymer is in its "unimer" state, while an increase of the pH results in the formation of micelles. (2) pH-sensitive PDEA-microgels, which exhibit reversible swelling properties in water by adjusting the solution pH. At low pH the microgel particles are swollen, while an increase of the pH leads to hydrophobic latex particles. Metal nanoparticles were synthesized within both the micellar cores of the diblock copolymers and the microgels by the incorporation of the metal precursor, i.e., by the addition of H_2PtCl_6 and the subsequent metal reduction, for various metal-to-polymer ratios.[1-3] Herein we report the structural study of aqueous solutions of these systems by Small Angle X-ray Scattering (SAXS) during the three steps of the metal nanoparticle synthesis: the original polymer dispersions in water, the metal – loaded polymer matrices and the metal nanoparticle-containing polymers after reduction.

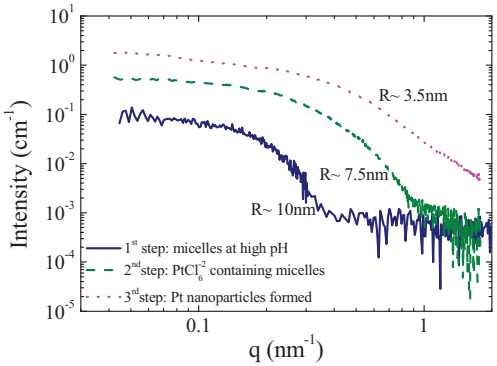

Figure 1. The SAXS patterns of the micellar matrices for the three synthetic steps.

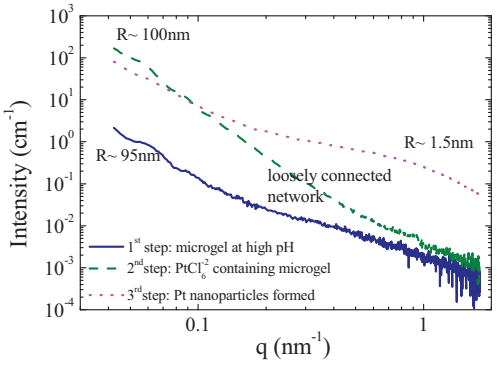

Figure 2. The SAXS patterns of the microgel matrices for the three synthetic steps.

SAXS measurements have been carried out at the Dutch-Belgian Beamline (DUBBLE) at the European Synchrotron Radiation Facility (ESRF) in Grenoble, France, covering a very wide scattering vector range $0.04 < q < 4$ nm^{-1}. The scattered intensity was corrected for background and transmission whereas measurement of a standard sample (Lupolen) was utilized for intensity normalization. For dilute systems like those under study, the q-dependence of the SAXS scattered intensity corresponds directly to the form factor of the scatterers and, thus, information about the shape, the size and the number density for both the metal loading and the polymeric matrices can be obtained simultaneously. The complexity of the final system requires the characterization of all three steps, each one providing information for a different phase.

Figure 1 presents the SAXS patterns that correspond to the three steps of the Pt nanoparticle formation within the PHEGMA-*b*-PDEA micelles for metal-to-polymer ratio 1/2. In the first step, the form factor acquired corresponds to a spherical structure with radius R~10nm, while in the second step the radius decreases to 7.5nm, indicating that the metal loading is located only in the micellar core. The form factor of the reduced sample exhibits higher intensity and is shifted towards higher q values, indicating that metal nanoparticles with R ~ 3.5nm are formed.

Figure 2 presents the respective SAXS curves for an aqueous solution of pH-sensitive PDEA-microgels at high pH. The complex form factor of the spherical microgels possessing a loose network interior structure is acquired for the first sample, while in the presence of H_2PtCl_6 the scattered intensity increases due to the strong contrast induced by the metal loading of the matrix. The radius increases slightly due to electrostatic interactions. The scattering curve obtained for the reduced sample contains information on both the polymeric matrix and the Pt nanoparticles that were formed.

We investigate the effect of the metal-to-polymer loading on the nanoparticle size in order to use it as a control parameter for tailoring the size and maybe the number density of the nanoparticles during synthesis. We anticipate that due to the spatial constraints one nanoparticle is formed within each micellar structure, while a higher number of nanoparticles are incorporated within the polymeric microgel particles; however, the analysis of the forward scattered intensity is expected to provide direct evidence for this.

References

1. Vamvakaki, et al., *Faraday Discuss.* **2005,** *128,* 129.
2. Bronstein, et al., *Langmuir* **2005,** *21,* 9747.
3. Palioura, D.; Armes, S. P.; Anastasiadis, S. H.; Vamvakaki, M. *Langmuir* **2007,** *23,* 5761.

* Acknowledgments: Part of this research was sponsored by the Greek General Secretariat for Research and Technology (ΠΕΝΕΔ 2003 programme 03ΕΔ581)

Oral 26

Complexation of anionic polyelectrolytes with Cu^{2+} ions and/or cationic surfactants : Design of the polymer architecture to control the behavior in aqueous solution

Zacharoula Iatridi,[1] Eudokia K. Oikonomou,[1,2] Charalambos Daktyloudis[1], Georgios Bokias[1]

[1]*Department of Chemistry, University of Patras, GR-26504 Patras, Greece*
[2]*Foundation of Research and Technology Hellas, Institute of Chemical Engineering and High-Temperature Chemical Processes (ICE/HT FORTH), P.O. Box 1414, GR-26504 Patras, Greece*

Water-soluble polymers may be considered as “intelligent” soft materials, able to respond to external stimuli or presenting multifunctional properties in aqueous solution, as the water-soluble group may be chosen among a large variety of functional groups. For instance, the carboxylate anions in the case of neutralized poly(acrylic acid) (PAA) or sulphonate groups in the case of poly(sodium styrene sulphonate) (PSSNa) make these polymers functional towards multivalent metal ions through coordination or electrostatic interactions, respectively, or towards cationic surfactants, like N,N,N,N-dodecyltrimethylammonium chloride (DTAC), through the synergistic action of electrostatic and hydrophobic interactions. Moreover, as a result of the weak acidic character of PAA, pH-sensitive characteristics are introduced in these polymer-metal ion or polymer-surfactant complexes. In addition, other properties may also be introduced, for instance using the thermosensitive polymer poly(N-isopropylacrylamide), PNIPAM provides such systems with temperature-sensitive (–responsive) properties.

In this presentation some examples of our efforts to tune or combine such stimuli-sensitive properties or functionalities by designing adequate copolymers will be given. To this purpose, two copolymer architectures are mainly used : either simple random copolymers or comb-like products prepared by appropriate grafting reactions.

A usual problem when multivalent metal ions, like Cu^{2+} ions form complexes with polymers containing carboxylate groups, like acrylic acid (AA) or maleic acid (MAc), is the low solubility of the polymer-metal complexes formed, leading finally to phase separation.

As a first approach to avoid this problem, random copolymers of these monomers with other, more or less hydrophilic, monomers were envisaged. Thus, it is found that phase separation is indeed inhibited when copolymers of MAc with sodium styrene sulphonate, SSNa, are used. Polymer-metal ion complexation, nevertheless, did occur using such copolymers as evidenced by physicochemical studies in aqueous solution, like UV-vis spectroscopy and dilute solution viscometry. An interesting finding here was that the electrostatic binding of Cu^{2+} ions by the sulphonate groups is, in fact, competing with the complexation of these ions with the carboxylate groups of the copolymers.

On the other hand, when hydrophobic comonomers, like vinyl acetate (VAc) or ethylene (Eth) are copolymerized with MAc, phase separation apparently can not be avoided in dilute solution. However, when the copolymer P(Eth-co-MAc) was used in slightly more concentrated solution the formation of stiff gels was observed prior to phase separation. Gelation was found to be time-dependent, while the gelation window depends on polymer concentration and the method of the introduction of Cu^{2+} ions, neutralization of $Cu(OH)_2$ or mixing with $CuSO_4$.

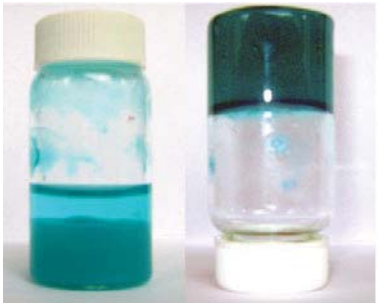

Figure 1. Phase separation (left) or gelation (right) observed upon the complexation of Cu^{2+} ions with P(Eth-co-MAc) copolymers, depending on the concentration of Cu^{2+} ions.

The second approach to inhibit phase separation upon polymer-metal complexation was based on the use of comb-like copolymers, PAA-g-PDMAM, consisted of a neutralized PAA backbone and hydrophilic poly(N,N-dimethylacrylamide), PDMAM, side chains. It is found that when the PDMAM content is high enough, the polymer-metal complex formed is again water-soluble. The viscometric, ζ-potential and dynamic light scattering studies give sufficient evidence that now hybrid polymer-metal nanoparticles are stabilized in aqueous solution. The polymer-Cu^{2+} complex form the compact core of the nanoparticle, stabilized in water by a hydrophilic corona formed by the pendent hydrophilic PDMAM side chains.

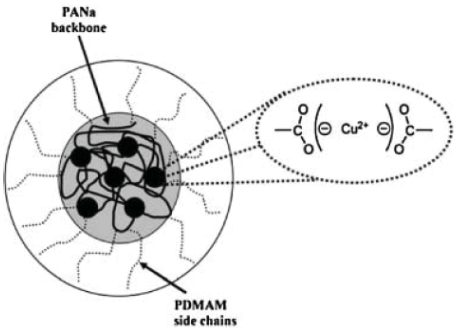

Figure 2. Schematic depiction of the water-soluble nanoparticles formed upon complexation of Cu^{2+} ions with the comb-like PAA-g-PDMAM copolymers

The same approach, namely using the comb-like PAA-g-PDMAM copolymers, was applied to control the complexation of these negatively charged polymers with the cationic surfactant DTAC. As a result, of the hydrophobic nature of the polymer-surfactant complex formed between linear polyelectrolytes and oppositely charged surfactants, phase separation is an often complication in this case also. However, using the aforementioned graft copolymers, phase separation can indeed be inhibited due to the formation of similar to Figure 2 nanostructures, where the PAA-DTAC complex consists now the insoluble core.

The achievement of water-solubility for both kinds of complexes using comb-like copolymers makes possible the study of ternary polymer-Cu^{2+}-DTAC systems, in order to get a closer look in the competition of the complexing species, Cu^{2+} and DTAC, for the same binding sites of the copolymer, namely carboxylate anions. Moreover, the ability of the hydrophobic polymer-surfactant complexes to host fluorescent probes like pyrene offers the possibility to control fluorescence through Cu^{2+}-binding, as these ions act as quenchers for pyrene. In addition, the different pH-sensitivity of PAA-Cu^{2+} complexes and PAA-DTAC complexes makes possible the pH-control of the pyrene fluorescence and the development of simple water-soluble “ON-OFF” fluorescent switches.

When the PDMAM side chains are replaced by the thermosensitive PNIPAM side chains, temperature-sensitivity is, in addition, introduced in the complexes formed between Cu^{2+} ions and/or DTAC with the comb-like PAA-g-PNIPAM copolymers. In these systems, the temperature effect is revealed as macroscopic phase separation upon heating the aqueous solution above 33^{o}C. However, phase separation can be restricted to a microscopic level if doubly grafted comb-like copolymers are used, i.e. copolymers containing both hydrophilic PDMAM and thermosensitive PNIPAM side chains.

Acknowledgments Financial support through the program PENED 2003, 03ED825, ‘Design and Development of new paints with controlled release of biocides for submarine applications’ co-financed by E.U.- European Social Fund (75%) and General Secretariat for Research and Technology (GSRT), Greece, is greatly acknowledged. Partial support from Chrotex S.A., Greece, is also acknowledged.

Invited Lecture 10

From chemical structure to physical properties of polymers via hierarchical modelling

Doros N.Theodorou
School of Chemical Engineering, National Technical University of Athens, 9 Heroon Polytechniou Street, Zografou Campus, 157 80 Athens, Greece

Predicting the physical properties of polymeric materials from their chemical constitution is highly desirable, but also very challenging, because of the extremely broad spectra of length and time scales governing their structure and molecular motion. This challenge can only be met through the development of hierarchical analysis and simulation strategies encompassing many interconnected levels, each level addressing phenomena over a specific window of time and length scales.

In this presentation we will discuss the fundamental underpinnings and example applications of new methods and algorithms for the hierarchical modelling of polymers.

We will start from connectivity-altering Monte Carlo methods, which have enabled full equilibration of long-chain polymer systems at all length scales. Recently, using these methods along with detailed, united-atom models, it has been possible to quantify how chain dimensions and packing in molten polyethylene are affected by short-chain branching.[1]

For polymers possessing bulky, inflexible groups, a successful strategy for equilibration is to first coarse-grain from a detailed representation employing many explicit atoms to one cast in terms of fewer multiatom interaction sites; equilibrate at the coarse-grained level; and finally reverse-map back to the atomistic level. Recently, atactic polystyrene melts of molar mass up to 200,000 g mol^{-1} have been simulated using this strategy.[2] Coarse-graining was based on Iterative Boltzmann Inversion of distribution functions obtained from atomistic simulations of oligomers. Equilibration at the coarse-grained level was accomplished using connectivity-altering Monte Carlo. Reverse mapping involved local Monte Carlo moves designed to respect the chirality and torsion angle distribution of the atomistic chains, along with molecular dynamics.

Well-equilibrated polystyrene configurations have served as starting points for predicting sorption equilibria of CO_2 in atactic polystyrene over a wide range of pressures and temperatures, above and below the glass temperature. For this purpose, molecular dynamics was combined with a void mapping/molecular exchange scheme that ensures efficient sampling of all cavities in the polymer by the sorbed molecules. The solubility was computed via a particle deletion (inverse Widom) algorithm,[3] which avoids molecular insertions. Predicted sorption isotherms and swelling effects are in very favourable agreement with experiment. A study of segmental dynamics at various CO_2 concentrations reveals devitrification at high penetrant activities.

Topological analysis of well-equilibrated long-chain melt configurations using the CReTA algorithm[4] yields estimates of the entanglement molar mass and of the entanglement tube diameter which agree with experimental plateau modulus measurements. Furthermore, it reduces atomistic configurations to entanglement networks that can serve as starting points for mesoscopic slip-link-based simulations of terminal relaxation and flow.

Structural relaxation in the glassy state presents a formidable challenge for molecular simulation, because of its extremely long characteristic times. We will outline a strategy, based on the energy landscape picture of glasses, to overcome this challenge. Relaxation is viewed as resulting from infrequent transitions between “basins” that surround local minima of the energy in configuration

space. The rate constants for such transitions are computed from an atomistic model of the glass, based on infrequent event theory. The evolution of the glassy system in the network of basins is tracked via analytical solution of a master equation for the probabilities of occupancy of the basins, the network being augmented "on the fly," as needed, based on a first passage criterion.[5] Through this "Dynamic Integration on a Markovian Web" (DIMW) strategy one can expand the time spans that can be simulated by many orders of magnitude relative to "brute-force" molecular dynamics. Application to glassy atactic polystyrene has yielded promising results for the characteristic frequencies and mechanisms of sub-glass relaxation transitions.

References

1. Ramos, J.; Peristeras, L.D.; Theodorou, D.N. "Monte Carlo Simulation of Short Chain Branched Polyolefins in the Molten State" *Macromolecules* **2007**, *40*, 9640-9650.
2. Spyriouni, T.; Tzoumanekas, C.; Theodorou, D.N.; Müller-Plathe, F.; Milano, G. "Coarse-grained and reverse-mapped united-atom simulations of long-chain atactic polystyrene melts: structure, thermodynamic properties, chain conformation, and entanglements" *Macromolecules* **2007**, *40*, 3876-3885.
3. Boulougouris, G.C.; Economou, I.G.; Theodorou, D.N. "Calculation of the chemical potential of chain molecules using the staged particle deletion scheme" *J. Chem. Phys*. **2001**, *115*, 8231-8237.
4. Tzoumanekas, C.; Theodorou, D.N. "Topological analysis of linear polymer melts: A statistical approach" *Macromolecules* **2006**, *39*, 4592-4603.
5. Boulougouris, G.C.; Theodorou, D.N. "Dynamical Integration of a Markovian Web: A first passage time approach" *J. Chem. Phys.* **2007**, 127, 084903.

Oral 27

A Poly(dimethylsiloxane) Quantum Mechanical Force-Field: Molecular Dynamics calculations for the prediction of physical properties

Konstantinos D. Papavasileiou[1], Vasilios E. Raptis[1, 2] and Vasilios S. Melissas[1]

[1]*Department of Chemistry, University of Ioannina, GR–451 10 Ioannina, Greece*
[2]*Department of Materials Science and Engineering, University of Ioannina, GR–451 10 Ioannina, Greece*

Expansion of the membrane based separation technology is leading to a growing interest in the study of polymer or other kinds of membrane materials. Molecular simulation methods based on reliable force-fields constitute an important aspect of such research. Quantum mechanical calculations provide substantial information for developing novel force-fields[1].

Poly(dimethylsiloxane), PDMS, a rubbery polymer with attractive permeance properties, is studied by means of molecular simulation methods, in order to determine its permeability capabilities to various gases of industrial interest. *Ab initio* calculations were performed so as to determine the geometry and energetics of hexamethyltrisiloxane, HMTS, an oligomer of PDMS. A systematic approach, already established in the study of other organosilicon polymers[2, 3], was employed.

Initially, the global minimum of the molecular energy was located, with respect to all degrees of freedom. Constrained optimizations were then performed, by varying the principal backbone dihedral and bonding angles, each time with respect to the remaining degrees of freedom. This strategy yielded a representative set of molecular conformations. All calculations were performed at the MP2(full)/cc-pVDZ [4] level of theory. Consecutively, force-field parameters were determined via a least squares fitting procedure, against the *ab initio* calculated energies.

Constrained geometry optimizations of the oligomers, via molecular mechanics, were performed to confirm reproduction of the molecule's quantum mechanical conformational behaviour. Excellent agreement between quantum mechanical and force-field optimized energetics and geometrical parameters was achieved for all HMTSh conformations under consideration.

Molecular dynamics simulation runs were subsequently performed, employing the newly developed force field, by means of the DL-POLY MD simulation package[5]. At first, bulk HMTSh systems were simulated at various temperatures and atmospheric pressure and MD predictions successfully compared with available thermophysical data. Then, simulations were extended to pure poly(dimethylsiloxane) systems in order to study polymer thermodynamic and transport properties. The trajectories obtained, were also employed in the prediction of normal alkane solubilities, S, at the dry limit, by means of the Widom insertion method. Finally, mixtures of PDMS with normal alkanes were studied, to determine diffusivity, D, of the latter through the polymer. Thus, permeability of gases, P = DS, was calculated, along with permselectivity $a_{A/B} = P_A/P_B$, i.e. the permeability of each gas A with respect to another gas B.

References:

1. (a) J.R. Maple, M.-J Hwang, T.P Stockfish, U. Dinur, M. Waldman, C. Ewig, A.T. Hagler, *J. Comp. Chem*. **1994**, *15*, 162, (b) M.-J. Hwang, T.P Stockfish, A.T. Hagler, *J. Am. Chem. Soc*. **1994**, *116*, 2515. (c) G.D. Smith, K.J. Bharadwaj, *Phys. Chem. B* **1999**, *103*, 3570, (d) G.D. Smith, R.L. Jaffe, D.Y. Yoon, *J. Phys. Chem*. **1993**, *97*, 12752. (d) G.D. Smith, W. Paul, *J. Phys. Chem. A* **1998**, *102*, 1200. (e) G.D. Smith, O. Borodin, D. Bedrov, *J. Phys. Chem. A* **1998**, *102*, 10318. (f) J.S. Smith, O. Borodin, G.D. Smith, *J. Phys. Chem. B* **2004**, *108*, 20340.
2. (a) V.E Raptis, I.G. Economou, D.N. Theodorou, J. Petrou, J.H. Petropoulos, *Macromolecules* **2004**, *37*, 1102, (b) A. Alentiev, I.G. Economou, E. Finkelshtein, J. Petrou, V. E. Raptis, M. Sanopoulou, S. Soloviev, N. Ushakov, Y. Yampolskii *Polymer*, **2004**, *45*, 6933, (c) I.G. Economou, V.E. Raptis, V. S. Melissas, D.N. Theodorou, J. Petrou, J.H. Petropoulos, *Fluid Phase Equilib*. **2005**, *228-229*, 15.
3. (a) V.E Raptis, V.S. Melissas, *J. Phys. Chem. B*. **2006**, *110*, 14929, (b) Z.A. Makrodimitri, V.E. Raptis, I.G. Economou, *J. Phys. Chem. B* **2006**, *110*, 16047.
4. (a) C. Møller, M.S. Plesset, *Phys. Rev*. **1934**, *46*, 618, (b) T.H. Dunning Jr., *J. Chem. Phys*. **1989**, *90*, 1007.
5. (a) http://www.ccp5.ac.uk/DL_POLY/ (b) W. Smith (Guest Editor), Molecular Simulation, **2006**, *32* 933.

Oral 28

Structure and Dynamics of Entangled Polystyrene Melts Through Hierarchical Multi-Scale Dynamic Simulations

Vagelis Harmandaris[1,2] and Kurt Kremer[1]

1. Max-Planck Institute for Polymer Research, Mainz, Germany

2. Department of Applied Mathematics, University of Crete, Greece

Results from a detailed study of polymer melts through a hierarchical methodology that combines atomistic and coarse-grained (CG) simulations are presented. As a test case we study polystyrene (PS). First a CG PS model is developed and tested against structural and dynamical properties of short PS oligomers, resulting from long detailed atomistic simulations [1-3]. A proper time mapping, based on mean-square displacement of short PS chains, allows for the quantitative prediction of polymer dynamics through the CG simulations. The overall speed-up factor of the CG dynamic simulations, turns out to be more than 3 orders of magnitude compared to detailed atomistic MD ones.

In a second stage, long entangled PS melts are studied with CG MD simulations [4]. Systems with molecular weight up to 50kDa are simulated and the polymer chain self-diffusion coefficient is calculated. With the proper time mapping, we present, for the first time, *quantitative* predictions of polymer chain diffusion using CG simulations *without any adjustable parameter*. The simulation data are in excellent agreement with experimental measurements. The CG simulation data are also mapped onto chain primitive paths (PP), through a recently developed topology analysis [5,6]. This allows us to calculate the entanglement molecular weight, the tube diameter, as well as the plateau modulus of the PS melts. All the results are compared to experimental data [4].

REFERENCES

1. V. Harmandaris, N. Adhikari, N. van der Vegt and K. Kremer, Macromolecules 39, 6708 (2006).

2. V. Harmandaris, D. Reith, N. van der Vegt and K. Kremer, Macrom. Chem. and Physics, 208, 2109 (2007).

3. V. Harmandaris, N. Adhikari, N. van der Vegt, K. Kremer, B. Mann, R. Voelkel, H. Weiss, C. Liew, Macromolecules, 40, 7026 (2007).

4. V. Harmandaris and K. Kremer, submitted.

5. V. Harmandaris and K. Kremer, manuscript in preparation.

6. R. Evereaers, S.K. Sukumaran, G.S. Grest, C. Svaneborg, A. Sivasubramanian, K. Kremer, Science, 303, 823 (2004).

Oral 29

Topological and Dynamical Mapping of Atomistic Simulation Data Onto the Tube Model for Entangled Polymer Melts

Pavlos S. Stephanou, Chunggi Baig, Georgia Tsolou and Vlasis G. Mavrantzas
Department of Chemical Engineering, University of Patras & FORTH-ICE/HT, Patras, GR26504 Greece
Martin Kröger
Polymer Physics, ETH Zürich, Department of Materials, Zürich, Switzerland

The notion of the primitive path (PP) is central in tube models underlying all reptation theories for the dynamics of entangled polymer melts proposed so far.[1] The primitive path is defined as the shortest path connecting the two ends of a (linear) chain having the same topology and developing under the same constraints as the chain itself;[1] it can be crudely visualized as the curvilinear axis of a mean field tube highlighting the part of the space spanned by the chain as it diffuses through the network formed by the entanglements with surrounding chains. Mathematically, it is specified by the average tube diameter *d*, the calculation of which has been the subject of extensive studies (experimental and theoretical) over the years. Then, the analysis in most reptation theories proceeds by specifying the function $\psi(s,t)$ giving the probability that a given segment *s* along the PP has remained within the initial tube (constructed at time t=0) after time *t*.

From the point of view of computer simulations, today there exist a number of methods for reducing an ensemble of atomistically detailed chains of entangled polymer melts to an ensemble of PPs.[2-5] Given such an ensemble of PPs through (e.g.) Kröger's Z1 code,[3,4] we present here a methodology which leads directly to the calculation of all linear viscoelastic (LVE) properties of entangled polymer melts. The method involves the following steps: (a) First, an estimate is obtained for the average tube diameter *d* or tube radius *a* in the entangled melt based either on the maximum displacement of PP points perpendicularly to the tube axis at short times or at the intersection of the curves in the plot of the mean-square displacement (msd) of chain segments (in a log-log plot) corresponding to the early anomalous diffusion in free space and the subsequent Rouse dynamics restricted by the tube constraints, with slope equal to ½ and ¼, respecively.[6] Knowing the value of *d* or *a*, the original tube around each PP is then constructed. (b) In a second step, we monitor the time displacement of PP points perpendicularly to the axis of the original PP and we check whether or not a segment *s* along the PP (*s* takes values between 0 and 1) has escaped the tube. This is based on the calculation of the shortest distance *x* from the axis of the original PP after time *t*: If $x>a$, this point has escaped the original tube (constructed at t=0) whereas if $x\le a$ it is still confined within the original tube. In fact, in the latter case, one has to be more careful since it should also be checked if the given point *s* has escaped from the tube laterally. This will have happened if the distance that the segment diffused up to time *t* is larger than the remaining distance from *s* to either end of the PP at time t=0. This is more probable to occur for points *s* close to the two ends of the PP but as time goes by such a possibility applies in general to all points *s*. By averaging over all PP in the system and over a large number of accumulated trajectories, such an analysis allows us to calculate the probability $\psi(s,t)$ that a segment *s* has remained in the original tube after time *t*. To improve statistics, we have made use of the trick of multiple time origins; we have also taken advantage of the symmetry of function $\psi(s,t)$ with respect to middle segment s=0.5, since $\psi(s,t)=\psi(1-s,t),\forall s\in[0,½],\forall t$, as the two chain ends are equivalent. (c) Having calculated the function $\psi(s,t)$, we can easily obtain next the function $\Psi(t)$ representing the unrelaxed portion of the tube through a simple integration over *s*, $\Psi(t)\equiv\int_0^1\psi(s,t)ds$. The function $\Psi(t)$ is directly related to the shear relaxation modulus $G(t)$ through $G(t)=G_N^0\Psi(t)$ [1], where G_N^0 denotes the plateau modulus. For the calculation of G_N^0, we have used the expression

$G_N^0 = \frac{4}{5}\frac{\rho RT}{M}\frac{\langle L\rangle}{\alpha_K}\left[1-\sqrt{\frac{\langle L^2\rangle}{\langle L\rangle^2}-1}\right]$, where α_K denotes the Kuhn length of the PP while the term in the brackets on the right-hand-side accounts for corrections due to contour length fluctuations (CLF). Having calculated $G(t)$ it is then a matter of simple algebraic calculations to obtain the rest of the LVE properties of the melt. For example, the zero-shear-rate viscosity η_0 is computed through $\eta_0 = \int_0^\infty dtG(t)$, the steady-state compliance J_e^0 through $J_e^0\eta_0^2 = \int_0^\infty dtG(t)t$, and the storage G' and loss G'' moduli through $G'(\omega) = \omega\int_0^\infty \sin(\omega t)G(t)dt$ and $G''(\omega) = \omega\int_0^\infty \cos(\omega t)G(t)dt$, respectively.

Results will be presented from calculations with such a methodology for two different polymers, cis-1,4-polybutadiene (PB) and polyethylene (PE), as a function of chain length, together with experimental data from rheological measurements. We will show how our predictions for the viscosity of two different chain length PE melts (C_{320} and C_{400}) as obtained from the present PP analysis at 175 ^oC, compare with measured rheological data.[7-9] We will also show how the computed G' and G'' moduli for two different cis-1,4-PB systems (with chain length equal to C_{320} and C_{400}, respectively) compare against experimentally measured spectra on similar chain-length PB samples. The simulations have been made at 450K and the computed spectra have been shifted to the experimental temperature using known shift factors reported in the literature for PE and PB.

In conclusion, we will present a new methodology that combines computer simulations with geometric methods to reduce atomistically details chains to PPs and then mapping onto the reptation model of polymer melts in order to calculate the LVE data of two different polymers: linear PE and cis-1,4-PB, including a thorough comparison against available experimental rheological data.

References

1. Doi M. and Edwards S. F., *The Theory of Polymer Dynamics*, Clarendon Press, Oxford, **1986**.
2. Everaers R., Sukumaran S. K., Grest G. S., Svaneborg C., Sivasubramanian A. and Kremer K., *Science*, **2004**, 303, 823.
3. Kröger M., *Comput. Phys. Commun*., **2005**, 168, 209.
4. Foteinopoulou K., Karagiannis N. Ch., Mavrantzas V. G. and Kröger M., *Macromolecules*, **2006**, 39, 4207.
5. Tsoumanekas C. and Theodorou D. N., *Macromolecules*, **2006**, 39, 4592.
6. Likhtman A. E. and McLeish T. C. B., *Macromolecules*, **2002**, 35, 6332.
7. Harmandaris V. A., Mavrantzas V. G., Theodorou D. N., Kroger M., Ramírez J., Öttinger H. C. and Vlassopoulos D., *Macromolecules*, **2003**, 36, 1376.
8. Pearson D. S., Fetters L. J., Graessley W. W., Ver Strate G. and Von Meerwall E., *Macromolecules*, **1994** 27, 711.
9. Pearson D. S., Ver Strate G., Von Meerwall E. and Schilling F. C., *Macromolecules*, **1987**, 20, 1113.

Oral 30

Molecular Dynamics Simulations of Diblock-Arm Star Copolymers

Anastassia N. Rissanou[1,3], Dimitris Vlassopoulos[1,2], Christos N. Likos[3]

[1]*FO.R.T.H., Institute of Electronic Structure and Laser, GR-71110 Heraklion, Crete, Greece.*
[2]*University of Crete, Department of Materials Science and Technology. GR-71003 Heraklion, Crete, Greece.*
[3]*Institut für Theoretische Physik II Weiche Materie, Heinrich-Heine-Universität, D40225 Düsseldorf, Germany.*

Amphiphilic star copolymers (stars with di-block arms, A-type and B-type) are interesting polymeric materials with a number of potential applications.
In this work, Molecular Dynamics simulations have been carried out in order to extract the effective interaction, in terms of a pair potential, between two star-polymers consist of di-block arms. In the simulation model employed, we represent attractive interactions (i.e., poor solvent conditions) with a Lennard-Jones potential acting between the same beads (*A)* of the inner blocks (n_1) while good solvent conditions are represented via a purely repulsive Lennard-Jones potential (truncated and shifted) acting between the same beads (*B)* of the outer blocks (n_2), as well as between beads of different blocks. For connected monomers along each star arm the attractive FENE-potential is added to the interaction.
The system we study first consists of two star polymers with (functionality) f = 5 and (number of monomer per arm) n = 100. Star arms comprise of two types of beads with equal lengths n_1=n_2=50 (*i.e.,* n_1/n_2=1), the inner beads realize poor solvent conditions while the outer beads are under good solvent conditions. This separation leads to the formation of a globule, consist by the internal monomers, which is surrounded by extended chains which are the external beads.

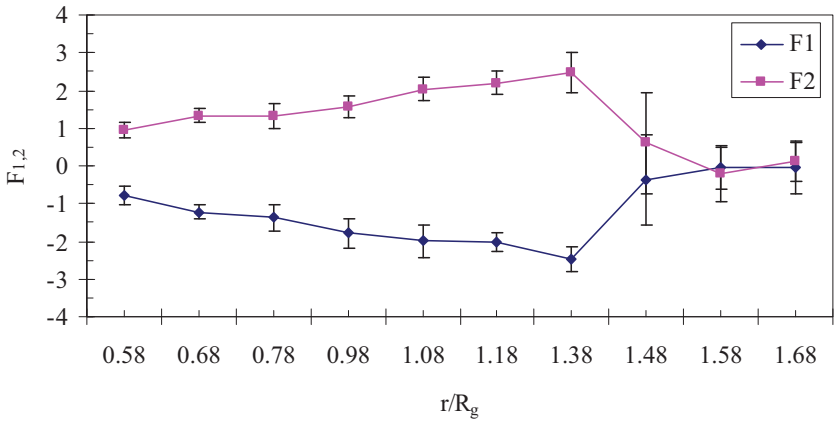

Figure 1: The effective force on each star center as a function of their distance for two stars with f=5 di-block arms of N=100 beads and n_1=n_2=50. The error bars were obtained by averaging over the results of 8 independent simulations.

Forces on the star centers are calculated as the statistical average over all monomers. The effective force on each star center as a function of their distance r in units of R_g (radius of gyration) is presented in Figure 1, where it is obvious that $\vec{F}_1 = -\vec{F}_2$ due to symmetry. Attraction dominates in forces for center to center distances up to $1.38R_g$, so force appears to be a decreasing function of the distance between the stars. This feature provides important information for the studied system which is an unstable system and is led to flocculation. Typical snapshots of two stars at distances

0.58 and *1.68* R_g respectively, are depicted in Figure 2, where flocculation is obvious at the small distance.

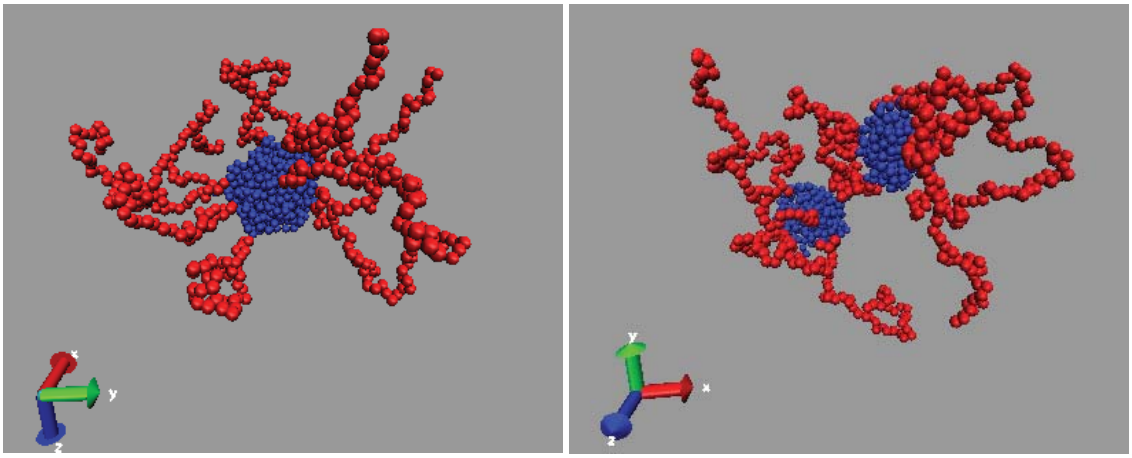

Figure 2: Configuration of two stars with f=5 di-block arms of n=100 beads and $n_1=n_2=50$. *The distance between the star centers are 0.58 and 1.68* R_g *in panels (a) and (b), respectively.*

A very substantial question which comes from the above results is: what is the critical number of arms which prevents flocculation? Another interesting issue could be the exploration of the critical ratio n_1/n_2, if exists, for the avoidance of flocculation. All these questions are currently under investigation.

Preliminary results for a much larger system: $f = 64$, $n = 100$, and $n_1/n_2=65/35$ show a completely different behavior of forces. The system is stable in this case, as observed in Figure 3 where, a snapshot of two stars at a distance equal to $1.06R_g$ is presented.

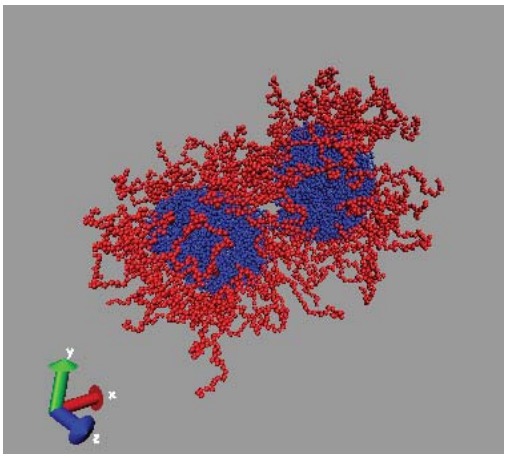

Figure 3: Configuration of two stars with f=64 di-block arms of n=100 beads and $n_1/n_2=65/35$, *at a distance between the star centers equal to* $1.06R_g$.

Oral 31

Atomistic Simulation of Poly(dimethylsiloxane) Permeability Properties to Gases and n- Alkanes

Zoi A. Makrodimitri and Ioannis G. Economou

Molecular Thermodynamics and Modeling of Materials Laboratory,
Institute of Physical Chemistry, National Center of Scientific Research "Demokritos",
GR – 153 10 Aghia Paraskevi Attikis, Greece
economou@chem.demokritos.gr

The accurate knowledge of the transport properties of polymeric materials based on their chemical structure is crucial for technological applications, since these properties govern the behavior of the materials at end-use conditions. In this work, a united atom (UA) force-field[1] is developed for the calculation of microscopic structure, thermodynamic and conformational properties of pure PDMS melts over a wide temperature and pressure range. Force field parameters are based on existing force fields proposed in the literature[2] and on experimental data for PDMS. The force field is used subsequently for the calculation of the solubility and diffusion coefficient of organic penetrants and small gases in PDMS. Permeability coefficients as obtained from MD are compared to recent experimental data. Both pure and mixed-penetrant systems are examined.

For the calculation of pure PDMS properties, Molecular Dynamics (MD) simulations were performed at the isobaric-isothermal (*NPT*) statistical ensemble using Nosé and Klein extended method. The *PVT* properties, such as density, isothermal compressibility and solubility parameter of polymer melts were simulated over an extensive temperature and pressure range. The agreement between experimental data and simulation was very good.

The solubility of *n*-alkanes (CH_4 to *n*-C_6H_{14}), perfluorocarbons (CF_4 to *n*-C_4F_{10}) and light gases (He, Ar, Ne, Kr, Xe, N_2, O_2) in PDMS at 300 K and 450 K and ambient pressure was calculated using the Widom test particle insertion method. The agreement with the experimental data[3] was very good in all cases. In figure 1, the infinite dilution solubility coefficient of *n*-alkanes and perfluoroalkanes in PDMS at the two different temperatures is shown. It is obvious that fluorocarbon solubilities in PDMS are lower than those of their hydrocarbon analogs. Similar experimental results have been reported in literature.

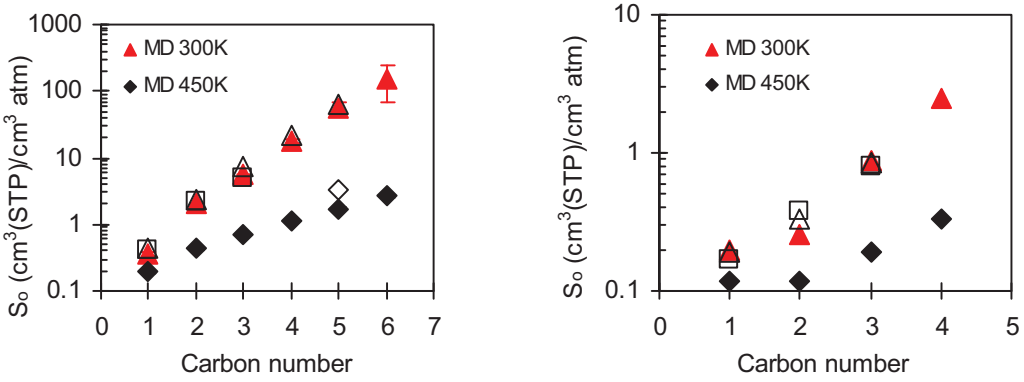

Figure 1. Infinite solubility coefficient S_o of (a) *n*-alkanes and (b) perfluoroalkanes in PDMS. Open symbols are experimental data and solid symbols are simulations.

Extensive MD simulations[4] on the order of 100 ns were performed for the estimation of the diffusion coefficient of light gases, n-alkanes and binary n-alkane mixtures in PDMS. As regards the diffusion and permeability coefficients, simulation predictions were lower than experimental data. However, the ideal separation factor for a number of n-alkane mixtures in PDMS at 300 K agrees remarkably well with the experiment. In Figure 2(a) temperature dependence on permeability selectivity of the pure binary system n-C_4H_{10}/CH_4 in PDMS is presented.

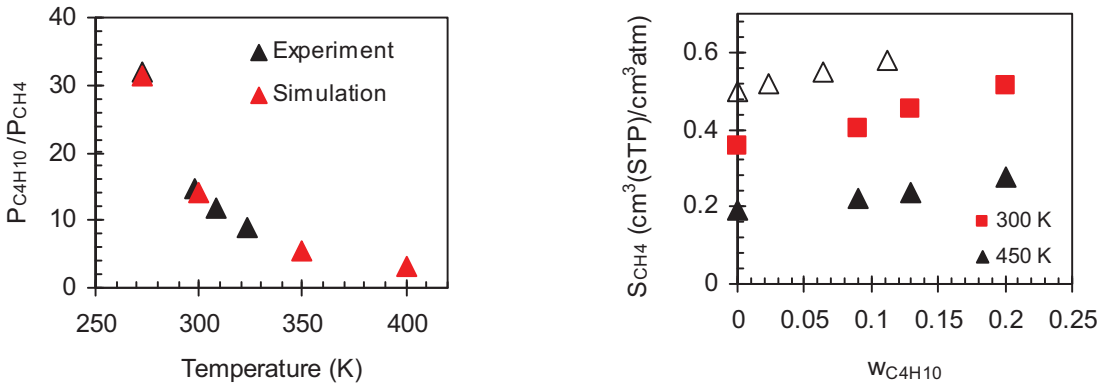

Figure 2. (a) Effect of temperature on pure *n*-C_4H_{10} – CH_4 permeability selectivity and (b) mixed gas CH_4 solubility in PDMS at 300 K and 450 K as a function of *n*-C_4H_{10} weight fraction in PDMS predicted by molecular simulation. Open triangles are experimental data at 298 K.

The effect of penetrant concentration on the diffusion coefficient value was also examined. MD simulations for PDMS – CH_4 and PDMS – *n*-C_4H_{10} mixtures at 350 K and various compositions were performed. In both systems, diffusion coefficient increases with penetrant concentration.

For the accurate design of a polymer membrane for the separation of a real mixture, mixture permeability data are needed. In this work[4], molecular simulation sorption calculations were performed for the *n*-C_4H_{10} – CH_4 mixture in PDMS. Predictions depicted in Figure 2(b) indicate that at both temperatures, CH_4 solubility increases as *n*-C_4H_{10} concentration in the polymer increases. Clearly, the presence of *n*-C_4H_{10} molecules in the polymer creates a more favorable environment for CH_4 sorption, which enhances CH_4 solubility. This behavior is consistent with the recent experimental data of Raharjo et *al*.[5] at 298 K shown in Figure 2(b).

References

1. Makrodimitri, Z.A.; Dohrn, R.; Economou, I.G. *Macromolecules* **2007**, *40*, 1720.

2. Sok, R. M.; Berendsen, H. J. C.; van Gunsteren, W. F. *J. Chem. Phys.* **1992**, *96*, 4699.

3. Kamiya, Y.; Naito, Y.; Hirose, T.; Mizoguchi, K. *Macromolecules* **2000**, *33*, 3111.

4. Makrodimitri, Z.A.; Economou, I.G. *Macromolecules* **2008** (in press).

5. Raharjo, R.D.; Freeman, B.D.; Paul, D.R.; Sarti, G.C.; Sanders, E.S. *J. Membr. Sci.* **2007**, *306*, 75.

Oral 32

Steady Capillary Flow of Polytetrafluoroethylene (PTFE) Paste: Experiments and Simulations

E. Mitsoulis (a), Th. Zisis (a), and S.G. Hatzikiriakos (b)

(a) School of Mining Engineering and Metallurgy, National Technical University of Athens, Athens, Greece
(b) Department of Chemical and Biological Engineering, The University of British Columbia, Vancouver, BC, Canada

Abstract

In the process of paste extrusion of PTFE, a paste is first formed by mixing the PTFE resin with a lubricant whose concentration varies from 16% to 40% wt., depending on the resin and the geometrical characteristics of the extrusion die. The system behaves like a semi-solid material when it is extruded at 35°C at various piston velocities in tapered capillary dies. During extrusion, the steady-state pressure in the system goes through a minimum at a certain tapered angle of the extrusion die for a given flow rate. To solve numerically such problems of semi-solid processing, it is important to include in the constitutive modelling the compressibility of the paste and its massive slip at the walls. Such a model is used here to predict the pressure behaviour in steady-state capillary flow of PTFE paste.

1 Introduction

Poly-tetra-fluoro-ethylene (PTFE or $-(CF_2\text{-}CF_2)_n-$) is a linear polymer of helical molecular conformation, high molecular weight (10^6-10^7), high melting point (342°C), and high melt viscosity (1-10 GPa·s at 380°C). The last two characteristics introduce an obstacle in its processing. So it is not possible to process PTFE resins by using polymer melt processing. There is still an advantageous alternative: because of its transition temperatures in its phase diagram at 19°C and at 30°C, above 19°C PTFE changes its crystallinity and becomes highly deformable. Then it can be processed as a paste by extrusion, mixed with appropriate lubricants in amounts of 16-40% wt.[1,2] After paste extrusion, the extrudate is dried and sintered.
In the present study, such a PTFE paste is studied rheologically by extrusion through capillary dies. The steady-state pressures are recorded for different tapered dies and processing conditions. Finally, an attempt is made at modelling the material through a rheological model that encompasses most of the phenomena encountered in paste extrusion.

2 Experiments

The experiments are carried out first by premixing the lubricant with the polymer at 25°C. The lubricant must coat the resin particles, must have a high vapor pressure, and must not leave a residue after evaporation.[1] The viscosities of the different types of lubricants range between 0.51-7.50 mPa·s. During preforming the two-phase mixture (resin and lube) is compressed and the lubricant migrates in all directions. Then during extrusion through a typical capillary rheometer, the pressure is recorded for different conditions. A typical behavior is shown in Fig. 1(a) for a given apparent shear rate. Figure 1(b) shows results for different apparent shear rates. Rich phenomena are observed, with the pressure going through a minimum at a given entrance angle, while the steady-state values for different apparent shear rates increase linearly as expected.

3 Mathematical modeling

We consider the steady-state Navier-Stokes equations for mildly compressible materials. The rheology of the material obeys a generalized Newtonian fluid with shear-thinning and shear-thickening terms:[3]

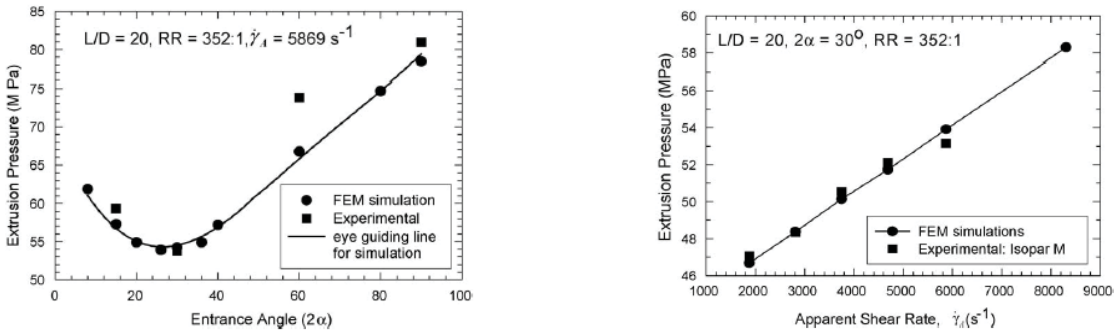

(a) (b)

Fig. 1: PTFE paste extrusion at 35°C: (a) effect of entrance angle of the tapered capillary die, (b) effect of apparent shear rate on the pressure (RR=area reduction ratio).

(mass conservation) $$\bar{u}\cdot\nabla\rho+\rho\left(\nabla\cdot\bar{u}\right)=0 \quad (1)$$

(momentum conservation) $$0=-\nabla p+\nabla\cdot\bar{\bar{\tau}} \quad (2)$$

(rheological model) $$\bar{\bar{\tau}}=\eta\left(|\dot{\gamma}|\right)\left(\bar{\bar{\dot{\gamma}}}-\frac{2}{3}\left(\nabla\cdot\bar{u}\right)\bar{\bar{I}}\right) \quad (3)$$

(viscosity model) $$\eta=(1-\xi)\eta_1+\xi\eta_2 \quad (4a)$$

(Carreau viscosity model) $$\eta_i=\eta_{0,i}\left[1+\left(\lambda_i|\dot{\gamma}|\right)^2\right]^{(n_i-1)/2} \quad (4b)$$

(convective transport equation) $$\bar{u}\cdot\nabla\xi=|\dot{\gamma}|\left(\sqrt{\psi}-\xi\right) \quad (5)$$

(linear equation of state) $$\rho=\rho_0\left(1+\beta P\right) \quad (6)$$

(linear slip law) $$u_{sl}=-\beta_{sl}\tau_w \quad (7)$$

In eq. (5), ξ is a structural parameter related to the creation of fibrils, and ψ is a flow-type parameter related to the type of flow in the die.[3] The values of the constants can be found in Ref. [3]. For the compressibility effects, ρ_0=1.6 g/cm^3, β=0.02 MPa^{-1} (for 0<P<100 MPa). The apparent shear rate is given by: $\dot{\gamma}_A=4Q/\pi R^3$.

Results are shown in Fig. 1 for the pressure drop in comparison with the experiments. In Fig. 1(a) a minimum is observed around 2α=30°, while a linear increase with flow rate is observed in Fig. 1(b). Figure 2 shows typical results for contours of the structural parameter, ξ, and the flow-type parameter, ψ. These developments are due to the combined effect of compressibility and slip, since neither of them alone can produce the phenomena found experimentally.

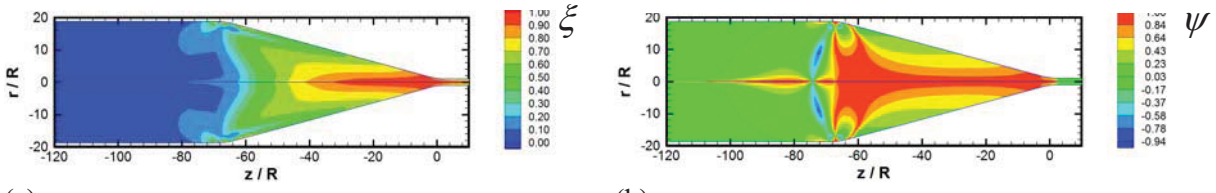

(a) (b)

Fig. 2: Steady simulation results for R_{res}/R=18.75, R=0.254 mm, $\dot{\gamma}_A$ =5869 s^{-1}, convergence angle 2a=30°: (a) structural parameter, ξ, (b) flow-type parameter, ψ.

References

1. A.B. Ariawan, S. Ebnesajjad, and S.G. Hatzikiriakos, *Paste Extrusion of Polytetrafluoro-ethylene (PTFE) Fine Powder Resins*, Can. J. Chem. Eng., **80**, pp.1153-1165 (2002)
2. A.B. Ariawan, S. Ebnesajjad, and S.G. Hatzikiriakos, *Properties of Polytetrafluoroethylene (PTFE) Paste Extrudates*, Polym. Eng. Sci., **42(6)**, pp.1247-1259 (2002)
3. P.D. Patil, J.J. Feng, S.G. Hatzikiriakos, *Constitutive Modeling and Flow Simulation of Polytetrafluoroethylene (PTFE) Paste Extrusion*, J. Non-Newtonian Fluid Mech., **139**, pp.44-53 (2006)

Oral 33

Thermal degradation kinetics of light-cured dimethacrylate resins used as biomaterials in dental applications

Dimitris S. Achilias, Maria M. Karabela, Irini D. Sideridou
Laboratory of Organic Chemical Technology, Department of Chemistry, Aristotle University of Thessaloniki, GR-541 24, Thessaloniki, Greece, E-mail: axilias@chem.auth.gr

Introduction

Thermal degradation kinetics of resins based on bis-phenol A glycidyl dimethacrylate (Bis-GMA), bis-phenol A ethoxylated dimethacrylate (Bis-EMA), urethane dimethacrylate (UDMA) and triethylene glycol dimethacrylate (TEGDMA) was investigated using thermogravimetric analysis (TGA) as a means to provide specific information regarding internal structures of these polymers. Dimethacrylate-based resins are materials forming highly crosslinked three-dimensional network structures, which find wide applications as biomaterials in dental applications. The study of thermal degradation of these polymers is a difficult task and owing to the complexity of the process only a few reports have been reported so far in literature[1-2]. In this investigation, thermal degradation kinetics of both homo- and co-polymers based on Bis-GMA, Bis-EMA, UDMA or TEGDMA was examined. Thermogravimetric scans were taken at four different heating rates in order to have adequate data to perform an isoconversional analysis to determine the change of the effective activation energy as a function of conversion[3]. Both differential and integral methods were employed.

Experimental

Polymers were prepared by mixing monomer(s) and the photoinitiator system (CQ 0.2% mass fraction and 4EDMAB 0.8% mass fraction), followed by heating in the dark at 60±0.5^{o}C until the photo-initiator components were dissolved in the monomer. Then the mixture of monomer was cured in Teflon molds using a XL 3000 dental photocuring unit (3M Company). This source consisted of a 75-W tungsten halogen lamp, which emits radiation between 420 and 500nm and has the maximum peak at 470 nm. The samples were irradiated for 200 sec on each side[4]. TGA was performed on a Pyris 1 TGA (Perkin Elmer) thermal analyzer. Samples of about 8mg were used. They were heated from ambient temperature to 600^{o}C under a 20 ml/min nitrogen flow. TGA measurements of each sample were performed at different heating rates of 2.5, 5, 10 and 20^{o}C min^{-1} and sample mass versus temperature was continuously recorded.

Results and Discussion

The effect of the resin chemical structure on the TGA scans appear in Figure 1.

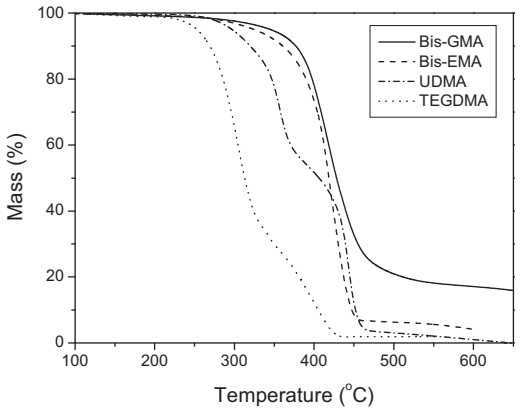

Fig. 1 Effect of the resin chemical structure on the TGA scans at 10^{o}C/min.

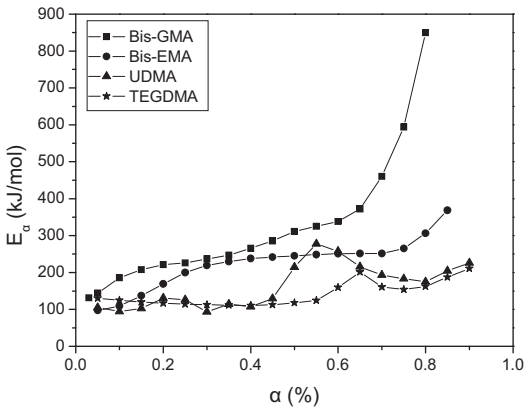

Fig. 2 Effect of the resin chemical structure on the activation energy as a function of the extent of degradation (method of Friedman).

The observed differences were interpreted in terms of degradation mechanisms, which are highly depended on the structural characteristics of the corresponding resin. When multifunctional monomers are polymerized, a pendant double bond can react intramolecularly with the radical in its propagating chain to form a loop in a primary cyclization reaction (Scheme 1). As both Bis-GMA and Bis-EMA resins contain the kinked and rigid bisphenol A core structure, it is expected that this connecting-group rigidity is primarily responsible for a reduction in the amount of cyclization reactions. In contrast, TEGDMA and UDMA due to their non-aromatic nuclei are more flexible monomers and therefore their pendants can cycle more readily after they are created.

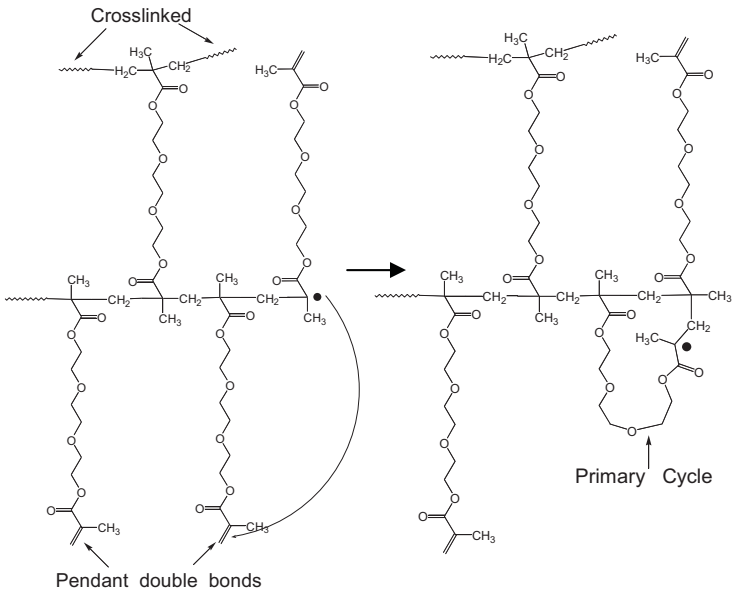

Scheme 1. Primary cyclization reaction occurring during polymerization of TEGDMA

The existence of only a small number of defects in the network structure of Bis-GMA and Bis-EMA resins together with their stiff aromatic nuclei lead to the formation of a rigid network with high thermal stability and to decomposition in one step. In contrast, inhomogeneities in the network structure of TEGDMA and UDMA resins, mainly due to the formation of primary cycles during polymerization, result in a two-step degradation mechanism at much lower temperatures. The hydrogen bonding ability of Bis-GMA and UDMA monomer units was also found to play an important role during thermal degradation of these resins. These results were also verified from isoconversional kinetic analysis and estimation of the activation energy as a function of the extent of degradation (Figure 2)[4].

Finally, some indicative results on the effect of the relative amount of each monomer during thermal degradation of Bis-EMA / TEGDMA based copolymers appear in Figure 3a and b

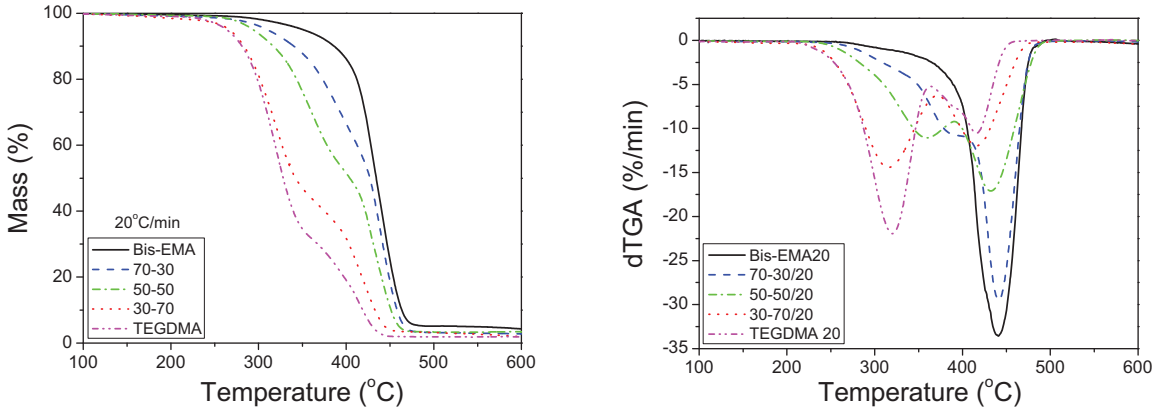

Fig. 3 Effect of the relative amount of monomer on the TGA (a) and DTGA (b) curves of Bis-EMA / TEGDMA resins at a heating rate of 20°C/min.

References

1. K. Pielichowski, J. Njuguna, Thermal Degradation of Polymeric Materials Rapra Technology, 2005
2. I.C. Rigoli, C.C. Cavalheiro, M.G. Neumann, E.T. Cavalheiro. J. Appl. Polym. Sci. 105 (2007) 3295.
3. S. Vyazovkin, N. Sbirrazzuoli, Macromol. Rapid Commun. 27 (2006) 1515-32
4. I.D. Sideridou, D.S. Achilias, M.M. Karabela, Thermochimica Acta in press (2008).

Oral 34

Study of polyblends containing plastics used in electrical and electronic applications

P.A. Tarantili, A.N. Mitsakaki, M.A. Petoussi, A.G. Andreopoulos
Laboratory of Polymer Technology, School of Chemical Engineering, Sector IV, National Technical University of Athens
9 Heroon Polytechniou Str., Zografou Campus, GR-15780, Athens, GREECE

ABSTRACT

Acrylonitrile-butadiene-styrene (ABS), polycarbonate (PC) and high impact polystyrene (HIPS) are high performance polymers widely used in electrical and electronic equipment (EEE). Recycling of these materials is of great interest, due to their high cost and availability as waste products. Obviously, it is not feasible that a recycled material shows similar properties to virgin resins, but a good balance between properties, processability and cost would always be desired.

In this work, polyblends based on ABS/PC and ABS/HIPS were prepared and studied, in an attempt to explore the performance of mixtures deriving from the recycling of waste electrical and electronic equipment (WEEE). The above mixtures were processed by melt mixing in a co-rotating twin-screw extruder (Haake PTW 16) and then, tested for their thermal (Differential Scanning Calorimetry, DSC), rheological (Melt flow rate, MFR) and mechanical (tensile test) properties.

The results showed that ABS/PC system displays two glass transition temperatures (T_g) at 50/50 w/w composition, which indicates partial miscibility of the two components, a parameter depending on the composition of the mixture (Fig. 1). The obtained MFI values for ABS/PC systems indicate that the behaviour of this system is controlled by the rheological characteristics of PC (Table 1).

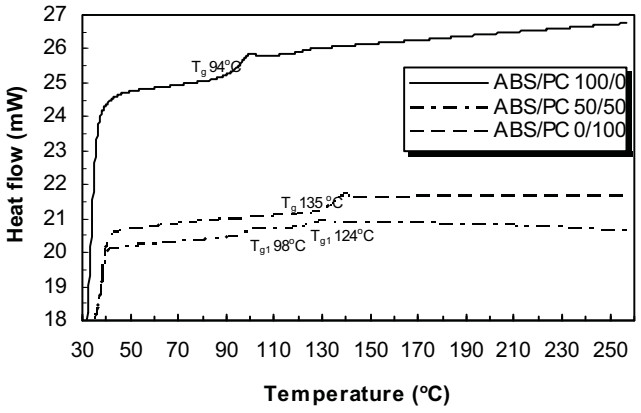

Figure 1. Comparative DSC thermographs of ABS/PC blends (2nd heating cycle).

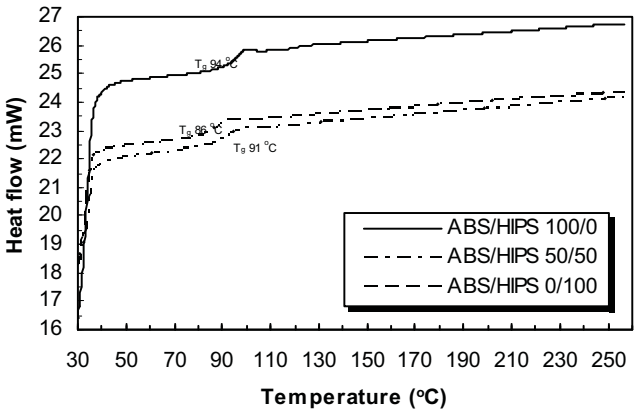

Figure 2. Comparative DSC thermographs of ABS/HIPS blends (2nd heating cycle).

Tensile tests (Table 2) show that the extrusion process of ABS does not significantly affect the strength of the material, which is in agreement with the related literature[1]. The incorporation of ABS in PC leads to a decrease of its tensile strength and ultimate elongation and this effect seems to be proportional to the ABS content in the polyblend (rule of mixtures). On the other hand, the modulus of elasticity was improved by this addition, with the highest value corresponding to 20 wt% PC content. According to the results of other researchers[2], this composition is the most interesting for the design of materials with balanced properties, that would become potential industrial products. In that composition the mechanical properties are acceptable and the processing conditions are similar to those of other widely used vinyl polymers.

A single T_g was recorded in the case of ABS/HIPS blends (Fig. 2), in accordance with the Fox equation. This suggests complete miscibility of the blend components and furthermore, an efficient homogenization taking placing during the mixing procedure in the co-rotating twin-screw extruder[3]. The changes of MFI values show again a linear dependence on the mixture composition (% PC content).

ABS/PC,HIPS	ABS/PC		ABS/HIPS	
(w/w)	MFI (g/10min)	MFI*	MFI (g/10min)	MFI*
0/100	2.564 ± 0.135	-	5.669 ± 0.355	-
20/80	4.608 ± 0.265	2.104	6.029 ± 0.192	5.258
50/50	2.012 ± 0.277	1.339	4.225 ± 0.231	3.962
80/20	2.018 ± 0.090	0.680	2.321 ± 0.090	2.687
100/0	0.227 ± 0.008	-	1.836 ± 0.127	-

Table 1: MFI measurements of ABS/PC and ABS/HIPS blends. **accord. to rule of mixtures*

ABS/PC (w/w)	Tensile strength (MPa)	Modulus of elasticity (MPa)	Strain at break (%)
0/100	68.973±0.233	1956.429±24.220	57.241±4.864
20/80	63.945±0.675	2074.500±111.015	36.949±8.683
50/50	61.657±1.035	2040.286±141.475	28.395±13.247
80/20	57.878±1.101	2178.200±84.384	10.078±4.278
100/0	50.654±4.742	1918.571±261.848	4.410±2.002

Table 2: Tensile test results for ABS/PC blends.

As can be seen in Table 3, the incorporation of HIPS in ABS decreases the tensile strength, whereas the strain at failure increases according to the rule of mixture. A synergistic effect was observed for the modulus of elasticity at compositions beyond 50% w/w in ABS.

ABS/HIPS (w/w)	Tensile strength (MPa)	Modulus of elasticity (MPa)	Strain at break (%)
0/100	32.400±1.344	1322.600±41.651	40.472±9.276
20/80	34.888±0.653	1409.750±14.210	39.705±10.523
50/50	40.867±0.510	1975.571±56.824	22.596±5.583
80/20	47.419±0.389	2045.143±121.424	20.772±5.578
100/0	50.654±4.742	1918.571±261.848	4.410±2.002

Table 3: Tensile test results for ABS/HIPS blends.

Based on the above, we can conclude that homogeneous polyblends containing plastics used in EEE can be prepared by melt mixing in a twin screw extruder. Depending on the blend composition, these products can give acceptable final properties, which allows their potential applications as recycled materials. The use of polyblends for this purpose has the additional advantage of skipping the separation and classification stage during recycling process, with obvious operational and economical benefits for the overall procedure.

References

1. A. Boldizar, K. Möller, *Degradation of ABS during repeating processing and accelerated ageing*, Polymer Degradation and Stability, **81**, 359 (2003).
2. R. Balart, J. López, D. García, M.D. Salvador, *Recycling of ABS and PC from electrical and electronic waste. Effect of miscibility and previous degradation on final performance of industrial blends*, European Polymer Journal, **41**, 2150 (2005).
3. L.B. Brennan, D.H. Isaac, J.C. Arnold, *Recycling o Acrilonitrile-Butadiene-Styrene and High-Impact Polystyrene from Waste Computer Equipment*, Journal of Applied Polymer Science, **86**, 572 (2002).

Oral 35

Porous materials from polysaccharide gels processed by supercritical CO_2

Costas Tsioptsias, Costas Panayiotou
Department of Chemical Engineering, Aristotle University of Thessaloniki, 54124 Thessaloniki, Greece

Supercritical carbon dioxide (CO_2) has been widely used for processing polymeric materials in a variety of applications. However, systematic investigations on the interactions of polymeric hydrogels with supercritical CO_2 have not been carried out so far. By a modified mass loss analysis[1,2] we studied the sorption of supercritical CO_2 by chitin and cellulose hydrogels and methanogels (gels with methanol as solvent), and concluded that dissolution of CO_2 in the solvent is the main mechanism of CO_2 sorption by the gel. However, upon depressurization, significant foaming of the hydrogels was observed but not of the methanogels. This observation is in contrast to the much greater CO_2 solubility in methanol than in water. To explain the observed greater degree of foaming in hydrogel, the crystallinity of chitin and cellulose in hydrogel and methanogel was examined by x-ray diffraction and was found significantly greater in methanogel. These measurements provide evidence that, besides dissolution in water, CO_2 is sorbed by chitin and cellulose molecules in the hydrogel but not in methanogel. To further explore and understand the phenomenon, porous chitin structures were produced by foaming the hydrogel at different conditions and freeze-drying it in order to retain the porous structure. Parameters such as pressure, temperature, and depressurization rate, that influence pore size distribution in classical polymer foaming, were examined. Additional parameters, related to the nature of the hydrogel and that could influence pore size distribution, were also examined. The chitin and cellulose methanogels leads to nanoporous aerogels by the critical point drying technique.[3] Parameters that influence pore size, density and surface area of the aerogels were investigated.

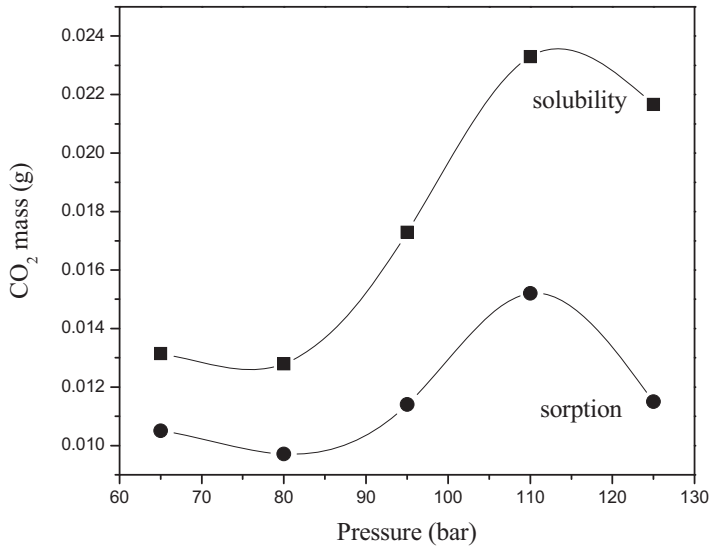

Fig. 1 Measured CO_2 sorption in chitin hydrogel and calculated CO_2 solubility in water from VLE data[4]

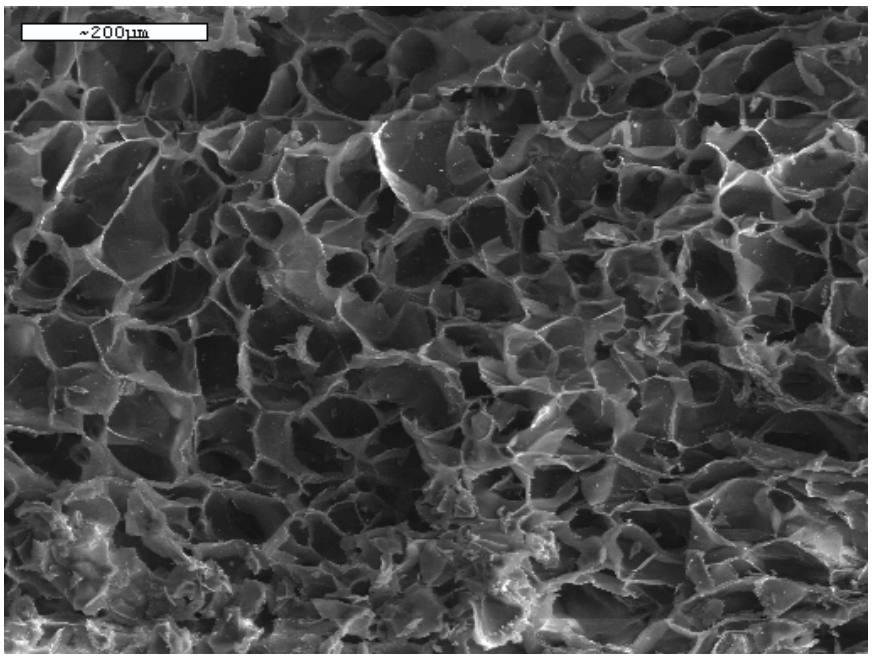

Fig. 2 Chitin porous structure produced by hydrogel foaming with CO_2

REFERENCES

1. M. Pantoula, C. Panayiotou. The Journal of Supercritical Fluids 37 (2006) 254-262.
2. A. Kumar, R. K. Gupta. "*Fundamentals of Polymers*", McGraw-Hill 1998, chap.7.
3. A. C. Pierre, G. M. Pajonk. Chemical Reviews 102 (2002) 4243-4265.
4. A. Bamberger, G. Sieder, G. Maurer. The Journal of Supercritical Fluids 17 (2000) 97-110.

Oral 36

Chemical modification of carbon fibers and its evaluation based on their composites with epoxy resin

L. Zoumpoulakis, V. Oikonomopoulou, J. Simitzis*
National Technical University of Athens, School of Chemical Engineering, Department III "Materials Science and Engineering", Laboratory Unit "Advanced and Composite Materials", 9 Heroon Polytechniou str., Zografou Campus, 157 73 Athens, Greece.
**e-mail: simj@orfeas.chemeng.ntua.gr*

1. INTRODUCTION

Fiber reinforced polymers have gained substantial interest over the last years, mainly due to their very high strength-to-weight and stiffness-to-weight ratios. These properties led to the use and application of composite materials in a lot of major industries with the aerospace and automotive industry taking the larger part[1]. Successful reinforcement of matrix materials can only be achieved if there is good stress transfer between the matrix and the fiber. Unfortunately, epoxy resins do not bond strongly to untreated fibers and have a negative effect on the properties of the composites. To overcome this, several pretreatments have been developed such as chemical oxidation[2], electrochemical oxidation[3,4] and oxidation in air at high temperatures[3]. One of the most often used chemically oxidizing solutions is the concentrated niric acid[5]. After the oxidation, an increase of the bands at 1720cm^{-1} of C=O stretching vibrations of carbonyl and carboxyl, at 1250-1400cm^{-1} of symmetric stretching vibrations of COO^- groups and the existance of C-O-C and C-OH bonds, OH deformation vibrations and C-O stretching vibrations are observed[6]. Also, an absorption increase at 730-900cm^{-1} is caused by the formation of cyclic anhydrides structures[5].The aim of this work is the chemical modification of carbon fibers and its evaluation based not only on structural characterization but also on their composites with epoxy resin.

2. EXPERIMENTAL

Commercial carbon fibers were chemically modified by two different methods using HNO_3 or $KMnO_4$. In the first method, the carbon fibers were treated with nitric acid (65%) at 110^{o}C for 70min, then the oxidized fibers were washed with distilled water for 3h and dried at 110^{o}C for 2h. In the second one, the carbon fibers were washed with acetone for 12h, dried under vacuum and then were immersed in an aq. solution of 0.3 wt% of sulfuric acid at room temperature. After 10 min, the reaction was initiated by adding dropwise 40ml of an aq. solution of 0.118g/ml of $KMnO_4$ and heating at 80^{o}C for 3h. The oxidized fibers were washed with warm water and were dried under vacuum at 120^{o}C for 2h[7].

The adsorptive ability of commercial and chemically treated carbon fibers was determined with the discoloration method using a proper aq. solution of methylene blue (MB). All carbon fibers were characterized by Fourier transform infrared spectroscopy (FTIR) and scanning electron microscopy (SEM). The prepreg method was used for the manufacture of composites with epoxy resin and treated or untreated carbon fibers. By using an appropriate arrangement, the impregnation of the fibers through the resin bath was achieved and they were continuously winded on a plate having constant distance. After setting the plate in an oven for partial curing of the resin at 60^{o}C for 20min, laminates were cut out. An appropriate number of laminates were placed into moulds in order to have 15%v/v of carbon fibers in the final composite and were cured by using a thermopress. The moulds were heated at 93^{o}C for 15min without pressure, then the pressure was increased up to 4000 kp/cm^2 and they remained under load for 2h. Different types of curing agent were used i.e. commercial one, triethylentetramine (TETA) and diethylentriamine (DETA). The mechanical properties (bending strength and interlaminar shear strength) of the manufactured composites were measured.

3. RESULTS AND DISCUSSION

Fig. 1 shows the FTIR spectra of the untreated (commercial) and treated carbon fibers. A peak at ~1800cm^{-1} (lactones) is observed for the treated fibers. The peak at ~1480cm^{-1} (aromatic ring) and at ~1050cm^{-1} (C-OH) of the treated fibers was decreased compared to the untreated ones. None of the bands of FTIR spectra of the fibers cannot be attributed to any kind of groups containing nitrogen. The nitric acid solution is an oxidizing agent that during reduction forms among others, nitrogen oxides and these oxides can oxidize carbons, however, they are reduced to N_2[5] evolved as gas. Fig. 2 shows the adsorption of MB from aqueous solution on carbon fibers. The carbon fibers treated with HNO_3 had greater adsorption ability than the others. Fig. 3 and 4 present the mechanical properties of the composites. Among the untreated carbon fibers, cured

with commercial curing agent (composite 1, C1), TETA (C2) and DETA (C3), the C1 had the highest values of the mechanical properties. It is obvious, that the type of the curing agent influences strongly the mechanical properties of the composites, therefore only the composites of the same group can be compared. The mechanical properties of C4 impregnated with water and cured with commercial curing agent were almost the same with C1. The C5 with fibers treated with HNO_3 and commercial curing agent had lower values of the mechanical properties than C1. The C6 with fibers treated with HNO_3 and TETA had slightly higher value of bending strength and lower shear strength than C2. The C7 with fibers treated with $KMnO_4$ and commercial curing agent had almost the same mechanical properties as C1. The C8 with fibers treated with $KMnO_4$ and TETA had lower mechanical properties than C2. The oxidation of carbon fibers with nitric acid decreased their mechanical properties, i.e. bending strength and shear strength, however such treated carbon fibers could be found applications in the medical sector as ligament and tendon prostheses or sutures[6]. Fig. 5-7 show the SEM images of the fibers. Fig. 5 and 6 show that the monofilaments of commercial carbon fibers are smooth and homogenous and have a “cordon” shape. Fig. 7 shows that the fibers had rough surface due to their chemical modification with HNO_3.

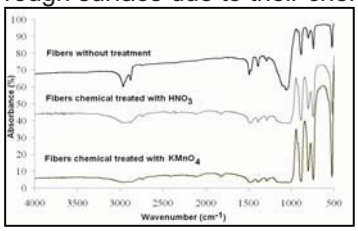

Fig. 1 FTIR spectra of fibers

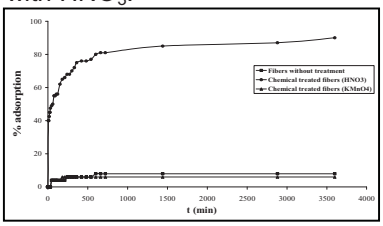

Fig. 2 Adsorption of MB from aqueous solution on fibers.

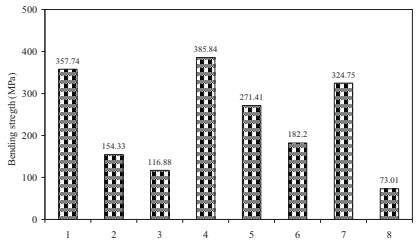

Fig. 3 Bending strength of the composites.

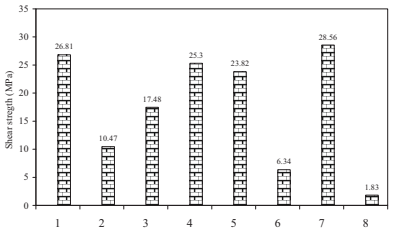

Fig. 4 Shear strength of the composites.

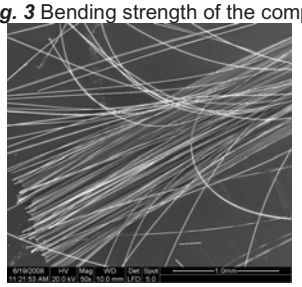

Fig. 5 SEM image of commercial fibers (magnification 50x).

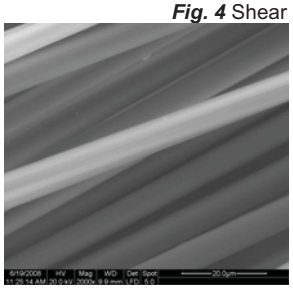

Fig. 6 SEM image of commercial fibers (magnification 2000x).

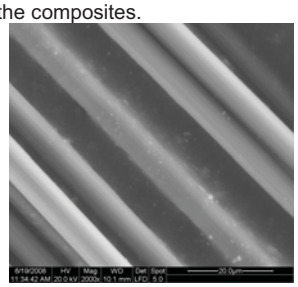

Fig. 7 SEM image of fibers chemical treated with HNO_3 (magnification 2000x).

REFERENCES

1. D.A. Papargyris, R.J. Day, A. Nesbitt, D. Bakavos. Comparison of the mechanical and physical properties of a carbon fiber epoxy composite manufactured by resin transfer moulding using conventional and microwave heating. Compos Sci Technol, 68, 2008, 1854-1861.
2. Elzbieta Pamula, Paul G. Rouxhet. Influence of surface properties of carbon fibers on the adsorption of catalase. Carbon, 43, 2005, 1432-1438.
3. Carol Jones. Effects of Electrochemical and Plasma Treatments on Carb. Fib. Surfaces. Sur and Inter Anal, 20, 1993,357-367.
4. Hailin Cao, Yudong Huang, Zhiqian Zhang, Jvtao Sun. Uniform modification of carbon fiber surface in 3-D fabrics using intermittent electrochemical treatment. Compos Sci Technol, 65, 2005, 1655-1662.
5. Jerzy Zawadzki. IR Spectroscopic Investigations of the Mechanism of Oxidation of Carbonaceous Films with HNO_3 Solution. Carbon, 18, 1980, 281-285.
6. Elzbieta Pamula, Paul G. Rouxhet. Bulk and surface chemical functionalities of type III PAN-based carbon fibers. Carbon, 41, 2003, 1905-1915.
7. Zhiwei Xu, Li Chen, Yudong Huang, Jialu Li, Xiaoqing Wu, Xueming Li, Yanan Jiao. Wettability of garbon fibers modified by acrylic acid and interfce properties of garbon fiber/epoxy. Europ Poly Journ, 44, 2008, 494-503.

Oral 37

Post-polymerisation in the solid state of sulfonated nylon 66 copolymers

S. N. Vouyiouka and C. D. Papaspyrides
Laboratory of Polymer Technology, School of Chemical Engineering, National Technical University of Athens, Zographou, Athens 157 80, Greece

ABSTRACT
The compositional effect caused by the incorporation of sodium 5-sulfoisophthalic acid in poly(hexamethylene adipamide) (nylon 66) was studied during solid state polymerisation (SSP). The comonomer presence induced severe process retardation found to be related to its ionic moieties, and SSP kinetics were appropriately modified to predict the copolyamide SSP performance.

INTRODUCTION
SSP can be applied to crystalline monomers as well as to prepolymers. It consists of an important finishing technique to prepare high molecular weight polyamides ($\overline{M_n}$ >25000 g mol^{-1}), suitable for spinning, extrusion and injection. It is applied to both nylon 6 and nylon 66 monomers and precursors, meanwhile its significance is enhanced in cases of specialty polyamides, such as nylon 46. Based on the reversible polycondensation reaction and on the restrictions set by SSP nature, one can identify several rate-determining steps, estimating also the influence of the main process variables, e.g. temperature, prepolymer molecular weight, crystallinity, reacting particle geometry and catalyst[1]. These parameters are thoroughly investigated in literature regarding homopolymers SSP[1-4], meanwhile the effect of the polyamide chemical composition on the process has not been fully studied, as in the case of ion-modified nylons, e.g. sulfonated copolymers. The pertinent ionomers (Fig.1) usually contain sodium 5-sulfoisophthalic acid (NaSIPA) as a comonomer (1-5 % mol) and are widely used due to the induced higher polyamide dyeability by cationic dyes and to the improved subsequent processing, which is not this way deteriorated by the presence of both pigment and copper[5].

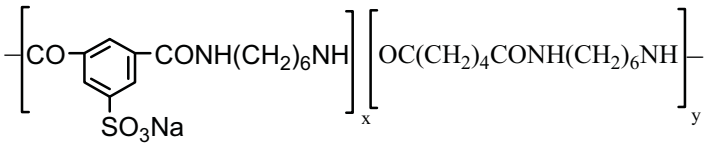

Fig.1. NaSIPA-containing nylon 66 copolyamide.(x: 0.01–0.05, y: 0.95–0.99)

EXPERIMENTAL
Batch SSP runs were performed under flowing (260 mL min^{-1}) and static nitrogen (N_2) in a solid bed reactor in the temperature range of 160–200 °C. NaSIPA-containing prepolymers (1, 2, 3 % wt. NaSIPA, flakes 10–12 Mesh) were kindly supplied by INVISTA™ Inc. and prepared through polycondensation of aqueous salt solutions in the absence of any other additive or catalyst[5].

RESULTS AND DISCUSSION
At each reaction temperature under flowing N_2, the copolyamides exhibited reduced SSP rate constants (k, kg^2 mmol^{-2} h^{-1}) for 3rd order kinetics, and more specifically, k decreased by 11–57 % as the amount of comonomer increased. The retarding effect of NaSIPA persisted also under static N_2 atmosphere runs, where the k values were found lower compared to flowing N_2 due to enhanced condensate removal limitations. This decrease under static N_2 did not significantly vary when comparing homopolymer and ionomers, showing that all grades experienced similar difficulty in removing the polycondensation water, despite the increased hygroscopic sites of the additive structure.

The observed retardation was correlated to partial deactivation of the polyamide protonated amine ends (NH_3^+) by the sulfonate units (SO_3^-), which exist in the amorphous regions of the

copolyamides, forming multiplets, clusters and finally a contiguous phase of restricted mobility[6]. As a result, in the ionomers, there are two types of end groups, active ($[NH_3^+]_a$) and inactive ($[NH_3^+]_{in}$) amine ends. The former are able to participate in the SSP polymerisation reaction and their concentration in the copolyamides is lower against nylon 66 homopolymer, resulting in reducing the reactant concentration and thus the reaction rate. The inactive amine species concentration is assumed to be a fraction of the total amine ends (experimentally measured) ($[NH_3^+]_t$) and depends on the SO_3^- content (C_s), the reaction temperature and the morphology of the ionomer. The two last parameters effect is depicted on a deactivation factor denoted as $\frac{1}{J}$.

Table 1. Modified kinetics for the post-SSP of NaSIPA-containing nylon 66.

Kinetics features	Expression
Active amine ends concentrations	$\left[NH_3^+\right]_a = \left[NH_3^+\right]_t - \left[NH_3^+\right]_t \frac{C_s}{J}$
SSP simple rate model	$\frac{-d[COO^-]}{dt} = k_{cop}\left[COO^-\right]^2 [NH_3^+]_t = k_{cop}[COO^-]^2 \frac{[NH_3^+]_a}{\left(1-\frac{C_s}{J}\right)}$
Correlation of apparent rate constants	$k_{cop} = k_{hom}\left(1-\frac{C_s}{J}\right)$ k_{hom} and k_{cop} the SSP rate constants of the homopolymer and copolyamide ($kg^2\ mmol^{-2}\ h^{-1}$), $[NH_3^+]$ in mmol kg^{-1}, C_s in mmol kg^{-1}, $\frac{1}{J}$ in kg $mmol^{-1}$

For all reaction temperatures, the ratio of k_{cop}/k_{hom} was plotted vs. C_s and the linearity (R^2 = 0.9538) verified the validity of the suggested mechanism. The deactivation factor was found equal to –0.0053 kg $mmol^{-1}$ and this value may be considered as the fractional decrease of the total amine ends in the copolyamide grades, i.e. for 1% NaSIPA the active amine ends are 82% of the experimentally measured value, for 2% NaSIPA 65%, and for 3 % NaSIPA 47%.

Considering the Arrhenius equation for nylon 66 homopolymer SSP, the compositional effect of NaSIPA on the SSP rate constant can be assessed when knowing C_s and T (eq.1). The slight effect of T on deactivation factor may be also introduced; eq.2 derives and can be used in SSP simulation models, especially since the relevant reaction rate constants are usually extrapolated from melt polymerization data despite the very different morphology of the solid polymer.

$$k_{cop} = 4.8\times10^{-6}\exp\left(\frac{70.41}{R}\left(\frac{1}{423}-\frac{1}{T}\right)\right)\times\left(1-\frac{C_s}{189}\right) \quad (1)$$

$$k_{cop} = 4.8\times10^{-6}\exp\left(\frac{70.41}{R}\left(\frac{1}{423}-\frac{1}{T}\right)\right)\times\left(1-6\times10^{-3}\exp\left(\frac{-4.587}{R}\left(\frac{1}{423}-\frac{1}{T}\right)\right)\times C_s\right) \quad (2)$$

where, T the reaction temperature (K), R the universal gas constant (kJ $mol^{-1}\ K^{-1}$).

REFERENCES

1. Vouyiouka S, Karakatsani E, Papaspyrides C. Prog. Polym. Sci. 2005;30:10-37..
2. Papaspyrides C. In The Polymeric Materials Encyclopedia, J. Salamone, Ed., CRC Press, Inc. 1996, pp.7819-7831.
3. Gantillon B, Spitz R, McKenna T. Macromol Mater Eng 2004;289:88-105.
4. Pilati F. In Comprehensive Polymer Science Pergamon, New York 1989, Vol.5, p. 201-216
5. Vouyiouka S, Papaspyrides C, Weber J, Marks D. Polymer 2007; 48(17):4982-4989.
6. Eisenberg A, Hird B, Moore R. Macromolecules 1990;23:4098-4107.

Oral 38

Evaluation of a polymer based chemocapacitive sensor array for the detection of vapor analytes and their mixtures

K. Manoli[a,b], E.Karonis[a], D.Goustouridis[a], S.Chatzandroulis[a], I.Raptis[a], M. Sanopoulou[b]

[a] *Institute of Microelectronics, NCSR "Demokritos", 15310-Aghia Paraskevi, Attiki, Greece*
[b] *Institute of Physical Chemistry, NCSR "Demokritos", 15310-Aghia Paraskevi, Attiki, Greece*
Email: kikimanoli@chem.demokritos.gr

Chemocapacitive sensors, and sensor arrays, based on changes in the dielectric properties of the sensing polymeric material due to sorption of analytes, are actively investigated for the detection of gases in complex vapor environments. Performance of such sensors is usually evaluated and interpreted on the basis of pure analyte-induced capacitance changes and on qualitative assessment of polymer-analyte interactions. In the approach presented here the capacitance responses of a four –component microfabricated InterDigital Chemocapacitive (IDC) sensor array, upon exposure to various concentrations of pure analytes and of their binary mixtures, is supplemented by data on the corresponding swelling response of the polymeric layers. The observed capacitance changes are well correlated to the permittivity changes calculated on the basis of the corresponding swelling data. PCA analysis showed that discrimination between the analytes and their mixtures at various concentrations is possible.

Microfabricated IDC sensor arrays are very promising devices in terms of fabrication costs, power consumption, integration with electronics and may be used for applications in quality control and quality assurance of foodstuffs, wine fermentation and similar consumer goods[1,2]. Towards the goal of a knowledge-base design of such devices for specific applications, essential steps are (i) interpretation of their behavior in terms of the physicochemical properties of analyte-polymer mixture[1-3] and (ii) to examine to what extend the sensor's response to multi-component mixtures can be evaluated from the corresponding response to the pure analytes.

The IDCs were fabricated from Al electrodes on Pyrex wafers by using conventional microelectronic processes[3]. A different polymeric material was selectively deposited on the comb electrodes of each sensor (Fig. 1 and Fig. 2) and the IDCs array response to various vapor concentrations of four analytes was determined (see Fig. 2). Based on the on the volume fraction of sorbed analyte, determined [by use of white light reflectance spectroscopy] from corresponding swelling $\Delta L/L_o$ of the polymeric films, the changes in permittivity of the polymer-analyte system was calculated by use of the Clausius-Mosotti equation and found, in most cases, in line with experimental trends in capacitance responses with type of analyte (see Fig. 3). It was found that (i) the sensors response to most binary mixtures was the sum of the pure components responses and (ii) the sensors can detect the removal of each one of the mixture component (see Fig. 4). Principal component analysis was applied to successfully discriminate the pure analytes, as well as their mixtures (see Fig. 5).

References

1. A.M. Kummer, A. Hierlemann, H. Baltes, “Tuning sensitivity and selectivity of complementary metal oxide semiconductor-based capacitive chemical microsensors”, Anal. Chem. vol. 76, p. 2470-2477, 2004
2. R. Igreja, C.J. Dias, “Dielectric response of interdigital chemocapacitors: The role of the sensitive layer thickness”, Sens. Act. B, vol. 115, p. 69-78, 2005
3. M. Kitsara, D. Goustouridis, S. Chatzandroulis, M. Chatzichristidi, I. Raptis, Th. Ganetsos, R. Igreja, C.J. Dias, “Single chip interdigitated electrode capacitive chemical sensor array” Sens. Act. B, vol. 127, p. 186–192, 2007

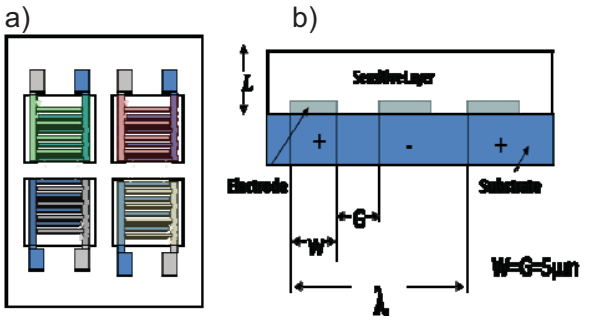

Fig. 1: Schematic (a) top view of IDC array and (b) side view of an IDC. Polymer layers, with L> λ/2, were used, in order to ensure that capacitance changes are solely determined by the dielectric constant change of analyte-polymer mixture.

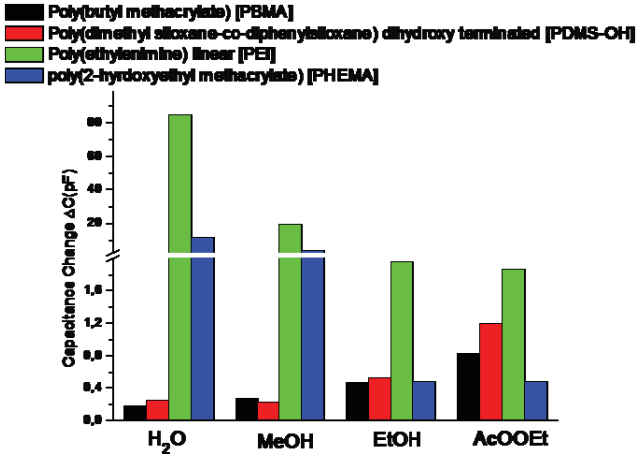

Fig. 2: Capacitance response of IDC array to 5000 ppm of each of the four analytes: moisture (H_2O), methanol (MeOH), ethanol (EtOH) and ethyl acetate (AcOOEt). Sensors initial capacitances C_o were in the range 47-80pF.

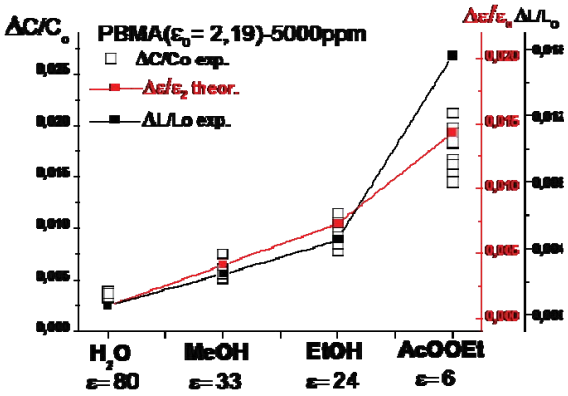

Fig. 3: Experimental capacitance ($\Delta C/C_o$) and swelling ($\Delta L/L_O$) changes and corresponding calculated permittivity ($\Delta\varepsilon/\varepsilon_o$) changes.

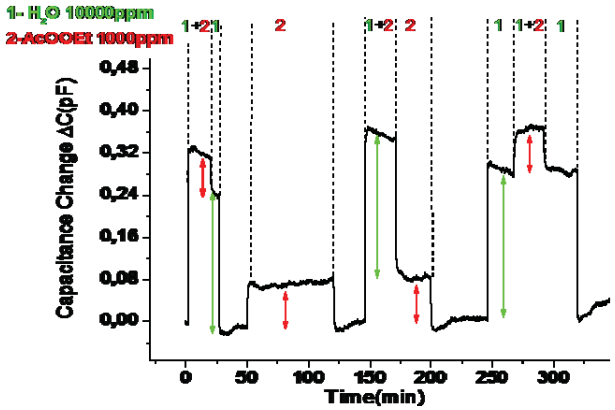

Fig. 4: Capacitance changes ΔC of PBMA-based sensor, upon successive exposures- removals of H2O, AcOOEt and their 1:10 mixture

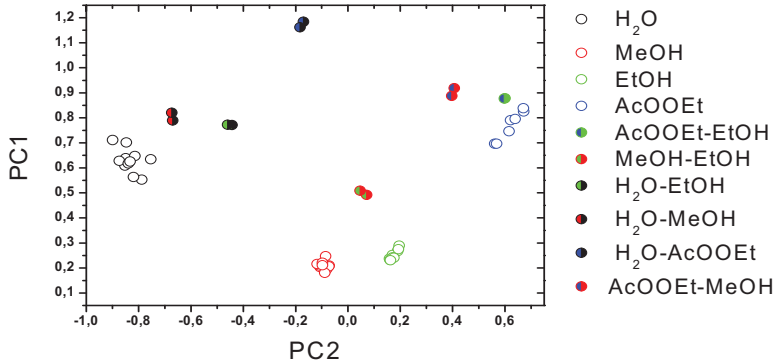

Fig. 5: Two dimensional Principle Component Analysis (PCA) of the equilibrium response results of the array, containing 92,68% of the total variance of the data. The array was exposed to 5000 ppm of the four analytes and their 1:1 mixtures.

Oral 39

Electrical Response of Polymer Matrix – Titanium Carbide Composites

C. G. Raptis, G. C. Psarras

Department of Materials Science, School of Natural Sciences, University of Patras,

Patras 26504, Hellas (Greece)

e-mail: G.C.Psarras@upatras.gr

Polymer matrix ceramic filler composites receive, recently, increased attention because of their interesting electrical, electronic and functional properties [1-3]. Integrated decoupling capacitors, acoustic emission sensors, electronic packaging, self-current regulators, self-heating systems and memory switches are some possible applications [1-3]. Moreover, electrical properties such as dielectric permittivity and conductivity can be suitably adjusted by simply controlling the type and the amount of ceramic inclusions. Composite systems consisting of a polymer matrix and conductive particles of titanium carbide have been considered as a novel class of smart materials [4,5].

In the present study, polymer matrix – ceramic TiC composites were prepared at different filler concentrations. Their electrical response was examined by means of Broadband Dielectric Spectroscopy (BDS), over a wide temperature range (40°C to 160°C) and in the frequency range of 10^{-1}Hz to 10MHz. Dielectric data are analyzed by means of electric modulus and ac conductivity formalisms. Pure matrix exhibits, at least, two distinct relaxation processes attributed, with ascending relaxation rate, to glass/rubber (α-mode) transition, and local motions of polar side groups (β-mode). An additional process has been detected in composite systems. The mechanism, present at low frequencies and high temperatures, is attributed to interfacial polarization or Maxwell-Wagner-Sillars effect. Figure 1 provides isothermal plots of the real and imaginary part of electric modulus as a function of frequency at 100°C for all the examined specimens. The presence of dielectric relaxation processes becomes evident via the formation of loss peaks. The first one, recorded in the intermediate frequency range, is related to the glass/rubber transition (α-mode) of the polymer matrix, while the second one recorded in low frequency region corresponds to interfacial polarization phenomena.

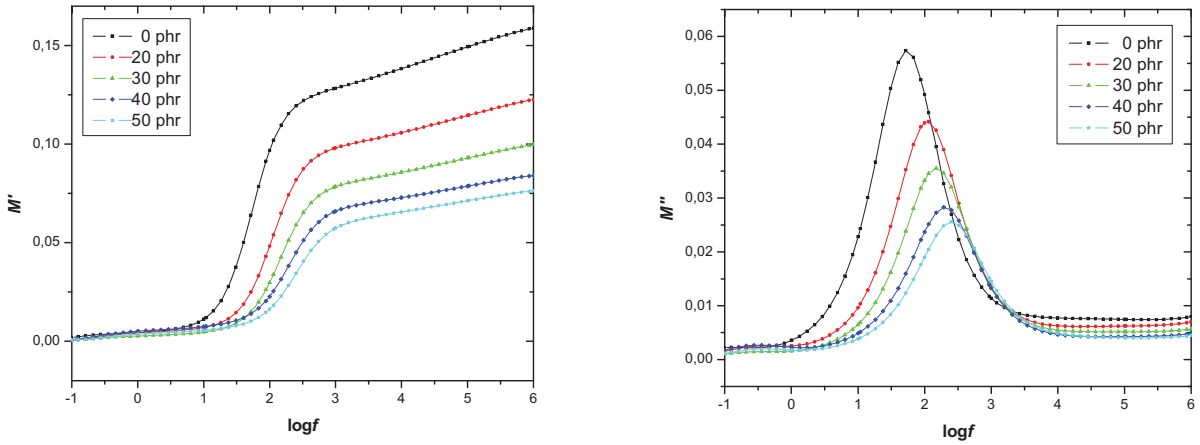

Fig. 1: Real (a) and imaginary part (b) of electric modulus as a function of frequency at 100°C, for all the examined systems.

As it can be seen in Figure 1b the loss peak position of α-mode shifts to higher frequencies as the TiC content increases. Such a variation is a clear indication for decreasing glass transition temperature (T_g) with the filler content.

Cole-Cole plots of Figure 2 give evidence for the existence of three relaxation mechanisms. The M''=f(M') plots are given at 150°C, and each of the formed semi-circles correspond to a relaxation process. Apart from the intensive semi-circle corresponding to glass/rubber transition, MWS relaxation is also present in the low frequency edge. The coincidence of the beginning of semi-circles with the origin of the graph is a clear indication that no other relaxation process is present, at lower frequencies, in all studied systems. MWS effect occurs in electrically heterogeneous systems [6-8] due to the accumulation of charges at the interface of the system, where large dipoles are formed. The inertia of the dipoles to follow the alternation of the applied electrical field is the physical origin of the observed relaxation process. Moreover the variation of the semi-circles radius, corresponding to α-mode, reflects the influence of the filler content. Finally, at the high frequency end, a tendency to form a third semi-circle is present. The corresponding relaxation mechanism is attributed to re-orientation polar side groups of the polymer chains.

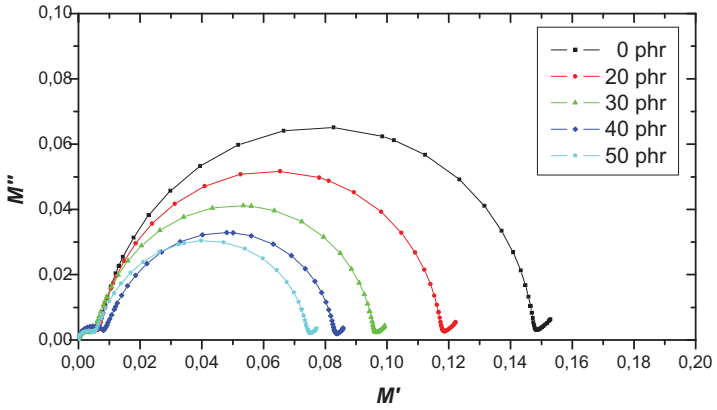

Fig. 2: Cole-Cole plots of all tested systems at 150°C.

References

1. P. Chahal, R. R. Tummala, M. G. Allen, M. Swaminathan, A novel integrated decoupling capacitor for MCM-L technology, IEEE Transactions on Components Packaging and Manufacturing Technology Part B-Advanced Packaging, 21 (2), 184-193 (1998) .
2. C. J. Dias, R. Igreja, R. Marat-Mendes, P. Inacio, J. N. Marat-Mendes, D. K. Das-Gupta, Recent advances in ceramic-polymer composite electrets, IEEE Transactions on Dielectrics and Electrical Insulation, 11 (1), 35-40 (2004).
3. G. A. Kontos, A. L. Soulintzis, P. K. Karahaliou, G. C. Psarras, S. N. Georga, C. A. Krontiras, M. N. Pisanias, Electrical relaxation dynamics in TiO2 – polymer matrix composites, eXPRESS Polymer Letters Vol.1, No.12, 781–789 (2007).
4. F. El-Tantawy, New Double Negative and Positive Temperature Coefficients of Conductive EPDM Rubber TiC Ceramic Composites, European Polymer Journal 38, 567 – 577 (2002).
5. K. F. Cai, D. S. McLachlan, N. Axen, R. Manyatsa, Preparation, Microstructures and Properties of Al2O3 – TiC Composites, Ceramics International 28, 217 – 222 (2002).
6. G. C. Psarras, Hopping conductivity in polymer matrix–metal particles composites, Composites: Part A 37, 1545–1553 (2006).
7. G. C. Psarras, Charge Transport Properties in Carbon Black/Polymer Composites, Journal of Polymer Science: Part B: Polymer Physics, Vol. 45, 2535–2545 (2007).
8. G. C. Psarras, K. G. Gatos, P. K. Karahaliou, S. N. Georga, C. A. Krontiras, J. Karger-Kocsis, Relaxation phenomena in rubber/layered silicate nanocomposites, eXPRESS Polymer Letters Vol.1, No.12, 837–845 (2007).

Poster A1

CONTRIBUTION TO OBTAIN THE GRAFT COPOLYMERS OF ALGINIC ACID WITH PNIPAM

Ciocoiu Oana-Nicoleta, Georges Staikos

Department of Chemical Engineering, University of Patras, GR-26504 Patras, Greece

Foundation for Research and Technology-Hellas, Institute of Chemical Engineering and High Temperature Chemical Processes (FORTH/ICEHT), Patras 26504, Greece.

Designing new materials with improved or tailored properties is one of the main goals of the chemists. Two common ways are mainly used to get a material with improved or new properties: chemical synthesis or blending. Chemical synthesis is an unlimited method to get new substances with well-defined properties even it is often time consuming and not seldom costly. [1]

In polymer chemistry random copolymerization of two different monomers results in the synthesis of a new polymer showing in average the properties of the two homopolymers. If the synthesis proceeds in such a way so that the copolymer prepared is comprised by sequences of the two monomers, the properties of both the homopolymers are presented on the same macromolecule.

We have synthesized new graft copolymers by grafting poly (N-isopropylacrylamide) (PNIPAM) onto a sodium alginate (NaAl) backbone. NaAl is a biopolymer with applications in food, pharmaceutical and medical industries. PNIPAM is a water-soluble polymer showing lower critical solution temperature (LCST) behavior in aqueous solution. [2] Generally, by heating in a semi-dilute aqueous solution, graft copolymers with LCST side chains on a hydrophilic backbone show a thermothickening behavior (i.e. viscosity increases as temperature increases), oppositely to most fluids that are characterized by the well-known Arrhenius thermothinning behavior (i.e. the viscosity decreases as temperature increases). [3]

Alginic acid is a polyuronide obtainable from brown seaweed, and composed of (1-4) linked β-D-mannuronic acid and α-L-guluronic acid. In alginic acid both residues exist in the form of homopolymer blocks (M block, G block) or at a heteropolymer block (MG block). Alginic acid is the only polysaccharide which naturally contains carboxyl groups in each constituent residue, and possesses various abilities for functional materials. Considering the potential amount as a natural resource and reproduction of alginic acid, it is meaningful to develop new possibilities for it as a chemical source.

In this work, PNIPAM chains were grafted on a NaAl backbone. For this purpose amino-terminated PNIPAM was prepared by radical polymerization in aqueous solution by using the redox couple 2-aminoethanethiol hydrochloride/potassium persulphate (AET/KPS) as initiator. The grafting reaction was then realized by means of 1-ethyl-3-(3-dimethylaminopropyl carbodiimide hydrochloride (EDC) as a condensing agent in the presence of N-hydroxybenzotriazole (HOBt) as a coupling agent, so the amide group was formed. We prepared three graft copolymers G33, G50, G67, named after their weight percentage composition in PNIPAM.

They were characterized by ^{1}H-NMR spectroscopy, elemental analysis and viscometry.

The products obtained are intended to exploit the phase separation behaviour of PNIPAM that phase separates from water when temperature increases above its LCST, approximately 32°C. Below LCST, PNIPAM chains are soluble in water, so are the graft copolymer chains. Above LCST, the PNIPAM chains aggregate resulting in interchain binding in semidilute solutions of the graft copolymers. This behaviour is reversible and can be modified by polymerizing the NIPAM monomer with more hydrophilic or more hydrophobic comonomers [4]

First we've measured the dynamic viscosity of semidilute solutions, C=1% (w/v), of the above three graft copolymers, G33, G50 and G67 in water as a function of temperature.

Figure 1-a show the viscosity results, obtained. The dynamic viscosity decreases slightly as temperature increases above 25^{0}C, fallowing an expected thermothinning behavior and then starts to increase showing an interesting thermothickening behavior. This behavior is mostly observed with the G50 and G67 samples of higher composition in PNIPAM, 50 and 67 w/w% respectively.

A minimum in viscosity is observed for the three copolymers above 32^{0}C, the LCST of PNIPAM aqueous solutions. The temperature values for the minimum observed, 32.5, 35 and 40^{0}C

for G67, G50 and G33 respectively are obviously related with the composition of each copolymer. They are closer to 32^0C as the copolymers composition in PNIPAM is higher.

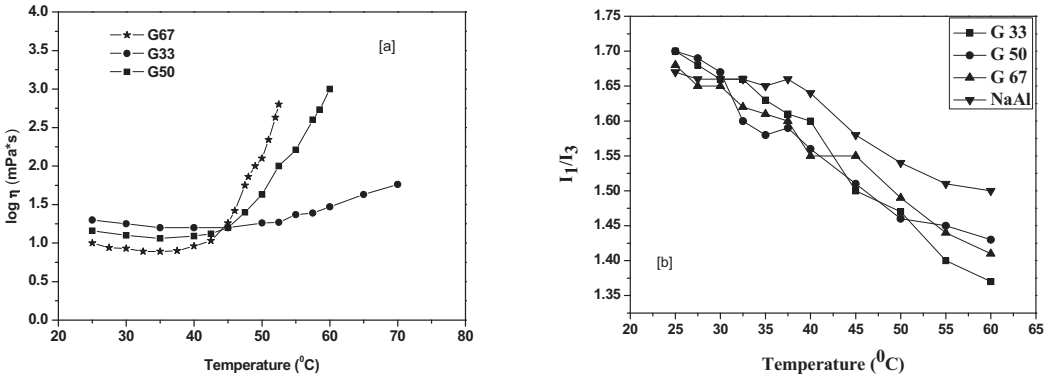

Figure 1. [a] Dynamic viscosity vs. temperature for semidilute solutions of all three graft copolymers in water, C=1% (w/v); [b] Variation of the pyrene fluorescence intensity ratio I_1/I_3 as a function of temperature for the three graft copolymers and NaAl in dilute solution, in water.

Moreover, we observe that even if at room temperature, 25^0C, G33 solution shows the highest viscosity value, it shows the less viscosity increase as temperature increases above 50^0C. Finally, at 52.5^0C η of the G67 solution increases 80 times, that of G50 8 times and of G33 1.2 times in comparison with their minimum values. This behavior indicates the critical rate composition of the graft copolymers in PNIPAM.

Fluorescence measurements (figure 2-b) were conducted by using pyrene was used as a micropolarity sensitive probe. The excitation wavelength was 334 nm. The change in the intensity ratio (I_1/I_3) of the first (I_1) vibronic band at 373 nm over the third vibronic band (I_3) at 384 nm, of the emission spectrum of pyrene was use detect hydrophobic microdomains. The measurements were taken place with dilute solutions in water prepared so that the PNIPAM concentration to be kept at 0.1%. The NaAl solution used was also 0.1%. The pyrene concentration was $5*10^{-7}$M, taken from a solution in ethanol $5*10^{-3}$M.

As we see, as temperature increases above 30^0C, I_1/I_3 starts gradually decreasing for all three graft copolymers, and forms a value of about 1.65 at 30^0C reach values at about 1.40 at 60^0C. This behavior is attributed to the formation of hydrophobic microdomains due to PNIPAM microphase separation at 32^0C.

Moreover, NaAl seems to be also somewhat sensitive in temperature as I_1/I_3 for its aqueous dilute solution decreases from about 1.65 by increasing temperature above 37.5^0C slowly at 1.50 at 60^0C, showing also some hydrophobic character.

Finally we can conclude that even if the fluorescence measurements show that in all three graft copolymers dilute aqueous solutions, hydrophobic microdomains, are formed due to PNIPAM microphase separation, as temperature increases above 30^0C, only the solutions of G50 and G67 show a considerable thermothickening behavior. This indicates the critical role of the PNIPAM side chains on the appearance of such a behavior. As they have the function of stickers their number is very important to ensure binding between the different chains.

References

1. “Polysaccharides- structural diversity and functional versatility”, Severian Dumitriu, 2005, chapter 21.
2. Heskins, M.; Guillet, J. E. J. Macromol. Sci. Chem. **1968**, A2(8),
3. Durand A.;Hourdet D. Polymer 40 (1999) 4941-4951,
4. Ranee A. Stile; Kevin E. Healy, Biomacromolecules 2002, 3, 591-600

Poster A2

High-temperature iminisation of crystalline poly(aryl ether ketones) using aromatic/aliphatic amines

Ioannis Manolakis and Howard M. Colquhoun
Department of Chemistry, University of Reading, Whiteknights, RG6 6AD, UK

The interest in chemical modification of crystalline poly(aryl ether ketones), PAEK's, and poly(ether ether ketone), PEEK, in particular, in order to facilitate their use as matrices in high-performance carbon fibre reinforced composites, has grown significantly in recent years[1-7]. The aim is to synthesize amorphous, soluble PAEK derivatives which would be easier to impregnate and subsequently regenerate the original polyketone from, without affecting its valuable properties.

Amongst other studies, the use of amine monomers and the subsequent synthesis of poly(aryl ether ketimines) has been reported[4-7]. However, only one attempt to directly functionalise polyketones with appropriate amines has been claimed[8]. The scarcity of similar studies should be attributed to the required use of strong acids (e.g. trifluoroacetic acid) to dissolve PAEK's. The presence of the acid would hinder the direct use of amines, due to their sensitivity to strong acidic environments. Therefore, a high-temperature (220-240 ^{o}C) reaction of PEEK with *p*-phenylene-diamine in diphenylsulfone (DPS) was employed, in the absence of any acid catalyst[8]. Nevertheless, this study was aiming towards improving the stiffness of the material in the T_g region by crosslinking, hence a crosslinking diamine was used. As a result, this chemical modification yielded an insoluble, crosslinked amorphous poly(ether ether ketimine).

In the present work, a high-temperature direct derivatisation route was investigated, employing non-crosslinking amines, which should yield amorphous, soluble PAEK derivatives. As long as this step was successful, it was then planned to reverse the reaction, i.e. cleave the ketimine group, while retaining all valuable properties of the polyketone intact during these protection-deprotection cycles.

The reaction with 2,2-diphenylethylamine (2,2-DPEA) and 3,3-diphenylpropylamine (3,3-DPPA) at 270 ^{o}C for 3h in diphenylsulfone as solvent proved to be quite successful for PEEK and PEK. ^{1}H-NMR, ^{13}C-NMR, IR, DSC and elemental analysis data were all consistent with the presence of an amorphous polymer bearing the C=N double bond and the flexible aliphatic/aromatic residue of the specific amines. Reaction schemes with PEEK are shown in Figure 1:

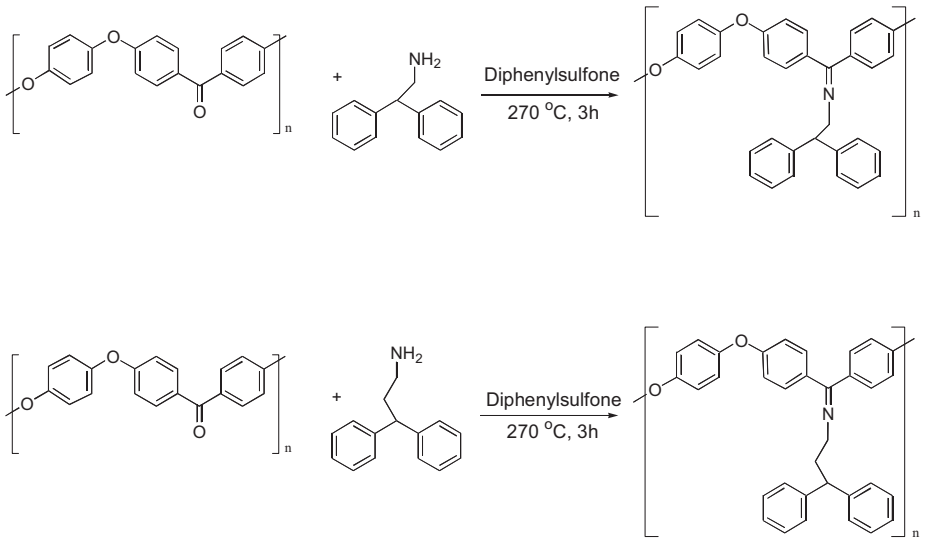

Fig.1. PEEK-2,2-DPEA and PEEK-3,3-DPPA synthesis

Table 1. Properties of imine derivatives of PEEK and PEK

Entry	Sample	T_g (onset) (°C)	M_n (RI)	M_w (RI)	T_m (°C)	η_{inh} in $CHCl_3$ (dL/g)
1	PEEK-2,2-DPEA derivative	128	27,800	49,300	-	0.25
2	PEEK-3,3-DPPA derivative	112	21,400	45,300	-	0.32
3	PEK-2,2-DPEA derivative	130	21,600	42,300	-	0.24
4	PEK-3,3-DPPA derivative	109	17,300	35,600	-	0.25

However, the deprotection of the imine derivatives of PEEK was not a trivial task. A wide range of acid- and base-catalysed, homogeneous and heterogeneous hydrolytic routes were investigated. Although deprotection was certainly achieved, in no case was it possible to obtain a deprotected PEEK with all its valuable properties intact. In most cases, chemical regeneration of the carbonyl groups occurred, but crystallinity and/or molecular weight were always significantly compromised. A characteristic set of data for the starting PEEK polymer and the corresponding protected-then-deprotected polymers, using different deprotection routes, is shown below:

Table 2. Characterisation of deprotected imine derivatives of PEEK

Entry	Sample	Acid hydrolysis route	T_g (onset) (°C)	T_m (°C)	M_n	M_w
1	Starting PEEK		144	342	28,900	81,100
2	Deprotected imine	Heterogeneous: 24h reflux in an aqueous 10% acetic acid solution	149	327	26,800	74,700
3	Deprotected imine	Homogeneous: 24h at r.t., dissolving in THF and adding 10% v/v of an aqueous 20% methane sulfonic acid solution	150	319	29,200	196,000
4	Deprotected imine	Same as entry 3	147	313	28,900	151,000
5	Deprotected imine	Same as entry 3	147	307	25,600	155,000

References

1. D.R. Kelsey, L.M. Robeson, R.A. Clendinning and C.S. Blackwell, *Macromolecules*, 1987, **20**, 1204.
2. W. Risse and D.Y. Sogah, *Macromolecules,* 1990, **23(18)**, 4029.
3. H.M. Colquhoun, F.P.V. Paoloni, M.G.B. Drew and P. Hodge, *Chem. Commun.*, 2007, 3365.
4. J. Roovers, J.D. Cooney and P.M. Toporowski, *Macromolecules*, 1990, **23**, 1611.
5. A.E. Brink, S. Gutzeit, T. Lin, H. Marand, K. Lyon, T. Hua, R. Davis and J.S. Riffle, *Polymer*, 1993, **34(4)**, 825.
6. B.E. Lindfords, R.S. Mani, J.E. McGrath and D.K. Mohanty, *Makromol. Chem., Rapid Commun.*, 1991, **12**, 337.
7. Y. Bourgeois, J. Devaux, R. Legras and I.W. Parsons, *Polymer*, 1996, **37(14)**, 3171.
8. S.A. Thompson and R.J. Farris, *J. App.Polym. Sci.,* 1988, **36**, 1113.

Poster A3

Synthesis, Characterization and Enzymatic Hydrolysis of Poly(propylene adipate)-co-poly(ε-caprolactone) block copolymers.

Stavroula G. Nanaki, Dimitrios N. Bikiaris
Laboratory of Organic Chemical Technology, Department of Chemistry, Aristotele University of Thessaloniki, 541 24, Thessaloniki, Macedonia, Greece.
e-mail: nanakistauroula@yahoo.gr

Introduction

PCL is an aliphatic polyester, biodegradable and biocompatible, with high crystallinity. It was found that when its molecular weight is above 15000 the biodegradation rate is negligible[1]. In order to reduce this disadvantage it was thought to prepare copolymers of PCL with aliphatic polyester that has higher biodegradation rate. As such it was selected PPAd[2]. Our intension was to produce biocompatible copolymers with a sufficient biodegradability rate that will found use as pharmaceutical matrices.

Experimental

Adipic acid (Ad) (purum > 99.5%) was purchased from Fluka, 1,3- propanodiol (1,3-PDO) (purum 99.6+%) and ε-caprolactone (ε-CL) (purum 99%) were obtained from Aldrich. Titanium(IV)butoxide (TBT) (purum 97%) was also purchased from Aldrich and was used as catalyst.
The aliphatic polyester poly(propylene adipate) (PPAd) was synthesized by the two-stage melt polycondensation method (esterification and polycondencation) in a glass reactor[3]. Esterification took place at 180 °C while polycondensation at 240 °C. Poly(ε-caprolactone) (PCL) was synthesized by ring opening polymerization of ε-CL. PPAd/PCL copolymers with various molar ratios, such as 10/90, 20/80, 30/70, 40/60, 50/50 and 75/25 were prepared by adding the proper amounts of PPAd and PCL and following the procedures made by Seretoudi et al[4].
Intrinsic viscosity [η] measurements were performed by using an Ubbelohde viscosimeter at 25 °C. All polymers and copolymers were dissolved at chloroform and at concentration 1 %w/v. Intrinsic viscosity [η] was calculated using the Solomon-Ciuta equation[5]

$$[\eta] = \{2[t/t_o - \ln(t/t_o) - 1]\}^{1/2} / c$$

where: c is the concentration of the solution and t and to is the flow time of the solution and of the pure solvent respectively.
Gel permeation chromatography (GPC) was used in order to determine the molecular weights of the prepared polymers and copolymers. The analysis was performed using a Waters 150C GPC equipped with differential difractometer as detector and three ultrastyragel (103, 104, 105 Å) columns in series. $CHCl_3$ was used as eluent (1mL/min) and the measurements were performed at 35 °C. Calibration was performed using polystyrene standarts with narrow molecular weight distribution. The polydispersity index M_w/M_n was also determined).
In order to study the enzymatic hydrolysis, thin films of polyesters were prepared in a hydraulic press. The films were 5 x 5 cm in size and about 0,15 mm thickness. They were incubated in Petries with a phosphate buffer solution (pH 7,2) containing 0.09 mg/mL Rhizopus delemar lipase and 0,01 mg/mL Pseudomonas Cepacia lipase. The incubation took place at 30 ± 1 °C and the media was replaced every day. After every incubation period the films were washed with distilled water and dried in a vacuum oven at 25 °C for 24h to constant weight. The degree of biodegradation was estimated from the weight loss.

Results and Discussion

A first observation made visually and was related to the colour of the prepared copolymers. PPAd is light brown in colour due to TBT which was used as catalyst or due to chromophore chemical groups formed by degradation reactions that happened during the polymerization procedure. On the other hand, PCL is white polyester. It was observed that as the amount of PCL to the copolymers became greater so their colour became whiter.

Concerning to the intrinsic viscosities of the prepared copolymers, it was found that they were lower to the pure polymers. The sample PPAd/PCL 20/80 was an exception and showed an intermediate value. In point of the molecular weights there was not a specific sequence. An observation is that all the prepared polymers and copolymers had low values of molecular weights. This was expected due to the fact that polycondensation procedure of PPAd took place at 240 °C, at a temperature higher than its melting point, so degradation reactions were dominant.

Table 1: Intrinsic Viscosity, Molecular Weights and Polydispersity Index of the neat polymers and copolymers with various molar ratios

Sample	[η] (dL/g)	Average M_n	Average M_w	M_w/M_n
PCL	0,53	15290	47724	3,12
PPAd/PCL 10/90	0,42	19332	50543	2,61
PPAd/PCL 20/80	0,53	12294	32831	2,67
PPAd/PCL 30/70	0,40	13212	34296	2,60
PPAd/PCL 40/60	0,41	16913	36076	2,13
PPAd/PCL 50/50	0,42	19418	38613	1,99
PPAd/PCL 75/25	0,43	11009	24918	2,26
PPAd	0,57	13745	28925	2,10

As can be seen by the following figure, PPAd shows a high biodegradation rate and in 3 days it was completely degraded. The same observation was done for the copolymer contained 50 %wt PPAd. As the amount of PPAd decreases the fully degradation time prolongs. For the copolymers containing 20 %wt and 10 %wt PPAd it was found that the weight loss is up to 60 and 35 % respectively for the period of 9 days. As it was expected for PCL its mass loss was imperceptibly and reaches at the slight amount of 5% even after 9 days.

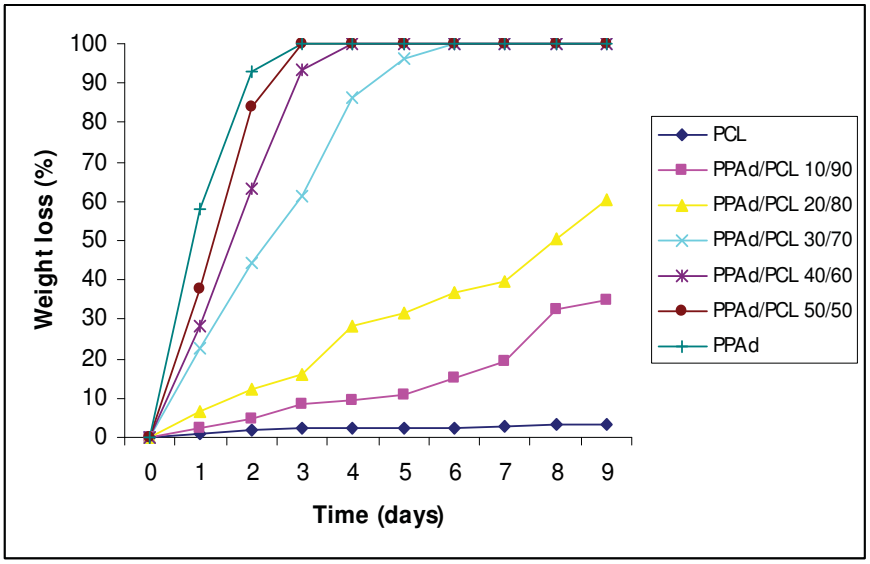

Figure 1: Weight loss caused by enzymatic hydrolysis

References

1. Fields, R. D.; Rodriguez, F. ; Finn, R. K., J Appl Polym Sci 1974, 18, 3571
2. Zorba T., Chrissafis K., Paraskevopoulos K.M., Bikiaris D.N. Polym Degrad Stab 2007, 92, 222.
3. Roupakias, C. P.; Bikiaris, D. N.; Karayannidis, G.P., J. Polym Sci Part A Polym Chem 2005, 43, 3998
4. Seretoudi G.; Bikiaris, D.; Panayiotou, C. Polymer 2002, 43, 5405.
5. Solomon, O. F.; Ciuta, I. Z. J Appl Polym Sci 1962, 6, 683.

Poster A4

Synthesis, solid state and enzymatic degradation of novel poly(propylene-co-ethylene succinate)s

George Z. Papageorgiou, Palazi Irini, Andria Poulheria, Charalampos A. Stergiou, Dimitrios N. Bikiaris,

Laboratory of Organic Chemical Technology, Department of Chemistry, Aristotle University of Thessaloniki, GR- 541 24, Thessaloniki, Macedonia, Greece.

Recent years, environmental protection has become of primary importance. Thus, more and more attention has been paid to development and applications of environmental friendly materials, like biodegradable polymers. The enzymatic degradation of biodegradable polyesters is sensitive to their chemical structure, the hydrophilic/hydrophobic balance within the main chain, molecular weight, the specific solid-state morphology and crystallinity. Copolymers are characterized by higher degradation rates.[1]

Poly(ethylene succinate) (PESu) is one of the most important synthetic biodegradable polyesters due to its sufficient mechanical properties as well as its high thermal stability and it is also commercially available.[2-3] On the other hand, poly(propylene succinate) (PPSu) is a relatively new biodegradable polymer, that is produced using monomers from renewable resources.[4,5] PPSu shows high biodegradation rates. However, since one of its monomers, namely 1,3-propanediol (PD) could not be produced till recently in sufficient quantities and purity, there were difficulties in its preparation and consequently, only recently a limited number of published works dealing with PPSu have been reported.[6,7] PPSu has higher biodegradation rate compared with the other two important succinate polyesters, poly(ethylene succinate) (PESu) and poly(butylene succinate) (PBSu).[8]

The aim of this work was to synthesize and study a complete series of fully biodegradable poly(propylene-co-ethylene succinate) (PPESu) copolymers. Synthesis and study of the correlation between enzymatic degradation and solid-state structure of such copolymers has not been reported before.

PPESu copolymers were synthesized following the two step polycondentation method in the melt state form succinic acid and ethylene glycol and 1,3-propanediol. The number average molecular weights of the prepared samples were found with GPC to be about 15000g/mol. The composition was determined with ^{1}H-NMR, while estimation of the degree of randomness of the copolymers from the ^{13}C-NMR spectra proved that they were essentially random. Mechanical properties decreased with increasing propylene succinate content (PSu). Multiple melting peaks were observed in DSC heating traces of copolymer samples after isothermal crystallization.

Extended analysis DSC and TMDSC experiments was carried out. It was concluded that the behaviour was associated with partial melting-recrystallization and final melting. Poly(propylene-co-ethylene succinate)s showed a eutectic behavior with the minimum melting point for 40mol% ethylene succinate content. Wide Angle X-ray Diffraction patterns showed that copolymers with more than 40mol% ethylene succinate form poly(ethylene succinate) crystals. Copolymers with less than 20mol% ethylene succinate content gave poly(propylene succinate) crystals while PPESu 60/40 and 70/30 were amorphous. The equilibrium melting points (Tm^{o}) of the copolyesters were determined using the Hoffman-Weeks extrapolation. Comonomer cocrystallization in PPESu copolyesters was thermodynamically analyzed using the Flory, Sanchez-Eby, Baur and Wendling-Suter It was found from both the thermodynamic analysis and shifts of the crystalline peaks in WAXD patterns that some extent of cocrystallization occurred. Insertion of ethylene succinate units in the PPSu is easier than insertion of the bulkier propylene succinate unit into the PESu crystal. Finally hydrolytic and enzymatic degradation in solutions containing mixture

of *Rhizopus delemar and Pseudomonas Cepacia* lipases were tested. Results showed accelerated biodegradation rates for copolymers of high propylene succinate content and low crystallinity compared to both PESu and PPSu. Thus, copolymers showed balanced mechanical/biodegradation characteristics.

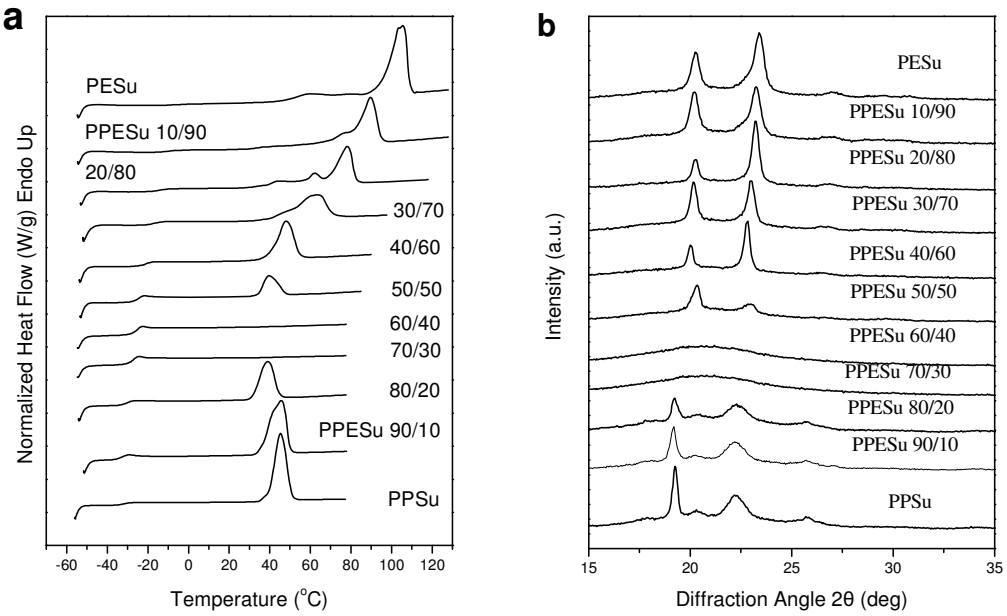

Figure 1. a) DSC heating traces and b) WAXD patterns of as received PPESu samples.

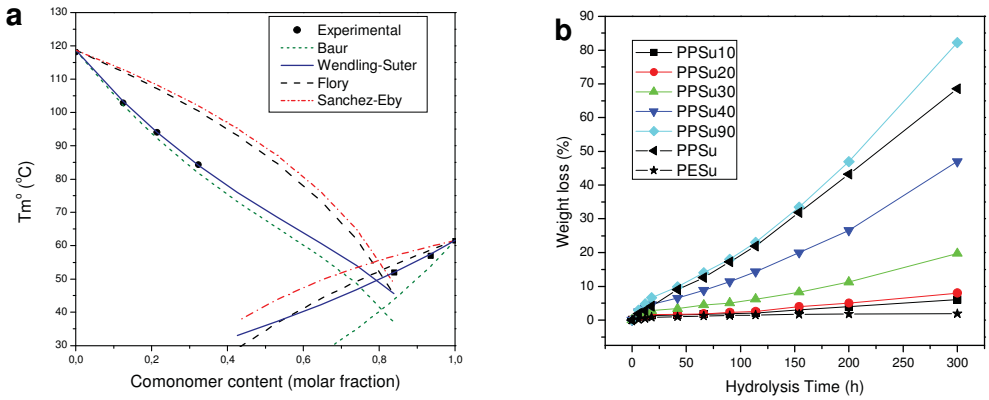

Figure 2. Melting point depression and weight loss in enzymatic hydrolysis of PPESu copolymers.

References

1. Rizzarelli, P.; Puglisi, C.; Montaudo, G. *Polym. Degrad. Stab.* **2004,** *85*, 855.
2. Z. Gan, H. Abe, Y. Doi, *Biomacromolecules* **2000**, *1*:704.
3. Z. Qiu, T. Ikehara, T. Nishi, *Polymer* **2003**, *44*, 5429.
4. Liu, Y.; Ranucci, E.; Söderqvist Lindblad, M.; Albertsson, A. C. *J. Polym. Sci. Part A: Polym. Chem*. **2001,** *39,* 2508.
5. Papageorgiou, G. Z; Bikiaris, D. N. *Polymer,* **2005,** *46*, 12081
6. Karayannidis, G.; Roupakias, C.; Bikiaris, D.; Achilias, D. *Polymer* **2003,** *44,* 931.
7. Hartlep. H.; Hussmann W.; Prayitno, N.; Meynial-Salles, I.; Zeng, A. P. *Appl. Microbiol. Biotechnol.* **2002**, *60*, 60.
8. Bikiaris, D. N.; Papageorgiou, G. Z.; Achilias, D. S. *Polym. Degrad. Stab.,* **2006**, *91*, 31.

Poster A5

β-Lactam functionalized amphiphilic block copolymers from poly(isoprene-b-ethylene oxide) copolymers

E.Kaditi, S. Pispas
Theoretical and Physical Chemistry Institute, National Hellenic Research Foundation
48 Vass. Constantinou Ave., 116 35 Athens, Greece

The ability of amphiphilic block copolymers (AmBC) to self-assemble into ordered structures, when dissolved in aqueous media has attracted research interest in the last years.[1] Micellar aggregates formed by AmBC are characterized by their unique core-shell architecture, where in an aqueous environment the hydrophobic blocks of the copolymer are segregated from the aqueous exterior to form the inner core, and the hydrophilic blocks form the corona or the outer shell. These assemblies have been successfully tested in several applications as nanocarriers, especially in drug delivery systems.[2] In such systems the nature of the core forming block and the composition of the copolymers play a decisive role in their self-assembly and encapsulation properties.

In this work β-lactam containing amphiphilic block copolymers were synthesized from poly(isoprene-b-ethylene oxide) diblock copolymer precursors, prepared by anionic polymerization high vacuum techniques, via reaction of the polyisoprene block with chlorosulfonyl isocyanate and subsequent reduction. The synthesis of the β-lactam containing amphiphilic diblock copolymers is shown, schematically, in Scheme 1.

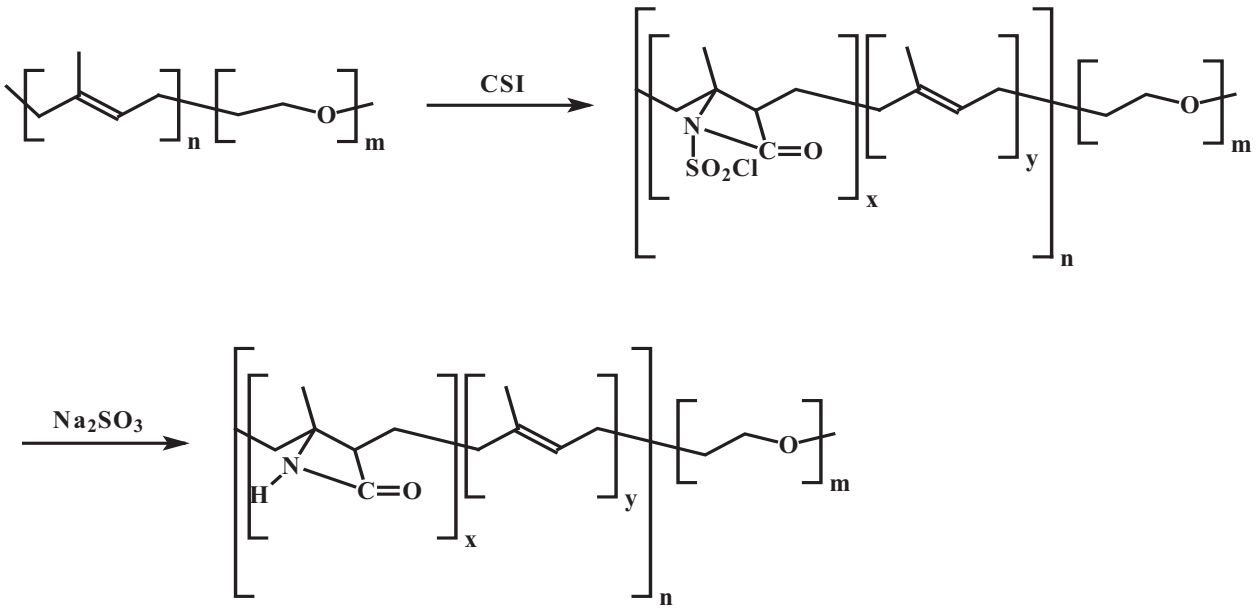

Scheme 1. Synthesis of β-lactam containing amphiphilic block copolymers from poly(isoprene-b-ethylene oxide) diblock copolymers.

The resulting block copolymers were characterized by FTIR and NMR spectroscopies, SEC and DSC, while their self-assembly in solutions was studied by dynamic light scattering (DLS) , static light scattering(SLS), fluorescence spectroscopy and AFM.

Representative ATR-FTIR spectra of the precursor and final copolymers are shown in Figure 1. In this figure the characteristic peaks of β-lactam absorptions at 1750 cm^{-1} and 3300 cm^{-1} can be clearly observed. The peaks at 1000-1100 cm^{-1} are derived from the C-O-C vibrations of the PEO block and in the regions 750-1000 cm^{-1} and 1200-1500 cm^{-1} the peaks are attributed to the carbonic chain. The spectra support the successful incorporation of the β-lactam moiety in the PI block of the copolymers.

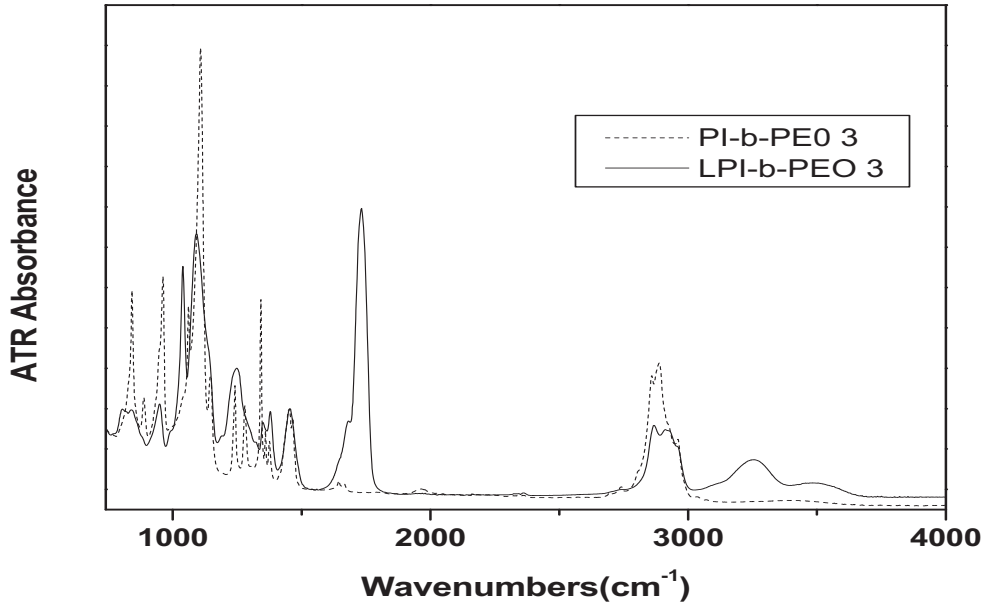

Figure 1. ATR-FTIR spectrum of poly(isoprene-b-ethylene oxide) precursor (PI-b-PEO) and β-lactam containing block copolymer (LPI-b-PEO).

From dynamic and static light scattering measurements in organic solvents it can be concluded that the β-lactam functionalized block copolymers form rather loose aggregates, due to interchain hydrogen bonding. Light scattering measurements in aqueous solutions show a lower aggregation number and larger dimensions for the β-lactam containing copolymers compared to the PI-b-PEO precursors. Fluorescence spectroscopy experiments, using a pyrene as a probe, indicate an increase in the cmc for the β-lactam functionalized copolymers. The results may be explained by the increased hydrophilic character of the PI block as β-lactam moieties are introduced.

References

1. Alexandridis, P.; Lindman, B., Eds *Amphiphilic Block Copolymers. Self Assembly and Applications*, Elsevier: Amsterdam, 2000.
2. N. Nishiyama, K. Kataoka Adv. Polym. Sci. 2006, 193, 67.

Poster A6

Responsive Polymer Brushes on flat surfaces by Surface – Initiated Polymerization

A. Mateescu[1,2] and M. Vamvakaki [2,3]
[1]*Department of Chemistry, University of Crete, 710 03 Heraklion, Crete, Greece*
[2]*Institute of Electronic Structure and Laser, Foundation for Research and Technology - Hellas, 711 10 Heraklion, Crete, Greece*
[3]*Department of Materials Science and Technology, University of Crete, 710 03 Heraklion, Crete, Greece*

Tethering of polymer brushes covalently onto a solid substrate is an effective method to tailor the chemical and physical properties of surfaces.[1] "Smart" polymer brushes exhibiting properties that change in response to external stimuli such as temperature, pH, electric or optical field can be used to create stimuli-responsive surfaces. The "grafting from" approach has been employed for the synthesis of well-defined polymer brushes of high grafting densities covalently anchored to the substrate.[2,3] Besides, Atom Transfer Radical Polymerization (ATRP) is a controlled/"living" radical polymerization that has gained great attention during the last decade because of its tolerance to a wide range of polymerizable monomers and its mild polymerization conditions.[4] Consequently, surface-initiated ATRP has been successfully used to polymerize homopolymer and block copolymer brushes from both organic and inorganic substrates.[5]

In this study, we report the synthesis and characterization of stimuli-responsive homopolymer and block copolymer brushes based on 2-(dimethylamino)ethyl methacrylate (DMAEMA), (hydrophilic and ionizable), 2-(diethylamino)ethyl methacrylate (DEAEMA), (hydrophobic and pH-sensitive) and tetrahydropyranyl methacrylate (THPMA), a methacrylate ester easily hydrolyzed to methacrylic acid (MAA) (hydrophilic and ionizable), on gold and silicon substrates by ATRP. The prepared polymeric films were characterized by ellipsometry, Atomic Force Microscopy (AFM), Attenuated Total Reflectance (ATR)-IR spectroscopy and contact angle measurements.

Experimental. The initiator self-assembled monolayer (SAM) was formed by immersing a gold or silicon substrate into a solution containing the appropriate initiator; ω-mercaptoundecyl bromoisobutyrate was used for the gold-coated substrate and 3-(2-bromoisobutyramido)propyl (trimethoxy)silane for the silicon surface. Next, the initiator coated substrate was placed in a reaction flask under a nitrogen atmosphere. A degassed solution of the monomer and the catalyst system (transition metal salt and the appropriate ligand) was added. The polymerization was allowed to proceed for the desired period of time, after which the reaction was quenched by exposure to air. For the synthesis of block copolymer brushes the above procedure was repeated by immersing a polymer coated substrate in a solution of the second monomer.

Results and Discussion. Table 1 summarizes the ATRP reaction conditions and the characteristics of the synthesized polymer brushes. The synthesis of acrylic and methacrylic acids by ATRP is problematic, due to the coordination of the carboxylic group with the copper catalyst. Thus, the acidic brushes were synthesized using the protected monomer, THPMA, followed by acid hydrolysis. For the amine-based brushes PDMAEMA and PDEAEMA, an increase of the dry polymer film thickness was observed with time, suggesting the controlled growth of the polymer chains. A high grafting density of 0.56 chains/nm^2 was calculated for the surface polymerized PDMAEMA on gold substrate after 2 h of reaction. In order to verify the livingness of our technique block copolymer brushes were also synthesized (Table 1). Ellipsometric measurements showed an increase in the film thickness after the polymerization of the second monomer, verifying that the homopolymer chains remained active and capable of reinitiation. Figure 1 shows the ATR-FTIR spectrum of a 20 nm PDMAEMA film on gold. The carbonyl group at 1740 cm^{-1}, the C-H symmetric and asymmetric vibration modes of the -CH_2- and –CH_3 groups at 2967 and 2930 cm^{-1} and the C-O stretching at 1255 cm^{-1} suggest the successful grafting of the polymer on the gold substrate.

Table 1. Polymer brushes synthesized by ATRP

Sample	Reaction Conditions	Reaction Time	Brush Thickness[a]	Film Roughness[b]
PDMAEMA*	Cu(I)/Cu(II)/Bpy, MeOH/H_2O = 4/1	30 min	5 nm	0.63 nm
		60 min	10 nm	0.74 nm
		120 min	20 nm	0.64 nm
PDEAEMA*	Cu(I)/1,1,4,7,10,10-hexamethyltriethylene tetramine (HMTETA), MeOH	3 h	22 nm	0.94 nm
		6 h	28 nm	0.66 nm
PTHPMA*	Cu(I)/HMTETA, MeOH	2 h	30 nm	0.56 nm
PDMAEMA**	Cu(I)/Cu(II)/Bpy, MeOH/H_2O = 4/1	3 h	6 nm	0.35 nm
		5 h	23 nm	0.5 nm
PDEAEMA**	Cu(I)/HMTETA, MeOH	4 h	16 nm	0.7 nm
PDMAEMA*	Cu(I)/Cu(II)/Bpy, MeOH/H_2O = 4/1	30 min	5 nm	0.63 nm
PDMAEMA*	Cu(I)/Cu(II)/Bpy, MeOH/H_2O = 4/1	120 min	19 nm	0.64 nm
PDMAEMA-*b*-PDEAEMA	Cu(I)/HMTETA, MeOH	60 min	32 nm	0.34 nm
PTHPMA*	Cu(I)/Cu(II)/Bpy, MeOH	5 h	7 nm	0.9 nm
PTHPMA-*b*-PDMAEMA	Cu(I)/Cu(II)/Bpy, MeOH/H_2O = 4/1	2 h	12 nm	0.52 nm

* on a gold substrate; ** on a silicon substrate; [a] by ellipsometry; [b] by AFM

AFM revealed the preparation of very smooth polymer films with a roughness below 1 nm (Table 1). The surface anchored film covered the surface completely and homogeneously, suggesting that the ATRP polymerization proceeded uniformly on the substrates. Contact angle measurements on the polymeric films were performed at pH 3 and 8. The amine-based polymer surfaces became more hydrophilic at pH 3 (~ 60° contact angle) compared to pH 8 (70° contact angle for PDMAEMA and 82° contact angle for PDEAEMA) due to the protonation of the tertiary amine groups at low pH (Figure 2), while the hydrophilicity of the MAA-based surface increased at high pH (contact angle 64° at pH 3 and 56° at pH 8) upon neutralization of the acid moieties.

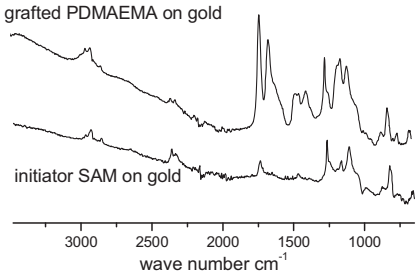

Figure 1. ATR-FTIR spectra of the grafted initiator and a PDMAEMA film on gold.

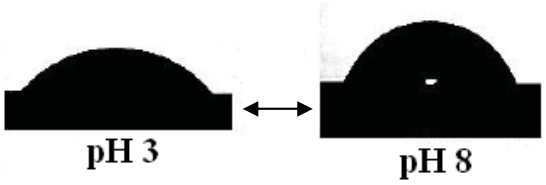

Figure 2. Contact angles on a grafted PDEAEMA film at pH 3 and 8.

Acknowledgments. Dr. G. Konstantinidis is acknowledged for the preparation of the gold substrates. We would also like to thank Prof. N. A. Chaniotakis for the use of the FTIR instrument. GSRT is acknowledged for funding (PENED 2003, 03EΔ623).

References

1. A. Bhattacharya, B. N. Misra, *Prog. Polym. Sci.* **2004**, *29*, 767-814.
2. N. Ayres, G. Boyes, W. J. Brittain, *Langmuir* **2007**, *23*, 182-189.
3. D. M. Jones, A. A. Brown, W. T. S. Huck, *Langmuir* **2002**, *18*, 1265-1269.
4. K. Matyjaszewski, J. Xia, *Chem. Rev.* **2001**, *101*, 2921-2990.
5. K. Matyjaszewski, P. J. Miller, N. Shukla, B. Immaraporn, A. Gelman, B. B. Luokala, T. M. Siclovan, G. Kickelbick, T. Vallant, H. Hoffmann, T. Pakula, *Macromolecules* **1999**, *32*, 8716-8724.

Poster A7

On the formation of apatite aggregates through precipitation from polymer-containing solutions

Vassiliki A. Kosma, Konstantinos G.Beltsios
Department of Materials Science and Engineering, University of Ioannina, Ioannina, Greece, GR-45110.

Abstract
Solution growth of apatite in the presence of gelatin is found to lead to a rich spectrum of morphologies, among them spherulitic aggregates of various types of morphological elements and tablet-based formations. Spherulite aggregates obtained under various conditions consist of radiating needles or radiating plates or dense packings of blocks or elaborate lacy elements. Tablets can be compact or contain parallel arrangements of needles or ribbons and constitute morphological intermediates for one of the spherulitic morphologies observed. Replacement of gelatin by appropriate water-soluble polymers also leads to related, though, usually, less perfect apatite-aggregate morphologies.

Introduction

The crystallization of any particular substance might be affected by the presence of the most disparate substances. The effect might pertain to one or more of various processes such as primary nucleation, preferential directional growth, formation of crystalline aggregates of regular or quasi-regular morphologies etc. High aspect ratio apatite particles constitute a familiar type of reinforcement of natural biocomposites[1]. In the case of apatite solution precipitation, usually monetite ($CaHPO_4$, Ca/P =1) forms first, octacalcium phosphate (OCP, $Ca_8(HPO_4)_2(PO_4)_4{\cdot}5H_20$, Ca/P= 1.33) follows and apatite (HAP, $Ca_{10}(PO_4)_6(OH)_2$, Ca/P = 1.67) occurs last[2]; somewhat different phase sequences and a wealth of morphologies are possible. Our basic approach is a polymeric extension of a HAP precipitation route used by Zhang et al[3]. The inclusion of polymers affects structural outcome in various ways one of which is interaction through hydrogen bonding. The latter interaction is, in principle, possible between amidic substances, such as biopolymeric gelatin, and apatite (or its precursor phases), but the employment of alternative water-soluble polymers bearing groups such as –OH, $-NH_2$, -NH-, -O- etc and including PVOH, PEO, PVP and polyacrylamide may also be considered.

Experimental

A basic recipe including calcium and phosphate sources and urea[3] was modified through addition of water-soluble polymers at levels ranging from 0.2 % to the polymer solubility limit. Most reactions were carried for 48 hrs ($t_{standard}$, time sufficient for full conversion in the absence of a polymer) but both shorter and longer times were also examined. Products obtained were examined by SEM, XRD and IR.

Results and Discussion

The polymer-free version of precipitation leads to the formation of loose HAP needles, while most of the polymers added favor the formation of precipitant clusters, frequently of the radiating type. In addition, polymers favor slower conversion; the effect tends to be stronger for higher polymer concentrations and molecular weights, possibly a refection of reduced diffusion coefficients pertinent to one or more diffusion-controlled reaction steps. Figure 1 shows the effect of polymer concentration in the case of gelatin and a fixed reaction time. Increasing gelatin content shifts product from pure HAP (0 % gelatin) to pure monetite early precursor phase (20 % gelatin). Figure 2 shows representative corresponding morphologies: (a, 5% gelatin) gives radiating clusters of needles with a Ca/P ca.1.55-1.60 (: approaching HAP composition), (b, 10 % gelatin) yields platelet clusters with a Ca/P ca. 1.05 (: close to monetite) plus surface sponges with a Ca/P ca. 1.45, while (c, 20% gelatin) offers a 2-D radial arrangement of blocks with Ca/P = 1.01 (: monetite). The effect of 5% additions of polymers other than gelatin is shown in Figure 3, for PVOH, PEO (: weakest effect) and polyacrylamide.

Clusters of high aspect ratio particles achieved in all cases might be appropriate for polymer reinforcement, with a processing benefit, when compared to the addition of loose high aspect ratio particles.

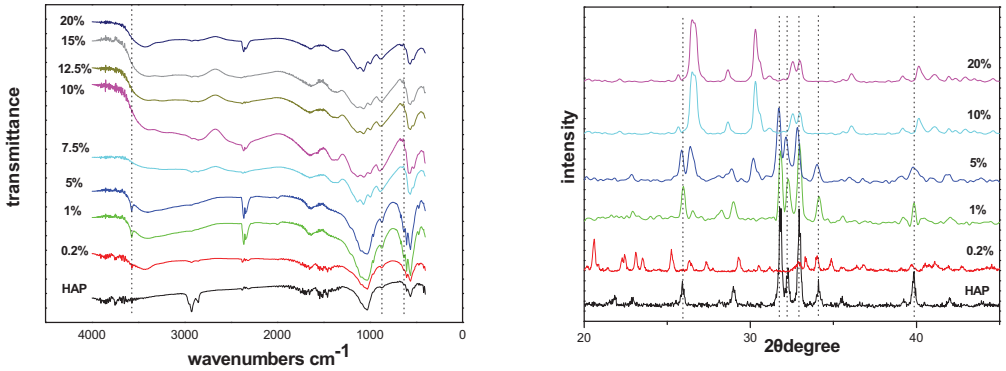

Figure 1: FTIR spectra and XRD patterns of samples with different gelatin addtions

Figure 2: a, b, c are morphologies for 5, 10 and 20% w/w gelatin respectively

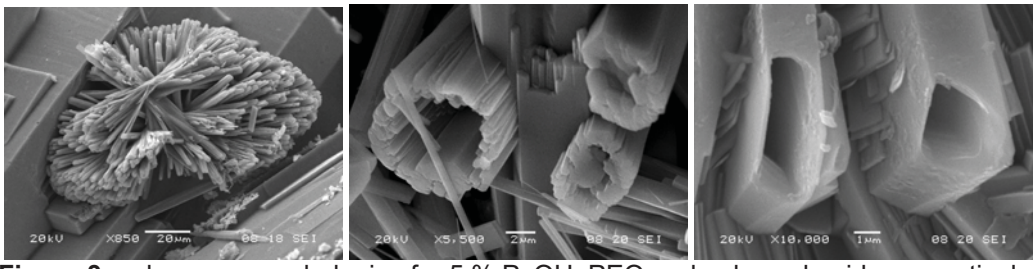

Figure 3: a, b, c are morphologies for 5 % PvOH, PEO and polyacrylamide respectively.

Conclusions

Modification of a procedure of HAP solution precipitation by the addition of commercial polymers slows down conversion but offers diverse cluster morphologies of high aspect ratio particles, some of which might offer a processing benefit when used for polymer reinforcement.

References

1.J. F. V. Vincent, Structural Biomaterials, Revised Ed., Princeton U. Press, 1990
2.M. Mathew and S. Takagi, *Journal of Research of the NIST*, 106, 1035, 2001
3.H. Zhang, Y, Wang, Y. Yan and S. Lim, *Ceramics International*, 29, 413, 2003

Poster A8

A kinetic investigation of vinyl neo-decanoate bulk free-radical polymerization over the full monomer conversion

D.S. Achilias
Laboratory of Organic Chemical Technology, Department of Chemistry
Aristotle University of Thessaloniki, 541 24 Thessaloniki
E-mail: axilias@chem.auth.gr

Introduction

Vinyl neo-decanoate (VnD) or vinyl versatate is a vinyl ester of versatic acid, a synthetic saturated monocarboxylic acid of highly branched structure containing ten carbon atoms. VnD is usually used as a modifying co-monomer in the preparation of vinyl acetate (VAc) based polymer lattices, which find applications in the manufacture of specialty emulsion paints due to the very good alkali resistance, UV resistance and hydrophobicity that offer to the final polymer latex[1]. Emulsion copolymerization of VnD with VAc results in a latex with improved hydrolytic stability owing to a protection that each branched vinyl ester group offers to the VAc groups by an "umbrella effect". Also, VnD is used as co-monomer with acrylates for the production of emulsion, solution and bulk polymers such as acrylic automotive and powder coatings[1]. Since the glass transition temperature of VnD is around -3^{o}C, adding VnD in VAc (Tg=33^{o}C) or methyl methacrylate (MMA) (Tg=105^{o}C) provides the emulsion with elastomeric properties.
Despite its commercial importance very few papers dealing with the polymerization kinetics of this monomer have been published in literature[2]. In this investigation, the free radical polymerization kinetics of VnD in bulk is examined in detail using Differential Scanning Calorimetry (DSC). Azo-bis-isobutyronitrile (AIBN) was used as a free radical initiator and a wide range of temperatures and initial initiator concentrations were considered.

Experimental

Experiments were performed in a nitrogen atmosphere using the DSC-Pyris 1 (Perkin-Elmer) equipped with the Pyris software for windows. The reaction temperature was continuously recorded and maintained constant (within $\pm$ 0.01 ^{o}C) during the whole conversion range. The reaction exotherm (in normalized values, W/g) at a constant temperature was recorded as a function of time. The rate of heat release (d(ΔH)/dt) measured by the DSC was directly converted into the overall reaction rate (dx/dt) using the following formula:

$$\frac{dx}{dt} = \frac{1}{\Delta H_T}\frac{d(\Delta H)}{dt}$$

where ΔH_T denotes the total reaction enthalpy.
The degree of conversion was calculated by integrating the area between the DSC thermograms and the baseline established by extrapolation from the trace produced after complete polymerization (no change in the heat produced during the reaction). All the experimental were repeated twice.

Results and Discussion

Initially the evolution of reaction rate with time of VnD was compared to that of VAc, MMA and butyl acrylate (BuA), (monomers which are used in the formation of emulsion coatings and primers) and is illustrated in Figure 1. As it can be seen, the reaction rate curve of VnD resembles that of VAc although not exactly the same. MMA polymerization exhibits no induction time in contrast to BuA polymerization. Moreover, VnD exhibited the lower maximum reaction rate and polymerization continuous for a longer time with a double bond conversion less than 90% achieved even after 60 min of reaction.
Furthermore, the effect of initial initiator concentration and reaction temperature on the reaction rate variation as a function of time appears in Figures 2 and 3, respectively. As it was expected,

reaction rate was favored by increased temperatures and initial initiator concentrations. These data are useful to estimate kinetic rate constants under different experimental conditions.

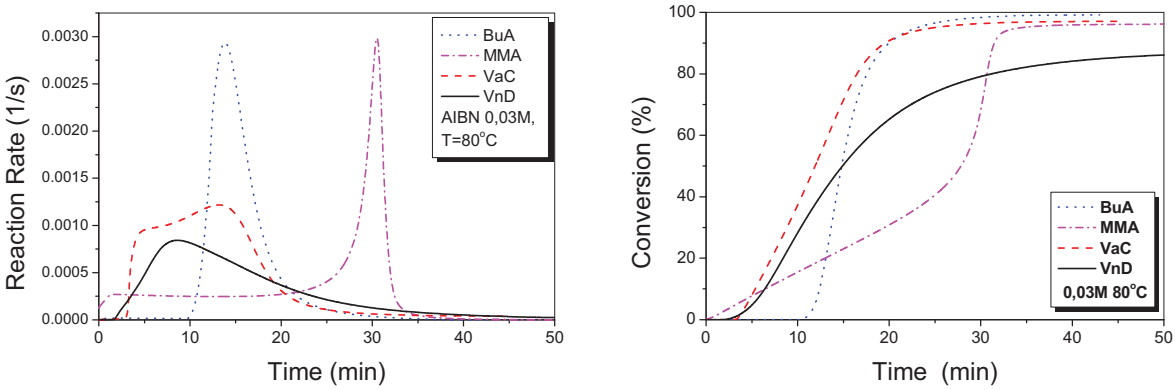

Fig. 1 Effect of the monomer chemical structure on the variation of reaction rate versus time (a) or conversion versus time (b), Initiator AIBN 0.03 M and temperature 80°C.

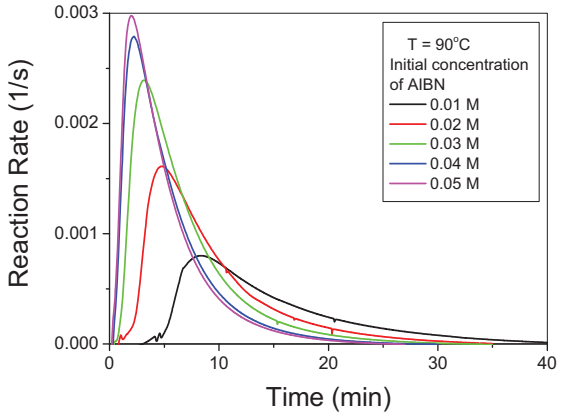

Fig. 2 Effect of initial initiator concentration on the variation of reaction rate versus time

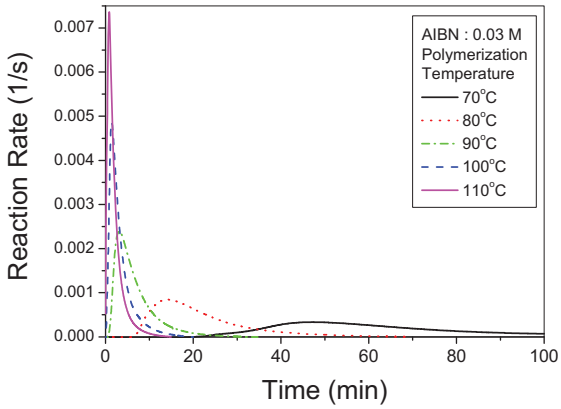

Fig. 3 Effect of temperature on the variation of reaction rate versus time

The glass transition temperature of the all VnD samples measured with DSC, was in the range of -2 to -5°C, which makes it an elastomeric material.
Furthermore, a simple mathematical model was developed to predict the polymerization kinetics over the full monomer conversion range using parameters already published, as well as estimated in this investigation. Chain transfer reactions were found to play an important role.
Finally, in order to simulate the performance of this monomer in commercial applications, several copolymerizations were carried out using as co-monomer vinyl acetate, methacrylate (MMA) and an acrylate monomer (BuA). The results showed that copolymerization with VAc results in homogeneous polymers with similar reactivity ratios. In contrast, when VnD was copolymerized with MMA, the large differences in the reactivity ratios result into a two stage reaction with bimodal MWD.

References

1. P.A. Lovell and M.S. El-Aasser, Eds. Emulsion Polymerization and Emulsion Polymers, J.Wiley and Sons, W. Sussex, 1997.
2. B.T.T. Pham, M. P. Tonge, M. J. Monteiro, and R. G. Gilbert, Grafting Kinetics of Vinyl Neodecanoate onto Polybutadiene, *Macromolecules* 2000, *33,* 2383-2390

Poster A9

SYNTHESIS AND CHARACTERIZATION OF 2nd GENERATION DENDRITIC TERPOLYMER

Rangou S.[1], Thomas E. L.[2] and Avgeropoulos A.[1*]
[1]*Department of Materials Science & Engineering, University of Ioannina, University Campus, 45110 Ioannina, Greece*
[2]*Department of Materials Science & Engineering, and Institute of Soldier Nanotechnologies Massachusetts Institute of Technology, 77 Mass. Ave., 02139 Cambridge, MA, USA*

Introduction

Advances in synthetic polymer chemistry and nanotechnology applications of polymers lead to the necessity of designing complex architectures in order to combine the observed properties of the more simple structures. Some of the new potentials are ascribed to the new physical and chemical properties which are very much affected by the long-chain branching when compared to the corresponding linear structures.

We report the synthesis of 2nd generation dendritic terpolymer consisting of polybutadiene (PB) of 1,4 microstructure, polyisoprene (PI) enriched in 3,4 microstructure (at least 55% $PI_{3,4}$) and polystyrene (PS). The main aspect was the synthesis of polymers exhibiting high molecular and compositional homogeneity. The preparation of these materials was achieved via anionic polymerization techniques in combination with chlorosilane chemistry potentials. The molecular characterization of the intermediate products and the final dendritic material was accomplished via Size Exclusion Chromatography (SEC), Membrane Osmometries (MO), Dilute Solution Viscometry Differential Scanning Calorimetry (DSC) and Proton Nuclear Magnetic Resonance Spectroscopy (^{1}H-NMR), leading to the conclusion that they can be considered model polymers. Morphological studies have been conducted via Transmission Electron Microscopy (TEM) to the terpolymer sample exhibiting microphase separation between the polydiene segments leading to possibly new 3-phase morphologies. It should be mentioned that the synthesis approach described in this study is different from the corresponding procedures reported by the Hadjichristidis' group[1,2] and has been used already for both dendritic homopolymers and copolymers reported in earlier research studies[3,4] by our group.

Results

The purification of all reagents (monomers, solvents, initiator, linking and termination reagents) was carried out following the standards required for anionic polymerization procedures. The molecular characterization instrumentation used (SEC, MO, Viscometry and ^{1}H-NMR) is described analytically elsewhere[3]. The DSC experiments were carried out, employing a TA Instruments DSC 2910 modulated DSC, in order to obtain preliminary information concerning the microphase separation of the three components.

Synthesis and Molecular Characterization of Dendritic Terpolymer of the [(PS)(PB)(PI)]$_3$ Type

The synthetic procedure of the dendritic terpolymer of the [(PS)(PB)(PI)]$_3$ type is exhibited in Figure 1. The number average molecular weight of the final dendritic terpolymer was 198.000 g/mol. Due to impurities and steric hindrance phenomena the final product was separated from the initial and intermediate products by fractionation in a solvent/non-solvent system (toluene/methanol respectively). The molecular characterization of the final neat

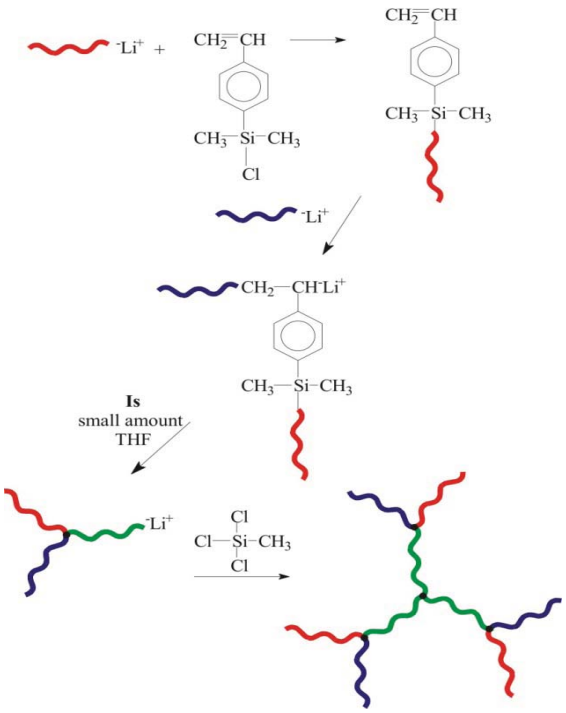

Figure 1. Synthesis reactions of the [(PS)(PB)(PI)]$_3$ 2nd generation dendritic terpolymers.

terpolymer lead to the conclusion that it can be considered a model polymer, since it exhibits increased molecular and compositional homogeneity.

Morphological Characterization of Dendritic Terpolymer of the [(PS)(PB)(PI)]$_3$ Type

Three different glass transition temperatures were exhibited from the DSC experiments. The values were approximately T_{g1}~-80 °C, T_{g2}~-30 °C, and T_{g3} ~ 100 °C. According to the literature[6] the first and last values correspond approximately to 1,4-PB and PS, respectively. If the chains were mixed, the values would be higher for the PB and lower for the PS, which is not observed, leading to the conclusion that the third T_g corresponds to the high 3,4-PI component. The T_g of the PI segment (with increased 3,4 microstructure) is significantly different compared to that of high 1,4-PI (~-60 °C) and that of the 1,4-PB (~-80 °C). The observation of three different glass transition temperatures thus suggests a well microphase-separated system. The morphological study with Transmission Electron Microscopy (TEM) on the terpolymer has proven that the two dienic segments exhibit microphase separation. Until recently it was believed that all polydiene blocks stain identically. However, OsO_4 staining depends on the detailed microstructure of a particular polydiene block. For example, with high 3,4 content (~55-60%) the PI block can stain less than the PB component with approximately 92% of 1,4-microstructure, probably due to steric hindrance, as observed via TEM and has already been reported in the literature[5]. A distinct contrast derives from the TEM images showing three different areas. The grey area is attributed to the PI segments, the black to the PB chains and the white to the PS phase. The grey areas are of greater extent and this is due to the majority of the PI branch. The white and black areas are of the same extent since the molecular weight of the PB and PS chains are approximately equal. The results from TEM are observed in Figure 2. A perforated lamellae structure is possibly exhibited (Figure 2 left image) and verified by the hexagonal packing of the two out of 3 segments corresponding to PS and PB respectively in a grey matrix (Figure 2 right image).

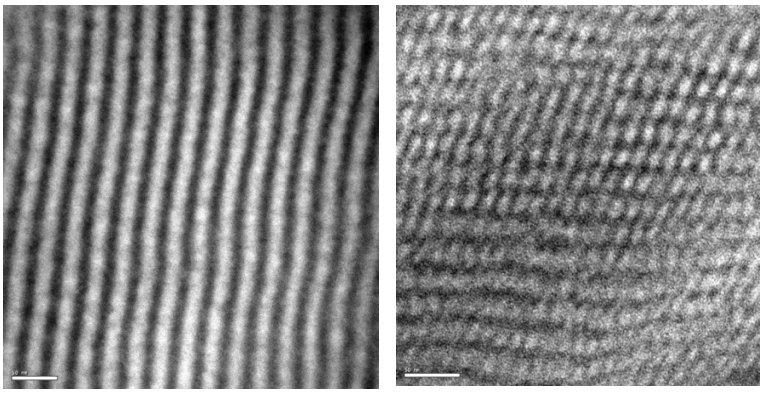

Figure 2. TEM images of the dendritic terpolymer.

It should be mentioned in this study that Small-Angle X-ray Scattering (SAXS) measurements must be employed in order to verify the specific structure. If perforated lamellae are exhibited that will lead to a new phase never observed previously for such complex systems and not predicted by theory.

Conclusions Therefore, it is very easily understood that such complex architectured materials as 2nd generation dendritic terpolymers are synthesized by employing anionic polymerization and chlorosilane chemistry leading to terpolymers with molecular and compositional homogeneity. Due to the complexity of the synthesis only one sample was prepared. The morphological characterization leads to new structures for such architectures never anticipated by theory or experiment.

References

1. I. Chalari, N. Hadjichristidis, *J. Polym. Sci. Polym. Chem.,* **40,** 1519, (2002).
2. K. Orfanou, H. Iatrou, D. J. Lohse, N. Hadjichristidis, *Macromolecules,* **39,** 4361, (2006).
3. S. Rangou, P. E. Theodorakis, L. N. Gergidis, A. Avgeropoulos, P. Efthymiopoulos, D. Smyrnaios, M. Kosmas, C. Vlahos, Th. Giannopoulos, *Polymer* **48**, 652, (2007).
4. A. Avgeropoulos, S. Rangou, V. Krikorian, E. L. Thomas, *Macromol. Symp*.,. accepted
5. A. Avgeropoulos, S. Paraskeva, N. Hadjichristidis, E. L. Thomas, *Macromolecules,* **35**, 4030, (2002).
6. *Polymer Handbook*, 4th ed, J. Brandrup, E. H. Immergut, E. A. Grulke, Wiley-Interscience: New York 1999, Vol 1-2, Ch IV-VI.

* To whom correspondence should be addressed
Email: aavger@cc.uoi.

Poster A10

Synthesis of Poly(α-methylstyrene-b-4-hydroxystyrene) Diblock Copolymers Via Anionic Polymerization

Evangelou G., Ntaras C., Rangou S. and Avgeropoulos A*.

Polymers' Laboratory, Department of Materials Science & Engineering, University of Ioannina, University Campus-Dourouti 45110 Ioannina, Greece

Model diblock copolymers of poly(α-methylstyrene-b-4-hydroxystyrene) were synthesized via anionic polymerization in a polar environment[1]. The preparation of these diblock copolymers was achieved by the hydrolysis of the corresponding poly(α-methylstyrene-b-t-4-butoxystyrene) diblock copolymers, since protection of the –OH group in the second monomer is needed for the successful synthesis. The molecular formulas of the two monomers are given in Figure 1. Molecular characterization of the initial diblocks as well as the modified ones was achieved via Size Exclusion Chromatography (SEC) and Proton Nuclear Magnetic Resonance Spectroscopy (^{1}H-NMR).

Figure 1. Schematic presentation of the molecular formula of: a) a-methylstyrene b) 4-tert-butoxystyrene

All reagents (monomers, solvent, terminating reagents and the initiator) were purified and prepared to the standards required for anionic polymerization and are described elsewhere[1,2,3].

The specific materials were synthesized by employing anionic polymerization techniques at specific conditions by adopting a specifically modified pyrex glassware apparatus. α-Methylstyrene was polymerized initially for 12 hours in THF at -78 ^{o}C and 4-t-butoxystyrene was then added into the polymerization reactor and was polymerized under the same conditions. An aliquot was removed and tested via SEC for determining the molecular characteristics of the first chains. The reaction was terminated after 12 hours with degassed methanol. It should be noted that the two monomers were purified under the same conditions [CaH_2 and $(Bu)_2Mg$] and were collected into calibrated ampoules selectively stored at -20 ^{o}C prior to use. The reaction scheme used is exhibited in Figure 2. The resulting diblock copolymer was converted to poly(α-methylstyrene-b-4-hydroxylstyrene) by incorporating a hydrolysis reaction (Figure 3).

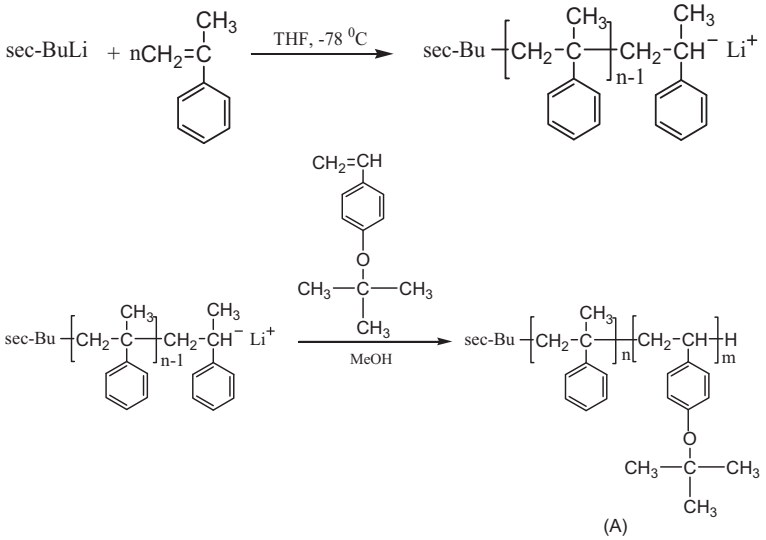

Figure 2. Synthesis reaction of the initial synthesized diblock copolymer of the PαMeS-b-PtBuOS.

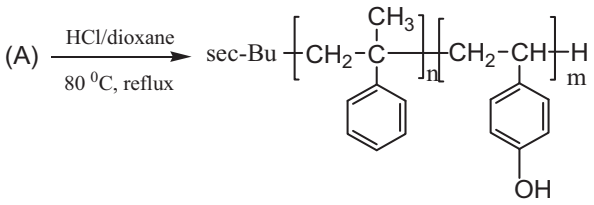

Figure 3. Hydrolysis reaction for the synthesis of the linear aphifilic diblock copolymer.

The chemical composition of the initially synthesized diblock copolymers and the finally modified (after hydrolysis) were determined by Proton Nuclear Magnetic Resonance Spectroscopy (^{1}H-NMR). The spectra for PαMeS-b-PtBuOS is exhibited in Figure 4. The SEC chromatographs in Figure 5 show the protected poly(a-methylstyrene-b-t-4-butoxystyrene) block copolymer obtained after polymerization, with narrow molecular weight distribution.

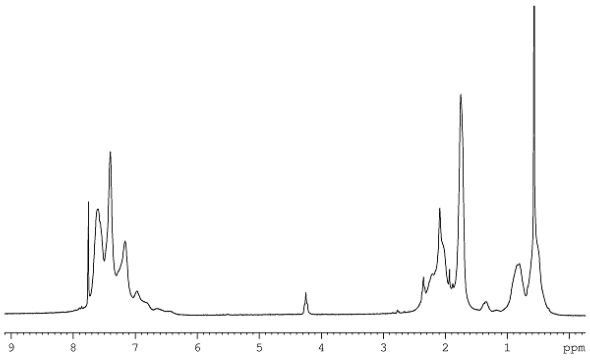

Figure 4. ^{1}H-NMR spectra of a PaMeS -b- PtBOS diblock copolymer.

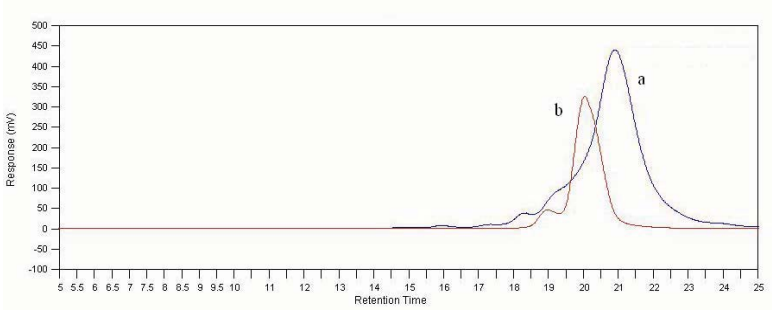

Figure 5. SEC chomatographs of: a) PaMeS and b) PaMeS -b- PtBOS.

References

1. Mingqi Li, Katsuji Douki, Ken Goto, Xuefa Li, Christopher Coenjarts, Detlef M. Smilgies, and Christopher K. Ober, Chem.Mater. **2004**, 16, 3800
2. Uhrig, D.; Mays, J.,W.; J. Polym. Sci. Part A: Polym. Chem. **2005**, 43, 6179
3. Hadjichristidis N., Iatrou H., Pispas S., Pitsikalis M., J. Pol. Sci. : Part A : Polym. Chem. **2000**, 38, 3211

*To whom correspondence should be addressed
E-mail: aavger@cc.oui.gr

Poster A11

Synthesis of Graft Copolymers with Divinyl – Terminated Poly(dimethylsiloxane) and Polystyrene ("Grafting to" Approach)

Ntaras C.[1], Evangelou G.[1], Rangou S.[1], Avgeropoulos A.[1*] and Hill R.M.[2]

[1]*Polymers' Laboratory Department of Materials Science & Engineering, University of Ioannina, University Campus-Dourouti 45110 Ioannina, Greece*
[2]*Dow Corning Corporation, Midland, Michigan 48686, USA*

Introduction: Model graft copolymers of divinyl-terminated poly(dimethylsiloxane) (PDMS) with polystyrene (PS) were synthesized in-situ without the incorporation of specific catalysts (e.g. Karstedt's catalyst) and hydrosilylation reactions (with either $HSiMe_2Cl$ or $HSiMeCl_2$) by using the "grafting to" approach. Specifically, the two vinyl bonds at both ends of the PDMS segments were used as new functional sites upon which the polymerization of styrene took place. It was indicated via molecular characterization techniques (Size Exclusion Chromatography or SEC and Proton Nuclear Magnetic Resonance or ^{1}H-NMR) that the polymerization and grafting of the PS chains was successful leading to a triblock copolymer of the PS-g-PDMS-g-PS type with severely decreased polydispersity index (1.22) when compared to the initial divinyl-terminated PDMS (1.61). Divinyl-terminated PDMS (the chemical formula of which is exhibited in Figure 1) was kindly provided by Dow Corning Corporation and was used without further purification. All other materials [styrene, tetrahydrofuran, methanol and initiator (sec-BuLi)] were purified and used according to procedures already described in the literature[1,2]. The reactions used for the successful synthesis are given in Figure 2.

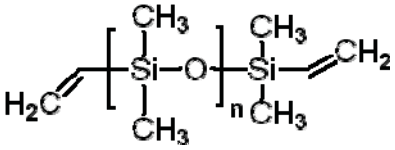

Figure 1. Molecular formula of Divinyl-terminated PDMS

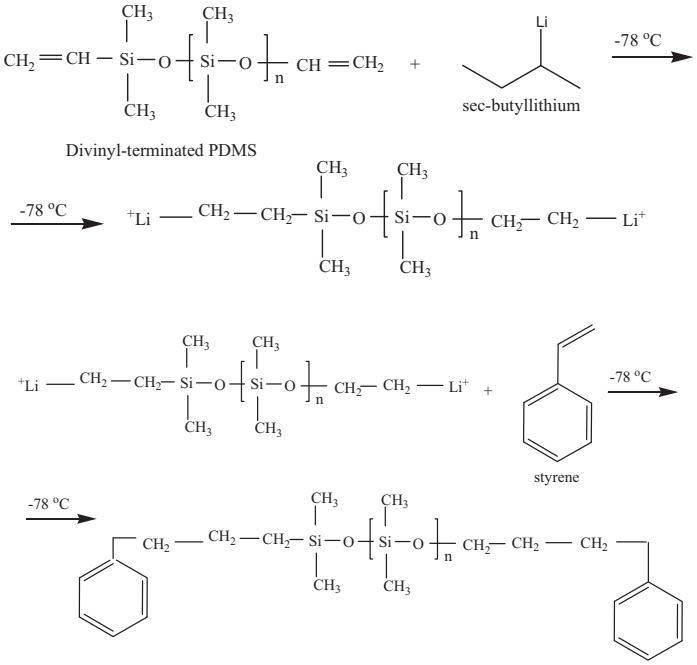

Figure 2. Reactions used for the synthesis of triblock copolymer of the PS-g-PDMS-g-PS type

The apparatus used for the completion of the polymerization is given schematically in Figure 3, where the polymerization reactor with the ampoules (left flask) and the purge section (right flask) are observed.

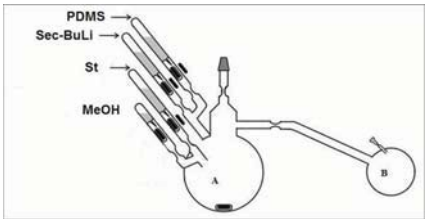

Figure 3. Schematic illustration of the specifically modified glassware Pyrex apparatus used for the synthesis of PS-g-PDMS-g-PS triblock copolymer

Molecular Characterization: From the Size Exclusion Chromatography (SEC) results (as observed in Figure 4) it is easily understood that there is a major decrease in polydispersity from 1.61 to 1.22 and an increase in molecular weight, which verifies consequently the polymerization of styrene and its grafting on the two vinyl ends of the PDMS' backbone.

Finally the results from Proton Nuclear Magnetic Resonance (^{1}H-NMR) indicates and verifies the success of the "grafting to" approach since the chemical shift at 7-7.5 pm and at 0-0.14 ppm corresponding to the 5 protons of the aromatic ring (of PS) and the 6 protons of the two methyl groups (of PDMS) respectively are observed.

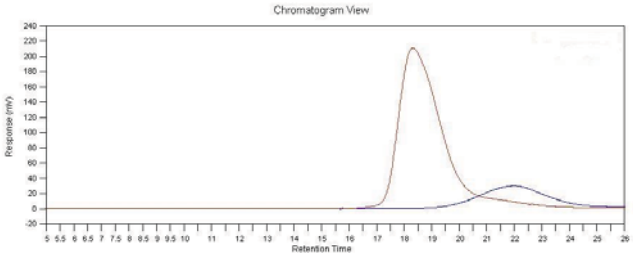

Figure 4. SEC chromatograph of the final copolymer of the PS-g-PDMS-g-PS (left) and the initial divinyl-PDMS (right)

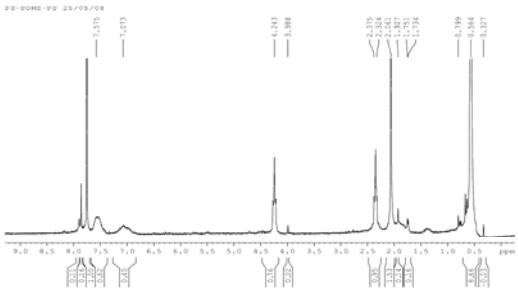

Figure 5. ^{1}H-NMR spectra of the triblock copolymer PS-g-PDMS-g-PS

References

1. Uhrig, D.; Mays, J.,W.; J. Polym. Sci. Part A: Polym. Chem. **2005**, 43, 6179
2. Hadjichristidis N., Iatrou H., Pispas S., Pitsikalis M., J. Pol. Sci. : Part A : Polym. Chem. **2000**, 38, 3211

* To whom correspondence should be addressed.
E-mail: aavger@cc.uoi.gr

Poster A12

Synthesis of Block Copolymers With Poly(Methyl Methacrylate) and 2-(Trimethylsilyloxy) Ethyl Methacrylate [PMMA-b-(TMS-HEMA)]

Constantinou M., Georgopanos P. and Avgeropoulos A.*

Polymers' Laboratory, Department of Materials Science & Engineering, University of Ioannina, University Campus, 45110 Ioannina, Greece.

By using anionic polymerization we were able to synthesize diblock copolymers [PMMA-b-P(TMS-HEMA] which are consisting of methyl methacrylate (MMA) and 2-(trimethylsilyloxy) ethyl methacrylate (TMS-HEMA) (Figure 1) monomers. To date there are no studies reported in the literature investigating the synthesis of PMMA-b-P(TMS-HEMA) using anionic polymerization techniques under high vacuum environment. Anionic polymerization provides the opportunity to synthesize such type of diblock copolymers exhibiting molecular and compositional homogeneity, therefore they can be considered "model" polymers, since they exhibit narrow molecular weight distribution and predictable molecular weight.

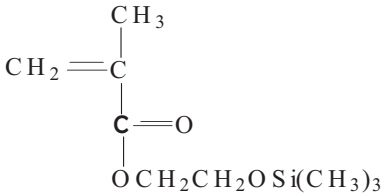

Figure 1. Molecular formula of 2-(trimethylsilyloxy) ethyl methacrylate (TMS-HEMA).

During its anionic polymerization, the monomer 2-hydroxyethyl methacrylate (HEMA) needs to be protected by incorporating a trimethylsilyl group[1]. Particularly, (HEMA) consists of functional hydroxyl groups which contain active protons. As a result, they can not be directly employed since they react immediately with the initiators before polymerization leading to unwanted byproducts[2]. Also, another difficulty during the polymerization of this monomer is its high boiling point; in order to succeed the highest purificication of the monomer, TMS-HEMA was degassed by three freeze-pump-thaw cycles. The addition of a small amount of trioctylaluminium solution until the color changed to light yellow, indicated the complete removal of water[3]. The monomer 2-(trimethylsilyloxy) ethyl methacrylate (TMS-HEMA) the last decade has attracted increased interest due to its practical use as a biomedical material.

Sequential addition of monomers was employed for the successful synthesis of the diblock copolymers by adopting the use of specific made in-situ glassware pyrex apparatuses. It is demonstrated that the anionic polymerization of most alkyl methacrylates proceeds in an ideal manner when the reaction is carried out in a polar environment such as tetrahydrofuran (THF) at low temperatures (-78 ^{0}C)[4]. In particular, sec-BuLi was used as the initiator and 1,1-diphenyl ethylene (1,1-DPE) for the protection of the carboxyl groups for the two monomers. The reaction between sec-BuLi and 1,1-DPE resulted to the formation of the initiator 1,1-diphenyl-3-methylpentyl-lithium. The polymerization started as soon as the methyl methacrylate (1st monomer) was added in the mixture followed by the addition of 2-(trimethylsilyloxy) ethyl methacrylate. The polymerization time for each monomer was estimated to last approximately one hour. Finally, the reaction mixture was terminated with the incorporation of a small amount of methanol. The reactions which took place during the synthesis of PMMA-b-P(TMS-HEMA) are exhibited in Figure 2:

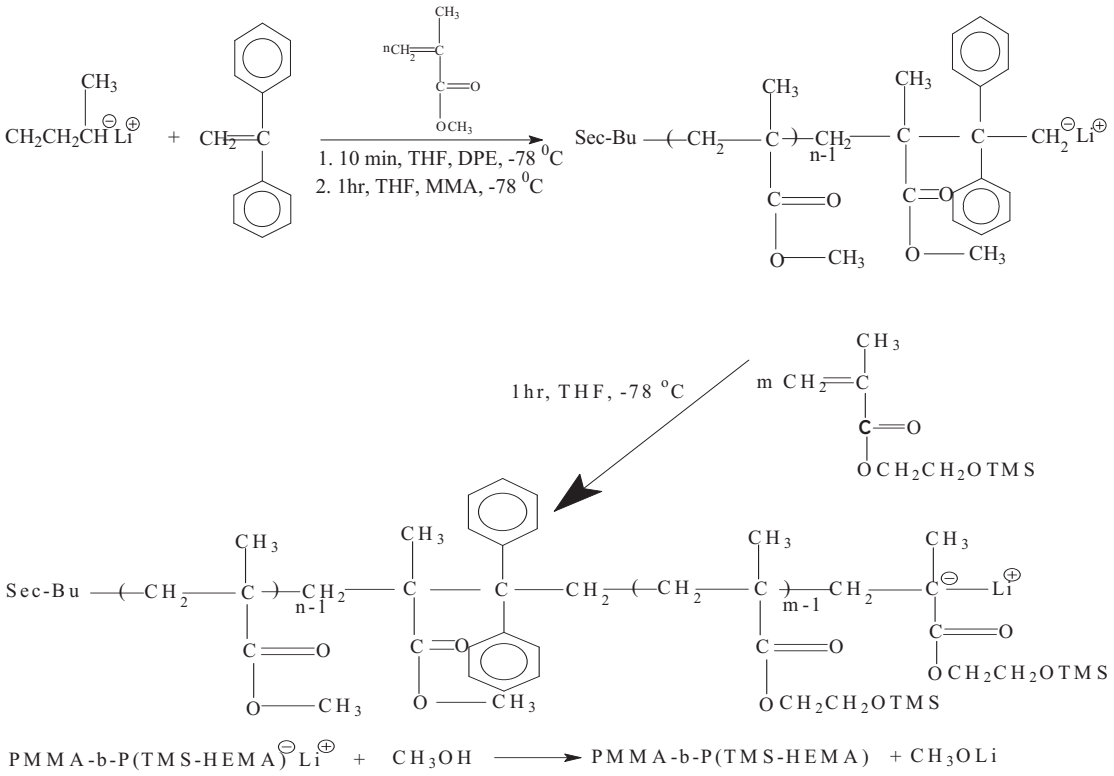

Figure 2. Synthesis reactions for the diblock copolymers of the PMMA-b-P(TMS-HEMA) type.

Four samples were synthesized with different compositions and the results are given in Table 1. Molecular characterization was accomplished with Gel Permeation Chromatography (GPC), Membrane Osmometry (MO) and ^{1}H-Nuclear Magnetic Resonance (NMR) Spectroscopy leading to the conclusion that the synthesized polymers exhibit molecular composition and homogeneity.

Samples	$\overline{M}_n^{PMMA}$ (kg/mol)	I_{PMMA}	$\overline{M}_n^{P(TMS\text{-}HEMA)}$ (kg/mol)	$\overline{M}_n^{PMMA-b-P(TMS-HEMA)}$ (kg/mol)	$I_{copolymer}$	$\overline{M}_w^{PMMA-b-P(TMS-HEMA)}$ (kg/mol)	wt_{PMMA}% (calc.)
PMMA-b-P(TMS-HEMA) - 1	11.2	1.08	26.6	37.8	1.11	41.9	29.6
PMMA-b-P(TMS-HEMA) - 2	34.3	1.09	9.7	44.0	1.13	49.7	78.0
PMMA-b-P(TMS-HEMA) - 3	10.2	1.07	38.0	48.2	1.15	55.4	21.2
PMMA-b-P(TMS-HEMA) - 4	40.4	1.11	11.1	51.5	1.14	58.7	78.4

Table 1. Molecular characterization results

References

1. Breiner T., Schmidt H. W., Müller A. H. E., *e-Polymers,* **2002***,* No 22.
2. Hirao A., Kroto H., Yamaguchi K., Nakahama S., *Macromolecules*, **1986**, 19, 1294.
3. Zhang M.F., Breiner T., Mori H., Müller A. H. E., *Polymer*, **2003**, 44(5), 1449-1458.
4. Müller A.H., *ACS Symposium Series*, **1981**,166, 441.

* To whom correspondence should be addressed
Email: aavger@cc.uoi.gr

Poster A13

Synthesis, Molecular and Morphological Characterization of Modified Diblock Copolymers with Organic Acid Chloride Derivatives

Politakos N[1]., Weinman C.J[2]., Ober C.K[2]. and Avgeropoulos A[1,*]
[1]*Polymers' Laboratory, Department of Materials Science & Engineering, University of Ioannina, University Campus-Dourouti, 45110 Ioannina, Greece*
[2]*Department of Materials Science & Engineering, Cornell University, Ithaca, New York 14853-1501, USA*

Introduction. The major scope of the presented work is the synthesis and characterization of novel copolymers of the PS-b-$PB_{1,2}$ type, where PS is polystyrene and PB is polybutadiene exhibiting 100% 1,2-microstructure as well as their modification with heptanoyl chloride and perfluorooctanoyl chloride. For the development of low energy materials it is a usual approach to attach fluorinated groups onto a polymer backbone, in order to create fluorinated surface coating. The fluorinated groups can possibly orient in a smectic layer structure, exhibiting extremely low critical surface tension (8mN/m)[1].

Synthesis of PS-b-$PB_{1,2}$. Styrene, benzene, butadiene and methanol were purified with known techniques used for anionic polymerization and described analytically elsewhere [2]. 1,2-Dipiperidinoethane was used as the polar medium in order to achieve absolute yield 1,2 microstructure for the PB reagent[3,4]. The polymerization of styrene was carried out at ambient conditions but that of butadiene was achieved at 8^0C, for 24 hrs. The reactions scheme employed as well as the molecular characterization results are exhibited in Figure 1 and Table 1 respectively.

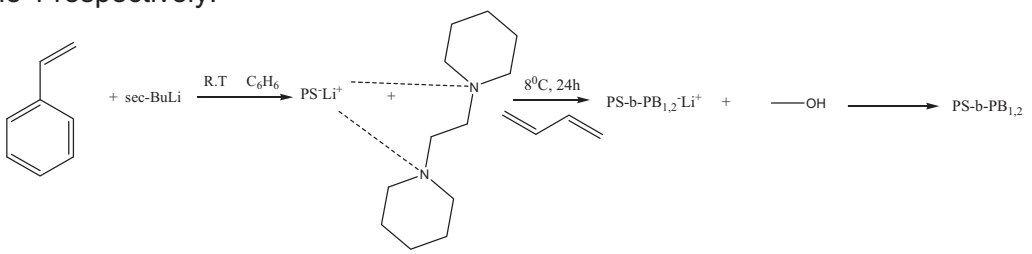

Figure 1: Reaction synthesis of PS-b-PB1,2

Table 1: Molecular Characterization results from SEC, MO, ^{1}H-NMR, as well as predicted morphologies

Sample	$\overline{M_n}$ (PS) g/mol	$\overline{M_n}$ (PB) g/mol	$\overline{M_n}$ (tot) g/mol	I	wt% PS	Predicted morphology
1	63,300	5,700	69,000	1.03	91.7	Bcc
2	37,400	12,300	49,700	1.03	75.3	Hcp
3	28,500	8,600	37,100	1.03	76.8	Hcp
4	10,800	7,300	18,100	1.06	59.7	Lam
5	10,300	9,600	19,900	1.04	51.8	Lam
6	58,500	2,000	60,500	1,05	96.7	Bcc
7	43,500	22,300	65,800	1,05	66,1	Lam

Hydroboration and Oxidation of PS-$PB_{1,2}$. The hydroboration and the oxidation of the PB block were carried out under inert atmosphere. For the hydroboration 9-borabicyclo[3.3.1]nonane (9-BBN) was used and for the oxidation hydrogen peroxide (H_2O_2) respectively. The hydroxylated polymer was precipitated into a mixture of water/NaOH and was rinsed with such a mixture for several times.

Modification with Various Organic Acid Chlorides. The hydroxylated polymer was reacted with the heptanoyl or perfluorooctanoyl chloride dissolved in THF. Finally, methanol was added to terminate the reaction. The fluorinated polymer was precipitated in a mixture of MeOH/water and washed with that solution several times. The hydroboration, oxidation and modification reactions of the dienic segments are exhibited in Figure 2.

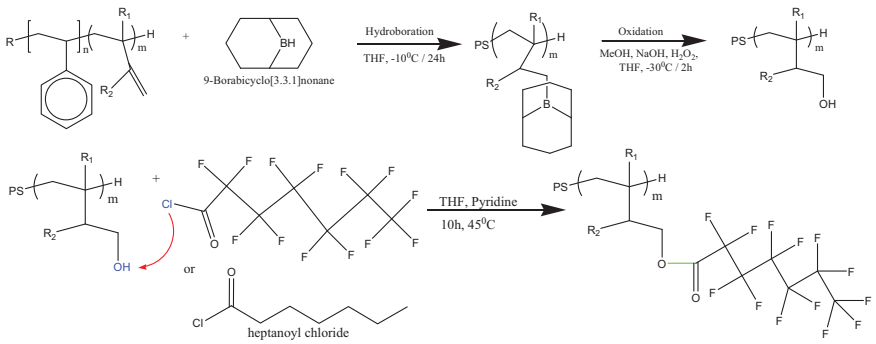

Figure 2. Hydroboration-oxidation (up) and modification (bottom) of the PS-b-$PB_{1,2}$ diblock copolymer

Characterization of the Polymers (Figure 3). Characterization was carried out with Size Exclusion Chromatography (SEC), Proton Nuclear Magnetic Resonance spectroscopy (^{1}H-NMR) for every stage of the synthesis and modification, with IR spectroscopyfor the hydroxylated and the modified polymer and with Transmission Electron Microscopy (TEM) for the 'raw' material and the modified polymer in order to study the self-assembly behavior and the kind of morphology incorporated.

IR results. From the IR spectra a very characteristic peak at 3500cm^{-1} for the hydroxylated product corresponding to –OH group is completely eliminated after the modification reaction. Additionally new peaks corresponding to $–CF_2$ and $–CF_3$ (1150-1350cm^{-1}) are also observed leading to the conclusion of the successful modification.

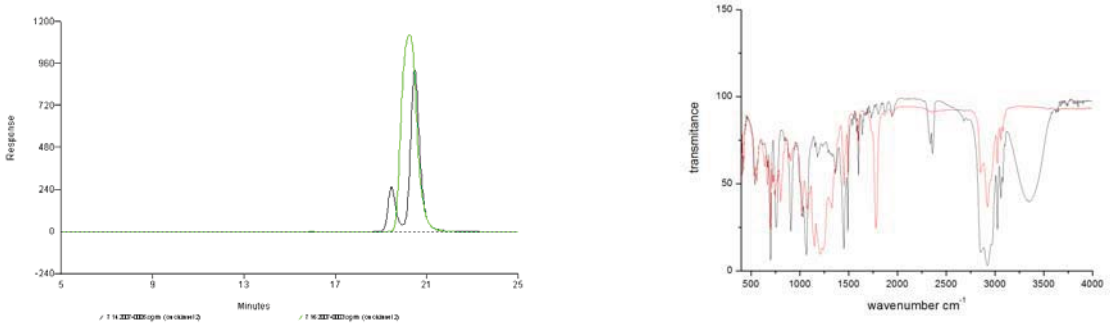

Figure 3. SEC chromatograph of the PS-$PB_{1,2}$-4 and IR spectra for the hydroxylated polymer and for the modified with the fluorinate acid

TEM results. TEM was used in order to verify the morphologies as well as the alteration from one morphology to the other due to the increased molecular mass of the PB modified monomeric unit.

Conclusions. It is a fact that the PB block exhibited high yield in 1,2 microstructure (~100%) as confirmed by ^{1}H-NMR and the diblock copolymers show increased molecular and compositional homogeneity. Also the successful hydroxylation and modification of the PB block was confirmed by IR and ^{1}H-NMR spectroscopies. Finally, the alteration of the morphologies due to enhancement of the molecular weight of the PB segment was verified via TEM instrumentation.

References

1. Ober C., *Macromolecules*, 30, 1906-1914, (**1997**).
2. Hadjichristidis N., *Journal of Polymer Science: Part A: Polymer Chemistry*, Vol 38, 3211-3234,(**2000**)
3. Bywater S., *Makromol. Chem., Rapid Commun.*, 3, 239-242, (**1982**)
4. Bywater S., *Journal of Polymer Chemistry Edition*, Vol. 23, 1997-2003, (**1985**)

*To whom correspondence should addressed
E-mail: aavger@cc.uoi.gr

Poster A14

Synthesis, Molecular and Morphological Characterization of Linear Triblock Terpolymers Where One of The Blocks is Poly(cyclohexadiene)

Misichronis K.[1], Rangou S.[1], Aschroft E.[2], Mays J. W.[2] and Avgeropoulos A.[1,*]

[1]*Polymers' Laboratory, Department of Materials Science & Engineering, University of Ioannina, University Campus, 45110 Ioannina, Greece*

[2]*Polymers' Laboratory, Department of Chemistry, University of Tennessee at Knoxville, TN, 37919, USA*

In this study six (6) linear triblock terpolymers were synthesized through sequential anionic polymerization, where three (3) samples were of the PS-b-PI-b-PCHD type, one of the PS-b-PB-b-PCHD type, one of the PB-b-PS-b-PCHD type and one of the PB-b-PI-b-PCHD type. The major aim was for the PCHD block to exhibit a high 1,4-microstructure (~90%). This was accomplished by using DABCO (1,4-diazodicyclo[2,2,2]octane) as a polar reagent. The synthetic route followed is shown in Figure 1 below.

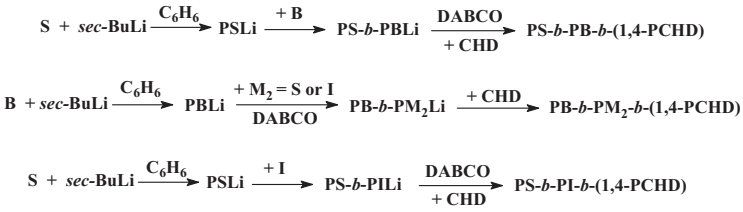

Figure 1: Synthesis reactions of the linear triblock terpolymers.

For the complete synthesis of the final terpolymers, high vacuum techniques were adopted, Size Exclusion Chromatography (SEC) was employed for the molecular characterization of the samples and especially for calculating the molecular weight distribution, Membrane Osmometry (MO) to confirm the $\overline{M_n}$ values and Proton Nuclear Magnetic Resonance Spectroscopy (^{1}H-NMR) to verify the type of the predicted polydiene microstructure and the composition of each block. One SEC chromatograph and two ^{1}H-NMR spectra are exhibited in Figure 2. In Table 1 are shown the molecular characterization results.

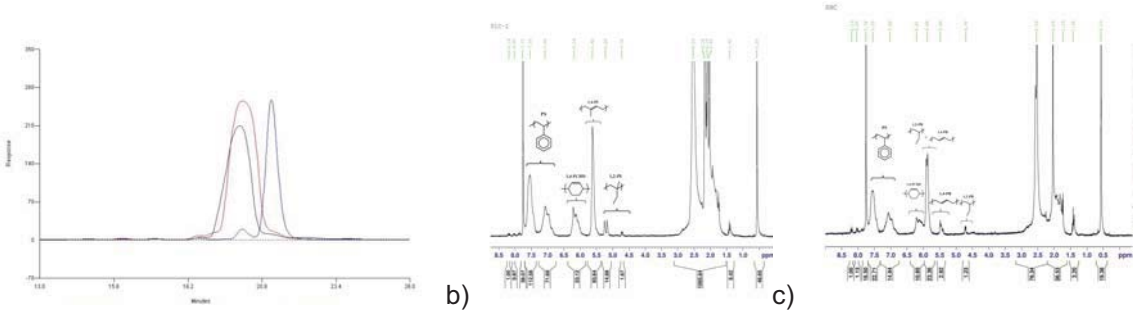

Figure 2: a) SEC chromatograph of the synthetic route of the SIC-2 (30/26/14) sample. The blue graph corresponds to the PS block, the red graph to the diblock and the black graph to the triblock respectively. b) ^{1}H-NMR spectra of the SIC-1 (17/35/10) triblock. c) ^{1}H-NMR spectra of the SBC triblock.

Samples	$\overline{M_n}^a$ 1st block (Kg/mol)	$\overline{M_n}^a$ 2nd block (Kg/mol)	$\overline{M_n}^a$ 3rd block (Kg/mol)	$\overline{M_n}^a$ triblock (Kg/mol)	$\overline{M_w}^b$ triblock (Kg/mol)	$I_{triblock}$ c
SIC-1	17	35,2	10	62,2	67,2	1,08
SIC-2	30	26,1	14,3	70,4	74,7	1,06
SIC-3	43,2	45	15,2	103,4	110,8	1,07
SBC	15	9,8	7,2	32	34,5	1,08
BSC	19	25,2	8,9	53,1	57	1,07
BIC	23	7,2	5,9	36,1	38,3	1,06

Table 1: Molecular Characterization Results.[α] Membrane Osmometry (MO) in toluene at 35^{0}C.[b] Two Angle Laser Light Scattering (TALLS) in THF at 30^{0}C. Size Exclusion Chromatography (SEC) in THF at 30^{0}C

The molecular characterization results lead to the conclusion that the synthesized terpolymers are well-defined since they exhibit low molecular weight distribution as well as molecular and compositional homogeneity[1,2,3].
The morphological characterization was accomplished via Transmission Electron Microscopy (TEM) as exhibited in Figure 3 for two of the six synthesized triblocks. Staining with OsO_4 was acquired for all TEM samples in order to achieve the required contrast between the chemically different blocks. The polydiene phases appear gray or dark while the polystyrene phase brighter.

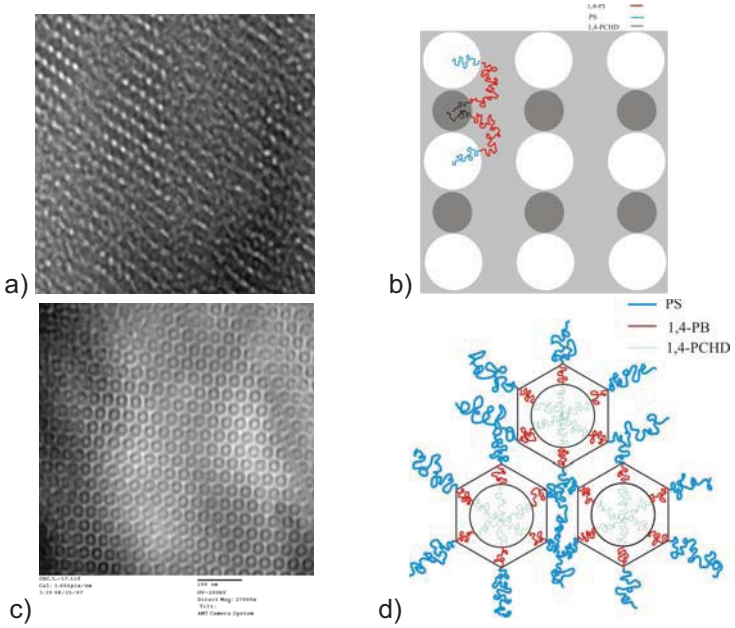

Figure 3: a) TEM micrograph image of the SIC-1 (17/35/10) triblock. The black regions correspond to the 1,4-PCHD block, the gray regions to the PI block and the white regions to the PS block. b) Schematic representation of the observed morphology for the SIC-1 triblock. c) TEM micrograph image of the SBC triblock. The black regions correspond to the PB block, the gray regions to the 1,4-PCHD block and the white regions to the PS block. d) Schematic representation of the observed morphology of the SBC triblock.

The morphological characterization for the SIC-1 triblock showed that the PI block constitutes the matrix and appears gray. A sequence of closed packed cylinders of PS block appears white forming an almost perfect square, while among them and adjacently 1,4-PCHD black cylinders are exhibiting the same structure as well. Such behavior has never been predicted before or reported in the literature. The morphological characterization for the SBC triblock showed that the morphology of the synthesized sample was concentric hexagonally closed packed cylinders, where the inner round 1,4-PCHD cylinders (grey) are surrounded from the hexagonally shaped PB cylinders (black), in a PS matrix (white).
It can be concluded that there is a significant dependence of the self-assembly from the χ interaction parameter and the polymerization degree for the majority of the synthesized samples. It seems that minor or even no effect at all is employed from the molecular weights alternation.

References

1. Mays, J. W.; Hong, K.; *Macromolecules* **2001**, 34, 782.
2. Hong, K.; Mays, J. W.; *Macromolecules,* **2001**, 34, 3540.
3. Tsoukatos, T.; Avgeropoulos, A.; Hadjichristidis, N; Hong, K; Mays, J. W.; Macromolecules, **2002**, 35, 7928

*To whom correspondence should be addressed.
E-mail: aavger@cc.uoi.gr

Poster A15

Synthesis and Characterization of High Molecular Weight Linear Triblock Terpolymer Consisting of Polystyrene, Polybutadiene and Polyisoprene with Different Isomerisms

Zapsas G.[1], Rangou S.[1], Avgeropoulos A.[1]* and Thomas E. L.[2]

[1]*Polymers' Laboratory, Department of Materials Science & Engineering, University of Ioannina, University Campus-Dourouti, 45110 Ioannina, Greece*
[2]*Department of Materials Science & Engineering and Institute of Soldier Nanotechnologies, Massachusetts Institute of Technology, Cambridge, MA 02139, USA*

The synthesis and characterization (molecular-morphological) of a high molecular weight linear triblock terpolymer of polystyrene (PS), polyisoprene with ~60%-3,4 microstructure ($PI_{3,4}$) and poly(butadiene) with ~90% -1,4 microstructure (PB) is studied. The sample prepared exhibits a specific sequence: PS / PB / $PI_{3,4}$ with corresponding ratio of volume fractions approximately equal to: 24 / 10 / 66.

The synthesis was accomplished by employing the sequential addition of monomers through anionic living ends (anionic polymerization). Specifically three monomer additions are employed with high purity in modified vacuum apparatuses, where it is possible (but not wanted) to have partial termination of the living ends during the addition of the second and third monomer. This is observed due to possible impurities which may exist in the used monomers, the initiator or even in the polymerization solvents and also due to impurities which may arise during the polymerization procedure.

For the molecular characterization Size Exclusion Chromatography (SEC) was used in combination with Membrane Osmometry (MO) and Proton Nuclear Magnetic Resonance (^{1}H-NMR) from which satisfactory results were obtained (identical molecular weights, weight and volume fractions). It is the first time that high molecular weight triblock terpolymer has been reported in the literature. The final material appears photonic (again first time observed such behavior in the corresponding terpolymers) as exhibited in Figure 1. Initial results from Transmission Electron Microscopy (TEM) are exhibited in Figure 2.

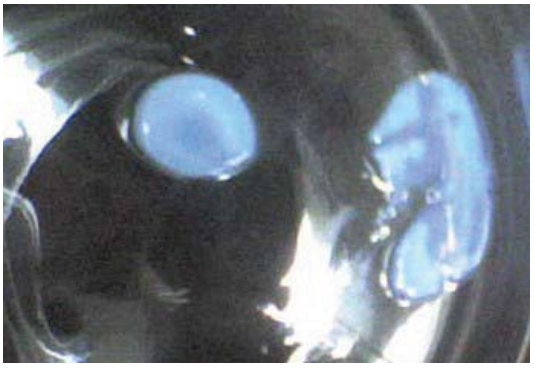

Figure 1. Photonic behavior for the linear triblock terpolymer of the PS-b-PB-b-$PI_{3,4}$ type in an almost non-selective solvent for all segments (toluene).

The major aim of the synthesis of these polymers was to combine the cases of linear triblock terpolymers from the literature where only low molecular weight segments were used in order to examine and compare the properties and behavior.

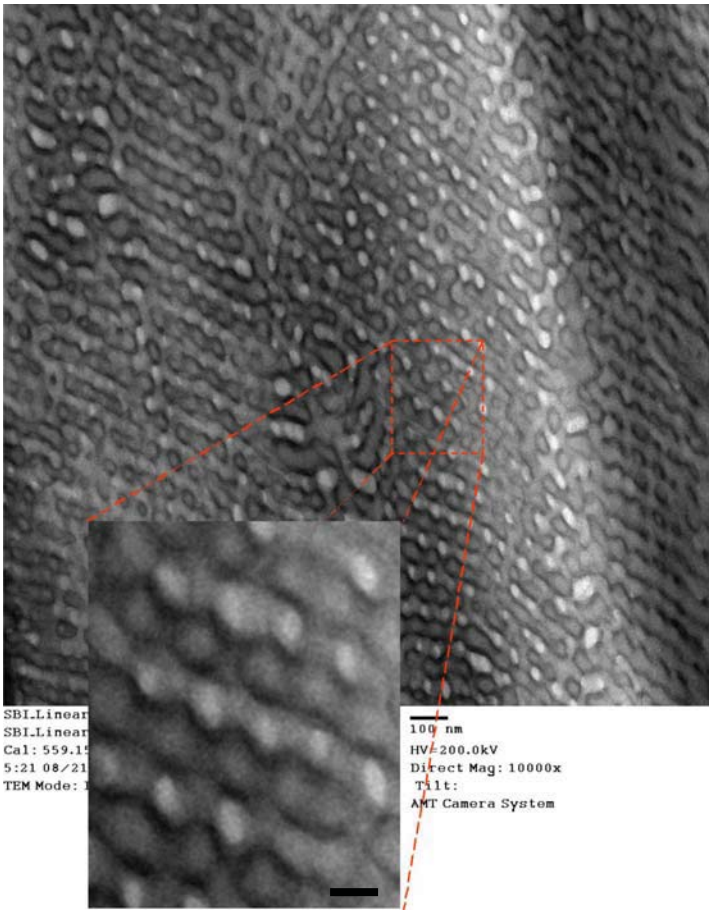

Figure 2. TEM image for the linear triblock terpolymer of the PS-b-PB-b-$PI_{3,4}$ type. OsO4 was used for the staining procedure (30 minutes and the PB appears black where as the PI appears grey and the PS remains white). The magnified image exhibits a scale bar with length of 1cm corresponding to 25 nm.

* To whom correspondence should be addressed
E-mail: aavger@cc.uoi.gr

Poster A16

Nanostructures From Well Defined Diblock Copolymers of Polystyrene (PS) and Poly(dimethylsiloxane) (PDMS)

Georgopanos P.[1], Chao C. C.[2] , Ho R. M.[2,3] and Avgeropoulos A.[1,*]

[1]*Polymers' Laboratory, Department of Materials Science & Engineering, University of Ioannina, University Campus, 45110 Ioannina, Greece*

[2]*Institute of Microelectromechanical System, National Tsing Hua University, Hsinchu 30013, Taiwan, R.O.C.*

[3]*Department of Chemical Engineering, National Tsing-Hua University, Hsinchu 30013, Taiwan, R.O.C.*

Well-defined linear diblock copolymers of polystyrene and poly(dimethylsiloxane) (PS-b-PDMS) were synthesized through sequential anionic polymerization of styrene (St) and hexamethylcyclotrisiloxane (D_3), employing high vacuum techniques. The aim was to synthesize copolymers exhibiting various microphase-separated nanostructures that could be identified with nanotechnology instumentations.

Two synthetic schemes were employed. The first scheme corresponds to the approach already described by Zilliox et al.[1] and Hadjichristidis et al.[2] and the second incorporates the use of two-fold excess of D_3. The reactions for both synthesis approaches are shown in Figure 1.

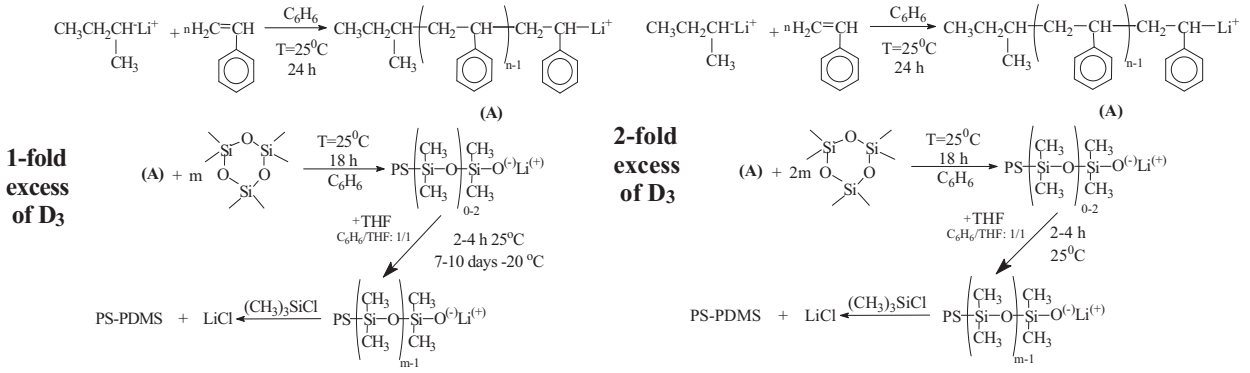

Figure 1: Synthesis schemes of the PS-b-PDMS copolymers.

Gel Permeation Chromatography (GPC), Membrane Osmometry (MO) and ^{1}H-Nuclear Magnetic Resonance (NMR) Spectroscopy were employed for the molecular characterization studies, and the results are given in Table 1. The results lead to the conclusion that the synthesized copolymers are well-defined since they exhibit molecular and compositional homogeneity. The morphological characterization was accomplished via Transmission Electron Microscopy (TEM) and Small Angle X-Ray Scattering (SAXS) as exhibited in Figure 2 for a series of the synthesized PS-b-PDMS block copolymers, including one PS-rich and one PDMS-rich materials. No staining was acquired for the TEM observed images since the microdomains of the PDMS segment appear relatively dark due to mass-thickness contrast while the PS microdomains appear brighter.

Samples	$\overline{M}_n^{PS}$ (kg/mol)	I_{PS}	$\overline{M}_n^{PDMS}$ (kg/mol)	$\overline{M}_n^{PS-b-PDMS}$ (kg/mol)	$I_{PS-b-PDMS}$	$\overline{M}_w^{PS-b-PDMS}$ (kg/mol)	wt_{PS} % (calc.)	wt_{PS} % (^{1}H-NMR)	φ_{PS}%
PS-b-PDMS 1	15.0	1.03	6.4	21.4	1.04	22.3	70.1	72.4	67.3
PS-b-PDMS 2	12.0	1.02	23.0	35.0	1.06	37.1	34.3	33.1	31.4
PS-b-PDMS 3	33.2	1.03	14.0	47.2	1.04	49.1	70.3	73.1	67.5
PS-b-PDMS 4	47.0	1.01	12.5	59.5	1.02	60.7	79.0	77.3	76.7
PS-b-PDMS 5	20.0	1.03	44.2	64.2	1.03	66.1	31.2	32.7	28.4
PS-b-PDMS 6	28.5	1.04	37.5	66.0	1.04	68.6	43.2	41.8	40.0

Table 1: Molecular Characterization Results

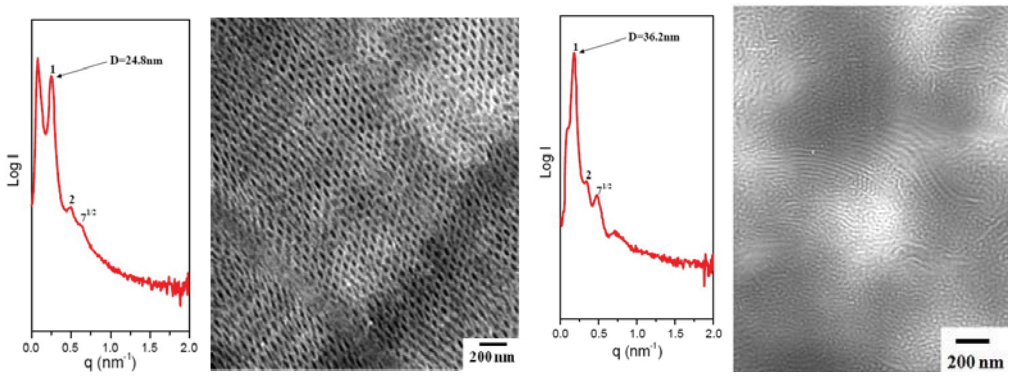

Figure 2: The TEM micrographs of solution-cast PS_{15}-$PDMS_{06}$ (f_{PS}^{v}=0.72) and PS_{12}-$PDMS_{23}$ (f_{PS}^{v}=0.34) left and right images respectively. The corresponding azimuthally scanned one-dimensional SAXS profiles are also given in the same manner.

The morphological characterization lead to the fact that the morphology of the synthesized copolymers was hexagonally closed packed cylinders of the minority phase in the matrix of the majority segments. This morphology was ideal for nanotechnology applications and especially nanolithography[3]. When the morphological characterization was accomplished the samples were spin casted on silicon wafers and then treated via etching techniques in order to remove the polystyrene fraction almost quantitatively. The main purpose was to create nanoporous or nanorelief structures, depending on the composition of the copolymer. The techniques employed were Reactive Ion Etching (RIE) in the presence of O_2, CF_4 or SF_6 and Physical Vapor Deposition (PVD). Further morphological characterization was accomplished on the etched samples via Field Emission Scanning Electron Microscopy (FESEM) and Atomic Force Microscopy (AFM) in order to study the microstructures that were adopted after the etching process. Figure 3 represents some of the results adopted after the etching process.

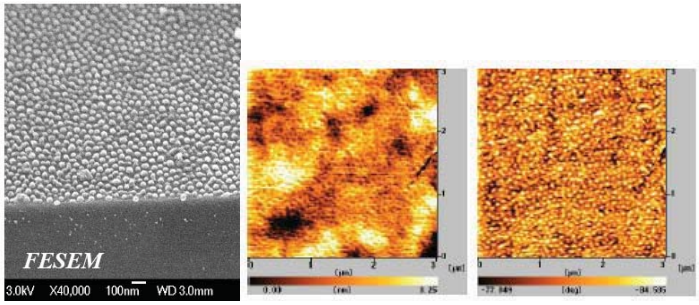

Figure 3: Further morphological characterization on sample PS_{15}-$PDMS_{06}$ (f_{PS}^{v}=0.72). An FESEM image demonstrating the nanoarrays from the PDMS fraction, and two AFM images of the same material (two different resolutions) also demonstrating the same nanostructure. Nanodots of the PDMS are shown fraction are shown laying on the silicon wafer (grey colored at the FESEM image).

References

1. Zilliox J. G., Roovers J. E. L., Bywaters S., *Macromolecules* **1975**, 8, 573.
2. Bellas, V., Iatrou, H., Hadjichristidis, N., *Macromolecules* **2000**, 33, 6993.
3. Park C., Yoon J., Thomas E.L., *Polymer* **2003**, 44, 6725.

* To whom correspondence should be addressed
Email: aavger@cc.uoi.gr

Poster A17

Thiophene Conducting Copolymers

Grana E.[1], Goulas V.[2], Katsoulidis A.[3], Makris T.[4], Katsigiannopoulos D.[1], Skouras E.[4], Pomonis P.[3] and Avgeropoulos A.[1*]

[1]*Polymers' Laboratory, Department of Materials Science & Engineering, University of Ioannina, University Campus, 45110 Ioannina, Greece*

[2]*Section of Organic Chemistry & Biochemistry, Department of Chemistry, University of Ioannina, University Campus, 45110 Ioannina, Greece*

[3]*Section of Industrial Chemistry, Department of Chemistry, University of Ioannina, University Campus, 45110 Ioannina, Greece*

[4]*Nanotechnology Laboratory, Department of Materials Science & Engineering, University of Ioannina, University Campus, 45110 Ioannina, Greece*

Introduction

Conducting polymers exhibit unique and remarkable applications due to their conducting and electroactive properties. More specifically, since their electrical and optical properties are precisely controlled via oxidation and/or reduction their applicable state can be altered as well. Some examples of their applications are: polymer rechargeable batteries[1], microtweezers, microvalves, actuators for micromechanical sorting, nanowires[2] etc. Polythiophene (PT) could be used as a microvalve in a membrane's pores and therefore alter their state by using electrical charge which will eventually modify the polymer's oxidation state. A range of volatile compounds with concentrations of 10 ppm or less can be detected by PT sensors[3], therefore they can be used in environmental chemistry for the increased absorption and removal of various types of pollutants. Several applications of conducting polymers have been reported, but their solubility and processability remains an important challenge. Synthesis of more soluble substituted polythiophene derivatives seems to be promising but it is considered that their electrical properties are degraded[4]. François and Olinga[5] have reported that ''an alternative way to maintain doped conducting polymer sequences in solution is the synthesis of copolymers in which these sequences are chemically bonded to soluble sequences of 'classical' polymer such as polystyrene''.

In this work the synthesis of diblock copolymers of PS-b-PT (where PS is polystyrene) and PI-b-PT (where the PI is either rich in 3,4 or 1,4 microstructure) and a triblock terpolymer of the PS-b-PI-b-PT sequence were prepared by combining anionic polymerization under high vacuum conditions and chemical oxidative polymerization technique using iron trichloride ($FeCl_3$) as the oxidant reagent[6]. Controlled modification of the living polymer ends was achieved by 2-bromothiophene in the presence of a polar solvent (Tetrahydrofuran or THF). Molecular characterization was accomplished by Size Exclusion Chromatography (SEC), Membrane Osmometry (MO), and Carbon Nuclear Magnetic Resonance Spectroscopy (^{13}C-NMR), whereas the microstructure/morphology was studied via Scanning Electron Microscopy (SEM). Specific conductivity (σ) was measured using the standard four-probe method. Additionally, the synthesis of diblock copolymers, where at least one block is polythiophene, led in most cases to final products which can be characterized as 'model' materials, exhibiting compositional and molecular homogeneity, with small molecular weight distributions and have never been reported in the literature. Finally, the synthesis of diblock copolymers of the PI-b-PT type and the triblock terpolymer PS-b-PI-b-PT is proved to be successful and original as well. The reactions used for the synthesis of the copolymers are given in Scheme 1:

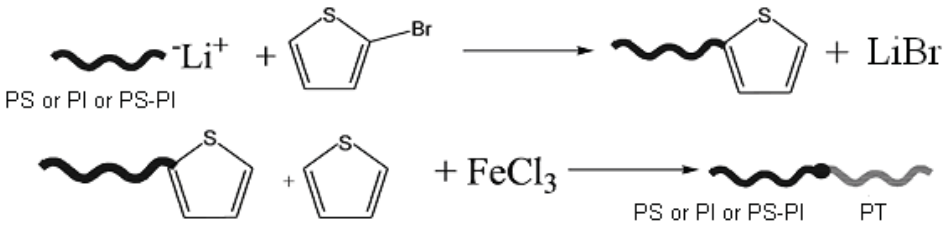

Scheme 1. Synthesis reactions of the end-functionalized polymer and the final copolymer.

Experimental Part

First, a living polymer chain (PS^-Li^+, $PI_{1,4}^-Li^+$, $PI_{3,4}^-Li^+$, PS-b-PI^-Li^+), synthesized via anionic polymerization and standard procedures well-established in the literature[7], reacts with a halogenated thiophene derivative (2-bromothiophene or 2-BrT) in order to produce a functionalized polymer with thiophene end groups. The end-functionalized polymer is then dissolved in chloroform, and a small amount of methanol is added in order to terminate the living polymer chain ends that have not been functionalized. The solution is transferred into a beaker, where under ambient conditions it reacts with the appropriate quantity of thiophene monomeric units and iron trichloride ($FeCl_3$). Four hours later, the reaction is completed and the copolymer is finally synthesized. A distinct dark solution is obtained, with a black precipitate in most cases due to the excess of the $FeCl_3$ used. The solution is filtered through a Büchner funnel, and the filtration product is then precipated in an excess of methanol. The precipitated material is purified through continuous rinsing with methanol until the filtration product becomes clear (no colour indicated) since the excess of $FeCl_3$ is removed. Actually, the filter retains both the unreacted initial living chain and the copolymer. By controlled fractionation of this product in a mixture of solvent/non solvent it is possible to obtain the pure copolymer.

In most cases in the past[5] the reason for synthesizing PS-b-PT copolymers was exclusively to obtain pure PT films through thermal treatment from the copolymer corresponding films. In this research work the copolymer films are examined without thermal treatment in order to discover possibly new properties and applications. Morphological characterization has shown that generally the copolymers form fibers (Figure 1) that are better defined when the molecular weight of the copolymer is enhanced or increased.

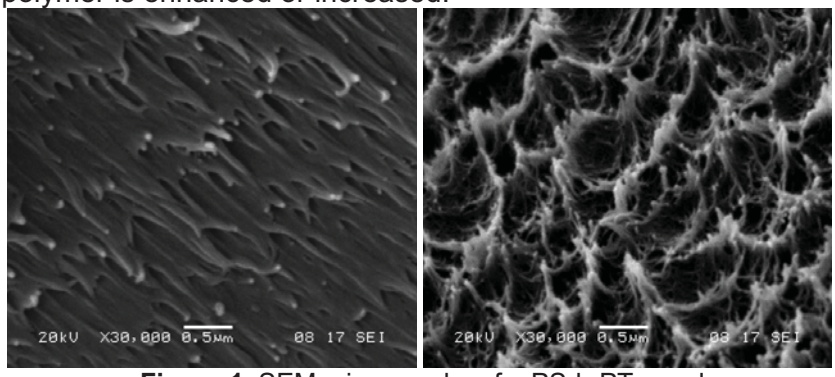

Figure 1. SEM migrographs of a PS-b-PT copolymer.

Conductivity measurements have proven that the copolymers are conductive and conductivity depends on the molecular weight of the PT block and the copolymer as well.

Conclusions

Diblock copolymers as well as triblock terpolymers with at least one segment being PT were synthesized by combining anionic and chemical oxidative polymerizations. The final products exhibited molecular and compositional homogeneity. Finally, we were able to study the structure via SEM of the whole neat material without the incorporation of any thermal treatment as reported in the literature.

References

1. Ciric-Marjanovic G., Mentus S. J. Appl. Electrochem. 1997;28:103.
2. Bjørnholm T., Hassenkam T., Greve D. R., McCullough R. D., Jayaraman M., Savoy S. M., Jones C. E., McDevitt J. T. Adv. Mater. 1999;11:1218.
3. Chang J., Liu V., Subramanian V., Sivula K., Luscombe C., Murphy A., Liu J., Fréchet J. M. J. J. Appl. Phys. 2006;100:014506.
4. Roncali, J. Chem. Rev. 1992;92:711.
5. Francois B., Olinga T. Synth. Met. 1993;57:3489.
6. Grana, E.; Katsigiannopoulos, D.; Avgeropoulos, A.; Goulas, V.; Int. J. Polym. Anal. Charact. 2008;13:108.
7. Uhrig, D.; Mays, J.,W.; J. Polym. Sci. Part A: Polym. Chem. 2005;43:6179.

* To whom correspondence should be addressed
E-mail: aavger@cc.uoi.gr

Poster A18

Incorporation of Magnetic Nanoparticles in a $PI_{3,4}$-b-$PB_{1,4}$ Polymeric Matrix

A. Tomou[1], A. Enotiadis[1], S. Rangou[1], M. Kitsas[1], A. P. Douvalis[1,2], A. Avgeropoulos[1], I. Panagiotopoulos[1], D. Gournis[1] and T. Bakas[2]

[1] *Department of Materials Science and Engineering, University of Ioannina, 45110 Ioannina, Greece*
[2] *Department of Physics, University of Ioannina, 45110 Ioannina, Greece*

Abstract

Magnetic nanoparticles and polymers are materials with very wide ranges of technological applications[1]. New hybrid materials were produced with γ-Fe_2O_3 magnetic nanoparticles attached to $PI_{3,4}$-b-$PB_{1,4}$ which was used as a polymeric matrix. Capped γ-Fe_2O_3 nanoparticles were synthesized by oxidative transformation of an iron hydroxide gel using $Na_2S_2O_4$[2]. The capped as-prepared γ-Fe_2O_3 nanoparticles and the hybrid materials were characterized and studied by X-ray diffraction, Mössbauer spectroscopy, magnetization measurements and thermogravimetric analysis.

Introduction

Magnetic nanoparticles have technologically important applications, like magnetic data recording media, cell separation methods, radioactive therapies and carriers for drug delivery[1]. A large amount of research in polymers involves the use of them as template building materials for a wide range of applications. In this work, in order to achieve a well dispersion and thermal protection of magnetic nanoparticles new hybrid materials were obtained by attaching capped magnetic γ-Fe_2O_3 nanoparticles to $PI_{3,4}$-b-$PB_{1,4}$ copolymer. Hybrids were characterized using a combination of experimental techniques, such as thermal analysis (DTA/TGA) X-Ray diffraction (XRD), magnetization measurements and Mössbauer spectroscopy.

Experimental

$PI_{3,4}$-b-$PB_{1,4}$ polymeric matrix was synthesized by anionic polymerization and high vacuum techniques. The magnetic capped nanoparticles ware produced via oxidative transformation of an iron hydroxide gel using $Na_2S_2O_4$ solution as oxidant. Capping with oleic acid is established simultaneously in one step by adding a toluene solution of the capping agent and refluxing the resulting biphase system[2]. Nanoparticles solution was then added to the toluene solution of the copolymer in different nanoparticle to polymer mass ratios [1:1 (M10 Hybrid), 1:2 (M20 Hybrid), 1:3 (M30 Hybrid)]. The mixture was stirred for 40 minutes, and precipitated with methanol and air-dried. Finally, the solid samples were heated for 2 hours under vacuum at 140^{o}C for the efficient removal of the solvent.

Results and Discussion

From the XRD patterns (Fig.1a) the peaks of maghemite (JCPD # 39-1346) are clearly observed in agreement with the Mössbauer spectra. The average particle size was estimated from the XRD patterns using the 'Scherrer' formula. The nanoparticle assembly has a range of particle sizes, with a mean value of ~3 nm. The thermogravimetric analysis measurements (Fig.1b) of the free as-made magnetic γ-Fe_2O_3 nanoparticles showed only one exothermic peak at 265 ^{o}C due to oxidation of the organic surfactants (oleic acid). The DTA curve of the hybrid sample shows a region of exothermic peaks in the range of 400-450 ^{o}C which is attributed to the oxidation of the copolymer. However, in the same curve the exothermic peak of the nanoparticles oxidation is not visible since the copolymer provides thermal protection to capped nanoparticles.

Mössbauer spectra (Fig 2.) collected at different temperatures reveal the presence of only trivalent (Fe^{+3}) iron ions, which indicate – in combination with the XRD results – that the magnetic nanoparticles have the structural characteristics of maghemite.

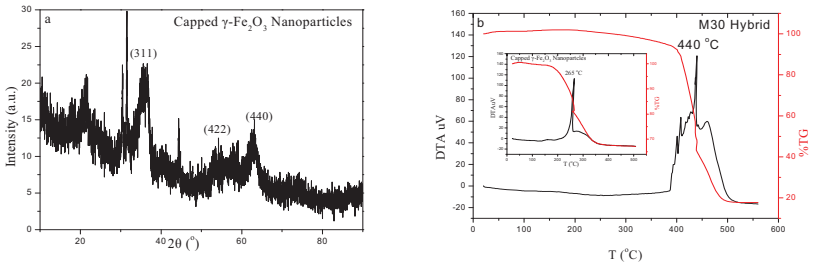

Figure 1. a. XRD patterns for free as-made capped magnetic γ-Fe_2O_3 nanoparticles **b.** DTA-TGA curves of the hybrid material and the as-made capped magnetic γ-Fe_2O_3 nanoparticles

A distribution of particle sizes is evident from the appearance of both magnetically split (sixtets) and paramagnetic (doublets) components at all samples, the area of which is temperature dependent. This confirms the nanostructured nature of the particle assembly and suggests that superparamagnetic phenomena are important for the interpretation of their magnetic properties. The magnetization loops (Fig. 3), collected at room temperature (RT), of all samples containing the γ-iron oxide nanoparticles show ferromagnetic behaviour, while that of the copolymer is diamagnetic. However the relative large slope at high fields and the vanishing coercivity of the free nanoparticles sample are characteristics of the

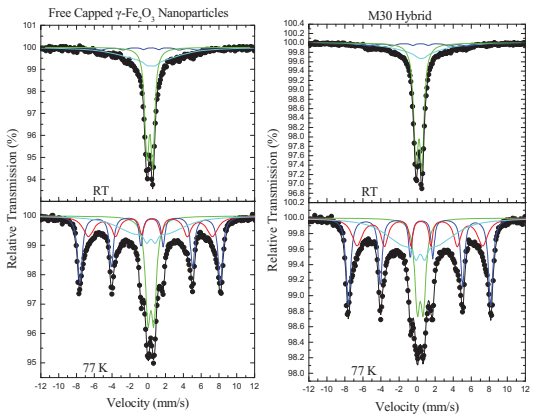

Figure 2. Mössbauer spectra of the hybrid material and the as-made capped magnetic γ-Fe_2O_3 nanoparticles

superparamagnetic nature of this assembly at RT. These characteristics are retained completely when the particles are attached to the copolymer (samples M10, M20, M30), indicating that all hybrid materials contain the same dispersion of nanoparticles as the free nanoparticle assembly. The magnetic moment tends to increase as the loading of the nanoparticles increases. However a saturation effect of the nanoparticles's loading above 20 % wt is observed, which shows a corresponding saturation in the receptivity of the nanoparticles from the copolymer. These results come in perfect agreement with the Mössbauer spectroscopy results.

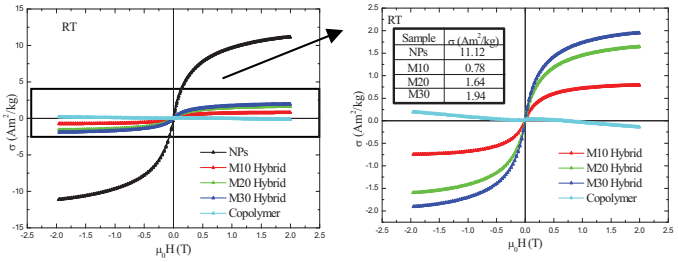

Figure 3. Magnetic Measurements of the hybrid materials, the copolymer and the as-made capped magnetic γ-Fe_2O_3 nanoparticles

Conclusions

Capped γ-Fe_2O_3 were synthesized and attached to the $PI_{3,4}$-b-$PB_{1,4}$ copolymer at different loadings (up to 30% wt). The nanoparticles's loading presents a saturation limit at 20% wt. Above this limit, the increase of the magnetization moment is not proportional. Thus indicates that the receptivity of the copolymer has an upper limit which prohibits the attachment of the nanoparticles.

Acknowledgements. A.E. gratefully acknowledges Academy of Athens for a PhD fellowship.

References

1. G. Reiss et al. Nature Materials, 4, 725 (2005)
2. A. B. Bourlinos et al. J. Mat. Science, 41, 5250 (2006)

Poster A19

Intercalation of an Amphiphilic Diblock Copolymer in Layered Materials

Enotiadis A.[1], Sotiriou I.[1], Douli E.[2], Georgopanos P.[2], Avgeropoulos A.[2] and D. Gournis[1]
[1]*Ceramics and Composites Laboratory, Department of Materials Science and Engineering, University Campus, 45110 Ioannina, Greece*
[2]*Polymers' Laboratory, Department of Materials Science & Engineering, University of Ioannina, University Campus, 45110 Ioannina, Greece*

Abstract
Nanocomposites of poly (styrene-*b*-ethylenoxide) (PS-*b*-PEO) block copolymer with layered smectite clays (montmorillonite SWy) were synthesized by the solution intercalation method to create a new class of hybrid organic-inorganic materials. The hydrophilic block of the PS-b-PEO has the tendency to intercalate within the clay interlayers while the hydrophobic block (PS) stands outside the clay galleries forming a new type of nanocomposite the "hairy clay". X-Ray powder diffraction (XRD) and FT-IR spectroscopy were used for the structural characterization of the nanocomposites while the thermal properties were measured by Differential Scanning Calorimetry (DSC).

Introduction
In polymer nanocomposite research, the basic aim is to enhance several properties of polymeric components using molecular or nanoscale reinforcements. The presence of two dimensional silicate layers in the matrix of a polymer was a major interest due to the significant gains in thermal stability, mechanical properties and electric conductivity.[1] Typical preparation methods of these nanocomposites include solution intercalation, melt intercalation, and in-situ polymerization. In the present work, we developed nanocomposites of PS-*b*-PEO with montmorillonite (SWy-2) in different clay/polymer loadings. The copolymer is an amphiphilic polymer containing two different blocks, one hydrophobic block (PS) and one hydrophilic (PEO). In the SWy / PS-*b*-PEO nanocomposite, the chains of PEO block are fully intercalated between the clay sheets while the PS block forms a spring that keeps the clay platelets apart forming a "hairy clay" (Fig. 1). Similar, hairy clay was observed in laponite/poly(ethylene oxide-*b*-isoprene) (PEO-PI) clay/block copolymer nanocomposites.[2]

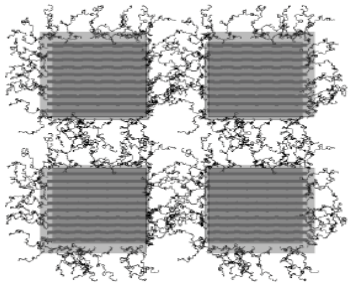

Figure 1. Schematic representation of a "hairy clay"

Experimental
The clay used in this work was a sodium-montmorillonite (SWy-2). The diblock was prepared by anionic polymerization using high vacuum techniques. The polymer consists of 85% PEO block and 15% of polystyrene. The polydispersity index is about 1.06 and the average molecular weight per number is 110 kg/mol. Polymer-clay nanocomposites (PS-*b*-PEO/SWy) were prepared as follows: 50mg of PS-*b*-PEO were diluted in a mixture of pure aceton/H_2O and added to aqueous clay suspension in different polymer to clay ratios *R*= 1, 2, 5 and 10 (where, *R* = [mass of PEO]/[mass of clay]).

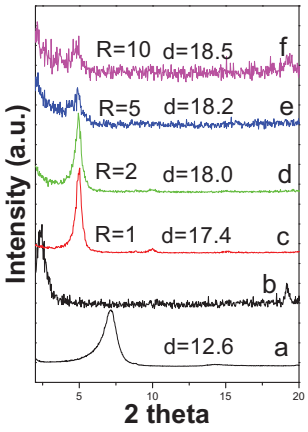

Figure 2. XRD patterns of SWy (a), PS-*b*-PEO (b), and nanocomposites with R=1 (c), 2 (d), 5 (e), and 10 (f)

Results & discussion
The intercalation capability of PS-*b*-PEO in montmorillonite was evaluated by powder XRD measurements (Fig 2). An increase of the basal spacing (d_{001}) of the clay is observed after the

insertion of the polymer from 12.6 Å in the pristine clay to 17.4 Å in the nanocomposite with R=1. This value corresponds to an intersheet separation of 17.4 – 9.6 = 7.8 Å, where 9.6 Å is the thickness of the clay layer. This increase in the interlayer space may attributed to the intercalation of the hydrophilic PEO chains in the clay galleries due to their close affinity with the hydrophilic environment of montmorillonite. In contrast, the hydrophobic PS block remain out of the clay interlayers forming a spring that keeps the clay platelets apart ('hairy clay', Fig. 1). As the polymer concentration increases the d_{001} spacing is increasing since more PEO chains are entering the lamellar space of the clay mineral. Moreover, in nanocomposites with R=1 and 2 the 001 diffraction peaks are sharper compared to pure montmorillonite indicating that the average stacking height of montmorillonite is higher in the nanocomposites. The elasticity provided by the PEO chains plays an important role in adjusting the layer spacing, improving therefore the layer correlation length. However, at higher polymer concentrations (R=5 and 10), the d_{001} reflection is broader indicating that the ordered structure of the layered mineral is destructed as the number of the intercalated PEO chains is increased. Fig 3 shows us the FT-IR spectra of the nanocomposites, in comparison with the pristine clay and the neat copolymer. The spectra of all nanocomposites present all the characteristics bands of the copolymer and the clay without significant changes. Specifically, the appearance of the peaks at 465 and 1036 cm^{-1} which correspond to Si-O and Si-O-Si vibrations of the clay lattice are indicative of the existence of the phyllomorphous mineral in the final composites. Finally, the thermal properties of the nanocomposites are studied by DSC. Fig. 4 shows the differential heat flow curves of the nanocomposites at different polymer loadings (R=2, 5 and 10). The crystallization/melting temperatures are observed during the cooling/heating cycle and the degree of crystallinity (*X*c) can be calculated for the PEO block. The crystallization temperature is increasing with the concentration of copolymer while the melting point of the nanocomposites doesn't change drastically. The increase of crystallization temperature of composites with the concentration is because that clay platelets can act as a nucleation agent in the melting polymer matrix, which causing the crystallization of melting polymer more easily and begin to crystalline at higher temperature in the cooling process. Finally, the highest degree of crystallinity (X_c = 66.15%) is observed for the nanocomposite with R=5 while the neat polymer shows a 57% crystallinity.

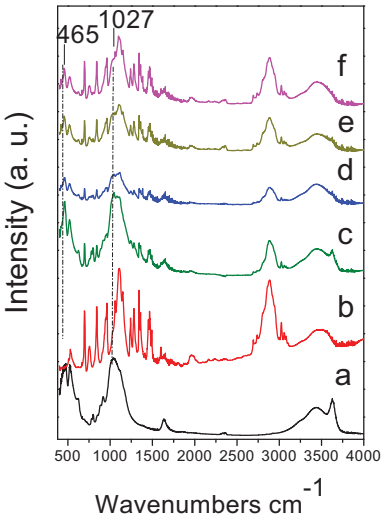

Figure 3. FT-IR spectra of SWy (a), PS-PEO (b), nanocomposites with R=1 (c), 2 (d), 5 (e), and 10 (f)

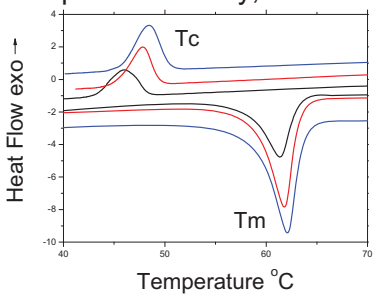

Figure 4. DSC curves of nanocomposites with R=2 (black), 5 (blue), and 10 (red).

Conclusions

In summary, we have investigated the behavior of the amphiphilic copolymer in the presence of montmorillonite platelets. Results showed the successful intercalation of the PEO block in the lamellar space of the clay mineral while the PI chains stands outside of the interlayer space keeping the plates apart.

Acknowledgements. A.E. gratefully acknowledges Academy of Athens for a PhD fellowship.

References

1. Litina K, Miriouni A, Gournis D, Karakassides M, Georgiou N, Klontzas E, Ntoukas E, Avgeropoulos A, *Eur. Polym. J.* **2006**, 42, 2098
2. Gournis D, Floudas G. *Chem. Mater.* **2004**, 16, 1686.

Poster A20

SYNTHESIS AND CHARACTERIZATION OF PROTON EXCHANGE MEMBRANE NANOCOMPOSITES FOR HIGH TEMPERATURE FUEL CELLS

I. Kalamaras[1], J. K. Kallitsis[2,3] and V. G. Gregoriou[1,2]
[1]*Foundation for Research and Technology-Hellas, Institute of Chemical Engineering and High Temperature Chemical Processes (FORTH/ICEHT), Patras 26504, Greece.*
[2]*Advent Technologies S. A., Scientific Park of Patras, Patras 26504, Greece.*
[3]*Department of Chemistry, University of Patras, Patras 26500, Greece.*

Fuel cells are a more efficient and environmentally friendly technology of power generation than current power sources. Among others, polymer electrolyte membrane fuel cell (PEMFC) is one of the most promising candidates and has been receiving increased attention due to its certain advantages. Applications of PEM fuel cells are seen in vehicular transportation, electric utility and other applications requiring clean, quiet and portable power. Operating above 150ºC has many advantages such as increased reaction rate, flexibility to use not so pure hydrogen as fuel and/or lower loading of the expensive metal (Pt) on the electrode.
Research is underway to optimize the performance of the high temperature PEM fuel cells by finding the electrolyte material that combines certain prerequisites. The ideal polymer electrolyte, for this type of cell, should exhibit long term durability, good mechanical properties and high thermal and oxidative stability in order to be applicable in the particular conditions under which the cell operates. Moreover it should be able to be doped with a strong acid like phosphoric acid in order to posses high proton conductivity. Advent TPS® is an electrolyte for high temperature PEMFC that exhibits excellent film-forming properties, mechanical integrity, high glass transition temperature (280^0C) as well as high thermal stability up to 400^0 C. In addition to the above properties, Advent TPS® shows high oxidative stability and acid doping ability, enabling proton conductivity in the range of 10^{-2} S/cm[1].
In this work we synthesized nanocomposite membranes by adding inorganic, hydrophilic fillers, such as modified montmorillonite (H^+-MMT), into the polymer matrix of Advent TPS® in order to fabricate an hybrid membrane that reveals the ability to absorb water. The hydration of electrolyte can increase the proton conductivity. The nanocomposite membranes showed doping water ability (Figure 1), oxidative stability and proton conductivity in the range of 10^{-2} S/cm.

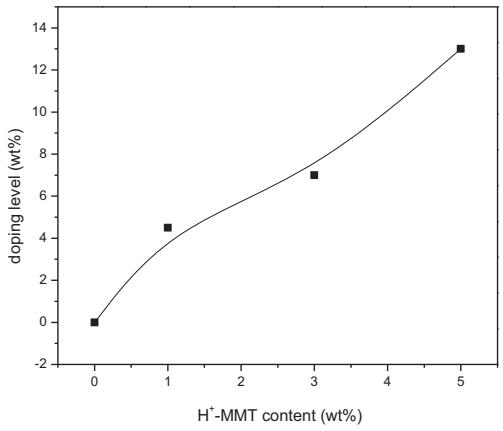

Figure 1: Doping level in water of the membranes versus H^+-MMT content

Furthermore, the nanocomposite membranes with H^+-MMT can retain the acid into the membrane, reducing the leaching problem during the cooling process of the cell. Finally the hybrid membranes were characterized with conventional techniques and showed thermal and mechanical stability (Figure 2).

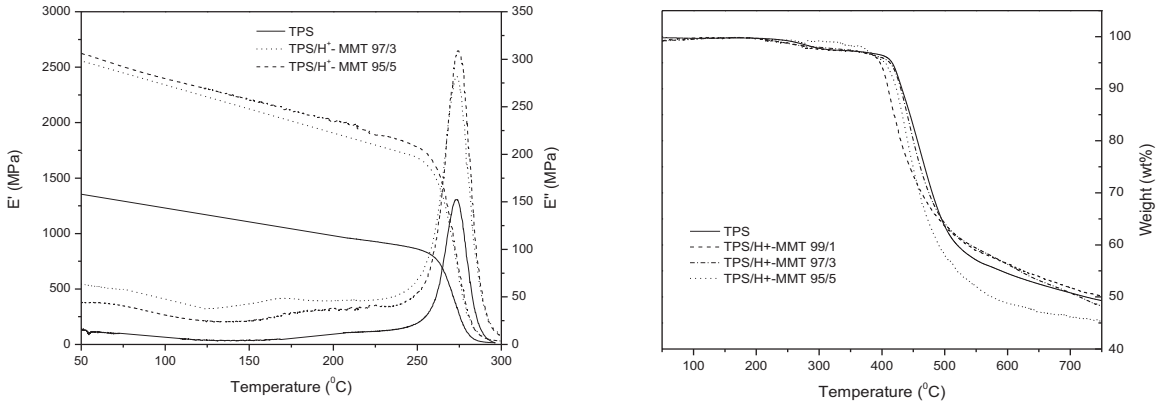

Figure 2: Storage and Loss modulus versus temperature and TGA curves for the membranes.

References

1.E. K. Pefkianakis, V. Deimede, M. K. Daletou, N. Gourdoupi, J. K. Kallitsis, Macromol.Rap.Commun., 26:1724 (2005)
2.V. Deimede, G. Kandilioti, J.K. Kallitsis, V.G. Gregoriou, Macromol. Symp. 230: 33 (2005).

Poster A21

Crosslinked 2-carboxybenzylchitosan: Synthesis, Characterization and Potential Use for Transdermal Delivery of Fluconazole.

Konstantinos P. Koutroumanis, Dimitrios N. Bikiaris

Laboratory of Organic Chemical Technology, Department of Chemistry, Aristotle University of Thessaloniki, 541 24 Thessaloniki, Greece.

Introduction

Hydrogels are gaining special interest as substances that exhibit phase transition (i.e., volumechange) in response to changes in external conditions such as pH, ionic strength and temperature, all of which are widely encountered in drug delivery systems. Chitosan (CS) [poly-b-(1→4)-D-glucosamine], a natural polymer obtained by alkaline deacetylation of chitin, is nontoxic and biocompatible. Chitosan dissolves in acidic solutions since it has a number of amino groups, but it is insoluble under higher pH conditions due to the deprotonation of amines. Chitosan is also of limited solubility in organic solvents. In order to overcome the above problems, some novel polyampholyte derivatives based on chitosan have been prepared by introducing various groups. The water-soluble derivative of chitosan, N-(2-carboxybenzyl)chitosan (CBCS) is synthesized and evaluated. The chemical structure of CBCS was characterized by FTIR, ^{1}H NMR and UV spectra. The DS of N-2-carboxybenzyl was determined by acid-base titration and UV spectrometry. When introducing 2-carboxybenzyl groups onto the $–NH_2$ groups of chitosan, an amphoteric polyelectrolyte containing both cationic and anionic fixed charges was prepared. CBCS crosslinked with glutaraldehyde (CBCSG) was prepared in this work. Finally, the release profiles of a model drug (Fluconazole) from the prepared hydrogels was studied.

Experimental

High-molecular-weight CS was obtained from Sigma-Aldrich. 2-Carboxybenzaldehyde (CBBA, 99%) was purchased from ACROS and sodium borohydride (SB, 'BAKER' grade) from J.T. Baker. Glutaraldehyde (GA, 50 wt % in water) was received and used as reagent grade from Sigma-Aldrich. All solvents were of analytical grade. Synthesis of CBCS was carried out as shown in Fig. 1. Chitosan powder was dissolved in 0.7% (v/v) aq. CH_3COOH, to which an appropriate amount of a solution of 2-carboxybenzaldehyde (3.6 g) in EtOH was added dropwise. After stirring in a water bath at specified temperature and time period the mixture was cooled down to R.T., and then an aq. solution of SB was added dropwise to bring about reduction of the Schiff base. Stirring was continued at R.T. The mixture was poured into an excess of acetone and the precipitate thus produced was filtered and washed with acetone. The partially derivatized product was dialyzed against deionized water for 3 days and precipitated by adding an adequate amount of acetone to obtain the purified CBCS, which was then dried under vacuum to constant weight. For the preparation of crosslinked CBCS, a solution of CBCS was prepared in distilled water and 0.7% (v/v) aq. CH_3COOH. A specific amount of crosslinking agent (GA) was added under intense stirring and after setting the bubble-free solutions were poured into shallow dishes at R.T. and let to stand overnight for gel formation. The hydrogels (CBCSG) were then dried in a freeze-dryer to yield the xerogels. The xerogels were then placed in drug solutions in ethanol of varying

concentrations, in which they swelled, and the mixture was left to dry at R.T. and constant stirring.

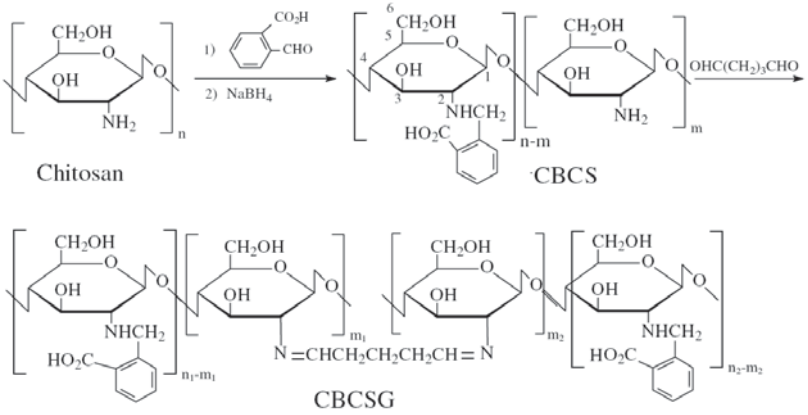

Fig. 1. Synthetic scheme for CBCS and CBCSG.

The degree of substitution was determined with both acid-base titration of the carboxylic groups on CBCS and UV spectrometry by measuring the absorption of the aromatic ring of 2-carboxybenzaldehyde. A Phillips 1710 Powder X-ray diffractometer was used for the identification of the crystal (structure and changes) of the polymers and also drug in case of solid dispersion. Dissolution Apparatus I basket method was used (PBS=7 , 37 °C), Drug loaded CBCSG powder was placed in a dialysis cellulose membrane bag, with a molecular weight cut-off 12.400, tied, and placed into the baskets. At predetermined time intervals 1 mL of aqueous solution was withdrawn from the release media. The samples were filtered and the quantification analysis was performed using HPLC method and an appropriate calibration curve.

Results

The in vitro release study showed zero release kinetics for fluconazole (Fig. 2).

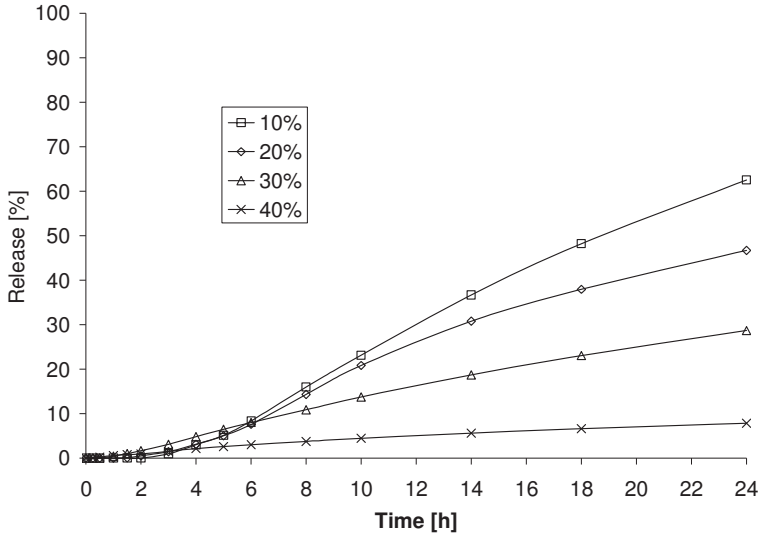

Fig.2. In vitro drug release profile of fluconazole.

Poster A22

Synthesis of copolyesters based on adipic acid, glycolic acid and 1,4-butanediol and their hydrolytic degradation

Sofia Papadaki, Despina Triantou, Johannis Simitzis*
National Technical University of Athens, School of Chemical Engineering, Department III "Materials Science and Engineering", Laboratory Unit "Advanced and Composite Materials", 9-Heroon Polytechniou str., Zografou Campus, 157 73 Athens, Greece.
*e-mail: simj@orfeas.chemeng.ntua.gr

1. INTRODUCTION

Aliphatic polyesters are among the most used biodegradable polymers in medical applications and have been extensively investigated in the past.[1] Homopolymers and copolymers of lactic acid (LA) with glycolic acid (GA) are used for surgical sutures, drug delivery devices, and other body implants. Random and block copolyesters of PLA and PGA as well as their blends have been investigated with regard to the regulation of biodegradation and improvement in the mechanical properties[1]. These polyesters degrade by hydrolytic attack of their ester bonds. Degradation denotes mass loss accompanied by a decrease of molecular weight of polyester and other structural changes. The mechanical properties and the degradation are affected by the combined effects of the crystallinity, the molecular weight, etc[2,3].

The aim of this work is the synthesis of copolyesters based on adipic acid, glycolic acid and 1,4-butanediol using different molar ratios and the study of their hydrolytic degradation.

2. EXPERIMENTAL

Polyesters were synthesized using glycolic acid, adipic acid and 1,4-butanediol in different molar ratios. The polyesterification was carried out in a 0.5 L vapor reflux reactor by the azeotropic distillation method and heating the reaction mixture up to 200 ^{0}C [4,5]. Since butanediol is volatile and is removed from the reactor together with the water, the necessary amount of glycol was in a molar excess of 5 % over the stoichiometry. The acid number (A.N.) of the polyesters, dissolved in toluene/ methanol (1/ 2 v/v), was determined by titration with 0.1 N KOH alcoholic solution and it characterizes the progress of the polyesterification [1,4,5]. The molecular weight of the polyesters, $\overline{M}_n$, was estimated from the acid number. The crystallinity of the polyesters were determined by X-Ray Diffraction analysis (XRD) using a Siemens D5000 diffractometer with CuK_α radiation. The hydrolytic degradation of polyesters in the form of discs (diameter: 20 mm, height: about 1 mm) was studied in deionized water at 50 °C for 180 h.

3. RESULTS AND DISCUSSION

Copolyesters based on glycolic acid (G) combined with adipic acid (A) and 1,4-butanediol (B) were synthesized in different percentage of molar ratios (A: 100 - 0 % and G: 0 - 100 %). In Table 1, the composition of the monomers used for the synthesis of polyesters and some of their basic structural characteristics are presented. The acid number (A.N.) of the polyesters is below 40, as the commercial polyesters have [4,5]. Moreover, the molecular weight of the polyesters, $\overline{M}_n$, was estimated from the A.N. using the equation :

$$\overline{M}_n = \frac{56000}{A.N.}$$

The molecular weight of the polyesters is between 1700 and 2200. The homopolymers A100 and G100 have higher degree of crystallinity than the copolymers, due to the single type of structural units that they are consisted of , i.e. butane adipate units in A100 and glycolate units in G100.

Figure 1 shows the hydrolytic degradation expressed as W ($W=(W_o-W_t)/W_o$, where W_o : initial weight of specimen and W_t : weight of specimen at time t) versus time of the polyesters A100, A60G40 and G100. The hydrolytic degradation of the polyesters increases and after a certain

time (equilibrium time, t_{eq} = 30 up to 60 h) reaches is maximum value of $W_m = (W_o-W_{eq})/W_o$, where W_{eq}: weight of specimen at equilibrium time.

Table 1. Raw materials used for the synthesis of polyesters, their physical state at 25 °C, acid number (A.N.), molecular weight ($\overline{M}_n$) and degree of crystallinity (X_c %).

Code	Raw materials (Composition % molar ratio)			Physical state at 25 °C	Acid number	Molecular weight	Degree of crystallinity
	Adipic acid (A)	Glycolic acid (G)	Butanediol (B)		A.N.	$\overline{M}_n$	X_c (%)
A100	100	-	105.0	solid	34	1700	80
A80G20	80	20	84.0	solid	29	2000	60
A60G40	60	40	63.0	wax like	28	2100	50
A50G50	50	50	52.5	viscous liquid	34	1700	0
A40G60	40	60	42.0	viscous liquid	26	2200	0
A20G80	20	80	21.0	wax like	28	2100	30
G100	-	100	-	solid	*	-	65

* Polyester G100 is insoluble in toluene/ methanol

Figure 2 shows the degree of crystallinity, X_c and the maximum degradation of polyesters versus the molar feed ratio of adipic acid. The homopolymers A100 and G100 show lower degradation than copolymers, due to their high X_c. Starting from 100 % molar feed ratio of adipic acid and increasing the corresponding ratio of glycolic acid up to 60 % (polyester A40G60), the degradation of the copolyesters increases, due to the decrease of X_c. The polyesters A50G50 and A40G60, which are viscous liquids, show the highest degradation. Copolyester A20G80 that has crystallinity show lower degradation than the viscous liquid copolyesters.

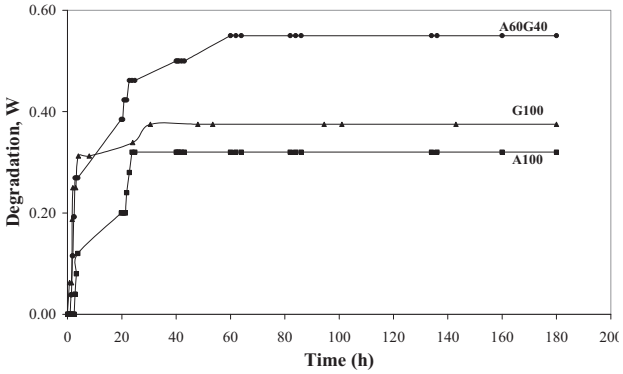

Figure 1. Hydrolytic degradation W, of the polyesters A100, A60G40 and G100 versus time

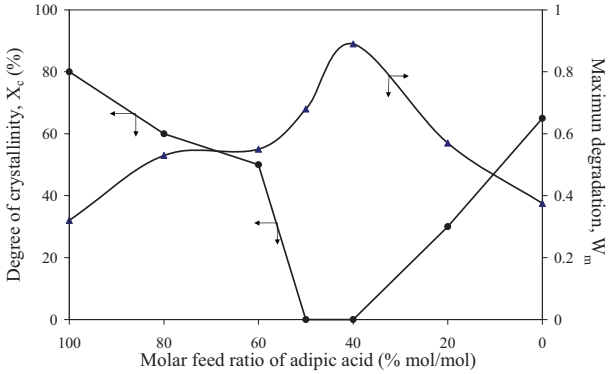

Figure 2. Degree of crystallinity, Xc and maximum degradation, W_m, versus molar feed ratio of adipic acid

In conclusion, the hydrolytic degradation of the polyesters is affected by their crystallinity, i.e. the polyester with high degree of crystallinity is more stable in degradation than the amorphous. The experimental data of hydrolytic degradation were fitted with exponential rise to maximum equations and the rate constant of hydrolytic degradation, k, of polyesters was determined.

References

1. A. C. Albertsson, I. K. Varma, Adv. Polym. Sci., 157 (2002), 1-40.
2. H. Sawada, *Depolymerization*, in **"Encyclopedia of Polymer Science and Technology"**, J.Wiley & Sons, 2007, pp. 1-26.
3. N. C. Billingham, *Degradation,* in **"Encyclopedia of Polymer Science and Technology"**, Vol. 6, J.Wiley & Sons, 2002, pp.1-49.
4. J. Pomakis, J. Simitzis, Angew. Makromol. Chem., 99 (1981), 145-170.
5. J. Simitzis, L. Zoumpoulakis, S. Soulis, Current Trends Polym. Sci., 8 (2003), 107-125.

Poster A23

Low Temperature Process for the Production of Long Chain Aliphatic Polyamides

A. C. Boussia, S. N. Vouyiouka, C. D Papaspyrides

Laboratory of Polymer Technology, School of Chemical Engineering,
National Technical University of Athens, Greece

Introduction

The polyamide structure and properties change when varying the monomer units, i.e. the diacid and/or the diamine. The use of long chain diacids in the formation of polyamide salts is anticipated to affect the properties of the resulting polyamides, such as melting point, moisture absorption and impact properties, through changing the hydrophilic/hydrogen bond site concentration [1].

Regarding the typical production of one of the most commercially important polyamides, PA 66, a starting intermediate is used, namely the salt of adipic acid and hexamethylenediamine, and a solution-melt polymerization technique is applied. Nevertheless, this method exhibits some disadvantages related to the use of high temperatures and to the expensive water cycle. Therefore, a low temperature two–step polyamidation profile has been suggested by our laboratory in a previous work, close to the melting point of the starting monomer, ensuring easy material handling due to solid starting monomer, end group balance and minimum thermal degradation in the produced prepolymer [2,3].

In this work long chain diacids, namely dodecanedioic acid, tridecanedioic acid and tetradecanedioic acid are used to form polyamide salts with hexamethylenediamine. The formed monomers are isolated in the solid state and characterized, in order to ensure their suitability for polymerization. In sequence, a two-step melt polymerization of the salts is carried out in an autoclave at low reaction temperature, in order to produce the respective long chain polyamides.

Experimental

The materials used were hexamethylenediamine (HMD) and adipic acid (AA) obtained from Merck (Darmstadt, Germany), dodecanedioic acid (DC12), tridecanedioic acid (DC13) and tetradecanedioic acid (DC14) provided by Cathay Biotechnology, China.

The preparation of polyamide salts involved combining the diacids with hexamethylenediamine in exactly molecular proportions, by bringing together ethanol solutions of equivalent amounts of the reactants [4], according to the reaction scheme:

$$HOOC–(CH_2)_n–COOH + H_2N–(CH_2)_6–NH_2 \rightarrow {}^-OOC–(CH_2)_n–COO^- \cdot {}^+H_3N–(CH_2)_6–NH_3^+$$

n=4, 10, 11, 12

Precipitation of the polyamide salts took place in all cases. The precipitates were filtered, thoroughly washed and dried *in vacuo* for 4 h (50 ^oC).The characterization of the obtained salts involved determination of mass yield, DSC and TGA analyses, pH of aqueous solution of the salts, amine end group concentration and XRD.

Following, the polymerization was carried out in a 50 ml stainless steel reactor (Parr Instr. Co.). The polymerization process was characterized by two stages. First stage involved heating under autogenous pressure maintenance (P_{max}= 4 bar) and at a temperature close to the melting point of the salt (T=200–225 ^{o}C). During the second stage, evacuation of the reactor accompanied with N_2 flow (300 mL min^{-1}) took place, and the temperature was raised, but still remaining at a benign range (T = 225–250 ^{o}C). The produced PA 66, PA 612, PA 613 and PA 614 were extracted as solids and characterized. For this purpose, the grades underwent DSC, RV measurement, NH_2 determination and XRD analysis.

Results and Discussion

PA salts were synthesized combining hexamethylenediamine and different diacids. The prepared PA 66, PA 612, PA 613 and PA 614 salts were isolated in the solid state and characterized. The salts were balanced and revealed different crystalline structures, characterized by diminishing thermal stability and melting point with increasing diacid chain length, whereas in some cases solvent inclusion in the crystal lattice occurred.

According to their melting points, which were in the range of 177 ^{o}C to 195 ^{o}C, the synthesized salts underwent polymerization at a low temperature polyamidation profile, with maintenance of autogenous pressure during the first stage, which ensured prepolymer products with minimum thermal degradation and molecular weight suitable for post polymerization. The melting points of the long chain polyamides varied from 205 ^{o}C to 262 ^{o}C, revealing a correlation with the amide group density, as were diminishing with diacid length increase.

The low temperature polyamidation technique was evaluated, as it can result in prepolymers of sufficient molecular weight, minimum thermal degradation accompanied with environmentally and energetically friendly profile, due to absence of the expensive water cycle and high temperatures.

Acknowledgements

The authors would like to thank Cathay Industrial Biotech Ltd. for the kind supply of long chain diacids.

References

1. P. Caswell, Polyamide 2005, The Polyamide Chain, 6th World Congress Düsseldorf, Germany, Conference Proceedings, 2005.
2. C. Papaspyrides; S. Vouyiouka; I. Bletsos, J. Appl. Pol. Sci., 2004, 92(1), 301-306.
3. D.G Tynan; C.D Papaspyrides; I.V. Bletsos, U.S. Patent 5941634, 1999.
4. A. C. Boussia; S. N. Vouyiouka; C. D. Papaspyrides, 9th European Symposium on Polymer Blends, Conference Proceedings, 2007, 97.

Poster A24

Titanium catalyzed ring opening polymerization of lactides. A route to novel macromolecular architectures

N. Petzetakis, D. Let, V. Kotzabasakis, M. Pitsikalis and N. Hadjichristidis
Industrial Chemistry Laboratory, Dept. of Chemistry, University of Athens
Panepistimiopolis Zografou, 15771 Athens Greece

Abstract

Titanium complexes have been widely used in the field of polymer chemistry since the discovery of the Ziegler-Natta catalytic systems for the synthesis of polyolefins with controlled stereochemistry[1]. More recently, half-titanocenes, titanocenes and other titanium complexes in combination with suitable cocatalysts have been employed for the polymerization of a wide variety of non-polar and polar monomers[2]. In the present study, rac-lactide and l-lactide have been polymerized in a very well controlled manner employing the titanium catalyst $CpTiCl_2OR$ [Cp=cyclopentadiene, and R= $-OCH_2CH_3$] leading to quantitative yields and products of narrow molecular weight distributions (M_w/M_n values lower than 1.1). The polymerization was conducted in toluene at 130°C. The reaction's kinetics was studied revealing that the polymerization yield and the molecular weight increase linearly with time. Using this methodology diblock copolymers of poly(L-lactide), PLLA with polystyrene, PS, PS-*b*-PLLA and triblock terpolymers with PS and polyisoprene, PI, of the type PS-*b*-PI-*b*-PLLA and PI-*b*-PS-*b*-PLLA were synthesized by a combination of coordination with anionic polymerization. Methacrylate-ended PLLA macromonomers have been prepared by polymerizing LLA with a suitable functionalized titanium catalyst. The macromonomers were copolymerized with methyl methacrylate, MMA, by conventional free radical polymerization techniques to provide the PMMA-g-PLLA graft copolymers. ATRP was also employed for the copolymerization offering a much better control over the molecular characteristics of the graft copolymers. The products are well-defined as concluded from the thorough characterization by size exclusion chromatography, equipped with refractive index and two-angle light scattering detectors, membrane osmometry, NMR and IR spectroscopy. Micelle formation was investigated for the diblock and triblock copolymers in acetonitrile, which is selective for the PLLA blocks. Static and dynamic light scattering were employed for this study.

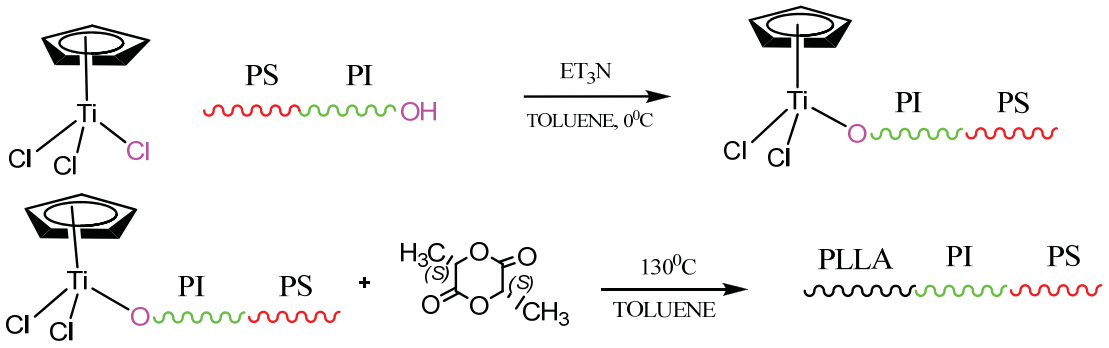

References

1. (a) Soga, K.; Shiono, T. *Progr. Polym. Sci.* **1997**, *22*, 1503. (b) Jenny, C.; Maddox, P. *Curr. Opin. Solid State Mater. Sci.* **1998**, *3*, 94. (c) Corradini, P.; Guerra, Cavallo, L. *Acc. Chem. Res.* **2004**, *37*, 231. (d) Coates, G.W. *Chem. Rev.* **2000**, *100*, 1223. (e) Bajgur, C.S.; Sivaram, S. *Curr. Sci.* **2000**, *78*, 1325, (f) Coates, G.W.; Hustad, P.D.; Reinartz, S. *Angew. Chem. Int. Ed.* **2002**, *41*, 2236. (g) Mülfaupt, R. *Macromol. Chem. Phys.* **2003**, *204*, 289.
2. (a) Kuran, W. Principles of Coordination Polymerization; John Wiley & Sons 2001 (b) Patten, T.E., Novak, B.M., *J.Am.Chem.Soc.* **113,** 5065 (1991). (c) Touris, A., Kostakis, K., Mourmouris, S., Kotzabasakis, V., Pitsikalis, M., Hadjichristidis, N., *Macromolecules* **41** (7), 2426-2438 (2008).

Poster A25

Synthesis of symmetric and asymmetric miktoarm star copolymers $(PI)_2(PEO)_2$

Vasilakopoulos Theodoros, Iatrou Hermis, Hadjichristidis Nikos

Department of Chemistry, University of Athens, Panepistimiopolis Zografou, 15771, Athens, Greece. (E-mail:tedhop82@gmail.com)

Abstract:

Symmetric and asymmetric 4-miktoarm star copolymers of PI (polyisoprene) and PEO (polyethyleneoxide) have been synthesized using anionic polymerization high vacuum techniques and appropriate linking chemistry (scheme).

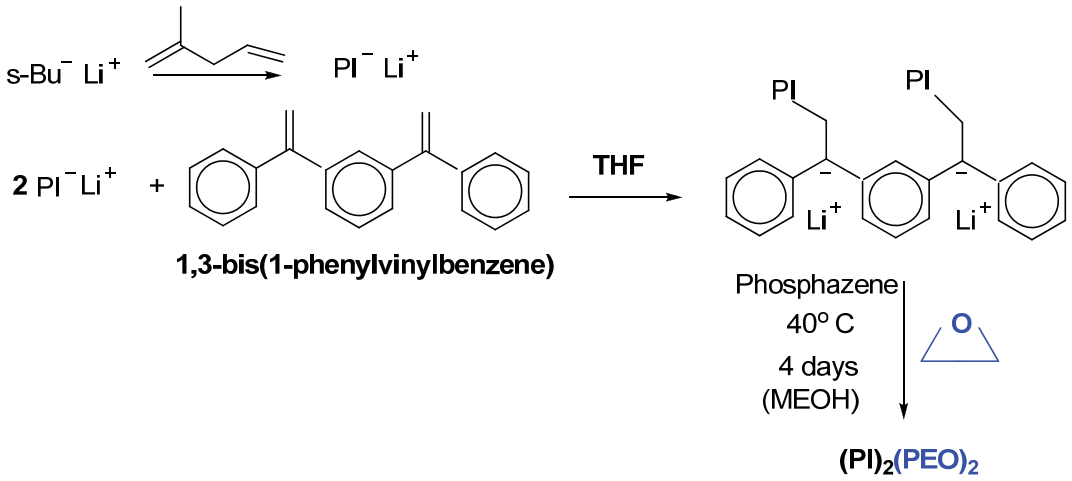

The molecular weight of each arm varied from 6k to 12k as determined by ^{1}H-NMR and size exclusion chromatography (SEC).The most crucial stage of this synthesis is the linking reaction of poly(isoprene)lithium with the coupling reagent PEB[1,3 bis(1-phenylethenyl)benzene].The yield of this reaction was almost quantitative. These miktoarm star copolymers will be used in order to examine the effect of architecture on surfactant efficiency in three-component microemulsions (oil, water and non-ionic surfactant).

References:
(1) Fernyhough, C.M., Young, R.N., Tack, R.D. *Macromolecules* **1999,** *32*, 5760-5764.
(2) Quirk, R.P., Lee, B., Schock, L.E. Makromol.Chem., Macromol.Symp. *53,* 201-210 **(1992**).

Poster A26

Synthesis of well defined graft polymers

Nikopoulou Anastasia, N. Hadjichristidis.

Industrial Chemistry Laboratory, Dept. of Chemistry, University of Athens
Panepistimiopolis Zografou, 15771 Athens Greece
(nnikopoulou@yahoo.gr)

Abstract

A series of well-defined H-4 branches, H-5 symmetric and H-5 branches asymmetric polybutadienes (Scheme 1) was synthesized by combining the anionic polymerization-high vacuum techniques and the dual functional linking agent 4-(dichloromethylsilyl)diphenylethylene (DCMSDPE)[1,2]. The synthetic approach of the H-4 branches PBd involves the coupling of two living 3-arm PBd stars with dichlorodimethyl silane. The H-5 branches PBd homopolymers were synthesized by reaction of two living stars with DCMSDPE in order to produce a new macromonomer, followed by addition of s-BuLi to the double bond and Bd monomer in order to be polymerized by the newly created anion. Finally H-5 branches asymmetric polybutadienes were prepared via reaction of two different living stars with DCMSDPE to produce a new macromonomer and then addition of s-BuLi and Bd monomer (Scheme 2). The living stars, the precursors of all polymers, were synthesized by performing the following steps:

a. Selective reaction of two equivalents of living chains with DCMSDPE in order to produce a macromonomer,
b. Addition of s-BuLi to the double bond of the in-chain macromonomer,
c. Polymerization of Bd from the newly created anionic site to create the third arm in order to synthesize the living star

Intermediate and final products were characterized via Size Exclusion Chromatography (SEC), Membrane Osmometry (MO), Low angle Lazer Light Scattering (LALLS) and proton Nuclear Magnetic Resonance(^{1}H-NMR).

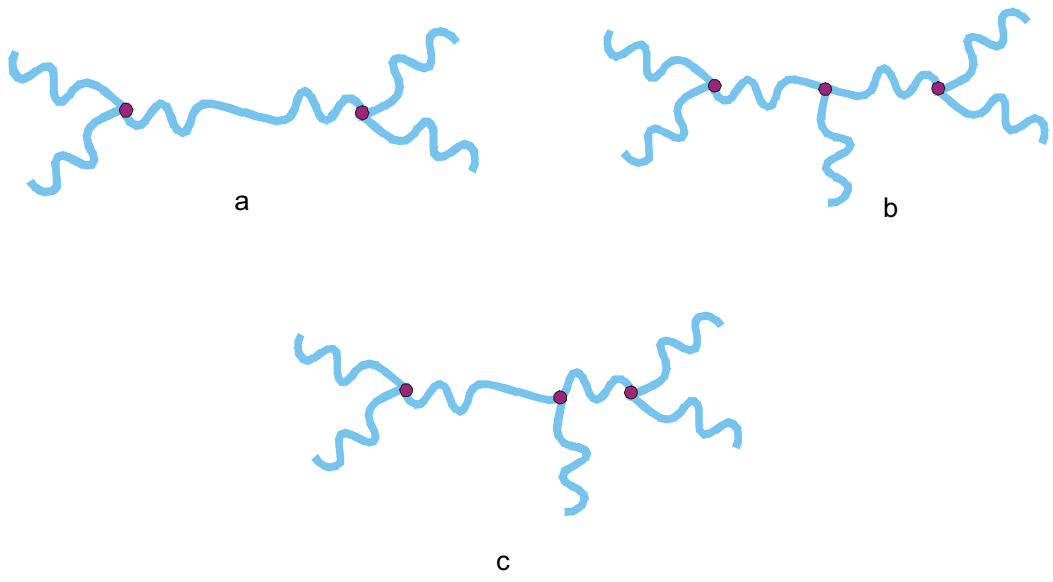

Scheme 1: Structures of the synthesized polymers,a)H-4 branches,b) H-5 branches symmetric and c)H-5 branches asymmetric

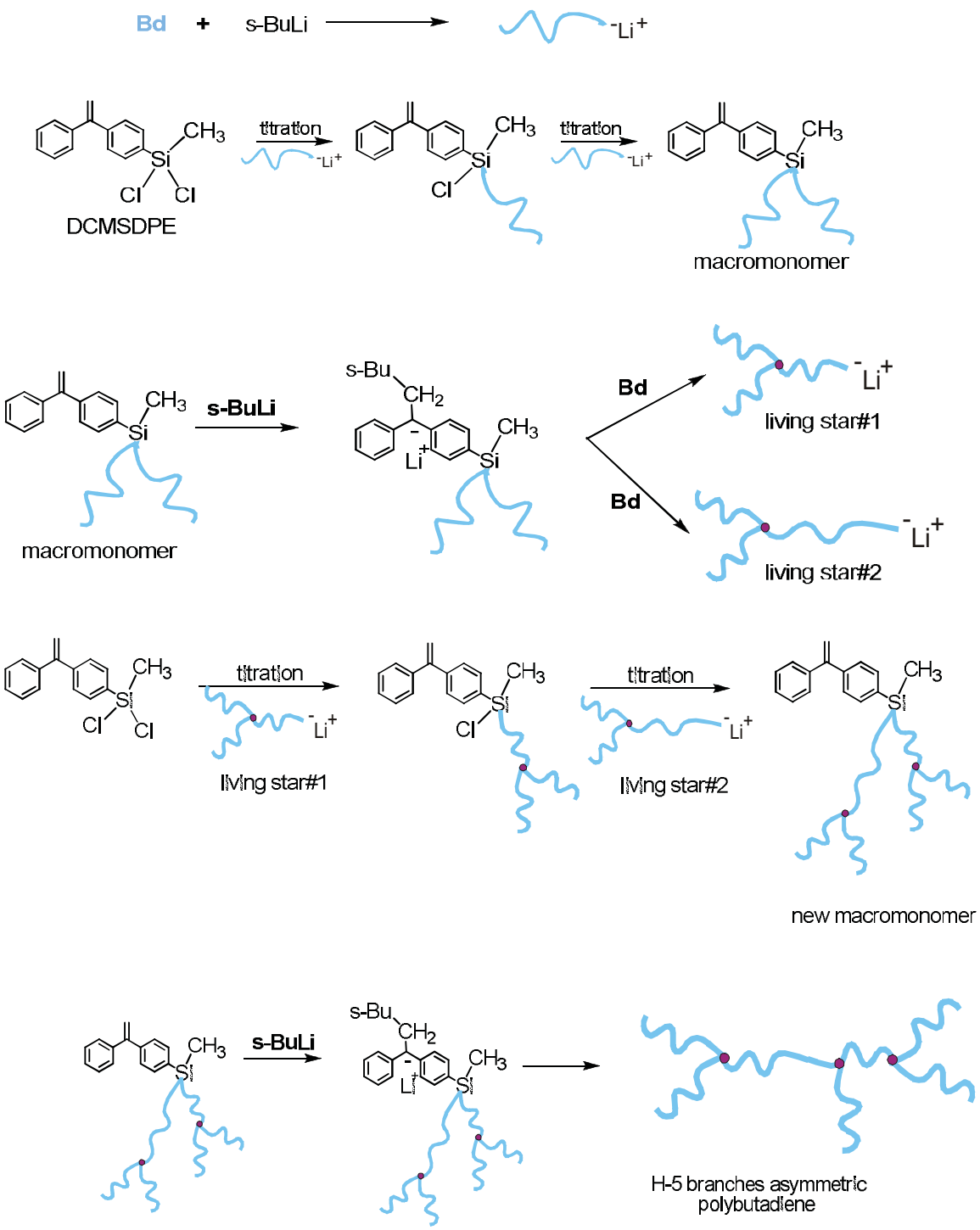

Scheme 2: Reaction scheme for the synthesis of H-5 branches asymmetric polybutadienes.

Refrences:

1. Zhou, Q., Wang, S., Fan, X., Advincula, R., Mays, J., *Langmuir* **2002**,18,3324.
2. Quirk, R., Mathers, R.,Cregger, T., Foster, M.D., *Macromolecules* **2002**,35,9964.

Poster A27

New approach to 'click chemistry' – Combination of 'click chemistry' and anionic polymerization

Athanasios Touris, Nikos Hadjichristidis

Department of Chemistry, University of Athens, Panepistimiopolis Zografou, 15771 Athens, Greece

ABSTRACT: Two novel anionic initiators containing a silyl-protected triple bond were synthesized. GCMS, ^{1}H NMR and ^{13}C NMR analysis showed that the synthesized initiators meet the standards of anionic polymerization in terms of purity. By using the above initiators, well defined α,ω-difunctionalized polymers (polymers that bear both the living anionic site and the chain-end 'clickable' triple bond) with narrow molecular weight distributions (I<1.1) were acquired. The existence of the chain-end triple bond was justified by several techniques (IR, ^{1}H NMR, ^{13}C NMR and MALDI TOF-MS analysis), showing the advantage of anionic polymerization upon other methods for synthesizing well defined polymers containing *quantitatively* functional groups susceptible to post polymerization reactions, like 'click' reactions.

Poster A28

Controlled Functional Nanoparticles

* E. Driva,[2] G. Sakellariou,[2] D. Baskaran,[2] J. W. Mays[1,2]
[1]*Chemical Sciences Division and Center for Nanophase Materials Science, Oak Ridge National Laboratory, Oak Ridge, TN 37831*
[2]*Department of Chemistry, University of Tennessee, 552 Buehler Hall, Knoxville, TN 37996*

Introduction

Functional polymeric nanoparticles with controlled sizes were synthesized using self-assembled poly(4-vinylbenzocyclobutene-b-butadiene) diblock copolymer precursor in tetradecane. The nanoparticles were formed by cross-linking the benzocyclobutene side groups at the core of the micelles and cleaving the polybutadiene corona block via ozonolysis. Dynamic and static light scattering confirmed the formation of micelles with core radius ranging from 2 to 8 nm. Benzocyclobutene side groups at the core were thermally cross-linked through inter/intra molecular Diels-Alder adduct formation at 200-240 °C in tetradecane. The ozonolysis of polybutadiene block of the core cross-linked micelles generated hydroxyl-functional groups at the surface of the nanoparticles. Transmission electron microscopy of the nanoparticles showed the presence of discrete nanoparticles ranging from 2 to 4 nm along with agglomerated nanoparticles ranging from 15 to 30 nm in diameter. Functional polymeric nanoparticles were also synthesized by intramolecular cross-linking of the middle styrenic block of poly (Bd-b-(St-co-VBCB)-b-Bd) linear, triblock copolymers. Ozonolysis of polybutadiene blocks led to organic nanoparticles that consist of only one chain and bear two hydroxyl groups on their surface.

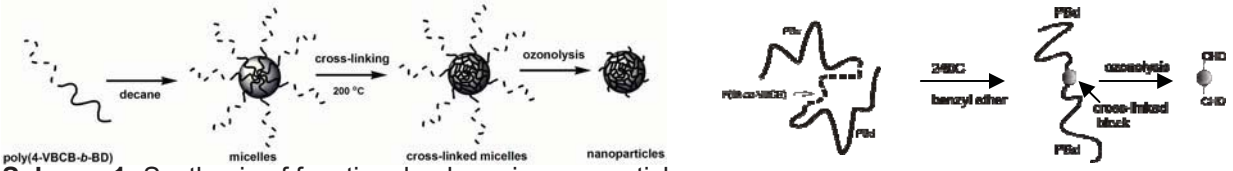

Scheme 1: Synthesis of functional polymeric nanoparticles

Experimental

Synthesis of poly(4-vinylbenzocyclobutene-b-butadiene):
The sequential block copolymerization of 4-vinylbenzocyclobutene and 1,3-butadiene was performed using standard all-glass high vacuum techniques as described in reference (Sakellariou et al, Macromolecules, 2006, 39, 3525).
Cross-linking reaction-Cleavage of polybutadiene segments through ozonolysis:
as described in reference (Sakellariou et al, Macromolecules, 2006, 39, 3525).

Results and Discussion

Benzocyclobutene side groups of poly(VBCB) are known to undergo thermal cross-linking via inter/intramolecular Diels-Alder adduct formation through an o-quinodimethane intermediate. Nanoparticles could be formed by cross-linking the micelles at the core and cleaving the 1,4-polybutadiene corona segments via ozonolysis. To accomplish this task, several diblock copolymers were synthesized through sequential living anionic polymerization using high vacuum technique (Table 1). Static and dynamic light scattering (DLS) of the micelles indicated the existence of uniform spherical micelles with aggregation numbers (N_w) ranging from 11 to 78. Hydrodynamic radius (R_h) of the micelles is in the range of 8-24 nm which increases with increasing the M_w of diblock and the N_w of micelles (Table 1, Fig. 2a-i). The drop wise addition of micelles into decane at 240 ºC was anticipated to minimize dissociation of micelles into unimers at high temperature. The SEC traces of core cross-linked micelles in THF showed a substantial shift to lower elusion volume as compared to diblock copolymer indicating formation of stabilized micelles without dissociation into unimers. The polydispersities of core cross-linked micelles were moderately narrow (M_w/M_n = 1.5) and free from unimers (Fig. 1). However,

dissociation of micelles into unimers up to about 10-15 % was detected when the cross-linking was performed at 200 ºC.

Table 1: poly(VBCB-b-BD) copolymers micelles and core cross-linked micelles in THF.

Micelles in decane					Cross-linked micelles in THF	
R_h(nm)	$M_{W,LS}$ x 10^{-3} (g/mol)	N_W	R_g/R_h	R_{core}(nm)	R_h(nm)	R_{core}(nm)
7.9	101.0	11.0	0.52	2.4	11.0	3.0
15.9	607.0	50.0	0.65	6.0	33.0	7.6
24.1	1800.0	78.0	0.65	7.7	44.1	9.7

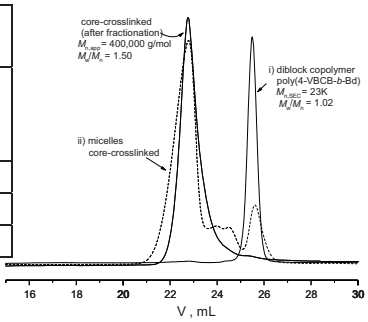

Figure 1. Size exclusion chromatography of core cross-linked micelles; i) poly(VBCB-b-BD) diblock copolymer, ii) after cross-linking at 240 ºC, M_w/M_n = 1.50, iii) after fractionation.

Molecular characteristics of the triblock copolymer that was synthesized and used for the preparation of intramolecularly crosslinked nanoparticles are shown in SEC chromatograms in Figure 2.

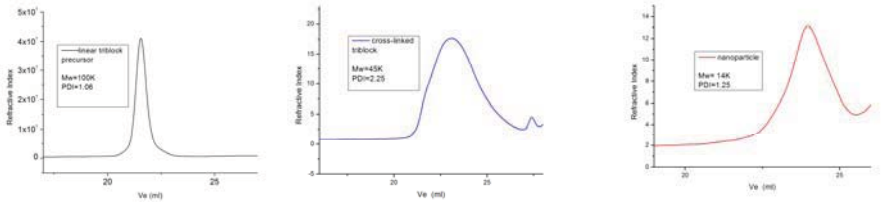

Figure 2. respectively linear triblock copolymer, cross-linked triblock, nanoparticle

The cross-linking was confirmed by H NMR and differential scanning calorimetry which showed an absence of cyclobutene signals and disappearance of T_g at ~120 ºC of poly(VBCB) block, respectively. In order to obtain functional nanoparticles, the core cross-linked micelles were subjected to ozonolysis to cleave the 1,4-polybutadiene corona segments in dichloromethane at -78 ºC. The nanoparticles obtained are insoluble in solvents and form agglomerated clusters. The FT-IR spectra of the nanoparticles show absorbance at 1740 cm^{-1}, 3000 cm^{-1} and 3400 cm^{-1} confirming the presence of aldehyde, aromatic and intermolecularly hydrogen bonded hydroxyl groups respectively. The nanoparticles decompose in air step wise from 200 to 600 ºC. The initial decomposition from 200 to 400 ºC is attributed to the decomposition of functional groups at the surface along with the residual fragments attached to the periphery of nanoparticles (Fig. 2). The nanoparticles were dispersed in methanol/dimethylformamide under sonication and drop coated on a carbon grid for TEM characterization. TEM images show discrete nanoparticles ranging from 2 to 4 nm along with agglomerated nanoparticles ranging from 15 to 30 nm in diameter. In conclusion, we have shown a new strategy for a controlled synthesis of functional organic nanoparticles using poly(VBCB) copolymers as precursor. This strategy could be used to tailor the size and the functionality of nanoparticles in several applications.

Acknowledgements. The authors of this paper would like to thank U.S. Army (DAAD19-01-2-002) and DOE (DE-AC05-00OR22725) for financial support. We gratefully appreciate Dow Chemicals, USA for a generous supply of 4-bromobenzocyclobutene.

References:

[1] G. Schmid, Wiley-VCH, Weinheim, **2004**.
[2] A. Einstein, Ann. Phys. (Leipz.) **1906**, 19, 371.
[3] M. E. Mackay, T. T. Dao, A. Tuteja, D. L. Ho, B. V. Horn, H. Kim, C. J. Hawker, Nature Materials **2003**, 2, 762.
[4] B. R. Cuenya, S. H. Baeck, T. F. Jaramillo, E. W. McFarland, J. Am. Chem. Soc. **2003**, 125, 12928.
[5] R. W. J. Scott, C. Sivadinarayana, O. M. Wilson, Z. Yan, D. W. Goodman, R. M. Crooks, J. Am. Chem. Soc. **2005**, 127, 1380.

Poster A29

Synthesis of Water Soluble Polypeptides Containing (L)-Proline

Gkikas Manos , Iatrou Hermis, Hadjichristidis Nikos
Department of Chemistry, University of Athens, Panepistimiopolis Zografou, 15771, Athens, Greece.

Abstract. In order to study the behavior and the conformation of water soluble polypeptides, we have managed to synthesize Poly-(L)-Proline[1] in high yields and purities by ring opening polymerization (ROP) of (L)-proline N-carboxyanhydride (NCA) using hexylamine as initiator and high vacuum techniques[2]. The (L)-proline NCA was prepared from (L)-proline and triphosgene in the presence of triethylamine or cross-linked polystyrene with dimethyl-amino groups[3].

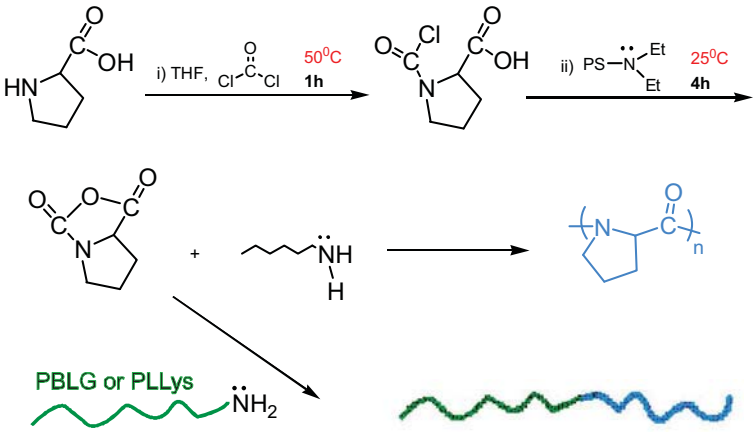

The use of high vacuum techniques allowed the purification of all chemicals involved in the polymerization (monomer, initiator, solvent) and the successful preparation of well-defined polypeptides. Taking advantage of the living character of polymerization we have synthesized proline based diblock copolypeptides by sequential ROP. These copolypeptides are very interesting because they combine the rigidity of the stable polyproline helicoidal conformation with the properties of the other polypeptides. We intent to study the conformational changes[4] and self-assembly behavior of the proline-based copolypeptides in water and other solvents, emphasizing in the role of polyproline in the architecture.

References

(1)Berger, A. ; Kurtz, J. ; and Katchalski, E. *J. Am. Chem. Soc.* **1954**, *76,* 5552-5554.
(2)Aliferis, T. ; Iatrou, H. ; Hadjichristidis, N. *Biomacromolecules* **2004**, *5*, 1653-1656
(3)Gulin, O.P ; Rabanal, F. ; Giralt, E. *Org. Lett.* **2006**, *8*, 5385-5388
(4)Müller, D. ; Stulz, J. ; Kricheldorf, H. *Makromol.Chem.* **1984**, *185*, 1739-1749

Poster A30

Synthesis and characterization of triblock copolymers by combination of anionic and atom transfer radical polymerization

Lucy-Fotini Arakelian, Marinos Pitsikalis and Nikos Hadjichristidis

Industrial Chemistry Laboratory, Department of Chemistry, University of Athens, Panepistimiopolis Zografou, 15771 Athens, Greece
(lucy_fotini@yahoo.com)

Abstract: Combination of anionic[1] and atom transfer radical polymerization[2] (ATRP) techniques were employed for the synthesis of poly(methyl methacrylate)-b-polybutadiene-b-poly(methyl methacrylate), PMMA-b-PBd-b-PMMA, poly(dimethylaminoethyl methacrylate)-b-polybutadiene-b-poly(dimethylaminoethyl methacrylate), PDMAEMA-b-PBd-b-PDMAEMA, and poly(methyl methacrylate)-b-polyethylene-b-poly(methyl methacrylate), PMMA-b-PE-b-PMMA, triblock copolymers. α, ω Difunctional polybutadienes bearing hydroxyl end-groups were synthesized by anionic polymerization high vacuum techniques using a difunctional initiator and reaction of the produced living polymers with excess ethylene oxide. Catalytic hydrogenation of these PBds provided the corresponding end-functionalized polyethylenes. The end-hydroxyl groups were subsequently esterified by reaction with 2-bromoisobutyryl bromide affording initiation sites for the ATRP of MMA or DMAEMA. The polymerizations were performed in THF using CuBr as the catalyst and 1,1,4,7,10,10-hexamethyltriethylenetetramine (HMTETA) as the ligand. The products were characterized by size exclusion chromatography, NMR spectroscopy, static light scattering and differential scanning calorimetry.

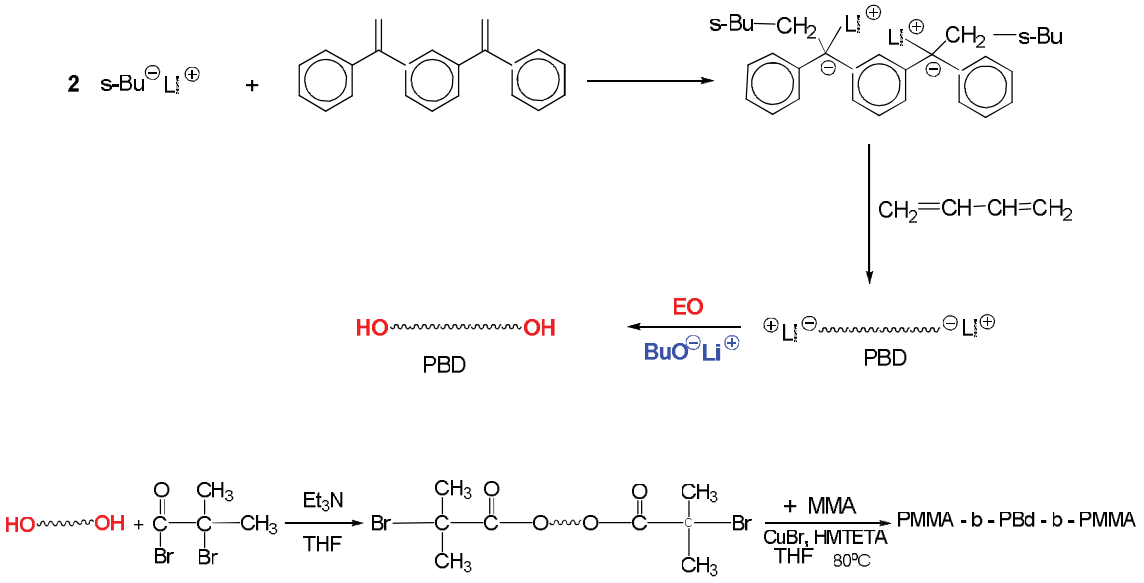

Scheme 1: Reaction scheme for the synthesis of PMMA-b-PBd-b-PMMA.

References:
1. N. Hadjichristidis, H. Iatrou, S. Pispas, M. Pitsikalis, J. Polym. Sci., Part A : Polym. Chem. 38, 3211 (2000).
2. K. Davis, K. Matyjaszewski, Macromolecules 2000, 33, 4039-4047

Poster A31

Terpyridine-Ruthenium Complexes for the Decoration of CNTs, Semiconducting Oligomers and Polymers.

A. K. Andreopoulou,[1,2] A. A. Stefopoulos,[1,2] E. K. Pefkianakis,[1,2] N. P. Tzanetos,[1,2] C. Papagellis,[3] M. Hammond,[4] R. Mezzenga,[4] J. K. Kallitsis[1,2]

1) Department of Chemistry, University of Patras, GR-26500 Rio-Patras, Greece;
2) Foundation of Research and Technology Hellas, Institute of Chemical Engineering and High Temperature Processes, P.O. Box 1414, GR-26500 Rio-Patras, Greece;
3) Department of Materials Science, University of Patras, 26504 Rio, Patras, Greece;
4) Department of Physics and Fribourg Center for Nanomaterials, University of Fribourg, Perolles Fribourg, CH-1700 Switzerland

The combination of metal ions, polymers, semiconducting species and furthermore carbon nanotubes is a triggering idea as well as a promising route for nanostructured composite materials with the properties needed in many modern and highly demanding technological applications. Metal-ligand coordination bonding, especially the bi and terpyridine transition metal complexes have been extended into a particularly useful tool towards supramolecular structures.[1] On the other hand carbon nanotubes (CNTs), single or multi walled, provide extraordinary mechanical, electrical and thermal properties.[3] Their surface modification towards soluble and processable functionalized CNTs has been the top priority of material scientists during the past decade. Several methodologies have been reported so far using covalent or non-covalent modifications of CNTs with polymers, organic, inorganic and biological molecules, thus many nanocomposites have been successfully prepared. The covalent modification can be categorized into two main routes the "*grafting to*" and the "*grafting from*" ways, that correspond to whether the functional group will be attached to the nanotube backbone or if it will be synthesized/polymerized onto the nanotube modified sites. [2]

Herein, both the "*grafting to*" and the "*grafting from*" routes were utilized for the functionalization of carbon nanotubes (CNTs) with terpyridine-Ru(II)-terpyridine moieties (tpy-Ru(II)-tpy). In particular SWCNTs (**Scheme 1a, 1b**) and MWCNTs (**Scheme 1c**) were modified with monomeric or polymeric tpy-Ru(II)-tpy dicomplexes through ATRP conditions[3] or aryl diazonium chemistry, respectively. For solubility reasons of the ruthenium complexes and metallopolymers used herein, long aliphatic chains were attached on the terpyridines, which subsequently acted as efficient solubilizers of the final hybrid metallo-CNTs.

Such long aliphatic substituents have led to improved solubilities of metallopolymers having high metal loadings and also when located on the outer sphere of dendrimers and dendronized polymers enhanced organizational features have been reported.[4]

The same functionalization approach was also applied onto other semiconducting species, oligomers or polymers, by proper end-functionalization with alkoxy bearing tpyRu(II)tpy complexes (**Scheme 1d**) indeed leading to their organization in the nanometer scale (**Figure 1b**).

Characterization of the modified CNTs was performed with TGA, UV-vis and Raman techniques while for the semiconducting oligomes additional NMR, PL and AFM characterizations were performed.

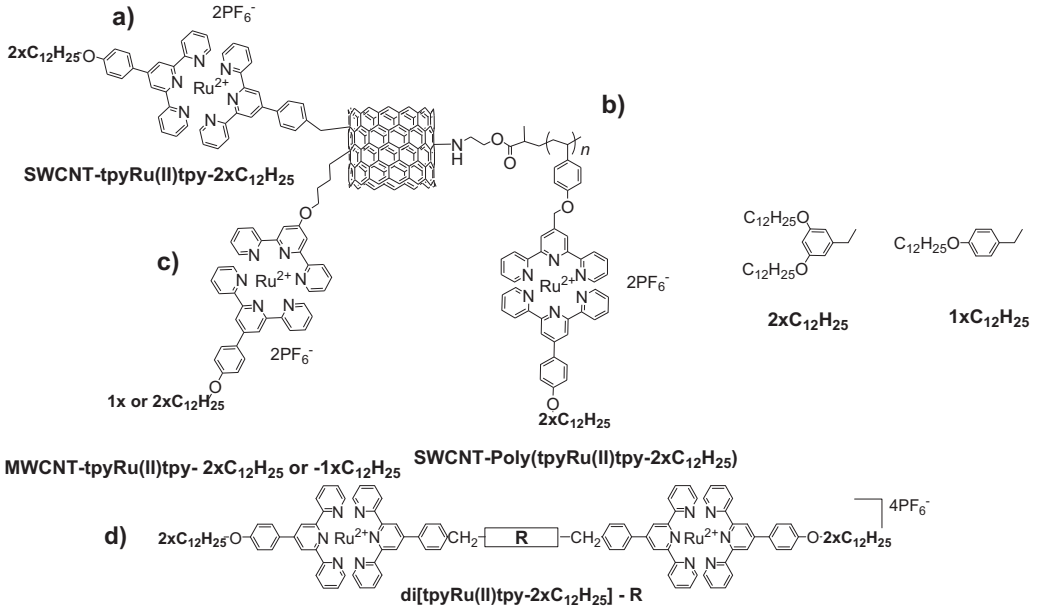

Scheme 1: CNTs and Semiconducting oligomers decorated with alkoxy-tpyRu(II)tpy complexes, R=distyrylanthracene, quinquephenyl, fluorene, trifluorene.

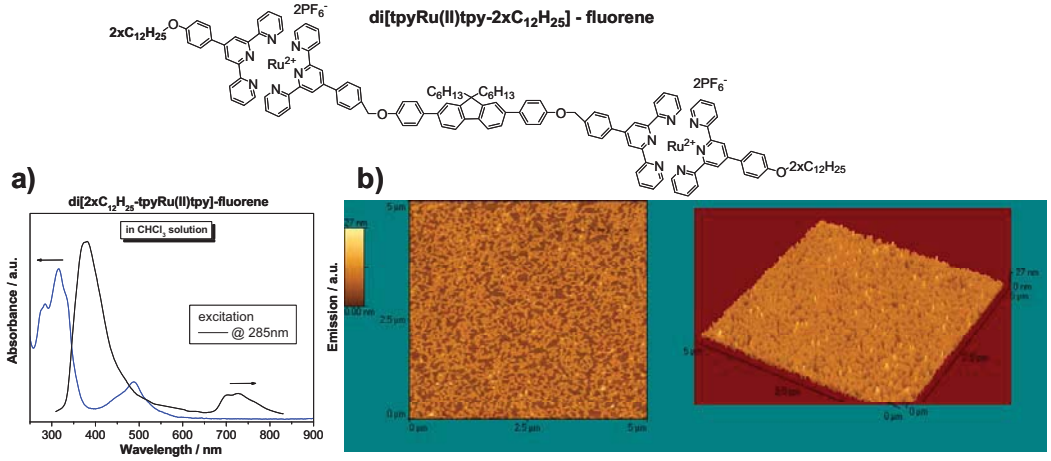

Figure 1: Semiconducting complex **di[tpyRu(II)tpy-2xC$_{12}$H$_{25}$]-fluorene** (**a**) UV-vis and PL spectra in $CHCl_3$ solutions 10^{-6} M, (**b**) AFM image of ~10^{-6} M solution spin coated on mica.

References:

1. U.S. Schubert, C.Eschbaumer, *Angew Chem Int Ed*. **2002**, *41*, 2892.
2. (a) D. Tasis, N. Tagmatarchis, A. Bianco, M. Prato, *Chem. Rev.* **2006**, *106*, 1105. (b) S. Iijima *Nature*, **1991**, *354*, 56. (c) A. Hirsch, O. Vostrowsky, *Top Curr. Chem.* **2005**, *245*, 193.
3. (a) D. Baskaran, W.J. Mays, S.M. Bratcher, *Angew. Chem., Int. Ed.* **2004**, *43*, 2138. (b) H. Kong, C. Gao, D. Yan, *J. Am. Chem. Soc.* **2004**, *126*, 412. (c) C.L. Chochos, A.A. Stefopoulos, S. Campidelli, M. Prato, V.G. Gregoriou, J.K. Kallitsis *Macromolecules*, **2008**, *41*, 1825. (d) A.A. Stefopoulos, C.L. Chochos, M. Prato, G. Pistolis, K. Papagelis, F. Petraki, S. Kennou, J.K. Kallitsis, *Chem. Eur. J*. **2008,** accepted.
4. (a) N.P. Tzanetos, A.K. Andreopoulou, J.K. Kallitsis *J. Polym. Sc.: Part A: Polym. Chem.*, **2005**, *43*, 4838. (b) A.K. Andreopoulou, J.K. Kallitsis *Eur. J. Org. Chem.* **2005**, 4448. (c) A.D. Schluter, *Top. Curr. Chem.* **2005**, *245*, 151. (d) A.K. Andreopoulou, B. Carbonnier, J.K. Kallitsis, T. Pakula, *Macromolecules*, **2004**, *37*, 3576 (e) V. Percec, B.C. Won, M. Peterca, P.A. Heiney *J. Am. Chem. Soc.* **2007***, 129*, 11265

Aknowledgement: We gratefully acknowledge “Nanothinx S.A.” for the MWCNTs. This project was partially supported from the Greek Ministry of Development under the research grant PENED 03ED118 “Organic Solar Cells” co-financed by E.U.-European Social Fund (75%) and the Greek Ministry of Development-GSRT (25%).

Poster A32

Synthesis of copolymers based on benzene and biphenyl and their characterization by XRD and DSC

Despina Triantou, Spyridon Soulis, Johannis Simitzis*
National Technical University of Athens, School of Chemical Engineering, Department III "Materials Science and Engineering", Laboratory Unit "Advanced and Composite Materials", 9-Heroon Polytechniou str., Zografou Campus, 157 73 Athens, Greece.
* e-mail : simj@chemeng.ntua.gr

1. INTRODUCTION

Conducting polymers, due to their low cost, low density, mechanical flexibility and easy processabilty are promising candidates for electronic, electrooptical and electrochemical applications [1]. Poly(p-phenylene), PPP, has attracted much interest among various conducting polymers, because of its high stability in air even at high temperatures, due to the aromatic repeat units [2]. Polyphenylenes can be prepared using benzene or other aromatic compounds, such as biphenyl, chemically in the form of powder or electrochemically as film. A principal advantage of chemical polymerization compared to the electrochemical one is the possibility of mass production at a reasonable cost. The para-coupling of the benzene ring leads to poly(p-phenylene), which is infusible and insoluble. Fusible and soluble polyphenylenes can be prepared from several aromatic compounds, such as biphenyl, because the resulting isomeric polyphenylenes have ortho-, meta- and para- couplings and therefore they are easier to be processed compared to the insoluble and infusible PPP [2,3] . In order to improve the processability of PPP, apart from the isomeric polyphenylenes, other approaches have been developed, where copolymerization is one of the most important [4].

The aim of this work is the synthesis of copolymers based on benzene and biphenyl and their characterization by XRD and DSC.

2. EXPERIMENTAL

Benzene (Benz) or biphenyl (Biph) were polymerized by oxidative cationic polymerization based on Kovacic method in order to produce polyparaphenylene (H-PPP) and o,m,p-polyphenylenes (H-PP), respectively. In the polymerization, copper chloride, $CuCl_2$, was used as oxidizer and aluminum chloride, $AlCl_3$, as catalyst [5,6]. Concerning the copolymerization of benzene with biphenyl, a series of preliminary experiments were carried out, in order to define the copolymerization conditions. Specifically, the optimum molar ratio of raw materials was determined as: [sum of the monomers] / [$CuCl_2$] / [$AlCl_3$] = 1/ 2 / 1.5 and the optimum copolymerization temperature as 55 ^oC. Two copolymers, C_1 and C_2, were produced using the molar ratio of benzene to biphenyl, [Benz] / [Biph] = 0.5 / 0.5 and 0.7 / 0.3, respectively [6]. The polyphenylenes produced were separated in the insoluble (H-PPP, H-PP-I, C_1-I, C_2-I) and the soluble (H-PP-S, C_1-S, C_2-S) in chlorobenzene polyphenylenes by extraction with chlorobenzene. The polyphenylenes were studied by X-Ray Diffraction (XRD) and Differential Scanning Calorimetry (DSC). XRD diffractograms were recorded on a Siemens D5000 diffractometer using samples in the form of powder, with CuK_α radiation and scan rate of 0.02 degrees per second. DSC measurements were carried out using a Netzch DSC 200 apparatus, in inert atmosphere of nitrogen, with a heating and reheating rate of 10 ^oC/min and cooling rate of 5 ^oC/min.

3. RESULTS AND DISCUSSION

Figure 1 shows the X-Ray difractograms of insoluble polyphenylenes. They have three main reflections, i.e. in the regions 19.1- 20.4^o, 21.0- 22.8^o and 26.3 - 28.0^o, where the latter reflection for the copolymers (C_1-I and C_2-I) appears as a double peak. Additionally, H-PP-I has three less intense reflections, i.e. at 16^o, 32^o and 39^o. From the X-Ray difractograms the degree of crystallinity, x_c (%) was determined. Table 1 presents the endothermic peaks of polyphenylenes at the temperature range from 268 up to 286 ^oC and their x_c (%). All polyphenylenes (homopolymers and copolymers) exhibit an endorhermic peak, except from homopolymer H-PPP, which has a rigid structure and it is infusible [2,3]. Moreover, they have x_c between 34.4 and 66.7 %, except from H-PP-S which has a low value. For the interpretation of the endothermic peaks, it was investigated whether the polymers melt at temperatures below 300 ^oC. For this reason, polyphenylenes in the form of discs were placed into furnace at 300 ^oC for 1.5 h, where it was observed that the soluble ones, i.e. H-PP-S, C_1-S and C_2-S, melt. Therefore, the endothermic peak

of soluble polyphenylenes, which have crystallinity, can be attributed to the melting of their crystallites. On the other hand, insoluble polyphenylenes, that they have also crystallinity they did not melt. In order to interpret these peaks, it is necessary to study the reversibility of the DSC peaks.

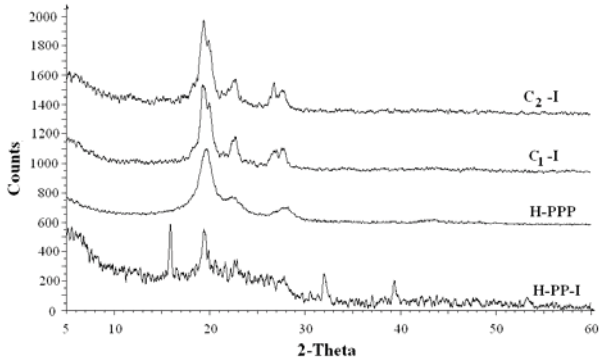

Figure 1. X-Ray difractograms of insoluble polyphenylenes

Table 1. Endothermic peak (°C) and degree of crystallinity, x_c (%) of polyphenylenes

Polyphenylene	Endothermic peak (°C)	Degree of crystalllinity, x_c (%)
H-PPP	-	47.5
H-PP-I	268.9	34.4
H-PP-S	278.0	practically amorphous (3.0 %)
C_1-A	280.0	66.1
C_1-S	281.4	57.1
C_2-A	277.8	66.7
C_2-S	286.4	44.6

Figures 2 and 3 show the DSC curves for the copolymers C_1-I and C_2-I, respectively. C_1-I during heating exhibits an endothermic peak at 280 °C, during cooling an exothermic peak at 236 °C and during reheating an endothermic peak at 265 °C. Similarly, C_2-I during heating exhibits an endothermic peak at 277.8 °C, whereas during cooling an exothermic peak at 241 °C. As it was previously mentioned, C_1-I and C_2-I have cystallinity but they did not melt. Their endothermic peaks seem like melting, which is a 1st order thermodynamic transition, whereas the 2nd order thermodanymic transitions, such as the glass transition temperature T_g are single phase transitions [7]. According to the literature[8], oligophenylenes exhibit thermal transitions near or above their melting point, which are endothermic and were attributed to liquid crystal transitions.

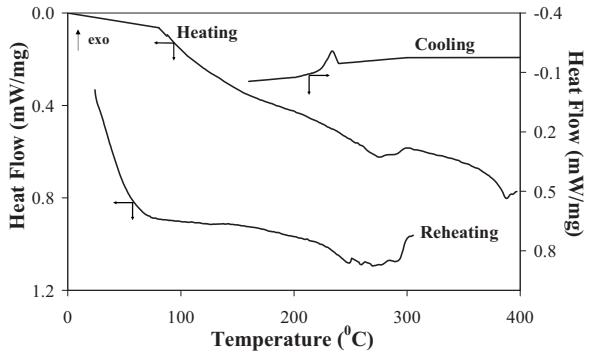

Figure 2. DSC curves of C_1-I

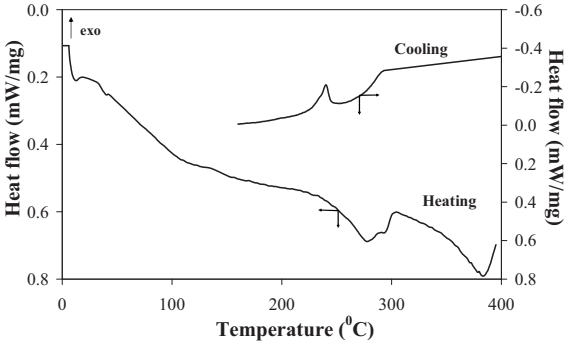

Figure 3. DSC curves of C_2-I

Thus, the endothermic peaks exhibited in the DSC of insoluble polyphenylenes from 268 up to 286 °C are attributed to liquid crystal transitions, whereas that of soluble polyphenylenes are attributed to the melting of their crystallites.

References

1. P. J. S Foot, A. B. Kaiser, *Conducting Polymers*, in **"Kirk-Othmer Encyclopedia of Chemical Technology"**, Vol. 7, J. Wiley, New York, 2004, pp. 513-550.
2. P.C. Lacaze, S. Aeiyach, J. C. Lacroix, *Poly(p-phenylenes): Preparation Techniques and Properties*, in **"Handbook of Organic Conductive Molecules and Polymers"**, ed. H. S. Nalwa, J. Wiley: New York, 1997, pp. 205-20.
3. A. C. Grimsdale, K. Müllen, Adv. Polym. Sci., 199 (2006), 1-82.
4. I. Cianga, Y. Yagci, Prog. Polym. Sci., 29 (2004), 387-399.
5. J. Simitzis, C. Dimopoulou, Makromol. Chem., 185 (1984), 2553-2568.
6. J. Simitzis, D. Triantou, S. Soulis, J. Appl. Polym. Sci., (2008), in press.
7. H-G. Elias, **"Makromolekuele"**, Huething Verlag, Basel, 1981, pp. 321-324.
8. K. N. Baker, A. V. Fratini, T. Resch, H. C. Knachel, W. W. Adams, E. P. Socci, B. L. Farmer, Polymer, 34 (1993), 1571-1587.

Poster A33

ELECTROCHEMICAL SURFACE TREATMENT OF LABORATORILY PRODUCED CARBON FIBERS BY CYCLIC VOLTAMMETRY

P. Georgiou, A. Photiou, S. Soulis, J. Simitzis *

National Technical University of Athens, School of Chemical Engineering,Department III, "Materials Science and Engineering", Laboratory Unit "Advanced and Composite Materials", 9 Heroon Polytechniou str., Zografou Campus, 157 73 Athens, Greece
**E-mail : simj@orfeas.chemeng.ntua.gr*

1. INTRODUCTION

Carbon fibres consistute one of the most important new age materials with their main application as reinforcement in advanced composite materials[1]. They are produced by pyrolyzing proper organic precursors above 1000 ^{o}C, the most important being the polyacrylonitrile (PAN) fibres. PAN fibres themselves, without pre-treatment cannot be carbonized because they lose more than half their weight when heated up to 500 ^{o}C. Thus, before pyrolysis they undergo a thermal oxidative treatment, which is usually called "oxidative stabilization", because PAN fibres are transformed into an infusible, inflammable material, which can then be efficiently transformed into carbon fibres[2,3]. The surface of carbon fibres is smooth and generally inert in nature. In order to increase their cohesion with the composite matrix, the carbon fibres are subjected to various surface treatments mainly with electrochemical methods[2,4]. These treatments form oxygen-containing functional groups such as carboxyl, carbonyl, lactone and/or hydroxyl groups on the surface of the fiber[1,4].
The aim of this work is the electrochemical surface treatment of laboratorily produced carbon fibres by cyclic voltammetry, using acidic electrolyte and the qualitative characterization of the functional groups formed on their surface.

2. EXPERIMENTAL

The precursor for the production of carbon fibres is commercial PAN (homopolymer Dralon-T) fibres (DT) in the form of untwisted yarn of 150 monofilaments. The fibres are isothermally treated following a heating programme of four stages in air atmosphere (1st:180ºC/60min/20g load, 2nd:220ºC/60min/12.5g load, 3rd:270ºC/60min/5g load, 4th:300ºC/20min/5g load), in a properly designed and constructed air circulation oven. The resultant oxidized PAN fibres (ODT) are subsequently carbonized / pyrolyzed under inert atmosphere up to 1000 ^{o}C and remained at this temperature for 30 min. The carbon fibers produced (PDT) are then electrochemically treated by cyclic voltammetry for 20 cycles, using 5 % w/w aqueous H_2SO_4 solution, in the potential sweep range between a) -1 V→+1.5 V→-1 V, narrow (PDT-N) (33.33 min of treatment) and b) -3 V→+3 V→-3 V, wide (PDT-W) (80 min of treatment) with sweep rate of 50 mV/s. Some of the oxygen-containing functional groups, created on carbon fibres surface after their electrochemical treatment, were indirectly characterized by FTIR spectroscopy and by their adsorption ability of anionic / cationic dyes from aqueous solutions (initial concentration of dye 0.032 g/l, 25 ºC). Additionally, for correlating purposes, the FTIR spectrum of carbon fibre DT isothermally treated at 270ºC for 2h is given (DT-270-2h).

3. RESULTS AND DISCUSSION

Figure 1a shows the cyclic voltammogram of carbon fibre PDT-N. In the forward sweep a broad anodic peak is observed in positive potentials between 0.2–0.6 V with maximum at 0.47 V for the 1st cycle and 0.29 V for the 20th cycle, due to the formation of oxygen containing groups on the fibre. In the reverse sweep a cathodic peak is observed in negative potentials at -0.41 V for the 1st cycle and -0.38 V for the 20th cycle, due to the partial reduction of the groups formed during forward sweep. Figure 1b shows the cyclic voltammogram of carbon fibre PDT-W. In the forward sweep a broad anodic peak is observed in positive potentials between 1.4 to1.7 V, with maximum at 1.52 V for the 1st cycle and between 1.7 to 2.2V, with maximum at 1.85 V for the 20th cycle. In the reverse sweep a broad cathodic peak is observed in negative potentials between -1.5 to -1.8 V with maximum at -1.64 V for the 1st cycle and between -1.1 to -1.5 V, with maximum at -1.31 V for the 20th cycle. Correlating the redox reactions of PDT-N, the anodic reaction begins earlier (shift to less positive potentials) and the cathodic one begins later (shift to more negative potentials) from the 1st cycle to the 20th. Correspondingly, for the PDT-W, the anodic reaction begins later (shift to more positive potentials) and the cathodic one begins also later (shift to more negative potentials) from the 1st cycle to the 20th. These shifts indicate a remotion from reversibility of the redox reactions with increasing cycles. The oxidation of carbon fibres surface proceeds by electron transfer reactions between the electrolyte and the fibres and by chemical reactions with the nascent oxygen formed during water decomposition[5] above 1.7 V.

Based on Figure 2, the fibre DT-270-2h exhibits low intensity absorption bands of C≡N groups at 2240 cm^{-1} and of C-H groups at 2930 cm^{-1} and 2865 cm^{-1}, whereas that of conjugated C=C groups at 1620 cm^{-1} is of high intensity. The fibre ODT exhibits a broad absorption band at 1596 cm^{-1} and low intensity absorption bands at 2927 cm^{-1} and 2853 cm^{-1} for C–H and at 2241 cm^{-1} for C≡N. The decrease of C–H can be attributed to the accomplishment of dehydrogenation reactions and the decrease of C≡N is due to cyclization reactions of most of the nitrile groups. The absence of C=O groups indicates that these groups 'accomplished their role' in the realization of cyclization reactions. According to FTIR spectrum of PDT, C≡N and C=O (1700 cm^{-1}) groups are not present, whereas the absorption band at 1638 cm^{-1} indicates the presence of conjugated bonds of >C=C< or C=N of the aromatic ring. Moreover, the absorption band at 3448 cm^{-1} is attributed to –OH groups. FTIR spectrum of PDT-W shows rather low intensity at 3448 cm^{-1} for the absorption band of OH groups, whereas the absorption bands of C=O groups and of conjugated >C=C< bonds of the aromatic ring are shifted leftwards (at 1682 and 1542 cm^{-1}, respectively).

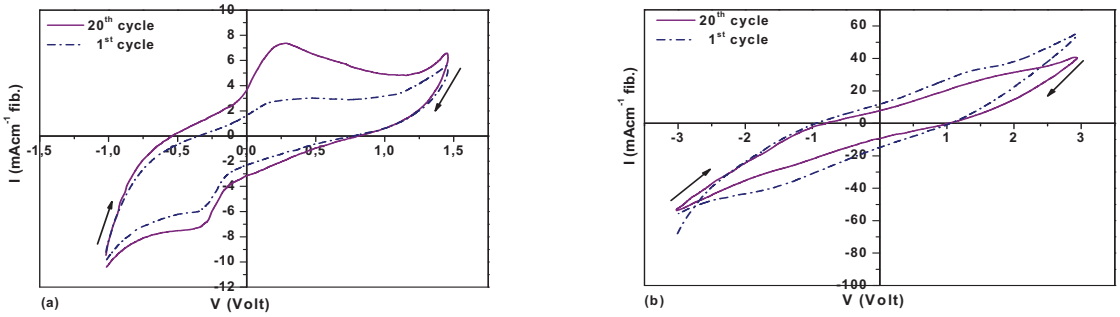

Figure 1. Cyclic Voltammograms of carbon fibres treated in H_2SO_4 5%w/w in the potential sweep range between a) -1V→+1.5V→-1V and b) -3V→+3V→-3V, with sweep rate at 50 mV/s for 1 and 20 cycles

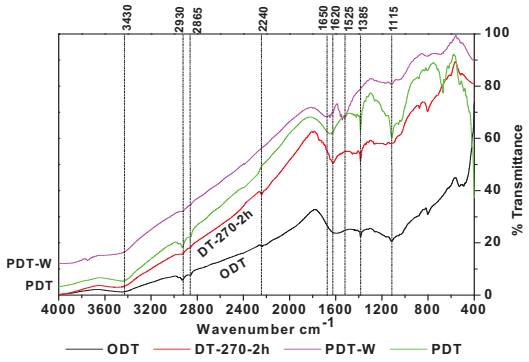

Figure 2. FTIR spectra of fibres ODT, DT-270-2h, PDT and the PDT-W

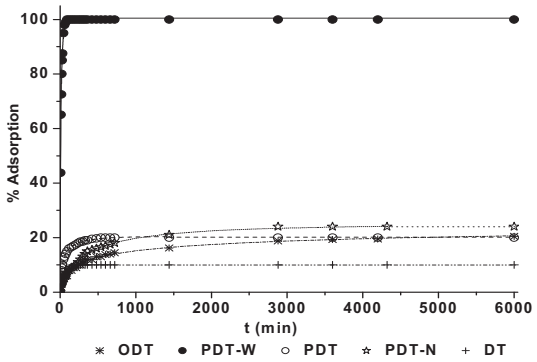

Figure 3. Adsorption of methylene blue by fibres ODT, PDT, PDT-N and PDT-W

Figure 3 configurates the discolouration ability of the untreated fibre DT, the oxidized fibre ODT, the pyrolyzed firbe PDT and the surface modified carbon fibres PDT-N, PDT-W. The fibres DT, ODT, PDT and PDT-N exhibit slight discolouration (10%, 20.5%, 20% and 24%, respectively). The PDT-W exhibits 100% discolouration only after 90 min. The ability of carbonaceous materials to adsorb dyes from their aqueous solutions can be used for the characterization of functional groups present on them. The dye adsorption taking place, is based on the concept of "electron donor-acceptor interactions" between the adsorbent and the adsorbate. Based on these, the discolouration of methylene blue solution, which mainly contains electron donating groups (EDG) in its molecule, is favoured by the presence of electron withdrawing groups (EWG) on fibre surface[6,7]. In conclusion, only after electrochemical treatment in the wide potential sweep range, EWG groups are sufficiently formed on the fibre surface.

References

1. L.B. Nohara, G.P. Filho, E.L. Nohara, M.U. Kleinke, M.C. Rezende, Materials Research, 8, 3, 2005, 281-286
2. M. Jing, C.-G. Wang, Y.-J. Bai, B. Zhu, Y.-X Wang, Polymer Bulletin 58, 2007, 541– 551
3. S. Soulis and J. Simitzis, Polym. Int., 54, 2005, 1474 – 1483
4. J. Gulyas, E. Foldes, A. Lazar, B. Pukanszky, Composites: Part A 32, 2001, 353–360
5. A. Bismarck, M.E. Kumru, J. Springer, J. Simitzis, Applied Surface Science 143, 1999, 45–55
6. C.U. Pittman, Jr.W. Jiang, Z.R. Yue, S. Gardner, L. Wang, H. Toghiani and C.A. Leon y Leon, Carbon, 37, 1999, 1797-1807
7. J. Simitzis, Acta Polymer., 45, 1994, 104-109

Poster A34

Nanofiller Effect On The Thermal Response Of Poly(3-Hydroxybutyrate) Nanocomposites And Isoconversional Kinetic Analysis Of The Thermal Degradation

E. Panayotidou[1,2], S. I. Marras[1], I. Zuburtikudis[1*], D. S. Achilias[2]
[1]*Department of Industrial Design Engineering, TEI of Western Macedonia, 50100 Kozani, Greece*
[2]*Department of Chemistry, Aristotle University of Thessaloniki, 54124 Thessaloniki, Greece*
[*] *izub@teikoz.gr*

Research on polymer-clay nanocomposites is currently expanding, because these hybrid materials exhibit improved properties over both their conventional counter-parts and the virgin polymers[1]. They consist of a polymer matrix in which inorganic particles with at least one dimension in the nanometer scale are homogeneously dispersed. The high aspect ratio particles interact with the polymer matrix and improve substantially many physical properties of the pristine polymer including enhanced mechanical characteristics and barrier resistance, decreased flammability and increased biodegrability in the case of biodegradable polymers.

Recently, biodegradable and biocompatible polymers have received significant attention because they are environmentally friendly and are extensively used in biomedical applications[2,3]. Poly(3-hydroxybutyrate) (PHB) is rapidly gaining recognition as one of the most promising biopolymers. PHB is a linear, aliphatic polyester produced by different types of microorganisms. However, the poor thermal stability at temperatures slightly higher than its melting point restricts the application field of PHB.

In the present work, various loadings of montmorillonite organically modified by octadecylamine (C_{18}MMT) were dispersed in PHB using a microexruder-compounder. The aim was to produce hybrid material with improved thermal properties over the pristine PHB. Constant nitrogen flow during nanocomposite preparation prevented thermal decomposition of the matrix.

Morphological characterization of the composites by X-ray diffraction analysis (XRD) indicated that the peak corresponding to the basal spacing of the inorganic material is shifted towards lower 2θ values which implies that polymer chains diffused into the clay galleries expanding the clay structure (Figure 1).

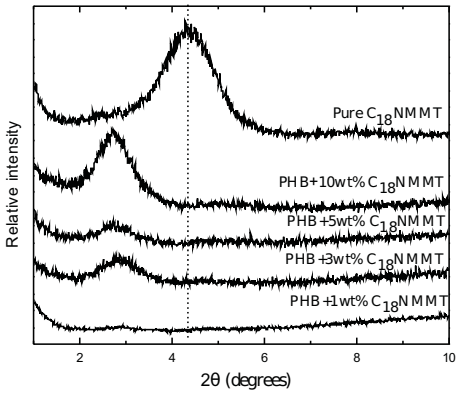

Figure 1: X-ray diffraction patterns of neat and nanocomposite materials

The effect of clay content on the thermal properties of the material was studied by differential scanning calorimetry (DSC) and thermogravimetric analysis (TGA). TGA analysis was performed

under nonisothermal (on heating) and isothermal conditions. It was found that organoclay incorporation significantly enhances the thermal stability of the polymer by retarding its decomposition rate, as shown in Fig. 2 and Fig. 3. Also, decomposition occurs in only one step starting at approximately 230°C

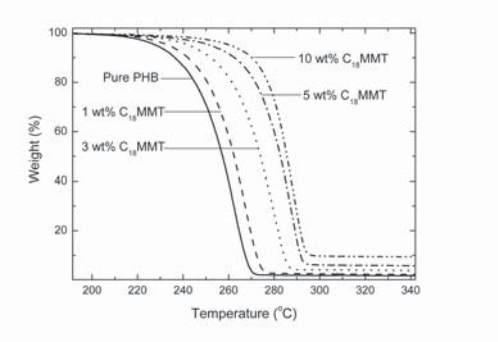

Figure 2: TGA curves for pure and nanocomposite PHB with various loading of C_{18}MMT in oxidant atmosphere.

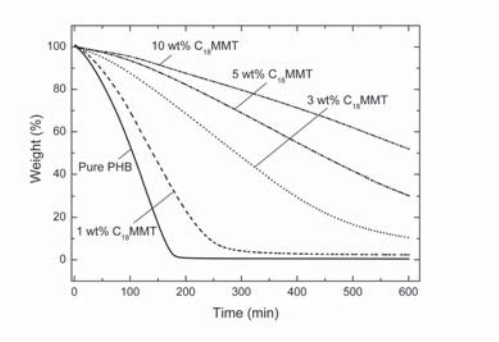

Figure 3: Effect of organoclay content on PHB nanocomposite mass loss in oxidant atmosphere and isothermal conditions (190°C).

Furthermore, in order to provide more insight into the thermal degradation mechanism a kinetic analysis was performed. Several different theoretical models were investigated according to their ability of simulating the experimental data. In addition, thermogravimetric scans were taken at four different heating rates for every sample in order to have adequate data to perform an isoconversional analysis. Effective activation energies were estimated as a function of the extent of degradation employing both a differential and an integral method. The effect of the amount of nanomaterial on the effective activation energy of the process is elucidated.

Acknowledgements
This work was supported by the Region of Western Macedonia (Greece) through the PEP grant with MIS 105545 to I. Z.

References

1. S.I. Marras, I. Zuburtikudis, C. Panayiotou *European Polymer Journal,* 43(6), 2191-2206, 2007.
2. S.I. Marras, K. P. Kladi, I. Tsivintzelis, I. Zuburtikudis, C. Panayiotou *Acta Biomaterialia,* 4, 756-765, 2008.
3. Tsivintzelis, S.I. Marras, I. Zuburtikudis, C. Panayiotou *Polymer,* 48(21), 6311-6318, 2007.

Poster A35

Periodic nanodot formation on polymers with plasmas: Towards plasma-directed polymer self-assembly?

D. Kontziampasis [a], N. Vourdas [a], G. Boulousis [a], V. Constantoudis [a], A. Tserepi [a], E. Gogolides[a].

[a] *Institute of Microelectronics NCSR Demokritos, Aghia Paraskevi, 15310, Greece*

Periodic, well-defined, features in the nano-scale are essential in several fields, such as photonics, optical applications, nanoelectronics, high-density information storage media, catalysis, bioanalytics, medicine etc. A variety of bottom up methods may be employed to attain the desired patterning such as block-copolymers[1], poly(styrene)-PS nano-beads[2], colloidal particles[3]. Also recent works have shown that sputtering with energetic ions (e.g. 1keV) may produce similar periodic structures after several hours of treatment [4, 5].

We present a new, fast, low ion energy, plasma-aided method of fabricating periodic nano-structures with controlled geometrical characteristics on polymer/plastic materials under appropriate plasma conditions[6].

Figure 1 is a 2x2 um^2 Atomic Force Microscopy (AFM) image, where the morphology of the plasma treated PMMA plate is unveiled; a mound-like surface of uniformly spaced and sized nanodots. Scaling analysis based on the height-height correlation function, G(r), shown in Figure 2 provides information on the correlation length (ξ), the average spacing (L) (1st min in G(r)) and width (W) (as 2ξ) of the nanodots. The periodic state of the surface is revealed by the existence of distinct minima of the G(r) function; at 45, 86, 121, 165 and 205 nm. Periodicity, L and W are plasma process- and reactor- dependent parameters and may be altered, by altering key-critical process and material parameters. The intense peak of F(k) function in Figure 3 at 0.02 nm^{-1} is in accordance with the G(r)-based results (1/0.02=50 nm periodicity). In figure 4 a 3D zoom of the AFM of Figure 1 is shown, unveiling the periodic nano-dots that are formed. PMMA films may also be etched down to the substrate. Figure 5 shows a 2x2 um^2 AFM image, where the morphology of the plasma treated PMMA film is unveiled. The film has been etched down to the Si substrate leaving only nano-dots of PMMA. Figure 6 shows also a peak of F(k) function at 0.009 nm^{-1} (1/0.009=111 nm periodicity) revealing the periodicity.

Analysis of the AFM images shows that only short range order has been achieved with the current choice of method parameters. We continue our work towards better control of long range order by altering and studying the effect of all process parameters. Also new polymeric materials (as well as PMMA with different M_w) will be studied as to their ability to form these nano-dots with this process. We are working towards using the nano-dots as a mask for pattern transfer on Silicon. Finally, we intent to check if long range order may be achieved with the use of a well known method such as grapoepitaxy[1].

Our results suggest that under the proposed process, spontaneously formed, self-organized, periodic nano-texturing is produced, with no special pretreatment. We propose to name this technique plasma-directed self-assembly of polymers.

[1] C. Park, J. Yoon, E.L. Thomas, Polymer, 44, 6725 (2003).

[2] S. Khvana, J. Kima, S.S. Lee, Journal of Colloid and Interface Science, 306, 2007, 22–27.

[3] A. K. Boal, F. Ilhan, J. E. DeRouchey, T. Thurn-Albrecht, T. P. Russell, V. M. Rotello, Nature, 404, 746 (2000).

[4] F. Frost, B. Ziberi, A. Schindler, B. Rauschenbach, Applied Physics A: Materials Science and Processing 91 (4), pp. 551-559.

[5] J. Muñoz-García, L. Vázquez, R. Cuerno, J.A. Sánchez-García, M. Castro, and R. Gago, Self-organized surface nanopatterning by ion beam sputtering, to appear in: Lecture Notes on Nanoscale Science and Technology, Edited by Zhiming M. Wang. (Springer, Heidenberg 2007, in press).

[6] N. Vourdas, E. Gogolides, A. Tserepi, V. Constantoudis, G. Boulousis, M. Vlahopoulou, K. Tsougeni, D. Kontziampasis, Greek patent application (under submission)

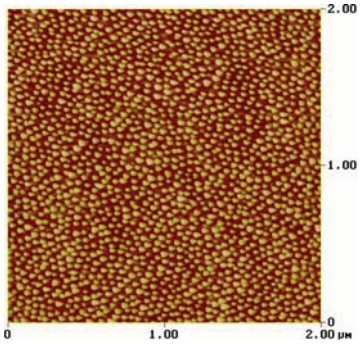

Fig 1. 2x2 um2 AFM image of PMMA plate surface after O_2 plasma treatment. RMS is 10.2 nm. (Nanoscope III AFM, tapping mode from Digital Instruments).

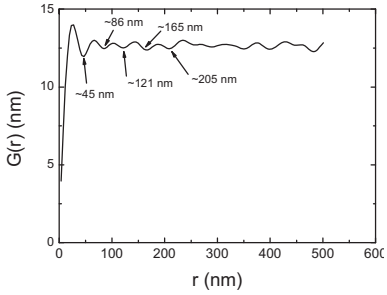

Fig 2. Height-height correlation function G(r) of the AFM image of Fig. 1.

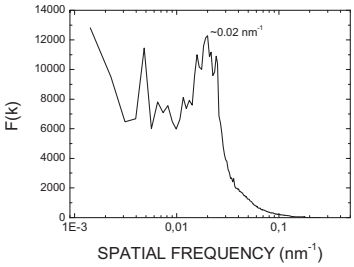

Fig 3. Circularly averaged fast Fourier transform of the AFM image of Fig.1

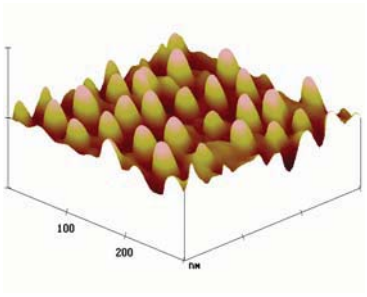

Fig 4. 300x300 nm AFM image (3-D) of the same sample as Fig.1.

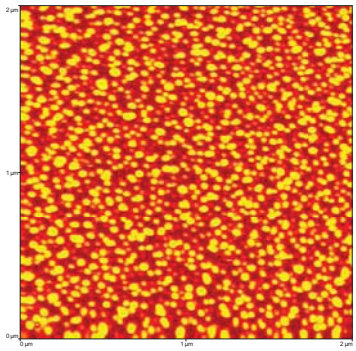

Fig 5. 2x2 um2 AFM image of PMMA film surface after O_2 plasma etching down to Silicon substrate. RMS is 8.6 nm. (CP-II AFM, tapping mode, from Veeco)

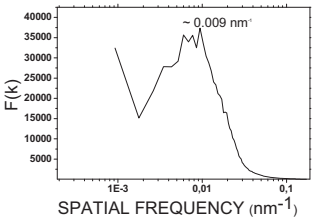

Fig 6. FFT of the AFM image of Fig.5

Poster A36

STOCHASTIC PREDICTION OF THE EXACT TOPOLOGICAL CHARACTERISTICS OF LDPE PRODUCED IN TUBULAR REACTORS

D. Meimaroglou[1,2], P. Pladis[2], A. Baltsas[2] and C. Kiparissides[1,2]

1. Department of Chemical Engineering, Aristotle University of Thessaloniki and
2. Chemical Process Engineering Research Institute, Centre for Research and Technology Hellas, P.O. Box 472, Thessaloniki, Greece 541 24

A well-known approach for the calculation of the distributed molecular properties of polymers (e.g., molecular weight distribution, MWD, long chain branching distribution, LCBD, copolymer composition distribution, CCD, etc.), is the use of bivariate population balance equations (PBEs).[1] In principle, based on the polymerization kinetic mechanism, one can derive dynamic PBEs to describe the time evolution of the "live" and "dead" polymer chains in a polymerization reactor. The resulting PBEs can be solved numerically using well-established numerical methods (i.e., 2-D fixed pivot, orthogonal collocation on finite elements, etc.). A major limitation in the application of these methods is the fact that they are extremely complex mathematically and they cannot be extended to more than two dimensions (i.e., they cannot be applied to trivariate or multi-dimensional problems).

To deal with the above limitation, a novel Monte Carlo (MC) algorithm was developed. The proposed algorithm can be used for the accurate prediction of the complete topological characteristics of the polyethylene polymer chains produced in a high pressure (LDPE), tubular polymerization reactor. Via the MC algorithm, it is possible to predict the exact size and position of every single branch (either short- or long-chain) that is attached to a given polymer chain in the reacting mixture, thus leading to the calculation of the complete topological structure of the polymer chains. Furthermore, no prior information on the distributional form of the "live" or "dead" polymer chains is required, neither any other kind of simplifying kinetic assumptions. The algorithm considers the evolution of both "live" and "dead" polymer chain populations and proceeds in complete conjunction with the polymerization kinetic mechanism.

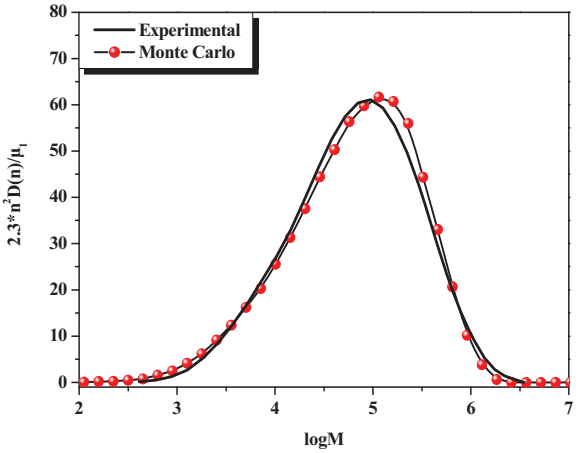

Fig. 1: Comparison between theoretical and experimental MWD of LDPE

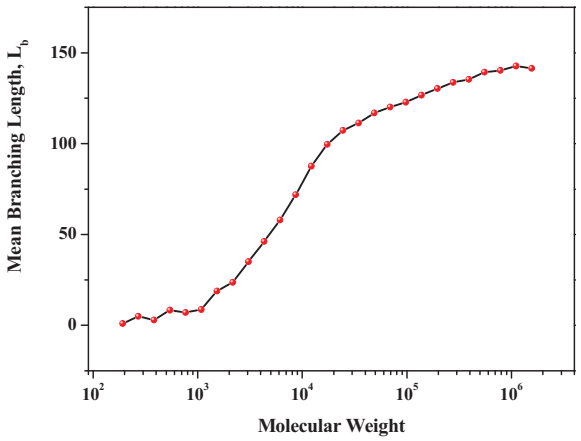

Fig. 2: MC calculated branching length distribution of LDPE

The proposed MC algorithm was successfully applied to the free-radical polymerization of LDPE in a tubular reactor, for the prediction of a series of distributed and topological properties of the polymer chains. The validity of the mathematical model was initially verified through a direct

comparison of MC predictions with available experimental measurements on the MWD of the polymer (see Fig. 1). Moreover, the MC calculated average molecular properties (i.e., M_n, M_w, etc.) were directly compared with theoretical predictions from the application of the well-established method of moments[2], in order to further verify the predictive capabilities of the method. The prediction of the mean branching length distribution (Fig. 2), the dynamic evolution of the seniority-priority distribution (Fig. 3) and the mean radius of gyration are some of the characteristic results obtained by the MC algorithm. The information obtained by the proposed algorithm can be further employed for the prediction of the viscoelastic properties of the polymer melts.

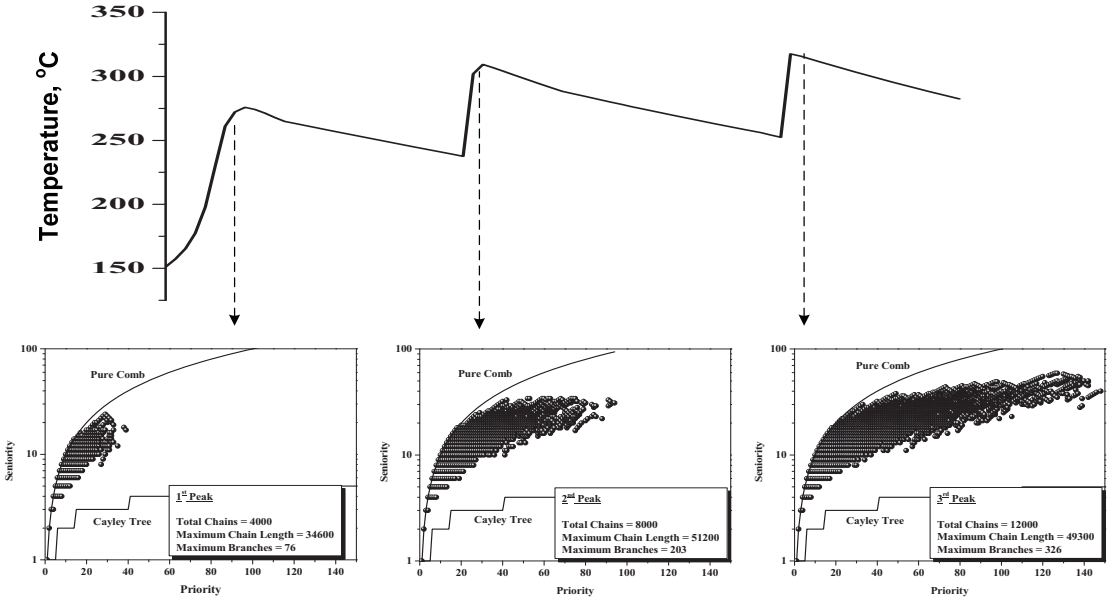

Fig. 3: Dynamic evolution of the seniority-priority distribution of LDPE

References

1. Kiparissides, C. J., Process Control 2006, 16, 205.
2. Kiparissides C., Baltsas A., Papadopoulos S., Congalidis J.P., Richards J.R., Kelly M.B. and Ye Y., Ind. Eng. Chem. Res. 2005, 44, 2592.

Poster A37

Effect of Reaction Conditions and Catalyst Design on the Rheological Properties of Polyolefins Produced in Gas-phase Olefin Polymerization Reactors

P. Pladis[2], V. Kanellopoulos[2] C. Chatzidoukas[2] and C. Kiparissides[1,2]*

1. Department of Chemical Engineering, Aristotle University of Thessaloniki and
2. Chemical Process Engineering Research Institute, Centre for Research and Technology Hellas, P.O. Box 472, Thessaloniki, Greece 541 24

Polyolefins are the most widely used plastics today due to their low production cost, reduced environmental impact, and wide range of applications. Polyolefins are commonly produced in low-pressure catalytic (e.g., Ziegler-Natta, metallocenes, etc.) bulk, slurry, and gas-phase reactors. The solid catalyzed gas-phase polyolefin production usually takes place in continuous fluidized bed reactors (FBR). In this process, prepolymerized catalyst (e.g., 20-80 μm) or polymer particles (e.g., 50-300 μm, produced in an upstream reactor) are continuously fed into the FBR at a point above the gas distributor and react with the incoming fluidizing gas mixture of monomer(s) and nitrogen to form a broad distribution of polymer particles in the size range of 100-5000 μm which are continuously withdrawn from the reactor at a point, preferably, close to the bottom of the bed.

In the present study, a multi-scale, integrated dynamic model is developed to assess the effect of polymer distributed properties on the rheological behavior of PE produced in a catalytic Ziegler-Natta gas-phase olefin copolymerization FBR[2]. The proposed multi-scale reactor description comprises a detailed kinetic model for the prediction of molecular weight distribution (MWD) and copolymer composition distribution (CCD), a random pore polymeric flow model (RPPFM) to follow the growth of individual polymer particles in the reactor and a population balance model to follow the dynamic evolution of PSD.

A detailed rheological model that includes reptation and Rouse relaxation terms[1,2] has been employed in the present study. It is well-known that the proposed rheological model can provide quantitative predictions of polymer rheological properties in terms of the molecular properties (e.g., MWD, CCD, etc.). Numerical simulations were initially carried out, using the multi-scale model, to investigate the effect of reactor conditions, polymer crystallinity and catalyst design specifications on the distributed molecular properties as well as on the rheological behavior of PE. The model MWD were then used to calculated the rheological properties of the produced polymer.

The ability of the proposed model to quantitatively predict the viscoelastic behaviour of linear polymer melts is examined in relation to the operation of a Ziegler-Natta olefin polymerization fluidized bed reactor. In Figure 1 the dynamic evolution of the MWD of the polyethylene produced in a fluidized bed reactor is illustrated. As it can be seen, during the reactor start-up the molecular weight moves to higher values until it reaches its steady-state value. The corresponding rheological curves of the produced polymer is shown in Figure 2. It is clear that the Newtonian plateau viscosity value molecular weight is moving toward higher values. Using the present modeling methodology it is possible to obtain a quantitative relationship between the molecular properties (e.g., MWD, etc.) and a polymer end-use property (e.g., viscosity, MFI) and control of this property to ensure the production of polymers with desired molecular characteristics.

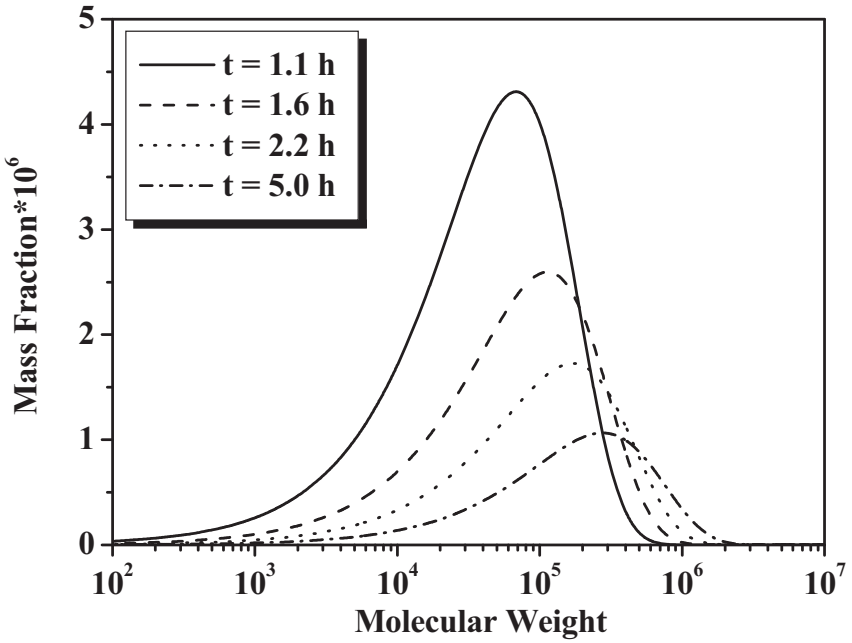

Fig. 1: Dynamic evolution of the MWD of the produced PE during reactor start-up.

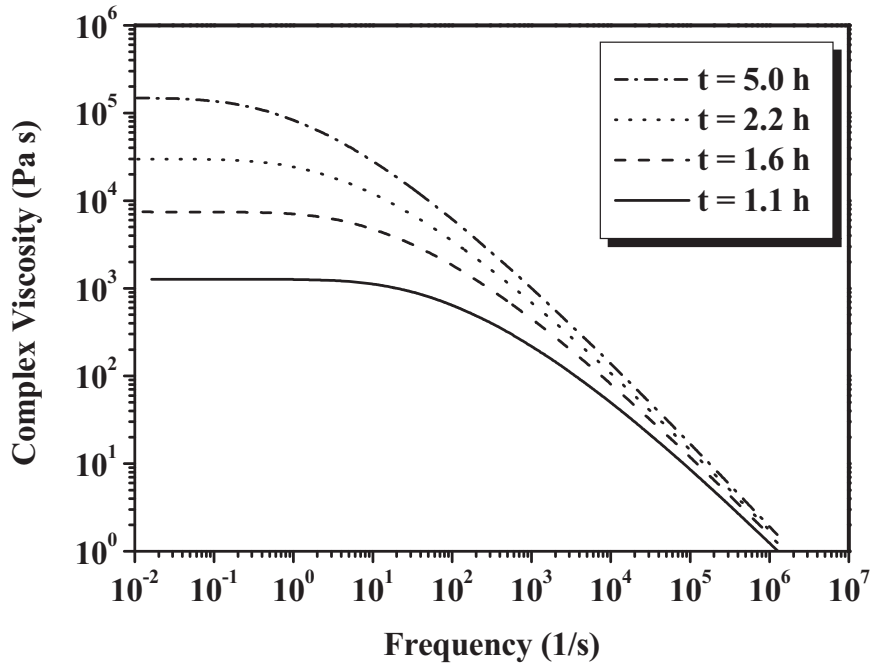

Fig. 2: Dynamic evolution of the rheological curve during reactor start-up.

References

1. Dompazis, G.; Kanellopoulos, V. Kiparissides, C. (2005) Macromol. Mater. & Eng. 290, 525.
2. Doelder, J. Den, (2006), Rheologica Acta, 46, 195.
3. Ruymbeke, E. Van, Keunings, R.,Stephenne, V., Hagenaars, A. and Bailly C. (2002) Macromolecules, 35, 2689-2699.

Poster A38

Modeling of Industrial Catalytic Olefin Polymerization Slurry Reactors

Touloupides Vassileios[1,2], Kanellopoulos Vassileios[2], Pladis Prokopis[2], Krallis Apostolos[2] and Kiparissides Costas[1,2]

1. Department of Chemical Engineering, Aristotle University of Thessaloniki, and
2. Chemical Process Engineering Research Institute, Centre for Research and Technology Hellas, P.O. Box 472, Thessaloniki, Greece 541 24

Slurry reactors are widely used for the polymerization of olefins because of their simple design and operation, their well-defined mixing conditions, their excellent heat transfer capabilities, low power requirements and high conversion rates.

In the present study, a comprehensive mathematical model is developed for the prediction of the polymer production rate and the polymer molecular properties in an industrial catalytic, slurry-phase copolymerization reactor series. Each reactor is modeled as a CSTR, while the product withdrawal rate from each reactor is directly controlled by the reactor pressure.

To calculate the monomer(s) and other molecular species consumption/production rates and molecular weight properties of polyolefins, a generalized multi-site Ziegler-Natta kinetic mechanism was employed. The kinetic mechanism comprised a series of elementary reactions including site activation, propagation, site transformation, site transfer reactions and site deactivation. To calculate the number of different types of catalyst active sites and the associated kinetic rate constants, a MWD deconvolution method was employed, using experimentally measured MWDs for different polyolefin grades obtained from the industrial reactor.

The polymerization mixture consisted of a liquid phase (i.e., solvent and monomer(s)) and a solid-polymer phase that included the polymer and the sorbed monomer, the co-monomer, the solvent and the chain-transfer agent. To calculate the equilibrium concentrations of the various species in the two phases, the degree of polymer crystallinity was also taken into account. The total reactor pressure was calculated using an EOS while the product removal rate was controlled via the operation of a feed-back pressure controller. All the thermodynamic calculations were carried out using the Sanchez-Lacombe Equation of State (S-L EOS). The S-L EOS binary interaction parameters were estimated by fitting the S-L EOS to binary equilibrium data obtained from the open literature.

Moreover, overall dynamic mass and energy balances were derived in order to predict the dynamic evolution of the various molecular species concentrations and temperature profiles in each reactor of the series. The distributed molecular properties (i.e. number- and weight-average molecular weight, M_n, M_w, molecular weight distribution, MWD) were also calculated using the well-known method of moments.

Extensive numerical simulations were carried out to investigate the effect of reactor operating conditions (i.e., inflow rates, reactor temperature, feed composition, etc.) on the dynamic evolution of the molecular properties (i.e., M_n, M_w, MWD) and polymerization rate as well as on other key reactor properties (i.e., pressure, densities in reactor, liquid and polymer phase, outflows etc.) in an industrial slurry reactor series.

In Fig. 1, the predicted MWDs are compared with the experimentally measured MWDs for a specific polyolefin grade at the exit of the first and second reactor of the series. In Fig. 2, the dynamic evolution of the polymerization rates in each reactor of the series is illustrated. In this figure, the continuous and broken lines show the model predictions while the discrete points

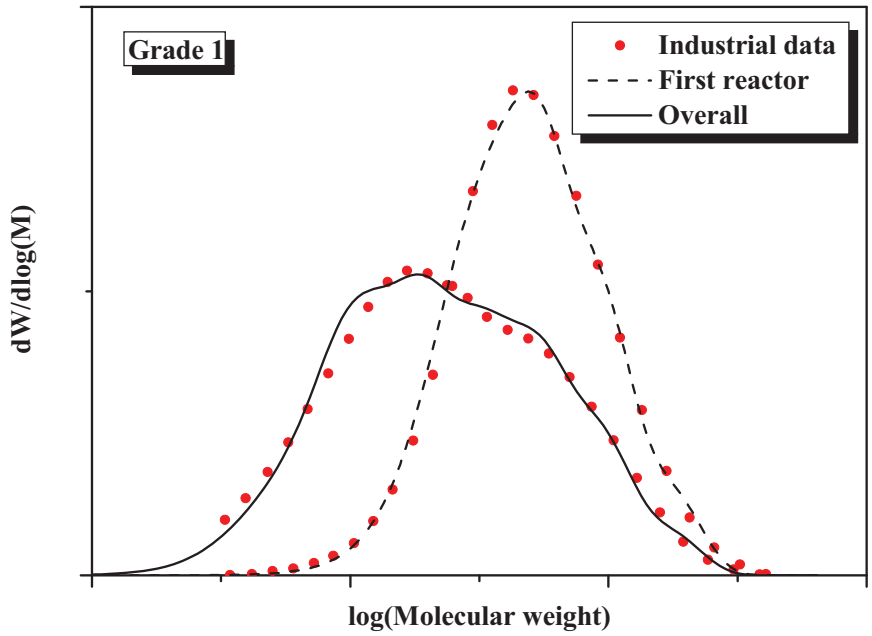

Fig. 1: Molecular weight distributions.

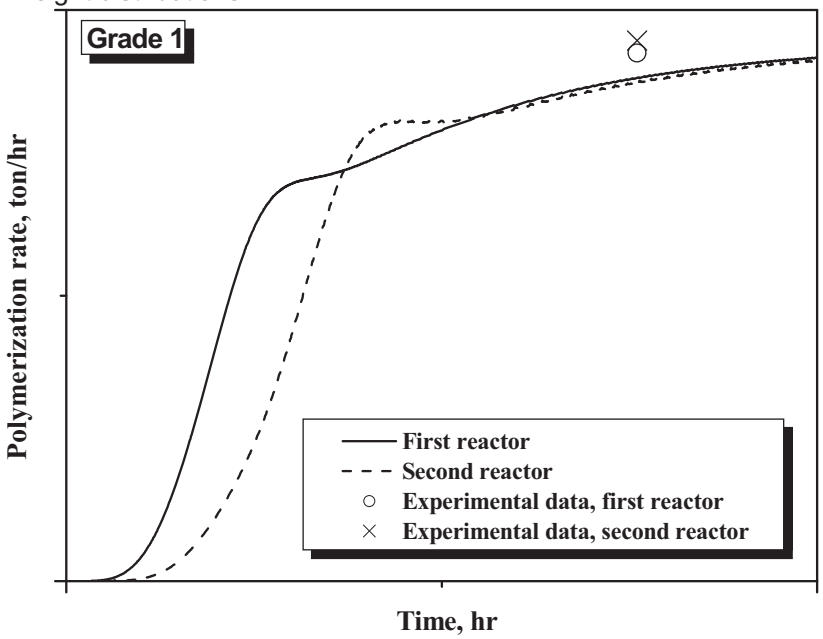

Fig. 2: Dynamic evolution of polymerization rate.

represent the experimentally measured steady-state polymerization rates in the first and second reactor of the series.

The successful application of the proposed model to different industrial grades, using the same kinetic and thermodynamic parameters, confirmed that the model is capable of accurately representing the dynamic behavior of the industrial unit.

References

1. Kanellopoulos., V., Mouratides., D., Pladis. P. and Kiparissides, C., *Ind. Eng. Chem. Res.*, 45, pp. 5870-5878, **2006**.
2. Reginato A. S., Zacca, J. J. and Secchi A. R., *AIChE Journal*, Vol. 49, No 10, pp. 2642-2654, **2003**.
3. Zacca, J. J. and Ray, H. W., *Chem. Eng. Sci.*, Vol. 48, No. 22, pp. 3743-3765, **1993**.

Poster A39

Viscoelastic tube inflation under constant rate of growth

Evangelos Voyiatzis, Christos Tsenoglou

School of Chemical Engineering and School of Applied Mathematics (Post-graduate Program in Mathematical Modelling in Modern Technologies and Finance)
National Technical University of Athens, Zografos, 157 80, Athens, Greece

The simultaneous radial inflation and axisymmetric extension of an incompressible viscoelastic tube is modelled analytically as an idealization of the blow molding process. The working fluid is supposed to obey the TVG integral constitutive model,[1] thus accommodating behaviour ranging from extreme strain hardening (akin to the Lodge-Maxwell model) to strain thinning leading to plastic flow. A crucial simplifying assumption is that axial and radial extension rates at the outer tube radius are kept constant, and that the tube is sufficiently long so that end effects may be neglected. In that respect, our work extends in the non-linear viscoelastic regime the results of an earlier study by Chung and Stevenson.[2] Analytical expressions are derived for the pressure difference ΔP across the tube wall and the axial force F required for sustaining the aforementioned tube inflation of constant stretch history; these results are further simplified for the case where the thin-shell approximation holds.

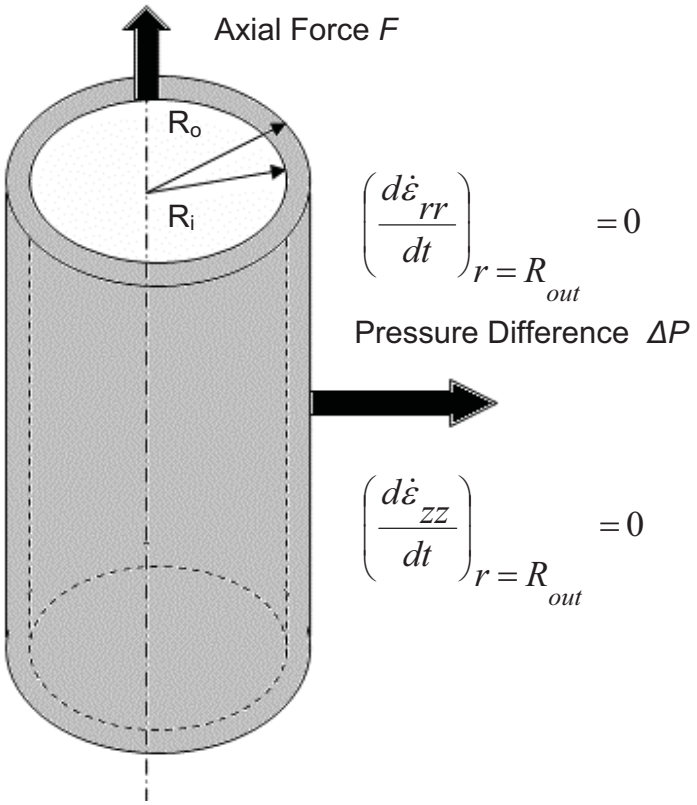

Figure 1 Schematic view of tube undergoing extension and inflation

References

1. Ch. J. Tsenoglou, E. Voyiatzis and A. D. Gotsis, Simple constitutive modelling of nonlinear viscoelasticity under general extension, Journal of Non-Newtonian Fluid Mechanics 138 (2006) 33-43
2. S.C.K. Chung and J.F. Stevenson, A general elongational flow experiment: inflation and extension of a viscoelastic tube, Rheol. Acta 14 (1975) 832-841.

Poster A40

On-line monitoring of the industrial formaldehyde resin production

D. Papapetros[1, 2], I. Katsampas[1], C. Panayiotou[2]

[1] *Chimar Hellas S.A., Sofouli 88, Kalamaria, Thessaloniki 55131, Greece*
[2] *Department of Chemical Engineering, Laboratory of Physical Chemistry, Aristotle University of Thessaloniki, Thessaloniki 54124, Greece*

Main concern of the wood based panel industry during the last years is the panel formaldehyde emission. The tendency to limit the allowable emitted formaldehyde has led to the decrease of the molar ratio of the formaldehyde resins used in board production. The resin industry follows new technologies producing resins, which despite their reduced molar ratio exhibit equal reactivity and mechanical performance with conventional molar ratio resins. In these new resin synthesis procedures, any deviation could lead to out-of-specifications resins with negative impact on the board production. In other words, the necessity of the reliable control of the whole resin synthesis is nowadays greater than ever before.

In the past the near infrared (NIR) technology has been applied to many fields of science, including the wood-based panels industry, for the on-line monitoring of many processes. Chimar Hellas, has successfully developed the GNOSSI methodologies in the field of resin industry, for the rapid, precise and reliable determination of the raw materials concentration and the properties of the resins as well as the in situ monitoring of the progress of resin condensation stage. However, despite all the efforts made, only traditional empirical techniques could be used so far to predict the end point of the condensation.

The aim of this paper is to present the latest improvements of GNOSSI technology that have already allowed its industrial application and the full monitoring of the whole synthesis procedure of a formaldehyde resin. It is the unique technique that can be used during production for in situ and real time determination of the molar ratio of the reaction mixture, each time a new component is inserted in the reactor as well as of the final molar ratio of the resin just before unloading the reactor. Moreover, the successful correlation of the NIR spectra with the progress of the molecular weight of the formed polymer, combined with the use of indices that follow up the gradual evolution of the condensation reaction allow the prediction of the end point of the condensation. The benefits of such an application lead to only one conclusion: “the time to install an eye inside the resin reactor has come”.

Poster A41

Effect of the Concentration of Silane-coupling Agent on Physical Properties of Dental Resin-Nanocomposites

M.M. Karabela, I.D. Sideridou
Laboratory of Organic Chemical Technology, Department of Chemistry,
Aristotle University of Thessaloniki, Thessaloniki, GR-54124, HELLAS.E-mail: siderid@chem.auth.gr

Introduction

Dental resin composites are consisted of a polymeric matrix admixed with silane treated reinforcing inorganic filler. Silane provides a crucial link between the matrix and the filler that can have a significant effect on the overall-performance of composite. It is worth to note that in the case of nanocomposites the silane phase plays an even more important role on properties of composite, since the nanoparticle fillers have an extremely high surface area-to-volume ratio and require a higher degree of silanization than larger particulate fillers. In this work it was studied the effect of the concentration of the silane-coupling agent on some physical properties of dental nanocomposites. These nanocomposites consisted of a Bis-GMA/TEGDMA (50/50wt/wt) matrix and silica nanoparticles (Aerosil OX50) as filler, silanized with various concentrations of silane. The silane used was 3-methacryloxypropyl-trimethoxysilane (MPS).

Experimental

The concentrations of silane was 1.0, 2.5, 5.0, 7.5, 10 wt-% relative to silica. The silanized silica nanoparticles were characterized by FTIR spectroscopy and thermogravimetric analysis (TGA). Then the silanized nanoparticles were mixed with the dimethacrylate matrix (60% filler by weight fraction), contained the system camphorquinone / ethyl-4-dimethylaminobenzoate as initiator for the light curing of the matrix. Then the composites were light cured. Degree of conversion was determined by FTIR analysis. The static flexural strength and static modulus were measured using a three-point bending set-up according to the ISO-4049 specification. The dynamic thermomechanical properties and glass transition temperature (T_g) were determined by DMA analyzer (bending, dual cantilever). Measurements were performed in samples stored in water 37^{o}C for 24 hours, immediately after curing. Sorption, solubility and volumetric change were determined after storage of composites in water or ethanol/water 75 vol-% for 1 day, 7 or 30 days. Thermogravimetric analysis of composites was performed in air and in nitrogen atmosphere from 50 to 800 ^{o}C.

Results

The FTIR spectra of the silica surface treated with MPS (5.0, 7.5, 10 wt-%) appear two peaks, one at 1720 cm^{-1}, due to the free carbonyl (-C=O) stretching vibration, and the peak at 1700 cm^{-1} characteristic of the carbonyl groups forming hydrogen bonds with the silica hydroxyls (Fig.1). These results indicate a multilayer coverage of silica by MPS molecules. The spectra of the silica surface treated with MPS (1.0, 2.5 wt-%) showed only one peak at 1700 cm^{-1} indicating that MPS forms a monomolecular layer and the molecules are oriented parallel to the silica surface. The amount of silane, chemisorbed and physisorbed to the nanosilica surface was quantitatively determined by TGA.

The degree of conversion (DC) attained values in range of 45-50% indicating that a high amount of residual monomer has remained. The mechanical properties of composites are summarized in Table 1. Sorption, solubility and volumetric change are shown in Table 2. In all composites the amount of sorbed ethanol/water solution is much higher than that of water. Thermogravimetric analysis showed that composite contains inorganic filler about 60 wt%. According to the TGA/DTGA curves (Fig.2), three decays can be distinquished, one around 200 to 340 ^{o}C, other from 340 to 470^{o}C and other one from 470 to 700^{o}C, indicating a three-step degradation process.

Table 1. Mechanical properties of the composites after stored in water 37°C for 24 hours, immediately after curing.

Composite	Flexure strength (MPa)	Static Modulus (GPa)	Dynamic Storage Modulus E' (GPa) 37°C	Dynamic Loss Modulus E'' (GPa) 37°C	tanδ	Tg (°C)
1.0 %	90 (10)	5.61 (0.08)	6.57 (0.02)	0.39 (0.00)	59.5 (0.85)	126.6 (0.3)
2.5 %	100 (8)	5.37 (0.07)	5.67 (0.01)	0.36 (0.02)	63.7 (3.68)	127.2 (2.7)
5.0 %	87 (7)	5.47 (0.08)	6.69 (0.01)	0.42 (0.00)	63.0 (0.42)	124.0 (0.9)
7.5 %	89 (6)	5.63 (0.11)	6.13 (0.00)	0.40 (0.04)	68.4 (1.84)	125.8 (0.0)
10 %	92 (5)	5.45 (0.10)	6.21 (0.31)	0.42 (0.04)	51.3 (4.67)	126.1 (3.0)

Table 2. Sorption/desorption parameters for the five composite materials, [mean (S.D.)]*, n = 4.

Concentration of MPS	% solution Sorption	% solution Desorption	% SoLubility	% Volume Increase	Swelling *f*
water					
1.0 %	1.87 (0.05)^{A,a}	1.83 (0.01)^{A}	0.26 (0.03)	1.69 (0.10)	0.54 (0.05)
2.5 %	1.77 (0.08)^{B,a,b}	1.68 (0.05)^{B,c}	0.21 (0.03)	1.35 (0.00)	0.41 (0.07)
5.0 %	1.68 (0.02)^{C,b}	1.63 (0.02)^{C,c}	0.28 (0.04)	1.32 (0.06)	0.47 (0.02)
7.5 %	1.74 (0.06)^{D,b}	1.70 (0.05)^{D,c}	0.31 (0.03)	1.36 (0.06)	0.47 (0.00)
10 %	1.73 (0.07)^{E,b}	1.67 (0.05)^{E,c}	0.29 (0.01)	1.27 (0.24)	0.44 (0.07)
Ethanol water solution 75 vol%					
1.0 %	3.80 (0.06)^{A}	3.68 (0.05)^{A}	0.44 (0.04)c	4.90 (0.14)^{d}	0.73 (0.07)^{f}
2.5 %	2.98 (0.29)^{B,a}	2.96 (0.25)^{B,b}	0.14 (0.00)	4.63 (0.32)^{d,e}	0.67 (0.03)^{f}
5.0 %	3.57 (0.02)^{C}	3.46 (0.09)^{C}	0.72 (0.05)	5.19 (0.02)	0.72 (0.03)^{f}
7.5 %	3.20 (0.06)^{D,a}	3.11 (0.06)^{D,b}	0.32 (0.02)	4.57 (0.11)^{e}	0.74 (0.02)^{f}
10 %	3.13 (0.17)^{E,a}	3.02 (0.15)^{E,b}	0.42 (0.03)c	3.44 (0.33)	0.62 (0.11)^{f}

**Common corresponding letters indicate no significant difference (p> 0.05).*

From these data, it was concluded that the highest coverage of methacrylate groups at the silica matrix interphase was not necessary to obtain composites with high strength; for each property an optimum concentration silane exists.

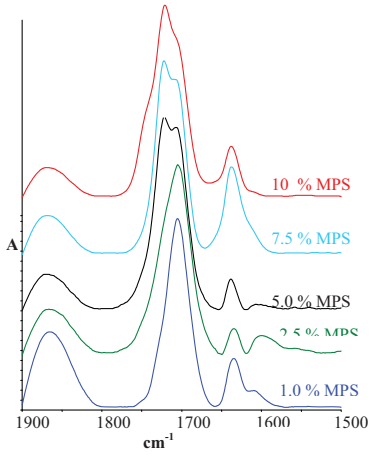

Fig.1 FT-IR spectra of silane treated silica surface

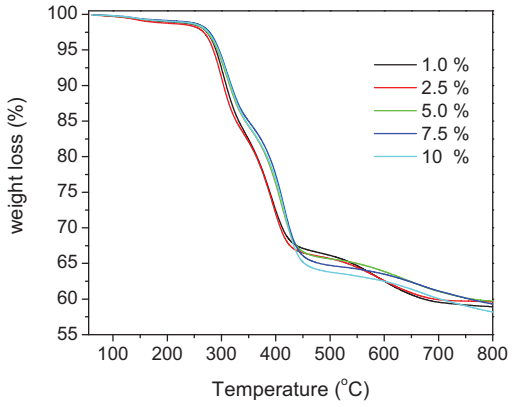

Fig. 2 Thermogravimetric curves of composites

References:
1. Maria M. Karabela, Irini D. Sideridou : Dental Materials, (2008) in press.
2. Kristen S. Wilson, Kai Zhang, Joseph M. Antonussi : Biomaterials, 26 (2005) 5095-5103.
3. British standard specification for resin-based filling materials, 2nd ed., ISO 4049; 1988.

Poster A42

Plain and modified phase inversion membranes for gas separation

George Karadimos, Vassiliki A. Kosma, Konstantinos G. Beltsios
Department of Materials Science and Engineering, University of Ioannina, Ioannina, Greece, GR-45110.

Abstract
Phase inversion (PI) in plain and modified versions is used for the fabrication of asymmetric polymeric membranes for gas separation. As asymmetric PI membranes frequently exhibit an unreliable ultrathin skin (= separation layer), emphasis is placed upon asymmetric versions with a thicker skin, either through control of single-step precipitation conditions or through development of an additional compact thin top-layer during a second precipitation step. Single-step asymmetric membranes considered are based on PMMA, PSf and CA, while the two-step approach is studied in the case of PMMA and PSf membranes. Preliminary air and methane permeability data are also included.

Introduction

While an endless range of membrane preparation methods is explored for more than 50 years[1,2], phase inversion remains the dominant method of membrane preparation, when membranes already finding industrial application are considered. Phase inversion (PI) is based on the precipitation of a biphasic and bicontinuous structure upon coagulation of a concentrated polymer solution. Upon drying, either a symmetric or an asymmetric porous membrane might result, depending on various processing choices (solution concentration, choice of solvent and non-solvent etc)[2]. In the case of gas separation membranes only asymmetric versions bearing a compact skin and a bicontinuous porous bulk are of practical interest. For the latter morphology, successful gas separation is possible only when the top layer (skin) is nearly defect-free and also capable of withstanding sizable pressure differentials; failure on one or both accounts is frequent in the case of PI membranes for gas separation. In this work we explore ways of thickening the top layer of a PI membrane either by properly modifying the one-step precipitation conditions or by developing an additional thin compact layer of the same polymer through a second precipitation step. In the latter case, it is necessary to avoid any of the following three possibilities: (a) very thick additional layer, (b) non-continuous additional layer, (c) destruction of the structural features of the main asymmetric membrane during solution deposition of the additional layer.

Experimental

Three grades of commercial atactic PMMA (very high, moderate and relatively low molecular weight), two grades of PSf purchased from Aldrich and one of cellulose acetate purchaced from Kodak were employed in the experiments. The solvents used were analytical grade acetone, chloroform and dimethylacetamide, while the main non-solvent employed was distilled water. Starting solutions (dopes) with 20 % wt. polymer content were used in all of the experiments performed. Membranes produced were characterised via SEM and permeability measurements.

Results and Discussion

PI membranes with an improved top layer were prepared through modified single-step precipitation or via standard PI and additional polymer deposition from dilute (1-3 % wt) solutions; convection heating and post-deposition annealing served as additional processing options. Both morphological examination (Fig. 1 and 2) and methane and air permeability measurements (Table 1) support the conclusion that defect-free membranes are obtained. 1-step processes applied lead to top layers with a thickness in the range of 1-10 microns, while successful top layers deposited through a second precipitation step are continuous with a thickness of 1-3 microns. The collection of a wide range of gas permeability and separation data is in progress.

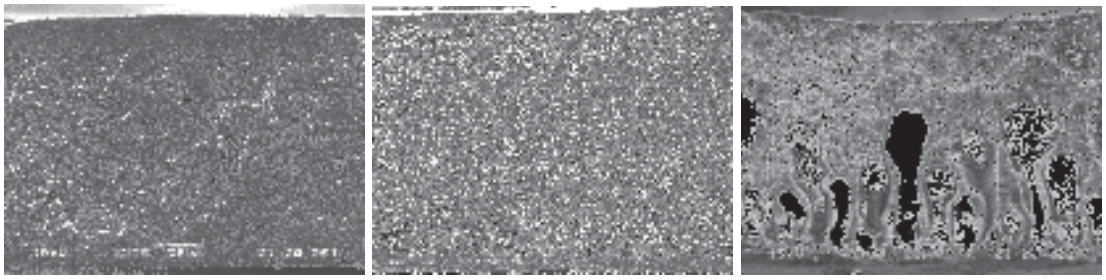

Figure 1: Cross-sections of single-step asymmetric PI membranes based on (a) PMMA, (b) Psf, (c) CA

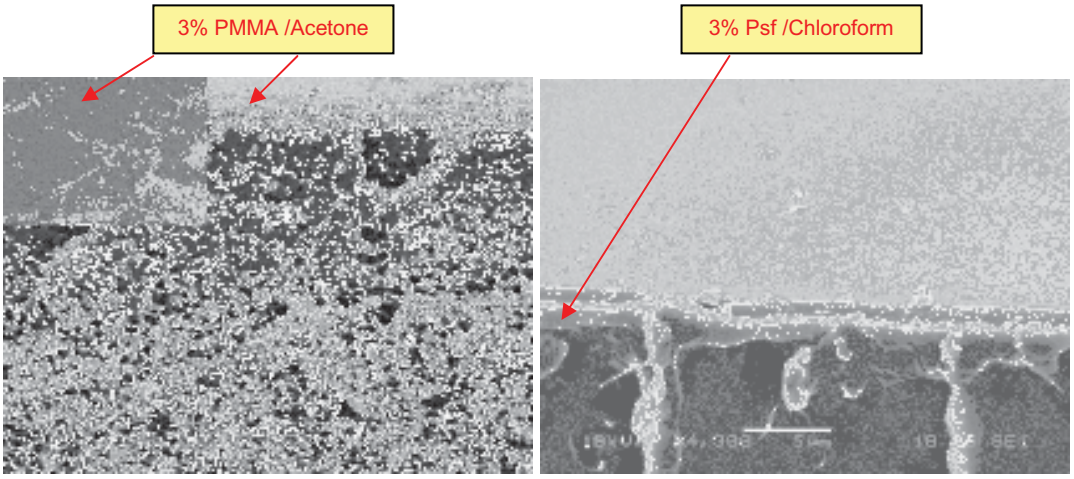

Figure 2: Cross-sections of two-step asymmetric PI membranes (a) Top from high MW (M_w=996.000) 3%/ACE PMMA, main membrane from medium MW (M_w=350.000) 20% PMMA/ACE/ethanol, (b) Top from 3% Psf/ chloroform (M_w=50.000), main membrane from 20% Psf/ chloroform /ethanol(M_w=26.000)

Membrane	Permeability(barrer)	
	CH_4	Air
PMMA /ACE /H_2O	1.043	6440
Psf/DMAc/ H_2O	44.1	4900
CA/ACE/ H_2O	31.9	2790
Psf/ $CHCl_3$(dense)	0.16	1600

Table 1: Methane and air permeability data (25 ^oC) for membranes shown in Figure 1

Conclusions

Gas separation PI membranes with defect-free separation layers are prepared by appropriate 1-step and 2-step processing conditions.

References

1.M.Mulder, “Basic Principles of Membrane Technology”, Kluwer Academic Publishers,1991

2.K.Beltsios et.al, ”Membrane Science and Applications”, Chapter in ‘Handbook of Porous Solids’, p.2281-2433, Wiley, 2002.

Poster A43

EFFECT OF THE ENVIRONMENTAL DEGRADATION ON THE VISCOELASTIC RESPONSE OF NANO MODIFIED EPOXIES AND CFRPs

N. M. Barkoula[1], E. Fiamegou[2], A. Paipetis[1]

[1] *Dept. of Materials Science & Engineering, University of Ioannina, GR-45110 Ioannina, GREECE*

[2] *Applied Mechanics Laboratory,Department of Mechanical Engineering and Aeronautics, University of Patras, Patras University Campus, 26500, Patras, Greece*

The introduction of nanoscaled reinforcement in otherwise conventional fibre reinforced composites has opened an exciting new area in composites research. The unique properties of these materials combined with the design versatility of fibrous composites may offer both enhanced mechanical properties and multiple functionalities.

One of the most attractive nanofillers for the matrix modification of fibre composites are Carbon Nanotubes (CNTs). CNTs possess unique properties such as elastic modulus at the terra scale, huge aspect ratio, as well as extremely large specific surface area (or interfacial area, when incorporated in the matrix). Moreover, the conductivity of such systems has been reported to directly correlate to (i) the macroscopic strain applied on the material and (ii) the internal damage that accumulates within the structural component throughout its service life[1]. Recent research has proven that when CNTs are used as an additive in the matrix of Carbon Fibre Reinforced Plastics (CFRPs) at weight fractions as low as 0.5% result to the spectacular improvement of the fracture toughness of the material[2], as well as the substantial prolongation of its fatigue life. According to these studies, the improvement of the damage tolerance of these systems is attributed to the incorporation of an additional interfacial area, i.e. that between the CNTs and the matrix. This interfacial area is expected to activate additional energy dissipation mechanisms related to interfacial sliding, fibre pull out and bridging as well as crack bifurcation and arrest at the nanoscale. Furthermore, five different blending techniques of incorporating MWCNTs into an epoxy matrix were examined recently[3]. In general the use of solvents together with sonication produced enhanced mechanical properties e.g. Young's Modulus, Bending Modulus and dynamic properties such as T_g and Storage Modulus.

However, one challenge for the applicability of CFRPs is related to their environmental durability. It is well known that epoxy matrix composites are susceptible to heat and moisture particularly when they operate in varying environmens. The amount of moisture absorbed by the matrix is significantly different to that absorbed by the reinforcing phase. The presence of moisture and stresses associated with moisture-induced expansion may deteriorate the matrix related properties of the composite and as a result, have an adverse effect on the damage tolerance and structural stability. The higher the temperature the higher the moisture uptake rate of the composites and the delamination nucleation. Furthermore the interfacial adhesion degradation is dependent on the conditioning temperature and exposure time. Among the properties of polymer matrix composites that are negatively affected by moisture uptake is the stiffness, the interfacial strength, the interlaminar interface, the damping ratio etc. Some of the mechanisms occurring during moisture absorption include weakening of the fibre-matrix interface, plasticization and swelling of the matrix and in some cases even softening of the matrix. From the above one can conclude that in the case of CFRPs, the properties dominated by the matrix or the fibre-matrix interface are degraded by moisture absorption, whereas the properties that are dominated by the fibres are less influenced.

Although CFRPs have received a lot of focus, very few papers have been published on the environmental degradation of CNTs-reinforced composites. No experimental results are available on the effect of moisture absorption on the water up-take and mechanical properties of CNT-reinforced CFRPs. In a recent communication[4] it was emphasized that that specific surface area of nanosized particles is huge, indicating that a large proportion of the surrounding matrix will be in contact with the interface or even a separate phase – the interphase- will be developed with properties different to those of the bulk matrix. One important point is that in crosslinking resins, the ability of CNTs to absorb or donate electrons may well affect the crosslinking densilty. As discussed above, matrix, and reinforcement-matrix interface are more

prone to absorb water and alter their properties. The fact that CNT-reinforced composites possess increased interfacial area may be beneficial for their fracture toughness; however, this could prove to be their weakest point in terms of in service durability.

Based on the above it is expected that the hygrothermal conditioning of the aforementioned systems will alter their viscoelastic response and more specifically their damping properties, glass transition temperature and dynamic modulus. Therefore, the purpose of this study is to evaluate the viscoelastic performance of the aforementioned materials in extreme environments. To this end, multi wall CNTs were incorporated in a commercial epoxy system via high shear mechanical mixing which was subsequently used for the manufacturing of quasi isotropic laminates CFRPs, using the wet lay up method. Modified matrices with CNT content varying from 0.1% to 1% were manufactured. All modified resins were used to manufacture un-reinforced rectangular cast specimens. The resin with the 0.5% CNT content was subsequently used for the manufacturing of the modified CFRPs. All systems were subjected to hydrothermal loading. During the environmental conditioning, the composites were weighted in specified intervals and the water absorption vs. time was recorded for both the modified and a reference system.

The conditioned composite systems were subsequently tested in tension and dynamic three-point bending in order to study their mechanical and viscoelastic behaviour. The properties of the modified systems were compared to the properties of unmodified composites that were subjected to identical conditioning.

REFERENCES

1. Sotiriadis G., Tsotra P., Kostopoulos V. and Paipetis, A., “Stiffness Degradation Monitoring Of Carbon Nanotube Doped Glass / Vinylester Composites Via Resistance Measurements”, *Journal of nanostructured Polymers and Nanocomposites*, No3 pp 90-95, 2007.
2. Kostopoulos V., Tsotra P., Vavouliotis A., Karappapas P., Nikolaou N., Paipetis A., Kempel F., Schledjewski R., “Damage Detection during Monotonic and Cyclic Loading of CNT Doped CFRPs via Resistance Measurements”, *Proceedings of the European Conference Composite materials (ECCM) 12*, Biarritz, France (2006).
3. Malandrakis G., Karapappas P., Vavouliotis A., Paipetis A., Kostopoulos V., “Mechanical and Electrical Properties of Carbon Nanotube Reinforced Polymers with Different Dispersion Techniques”, *Proceedings of COMP07: 6th International Symposium on Advanced Composites, Corfu, Greece (2007)*
4. Windle A., “Two Defining Moments: A Personal View by Prof. Alan H. Windle”, Composites Science and Technology, 67 pp 929-930, 2007.

Poster A44

Synthesis and characterization of acrylic bone cements reinforced with bioceramics

Diana-Elena Baciu, Dimitris Giannakopoulos, Spyridon Soulis, Johannis Simitzis*

National Technical University of Athens, School of Chemical Engineering, Department III "Materials Science and Engineering", Laboratory Unit "Advanced and Composite Materials", 9 Heroon Polytechniou str., Zografou Campus, 157 73 Athens, Greece.

e-mail: simj@orfeas.chemeng.ntua.gr

1. INTRODUCTION

Acrylic bone-cements of poly(methylmethacrylate) (PMMA) have been used for more than 40 years in dental implantology for expansion of dental implants, at maxillofacial prosthesis as gentamicin loaded beads, at prosthetics for fixing partial dentures and in orthopaedic surgery [1]. In orthopaedic surgery, bone cements serve as a mechanical interlock between the metallic prosthesis and the bone, acting as a load distributor between the artificial implant and the bone [2, 3]. Bioceramics such as zirconia, alumina, porcelains, glass–ceramics have been widely used in medical applications due to their superior biocompatibility, aesthetics, mechanical resistance, corrosive resistance and their ease fabrication of complex shapes [4].

The aim of this work was the synthesis and characterization of acrylic bone cements reinforced with zirconia acting as bioceramic and the investigation of their thermo-mechanical behavior.

2. EXPERIMENTAL

The acrylic bone cement reinforced with bioceramic was prepared by mixing beads of PMMA (produced by suspension polymerization), methylmethacrylate (MMA) as monomer, benzoyl peroxide (BPO) as free radical initiator and stabilized ZrO_2 powder as bioceramic. The latter was produced by the sol-gel method and stabilized in tetragonal phase by digestion treatment with 5M NaOH following heat treatment at 700 ^{0}C (tetragonal crystal zirconia). The homogenized mixture of PMMA, MMA, BPO with various proportions of ZrO_2 powder or without, was placed into small parallelepiped moulds and polymerized at 60 ^{0}C for 24 hours to give acrylic bone cement or acrylic bone cement reinforced with bioceramic (ZrO_2 powder in 22.5, 32.5 and 39 % w/w).

The produced PMMA was characterized by Fourier transform infrared spectroscopy (FTIR) and X-ray diffraction (XRD) and scanning electron microscopy (SEM). The structure of the tetragonal stabilized zirconia was investigated by FTIR, XRD and SEM. The acrylic bone cement reinforced with bioceramic (ZrO_2) was characterized by FTIR, XRD, SEM and dynamic mechanical thermal analysis (DMTA).

3. RESULTS AND DISCUSSION

Fig. 1 shows the SEM images of PMMA beads prepared by suspension polymerization. The PMMA beads have a spherical form. The diameter of the most beads is approx. 16 μm. *Fig. 2* shows the XRD diffractogram of the PMMA known as amorphous polymer having a major broad peak at 2Θ value of 11.62 ^{0}, a second one at 30. 67 ^{0} with much lower intensity and probably a third one at 41.96 ^{0}. The shape of the first most intense peak reflects the ordered packing of polymer chains while the second peak denotes the ordering inside the main chains [5]. According to the FTIR spectrum of PMMA, in *Fig. 3,* the main characteristic vibration bands of PMMA appear at 1756 cm^{-1} (C=O) and in the fingerprint at 1450 cm^{-1} (C–O).

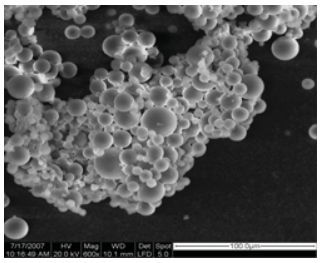

Fig. 1. SEM images of PMMA beads.

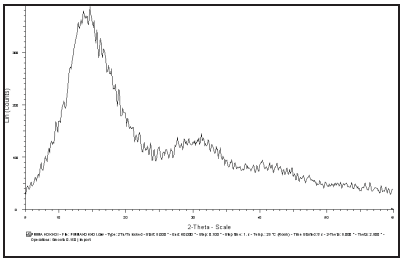

Fig. 2. XRD diffractogram of PMMA.

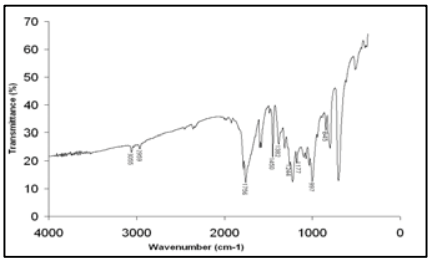

Fig. 3. FTIR spectrum of PMMA.

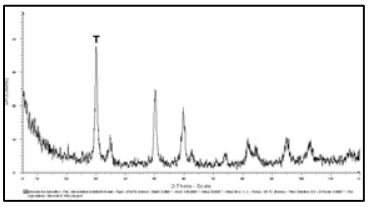

Fig. 4 shows the XRD diffractogram of ZrO_2 with peaks of various intensities at 2Θ values of 30.39 ^{0}, 34.85 ^{0}, 43.18 ^{0}, 50.46 ^{0}, 50.92 ^{0}, 59.50 ^{0}, 62.95 ^{0}, 72.99 ^{0}, 74. 40 ^{0}.The corresponding d (lattice spacing) of the 2Θ (^{0}) peaks are similar to that determined in the literature [6] for tetragonal crystal zirconia which is the stable phase of zirconia.

Fig. 4. XRD diffractogram of ZrO_2 (tetragonal crystal zirconia).

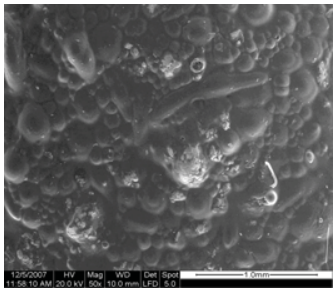

Fig. 5. SEM image of the acrylic bone cement reinforced with bioceramic (tetragonal zirconia powder in 22.5 % w/w).

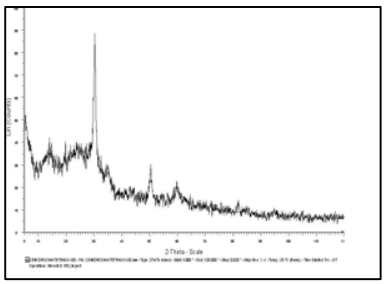

Fig. 6. XRD diffractogram of the acrylic bone cement reinforced with bioceramic (tetragonal zirconia powder in 22.5 % w/w).

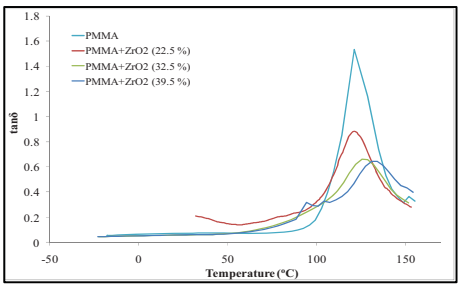

Fig. 7. tanδ versus temperature curves of acrylic bone cements without or with tetragonal crystal zirconia.

According to the Figure 5, the acrylic bone cement is a multiphase composite material. The PMMA beads retain their shape and are surrounded by the polymerized MMA monomer acting as binding agent. The small white particles are ZrO_2 powder. The peaks observed in *Fig. 6* at 2Θ value of 12.32 ^{0}, 30.39 ^{0} correspond to PMMA, while the peaks at 2Θ values of, 30. 39 ^{0}, 30.86 ^{0}, 34.85 ^{0}, 43.26 ^{0}, 50.86 ^{0}, 60. 38 ^{0}, 63.10 ^{0}, 73.30 ^{0} correspond to tetragonal phase of zirconia.

Figure 7 shows the tanδ versus temperature curves of the acrylic bone cements with different ZrO_2 percentage. The glass transition of PMMA is at 121 ^{0}C, whereas for the acrylic bone cements, T_g shifts to higher temperature and its intensity decreases with increasing the percentage of ZrO_2.

References

1. S. Daglilar , M.E. Erkan , O. Gunduz , L.S. Ozyegin , S. Salman , S. Agathopoulos , F.N. Oktar, “Water resistance of bone-cements reinforced with bioceramics”, Materials Letters 61, pp. 2295–2298, (2007).
2. E. Rusen, C. Zaharia, T. Zecheru, B. Marculescu,R. Filmon, D. Chappard, R. Badulescu, C. Cincu, “Synthesis and characterisation of core–shell structures for orthopaedic surgery”, Journal of Biomechanics 40, pp. 3349–3353, (2007).
3. I. Espigares, C. Elvira, J. F. Mano, B. Vazquez, J. S. Roman, R. L. Reis, “New partially degradable and bioactive acrylic bone cements based on starch blends and ceramic fillers”, Biomaterials 23, pp.1883–1895 (2002).
4. L. Yin, X. F. Song, Y. L. Song, T. Huang, J. Li, “An overview of in vitro abrasive finishing & CAD/CAM of bioceramics in restorative dentistry”, International Journal of Machine Tools & Manufacture 46, pp. 1013–1026 (2006).
5. S, Ahmad, S. Ahmad and S. A. Agnihotry, “Synthesis and characterization of *in situ* prepared poly (methyl methacrylate) nanocomposites”, Bull. Mater. Sci., Vol. 30, No. 1, pp. 31–35, February 2007.
6. Peter Southon, “Structural evolution during the preparation and heating of nanophase zirconia gels”, Ph. D. Thesis, University of Technology, Sydney, Chapter 5, Decomposition and crystallization with heating, p. 174, November 2000.

Poster A45

Processing effects on the dissolution properties of thin polymer based chemically amplified photoresist films

D. Drygiannakis[a,b], G. P. Patsis[a], K. van Werden[c], A. Boudouvis[b], I. Raptis [a]

[a] *Institute of Microelectronics, NCSR "Demokritos", 15310, Athens, Greece*
[b] *School of Chemical Eng., National Technical Uni. Athens Zografou 15780, Athens, Greece*
[c] *AZ Electronic Materials GmbH, Rheingaustrasse 190, 65203 Wiesbaden, Germany*

In the 22nm technology node, the resist film is anticipated to have a thickness of ~ 60nm, setting significant processing challenges due to the possible in-homogeneities of the resist film vs. depth i.e. glass transition temperature, free volume, photoacid generator (PAG) concentration etc. Among the properties, which should be understood and quantified in detail, resist dissolution mechanism poses a leading role, since at this processing step the resist profile is revealed and thus it has a great impact on the resolution, critical dimension, and LWR control.

The purpose of the current work is to study the effect of various processing parameters, such as film thickness, exposure dose, thermal processing conditions, on the dissolution of positive chemically amplified resists and also to provide the necessary input to stochastic simulators for the modeling of the influence of material and processes in the sub 50nm resolution scale (e.g. quantification of material interactions with substrate and developer, film morphology, dissolution rate).

For the present study, a FR-Dissolution (by Thetametrisis®, www.thetametrisis.com) dissolution rate monitor (Fig. 1) based on the concept of White Light Reflectance Spectroscopy (WLRS) was applied. The reflectance spectra are recorded every 100msec allowing the detailed observation of phenomena occurring during dissolution after the film is exposed even with high doses. The samples are consisted of three layers i.e. Si wafer (substrate), 1060nm SiO_2 layer (to provide the necessary interference fringes) and resist film, while the developer is considered as a fourth layer on the top (Fig. 2). Reflectance and transmittance equations are considered within each layer, and by applying the non-linear-recursive least-square method of Levenberg – Marquardt[1] on the reflectance spectrum the refractive index and thickness of the resist layer are calculated[2].

The evolution of the resist film thickness for two thicknesses and two exposure doses in the case of AZ DX6270 resist (AZ-EM) is illustrated in Fig. 3. Both films were treated at the same PAB and PEB conditions. For the high exposure doses the dissolution proceeds very fast and linearly while in the other dose an intermediate plateau is observed. In Fig. 4 the dissolution of 65nm thick films for a wide range of exposure doses is illustrated. The unexposed resist's thickness decreases ~10% after a development of 30sec (dark erosion). At the moderate exposure doses a plateau is observed which disappears for the high exposure doses. In this case the PAB was 120oC, 90sec and the PEB 130^{o}C, 90sec. The effect of PAB on dissolution of thin films of AZ DX6270 for low and high exposure dose is seen in Fig. 5. For low dose, PAB at high temperatures, increases dissolution time, due to the extra drying of the film from developer molecules, and the better relaxing of the polymer chains. At high exposure dose, PAB at ≥120oC causes a fast and linear dissolution process, thus such a temperature range seems to be adequate for the processing of such thin films.

From the simulation point of view of the dissolution process, detailed models of the resist film and the lithography process are employed[3], in a stochastic simulator which models the effects of dissolution process on the roughness evolution of pattern edges. Specifically, the Mack dissolution model is modified and adapted in the stochastic modeling approach of the resist film. Each polymer chain is treated separately by monitoring its dissolution rate, modeling it in terms of its size (radius of gyration) and location in the resist film.

References:

1. W. H. Press, S. A. Teukolsky, W. T. Vetterling, B. P. Flannery, Numerical Recipes in C, Uni. Press.
2. M.T.Spuller, R.S.Perchuk, D.W.Hess J. Electrochem. Soc. 152 G40 (2005).
3. G. P. Patsis, Polymer 46, 2404 (2005).

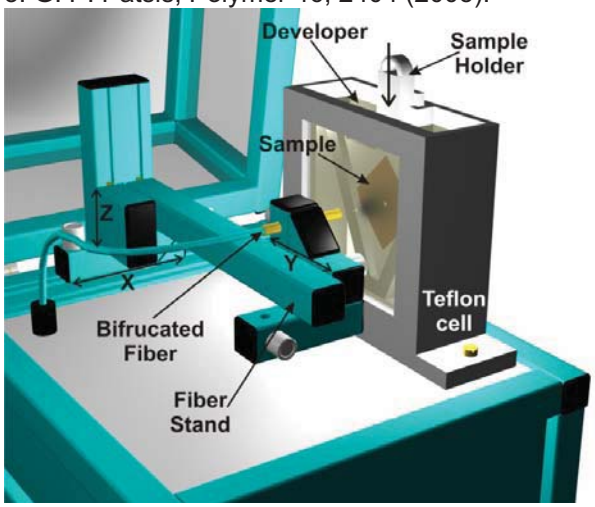

Fig. 1: Dissolution Monitoring setup. The sample is placed in a vessel filled with the developer. A Vis-NIR light source is constantly emitting light through optical fibers on the film surface. Another optical fiber collects the reflected light and transmits it into a PC controlled spectrometer.

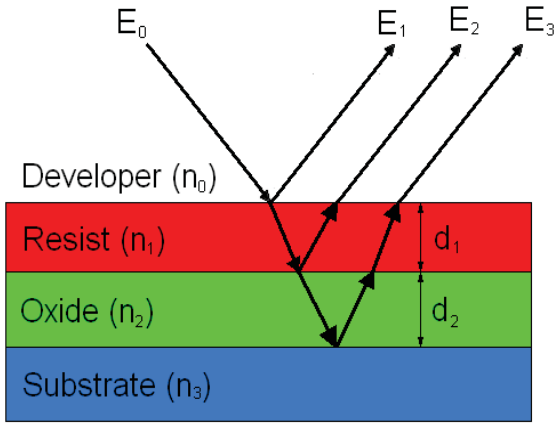

Fig. 2. (a) Film stack modeling. In the set-up used the light incidents with a very small angle respect to the vertical (1-2°)

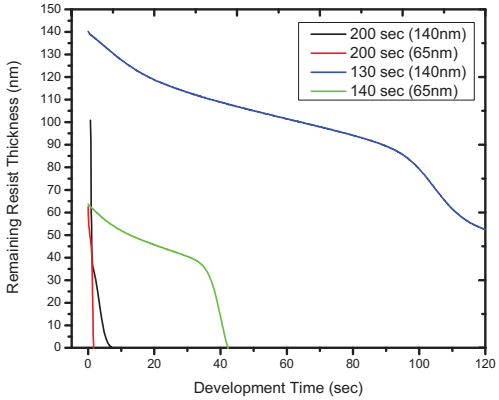

Fig. 3: Dissolution process for two exposure doses for two film thickness

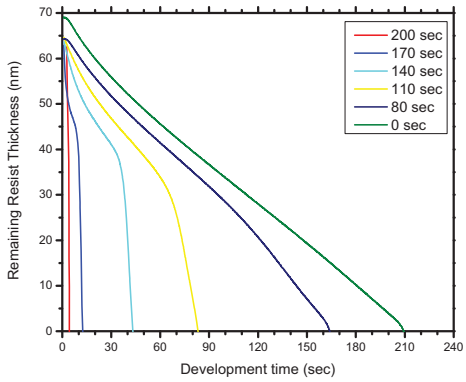

Fig. 4: Film thickness evolution of a 65nm thick AZ DX6270 film processed at PAB 120°C, PEB 130°C

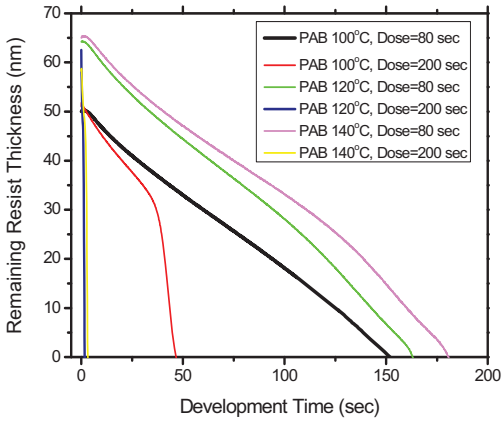

Fig. 5. Film thickness evolution of a 65nm thick AZ DX6270 film processed at various PAB conditions and for two exposure doses (low and high)

Poster A46

ELECTRICAL PROPERTIES OF POLYMERIC CARBONS PRODUCED FROM THE PRECURSOR SYSTEM OF NOVOLAC RESIN – NAPHTHALENE/CATALYST – OLIVE STONES BIOMASS

Anastasia Pikasi, Pantelitsa Georgiou, Johannis Simitzis*
National Technical University of Athens, School of Chemical Engineering, Department III
"Materials Science and Engineering", Laboratory Unit "Advanced and Composite Materials",
9 Heroon Polytechniou str., Zografou Campus, 157 73 Athens, Greece
*e-mail: simj@orfeas.chemeng.ntua.gr

1. INTRODUCTION

The conversion of organic materials into carbon is a complex process involving a wide variety of reactions and a vast number of intermediates. Considerable insight into the mechanisms of these reactions has been gained through studies of model aromatic compounds, such as naphthalene. The key step involves thermal polymerization, in which the aromatic starting material or rearranged intermediates are converted to oligomeric and polymeric components. This polymerization involves the loss of hydrogen and other substitute groups on the aromatic ring[1]. The carbonization of organic compounds by the addition of $AlCl_3$ has been reported to accelerate the formation of various types of cokes giving soft carbons[2, 3]. Production of value-added products from renewable sources is also attracting research efforts such as the production of carbons from renewable sources[4]. Alternative utilization processes involve olive stone. This source is pyrolyzed to obtain a valuable carbonaceous material. Olive stone is an important by - product generated in the olive oil extraction and pitted table olive industries[5]. The chemical and physical properties of the precursor system involved in the process of preparation, control the structure and properties of the final material[4]. Composite of olive stones biomass with novolac as binding agent had been fabricated under curing conditions and after the pyrolysis of the composites, carbonaceous adsorbents had been produced[6]. The aim of this work is the production of polymeric carbons of the precursor system of novolac resin - naphthalene/catalyst - olive stones biomass and the determination of the electrical properties of the final products.

2. EXPERIMENTAL

Carbonaceous materials were produced by pyrolyzing mixtures of novolac resin (N), agricultural by-product (olive stones biomass) (B) and aromatic substance (naphthalene) (A), mixed with catalyst ($AlCl_3$). Initially, the first precursor system consists of naphthalene (A) mixed with catalyst in ratio 1:0.1 mol and 1:1 mol, in the form of powder. Additionally, the second precursor system consists of naphthalene (A) / catalyst 1:1mol mixed with olive stones biomass (B) in three proportions: A : B equal to 20 : 80, 40 : 60 and 50 : 50 w/w, in the form of powder. The third precursor system consists of naphthalene (A) / catalyst 1:1 mol mixed with olive stone biomass (B) and novolac resin (N) in proportion 40 : 40 : 20 and 0 : 20 :80. The third precursor system before being pyrolyzed was cured as casting at 170 ºC for 30 min. All precursor systems (powders and specimens respectively) were pyrolyzed at 600 and 800 ºC with a heating rate of approximately 10 ºC/min, in a furnace under nitrogen flow (the residence time at these temperatures was 5 min.). The electrical conductivity of materials with constant current at room temperature was determined by the two-probe technique. These measurements were carried out either using disks after pressing the pyrolytic products of the first and the second precursor systems, or using the resulting pyrolyzed specimens of the third precursor system. Furthermore, non pyrolyzed or pyrolyzed at 350 ºC and 450 ºC olive stones biomass, were studied with FTIR spectroscopy.

3. RESULTS AND DISCUSSION

In Figure 1, the FTIR spectra of olive stones biomass and those pyrolyzed at 350 and 450 ºC are presented. According to the spectra, the OH absorption band at 3418 cm^{-1} for non pyrolyzed olive stones biomass, due to its component of cellulose, is strongly reduced during pyrolysis at 350 and 450 ºC. Similarly, the bands of C-H at 2855 cm^{-1} and 2920 cm^{-1} are also reduced after pyrolysis. The band at 1735 cm^{-1} of C=O stretching vibrations of the olive stones biomass disappeared after pyrolysis. The band at 1639 cm^{-1} of C=C without conjugation or conjugation in aromatic ring for olive stones biomass is shifted to 1615 and 1603 cm^{-1} for the pyrolyzed materials at 350 and 450 ºC, respectively (i.e. it is valid the absorption at 1600 cm^{-1} for aromatic ring). In the spectrum of olive stones biomass there is a high absorption band at 1380 cm^{-1} corresponding to CH_3 symmetric bending vibrations and a small absorption band at 1254 cm^{-1} possibly due to syringyl vibrations, both of which are reduced after pyrolysis at 350 ºC and practically disappeared at 450 ºC. The band of C-O stretching vibrations at 1050 cm^{-1} of the olive stones biomass disappeared after pyrolysis.

Table 1. Composition of precursor systems and their pyrolytic treatment.

Code of pyrolyzed materials		N % ↓	A % ↓	B % ↓	Temperature (ºC)
C1	1st prec. syst.	-	A100	-	600
C2		-	A100	-	800
C3		-	A100	-	600
C4		-	A100	-	800
C5	2nd prec. syst.	-	A20	B80	600
C6		-	A20	B80	800
C7		-	A40	B60	600
C8		-	A40	B60	800
C9		-	A50	B50	600
C10		-	A50	B50	800
C11	3rd prec. syst.	20	-	B80	800
C12		20	A40	B40	600
C13		20	A40	B40	800

N = Novolac
A = Naphthalene
B = Olive stones biomass

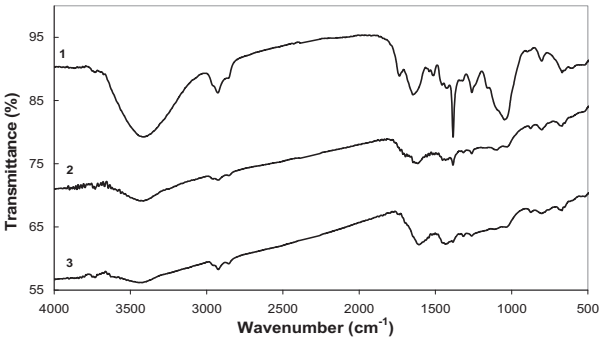

Figure 1. FTIR spectra of olive stones biomass, 1: non pyrolyzed, 2: pyrolyzed at 350 ºC and 3: pyrolyzed at 450 ºC

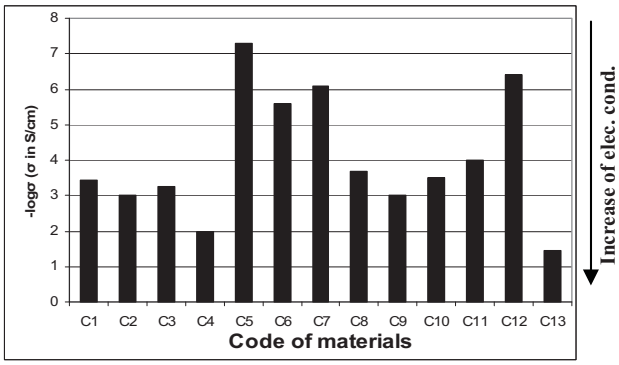

Figure 2. Conductivity of materials (for their code, see Table 1)

Table 1 presents the composition of precursor systems including also their pyrolytic treatment. Figure 2 presents the electrical conductivity (as a function of –logσ) of the previous materials.

According to Table 1 and Figure 2, correlating the C1 with C2 and C3 with C4 of the first precursor system, it is concluded that the electrical conductivity of the materials increases during the pyrolysis from 600 to 800 ºC. Although the amount of the catalyst is small, it contributes to a slight increase of the electrical conductivity of the pyrolysis residue at 600 ºC (C1 with C3) and to a higher increase at 800 ºC (C2 with C4). The electrical conductivity, σ of the first precursor system (pyrolyzed naphthalene) ranges from 10^{-4} to 10^{-2}.

In respect to the second precursor system (pyrolyzed naphthalene with biomass), by increasing the proportion of olive stones biomass, the electrical conductivity decreases (correlation of C5 with C7 and C9 for 600 ºC and C6 with C8 and C10 for 800 ºC). The electrical conductivity, σ, of the second precursor system ranges from 10^{-8} to 10^{-4}.

Concerning the third precursor system (pyrolyzed novolac with biomass and with or without naphthalene), the electrical conductivity of materials pyrolyzed at 800 ºC is high, comparable or better to that of the first precursor system. Therefore, the novolac due to its aromatic structure contributes to high conductivity, like as naphthalene. The highest electrical conductivity among all pyrolyzed materials has the C13 (σ = 3.6×10^{-2} S/cm, which contains not only novolac and naphthalene, but also olive stone biomass.

References

1. R.A. Greinke, I.C. Lewis, Carbon, 22, 1984, 305-314
2. I. Mochida, E.-I. Nakamura, K. Maeda, K. Takeshita, Carbon, 13, 6, 1975, 489-493
3. I. Mochida, K. Kudo, N. Fukuda, K. Takeshita, R. Takahashi, Carbon, 13, 2, 1975, 135-139
4. E. Genceli, E. Apak, M. Razvigorova, N. Petrov, V. Minkova, E. Ekinci, Fuel Processing Technology, 75, 2002, 97-107
5. G. Rodríguez, A.Lama, R. Rodríguez, A. Jiménez, R. Guillén, J. F.-Bolaños, Bioresource Technology, 2008, 5261-5269
6. J. Simitzis and J. Sfyrakis, Journal of Applied Polymer Science, 54, 1994, 2091-2099

Poster A47

NOVOLAC RESIN AND LIGNOCELLULOSIC MATERIALS AS PRECURSORS FOR CARBONACEOUS ADSORBENTS

Z. Ioannou*, J. Simitzis
*National Technical University of Athens, School of Chemical Engineering, Department III "Materials Science and Engineering", Laboratory Unit "Advanced and Composite Materials", 9-Heroon Polytechniou str., Zografou Campus, 157 73 Athens, Greece,*e-mail : zioan@mail.ntua.gr.*

1. INTRODUCTION

Natural polymers such as biomass, which consists of lignocellulosics have a great importance alone or in combination with synthetic polymers such as resins. Lignocellulosic materials are widely used in phenolic (i.e. novolac) and other thermosetting resins due to the decrease of shrinkage during moulding, the improved of impact strength and the reduced cost[1]. Such polymeric raw materials can be transformed to adsorbents by appropriate carbonization and activation. These materials are broadly used in different fields[2,3]. Specifically activated carbons are widely used in liquid and gas-phase adsorption of water and air pollution control and in various separation and purification processes[3]. Moreover, activated carbon adsorption helps to the removal of harmful substances from process solutions during treatment of polluted soils[4].

The aim of this work was the use of novolac resin and olive stones biomass, which is a lignocellulosic material, as precursors for the production of carbonaceous adsorbents and the investigation of the latter for its ability to adsorb dyes and for its functional groups determined by Fourier Transformed Infrared Spectroscopy (FTIR).

2. EXPERIMENTAL

Carbonaceous adsorbents were produced from novolac resin (N) and olive stone biomass (B). The resin was prepared by polymerization of phenol with formaldehyde using oxalic acid as catalyst and then follows drying and pulverization. The biomass consisted of the agricultural by-product that is left from olive stones after pressing and separation of the oil. Hexamethylenetetramine (hexa) was used as the curing agent whereas the proportion of novolac to hexa was 7/2 w/w. Hexa, novolac resin and biomass were separately ground and sieved to yield grains with a diameter less than 300μm. Then, the mixture was placed in small cylindrical moulds and cured at 170 ^{o}C for 30 min. The cured specimens were carbonized in a cylindrical tube oven at 1000^{o}C for 30 min under continuous flow of nitrogen. After the carbonization process, some specimens (as shown in Table 1) including commercial activated carbon (AC), were activated in a 45^{o} inclined oven using carbon dioxide. Nitrogen gas was inserted to avoid the inlet of oxygen into the oven.

FT-IR spectra were determined for the biomass, the cured, carbonized and activated materials. The discoloring abilities of carbonized and activated materials to adsorb dyes, were also determined, using methylene blue as dye from an aqueous solution of 0.032g/l, in a proportion of adsorbent to solution equal to 10/1 g/L.

Table 1. Composition of raw materials and conditions used for the production of carbonaceous materials

MATERIAL / Code	COMPOSITION OF RAW MATERIALS (w/w)			CURING (c)	CARBO NIZATION (C)	ACTIVATION (a)			
	Novolac (N) %	Olive stones biomass (B) %	N/hexa 7/2	170 °C 30 min	(1000 °C, 30 min)	Flow (ml/min) CO_2	Flow (ml/min) N_2	T_a (°C)	Residence time (sec)
B	-	100	-	-	-	-	-	-	-
N100-c	100	-	X	X	-	-	-	-	-
N20B-c	20	80	X	X	-	-	-	-	-
N40B-c	40	60	X	X	-	-	-	-	-
N20B-cC	20	80	X	X	X	-	-	-	-
N40B-cC	40	60	X	X	X	-	-	-	-
N20B-cCa	20	80	X	X	X	3.9	7.4	900-930	35
N40B-cCa	40	60	X	X	X	3.9	7.4	900-930	35
AC	-	-	-	-	-	-	-	-	-
AC-a	-	-	-	-	-	3.9	7.4	900-930	35

3. RESULTS AND DISCUSSION

According to the FTIR spectra presented in Fig. 1a, many differences were observed between olive stone biomass (B), cured novolac (N100-c) and cured mixtures of them, N20B-c and N40B-c. The most important differences are: a) the presence of C-O-CH_3 at 2850, 2848, 2849 cm^{-1} for B, N20B-c and N40B-c, respectively, COOH at 1749, 1730, 1727 cm^{-1} for B, N20B-c and N40B-c, respectively and their absence in cured novolac and b) the presence of hexa peaks at 1007, 1244 cm^{-1} for N100-c, 1011, 1235 cm^{-1} for N20B-c, 1007, 1234 cm^{-1} for N40B-c, respectively and their absence in B. The most intense

peaks between B, N100-c, N20B-c and N40B-c are the aromatic ring vibrations at 1509, 1605, 1508, 1504 cm^{-1} respectively, the presence of C=C at 1639, 1634, 1634 cm^{-1} for B, N20B-c and N40B-c respectively, C-H at 1029, 2920 for B, 2917 for N100-c, 1028, 2920 for N20B-c and 1033, 2919 cm^{-1} for N40B-c. Based on Fig. 1b for carbonized materials, the main absorption peaks for AC, N20B-cC and N40B-cC are C=O at 1547, 1398 and 1396 cm^{-1} respectively, C-H at 2915 cm^{-1} for N40B-cC, C=C at 1620 cm^{-1} for N20B-cC, 1618 and 1640 cm^{-1} for N40B-cC and OH at 3444 cm^{-1} the same for the three materials. Therefore the carbonized materials and the commercial activated carbon contain oxygen in the form of C=O and OH. The presence of oxygen in the form of other groups such as lactonic can not be detected from the FTIR spectra. Concerning the activated materials, Fig. 1c, their FTIR spectra presents a lot of similarities with carbonized.

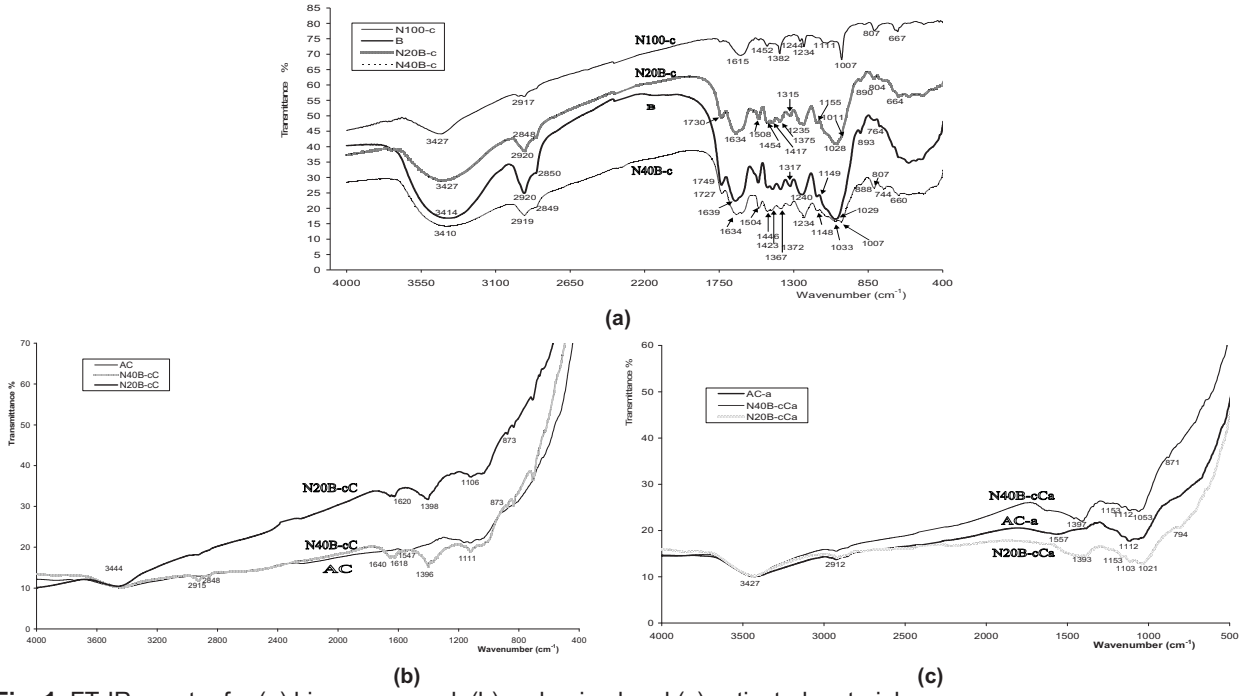

Fig. 1. FT-IR spectra for (a) biomass, cured, (b) carbonized and (c) activated materials.

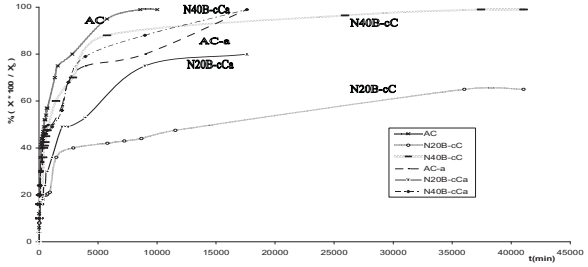

Fig. 2. Adsorption of methylene blue from aqueous solution on carbonaceous materials X_o: initial amount of methylene blue in solution before adsorption X: adsorbed amount of methylene blue.

It is concluded from Fig. 2 that the carbonized material presents generally lower adsorption ability than the respective activated except for AC which reveals better adsorption than AC-a for the same conditions. The N20B-cC presents the lowest adsorption compared to all other carbonized and activated materials. The N40B-cC presents similar adsorption compared to the respective activated specimens for the first seven days but then the activated materials (N40B-cCa) are discolored faster (in five days) than the carbonized. The N40B-cCa present similar adsorption behavior compared to AC-a specimens for the same proportions. The better adsorption ability for AC, N40B-cCa, N40B-cC and AC-a compared to the other materials indicate the presence of acceptor groups which interact with the donor groups of methylene blue leading to higher adsorption.

References

1. Simitzis J.; Karagiannis K.; Zoumpoulakis L.; Polymer International, **38** (1995) 183.
2. Simitzis J.; Sfyrakis J.; J. Applied Polymer Science, **54** (1994) 2091.
3. Ubago-Perez R.; Carrasco-Marin F.; Fairen-Jimenez D.; Moreno-Castilla C.; Microp. and Mesop. Materials , **92**, (2006), 64.
4. Forstner. U.; Chemiker – Zeitung, **110(10)**, (1986), 345.

Poster A48

New High Temperature Polymer Electrolyte Membranes. Influence of the Chemical Structure on their Properties.

N. Gourdoupi[1,3], K. Papadimitriou[1], S. Neophytides[2,3] J.K. Kallitsis[1,2,3]

[1] *Department of Chemistry, University of Patras, Patras 26500, Greece*
[2] *Foundation of Research and Technology-Hellas, Institute of Chemical Engineering and High Temperature Processes (FORTH-ICE/HT), Patras 26504, Greece*
[3] *Advent Technologies S.A., Patras Science Park, Stadiou Str.,Patras 26504, Greece*

Introduction

The search for new electrolytes, suitable for application in fuel cells, is one of the main interests in the field of energy related materials[1]. Especially in the case of polymeric fuel cells (PEM FC) the prerequisites for such materials are very demanding due to the chemically aggressive environment. Additionally, PEM fuel cells operating at temperature higher than 120℃ need polyelectrolytes which should be able to transport protons under non aqueous conditions. In such cases, one solution is the formation of acid-base complexes (PBI/H_3PO_4) using polymers bearing basic groups doped with strong acids giving materials with high ionic conductivity[2,3]. Another approach is the use of aromatic polyethers containing polar groups in the main chain which are also able to absorb strong acids and at the same time keep their mechanical and oxidative stability[4]. The synthesis of soluble high molecular weight polymers is a key issue[3,5], however this type of rigid polymers present inherent insolubility problems due to their structural characteristics.
In this work we report our attempt to synthesize soluble homopolymers and copolymers containing polar pyridine groups which can be eventually obtained in high molecular weight enabling the preparation of mechanically stable doped membranes. A study of the influence of the chemical structure on the properties of these materials in respect to their ability to be used in high temperature PEM fuel cells was made[6].

Synthesis of momomers and polymers

The combination of solubility and rigidity in polymers is a long lasting problem. In the case of aromatic polymers in order to overcome this difficulty we adopted two of the existing solubility strategies. The first includes the attachment of solubilizing side groups and the second the `incorporation of kinks in the polymeric main chain. Regarding the first route, we have synthesized a new monomer, the 1,4-[bis(4-hydroxyphenyl-2,5-pyridine)2,5-diethyloxy]benzene using the Suzuki coupling of 2,5 diethoxy 1,4-phenyl-bisboronic acid and the protected bromo phenyl pyridine. Homopolymers and copolymers incorporating the substituted diol were successfully synthesized. The second route involves the use of the bis(4-hydroxyphenyl) phenyl phosphinoxide for the synthesis of copolymers. The chemical structures of the synthesized polymers are shown in Scheme 1.

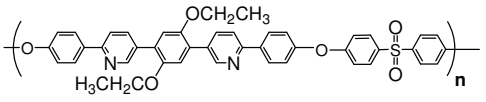

PQdPyEtO

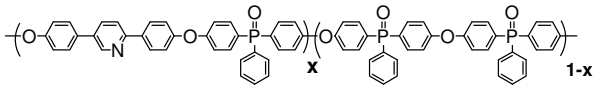

PPy(x)coPO

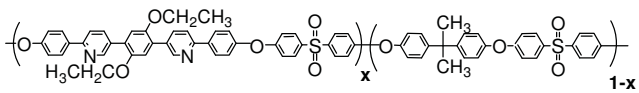

PQdPyEtO(x)coPSF

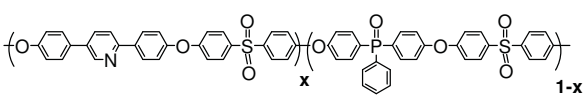

PPy(x)POcoPSF

Scheme 1 Chemical structures of the synthesized polymers

Characterization

Homopolymers and copolymers with high T_g values, high molecular weight, soluble in common organic solvents showing film forming properties were obtained as shown in Table 1. The influence of the polymeric structure in the T_g values shows that copolymer PPy(90)coPO possesses higher Tg value and higher thermal stability compared to the PQDPyEtO and PQDPyEtO(50)coPSF. The superior characteristics of PPy(90)coPO are due to the absence of side groups in its chemical structure and at the same time due to the existence of phosphinoxide moiety.

Table 1 Characterization of the synthesized polymers

Polymer	Mn	Mw	I	T_g (°C)	$T_{d\ (5\%)}$	Film quality
PQdPyEtO-iii	20300	43200	2.1	184	410	+
PQdPyEtO(70)coPSF-ii	19500	41800	2.1	-	-	+
PQdPyEtO(50)coPSF-i	34200	68400	2.0	208	410	+
PPy(90)coPO-iii	50700	116700	2.3	270	540	+
PPy(80)coPO-ii	16800	31500	1.8	-	-	+
PPy(50)POcoPSF	7000	19400	2.7	-	-	- -
PPyPO-iv	29000	63800	2.2	252	550	+

The synthesized polymers are easily doped with phosphoric acid. In our attempt to observe the influence of the polymeric matrix on the measured conductivity, we chose different polymeric materials that possessed the same phosphoric acid doping level. The results are depicted in Figure 1. As it is clearly shown their, even small changes on the polymeric structure have a significant influence on the conductivity values.

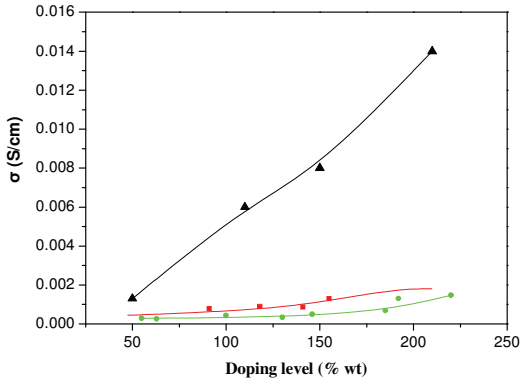

Fig.3 Doping level dependence of ionic conductivity of PPy(90)coPO (●), PPy(80)coPO (■) and PPyPO (▲) at room temperature and relative humidity 40%.

Conclusions

New monomers and polymers have been synthesized and tested in respect to their solubility, thermal and mechanical properties as well as their ability to absorb phosphoric acid. A detailed study of the influence of the various structural parameters on the polymer properties was made, in order to evaluate their ability to be used as polymer electrolytes in fuel cells operating at temperatures above 120 °C.

References

1. B.C.H.; Steele, A. Heinzel, *Nature* 2001, 414, 345.
2. Q. Li, R. He, J.O. Jensen, N.J. Bjereum, *Fuel Cells* 2004, 20, 147.
3. Y.L. Ma, J.S. Wainright, M. Litt, R.F. Savinell, *J. Electrochem. Soc* 2004, 151, 8.
4. N. Gourdoupi, A. K. Andreopoulou, V. Deimede, and J. K. Kallitsis, *Chem. Mater.* 2003, 15, 5044.
5. E.K. Pefkianakis, V. Deimede, M.K. Daletou, N. Gourdoupi, J.K. Kallitsis, *Macromol. Rapid Commun.* 2005, 26, 1724.
6. N. Gourdoupi, K. Papadimitriou, S. Neophytides J.K. Kallitsis, Fuel Cells 2008, in press.

Poster A49

The effect of nanoclay content on the electrospun fibrous structure of biodegradable polymer nanocomposites

A. Tsimpliaraki, S. Svinterikos and C. Panayiotou

Department of Chemical Engineering, Aristotle University of Thessaloniki, 54124 Thessaloniki, Greece
E-mail: cpanayio@auth.gr

Polymer/layered silicate nanohybrids have lately become the focus of academic and industrial attention. Incorporation of a small quantity (typically less than 10%) of inorganic nanosized materials which are highly anisotropic, such as clay platelets, can significantly improve mechanical and physical properties of the neat polymer[1,2]. The lower loadings also facilitate processing and reduce component weight.

Electrospinning has been widely used as an alternative technique in fabrication of membranes and filters and have fiber diameters ranging from few nanometers to few micrometers. This markedly simple and cost effective process operates on the principle that the solution is extracted under a high electric field. Once the voltage is sufficiently high, a charged jet is ejected following a complicated looping trajectory[3]. During its travel, the solvent evaporates within milliseconds and fibers are accumulated on the collector in a randomly oriented fashion. The combination of their nanometric dimensionality, high surface area, porosity, flexibility and mechanical integrity makes the electrospun fibers suitable for several value-added applications, such as tissue engineering, wound dressing, clothing protection, nanoscale and biological adsorption, filter and membrane technology.

In the present work, a novel polymer – clay nanocomposite system is studied. A bulk preparation of nanocomposite materials was initially conducted according to the same solution casting routine followed in our previous studies[1,2]. Specifically, various loadings of organically modified montmorillonite (Cloisite 25A), which ranged from 0-9 wt%, were dispersed in the commercial polyester poly(butylene succinate-co-butylene adipate) (PBSA) (Bionolle 3001) using dichloromethane as a solvent. Membranes consisted of nanosized fibers of pure and nanocomposite PBSA were subsequently prepared by electrospinning. The applied DC voltage was 15 kV, solution concentration of nanocomposite into dichloromethane was 18 %w/v, the flow rate of the solution was 1 ml/h and the distance between the capillary tip and the collector was kept at 8 cm in accordance with studies on similar systems[4,5]. Therefore, influence of the clay content into the polymer composites is chosen to be the focal point of this investigation.

The surface morphology of the fibrous mats was examined using scanning electron microscopy (SEM) and image processing of the micrographs was employed in order to determine the mean diameter of the fibers and their standard deviation utilizing an image analyzer. Fig. 1 presents SEM micrographs of the obtained membranes where the dependence of final fibrous structure on the clay content is evidently depicted. Increasing the clay loading from 0 to 5 wt% into the nanocomposite resulted in more uniform structures with non-beaded continuous fibers and narrower diameter distributions. Further increment of the clay content from 5 to 9 wt % had no major effect on uniformity of the observed structures apart from lower average fiber diameters (from 510 to 370 nm) and almost the same diameter distributions as concluded also from the magnified SEM photographs presented.

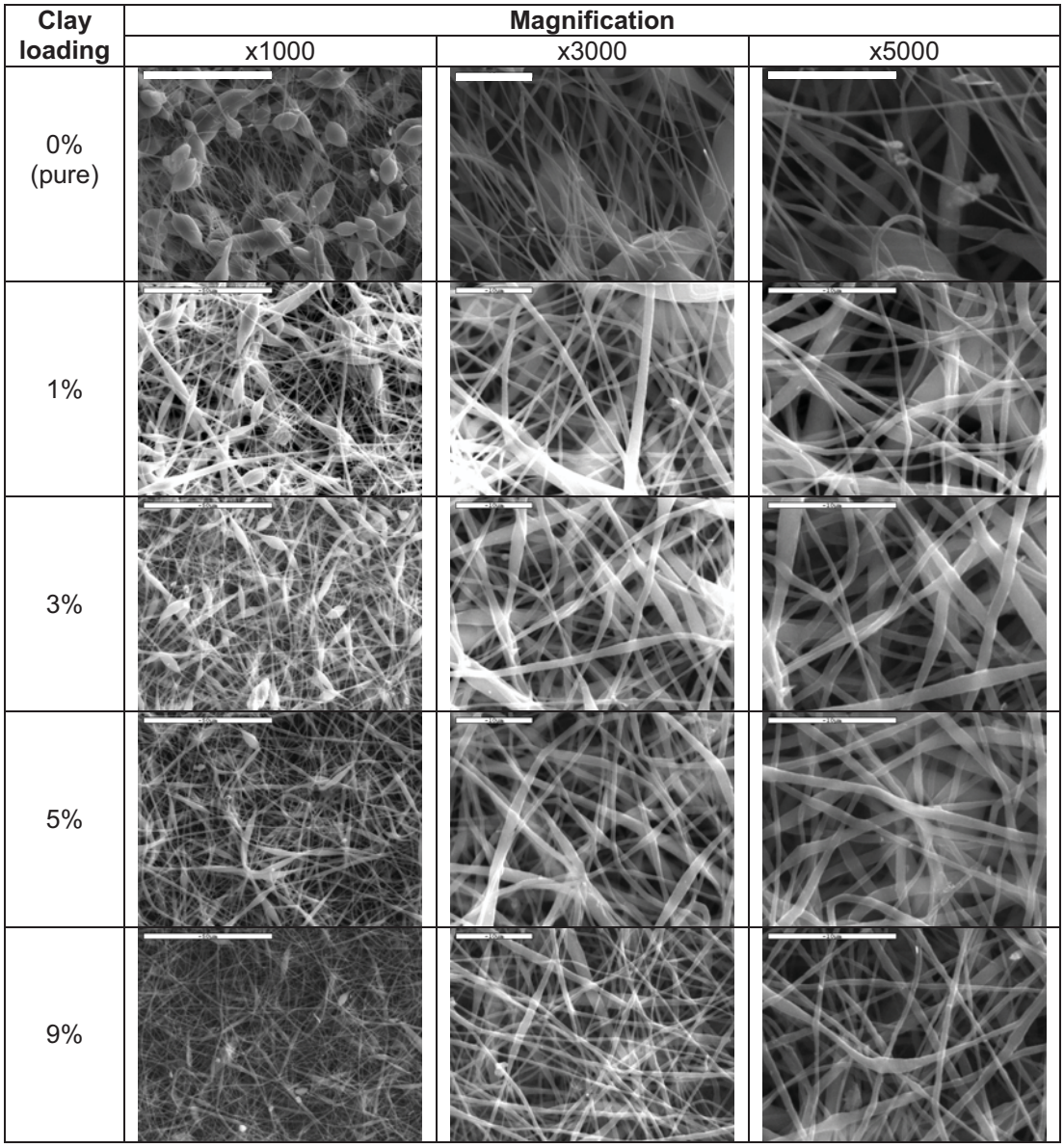

Fig. 1. SEM photographs of PBSA nanocomposite with clay content ranging from 0 to 9 wt%, scale bar is 50 μm at magnification x1000 and 10 μm at x3000 and x5000.

References

1. *"Surfactant-induced morphology and thermal behavior of polymer layered silicate nanocomposites"*, Marras SI, Tsimpliaraki A, Zuburtikudis I, Panayiotou C, J Phys: Conf Ser, **61**, 1366–1370(2007).
2. *"Morphological, thermal and mechanical characteristics of polymer/layered silicate nanocomposites: The role of filler modification level"*, Marras SI, Tsimpliaraki A, Zuburtikudis I, Panayiotou C, Pol Eng Sci, in press.
3. *"Bending Instability of Electrically Charged Liquid Jets of Polymer Solutions in Electrospinning"*, Reneker DH, Yarin AL, Fong H, Koombhongse S, J Appl Phys, **87**, 4531(2000).
4. *"Biodegradable polymer nanocomposites: The role of nanoclays on the thermomechanical characteristics and the electrospun fibrous structure"*, S. I. Marras, K.P. Kladi, I. Tsivintzelis, I. Zuburtikudis, C. Panayiotou, Acta Biomater, **4(3)**, 756-765(2008).
5. *"Preparation and characterization of electrospun poly(butylene succinate-co-butylene adipate) nanofibrous nonwoven mats"*, V. Tserki, I. Filippou, C. Panayiotou, Proc IMechE, Part N: J Nanoengineering and Nanosystems, **220(2)**, 71-79(2006).

Poster A50

Type II Photoinitiator Systems Based on Novel Fluorenone and Fluorene Chromophores. A Mechanistic Study by Laser Flash Photolysis

X. Asvos[1], M. G. Siskos[1], A. K. Zarkadis[1], O. Brede,[2] R. Hermann[2]

[1)] *Department of Chemistry, University of Ioannina, 451 10, Ioannina, Greece*
[2)] *Interdisciplinary Group Time-Resolved Spectroscopy, University of Leipzig, D-04303, Leipzig, Germany*

Photoinitiated free radical polymerization is a technologically important process of enormous commercial importance which involved in numerous applications such as coatings, printing inks, varnishes, adhesives, paints, microelectronics, etc. [1]

In recent years, there have been many new developments in the synthesis and photochemical studies of novel photoinitiator molecules which are the key to control the photopolymerization process. Free radical photoinitiators fall in two categories, the photofragmentating (*Type I*) initiators and the hydrogen-abstracting type (*Type II*) initiators. Photoinitiation by Type II initiators (mainly aromatic ketones) are based on the reaction of their triplet excited states with a hydrogen donor (usually an amine) producing the initiating radical.

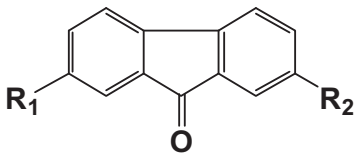

1

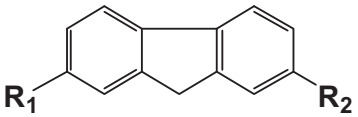

2

1, 2	R_1	R_2
a	H	H
b	H	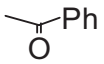
c		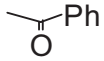

In the present report, we synthesized a series of novel fuorenone **(1)** and fluorene **(2)** based photoinitiators[2] which are used to study the photopolymerization reaction (*initiation efficiency, degree of polymerization, influence of solvent, concentration of amine*) of methylmethacrylate (MMA) using the triethylamine (TEA) as co-initiator. The *motivation* behind this work is *(i*) to ***synthesize*** novel photoinitiators, in which the chromophore unit *(fluorenone or fluorene)* is extended to the longer wavelength by introducing one or two benzoyl groups; *(ii)* to ***study*** their photophysical/photochemical properties and *(iii)* to ***investigate*** the mechanism of the photopolymerization reaction. For this study we have used techniques such as UV-visible and fluorescence spectroscopy, laser flash photolysis (LFP) (*ns-timescale*) and product analysis. Finally, this study is supported by *ab initio* and DFT calculations

References:

[1] Allen N. S. *"Photopolymerization and Photoimaging Science and Technology",* Elsevier Applied Science, London, **1989**; Fouassier J. P. *"Photoinitiation, Photopolymerization, and Photocuring, Fundamentals and Applications"*, Hanser, München, **1995;** [2] D. A. Tasis, M. G. Siskos, A. K. Zarkadis, *Macromol.Chem.Phys*.,199 (**1998**)1981-1987; Georgakilas V, Perdikomatis G. P., Triantafyllou A. S., Siskos M. G., Zarkadis A. K., *Tetrahedron*, **2002**, 58, 2441

Poster B1

Measurements of free volume in polymer nanocomposite coatings using Positron Annihilation Lifetime Spectroscopy

G. Choudalakis and A.D. Gotsis
Dept. of Sciences, Technical University fo Crete, 73100 Hania

Polymer nanocomposites materials are two-phase systems that consist of a polymeric matrix and dispersed inorganic particles of nanometer scale. The inorganic particles consist of stacked layers of 2:1 phyllosilicates. These layers have thickness of around 1 nm, lateral dimension from 30 nm to several μm and are separated ("exfoliated") to some degree in the polymer matrix. Thus the nanoparticles present a very high aspect ratio of width/thickness in the order of 10-1000. Even at very low filler concentrations the total interface between polymer and layered silicates is much greater than that in conventional composites.

The morphology of a nanocomposite depends on the strength of the interactions between the two phases. For strong interactions the layers can be fully separated resulting in an exfoliated morphology. For weaker interactions the separation is not complete and an intercalated morphology may be obtained. The presence of the particles and their shape alters the physical properties and the free volume characteristics of the polymer nanocomposite material. This is, a.o., due to the particles restricting the motions of the polymer chains in their vicinity, affecting, thus, the total free volume in the material. Additionally, ineffective packing in the large interfacial regions between the two phases may create extra free volume.

Exfoliated nanocomposites are used as barrier materials that prevent the permeation of small molecules in packagings, films and coatings.[1] The nano-platelets in these materials act mainly as geometrical barriers, forcing the permeant to follow a much longer tortuous path around them inside the matrix. The rate of permeation could be affected also by changes in the permeability of the polymeric matrix due to the effect of the filler on the free volume in the polymer.

These variations of the free volume characteristics can be detected experimentally using Positron Annihilation Lifetime Spectroscopy (PALS).[2] This technique is based on the measurement of the time scale for the formation of positronium (Ps) atoms in the low electron density sites of the material and their subsequent annihilation. A typical PALS spectrum of a polymer consists of three components coming from the three possible types of the annihilation process. The first process is the direct annihilation of the positron with an electron, the second type is the p-Ps annihilation, while the third is the o-Ps annihilation. The latter depends on the specific features of the free volume. From the measured lifetime $\tau_{\text{o-Ps}}$ and its relative intensity $I_{\text{o-Ps}}$ it is possible to extract an estimate of the number and the size of the free volume holes existing in the materia.[3,4]

In the present study, the PALS technique was applied in a nano-platelet/polymer composite material. The nanocomposites consisted of a crosslinked acrylic resin filled with organomodified laponite particles (width/thickness ratio of $\sim$30) at various concentrations (0,1,2,3,6 wt%). The results indicated that the life time of the positroniums and the relative intensity of their annihilation in the polymer remain almost unchanged with the addition of laponite particles. This indicates that the changes of the free volume in the system are very small. It seems that any decrease in free volume that may be caused by the restriction of the polymer (side-)chain motions near the particle interfaces is counterbalanced by the possible increase due to the extra interface. The final result is that the diffusion of gasses through the polymeric matrix is not accelerated by the presence of the nanoparicles and the effectiveness of the barrier properties of the nanocomposites are not reduced by this mechanism.[5]

Acknowledgements: We thank prof. S.J. Picken and dr. H. Schut of Delft University of Technology for helping with the use of the positron facilities at the Reactor Institute Delft. This research project has been supported by the European Commission under the 6th Framework Programme through the Key Action Strengthening the European Research Area, Research Infrastructures, contract nr: RII3-CT-2003-505925.

References:

1. G. Choudalakis and A.D. Gotsis, "Permeability of polymer/clay nanocomposites. A Review", subm. to Euro.Polym.J., June 2008.
2. R.A. Pethrick, "Positron annihilation -- A probe for nanoscale voids and free volume?", Prog.Polym.Sci., **22**, 1--47, 1997.
3. S.J. Wang, L.M. Liu, P.F. Fang, Z. Chen, H.M. Wang and S.P. Zhang, Microstructure of Polymer-Clay Nanocomposites Studied by Positrons, Radiation Physics and Chemistry, 76, 106-111, 2007.
4. P. Winderg, M. Eldrup, N. Pedersen, M. Van Es, F. Maurer, Free Volume Sizes in Intercalated Polyamide6/Clay Nanocomposites, Polymer, 46, 8239-8249, 2005
5. G. Choudalakis, S.J. Picken, H. Schut and A.D. Gotsis, "Free volume measurements in nanocomposites using PALS", to be published, 2008.

Poster B2

LIGHT INDUCED MICRO-FIBER FORMATION IN TRANSPARENT POLYMER SOLUTIONS

Emmanuel Anyfantakis[1,2], Benoit Loppinet[2], Christos Mantzaridis[3,4], Stergios Pispas[4] and George Fytas[2,3]

[1]*Chemistry Department, University of Crete, Heraklion, Greece*

[2]*Institute of Electronic Structure and Laser, FO.R.T.H., Heraklion, Greece*

[3]*Materials Science and Technology Department, University of Crete, Heraklion, Greece*

[4]*Theoretical and Physical Chemistry Institute, N.H.R.F, Athens, Greece*

Surprisingly, irradiation of transparent semidilute solutions of common entangled polyolefins (e.g. cis-1,4 polyisoprene) in organic solvents of lower refractive index (e.g. hexane, toluene) with visible laser light of mild power causes an alteration in the composition of the binary mixture leading to optical nonlinearities.[1] The local increase of the polymer concentration along the light propagation direction leads to optical nonlinearity and eventually laser beam self trapping. The process results in the formation of long fibers, which remain even after the laser light is turned off. This phenomenon is unrelated to photophysical and photochemical processes and presents some clear phenomenology. Analogy with optical spatial solitons observed in other non linear optical media is discussed.

The writing process of the long fibers in cis-1,4 polyisoprene and polybutadiene solutions in various solvents is studied by means of quantitative phase contrast microscopy where the spatial modulation of the polymer concentration is deduced from the imaged intensities. The influence of different parameters that affect the writing, such as irradiating conditions (power, beam waist) and solution properties (polymer-solvent refractive index difference, concentration) is reported. Noticeably, larger beam waist lead to multiple filaments formation with fiber diameter of the order of 5 μm, similar to the single filament diameter, rather independent of the writing conditions and polymer concentration. As to the fiber reversibility, while short writing time leads to structures that redissolve, fibers obtained for longer illumination appear to be permanent.

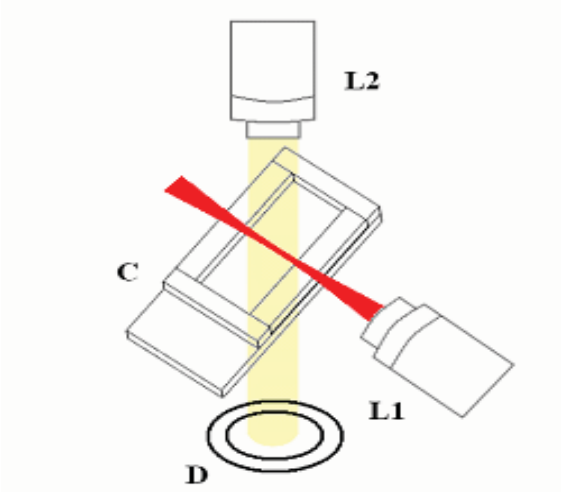

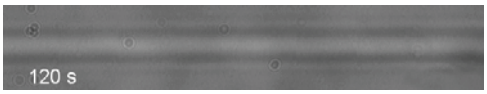

Fig.1. *Left:* A schematic view of the experimental set-up: L1: Writing lens focusing the laser light. L2: Microscope Objective lens, C: Homemade glass cell and D: Microscope illuminating white light.

Right: Filament created by irradiating a solution of cis-1,4 PI in decane, c= 2.42% wt with a red laser (λ= 671 nm) at a power of 29 mW for 120 s.

1. R. Sigel, et al. *Science* 297 (2002) 67

Poster B3

Does Brillouin light scattering probe the primary glass transition process?

Panayiotis Voudouris[1, 2] and George Fytas[1, 3, 4]*

[1]*FORTH/ Institute of Electronic Structure and Laser, P.O Box 1527, 71110 Heraklion, Greece*

[2]*Department of Chemistry, University of Crete, Heraklion, Greece*

[3]*Department of Materials Science and Technology, University of Crete, Heraklion, Greece*

[4]*Max Planck Institute for Polymer Research, Mainz, Germany*

The primary α-relaxation probed by either dielectric spectroscopy (DS) depolarized light scattering (DRS) and photon correlation spectroscopy (PCS) describes the torsional autocorrelation function of the molecular dynamics (MD) simulation. This function has a non-exponential shape and is characteristic time obeys the WLF equation. Another experimental light scattering technique, Brillouin Light Spectroscopy (BLS) operating in GHz frequency probes a fast (10-100ps) relaxation (dissipation of the phonon energy into the structure) of the longitudinal modulus M=K+(4/3)G. This relaxation function is assumed to be a single exponential decay (or Debye process) and its relaxation time is faster than the α-relaxation following an Arrhenius T-dependence. This available knowledge is based only on a single wave vector (frequency)[1]. To the best of our knowledge no specific molecular motion has been assigned to this fast process far above T_g (~T_g+100K) and the origin of the discrepancy with the α-relaxation process is not known. Any association to faster secondary (β,γ) species specific relaxations is ambiguous. Using a new spectrometer[2] we measured the phonon dispersion at GHz frequencies in molecular (ortho-terphenyl, OTP) and polymeric (polyisoprene, PI and polypropylene PP) glass formers. We found that the hypersonic dispersion relates to the glass transition dynamics but the disparity of its relaxation time from the α-relaxation time is system dependent. In PI and PP, the BLS relaxation time is more than one order of magnitude faster than the α-relaxation time whereas the two times become comparable in the case of OTP. The difference between the times scale appear to relate to the width of the relaxation time distribution function.

References:

[1] Polymer 32, 2307, 177-185, *1991*
[2] J. Chem. Phys. 119, 6883, *2003*

Poster B4

A thermal and dielectric study of molecular dynamics in Polyurethane-POSS hybrids

Konstantinos Raftopoulos[1], Christos Pandis[1], Lazaros Apekis[1], Bartlomiej Janowski[2], Krzystof Pielichowski[2] and Polykarpos Pissis[1]

[1] National Technical University of Athens, Department of Physics, Iroon Polytechneiou 9, Zografou Campus, 157 80, Athens, Greece
[2] Department of Chemistry and Technology of Polymers, Cracow University of Technology, ul. Warzawska 24, 31-155 Krakow, Poland

Introduction

Polymeric materials modified with inorganic nanoparticles either by mixing or by incorporation in the polymeric chain (organic-inorganic O-I hybrids) have attracted much attention due to their improved mechanical properties compared to their matrix as a pure polymer[1]. In particular, incorporation of Polyhedral Oligomeric Silsesquioxane (POSS) particles in the main chain of polymers is known to increase the glass transition and decomposition temperature, while decreasing flammability.

Materials

In this work 1,2-propanediol-heptaisobutyl-POSS (PHIPOSS) has been used to modify a common Polyurethane matrix. The latter has been synthesized by 4,4'-methylenebis(phenylisocyanate) (MDI) as isocyanate component and poly(tetramethylene glycol) (TERATHANE 1400 ®) with molecular weight of ~1400 as elastic component while 1,4-butanediol was used as chain extender. Appropriate quantity of the chain extender was substituted by the PHIPOSS particles to provide samples with PHIPOSS mass fraction in the range 2-10%.

Experimental

For the study of the local and segmental dynamics, Differential Scanning Calorimetry (DSC), Thermally Stimulated Depolarization Currents (TSDC) and Dielectric Relaxation Spectroscopy (DRS) were employed.

DSC was performed in the glass transition region of the polyurethane matrix and the hybrids revealed a monotonous increase of the glass transition temperature (T_g) upon addition of POSS (fig.1) indicating reduced mobility in the hybrids.

TSDC, is a special dielectric technique in the temperature domain. It has high resolving power due to its low equivalent frequency (10^{-3} Hz) [2]. Results by this technique indicate the existence of 3 relaxations. Starting from low temperatures, β relaxation is visible at -120°C and no indication of influence of POSS on it is observed. α relaxation that is visible in the region -80 ─ -40°C corresponds to the glass transition, and the peak temperature (T_α) is a good measure of the calorimetric T_g. In accordance with DSC, T_α increases systematically with POSS content (fig.1). The strength of the relaxation is significantly reduced upon addition of POSS, suggesting immobilization of the polymer, a result that should be clarified in future work. In the region of 0-10°C the interfacial Maxwell Wagner Sillars relaxation[3] is observed as a prominent peak.

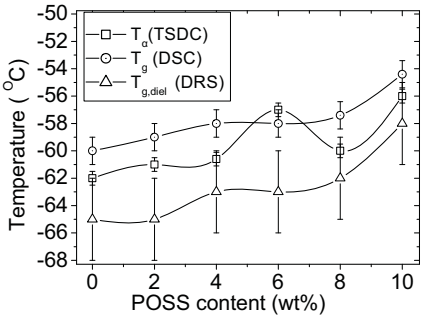

Fig. 1: *Glass transition Temperatures as measured by the three techniques employed in this study, as a function of POSS content. Lines are guides to the eye.*

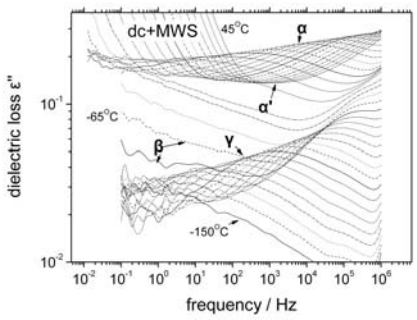

Fig. 2: *Dielectric loss spectra of a selected sample for various temperatures in step of 5 degrees.*

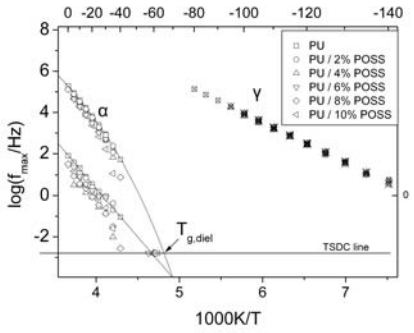

Fig. 3: *Arrhenius plot for the samples indica.ted on the plot. Solid lines are fits of Arrhenius (α') or VTF (α) equations for unmodified polyurethane.*

DRS spectra were obtained in a wide temperature and frequency range (-150 to 45°C and 10^{-1} to 10^{6} Hz respectively). Four relaxations are observed (Fig. 2). Starting from low temperatures, γ relaxation is visible in a wide temperature interval, followed by the weak β relaxation visible only in a short temperature interval (-70 ─ -55°C) before being masked by α relaxation (dynamic glass transition). Between α and the combined contribution of dc conductivity and MWS (steep decrease of ε´´(f) in the low frequency region) a weak relaxation (α') is present.
Spectra in the area of the combined α and α' peak were analyzed in terms of Havriliak-Negami[4] model functions.
In fig.3 the activation diagram is shown for α, α' and γ relaxations. TSDC peak temperatures are plotted at equivalent frequency $1.6 \cdot 10^{-3}$ Hz (τ=100sec)[3]. Time scale of γ is unaffected by modification and shows Arrhenius behavior with activation energy 0.39eV. α shows Vogel Tamman Fulcher (VTF)[3] behaviour and is clearly slowed down by addition of POSS in accordance to DSC and TSDC results. Temperatures obtained by extrapolation of VTF to frequency $1.6 \cdot 10^{-3}$ Hz ($T_{g,diel}$) coincide well with glass transition temperatures obtained by aforementioned techniques.
The trace of α' merges in the low frequency region with that of α, thus explaining its absence in TSDC thermograms as a standalone peak. This behaviour is typical of the so-called normal mode relaxation which is related to the presence of a dipole moment component along the chain contour (here Terathane 1400). In that case, the relaxation should show VTF rather than Arrhenius behavior and is a point that should be clarified in future work.

Conclusions

Polyurethane-POSS nanocomposites were studied regarding their molecular dynamics by three techniques, DSC, TSDC and DRS. One secondary relaxation and the dynamic glass transition were studied in detail. While the secondary γ relaxation seems unaffected, all three techniques verify that the dynamics of the glass transition becomes slower upon addition of POSS particles indicating reduced mobility in the composites.

Literature

1. L.Matejka, A.Strachota, J.Plestil, P.Whelan, M.Steinhardt, M.Slouf, Macromolecules, 37/25 (2004) 9449
2. Van Tournhut, in “Electrets” Topics in Applied Physics, edt.G.M.Sessler, Springer Berlin, 1980
3. J.P. Runt and J.J. Fitzgerald, Editors, Dielectric spectroscopy of polymeric materials, American Chemical Society, Washington, DC, 1997
4. S.Havriliak Jr, S.J.Havriliak, Dielectric and Mechanical Relaxation in Materials, Hanser, Munich, 1997

Poster B5

Dielectric – mechanical and thermal studies of molecular mobility and phase morphology in epoxy-amine / carbon black nanocomposites

E.Logakis[1], Th.V.Kosmidou[3], A.Kanapitsas[2], C.Tsonos[2], C.G.Delides[3], P.Pissis[1]

[1] National Technical University of Athens, Department of Physics, Zografou Campus, 15780 Athens, Greece

[2] Technological Educational Institute of Lamia, Department of Electronics, 35100 Lamia, Greece

[3] Technological Educational Institute of Western Macedonia, Laboratories of Physics and Materials Technology, 50100 Kila, Kozani, Greece

Abstract

In this work we focus on the effect of the filler content on the relaxation mechanisms and the dielectric, dynamic mechanical and thermal behaviour of epoxy-amine / carbon black nanocomposites. For the preparation of the nanocomposites diglycidil ether of bisphenol A (DGEBA) was used with triethylenetetramine (TETA) as a curing agent. As fillers carbon black (CB) nanoparticles with size from 25 to 75 nm used. The characterization was done using Dynamic Mechanical Analysis (DMA), Dielectric Relaxation Spectroscopy (DRS), Differential Scanning Calorimetry (DSC), Thermogravimetric Analysis – Differential Thermal Analysis (TGA/DTA) and electrical conductivity measurements. The dependence of the dynamic mechanical, dielectric and thermogravimetric parameters (E', E", tanδ, ε', ε'', σ, m) is associated with the filler content. Several relaxation mechanisms were observed: Main α-relaxation, secondary β relaxation and interfacial Maxwel-Wagner-Sillars relaxation probably due to the formation of aggregated microstructures in the bulk composite. The effect of the filler loading and the dispersion conditions on the molecular mobility is related to the enhanced polymer dynamics due to the network structure formed around the filler particles and to the extra free volume at the resin-filler interface. Results related with the interfaces formation between fillers and the polymer matrix were extracted, and their contribution on the behavior of the system were discussed.

References

1. Th.V.Kosmidou, A.S. Vatalis, C.G. Delides, E. Logakis, P. Pissis, G.C. Papanicolaou, express Polymer Letters **5(2)**, 364-372 (2008**)** .
2. E. Vassileva, K. Friedrich, J. Appl. Polym. Sci. **89**(14), 3774-85, (2003).
3. W. K. Goertzen, M.R. Kesler, Composites, Part A , **39,** 761-768, (2008).
4. J. Xu, C. P. Wong, Electronic Components and Technology Conference, IEEE (2005).
5. Y. Sun, Z. Zhang, K-S. Moon, C. P. Wong, J. Pol. Sci. Part B: Polymer Physics, **42**, 3849-3858 (2004).
6. J. G. Meier, M. Klupper, Macromol. Mater. Eng. **293**, 12-38 (2008).

Poster B6

Dynamics and rheology in suspensions and glasses of soft colloids.

Andreas Pamvouxoglou[1, 2] and George Petekidis[1, 2,*]

[1]FORTH/ Institute of Electronic Structure and Laser, P.O Box 1527, 71110 Heraklion, Greece

[2]Department of Materials Science and Technology, University of Crete, Heraklion, Greece

*georgp@iesl.forth.gr

Colloidal suspensions of soft particles consisting of a hard core and polymer grafted chains, with variable chain lengths have been investigated by dynamic light scattering and rheology. These particles can be used as a model system to study the fundamentals of soft particles dynamics and rheology as a function of volume fraction. Two different light scattering set-ups were used to probe the dynamics from the dilute limit up and well into the glassy state[1]. For volume fractions up to glass transition, 3D Dynamic Light scattering (3DDLS)[2] was used in order to suppress any possible multiple scattering, monitoring the relaxation of concentration fluctuations through cooperative and self-diffusion mechanisms. In glassy samples, Multispeckle Dynamic Light Scattering (MDLS)[3] was utilized to enable measurement of the proper ensemble average correlation function which allows the investigation of slow dynamics and aging effects. In both regimes cooperative and self diffusion coefficients were probed as a function of volume fraction and the effects of thermodynamics and hydrodynamics were monitored around the peak of the structure factor. Dynamic Light scattering in the glassy state was complemented by shear rheology to connect the microscopic frustration of particle motion with macroscopic liquid to solid transition.

In collaboration with: Kohji Ohno, Institute of Chemical Research, Kyoto University, Uji, Kyoto 611-0011, Japan

References:

[1] Ohno K. et al. , Macromolecules, 40, 9143 - 9150 , 2007
[2] Current Opinion in Colloid & Interface Science 4 (1999) 177-185
[3] J. Phys. : Condens. Matter 17 (2005) S3543-S3549

Poster B7

Thermal and electrical properties of multi-walled carbon nanotube nanocomposites prepared by diluting a masterbatch with various types of modified and non-modified polypropylenes

Emmanuel Logakis[1], Christos Pandis[1], Vasilios Peoglos[1], Polycarpos Pissis[1], Matej Mičušík[2], Mária Omastová[2], Jürgen Pionteck[3] and Petra Pötschke[3]
[1]*National Technical University, Zografou Campus, 157 80 Athens, Greece*
[2]*Polymer Institute, Slovak Academy of Sciences, 842 36 Bratislava, Slovakia*
[3]*Leibniz Institute of Polymer Research Dresden, 01069 Dresden, Germany*

Corresponding author's email: logmanos@central.ntua.gr

Carbon nanotubes (CNTs) have attracted big attention in academic and industrial research for the creation of electrical dissipative or conductive polymeric nanocomposites due to their challenging structures and exceptional properties. The major hitch to overcome for the production of such materials is the inherent tendency of nanotubes to form bundles or agglomerates due to strong inter-tube van der Waals interaction. In order to improve the state of dispersion of carbon nanotubes within a polymeric matrix the polymer-nanotube interface has to be properly modified. In the present study an improvement of the non-covalent interactions due to introduction of polar maleic anhydride (MA) units to the polymer was essayed.

The nanocomposites were prepared by melt mixing a masterbatch of polypropylene (PP) containing 20 wt.% multi walled carbon nanotubes (MWCNTs) with various types of polypropylene. Melt mixing was followed by compression moulding in order to shape the samples to plates.

The influence of the melt viscosity as well as of the modification of polypropylene with maleic anhydride on the dispersion and thermal and electrical properties of CNT composites is investigated. For this purpose two sets of non-modified and MA-grafted PP with different molecular weights, resulting in different melt viscosities, were used. An additional set of samples consisting of the same polypropylene like that in the masterbatch was prepared for comparison with the previously mentioned series of samples. The non-modified and the modified samples are labelled as PP_x/yCNT and PP-MA_x/y, respectively, where x is the melt flow index (MFI) of the polymer matrix and y the content of CNT in wt.%.

Thermal transitions and electrical/dielectric properties of the nanocomposites are investigated using differential scanning calorimetry (DSC) and dielectric relaxation spectroscopy (DRS) techniques, respectively. Scanning electron microscopy (SEM) and transmission electron microscopy (TEM) were used for the morphological characterization of the prepared composites.

Preliminary DSC results show that crystallization peak shifts to higher temperatures by the addition of CNT. This fact indicates that CNTs act as external nuclei sites and accelerate the crystallization process. In the case of non-modified series higher MFI leads to higher degree of crystallinity (X_c) (Fig. 1). Furthermore, as the amount of CNT increases the degree of crystallinity increases. A very interesting observation also is that all series exhibit a second crystallization peak when nanotubes were added. This peak can be attributed to trans-crystallinity. In the region far from the nanotubes the polymer crystals grow radially as spherulites, which is the most common supermolecular structure, whereas, near the nanotubes walls the crystals growth begins on the surface of CNT in a direction parallel to the normal of their surface. This special kind of morphology is known as trans-crystalline structure[1].

Special attention is paid to the investigation of percolation, the transition from the insulating to the conducting phase through a conducting pathway formed by CNTs, by conductivity measurements for the samples above the percolation threshold (p_c) and by dielectric function measurements for the samples below p_c. The percolation threshold can be then calculated from the following equations (Eq. 1 and 2) of the percolation theory[2]:

$$\sigma(p) \sim (p-p_c)^t \quad (1)$$

$$\varepsilon'(p) \sim (p_c-p)^{-s} \quad (2)$$

where σ is the electrical conductivity, ε′ is the real part of dielectric function ($\varepsilon^*=\varepsilon'-i\varepsilon''$), p is the volume fraction of carbon nanotubes, and t, s are critical exponents. As an example, the calculation procedure of p_c for the PP_{12}/CNT series (through conductivity) is given in Figs. 2 and 3. The best fit gives a value of 1.18 vol.% (corresponds to 2.3 wt.%) for the percolation threshold and s = 2.0. for the critical exponent. It is noted that the concentration of 2.0 wt.%, which diverges from the normal in Fig. 2, was not taken into account at the fitting procedure in Fig. 3.

By comparing the non-modified series we conclude that higher MFI leads to lower percolation thresholds. The lowest value for p_c was obtained for the PP_{12} series where the polymer used for the dilution is the same as the polypropylene of the masterbatch. Comparison between PP-MA_2 and PP_2 (same MFI) shows that percolation threshold decreases after the modification of the matrix.

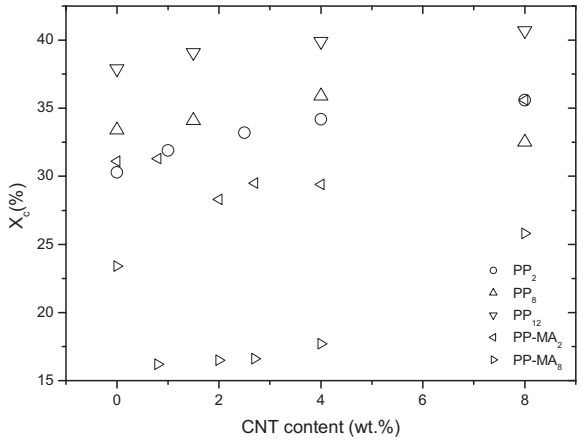

Fig. 1 Crystallization degree (X_c) as a function of CNT content for the series as indicated on the plot.

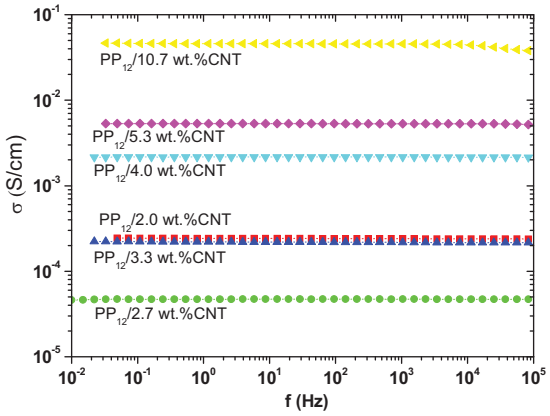

Fig. 2 ac conductivity (σ) against frequency at room temperature for the PP_{12}/CNT series.

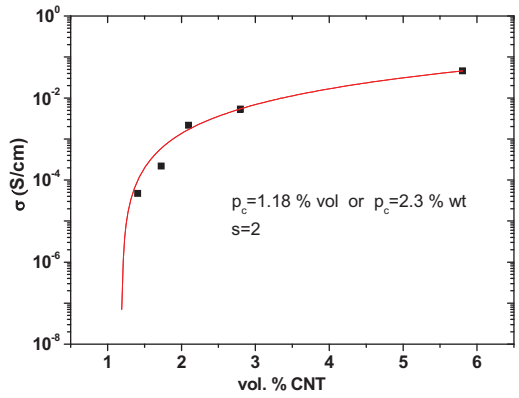

Fig. 3 σ against CNT content (vol.%) for the PP_{12}/CNT series at 1.19Hz. The line is a fit of equation (1).

References

[1]Zhang S., Minus L.M., Zhu L., Wong CP., Kumar, S. Polymer transcrystallinity induced by carbon nanotubes. Polymer 49 (2008) 1356-1364.
[2]D. Stauffer, Introduction to Percolation Theory, *Taylor and Francis*, London, (1985).

Acknowledgments

"This work has been funded by the project PENED 2003. The project is cofinanced 75% of public expenditure through EC - European Social Fund, 25% of public expenditure through Ministry of Development - General Secretariat of Research and Technology and through private sector, under measure 8.3 of OPERATIONAL PROGRAMME "COMPETITIVENESS" in the 3rd Community Support Programme."

Poster B8

Dielectric studies of molecular dynamics in swollen poly(ethyl acrylate) networks with non-polar solvents

A. Stathopoulos*[1], A. Kyritsis[1], P. Pissis[1], J.L. Gomez Ribelles[2], M. Monleon Pradas[2]

[1] *Department of Physics, National Technical University of Athens, Zografou Campus, 15780, Athens, Greece*

[2]*Department of Applied Thermodynamics, Universidad Politecnica de Valencia, 46022, Valencia, Spain*

It is well known that in swollen polymer networks with water or other solvents several effects on the α relaxation dynamics of the polymer and the thermal transitions of the solvent take place. These effects are not solely controlled by the specific polymer – solvent interactions but it seems that the increase of polymer network viscosity as the temperature of the system is lowered approaching Tg must be considered as well.

In this work a poly(ethyl acrylate) PEA network with 2wt% of curing agent ethylene glycol dimethacrylate EGDMA was swollen with non-polar p-xylene and toluene as solvents. Thermally Stimulated Depolarization Currents (TSDC) at a temperature range between -150 to 20^{o}C and Dielectric Relaxation Spectroscopy (DRS) at frequency range between 10^{-1}-10^{6}Hz and in the same temperature interval were employed for different contents of p-xylene and toluene. The sorption saturation level of *0.47* and *0.63* mass of p-xylene and toluene respectively to the mass of both polymer and solvent has been achieved at room temperature.

The study of the α relaxation indicate a strong shift to lower temperatures for the glass transition temperature of the network with increasing solvent content. This shift is well described by the Fox equation, independently on the type of the solvent. The shape and the dielectric strength of the α relaxation process have been found independent on the solvent content. In the case of the swollen PEA with p-xylene, crystallization of p-xylene affects drastically the α relaxation dynamics. Our results indicate that a fraction approximately 0.15 of p-xylene content is not able to crystallize at any p-xylene content. For p-xylene contents in the range of 0.20 to 0.27 cold crystallization of p-xylene has been observed whereas for higher solvent content crystallization of p-xylene during cooling occurs.

The results suggest that the swollen polymeric network can be treated as a homogeneous mixture in the whole solvent content range studied providing that no crystallization of the solvent occurs. The existence of non-freezable p-xylene can not be explained invoking any specific polymer-solvent interaction but is discussed in terms of increasing viscosity of the gel when approaching the glass transition temperature and of constraints imposed to p-xylene diffusion process.

Poster B9

DYNAMIC MECHANICAL AND TENSILE PROPERTIES OF THERMALLY OXIDIZED HOMOPOLYMER PAN FIBERS

Spyridon Soulis, Markella Pisania, Panagiotis Stergiou, Johannis Simitzis*
National Technical University of Athens, School of Chemical Engineering, Department III "Materials Science and Engineering", Laboratory Unit "Advanced and Composite Materials", 9-Heroon Polytechniou str., Zografou Campus, 157 73 Athens, Greece
*e-mail: simj@chemeng.ntua.gr

1. INTRODUCTION

The oxidative thermal treatment of polyacrylonitrile (PAN) fibers is the first step for the production of carbon fibers. During this process, PAN fibers (usually kept under tension) are heated at temperatures up to 300 °C for prolonged time, commonly in air. Thus, PAN macromolecules are converted into a "ladder polymer", consisting mainly of sequences of up to five fused heteroaromatic rings, interrupted by short linear parts of non- cyclized carbon backbone [1-3]. The process is also known as "oxidative stabilization", since ladder polymer is an inflammable material that can be effectively carbonized at temperatures above 1000 °C[1-3]. During the treatment, various chemical reactions take place, the most important being dehydrogenation, oxidation and nitrile cyclization reactions. The latter concern the highly exothermic conversion of the nitrile groups (-C≡N) into >C=N-, leading to the formation of the heteroaromatic rings[1,3-5]. Oxidative thermal treatment of PAN fibres depends on the treatment parameters (temperature, time, stress applied) accompanied by physical and chemical changes. As described in the literature[2,3], the treatment temperature - time combinations can be separated in three regions: (I) where only physical phenomena take place, (II) where dehydrogenation and oxidation reactions dominate and (III) where cyclization takes place. The aim of this work is to study the effect of thermal oxidative treatment to the static and dynamic mechanical properties of the oxidized PAN fibers. Since in region (I) the chemical structure of the fibers remain the same as the initial PAN fiber, two representative treated PAN fibers were selected from treatment regions (II) and (III).

2. EXPERIMENTAL

The fibers used in this work were commercial PAN fibers (type Dralon-T, code: DRT, from Bayer AG, Germany) in the form of untwisted yarn containing 150 monofilaments. These fibers were dry- spun from PAN homopolymer. The fibers were isothermally treated in air atmosphere using a specially designed and constructed air circulation oven. The fibers were treated at 150 °C for 3h with an applied load of 28 MPa (code: DRT-150) and at 220 °C for 2.5 h with an applied load of 4 MPa (code: DRT-220). The tensile test (according to ASTM D2101-79) of PAN and treated fibres was carried out using an Instron 4466 (Instron) tensile-testing machine, with a gauge length of 30mm and a nominal strain rate of 30mm min^{-1}. The breaking load (*F*) was determined as the maximum force applied to a specimen in a tension test carried through to rupture. In order to calculate the tensile strength of the fibres, the mean fiber cross-section area was microscopically determined. The dynamic mechanical properties of the PAN and the treated fibers were measured with a Perkin Elmer Pyris Diamond DMTA apparatus using the tension module, heating from room temperature up to 300 °C with a heating rate of 1°C/min. FTIR spectra of the fibers were recorded on a Perkin Elmer System Spectrum GX spectrometer using KBr discs.

3. RESULTS AND DISCUSSION

Figure 1 shows the Young modulus and the tensile strength of untreated and treated in different conditions PAN fibers. Even though the treated fibers have different kind of treatment, they have similar Young modulus and tensile strength, which are higher than the corresponding of the initial PAN fibers. It should be also noticed that the treated fibers have smaller mean monofilament cross section than the initial fiber. Namely, DRT has a mean monofilament cross section of 180 μm^2, whereas DRT-150 has 150 μm^2 and DRT-220 has 115 μm^2. In region (II), PAN homopolymer fibers undergo dehydrogenation reactions that lead to the formation of conjugated double bonds in the macromolecular backbone[2,3,6]. That structure is more rigid than that of PAN, a fact reflected to the increase of the Young modulus of DRT-150 fibers. Moreover, due to the sufficient applied load, these fibers did not shrink during their treatment (in fact, they were elongated for 1 %), i.e. the applied load caused the orientation of the fibers by their stretching. As a result of this treatment, the tensile strength of DRT-150 fibers is higher than that of DRT. In region (III), the nitrile cyclization reactions lead to even

more rigid, fused ring structures[2,3,6]. In this region the backbone degradation reactions can be severe and may cause an abrupt decrease of the tensile strength of the treated fibers. Since both Young modulus and tensile strength of the DRT-220 fibers are higher than that of DRT fibers, it can be deduced that during this treatment the degradation was not significant. Figure 2 shows the FTIR spectra of untreated and treated in different conditions PAN fibers. The recorded FTIR spectra of the fibers exhibit various peaks. The most prominent peaks in DRT are at 2940 cm^{-1} (CH_2 stretching), 2240 cm^{-1} (CN stretching), 1450 cm^{-1} (CH_2 bending) and 1250 cm^{-1} (wagging of C-H bond). Additionally, the treated fibers exhibit a peak at 1600 cm^{-1} due to the conjugated C=C and / or C=N double bonds, which are formed during the dehydrogenation and / or the cyclization reactions[2-4,6]. This peak is more intense for the DRT-220 fibers than for DRT-150, i.e. the extent of the treatment for the two fibers is not the same, even though their mechanical properties are similar.

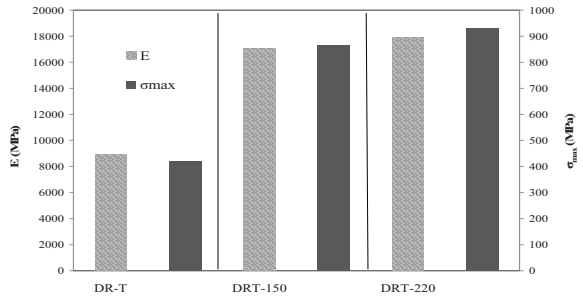

Figure 1. Young modulus (E) and tensile strength (σ_{max}) of untreated and treated PAN fibers

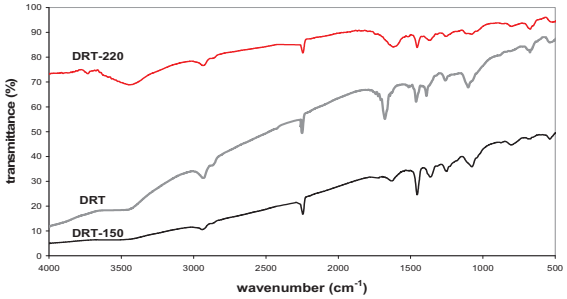

Figure 2. FTIR spectra of untreated and treated PAN fibers

Figure 3 shows the storage modulus (E') and Figure 4 the loss factor (tanδ) versus temperature, of untreated and treated in different conditions PAN fibers. The DRT and DRT-150 fibers exhibit a transition around 100 °C, where the storage modulus decreases by about 1.5 orders of magnitude. In the same temperature, DRT-220 fibers exhibit a similar transition, although the decrease of E' is less than 1 order of magnitude. The cyclization reactions are the reason for the increase of E' above 220 °C for all fibers, which also appear as a peak with maximum of tanδ at 280 °C. This peak is broader for DRT-220 fibers, i.e. cyclization reactions start at lower temperatures.

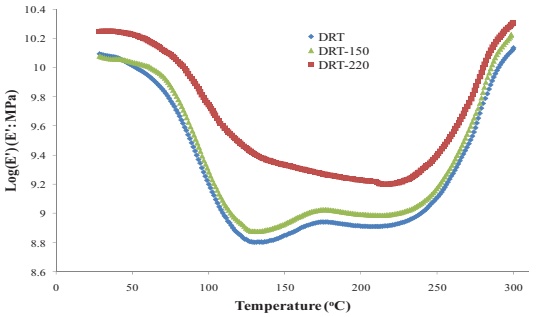

Figure 3. Storage modulus (E') of treated and untreated fibers. Frequency: 1 Hz.

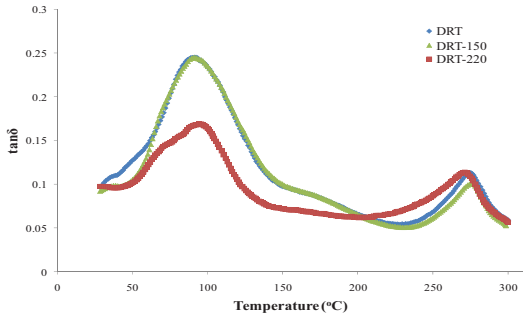

Figure 4. Loss factor (tanδ) of treated and untreated fibers. Frequency: 1 Hz.

Comparing the static mechanical properties and DMTA analysis, DRT-150 fibers have higher mechanical properties than DRT, but their dynamic mechanical behavior is similar. Contrarily, DRT-220 fibers have the same mechanical properties as DRT-150, whereas the former material, which has undergone cyclization, behaves as a more rigid material in DMTA than DRT-150 fibers which have undergone only dehydrogenation. Thus, the dynamic mechanical behavior of homopolymer PAN fibers is not affected by the dehydrogenation reactions (DRT-150 fibers), but is strongly influenced by the cyclization reactions (DRT-220 fibers).

REFERENCES

1. P. Bajaj, A.K. Roopanwal, J.M.S.-Rev. Macromol. Chem. Phys., C37 (1997) 97.
2. J. Simitzis, S. Soulis, Polym. Int., 57 (2008) 99.
3. S. Soulis, J. Simitzis, Polym. Int., 54 (2005) 1474.
4. J. Simitzis, *Polyacrylonitrile*, in "**Handbook of Thermoplastics**", O. Olabishi (ed.), M. Dekker, New York (1997), pp. 177-201.
5. K.E. Perepelkin, Fibre Chem., 35 (2003) 409.
6. M. Pisania, S. Soulis, J. Simitzis, 20th ISPAC, October 2007, Ag. Nikolaos, Crete, pp.85-87.

Poster B10

Synthesis and mechanical properties of A_nB_n star copolymers and $A_n(B\text{-}b\text{-}C)_n$ star terpolymers

G. Tsoukleri[1,2], G. Linardatos[1,3], J. Parthenios[1], C. Galiotis[1,2] and C. Tsitsilianis[1,3]

[1] *Foundation of Research and Technology Hellas, Institute of Chemical Engineering and High Temperature Processes, Stadiou str. Platani, P.O. Box 1414, Patras GR-265 04, Greece*
[2] *Department of Materials Science, University of Patras, University Campus, Patras GR-265 04, Greece*
[3] *Department of Chemical Engineering, University of Patras, University Campus, GR26500 Patras, Greece*

Keywords: Star copolymers, star terpolymers, mechanical properties, dynamic mechanical properties

Abstract

Over the last few years it has emerged that the mechanical, electronic, magnetic and optical properties of composite materials can be improved in some cases when their building blocks are engineered at the nano-, as opposed to the micro-scale.

In this study we are going to examine the mechanical (compression, ASTM D695 – 96 and tension, ASTM D882) and dynamical properties of casting-annealed hetero-arm stars copolymers PS_nPEMA_n, PS_nPHMA_n and terpolymers $PS_n(PHMA\text{-}PMMA)_n$ (Fig.1a), and compare them at first with pure PS and annealed linear PS-PHMA and PS-PHMA-PMMA and then with previous work, same hot pressed hetero-arm stars copolymers and terpolymers (Fig. 1b).

Finally, we will try to determine the effect of the molecular characteristics of each synthesized hetero-arm star copolymer and terpolymer by combining structural information obtained from TEM and AFM techniques and relate them to the static and dynamic mechanical behavior.

The results already have shown that hetero-arm stars copolymers and terpolymers show higher elastic modulus values than linear polymers. Triblock and star polymers exhibit the highest values of strength (in compression), where better values found for the “glassy” heteroarm star PS_n- $PEMA_n$. Concerning strain- to-failure (ductility), the presence of PHMA is crucial for conveying elastomeric character to linear and star-like polymer. Finally, triblock polymers show superior properties in terms of ductility.

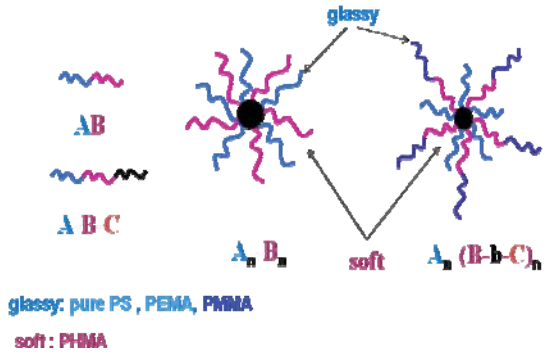

Σχ.1a Linear and hetero-arm star synthesized copolymers and terpolymers

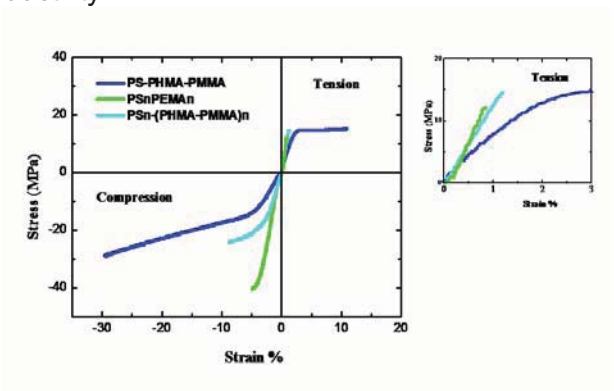

Σχ.1b Mechanical behavior of linear and hetero-arm star synthesized copolymers and terpolymers

Poster B11

Influence of maleic anhydrite component of cured polyesters on their relaxations determined by Dielectric Spectroscopy (DS) and Dynamic Mechanical Thermal Analysis (DMTA)

Georgios Mitsis, Despina Triantou, Spyridon Soulis, Johannis Simitzis*

National Technical University of Athens, School of Chemical Engineering, Department III "Materials Science and Engineering", Laboratory Unit "Advanced and Composite Materials", 9-Heroon Polytechniou str., Zografou Campus, 157 73 Athens, Greece.

* e-mail : simj@orfeas.chemeng.ntua.gr

1. INTRODUCTION

Unsaturated polyester resins (UP) are one of the widely used thermoset polymers in polymeric composites, because of their good mechanical properties and relatively inexpensive prices. They possess a wide range of properties and are used in marine, automobile, construction and furniture applications[1,2]. UP are produced by polycondensation of dioles (such ethylene glycol) and acids or anhydrides and degree of crosslinking can be controlled by the concentration of unsaturated acids or unsaturated monomers. The dense of crosslinks can be controlled to some degree by the concentration and type of cross-linking monomer and also by the type and concentration of initiators and catalysts used to affect the crosslinking reaction. Polyesters based on aromatic monomers, such as maleic anhydride are known to be heat resistant and thermally stable, due to their rigid backbone[2].

Relaxation phenomena of polymers are related to molecular fluctuations of dipoles due to the influence of electric field[3] or due to oscillating forces applied to the polymer[4]. At high temperature the α-relaxation can be observed, associated with the 'dielectric glass transition', but at lower temperatures β-relaxation or even γ-relaxation can be detected. The α-relaxation is associated to the beginning of segmental mobility within the polymer backbone, whereas the β and γ-relaxations are associated to fluctuations of a short side chain[4,5]. For the determination of relaxation temperatures of polymers Dielectric Spectroscopy (DS) and Dynamic Mechanical Thermal Analysis (DMTA) are used.

The aim of this work is to study the effect of maleic anhydrite for cured polyesters on their dielectric and mechanical relaxations.

2. EXPERIMENTAL

Unsaturated polyesters were synthesized by polycondensation of ethylene glycol with maleic anhydrite (MA) and phthalic anhydride (PA) in molar ratio of glycol to anhydrides 1.1:1.0. The molar ratios of the anhydrides were: 0.5/0.5, 0.7/0.3 and 0.3/0.7 for polyesters MA5PA5, MA7PA3 and MA3PA7, respectively. After production, the polyesters were mixed with styrene (30% w/w). In polyester- styrene mixture was added a proper initiator (methyl ethyl ketone peroxide, 3%v/w) and accelerator (cobalt naphthenate, 1% v/w), and then the homogenized mixture placed into an appropriate mould (cylindrical shape for DS with 55 mm diameter, 4 mm thick and orthogonal shape for DMTA with 50 mm length ,6 mm width, 2 mm thickness) and cured at room temperature for about 24 hours.

The dielectric relaxations of cured polyesters were studied by Dielectric Spectroscopy (DS) using an Impedance Analyzer (Hewlett Packard, type: 4192ALF) in a frequency range from 5 Hz up to 10^7 Hz at constant temperature, following also a heating program from 20 to 180 °C, with a step of 10 °C. The real part ε´ (which is related to the energy stored in the material), the imaginary part ε´´ (witch is related to the energy dissipated) and the loss tangent, tanδ = ε´´/ε´, were determined.

The mechanical relaxations of cured polyesters were studied by Dynamic Mechanical Thermal Analysis (DMTA) using a Perkin-Elmer Diamond analyser in a frequency range from 0,1 Hz up to 10 Hz, following also a heating program from -100 to 160°C. The storage modulus E', loss modulus E'' and tanδ=E''/E' were determined.

3. RESULTS AND DISCUSSION

Figure 1 presents the real part of dielectric constant, ε', versus logf of polyester MA5PA5 for different temperatures from DS. It is observed that ε' has an almost constant value for the whole frequency range at temperatures up to 40 °C. This indicates that the dipoles can not follow the alternating electrical field, i.e. the material is still in the glassy state. Above this temperature a decrease of ε' with increasing the frequency is observed, indicating that the dipoles can partially follow the electric field, i.e. the beginning of a relaxation[3]. Although the change of ε' has practical importance (e.g. for high frequency applications[6]),

more useful for the determination of the relaxations are the plots of loss tangent (tanδ) versus temperature at selected frequencies.

Figure 2 shows tanδ versus temperature for cured polyesters at the frequency of 10 KHz. All polyesters show a relaxation between 80 and 100 ^{o}C, determined from the peak maximum of tanδ. Specifically, MA3PA7 has a relaxation at 80 ^{o}C, MA5PA5 at 90 ^{o}C and MA7PA3 at 100 ^{o}C. It is clear that, by increasing the molar ratio of maleic anhydride (MA) in polyester composition, the relaxation shifts to higher temperature. The relaxations observed are attributed to the glass transition temperature, $T_{g.}$. Moreover, in polyester MA3PA7 the arrow indicates probably the final part of a curve (β-relaxation) which begins at very low temperature.

Figure 3 and 4 present the log of storage modulus E' and tanδ versus temperature from DMTA at the representative frequency of 10 Hz. Storage modulus starts decreasing from temperature above 40 ^{o}C(Figure 3), indicating the beginning of a relaxation. This decrease of storage modulus for MA3PA7 is about three orders of magnitude, about two orders of magnitude for MA7PA3 and has an intermediate value for MA5PA5. Concerning the tanδ (Figure 4), relaxations are observed for polyesters MA3PA7, MA5PA5 and MA7PA3 at 60 ^{o}C, 70 ^{o}C and 95 ^{o}C respectively, determined from the peak maximum of tanδ. For MA3PA7 an additional relaxation is observed (Figure 3, 4) at about -50 ^{o}C, indicated by arrow, which is attributed to β-relaxation.

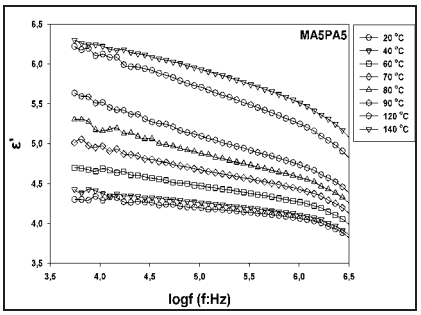

Figure 1.Real part of dielectric constant ε' versus temperature for MA5PA5(DS)

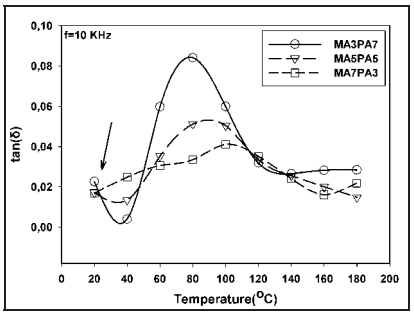

Figure 2.tanδ versus temperature for the polyesters (DS)

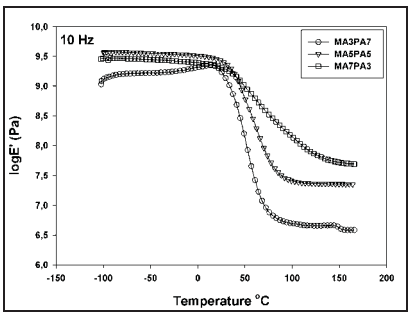

Figure 3.Storage modulus, E,' versus temperature for polyesters (DMTA)

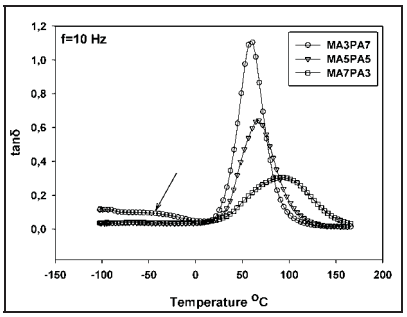

Figure 4.tanδ versus temperature for polyesters (DMTA)

The increase of molar ratio of MA (unsaturated monomer) in polyesters composition, shifts the glass transition temperature T_g to higher values because of the formation of more dense network . MA3PA7 has the lowest MA ratio, loose network and is the only polyester which exhibits a β-relaxation. Relaxations determined by DS are in accordance with that determined by DMTA.

References

1. *Ayman M. Atta, Ibrahim F. Nassar, Hamed M. Bedawy, ,Reactive and Functional Polymers, 67, July 2007, Pages 617-626.*
2. *S. Y. Tawfik, J. N. Asaad, M. W. Sabaa, Polymer Testing, 22, October 2003, Pages 747-759*
3. *"Broadband Dielectric Spectroscopy",F.Kremer,A.Schönhals (Eds.), Springer-Verlag Berlin, 2003, p.p. 1-3, 349-350.*
4. *F. Henry, L.C. Costa, M. Devassine, J. Eur. Polym. 41, 2005, 2122-2126.*
5. "Dynamic Mechanical Analysis – A Practical Indroduction", Kevin P. Menard, CRC Press, 1999 p.65, 95
6. "Makromolekuele",Hans-Georg Elias, Huething & Wepf Verlag, Basel, 1981,p.413.

Poster B12

Self-assembly and Dynamics of Discotic Liquid Crystals

Elmahdy, M.M.[a b *], Dou, X.[c], Mondeshki, M.[c], Floudas, G. [a b], Butt, H.J.[c], Spiess, H.W.[c], Müllen, K.[c]

[a] *Department of Physics, University of Ioannina, 451 10 Ioannina, Greece*
[b] *Foundation for Research and Technology-Hellas (FORTH), Biomedical Research Institute (BRI), Ioannina, Greece*
[c] *Max-Planck Institut fuï Polymerforschung, D-55021 Mainz, Germany*
** Present address: Department of Physics, University of Mansoura, 35516 Mansoura, Egypt*

Abstract: Among the different discotic LC hexa-*peri*-hexabenzocoronenes (HBCs) are particularly promising because their large aromatic core permits one of the highest values for the intrinsic charge carrier mobility [1]. Self-assembly and dynamics of discotic liquid crystals with applications in electronics and in flexible displays is studied aiming at providing answers to some open literature questions. For this purpose a series of un-functionalized and dipole functionalized HBCs are synthesized and examined by structural (X-ray, NMR, DSC, POM) and dynamic (DS, NMR) probes. Pertinent issues investigated include the effect of dipole substitution on the stability of the liquid crystalline phases, the core dynamics within the columns, the thermodynamic phase diagram and the evolution of structure formation (i.e., kinetics) following distinct paths in the thermodynamic phase diagram. The complete assignment of the "fast" and "slow" dynamics, the thermodynamic phase diagram and the evolution of structure formation following a jump from the liquid crystalline to the crystalline state is made here for the first time.

The un-functionalized HBCs (HBC-$C_{10,6}$ and HBC-$C_{14,10}$), despite their symmetric shape displayed a very weak dipolar relaxation with a non-Arrhenius temperature dependence that freezes at ~215 K [2]. Dielectric spectroscopy together with NMR revealed that the origin of this process is the freezing of the disc axial motion at the respective glass temperature (T_g) [2].

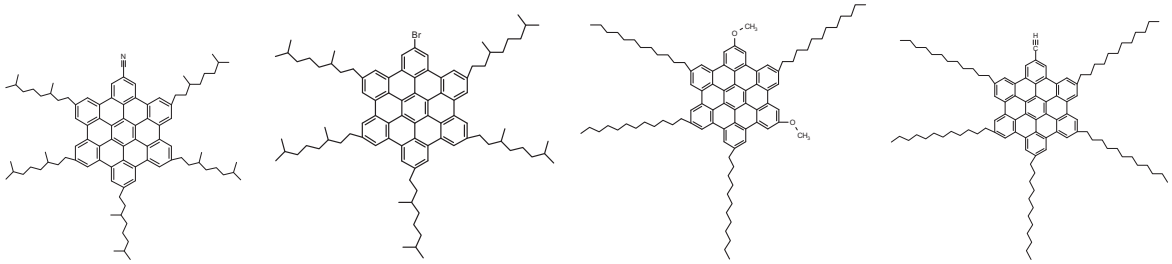

Scheme 1: From left to right: mono-cyano, mono-bromo, dimethoxy and mono-ethynyl HBCs

For the dipole substituted HBCs, four dipole functionalized HBC derivatives (Scheme 1) were studied bearing strong (mono-cyano and mono-bromo HBCs) to moderate (dimethoxy and mono-ethynyl HBCs) dipole moments [3,4]. The effect of dipole substitution with strong dipoles is to destabilize the columnar crystalline phase at low temperatures. On the other hand, substitution with weaker dipoles gives rise to a crystalline phase on cooling. It is shown that the strongly temperature-dependent *α*-process reflects the collective axial disc rotational dynamics. The freezing of the axial disc motion occurs at about 236 K for the discotics within the liquid crystalline phase (bearing stronger dipoles) and at 253 K for the discotics within the crystalline phase (bearing moderate dipoles) (Figure 1). The important conclusion from this study is that the phase state completely controls the dynamic response.

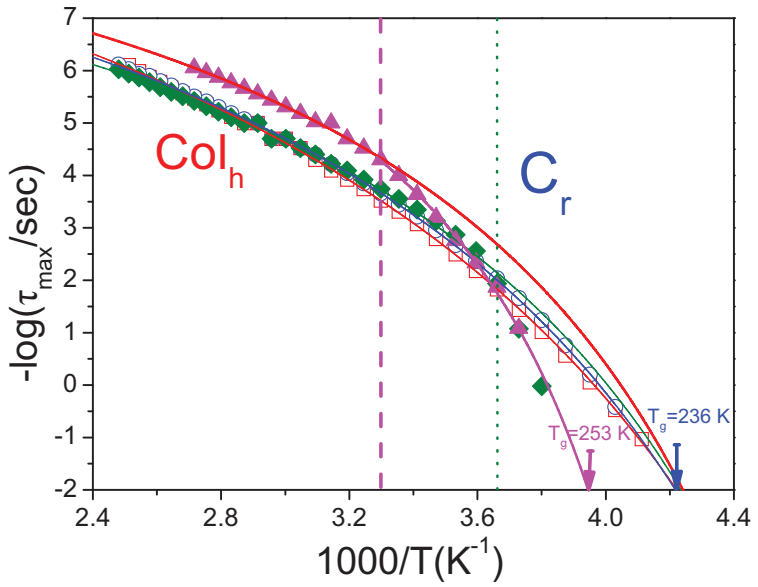

Fig. 1 Comparison of the *α*-process relaxation times for the different dipole functionalized discotics: (open squares): mono-cyano HBC, (open circles): mono-bromo HBC, (filled rhombus): mono-ethynyl HBC, and (filled up triangles): dimethoxy HBC. Notice the similarity in the $\tau(T)$ dependence within the Col_h phase and the steeper $\tau(T)$ within the C_r phase for the dimethoxy- (thick vertical line) and mono-ethynyl HBC (dotted vertical line).

Another pertinent finding is that the relaxation times and breadth of *α*-process have distinctly different temperature- and pressure-dependencies on entering the crystalline state. These features enable the construction of the first phase diagram (*T-P*) for HBCs.

The main outcome from this study is the increased stability of the crystalline phase at elevated pressures. Subsequently, the transformation of the liquid crystalline to the crystalline phase is studied by pressure jumps aiming at identifying possible intermediate states, nucleation sites and the existence of long-lived metastability. The results of the kinetic investigation reveaedl the absence of intermediate states but have shown long-lived metastability and fractional exponents that were strongly depended on the quench depth. Although most of these finding supported nucleation and growth, as the main mechanism of formation of the crystalline phase, the dependence of the kinetic times on the driving force was not typical for a nucleation and growth process.

References

1. Pisula, W.; Kastler, M.; Wasserfallen, D.; Mondeshki, M.; Piris, J.; Schnell, I.; Müllen, K. *Chem. Mater.* **18**, 3634 (2006).
2. Elmahdy, M.M.; Floudas, G.; Kastler, M.; Müllen, K. *J. Phys.: Condens. Matter* **20**, 244105 (2008).
3. Elmahdy, M.M.; Floudas, G.; Mondeshki, M.; Spiess, H.W.; Dou, X.; Müllen, K. *Phys. Rev. Lett.* **100**, 107801 (2008).
4. Elmahdy, M.M.; Dou, X.; Mondeshki, M.; Floudas, G.; Butt, H.J.; Spiess, H.W.; Müllen, K. *J. Am. Chem. Soc.* **130**, 5311 (2008).

Poster B13

Effect of architecture on the self-assembly and dynamics of model diblock and star copolypeptides

Gitsas A.[1,*], Floudas G.[1], Mondeshki M.[2], Butt, H.-J.[2], Spiess H. W.[2], Iatrou H.[3], Hadjichristidis N.[3]

1. University of Ioannina, Department of Physics, P.O. Box 1186, 451 10 Ioannina, Greece, and Foundation for Research and Technology-Hellas (FORTH), Biomedical Research Institute (BRI).
2. Max Planck Institute for Polymer Research, D-55021 Mainz, Germany.
3. University of Athens, Department of Chemistry, Panepistimiopolis, Zografou, 157 71, Greece.

Over the last years, a great effort has been made to understand the interplay between the primary structure and the resulting secondary structure and molecular dynamics in polypeptides.[1,2] Conformational studies of model polypeptides are an important step towards the understanding of protein folding. In particular, emphasis is given in the open questions of (i) the effect of confinement on the peptide secondary structure, (ii) the effect of nanophase separation on the persistence length of the secondary structure, and (iii) the effect of the chain topology on the secondary structure. In this framework, two approaches are presented in the present study.

In the first part, a series of poly(*γ*-benzyl-L-glutamate)-*b*-polyalanine (PBLG-*b*-PAla) diblock copolymers are investigated with respect to the phase state and the molecular dynamics.[3] It was found that both blocks form α-helices, with the α-helices/β-sheet ratio being increased in the copolymer compared to the pure homopolypeptides. The bulkier PBLG main chain drives the assembly of the attached PAla block. This suggests that confinement can serve as a tool for improving the secondary structure. WAXS showed that the α-helices assume a hexagonal arrangement within the nanophases. Phase separation is implied by the observance of reflections from both blocks in WAXS. Further support of nanophase separation is provided by DS. The segmental dynamics of PBLG are traced to be close to the bulk ones, while differential scanning calorimetry (DSC) scans provide the PAla T_g in the copolypeptides. The dielectrically stronger slow process shows that the helical structure of PBLG is improved in the copolypeptide compared to pure PBLG.[4]

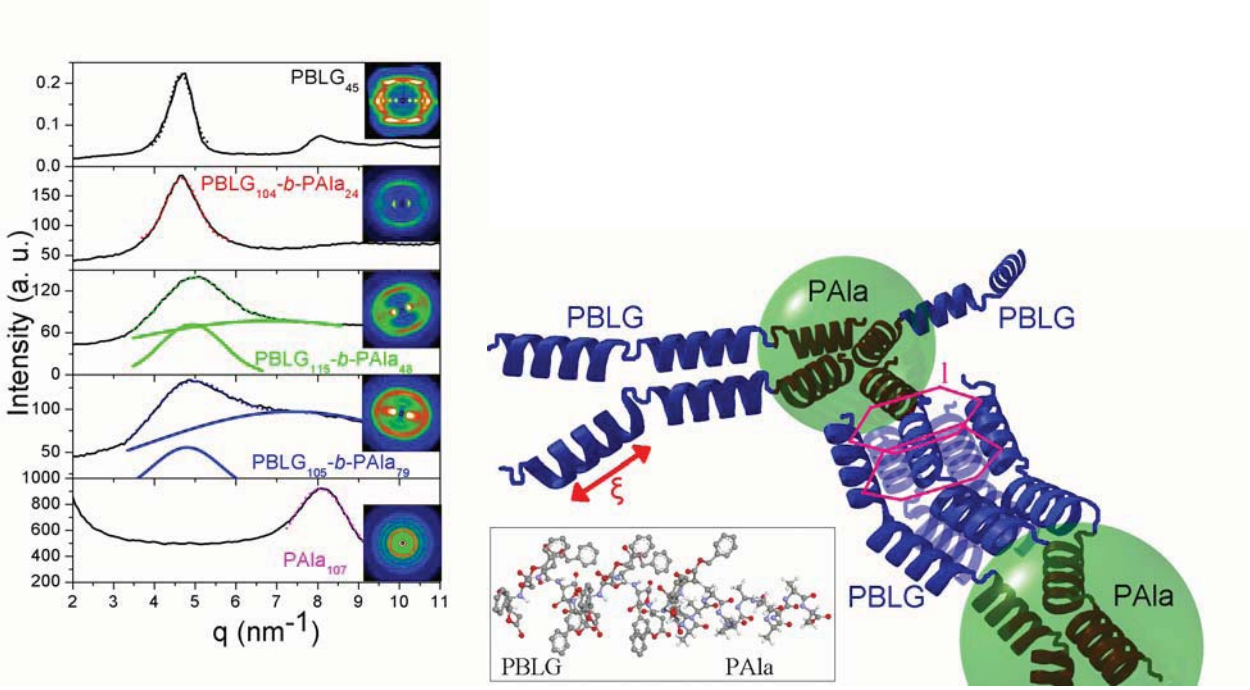

Figure 1. (Left) Equatorial WAXS intensity distributions of the homopolypeptides and the copolypeptides obtained from oriented fibers, along with the respective 2D images. Fiber orientation is along the vertical direction. In the copolypeptides, two reflections are present, coming from the respective blocks, indicating phase separation. (Right) Schematic representation of the copolymer morphology. Both blocks form α-helices (NMR), packed in a hexagonal cell (WAXS). DS gives a quantitative estimate of the helices

persistence length, ξ, to be increased in the copolypeptides. In the inset, a schematic of a $PBLG_{12}$-*b*-$PAla_{12}$ diblock copolymer in the "ideal" extended conformation (red: O; blue: N; grey: C).

Next, the effect of chain topology on the (i) the peptide secondary structure, (ii) the nanophase self-assembly, and (iii) the local segmental and global peptide relaxations has been investigated in a series of model diblock and 3-arm star copolypeptides of poly(ε-carbobenzyloxy-L-lysine) (PZLL) and PBLG with PZLL forming the star core.[5] Diblock copolypeptides are nanophase separated with PBLG and PZLL domains comprising α-helices packed in a hexagonal lattice. Star copolypeptides are only weakly separated, complrising PBLG and PZLL α-helices in a pseudohexagonal lattice. Phase mixing has profound consequences on the local and global dynamics. The relaxation of the peptide secondary structure speeds up, and the helix persistence length is further reduced in the stars, signifying an increased concentration of helical defects.

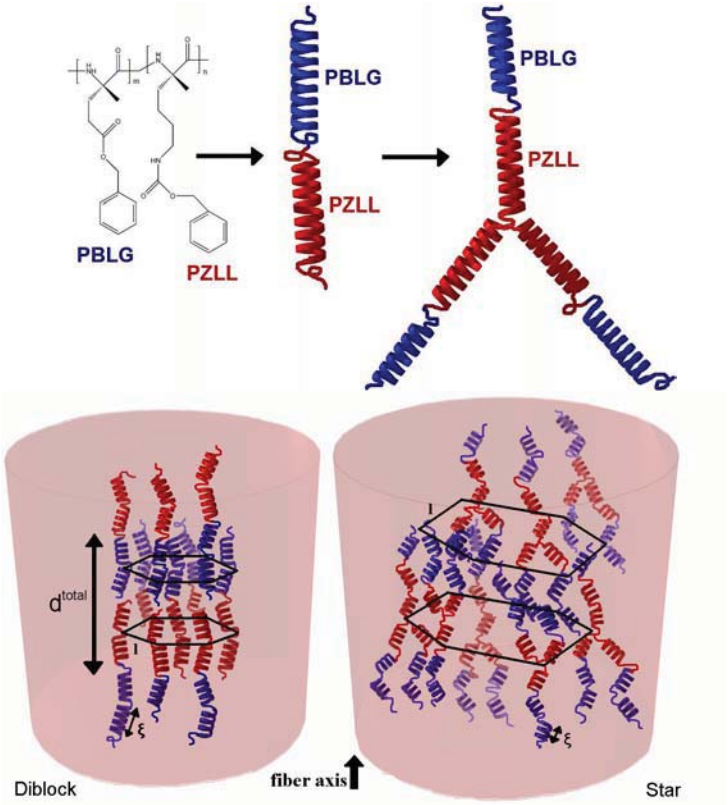

Figure 2. (Top) Idealized α-helical structures of diblock and 3-arm star copolypeptides of PBLG and PZLL blocks. The diblocks are used as star arms, with PZLL forming the core. (Bottom) Schematic representation of the self-assembly in the diblock and star cases, based on the combined experimental results. In the diblock, a lamellar nanostructure with a domain spacing d^{total} (SAXS) is composed of PZLL and PBLG domains both comprising α-helical segments (NMR, WAXS) that are hexagonally packed (WAXS). In the star, mixing between the PZLL and PBLG blocks occurs (SAXS). Despite this, both PZLL and PBLG form α-helices (NMR, WAXS), however, with a smaller persistence length, *ξ* (DS), that are packed in a pseudo-hexagonal lattice (WAXS).

References

1. Deming, T. J. *Nature* **1997**, *390*, 386.
2. Tuchscherer, G.; Scheibler, L.; Dumy, P.; Mutter, M. *Biopolymers* **1998**, *47*, 63.
3. Gitsas, A.; Floudas, G.; Mondeshki M.; Spiess, H. W.; Iatrou, H.; Hadjichristidis, N. *Macromolecules* **2008** in press.
4. Papadopoulos, P.; Floudas, G.; Klok, H.-A.; Schnell, I.; Pakula, T. *Biomacromolecules* **2004**, *5*, 81.
5. Gitsas, A.; Floudas, G.; Mondeshki M.; Butt, H.-J.; Spiess, H. W.; Iatrou, H.; Hadjichristidis, N. *Biomacromolecules* **2008**, *9*, 1959.

* e-mail: me01296@cc.uoi.gr

Poster B14

Modeling the lateral aggregation of membrane proteins

Marianna Yiannourakou*, Luca Marsella+, Frederick De Meyer+**, Berend Smit**
* *Demokritos, GR-153 10, Aghia Paraskevi Attikis, Greece*
+ *CECAM - Centre Europeen de Calcul Atomique et Moleculaire, 46 All´e d'Italie 69364 Lyon, France*
** *Department of Chemical Engineering, University of California, Berkeley, 1462 Berkeley CA*

Membranes are fundamental for the physiology of the cells[1]. Several membrane proteins form lateral aggregates, which are important to perform their biological functions[2]. Although many theoretical studies addressed already the problem of membrane proteins aggregation, a unified explanation of the mechanisms underlying the aggregation processes is still lacking. Venturoli et all[3] have applied a coarse-graining description of a lipid bilayer with embedded proteins with the numerical technique of Dissipative Particle Dynamics[4], in order to study the behavior of reconstituted biological membranes. Using this model, De Meyer et all[5] have proposed a realistic mechanism underlying the aggregation process. The Potential of Mean Force (PMF) of the lipid mediated interaction between two proteins was computed for different cases of hydrophobic mismatch.

In the present work, we studied the aggregation of integral membrane proteins through lipid mediated interactions in 2D systems, with the purpose of illustrating within a simplified framework the behavior of small proteins like gramicidin, where the negative hydrophobic mismatch with respect to the lipid bilayer is the main driving force. As input, we used the information obtained by simulations of the mesoscopic model mentioned above. The simplest way to simulate the behavior of the two dimensional system would be to use the PMF as a pairwise additive potential, neglecting many body interactions. However, three-body interactions among embedded proteins cannot be neglected, even at low density[6]. In order to evaluate the order of magnitude of the correction, we simulated the system of two aggregated proteins and a probe protein approaching them, computing the PMF between the aggregate and the probe. By comparing the results obtained (by the 2D and 3D models) from these simulations, the need to include many-body interactions is evident, since the three-body correction is not negligible. Due to this, we developed and used a screened potential (for the 2D model) which gives a good comparison even when we compared with the PMF computed for the system with a cluster of seven proteins interacting with a probe protein approaching. In this model, proteins are treated as hard disks (Fig.1). We compute the polar angles φ_1 and φ_2 of the centers of mass of i and j respectively, and the angles θ_1 and θ_2 defined by tangents to i and j from the center of k. A protein is shaded by another one, if:

$$\frac{\theta_1 + \theta_2}{2} < \left|\phi_1 + \phi_2\right| \quad (1)$$

Each protein interacts only with non-shaded ones and does not feel the presence of the shaded ones. The first neighbor of each protein cannot be shaded, while for all the rest the criterion given by Eq. 1 determines whether they are shaded by another protein or not.

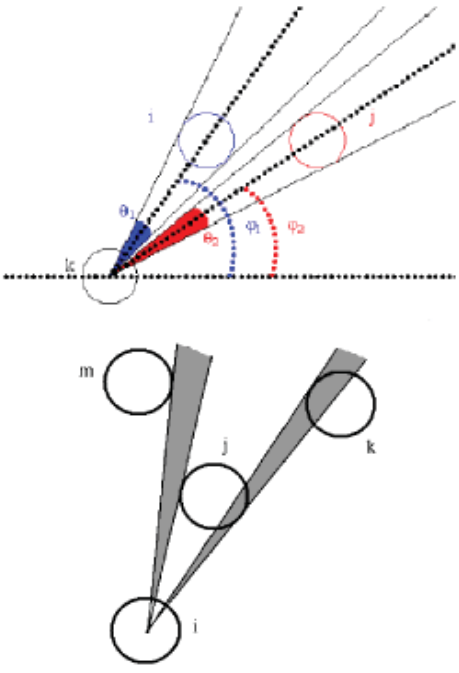

FIG. 1: (Up) Description of the screening in the 2D model, (Down) According to this model, protein k is shaded by protein j, protein m is not shaded by protein j. Protein interacts only with proteins j and m.

Monte Carlo simulations in the NVT ensemble, for small systems of up to 20 particles at low density, were performed. In these simulations all the proteins finally form one big cluster although some particles may leave the cluster for a while and rejoin it afterwards. In order to have a better understanding of whether phase separation is really favored, we have studied the ground state configurations of systems of up to 35 proteins. We focused on finding out if there is a critical cluster size for which the energy is minimum: that would indicate that for any temperature, phase separation would be entropically disfavored and clustering of proteins would take place with an upper limit of the cluster size[7]. The agreement between the two methods that were used[8,9] is satisfactory: as the number of proteins in the cluster increases, the energy per protein continues to drop, therefore no energy minimum exists (Fig. 2). This indicates that aggregation will be favored rather than the formation of a number of clusters.

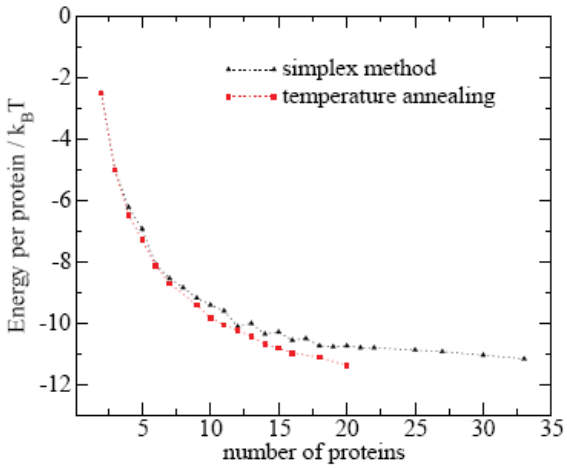

FIG. 2: Ground state energies of the system with negative mismatch

Long simulations were performed in large systems, containing 100 proteins, always at low density. Small clusters were formed very fast; those clusters continued to grow slowly. In the end, all proteins do aggregate into one cluster and the system appears to be stable. Single proteins continue to leave from the aggregate, but they join it again shortly after.

The results we obtain are in agreement with the known properties of gramicidin within phospholipid bilayers: in fact, previous experimental studies[10,11] have shown the tendency of gramicidin to form big aggregates even in the gel phase. This behavior has been confirmed as expected in the fluid phase, both by computer simulations of elastic models of reconstituted lipid bilayers[6,12,13] and by experiments[14], notwithstanding the difficulty to detect the tiny mismatch between the lipids in the fluid phase and gramicidin clusters with atomic force microscopy.

Financial support from the Marie Curie Excellence Grant (EXT) BiMaMoSi (MEXT-CT-2005-023311) and the Marie Curie Early Stage Training (EST) EuroSim (MEST-CT-2005-020491) is acknowledged.

[1] E. Sackmann, in Structure and Dynamics of Membranes, edited by R. Lipowsky and E. Sackmann (Elsevier, Amsterdam, 1995), pp. 1-65.
[2] J. Killian and B. D. Kruij_, Biochemistry 24, 7881 (1985).
[3] M. Venturoli, B. Smit, and M. Sperotto, Biophysical Journal 88, 1778 (2005
[4] R. Groot and P. Warren, J. Chem. Phys. 107, 4423 (1997).
[5] F. D. Meyer, M. Venturoli, and B. Smit, Biophys. J. (accepted) (2008).
[6] G. Brannigan, C. Lawrence, L. Lin, and F. Brown, Eur. Biophys. J. 35, 104 (2006).
[7] F. Cardinaux, A. Stradner, P. Schurtenberger, F. Sciortino, and E. Zaccarelli, EPL 77, 48004 (2007).
[8] W. H. Press, S. A. Teukolsky, W. T. Vetterling, and B. P. Flannery, Numerical Recipes: The Art of Scientific Computing (Cambridge University Press, Cambridge, UK, 1999).
[9] S. Kirkpatrick, C. Gelatt, and M. Vecchi, Science 220, 671 (1983).
[10] J. Mou, D. Czaijkowsky, and Z. Shao, Biochemistry 35, 3222 (1996).
[11] M. Diociaiuti, F. Bordi, A. Motta, A. Carosi, A. Molinari, G. Arancia, and C. Coluzza, Biophys. J. 82, 3198 (2002).
[12] H. Aranda-Espinoza, A. Berman, N. Dan, P. Pincus, and S. Safran, Biophys. J. 71, 648 (1996).
[13] K. Kim, J.Neu, and G. Oster, Biophys. J. 75, 2274 (1998).
[14] V. Ivanova, I. Makarov, T. Sch□a_er, and T. Heimburg, Biophys. J. 84, 2427 (2003).

Poster B15

Complexation of hen egg white lysozyme with sodium (sulfamate-carboxylate) isoprene polyelectrolytes

M. Karayianni, G. Mountrichas, S. Pispas, G. D. Chryssikos, V. Gionis

Theoretical & Physical Chemistry Institute, National Hellenic Research Foundation, 48, Vass. Constantinou Ave., Athens 11635, Greece

Recently the complexation of proteins with polyelectrolytes has attracted considerable attention, due to its importance in a variety of chemical and biological processes, such as protein purification and separation, drug delivery and biotechnology.[1] The complexation is mainly driven by electrostatic interactions, though hydrophobic interactions may also be involved. A number of parameters, including the polyelectrolyte molecular weight, charge density and chain stiffness, as well as the nature of the protein are important for complexation to take place. The polyelectrolyte/protein complexes can form monophasic or biphasic solutions, which can be clear or turbid, while in the latter case precipitation is often observed.

In this work we employ static, dynamic, and electrophoretic light scattering and fluorescence spectroscopy to study the solution behavior and structure of complexes formed between hen egg white lysozyme (HEWL) and sodium (sulfamate-carboxylate) isoprene polyelectrolytes (SCPI).[1,2] All experiments are performed at 25 °C, in aqueous solutions at pH 7 and 0.01M ionic strength (phosphate buffer solution). HEWL is a globular protein with a molecular weight M_r=14600, an isoelectric point pI=11 and a net charge of +8 at pH 7. Two SCPI polyelectrolytes were prepared by a post-polymerization functionalization reaction on polyisoprene homopolymers with M_W=54000 and M_W=21000. This reaction introduces sodium sulfamate and carboxylate groups in approximately 68% of the monomeric units of polyisoprene: [3]

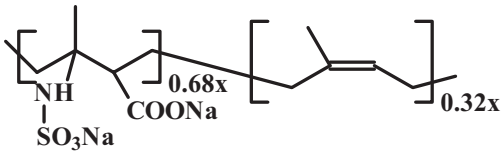

Figure 1 shows representative static and dynamic light scattering results from the complexes formed between HEWL and the two SCPI polyelectrolytes as a function of polyelectrolyte concentration, which is expressed as the nominal (polyelectrolyte/protein) charge ratio. HEWL concentration is kept constant at 0.25 mg/mL.

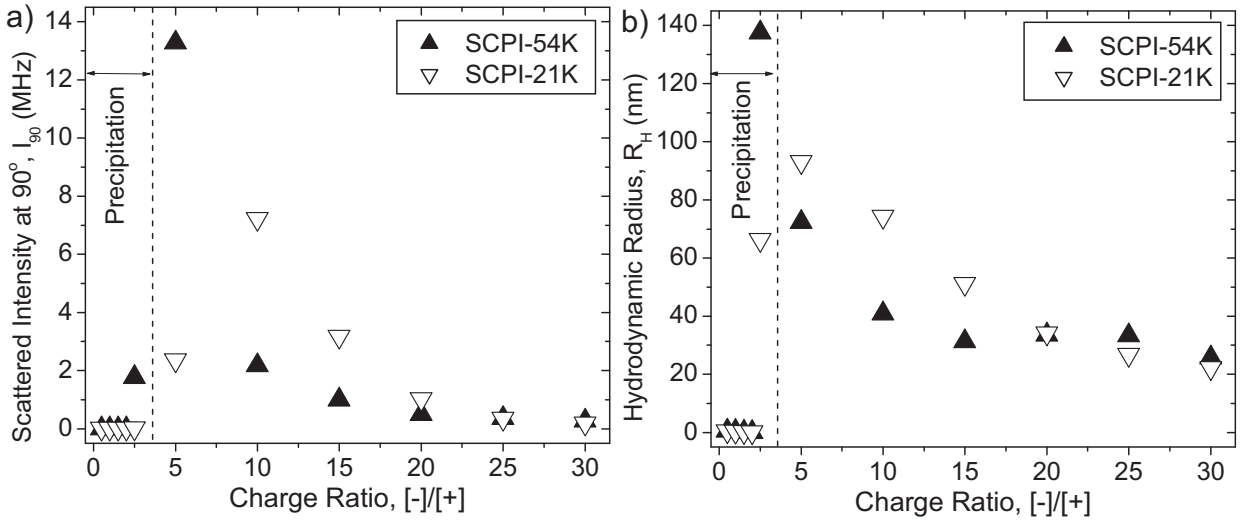

Fig. 1, a) Light scattering intensity at 90° and b) hydrodynamic radius, versus charge ratio for HEWL and SCPI-54K/SCPI-21K complexes at pH 7 and 0.01M ionic strength. For comparison HEWL I_{90}≈ 5 kHz & R_H≈ 1.5 nm, SCPI-54K I_{90}≈ 45 kHz & R_H≈ 28 nm and SCPI-21K I_{90}≈ 55 kHz & R_H≈ 21 nm.

With reference to Figure 1 we note that both the scattered intensity and the hydrodynamic radius of the SCPI/HEWL solutions are higher than the corresponding values for the pure component solutions, proving that complex formation is actually taking place. The mass (proportional to the scattered intensity) and the size of the complexes depend on the charge ratio and the molecular weight of SCPI. Maximum values are observed for a charge ratio about 5 and decrease at higher charge ratios. For charge ratios smaller than 5 precipitation occurs. Remarkably, at high charge ratios, the mass and size of the complexes become independent of the polyelectrolyte molecular weight.

Electrophoretic light scattering measurements for the same system (Figure 2a) show that the zeta potential is dependent on the molecular weight of the polyelectrolyte and exhibits increasingly negative values as the charge ratio increases. This behavior is indicative of increasing effective negative charge as the polyelectrolyte concentration increases.

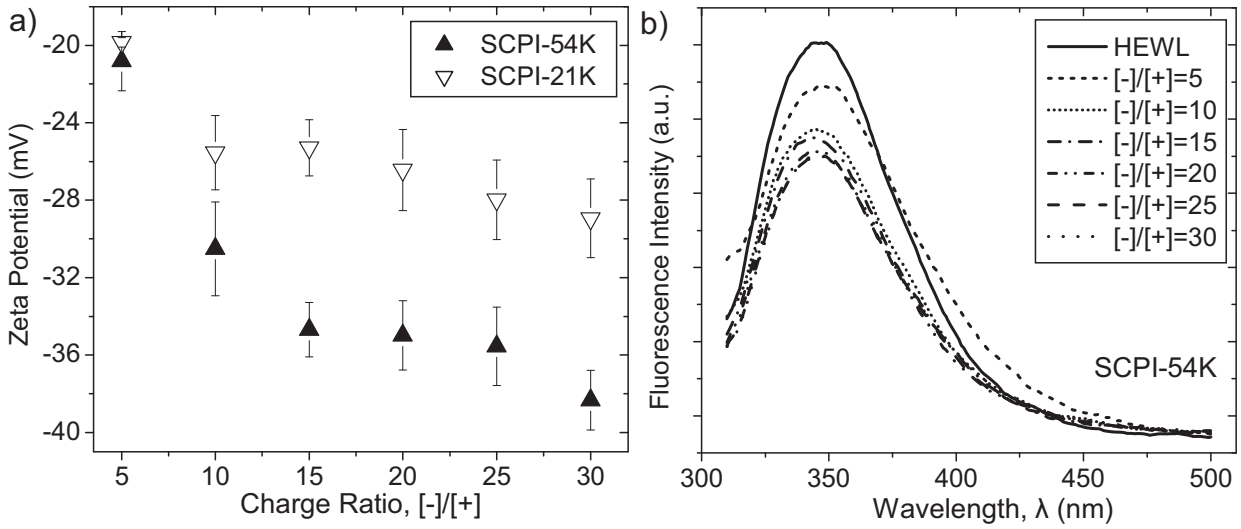

Fig. 2, a) Zeta potential values versus charge ratio and b) fluorescence spectra, for HEWL and SCPI complexes at pH 7 and 0.01M ionic strength.

Fluorescence spectroscopy was employed in order to investigate the conformational changes of HEWL upon complexation, by monitoring the fluorescence of the tryptophan residues in the protein.[4] The spectra for the HEWL/SCPI-54K are shown in Figure 2b (similar spectra were obtained for the HEWL/SCPI-21K system), the spectrum of free HEWL is included for comparison. Despite small intensity variations, all spectra exhibit a maximum at approximately 350 nm. This fact suggests that although minor changes of the environment around tryptophan cannot be excluded, no protein denaturation is observed upon complexation.

Further research in progress includes the detailed conformational characterization of HEWL by spectroscopic techniques, as well as the elucidation of the influence of the pH and the ionic strength of the medium on the formation and structure of the HEWL/SPCI complexes.

References

1. a) C. L. Cooper, P. L. Dubin, A. B. Kayitmazer, S. Turksen, *Curr. Opin. Colloid Interface Sci.*, 2005, *10*, 52 b) C. Tribet, In Surfactant Science Series, Vol. 99: Physical Chemistry of Polyelectrolytes, T. Radeva, Ed. Marcel Dekker: New York, 1999, Chapter 19, pp 687
2. S. Pispas, *J. Polym. Sci. Part A: Polym. Chem.*, 2007, *45*, 509
3. S. Pispas, *J. Polym. Sci. Part A: Polym. Chem.*, 2006, *44*, 606
4. M. van de Weert, M. B. Andersen, S. Frokjaer, *Pharm. Res.*, 2004, *21*, 2354

Poster B16

Study of the release kinetics of a drug and an MRI contrast agent from poly (vinyl alcohol) matrices

A. Hasimi, K. G. Papadokostaki, M. Sanopoulou
Institute of Physical Chemistry, NCSR "Demokritos, 153 10 Ag. Paraskevi Attikis

Poly(vinyl alcohol) (PVA) is a low-toxicity, biocompatible polymer, used or under investigation, in a wide range of biomedical applications, such as controlled release devices and tissue engineering. Matrix controlled release systems consist of a swellable polymer matrix incorporating the drug, and are activated by the ingress of water (swelling controlled systems[1,2]). Magnetic resonance imaging (MRI) is a non-invasive technique which can provide cross-sectional images from inside solid materials and living organisms. Thus, in the case of polymer-based, sustained drug release devices, the incorporation of an MRI contrast agent in the polymer matrix should allow, in principle, the use of MRI as a method of following the drug administration and distribution to the tissues.[3] The present work focuses on the study of the release of both a model drug and an MRI contrast agent from poly(vinyl alcohol) (PVA) matrices, and the effect of the presence of the contrast agent on the drug release kinetics.

The drug used was diphylline [7-(2,3-dihydroxypropyl)-theophylline] and the MRI contrast agent was the paramagnetic complex of Gadolinium, Diethylenetriaminepentaacetic acid gadolinium(III) dihydrogen salt hydrate (Gd-DTPA). Appropriate amounts of diphylline and Gd-DTPA were added to the aqueous casting solution of the polymer (10% wt/wt in PVA) to obtain rectangular matrices of thickness 2L=300-500 μm, loaded with diphylline, or Gd-DTPA or both. After water evaporation, the matrices were annealed at 130^0C for 20 min. The effect of the two solutes on the thermal properties of PVA was studied by Temperature Modulated DSC. Diphylline release kinetics in pure water were followed by UV spectroscopy (at 275 nm) and Gd-DTPA release kinetics were measured by spectorfluorimetry (excitation at 275 nm, emission at 316 nm). The diffusion coefficients of the two solutes in PVA were determined from desorption experiments from the fully swollen matrix. Finally, water uptake kinetics by PVA matrices was determined gravimetrically. All experiments were performed at 25±0.2 ^{o}C.

Comparison of release kinetics from Gd-DTPA-loaded, and from diphylline-loaded, matrices (Fig. 1 and full points in Fig. 2) indicates that the two solutes are released at comparable time scales, in line with the similar diffusion coefficients D_{SE} and D_{NE} (Table1). In both cases , the rate of release is relatively stable for more than 50% of the loaded solute (see inset of Fig. 2), as expected from the fact that solute release occurs at comparable time scales with the ingress of water in the matrix[1,2] (dashed line in Fig. 1).

Table 1. Diffusion coefficients of the solutes studied

Solute	Diffusion coefficient in swollen PVA matrices	Diffusion coefficient in pure water*
Diphylline	D_{NE} = (1.44±0.20) *10^{-7} cm^2/s	D_{NS} =8.4 *$10^{-6}$$cm^2/s$
Gd-DTPA	D_{SE} = (1.47±0.17) *10^{-7} cm^2/s	D_{SS} = 5.7*$10^{-6}$$cm^2/s$

*Determined on the basis of empirical relations (R.C.Reid, T.K. Sherwood, The Properties of Gases and Liquids, McGraw Hill, New York, 1975)

Release of diphylline from PVA is accelerated, in the presence of Gd-DTPA in the matrix (open points in Fig. 2), probably due to enhanced hydration of the matrix in this case. DSC analysis of the dry matrices indicated that the incorporation of Gd-DTPA does not materially affect the crystallinity of PVA, nor it has a plasticizing effect through reduction of the T_g of the polymer (Fig. 3). Thus, the observed acceleration of diphylline release (Fig. 2) could be possibly due to enhanced hydration of the matrix.

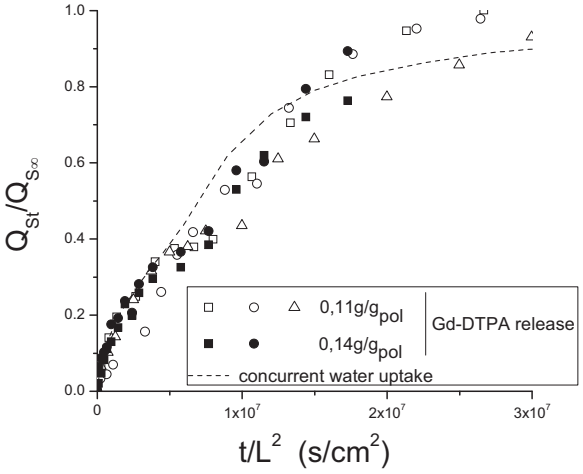

Fig. 1. Release kinetics of Gd-DTPA from dry PVA films on a time scale. The full line corresponds to concurrent water uptake.

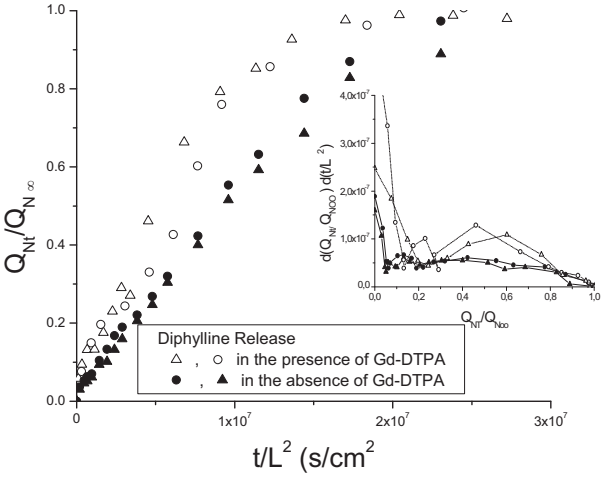

Fig. 2. Release kinetics of diphylline from dry PVA films in the presence (0.11 g/g PVA) or absence of Gd-DTPA on a t scale. Diphylline load: 0.11 g/g PVA. The inset presents the release rate of diphylline $d(Q_{Nt}/Q_{N\infty})/d(t/L^2)$ versus the fractional amount released ($Q_{Nt}/Q_{N\infty}$).

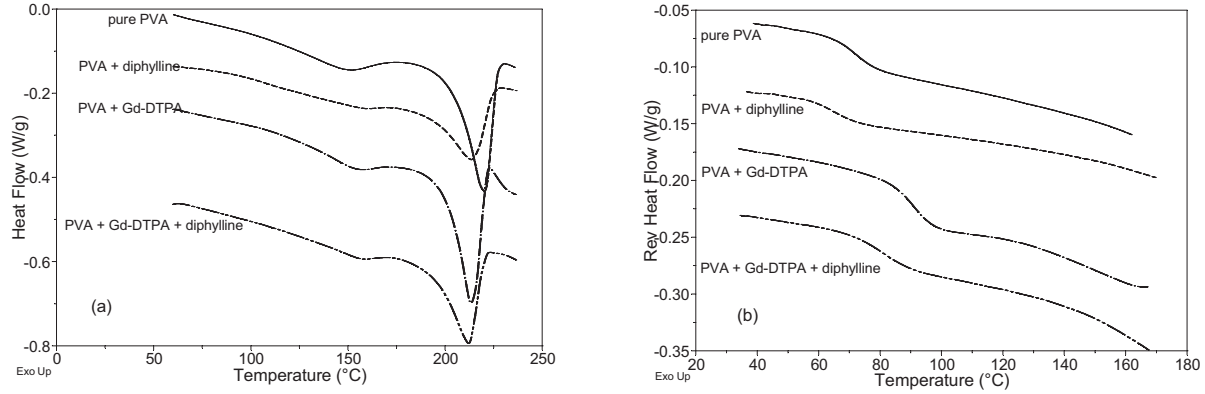

Fig. 3. (a) Total TMDSC signal during the first heating run and (b) reversing TMDSC signal during the second heating run of pure and drug-loaded PVA films containing 0.11 g diphylline or Gd-DTPA per g PVA. In the case of PVA loaded with both solutes, the content was 0.11 g/g PVA for each one.

The above results indicate that during the design of contrast agent-loaded, drug controlled release systems, the possible effect of the contrast agent on the drug release kinetics should be taken into account.

Acknowledgment

This work was partially financed by the European Union and the General Secretariat for Research and Technology, Greece, in the Framework of the Regional Operational Program of Attiki.

References

1. C. S. Brazel, N. A. Peppas, Polymer **40**, 3383 (1999).
2. K.G. Papadokostaki, A. Stavropoulou, M. Sanopoulou, J.H. Petropoulos, J. Membrane Sci. **312**, 193 (2008).
3. J.C. Richardson, R. W. Bowtell, K. Mäder, C.D. Melia, Adv. Drug Deliv. Rev. **57**, 1191 (2005).

Poster B17

Wetting, Optical Property and Protein Adsorption Control of Polymer Surfaces by Plasma Nanotexturing

[1] K.Tsougeni, [1] M.E.Vlachopoulou, [1] K. Kontakis, [1] D. Papageorgiou, [2] P.S. Petrou, [2] S.E. Kakabakos, [1] A.Tserepi, [1] E.Gogolides

[1] Institute of Microelectronics, [2] Institute of Radioisotopes and Radiodiagnostic Products NCSR "Demokritos", PO Box 60228, Aghia Paraskevi, Attiki, 153 10 Greece.

In the present work, we fabricate plasma-induced random columnar-like low- and high-aspect ratio nano-roughness on commercial polymers (which we term nanotexture). We examine the effect of nanotexture on the wetting and optical properties of the polymer and use them as substrates for protein adsorption. We demonstrate self-cleaning, optically transparent and antireflective polymer surfaces appropriate for widespread applications. Organic polymers such as Poly (methyl methacrylate) (PMMA), Poly (ether ether ketone) (PEEK), Poly (ethylene terephalate) (PET) and Polystyrene (PS) are textured in O_2 plasmas and inorganic polymers such as Poly (dimethyl siloxane) (PDMS) in SF_6 plasmas.

The height of nano-columns varies from tens of nm to tens of μm, by increasing the duration of plasma treatment, while their density is also affected, as aggregates of nanocolumns are created at longer treatment time [1-3]. In Fig. 1, we show PEEK and PDMS surfaces, as viewed with AFM images and at a tilt under scanning electron microscopy, after etching with O_2 and SF_6 plasmas respectively, under conditions ensuring high etch rates 660 and 750 nm/min, respectively. The images indicate high-aspect ratio columnar-like structures.

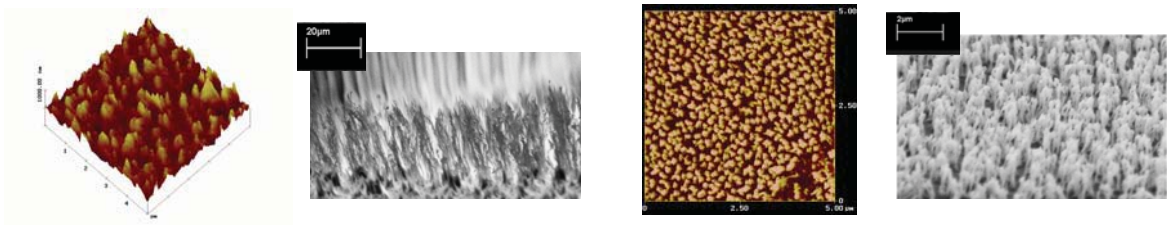

(a) (b)

Fig. 1 AFM and tilted SEM images of (a) PEEK after 4 min (z range ~ 662 nm, rms roughness ~ 75 nm) and 60 min and (b) PDMS surfaces after 2 min (z range ~ 793 nm, rms roughness ~ 133 nm) and 6 min SF_6 plasma etching respectively. Notice the creation of a porous surface.

After O_2 plasma organic polymer surfaces are super-hydrophilic (contact angle ~ 0°). After SF_6 plasma the contact angle of inorganic polymer such as PDMS, drops from 110° to ~ 60°. However, if before exiting the plasma reactor a 10 sec plasma deposition step with C_4F_8 gas is done, a fluorocarbon layer is deposited on the surface and hydrophobic as well as super-hydrophobic behaviour is attained.

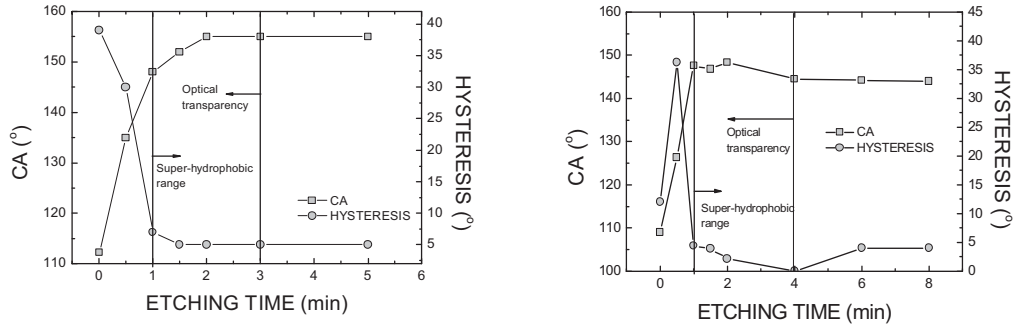

(a) (b)

Fig. 2(a, b). CA and CA hysteresis versus etching time for (a) PMMA and (b) PDMS surfaces, after deposition of fluorocarbon layer.

As seen in Fig. 2(a, b), FC coating on smooth surfaces attains ~110°. The contact angle (CA) increases with etching time due to the surface roughness formation from the etching step, reaching a plateau of ~150° within the first minute of processing. CA hysteresis lowers below 5° after the first minute. Thus super-hydrophobicity is attained within the first minute of etching, indicating a very fast process compared to other super-hydrophobic fabrication techniques. Further processing does not alter the wetting properties of both PMMA and PDMS surfaces. As a result such surfaces reveal self-cleaning properties.

For all polymer plasma treated surfaces that we study here, optical transparency remains intact until ~3 min of processing, while after 5 min of etching time, the surface becomes milky. The non-processed samples attain ~9% reflectance, which gradually decreases to ~7% after 1 and 2 min of O_2 plasma processing. Further plasma processing results in lower levels of reflection. However process time longer than 3 min results also in transmission decrease. From this we conclude that the maximum process time to attain antireflective, yet optically transparent substrates should be lower than 3 min. As for the case of PMMA, SF_6-treated PDMS surfaces for plasma durations between 1 and 3 minutes can be used as transparent and antireflecting coatings as for 4-minute SF_6 plasma treatment, transmittance at 600 nm has been decreased to 88%, while reflectance has been decreased to 3.5%.

Such nanostructured surfaces (without fluorocarbon layer deposition) are investigated as substrates for protein adsorption. We used both fresh and aged samples, since ageing affects surface wettability, a critical parameter in protein adsorption. To evaluate the protein adsorption ability of nanotextured surfaces, treated and untreated surfaces were coated with biotinylated-bovine serum albumin (BSA) and the fluorescence intensity after reaction with AlexaFluor 546 (AF546) labeled streptavidin was determined. An increase in biotinylated-BSA adsorption is observed on PMMA nano-columnar surfaces, compared to flat untreated PMMA surfaces, due to both modified surface chemistry and increased surface area as shown in Fig. 3. In detail, protein adsorption increases with protein concentration and with plasma duration, while even larger adsorption is observed for aged samples. Best homogeneity is obtained, however, for short plasma treatments, as shown in Fig. 4.

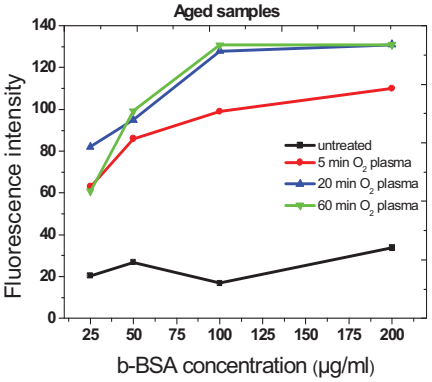

Fig. 3 Variation of fluorescence intensity of proteins on aged O_2 plasma treated surfaces for different plasma exposure time.

Fig. 4 Fluorescence images obtained from (a) untreated, (b) 5 min and (c) 20 min O_2 plasma-treated PMMA surfaces after coating with biotinylated BSA and reaction with AF546 labeled streptavidin. Similar images are obtained for fresh and aged samples, with aged samples having even higher intensity.

Plasma processing was implemented in nano-texturing polymeric surfaces and the use of the latter in the fabrication of hydrophobic or super-hydrophobic, or super hydrophilic yet transparent and antireflective polymeric surfaces has been demonstrated. These surfaces are appropriate for both applications in the micro-scale such as in microfluidics, cell/protein adsorption and/or macro applications, such as in panels for photovoltaics, solar cells, smart windows etc.

1. A. Tserepi, E. Gogolides, K. Misiakos, M. E. Vlachopoulou, and N. Vourdas, Greek Patent Application 20050100473; PCT Application Number GR2006/000011.
2. N. Vourdas, A. Tserepi, and E. Gogolides, Nanotechnology **18**, 125304 (2007).
3. A. Tserepi, M.E. Vlachopoulou, and E. Gogolides, Nanotechnology 17 (2006) 3977.

Poster B18

Bulk and interfacial dynamics of PDMS/Titania nanocomposites

Panagopoulou Anna, Spanoudaki Anna, Pissis Polycarpos, Bokobza Liliane
National Technical University of Athens, Department of Physics, Zografou Campus, 15780 Athens, Greece
Laboratoire de Physico-Chimie Structurale et Macromoléculaire ESRCI, 10 rue Vauquelin, 75231 Paris cedex 05, France

We present results of a study on the molecular dynamics of poly(dimethylsiloxane) (PDMS), a crosslinked semicrystalline polymer, with inclusions of titania nanoparticles. The nanoparticles were prepared in situ using the sol-gel method.

The aim was to investigate the degree to which the dynamics of the polymer are affected by the nanoparticles, as well as the mechanism through which this takes place. This study follows up on a previous study by our group on PDMS/silica nanocomposites, which showed that near the surface of the nanoparticles an interfacial layer with modified dynamics is formed [1,2,3].

The Thermally Stimulated Depolarization Currents (TSDC) technique due to its high resolving power has proven to allow the separation of relaxations that have similar frequencies. In particular, it allows the discrimination of the dynamics of the bulk polymer from those of the interfacial layer. Furthermore, it allows the separation of the α relaxation connected with the glass transition in the amorphous regions and the α_c relaxation attributed to the dynamics of polymer chains in the crystalline regions.

In Figure 1 characteristic TSDC thermograms are presented. Two different thermal protocols have been followed in order to separate α and α_c contributions. On the diagram, estimated regions of the relaxations observed, are highlighted.

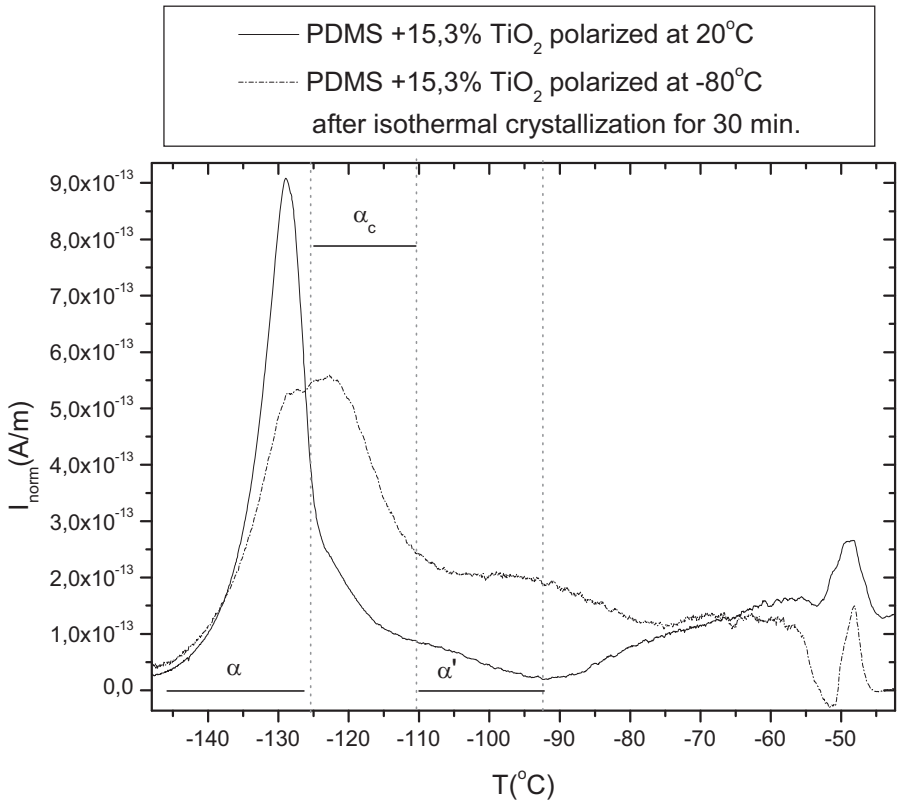

Figure 1: TSDC thermograms of a PDMS sample with 15.3% nanoparticles of Titania after different thermal protocols.

Dielectric Relaxation Spectroscopy on the other hand provides information on the molecular mobility over a large frequency range and the temperature dependence of the dynamics.
In the Arrhenius diagram of Figure 2 it is shown that different thermal protocols of the DRS measurements lead to separation of α and α_c relaxations. In addition, the relaxation of the interfacial layer is followed.

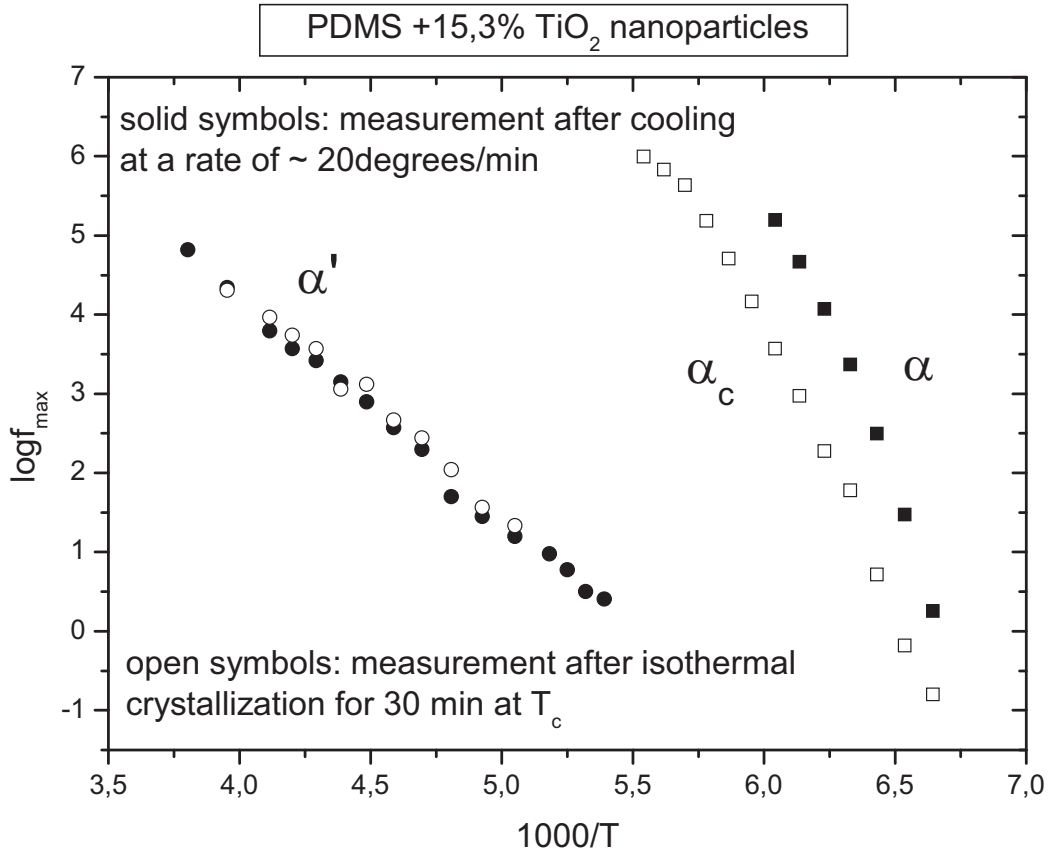

Figure 2: Arrhenius diagram of a PDMS sample with 15.3% nanoparticles of Titania.

Differential scanning calorimetry (DSC) was used complementarily in order to obtain information on the thermal properties of the samples and importantly on the state of the samples (crystallinity degree, quality of the crystals) depending on the thermal protocol used for the dynamic measurements.

1. D. Fragiadakis, P. Pissis, J. Non-Cryst. Solids, 353 (2007) 4344-4352
2. D. Fragiadakis, P. Pissis, L. Bokobza, J. Non-Cryst. Solids, 352 (2006) 4969-4972
3. D. Fragiadakis, P. Pissis, L. Bokobza, Polymer 46 (2005) 6001-6008

Poster B19

SYNTHESIS AND PROPERTIES OF UNMODIFIED LDPE/ORGANOSILICATES NANOCOMPOSITES

A.Giannakas[1], C.G.Spanos[1], P.Xidas[2], K.S.Triantafyllidis[2], A.Katsoulidis[3] and A.Ladavos[1,*]

[1]*School of Natural Resources and Enterprise Management, University of Ioannina, Agrinio 30100, Greece*
[2]*Department of Chemistry, Aristotle University of Thessaloniki, GR-54124 Thessaloniki, Greece*
[3] *Department of Chemistry, University of Ioannina, Ioannina 45110, Greece*

Polymer-layered silicate nanocomposites have attracted great interest due to their improved thermal, mechanical and gas barrier properties compared to conventional composites or neat polymers. Low density polyethylene (LDPE) is widely used for packaging applications and the synthesis of LDPE/inorganic nanocomposites with improved mechanical and barrier properties, is expected to further boost its use in that direction. However, the achievement of nanocomposite structures with highly dispersed inorganic nanoparticles in LDPE, is much more difficult than in HDPE because of the branched macromolecules (in LDPE) which hinder the penetration of the polymer chains into the clay galleries [1]. Nanocomposites based on LDPE and the use of a compatibilizer such as maleic anhydride-grafted PE or ethylene vinyl acetate (EVA) giving intercalated or partially exfoliated structures have been reported [2].

The objective of this study was to synthesize LDPE based nanocomposites, without any polymer modification using as filler two kinds of layered silicates, one with low aspect ratio (i.e. synthetic laponite) and another with high aspect ratio (i.e. montmorillonite). The effects of synthesis parameters, and the type of layered silicate on the structure and properties of the resulting LDPE / silicate (nano)composites have been systematically investigated.

The silicates used in this work were laponite (Lp), a synthetic hectorite obtained from Southern Clay Products Inc., with cation exchange capacity (CEC) 50 meq/100g of clay and organo-montmorillonite (OMt) NANOMER®-I.44P produced by Nanocor Company and supplied by Aldrich. Surface modification of the synthetic laponite carried out using, the same modifier as that used by Nanocor in NANOMER®-I.44P namely di(hydrogenated tallow) dimethylammonium chloride (Arquad® 2HT-75, supplied by Fluka). The polyethylene used for the nanocomposites preparation, was LDPE supplied by Aldrich, with Melt Index=25g/10min (190°C/2.16kg) and density 0.915 g cm^{-3}.

Two series of materials were prepared, one via solution blend method using CCl_4 as solvent and another by melt compound in an oven at 180°C. The organosilicate loadings were 2, 5 and 10 wt % for LDPE-OLp composites and 2 and 10 wt % for LDPE-OMt composites. XRD analysis took place on composite's films, using a D8 Advanced Brüker diffractometer with CuK_α radiation. The obtained diagrams are shown in Fig.1. Thermogravimetric (TGA) analysis and DSC measurements were carried out using a NETZSCH STA 449C apparatus. Tensile tests were performed on an Instron Tensile Testing Machine model 3344 according to ASTM D638 using dogbone-

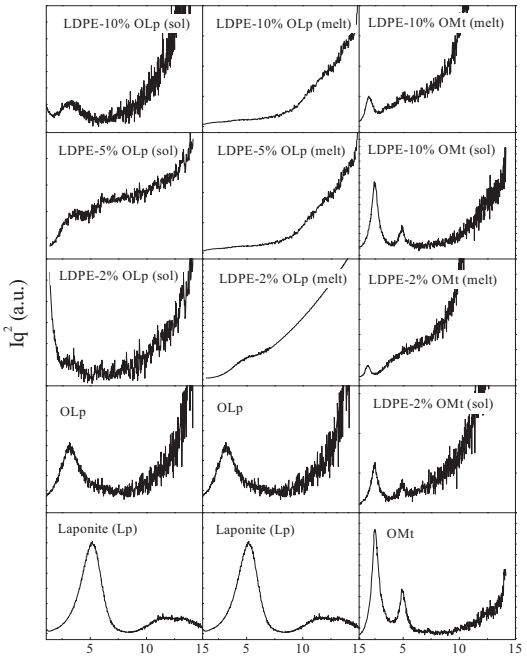

Fig.1. XRD patterns of various LDPE/organosilicate composites prepared by OLp and OMt in the form of $Iq^2=f(q)$ where I is the intensity and $q=4\pi \sin\theta/\lambda$, The patterns of pristine laponite, OLp and OMt samples are also shown for direct comparison.

shaped specimens with dimensions 22 x 5 x 0.22 mm at 50 mm/min crosshead speed. Three specimens from each sample were tested to establish reproducibility of the measurements. Basal spacing (d_{001}) of clays in the LDPE/organosilicate composites, crystallization (T_c) and melting (T_m) temperatures of composites and elastic modulus values for neat polymer and composites are tabulated in Table 1.

From the XRD patterns shown in fig 1 it is obvious that the use of melt process method is more effective for the preparation of nanocomposite structures, compared to solution blend method, which gives conventional composites. In particular using the melt process method in case of laponite, a low aspect ratio silicate (20-30), the absence of XRD peaks of LDPE/OLp nanocomposites is indicative of the formation of exfoliated nanostructure, while in montmorillonite, a high aspect ratio silicate (100-200), the shift of XRD peaks of LDPE/OMt nanocomposites to lower 2θ angles corresponds to intercalated nanostructure formation. For the composites prepared via solution blend method the presence of the XRD reflections at the same 2θ angles with those of the correspondent organosilicates, indicates that conventional phase separated composites have been formed. TG analysis results indicated that thermal stability increment was more prevalent for nanocomposites prepared using OMt as filler, compared to those prepared with OLp. DSC measurements for LDPE/OLp nanocomposites revealed a gradual increase in crystallization temperatures with increasing Laponite content, while for nanocomposites prepared using organo-montmorillonite, T_c values remained constant and similar to that of neat LDPE, irrespectively the preparation method for both series of materials. Tensile measurements evidenced an increase in elastic modulus of polymer with the addition of organosilicate. This increment was more prevalent for nanocomposites prepared by melt process using high aspect ratio silicate and high organosilicate content (i.e. 10 wt %), compared to conventional composites prepared by solution blend method.

Table 1. Basal spacing (d_{001}) of layered silicates in the LDPE/organosilicate composites, crystallization and melting temperatures of composites, and elastic modulus values for neat polymer and composites.

Material	d_{001} (nm)	T_c (^oC)	T_m (^oC)	Elastic modulus (MPa)
LDPE (neat)	-	100.2	115.2	288
LDPE-2%OLp(Solution)	1.99	101.7	115.1	286
LDPE-5%OLp(Solution)	1.99	102.1	114.7	295
LDPE-10%OLp(Solution)	1.99	102.6	114.2	215
LDPE-2% OLp (Melt)	n.p.*	102.1	114.5	269
LDPE-5% OLp (Melt)	n.p.	102.4	114.5	305
LDPE-10% OLp (Melt)	n.p.	102.6	114.7	345
LDPE-2%OMt(Solution)	2.51	100.9	115.5	311
LDPE-10%OMt(Solution)	2.51	100.9	115.4	350
LDPE-2% OMt (Melt)	3.49	100.6	115.7	303
LDPE-10% OMt (Melt)	3.39	100.9	115.5	423

n.p.* = no peak

Acknowledgments

This work was financed: 75% by the European Union-European Social Fund, 25% by the Greek Secretary of Research and Technology (GSRT) and by private funding under the programme's EPAN framework (PENED 03). The authors would like to thank the Ring of the Laboratory Units and Centers of the U.I. for the XRD and TGA experiments.

References

1. Liang, G., Xu, J., Bao, S., and Xu, W., "Polyethylene/ maleic anhydride grafted polyethylene/organic montmorillonite nanocomposites. I. Preparation, microstructure, and mechanical properties". *J. Appl. Polym. Sci.*, 2004; 91:3974-3980.
2. Morawiec J., Pawlak, A, Slouf, M., Galeski, A., Piorkowska, E.and Krasnikowa, N., "Preparation and properties of compatibilized LDPE/organo-modified montmorillonite nanocomposites". *European Polymer Journal*, 2005; 41: 1115-1122.

Poster B20

Organic – Inorganic Nanocomposites: A study of the structure and dynamics in confined geometry

S. Fotiadou[1], K. Chrissopoulou[2], B. Frick[3], S. H. Anastasiadis[1,2],

[1] *Materials Science and Technology Laboratory, Chemical Engineering Department, Aristotle University of Thessaloniki, 54124 Thessaloniki, Greece*

[2] *Institute of Electronic Structure and Laser, Foundation for Research and Technology-Hellas, P. O. Box 1527, 711 10 Heraklion, Crete, Greece*

[3] *Institut Laue Langevin, 6 rue Jules Horowitz, F38042 Grenoble, France*

The aim of the present work is the investigation of the structure and dynamics in polymer / layered silicate nanocomposites. Mixing polymers with inorganic layered materials can lead to three different types of structure, depending on the specific interactions between the two components; the phase separated, which is formed when the two components are immiscible, the intercalated, where the polymer chains enter the inorganic galleries forming thin polymer films (0.8-2.5nm) and the exfoliated structure, where the ordering of the inorganic material is destroyed and the silicate layers are dispersed in the polymer matrix.[1] The reason that these materials have attracted the scientific interest is related both with their unique properties that render them candidates for numerous technological applications and with the fact that they offer the opportunity to study the static and dynamic properties of macromolecules in nanoconfinement, using macroscopic samples and conventional analytical techniques.[2]

In this work we investigate the structure and dynamics of nanocomposites, composed of a hydrophilic, amorphous polymer, Poly(hexa ethylene glycol methacrylate), PHEGMA, (M_n=6100, T_g=-60°C) mixed with Na^+-MMT. Two methods, solution mixing and melt intercalation, were used to prepare a series of hybrids with PHEGMA / Na^+-MMT ratio between 0 and 100% w/w. In the first method, the polymer was dissolved in an appropriate solvent, then the inorganic component was added and finally the solvent was evaporated. In melt interclation, the two components were mixed in a vacuum oven at a temperature that is higher than the polymer flow temperature. The structure of the hybrids was studied with X-ray Diffraction (XRD), their thermal properties with Differential Scanning Calorimetry (DSC) and Thermogravimetric Analysis (TGA), while Quasi Elastic Neutron Scattering (QENS) was used in order to study the dynamics of both the pure components and the composites.

Figure 1 shows the XRD pattern of the PHEGMA nanocomposites that were prepared with solution intercalation. The peak that corresponds to the interlayer distance of the silicate shifts toward lower angles as the polymer concentration increases, indicating a respective increase of the interlayer distance. However, after annealing at 95°C for 2days, all the samples have the same interlayer distance that is independent of their concentration.[3] (Figure 2) Additionally, the interlayer distances that derive from the annealed nanohybrids agree with the values obtained for the samples that were prepared with melt intercalation, which show the same interlayer distance, independent of the polymer content.

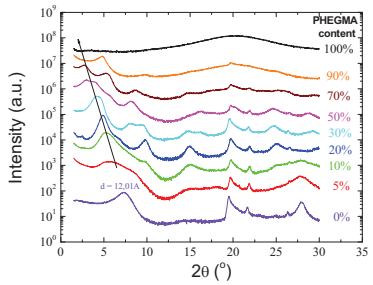

Figure 1. XRD pattern for the PHEGMA/Na^+-MMT nanocmposites before annealing at 95°C for 2days.

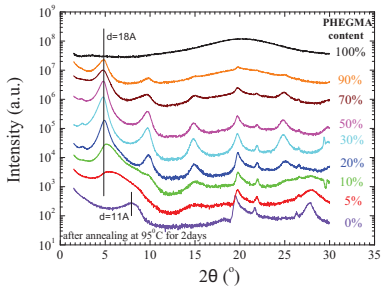

Figure 2. XRD pattern for the PHEGMA/Na^+-MMT nanocmposites after annealing at 95°C for 2days.

The dynamics of the nanocomposites was studied with QENS experimets that were poerformed at the IN16 backscattering spectrometer at the Institue Laue-Langevin in Grenoble. Figure 3 shows the temperature dependence of the elastically scattered intensity for the silicate, the polymer and the nanocomposite with 30wt% PHEGMA at various wavevectors normalized to the respective values at the lowest temperatures. It is estimated, that at this polymer concentration all the polymer chains are intercalated and there is no polymer outside the inorganic galleries. The elastic intensity for the polymer is almost constant for temperatures below its glass transition, T_g, and drops to zero within a temperature range of ~100K. The intensity of the nanocomposite on the other hand, shows a smaller but continuous decrease starting even at temperatures below and goes smoothly through the polymer T_g. This indicates enhanced mobility even at temperatures that the bulk polymer is frozen, but also dynamics within the experimental window at temperatures that the polymer dynamics has been too fast to be measured. The intensity of Na^+MMT shows a small decrease around 270K which is attributed to the mobility of water molecules that are present due to the hydrophilic character of the clay. These results are verified by the temperature dependence of the mean square displacement, as well.

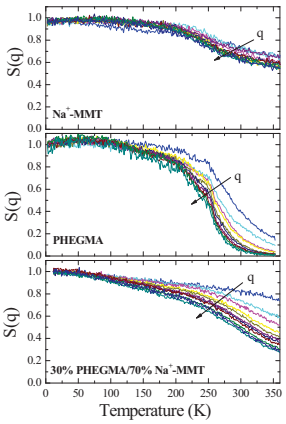

Figure 3. Elastic scans for different wavevectors for Na^+-MMT, PHEGMA and 30wt% PHEGMA + 70wt% Na^+-MMT.

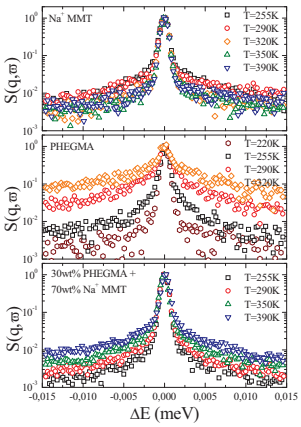

Figure 4. S(q,ω) of Na^+-MMT, PHEGMA and 30wt% PHEGMA + 70wt% Na^+-MMT for different temperatures at q=1.29A^{-1}

Figure 4 shows the incoherent structure factor S(q,ω) for Na^+-MMT, PHEGMA and the nanocomposite with 30wt% PHEGMA for different temperatures at wavevector q=1.29A^{-1}. The data are shown normalized to their maximum value. It is evident that the temperature dependence is quite different between the different samples. The S(q,ω) of PHEGMA consists of an elastic contribution that decreases strongly with temperature and a quasielastic part shown through the broadening of the spectra wings with dynamics that become faster with increasing temperature. This dynamics is attributed to the segmental motion that becomes unfrozen above the polymer's Tg. On the contrary, both the incoherent structure factor and thus the relaxation times of the nanohybrid show a much weaker temperature dependence. S(q,ω) for Na^+-MMT shows a broadening only around the melting temperature of water whereas it superimposes with the resolution function for higher temperatures, in agreement with the elastic measurements.

References
1. Giannelis E. P., Krishnamoorti R., Manias E., Adv. Polym. Sci. **138** :107 (1999)
2. Vaia R. A., Vasudevan S., Krawiec W., Scanlon L. G., Giannelis E. P. Adv. Mater. 7:154 (1995)
3. Fotiadou S., Chrissopoulou K., Anastasiadis S. H, Frick, B., in preparation (2007)

Acknowledgements: Part of this research was sponsored by the Greek General Secretariat for Research and Technology (ΠΕΝΕΔ Programmes 03ΕΔ581 and ΠΑΒΕΤ 05PAB96) and the EU (STREP NMP3-CT-2005-506621).

Poster B21

Glass transition, structural characterization and segmental dynamics in epoxy/carbon fillers nanocomposites

Th. V. Kosmidou[1], C.G Delides[1], C.A. Stergiou[2], A.S. Vatalis[1], and P.Pissis[3]

1. Technological Education Institute (TEI) of Western Macedonia, Laboratories of Physics and Materials Technology, Kozani, Greece, e-mail: kdelidis@yahoo.com

2. Aristotle University of Thessaloniki, Department of Electrical Engineering and Computers, ThessalonikiGreece,

3. National Technical University of Athens, Department of Physics, Zografou Campus, 15780 Athens, Greece

Nanocomposites based on Carbon Nanotubes (CNTs) ,either single wall (SWCNTs)or multiwall (MWCNTs),have received a tremendous amount attention during the last years. This unique carbon crystalline form shows remarkable physical and mechanical properties, such as high elasticity modulus and tensile strength, advanced thermal and electrical conductivity, etc.
In the field of electrical and electronic applications, where conductivity plays an important role, there is another commercially available carbon product that shows excellent performance characteristics: Carbon Black (CB). The main advantages of Carbon Black over CNTs are the low toxicity and the low price. The major challenge in the preparation of nanocomposites containing carbon products is the control of filler dispersion[1].

In the present work we compared the structure of two different carbon/epoxy nanocomposites, using Differential Scanning Calorimetry (DSC), Dynamic Mechanical Analysis (DMA), Scanning Electron Microscopy (SEM) and wide angle X-Rays Diffraction (XRD) techniques. For the preparation of the nanocomposites diglycidyl ether of bisphenol A (DGEBA) was used with triethylenetetramine (TETA) as a curing agent. As fillers *a*. CB, *b*. MWCNT were used. Carbon nanofillers were dispersed into the epoxy resin using a combination of mechanical and ultrasonication mixing and the samples were cured in two stages *a*: 60^{o}C for 2h and *b*: 150^{o}C for 2h.Full details are presented elsewhere[2].

From the XRD spectra we can see that the CB/epoxy composites are non crystalline as expected. They present a broad peak corresponding to 2θ=19^{o}, which is an indication of some loose segmental orientation of the matrix[2]. In addition the XRD patterns of composites containing CNTs show clear crystalline peaks due to CNTs

The effect of various nanofillers on the glass transition (T_g) in polymer composites is reported in the literature. In some cases an increases in the T_g was observed,[3-5] but the opposite result is also possible[6]. In many cases the amount, the dispersion and the surface conditions of the nanoparticles play important role in the changes in T_g[3,7].

In our case the T_g dependence on the CB and CNTs-content is presented in Table 1 for the two distinctly different fillers.

Table 1. Glass transition Temperatures of composites for CB(T_{gCB}) and CNT(T_{gCNT}) as filler.

Filler content [wt%]	0.0	0.2	0.5	1.0
T_{gCB} [^{o}C]	132	146	169	149
T_{gCNT}[^{o}C]	132	155	151	152

In the case of CB, at low filler contents T_g increases up to a maximum value (at about 0.5 % w/w) of filler content and afterwards decreases. This dependence is confirmed also by DSC measurements. This unexpected behavior shows a remarkable difference with the predictions of the statistical theory available for randomly dispersed and distributed fillers. A similar behaviour was observed in many other nanocomposites. It can be qualitatively explained by the coexistence of the two mechanisms (namely interfacial constrains and free volume

increase[8]) which can be responsible for the T_g shifting. In any nanocomposite the two mechanisms are in dynamic equilibrium. The equilibrium point depends on many factors (filler's amount, size, etc) and in that way it analogically affects the T_g.

According to the first mechanism, a short –range, highly immobilized layer of a few nm thick is developed near the surface of the fillers. In this interaction region of the polymer layer surrounding the particles, the conformational entropy and the chains kinetics are significantly altered. As the filler content increases the volume fraction of the interaction region in the nanocomposites increases too. The polymer chains in this region are under constrain because of the interfacial polymer-particle interactions and therefore T_g of the nanocomposites has been shifted to higher temperatures.

Based on the concept of free volume, the increase of the filler content increases the free volume due to loosened molecular packing of the chains. This extra created free volume assists the large – scale segmental motion of the polymer. . As a result, T_g of the nanocomposites decreases as the filler loading increases.

In our case, at low filler content the first mechanism (interfacial constrains) dominates and therefore contributes to a T_g increase with the filler loading. After a certain amount of filler (0.5 % w/w) the second mechanism (free volume increase) starts to be dominant and the T_g decreases with the filler content.

This inversion in the domination of the mechanisms which are responsible to T_g shifting could be explained as a consequence of a transition of the filler arrangement within the matrix. The critical value of CB content separates, in fact, a dispersed and an agglomerated state and can therefore not be compared with the one obtained through a purely random geometrical process. The CB particles have permanent electrical charges at their surfaces, which are probably responsible for this morphological structure.

In the case of CNTs the T_g appears to be maximum at the 0.2% of filler content, but the overall tendency remains the same as it seems to decrease again at higher concentrations.

Concerning the dependence of dynamic moduli (E´ and E´´) on the filler content it is clearly from the DMA spectra that E´ is slightly affected by the filler content in the glassy state and increases significantly in the rubbery one, either with CB or CNTs as fillers. E´´ decreases with filler concentration for all the composites, as expected.

References

1. A. Kelarakis, K. Yoon, R. Somani, I. Sics, X. Chen, B. S. Hsiao, B. Chu, Polymer **47** 6797-6807 (2006).
2. Th.V.Kosmidou, A.S. Vatalis, C.G. Delides, E. Logakis, P. Pissis, G.C. Papanicolaou, express Polymer Letters **5(2)**, 364-372 (2008**)**
3. Brown J., Rhoney I., Pethrick R. A., Polymer International, **53**, 2130–2137 (2004).
4. Cao Y. M., Sun J., Yu D. H, Journal of Applied Polymer Science,**83**, 70–77 (2002).
5. Pham J. Q., Mitchell C. A., Bahr J. L., Tour J. M., Krishanamoorti R., Green P. F., Journal of Polymer Science, Part B: Polymer Physics, **41**, 3339–3345 (2003).
6. Ash B. J., Schadler L. S., Siegel R. W., Materials Letters, **55**, 83–87 (2002).
7. Kotsilkova R., Fragiadakis D., Pissis P., Journal of Polymer Science, Part B: Polymer Physics, **43**, 522–533 (2005).
8. Bershtein V. A., Egorova L. M., Yakushev P. N., PissisP., Sysel P., Brozova L., Journal of Polymer Science, Part B: Polymer Physics, **40**, 1056–1069 (2002).

Poster B22

Dynamics of epoxy nanocomposites: The effect of filler's content and the size structure and geometry of the nanoparticles.

C.G.Delides
Technological Education Institute (TEI) of Western Macedonia, Laboratories of Physics and Materials Technology, Kozani, Greece e-mail: kdelidis@yahoo.com.

Abstract
The purpose of this work was to examine the effects of particles' characteristics of different fillers on the thermomechanical behaviour of epoxy nanocomposites. Dynamic mechanical analysis (DMA) and differential scanning calorimetry (DSC) measurements have been used. An attempt has been made to correlate the structure, the surface chemical modification, the size, the shape and the geometry of the particles and the content of the fillers to the dynamic properties.

Introduction

Among various polymers composites, epoxy nanosystems are very important materials for painting, packaging, adhesions, aircraft, space shuttle, electronics products, and many other industrial applications.
A variety of nanofillers namely: Carbon black (CB), carbon nanotubes (CNTs) either single (SWCNT) and/or multiwall (MWCNT), montmorillonite-based organoclays, metal oxides et al. have been widely used to create nanocomposites. Depending on the application, each of the filler has its own advantages and disadvantages in comparison to the others. CNTs for example are unique nanostructured material with remarkable physical and mechanical properties, such as high tensile strength and Young's modulus, as well as high thermal and electrical conductivity. Another illustrative example of nanofiller with unique properties is silica platelets widely used in packaging applications.
In this work, the effect of filler content, the size, the structure and the geometry of the particles and the contribution of the interface region on the dynamic mechanical behavior of epoxy nanocomposites using different fillers (CB, CNT, silica and montmorillonite clay) was investigated.

Experimental

Materials and sample preparation

The pre-polymer D.E.R.332 used in this study is diglycidyl ether of bisphenol A (DGEBA) supplied by Fluka SA, USA. The hardener used was triethylenetetramine (TETA) supplied by Sigma Aldrich, USA.. The extra conductive carbon black (particle size 25-75 nm) was obtained from Degussa, Germany.and the amine modified multiwall carbon nanotubes (average diameter 9.5 nm and average length <1 μm) was supplied by Nanocyl S.A. Belgium. The organically modified montmorillonite clay (Cloisite 25A) was supplied and characterized by Southern Clay USA and the silica CAB-O-SIL EH5 (particle size 0.2-0.3 μm) by Cabot Corporation, USA. All the components of the system are commercial products and were used without any purification. The recipe for sample preparation was presented elsewhere[4].

Methods: DMA Measurements using a Polymer Laboratories dynamic mechanical thermal analyzer MK III operating at a frequency of 10 Hz, a strain of 4x and a scanning rate of 2 ^{0}C/ min were performed from room temperature up to 200 ^{0}C
DSC measurements using a Perkin Elmer Differential Scanning Calorimeter (Pyris 6, DSC) was used under nitrogen atmosphere. The measurements were performed from room temperature to 200^{o}C at a programmed heating rate of 20^{o}C/min.

Results and discussion

The experimental results can be analyzed taking into account the main factors involved like the crosslink density, the size, the shape and the surface modification of the particles , the thickness and the behavior of interface ect. Briefly, the results can be summarized as follow:

A Effect of filler characteristics on T_g,

All T_gs were determined from the maximum temperature of tanδ peak. In general T_gs determined from DSC measurements are a few degrees lower in comparison to DMA ones.

The T_g dependence on the filler-content has as follow:

a) For the DGEBA/TETA/CB system , at low filler contents T_g increases from 132 ^oC for pure resin up to a maximum value 169^oC coresponding to about 0.7 % w/w of filler content and afterwards decreases. This dependence, which was also presented in other system[7] is confirmed by DSC measurements and can be explained taking into account the crosslink density, the free volume and the interface region formed around the nanoparticles.

b) For the DGEBA/TETA/MWCNTs system, T_g decreases slightly with filler content

c) For the DGEBA/TETA/silica system, the results show no significant change in T_g with silica content.

d) For the DGEBA/TETA/Choisite 25A system the results indicate very small decrease in the T_g with increasing concentration up to 20 wt% of Closite 25A.This is in agreement with the results already published[1,2].

B Mechanical Properties

E´ is slightly affected by the filler content in the glassy state and significantly increases in the rubbery one for all composites. In the case with CNTs the effect is more clear.

Tanδ decreases in all cases with filler content, indicating the existence of an interface around the nanoparticle. From some calculations based on tanδ height[5,6], it was found that the thickness of the interface ranges from 2 nm up to 7 nm.

Conclusions

The structure, the geometry, the size of particles, the surface modification, and the filler content influence the thermomechanical properties of epoxy nanocomposites. This dependence of the dynamic mechanical behaviour of the composites is a complex phenomenon, which needs more work to be completely clarified.

References

1. Sun Y., Zhang Z., Moon K.-S., Wong C.P.,J. Pol Sci. Part B: Polymer Physics. **42**, 3849–3858 (2004)
2. Brown J., Rhoney I., Pethrick R.A.: Polymer International, **53**, 2130-2137 (2004)
3. J.K Kim, Hu C.,Woo, R.S.C.,Sham I M-L, Compos Sci and Technol, **65**(6), 805-813 (2005)
4. Th.V.Kosmidou, A.S. Vatalis, C.G. Delides, E. Logakis, P. Pissis, G.C. Papanicolaou' express Polymer Letters **5(2)**, 364-372 (2008**)**
5. E. Vassileva, K. Friedrich, J. Appl. Polym. Sci. **89**(14), 3774-85, (2003).
6. W. K. Goertzen, M.R. Kesler, Cmposites, Part A, **39,** 761-768, (2008)
7. .Y.Breton, G. Desarmot, J. P. Salvetat, S. Delpeux, C. Sinturel, F. Bguin, S. Bonnamy, Carbon, **42**, 1027-1030 (2004).

Poster B23

Study of silicone rubber nanocomposites reinforced with organophilic montmorillonite

A. Voulomenou, P.A. Tarantili
Polymer Technology Lab., School of Chemical Engineering, National Technical Univ. of Athens, Heroon Polytechniou 9, Zografos Athens Greece, GR 15780

ABSTRAC

Poly(dimethylsiloxane) (PDMS) is one of the most interesting high performance elastomer and finds important applications as a composite material containing the appropriate reinforcing fillers, such as aerosilica. It was found that nanoparticles can strongly influence the properties of these composites, even at very low volume fractions, due to the interface characteristics and the subsequent changes in morphology. As a result, the desired property improvement is often achieved low filler volume fractions, which allows nanocomposite (NC) to retain the homogeneity and original density of the polymer. Because of the high cost of aerosilica and its tendency for conglomeration, researchers have focused on the development of other reinforcing fillers such as montmorillonite (MMT), as a candidate aerosilica substitute. In general, polymer nanocomposites containing clays have recently attracted a great deal of interest and, according to the arrangement of the silicate layers in the polymer matrix, can be classified into two categories: intercalated or exfoliated[1-3]. Exfoliated structures are recognized as the recommended morphology for high performance at low clay loadings, but are difficult to be achieved. For this reason, clays are generally modified with ammonium surfactants, as a means to reduce their hydrophilic character and promote miscibility with polymer matrix.

In the experimental part of this work, hydroxyl-terminated PDMS, (Silopren C1,Bayer) was vulcanized using tetrapropoxysilane (TPOS, Aldrich) as crosslinker and dibutyl tin dilaurate (Aldrich) as a catalyst. Cloisite 20A (Southern clay products), which is a natural MMT modified with dimethyl, dihydrogenated tallow ammonium chloride, was used as filler. Aerosil R 972 (Evonic Degussa), a hydrophobic fumed silica treated with dimethyldichlorosilane (specific surface area 130 m^2/g), was also used as reinforcing agent for comparison reasons.

The nanocomposites were prepared by sonicating mixtrures of PDMS with the appropriate amount clay, with an ultrasound probe. The crosslinking system was then added to the mixture and the samples were cast into moulds and cured at room temperature.

The prepared nanocomposite specimens were characterized by X-ray diffraction (XRD) using a Siemens X-ay diffractometer with Cu Kα (λ-1.52Å) radiation source operated at 40 KV and 100 mA.

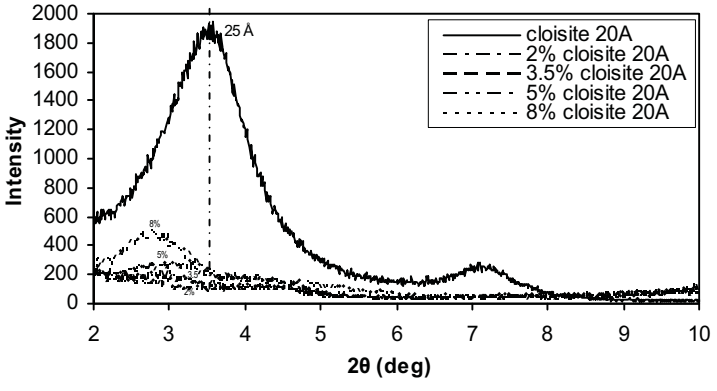

Fig.1: X-ray diffraction patterns of cloisite 20A/PDMS NC.

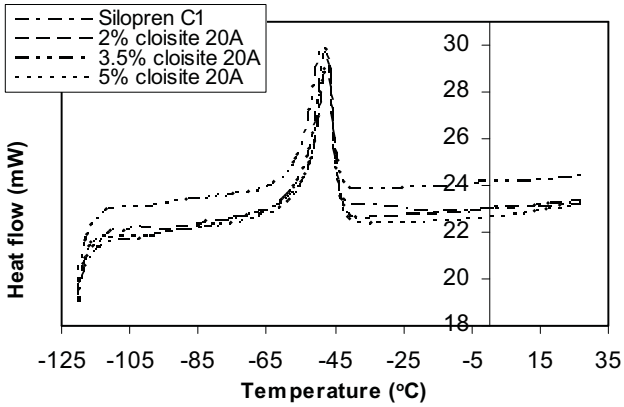

Fig.2: DSC curves of 20A/PDMS NC.

Some XRD patterns of PDMS composites containing various cloisite 20A loadings are shown in Fig. 1. The featureless pattern for loadings of 2 and 3.5 % OMMT suggest that exfoliation or delamination hybrids are present. The thermal transitions were determined using differential scanning calorimeter (DSC) cooled with liquid nitrogen, in an atmosphere of flowing nitrogen. Samples were scanned at a rate of 10 ^{o}C/min over a temperature range from -120 to 50 ^{o}C. Pure PDMS and cloisite 20A NC showed a melting point at -47^{o}C. The incorporation of MMT does not have any obvious effect on the thermal properties of PDMS (Fig.2).
IR spectra of silicone elastomer, pure and filled with different loading of MMT, are presented in Fig. 3. The fading of peaks at 1640 cm^{-1} (attributed to bending vibrations of O-H) reflect the elimination of inorganic water existing in the silicate layers of MMT.

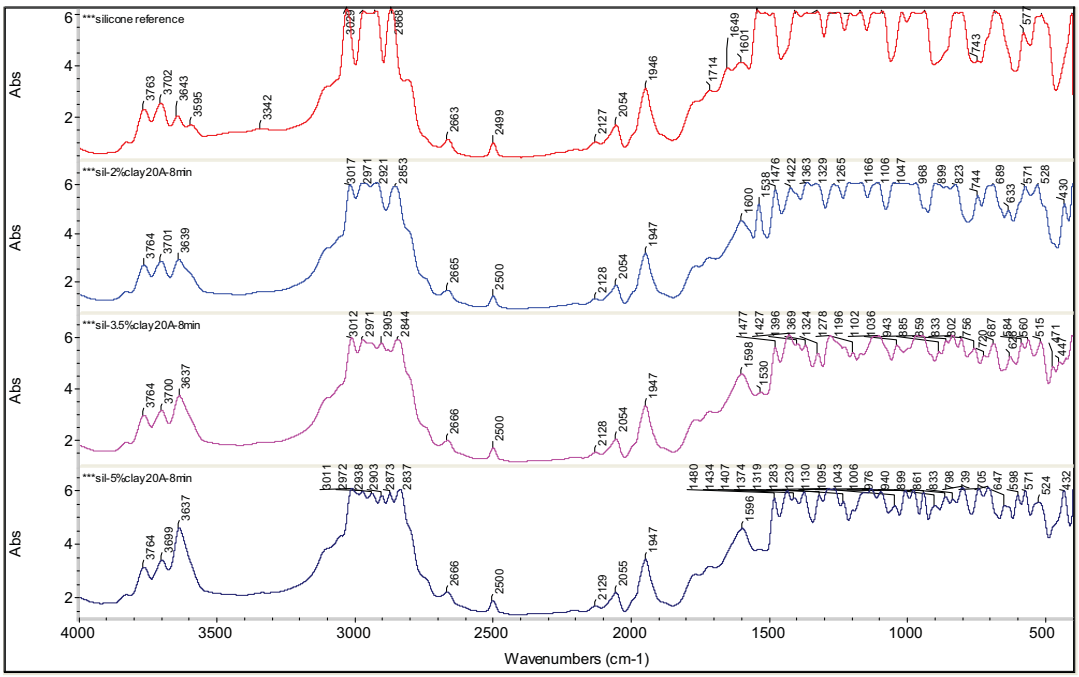

Fig. 3: FT-IR spectra of cloisite 20A/PDMS NC.

Tensile test measurements revealed that the incorporation of cloisite 20A increases the strength (48%) and modulus of elasticity (28%) of silicon rubber. Swelling experiments of PDMS NC immersed in toluene, showed that a decrease of solvent uptake takes place as compared with the unfilled PDMS matrix.
In conclusion, the results of this work showed that hydroxyl terminated silicone rubber containing organic modified MMT as reinforcing agent can produce nanocomposite structures under certain mixing conditions. Chemical characterization of the above nanocomposites revealed interactions between the organic reinforcement and PDMS elastomer, whereas no significant effect in thermal characteristics was observed. When efficiently dispersed, the nanolayer reinforcement improves tensile characteristics and solvent resistance of PDMS.

References

1. Burnside S.D., Giannelis E.P. Nanostructure and Properties of Polysiloxane-Layered Silicate Nanocomposites, *J. Polym Sci: Part B* **38** 1595-1604 (2000)
2. LeBaron P.C., Pinnavaia Th.J. Clay Nanolayer Reinforcement of a Silicone Elastomer, *Chem. Mater.* **13** 3760-3765 (2001)
3.Wang J., Chen Y., Jin Q. Preparation of a Novel Silicone Rubber Nanocomposite Based on Organophilic Montmorillonite, *High Perform. Polym.* **18** 325-340 (2006)

Poster B24

Molecular mobility studies in hybrid PCN clay nanocomposites

P.Maroulas[1*], S.Kripotou[1], P.Pissis[1], A.Fainleib[2], K.Gusakova[2]
[1]*Department of Physics, National Technical University, Zografou Campus, 157 80 Athens, Greece,*
[2]*Institute of Macromolecular Chemistry of National Academy of Sciences, 48, Kharkivs'ke shose, 02160 Kyiv, Ukraine*

[*]Correspondant author : pmaroul@mail.ntua.gr

Polycyanurate resins (PCNs) combine thermal and dimensional stability at solder temperatures, low outgassing, high adhesion to metals, low water absorptivity and low dielectric constant[1], and find many applications in electronics and aerospace industries. Despite their outstanding performance in many areas, their applications are limited because of their brittleness. Many efforts have been taken the last few years to modify the PCN network in a way that it would be less brittle keeping at the same time its outstanding physical properties[2,3]. In previous studies it was found that co-polymerization of cyanate esters with a flexible polymer such as polyoxytretramethylene glycol (PTMG) or polysulfone (PSF) lowers its brittleness but, at the same time, downgrades its mechanical properties. Studies are now moving forward in synthesis of hybrid clay nanocomposites where montmorillonite (MMT) is used as reinforcement material[4]. In the present work the results of molecular mobility studies in hybrid clay nanocomposites based on polycyanurate resins are presented in the frame of the structure-property relationships understanding.

Hybrid clay nanocomposites having as a matrix polycyanurate network modified though co-polymerization with polysulfone (PSF) and modified montmorillonite (I30E). MMT introduced in a solution of the PCN monomer and homogenized by stirring or and using ultrasound. Extraction of solvent follows and then the samples are cured using a step heating program at several temperatures.

Broadband dielectric spectroscopy revealed several relaxation mechanisms and retrieved information about molecular mobility. The techniques used are dielectric relaxation spectroscopy (DRS) in the frequency range of 0.1 to 10^6 Hz at several temperatures (-150^{o}C to 210^{o}C) and the technique of thermally stimulated depolarization currents (TSDC). Differential scanning calorimetry (DSC), performed at a heating/cooling rate of 20K/min, was used in order to study the thermal transitions in the samples, revealing phase separation of all hybrid systems.

1. T.Fang, D.Shimp, *Prog. Polym. Sci., Vol. 20, 1995, 61-118*
2. A.Fainleib, O.Grigoryeva, D.Hourston*, Int. J. Polym. Materials, 51, No* 1-2*,* 2002*, 2781-2791*
3. J.-Y.Chang, J.-L.Hong, *Polymer 42, 2001, 1525-1532*
4. I. Mondragon et al., *Poymer 47, 2006, 3401–3409*

Poster B25

A Theoretical Study on the Size and the Shape of Linear Dendronized Polymers in Good and Selective Solvents

Pavlos Efthymiopoulos, Marios Kosmas, Costas Vlahos

Department of Chemistry, University of Ioannina, 45110 Ioannina, Greece

The large degree of vacancies in the interior of dendritic polymers offer them the ability to encapsulate and release guest molecules which makes them successful delivery vehicles both for drugs but also for other cargos[1]. Their numerous end groups with the capability to be connected to various chemical functionalities at spatially defined locations with a varying degree of accessibility make them find applications in fields like catalysis[2] or solubility[3]. The interesting properties of dendritic polymers can even be better in more complex structures coming from the connection of dendritic polymers with a linear macromolecular chain. Such systems are the linear dendronized polymers[4,5] (LDPs) which are composed of many grafted dendrons emerging at regular intervals on the backbone chain. Their possibility to form objects with controllable dimensions, topology, structure, and chemical functionality on the nanometric scale makes them useful as building blocks in the manufacture of nanomaterials. A challenge is the determination of the way which various parameters affect the conformations of the backbone and the dendrons and thus the size and the shape of these macromolecules.

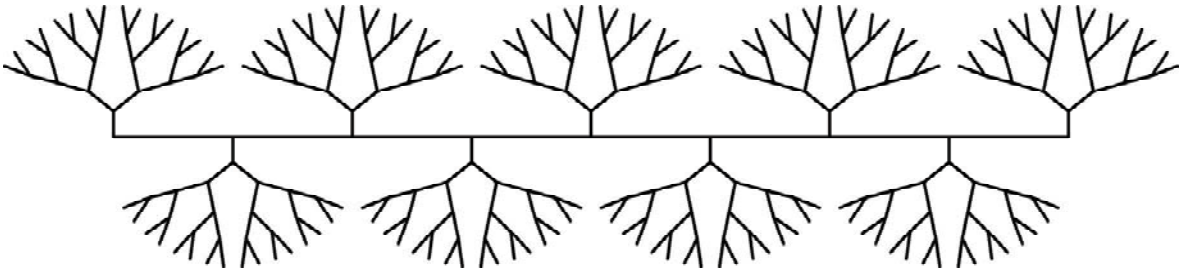

Fig. 1. Schematic representation of a LDP with n=8, g=4 and f=3.

Our previous developed analytical model[6] for dendritic homopolymers with a central core is extended to include dendritic structures emerging from a linear polymeric chain made of units of different chemical nature. In this work we study the ways that the number of dendrons (n+1), their number of generations (g), their branching point functionality (f), the molecular weight of each branch (N_d), the molecular weight of the backbone's spacer between two successive grafting points (N_b) as well as the quality of the solvent for both backbone and grafted dendrons affect the size and the shape of a LDP. Three interaction parameters u_{dd}, u_{bb} and u_{db} are used to describe the intensity of the interactions between two dendron, two backbone, and one dendron and one backbone branching points respectively. Positive and negative values of u's mean repulsions (good solvent) and attractions (poor solvent) respectively, while the value zero represents the Θ solvent conditions.

The expansion factor of the backbone α_b is mainly affected by the quality of the solvent for the dendrons. In a common good solvent the backbone is forced to elongate on increasing g, n and grafting density of the dendrons, while in a dendron selective solvent this extension is slightly smaller. In a backbone selective solvent the LDP collapses, which is caused by the strong attractions between the dendron segments. The expansion factor of the dendrons α_d shows a symmetrical dependence on the position along the backbone with the central dendrons being more affected, extended or shrinked, than the side ones. By choosing specific structural characteristics and solvent environment we can obtain fluctuations in the longitudinal structure of the LDP. In a good solvent the LDP could be described as an elongated cylinder or as a prolated ellipsoid while the expansion of the dendrons in the free space is increasing on increasing g, f and n or on decreasing N_b, but the α_d is much smaller than the α_b. In order to

study the shape of the LDPs we have defined their aspect ratio (*AR*) as the square root of the ratio of the mean square end-to-end distance of the central dendron to that of the backbone. Large and small values of *AR* means spherical and cylindrical shaped LDPs respectively. The *AR* of a LDP in a good solvent shows us that it reaches its cylindrical geometry at smaller values of *g* for larger *f* or grafting densities. In a backbone selective solvent the LPD collapses and adopts a spherical shape after a certain value of *g* or *n*.

References
1. Paleos, C. M.; Tsiourvas, D.; Sideratou, Z. *Mol. Pharm.* **2007**, *4*, 169−188.
2. Helms, B.; Fréchet, J. M. J. *Adv. Synth. Catal.* **2006**, *348*, 1125−148.
3. Gupta, U.; Agashe, H. B.; Asthana, A.; Jain, N. K. *Biomacromolecules* **2006**, *7*, 649−658.
4. Frauenrath, H. *Prog. Polym. Sci.* **2005**, *30*, 325−384.
5. Christopoulos, D. K.; Terzis, A. F.; Vanakaras, A. G.; Photinos, D. J. *J. Chem. Phys.* **2006**, *125*, 204907.
6. Efthymiopoulos, P.; Kosmas, M.; Vlahos, C.; Gergidis L. N. *Macromolecules* **2007,** *40,* 9164−9173.

This work was financially supported by the Greek Secretariat of Research and Technology (grant PENED 03ED856).

Poster B26

ON THE CONFORMATIONAL PROPERTIES OF A DNA CHAIN WITH LOOPS

Marios Kosmas* , Costas Vlahos
Chemistry Department
University of Ioannina
Greece

Abstract

We use statistical mechanics and a grand canonical ensemble to study the conformational properties of a long DNA chain capable to bear the formation of a certain amount of loops. We use a microscopic model where the DNA chain is described by a continuous line. The probability of formation of a loop, after the contact of two sites away along the chain, is based on Gaussian statistics which have been extensively used in the past. Beyond its persistence length it includes also a small length parameter which can describe the local structure of the DNA chain like its helical behavior. Based on this probability an optimum size of the loop is determined in accordance with previous more sophisticated theories and the results of enumerations of ring closures on a DNA chain. The average number of loops which goes as the probability of contact of two sites as well as the average size of the DNA chain are analytically described in terms of the size of the chain the chemical potential of formation of a loop and the largest possible number of loops. Cases with a small number of loops like in DNA various processes where a few sites are brought in close proximity and interact can properly be described. Cases with a larger number of loops leading to an overall expansion or condensation of the chain after the addition of condensing agents, can also be properly described. A comparison with existing experimental data based on single chain observations is included.

References

1)Kosmas, M.K. J. Phys. **A:** Math. Gen. 1981**,** 14,931-943; M. K.Kosmas,M.K. Macromolecules **1990**,23, 2061-2065;Efthymiopoylos,P.;Kosmas,M.;Vlahos,C.; Gergidis L.N. Macromolecules, **2007** ,40, 9164-9173

2)Morgan,M.A.;Okamoto, K.; Kahn,J.D.; English,D.S. Biophysical Journal **2005** **,** 89 , 2588–2596; Saecker,R.M.;Record Jr,M.T..Curr. Opin. Struct. Biol. **2002**,12,311-319;Mehta,R.A.; Kahn,J.D. J. Mol. Biol. **1999** , 294, 67-77;Edelman,L.M.;Cheong,R.; Kahn,J.D. Biophysical Journal **2003**,84 ,1131–1145

3) Sakaue,T. J.Chem.Phys.**2004**, 120, 6299-6305; Miyazawa,N.;Sakaue,T.; Yoshikawa,K.; Zana,R. . J.Chem.Phys.**2005**, 122, 044902-5

Poster B27

COLLAPSE TRANSITIONS IN THERMOSENSITIVE ALTERNATING COPOLYMERS: A MONTE CARLO STUDY

by
Anastassia N. Rissanou [(*,+)], Evangelos Manias[(#)] and Ioannis A. Bitsanis[(*)]

[*]Institute of Electronic Structure and Laser, Foundation for Research and Technology Hellas, GR-711 10 Heraklion, Greece
[+]Molecular Thermodynamics and Modeling of Materials Laboratory, Institute of Physical Chemistry, National Center for Scientific Research "Demokritos",GR-153 10, Aghia Paraskevi Attikis, Greece
[#]Department of Materials Science & Eng., Pennsylvania State University, University Park, PA, USA

Alternating copolymers are expected to exhibit a rich transition behavior in selective solvents. This behavior has implications in life sciences and applications to the design and material selection of thermo and pH-sensitive materials and membranes.
We have studied the transitions of model alternating copolymers via Monte Carlo (MC) simulations. Copolymers of the type $(AAA\ldots)_{n1}(BBB\ldots)_{n2}(AAA\ldots)_{n1}(BBB\ldots)_{n2}\ldots$ with blocks A and B chemically connected were simulated. In this work we study single chains of alternating copolymers in selective solvents. Our results demonstrated that the most important factor, which controls block copolymer response to external stimuli, is their chemical composition (i.e., the thermodynamic competition of the sequential blocks). We focused on the extreme case of a single polymer chain of $N = 1000$ units, distributed in alternate blocks of $n_1 = n_2 = 100$ units (A- and B- blocks). The solvent was quite selective, i.e. A-blocks (500 units) were soluble $E_{AA} = 0.10kT$ (good solvent, almost athermal) whereas, the B-blocks (500 units) were quite insoluble $E_{BB} = 0.45$ (poor solvent). In this case an extended critical region was observed, characterized by the presence of several distinct intermediate states between coil and globules, and by fluctuation strong enough to induce spontaneous transitions among these states.
Our findings underline that, even in a case of very high blockiness, the alternating architecture introduces qualitatively new phenomena. In particular, the collapse transition proceeds through stages not existing in the corresponding homopolymer and di-block copolymer transition.

Poster B28

Molecular dynamics of PAMAM dendrimers and their complexes with linear polymers in aqueous solutions

I.Tanis, K.Karatasos*
Department of Chemical Engineering, Aristotle University of Thessaloniki, 54124 Thessaloniki
e-mail:karatas@eng.auth.gr

The aim of this work was to obtain a deeper insight regarding the mechanisms responsible for the non-covalent complex formation between linear polymers and dendrimers in aqueous solutions at different pH levels of the solution. More specifically, the hydrogen-bonding-driven complexation was examined in detail. This mechanism is experimentally found to play a significant role in several biomedical applications of dendrimers, particularly to those related to their ability to capture/encapsulate substances of pharmaceutical interest for targeting delivery purposes.
To this end we have performed fully atomistic molecular dynamics simulations in aqueous solutions of different generation polyamidoamine PAMAM dendrimers as well as in solutions of their complexes with poly(ethylene oxide) (PEO) chains and studied their responsiveness to different solution pH. Based on titration data, three simulation conditions were designed to represent the effect of pH: no amines are assumed to be protonated above pH 10, all primary amines are protonated at pH 7, and all amines of a dendrimer are protonated below pH 4. Counterions were taken into account to ensure charge neutrality wherever needed.
A detailed description of the behavior of the systems under the above mentioned conditions was accomplished through evaluation of several static and dynamic properties. Both the excluded-volume interactions and the coulombic repulsions between the protonated primary and tertiary amines give rise to a systematic increase in dendrimer dimensions at various protonation levels. These changes in dendrimer size are accompanied by an augmented degree of penetration of solvent molecules within its interior, which appears moderately elevated in complexed systems. Particular attention was paid on the relevant lifetimes of the formed hydrogen bonds. Results indicate that the hydrogen bonds formed between PAMAM amine hydrogens and PEO ether oxygens exhibit longer average lifetimes compared to those formed between water and polymer molecules rendering hydrogen bonding interaction one of the crucial factors governing complex formation. Local scale dynamics was examined through the bond reorientation correlation function. Analysis reveals that full protonation of PAMAM accelerates the relaxation of carbonyl and amine bonds which remain unaffected by the presence of the linear chain. Different behavior was observed in dynamic size fluctuations which were probed by the autocorrelation function of the mean squared radius of gyration. Complex systems exhibit longer relaxation times compared to free linear chain models, an effect that is limited when protonation occurs.

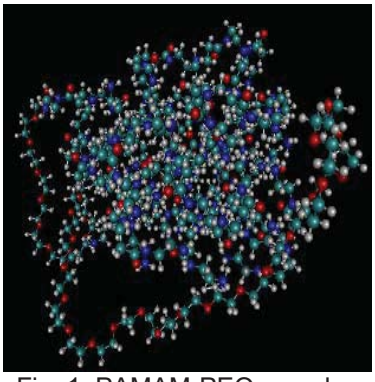

Fig. 1: PAMAM-PEO complex

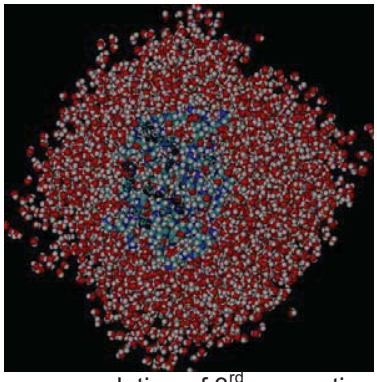

Fig. 2: Aqueous solution of 3rd generation PAMAM

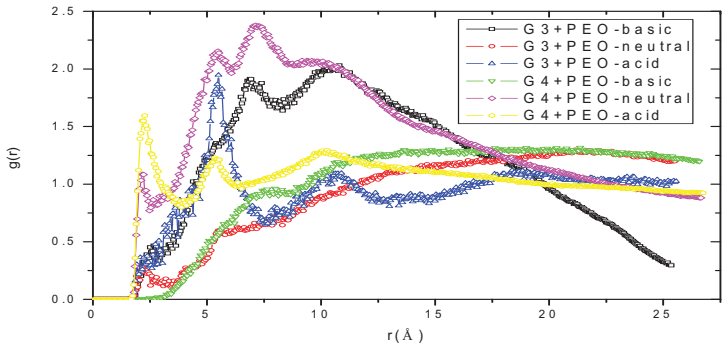

Fig. 3. Radial pair distribution function of amine hydrogen-ether oxygen in complex systems

Acknowledgements
Financial support for this work has been provided by the Greek GSRT / PENED 2003, code number 03EΔ716.

Poster B29

Off Lattice Monte Carlo Simulations of AB and ABA Hybrid Star Dendritic Copolymers

Leonidas Gergidis[1], Othonas Moultos, Costas Georgiadis, Marios Kosmas and Costas Vlahos *

[1]Department of Materials Science & Engineering, University of Ioannina,
Department of Chemistry, University of Ioannina, 45110 Ioannina, Greece

Dendrimers are highly branched macromolecules that are synthesized using a stepwise repetitive reaction sequence. This procedure leads to a very highly monodisperse polymer with a nearly perfect topology radiating from a central core and grown generation by generation. The unique molecular structure of dendrimers with a large number of terminal groups, well defined dimensions, surface and interior offers potential applications in drug delivery systems, gene transfection, molecular containers, chemical catalysis, etc. In solutions, amphiphilic dendrimers designed with lyophobic interior and lyophilic exterior, have size of few nanometers and behaves as unimolecular micelles. The quest for larger self-assembled, self organized systems in order to mimic the nature's wiseness is an intriguing aspect in dendrimer chemistry and physics. Due to the progress in controlled polymer synthesis new dendritic architectures by incorporated linear or star polymer chains are created[1] (Figure 1). These hybrid architectures combine the properties of dendrimers with those of flexible polymers. Hybrid copolymers are often designed to look like macromolecular amphiphilies, with well defined dendritic head that possesses hydrophobic or hydrophilic character and the linear or star chains possesses the opposite character. The addition of linear or star chains will drive the assembly behavior of these polymers in solution, in thin films and in the bulk resulting at first sight to many 'sophisticated' applications.

The conformational properties of hybrid star dendritic copolymers are also important. If we consider the dendrimer as a sphere with radius the mean radius of gyration and star branches with adequate size the hybrid star dendritic copolymers can be modeled as of 'hairy spheres' with linear chains grafted in a spherical surface. Numerical calculations based on the self constistent field theory (SCF) and Monte Carlo simulation results[2] obtained with the cooperative motion algorithm shows that the concentration profile of polymer units are sensitive both to the changes of interface radius and the surface coverage. For fixed chain length the monomer concentration profile changes from concave to convex as the radius of the sphere increases, and that the free chain ends are excluded from the neighborhood of the interface. The Monte Carlo simulations lead to a simple model of the end grafted chains. The first part of them tends to wrap around the sphere, the second gets coiled in the vicinity of the surface and the third forms the outer fraction of the elongated chains.

In previous studies[3] using off lattice Monte Carlo simulations we were able to simulate the conformational properties of dendrimers with polymeric length arms. The radii of gyration of different generations and the whole dendrimer, the end-to-end square distances and various angles which describe the penetration of the end groups in the interior and the vacancies in the interior and exterior regions have been calculated using the efficient Pivot algorithm. Our results were in good agreement with respective analytical and experimental results. In the current paper using the same algorithm we study the conformational properties of the hybrid AB and ABA star dendritic copolymers for various macroscopic states. The influence of the number and the molecular weight of star branches on the conformational averages of dendrimer and on the shape of the hybrid copolymer is studied.

Figure 1

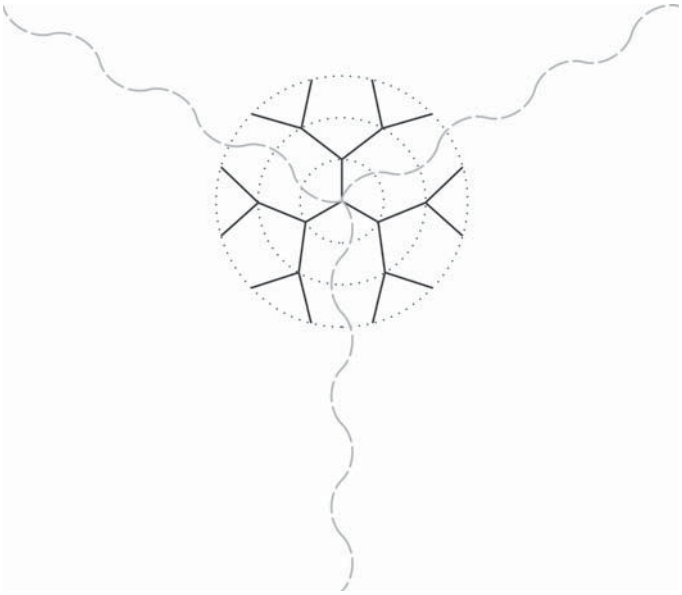

References

1. H. Frauenrath Progress in Polym Sci,2005,30,325.
2. J. Klos, T. Pakula, JCP 2003,118,7682..
3. Rangou, Theodorakis,Gergidis,Avgeropoulos,Efthymiopoulos,Kosmas, Vlahos, Giannopoulos Polymer, 2007,48,652

Poster B30

Neutron reflectivity and computer simulation studies of centrally adsorbed star polymer brushes.

Ioannis Hiotelis[1], Alexandros G. Koutsioubas[1], Nikolaos Spiliopoulos[1], Dimitris Anastassopoulos[1], Alexandros A. Vradis[1], Chris Toprakcioglu[1*], Alain Menelle[2], George Sakellariou[3], Nikos Hadjichristidis[3]

[1]Physics Department, University of Patras, Greece 26500

[2]Laboratoire Leon Brillouin, CEA SACLAY, 91191 Gif-sur-Yvette Cedex, France

[3]Chemistry Department , University of Athens, Panepistimioupoli Zografou 15771, Greece

We have used neutron reflectometry to study the adsorption of polymer brushes formed by star-like polymers with a varying number of arms, attached to a surface via their centre. Polystyrene stars in a good solvent (toluene) were centrally adsorbed onto a quartz substrate by means of a zwitterionic anchor group. Increasing the number of arms resulted in a substantial reduction of the equilibrium adsorbance. Replacement adsorption experiments in which a 3-armed star brush was replaced by linear chains revealed interesting equilibrium and kinetic features related to the architecture of star polymers. These results are compared with scaling theoretical calculations and Monte Carlo simulations of centrally adsorbed star polymers. The main features of the experimental results are reproduced in our simulation study.

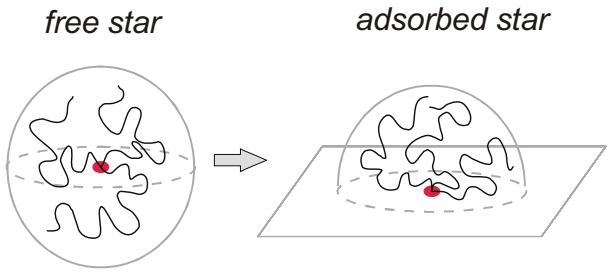

Poster B31

Detection of diffusive jumps of small penetrants dispersed in polymer systems

Theophanes E. Raptis[1], Vasilios E. Raptis[2, 3] and Jannis Samios[4]

[1]*Division of Applied Technology, NCSR "Demokritos" GR–153 10 Athens, Greece.*
[2]*Department of Chemistry, University of Ioannina, GR–451 10, Ioannina, Greece.*
[3]*Department of Materials Science and Engineeering, University of Ioannina, GR–451 10, Ioannina, Greece.*
[4]*Department of Chemistry, Laboratory of Physical and Theoretical Chemistry, University of Athens, Panepistimiopolis GR–157 01, Athens, Greece.*

In this work we report on the development and application of a novel method for analysing Molecular Dynamics simulation trajectories to detect jump events that contribute to the diffusive motion of small penetrant molecules through polymer or other amorphous matrices. The main idea of our method is to consider a time interval Δt that slides along the recorded trajectory, including $N(\Delta t)$ centre of mass positions of each penetrant, which constitute a "swarm" of observation points. Then, the swarm radius of gyration R_G is calculated, taken over all swarm points, and the jump events are identified as peaks observed in the R_G versus time curve.

The method can be further improved to account for the fact that certain jumps are "unsuccessfull" since the penetrant molecule may fail to settle to a neighboring free volume host cavity and instead, it returns to the original one. This possibility is taken into consideration by properly weighting the radius of gyration leading to a definition of jump length, λ, of the form

$$\lambda = \frac{\text{contour length of trajectory from 1 to N}}{\text{distance from 1 to N}} R_G$$

where 1 and N refer to the first and last observation points recorded during the time interval Δt. The weighting factor tends to zero for the molecule returning to its original position and it can be shown to be constant when the time interval value Δt exceeds a certain value. That value can be taken as a reliable measure of the jump duration.

Furthermore, one may calculate the average jump length square for each species diffusing through the polymer matrix and use it to derive a jump-induced self-diffusion coefficient via the formula

$$D_{\text{s, jumps}} = \frac{1}{6} \nu \langle \lambda^2 \rangle$$

where ν is the jump events frequency. This can be compared to the overall self-diffusion coefficient, $D_{\text{s, MSD}}$, calculated via the well known Einstein relation connecting the average mean square displacement, MSD, with time scales. If the latter is substantially larger than the former, this is a strong evidence that other diffusion mechanisms underlying the mass transport process, coexist with the jumps induced penetrant motion.

We have successfully employed the weighted R_G approach in simulations of gaseous alkanes diffusing in n-decane and n-eicosane[1]. Furthermore, we extend our study to amorphous systems of higher molecular weights, i.e. polymers, with gaseous molecules dispersed therein, simulated in the NPT ensemble, at atmospheric pressure and various temperatures well above the polymers melting point. The average jump length and frequency are shown to decrease with penetrant and polymer molecular weight, whereas the smaller values of $D_{\text{s, jumps}}$, with respect to $D_{\text{s, MSD}}$, in several cases, clearly show the coexistence of other contributions, such as smooth translocation, to the overall diffusion process, beyond the jumps mechanism.

References

1. T. E. Raptis, V. E. Raptis, J. Samios, *J. Phys. Chem. B*, **207**, *111*, 13683.

Poster B32

Investigation of Thermodynamic Properties of Polyethylene glycol by Inverse Gas Chromatography and Computer Simulations

G.S. Dritsas, I. Tanis, M. Stournara, K. Karatasos, C. Panayiotou*
Department of Chemical Engineering, Aristotle University of Thessaloniki, 54124 Thessaloniki
e-mail:cpanayio@auth.gr

Inverse gas chromatography is a useful and very versatile method for materials' characterization because it can provide information on thermodynamic properties and surface energy over a wide temperature range, while a combined study with molecular dynamic simulations allows a detailed view of the mechanisms involved in the manifestation of their thermodynamic behavior. The term "inverse" indicates that the stationary phase of the chromatographic column is of interest, in contrast to conventional gas chromatography. The chromatographic column contains the material under study. The method is simple, fast and efficient.

Polyethylene glycol is a water soluble polymer, so it can be used in a wide range of industrial applications, which include adhesives, pharmaceuticals, cosmetics packaging films, paper coatings, textile wraps, and lubricant additives. Also, it is used as a stationary phase for commercial GC columns.

In the present study, inverse gas chromatography and molecular dynamic simulations was applied to investigate thermodynamic and surface properties of polyethylene glycol. Data for weight fraction activity coefficient, Flory-Huggins interaction parameter, total, partial and corrected solubility parameters, dispersive component of the surface free energy, specific free energy of adsorption, as well as acidic and basic parameters were obtained.

Molecular dynamics simulations were performed in a system containing 20 polyethylene glycol chains in the bulk in the above mentioned range of temperatures. Analogous runs were carried out in systems of isolated PEG chains in the gaseous phase. AMBER forcefield was employed in order to provide the energy parameters of the systems. Hildebrand's total solubility parameter as well as Hansen dispersive + hydrogen bonding and polar components were determined. Results show that simulation values lie in relevant agreement with the experimental measurements.

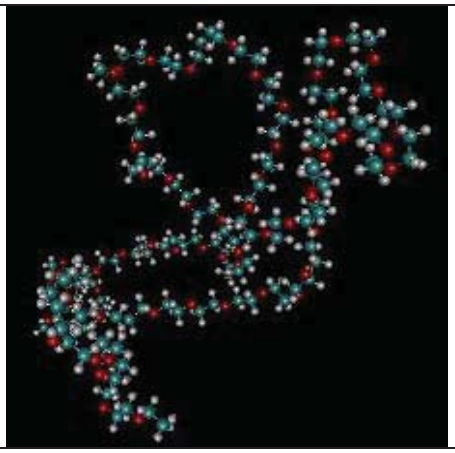

Fig. 1. Atomistic representation of PEG

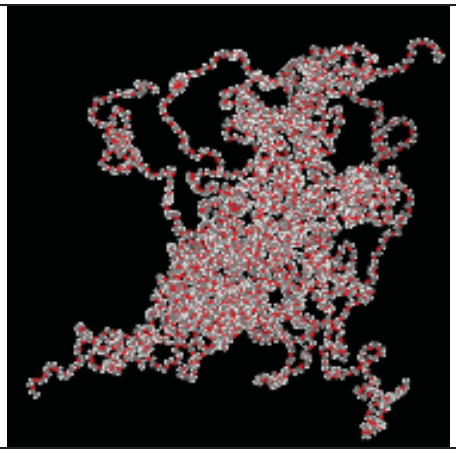

Fig. 2. PEG in bulk configuration

The analysis of the experimental results showed that the solubility parameter had a small decrease with increase in temperature Figure 3. Table 1 showed the relationship of the dispersive

surface energy of PEG with temperature. This is in agreement with earlier results reported by Al-Saigh[1].

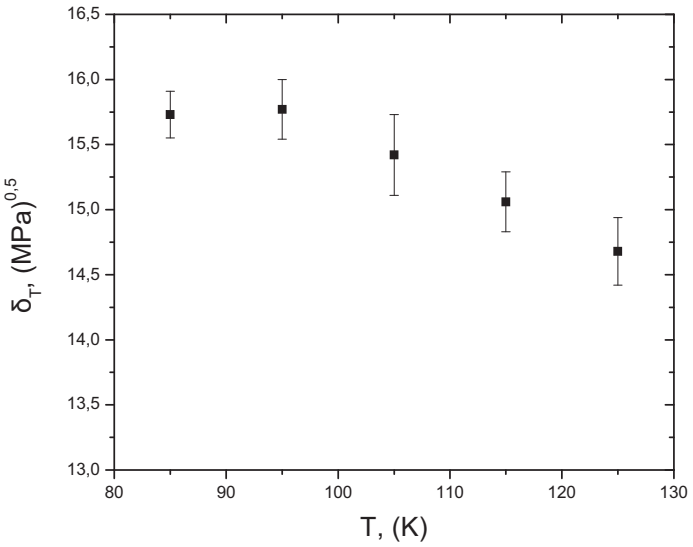

Fig. 3. Influence of temperature on the total solubility parameter, δ_T.

Table 1 Dispersive surface energy of PEG

Temperature (°C)	Surface energy, γ_s^d (mJ m^{-2})
85	21.49 ± 0.34
95	22.46 ± 0.58
105	23.53 ± 0.56
115	23.11 ± 0.81
125	22.76 ± 0.64

Acknowledgements
Financial support for this work has been provided by the Greek GSRT / PENED 2003, code number 03EΔ716.

References

1.Al-Saigh, Z. Y. Polymer 1999, 40, 3479-3485.

Poster B33

Atomistic simulation of the sorption of small gas molecules in polyisobutylene

Georgia Tsolou and Vlasis G. Mavrantzas
Department of Chemical Engineering, University of Patras & FORTH-ICE/HT, Patras, GR26504 Greece
Zoi A. Makrodimitri and Ioannis G. Economou
Molecular Thermodynamics and Modeling of Materials Laboratory, Institute of Physical Chemistry, National Center for Scientific Research "Demokritos", GR-15310 Aghia Paraskevi Attikis, Greece
Rafiqul Gani
CAPEC, Department of Chemical Engineering, Technical University of Denmark, Lyngby DK-2800, Denmark

Motivated by the remarkable properties and the wide applications of polyisobutelene (PIB) in rubber technology, lubrication and biomedical engineering, we have undertaken a systematic investigation of the conformational, structural, thermodynamic and permeability properties of model PIB systems containing up to 320 carbon atoms per chain at temperatures (T) from 600 K down to 300 K by executing long (up to 600 ns) parallel molecular dynamics (MD) simulations.[1] Furthermore, we designed and implemented a hierarchical simulation strategy for the prediction of the solubility of four gases (He, Ar, O_2 and N_2) in PIB and its temperature dependence. The method involves the following three steps: (a) equilibration of model PIB systems at various temperatures through a brute-force application of the parallel MD method by employing a new united-atom (UA) model[1] that correctly reproduces the volumetric, structural and conformational properties of PIB over a range of temperatures, (b) conversion of representative, fully equilibrated configurations from these MD simulations to all-atom (AA) PIB structures and thermal re-equilibration, and (c) sorption computational experiments at various temperatures for the estimation of the solubility parameter of the four penetrants.

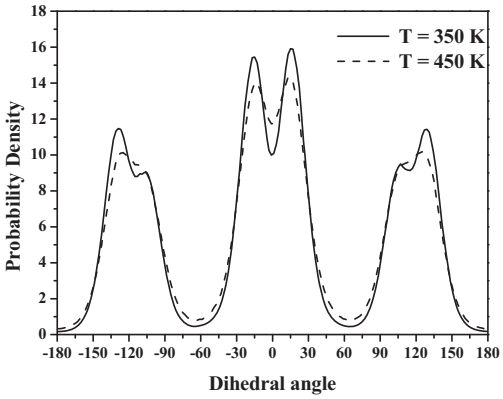

Fig. 1 MD predictions for the distribution of the torsion angles, ϕ, at two temperatures as obtained with the new UA force field introduced in this work.[1]

Proof of the capability of the new UA model to reproduce the correct conformational properties of PIB is given in Figure 1 where the distribution of torsion angles, ϕ, at two different temperatures (350 K and 450 K) is presented. Consistent with previous theoretical studies[2] and explicit molecular dynamics simulations,[3] six characteristic maxima are observed in the plot at ±15° corresponding to the two trans conformational states (t^+ and t^-) and at ±107° and ±128° corresponding to the two gauche conformational states (g^+ and g^-) and their splitting, which is more pronounced at the lower temperatures.[1]

The results of the sorption experiments are summarized in Figure 2 reporting the infinite

dilution solubility coefficient S_o of He, Ar, O_2 and N_2 in PIB as extracted from the present MD simulations with the UA (open circles) and the AA COMPASS force-field[4] (solid circles). Additional data corresponding to available experimental data[5] and macroscopic model predictions[6] have also been added in the Figure. Our results demonstrate that at room temperature O_2 is more soluble in PIB by about two times than N_2, and that He is less soluble than Ar by almost one order of magnitude. They also indicate a rapid decrease in O_2 solubility as the temperature is increased; in contrast, the solubility of N_2 remains practically unaffected. Similarly, the solubility of He increases rapidly with increasing temperature whereas that of Ar decreases. However, Ar remains always more soluble in PIB than He. From Figure 2, it is also clear that the solubility calculations of O_2, N_2 and Ar based on the UA model, although qualitatively correct, significantly overestimate the experimental data[5] and the AA model based simulation results (by a factor of 4 in some cases).

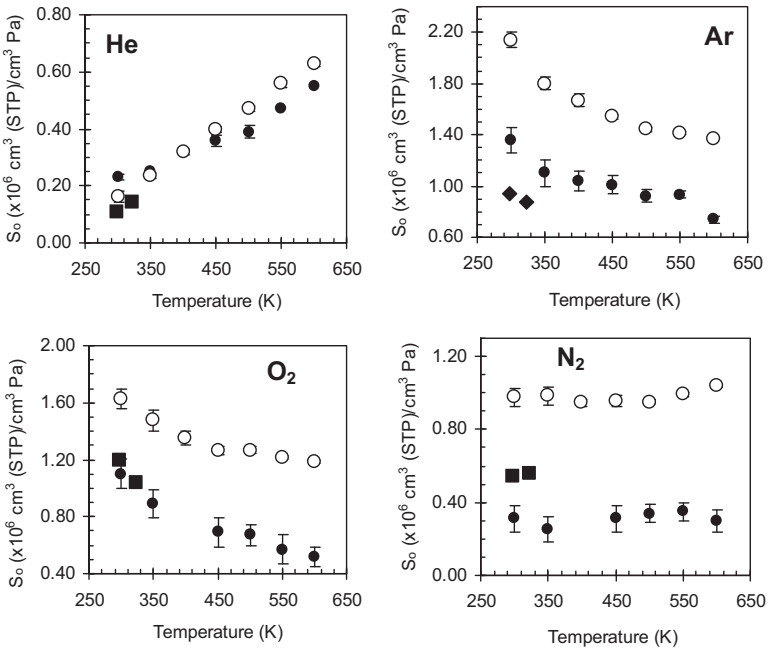

Fig. 2 Infinite dilution solubility coefficient S_o (cm^3(STP)/cm^3 Pa) of He, Ar, O_2 and N_2 in PIB from MD simulations based on a UA force-field (open circles) and the AA COMPASS force-field[4] (solid circles), and comparison with experimental data[5] and macroscopic model predictions.[6]

Currently work is in progress to address the diffusive properties of the four penetrants in PIB as a function of temperature, and the role of molecular packing and energetics on the barrier properties of PIB. This will help us understand why, at a given temperature, PIB exhibits so markedly different permeability properties in comparison to other elastomers such as (e.g.) polyethylene (PE).

References

1.Tsolou, G.; Mavrantzas, V. G.; Makrodimitri, Z. A.; Economou, I. G.; Gani, R. *Macromolecules*, submitted.
2. Suter, U. W.; Saiz, E.; Flory, P. J. *Macromolecules* **1983**, *16*, 1317.
3. Karatasos, K.; Ryckaert, J. P. *Macromolecules* **2001**, *34*, 7232.
4. Sun, H. J. *J. Phys. Chem. B* **1998**, *102*, 7338.
5. van Amerongen, G. J. *J. Polym. Sci.* **1950**, *5*, 307.
6. Thorlaksen, P.; Abildskov, J.; Kontogeorgis, G. M. *Fluid Phase Equilibria* **2003**, *211*, 17.

Poster B34

Studying the Elasticity of Biological Membranes through Theory and Simulations

V.Harmandaris, M.Deserno

Max Planck Institute for Polymer Research, Mainz, Germany

Email: harmanda@mpip-mainz.mpg.de

Biological membranes have been extensively studied in the past using both experimental techniques and simulations [1]. One of the main aspects that can be directly studied with simulation techniques is the curvature elasticity of membranes. The most common approach for measuring bending rigidities in simulations is from the spectrum of equilibrium membrane fluctuations, which is the analogous of the experimental “flicker spectroscopy” technique: by monitoring the fluctuations of vesicles as a function of wavelength by light microscopy the bending modulus, κ, can be determined [2]. Here we present an alternative novel method by measuring the force needed to pull nanoscale bilayer tubes (tethers) from vesicles [3]. Then, the tensile force along a cylindrical lipid bilayer tube is proportional to the membrane's bending modulus and inversely proportional to the tube radius. Using a coarse-grained bilayer model [2] we efficiently obtain bending rigidities that compare very well with complementary measurements based on an analysis of thermal undulation modes.

Membrane proteins can also experience mutual interactions mediated by the lipid bilayer. These occur whenever local protein-imposed changes in some membrane property excite fields which extend beyond their point of imprint. One example is membrane curvature, another is lipid composition. Interactions result because the stresses associated with these fields in turn induce forces on other proteins. By using a combination of coarse-grained simulations and analytical theory we illustrate how such interactions manifest themselves and which consequences they have. For instance, the curvature fields emanating from local membrane curvers can drive their spontaneous aggregation and subsequent vesiculation even in the absence of any direct protein-protein binding. Such physical forces therefore complement and assist specific interactions in their task of controlling protein and membrane organization [4,5].

References

1. “Structure and Dynamics of Membranes”, R. Lipowsky and E. Sackmann (Eds.), Elsevier, Amsterdam, 1995.
2. I.R. Cooke, K. Kremer and M. Deserno, Phys. Rev. E 72, 011506 (2005).
3. V. Harmandaris and M. Deserno, *J. Chem. Phys*. 125, 204905 (2006).
4. B. Reynolds, G. Illya, V. Harmandaris, M. Muller, K. Kremer and M. Deserno, *Nature* 447, 461 (2007).
5. V. Harmandaris, M. Deserno, under preparation.

Poster B35

Structural and Electronic Properties Of Nb Nanowires By Tight Binding Molecular Dynamics Calculations

M. Iakovidis and Ch.E.Lekka*

Department of Materials Science and Engineering, University of Ioannina 45110, Ioannina, Greece

** chlekka @cc.uoi.gr*

The structural and electronic properties of metallic nanowires have been the subject of numerous studies because of the cylindrical geometry and the strong two-dimensional confinement of electrons that make them particularly attractive as potential building blocks for nanoscale electronics and optoelectronics devices. Polycrystalline Nb nanowires templated by carbon nanotubes have shown superconducting properties. Nevertheless, a detailed study concerning the properties of crystalline Nb nanowires (NWs) is still lacking. In this work we present tight binding molecular dynamics calculations concerning Nb NWs with diameters varying from 0.5 to 2.5nm. We found that the NWs oriented along the [111] direction are energetically favored compared to the NWs along the [001] and [110] directions. The calculated electronic density of states revealed significant enhancement at energies around the Fermi level; the energy states of the smallest NWs are well localized, while the metallic character of the NWs increases with the diameter. Finally, with the exception of the smallest NW, we found electronic charge transfer from the surface atoms towards the interior of the NWs, a result that depends on the size of the NWs. These results could offer important information for the conception of nanostructured or nanoscaled materials having improved properties suitable for multiple technological applications.

References

1. A. Marcenkov, Z.Dai, C.Zhang, R.N.Barnett, U.Landman, PRL 98, 046802 (2007)
2. A.Rogachev, A.Bezryadin, APL 83, 512 (2003)
3. A. Rogachev, T.C.Wei, D.Pekker, A.T.Bollinger, P.M.Goldbart, A.Bezryadin, Cond.Mat.0604351 (2006)

Poster B36

Structural and Electronic Properties of Ti And TiO_2 on C Nanotubes by Ab-Initio calculations

M. Gialambouki and Ch.E.Lekka*

Department of Materials Science and Engineering, University of Ioannina 45110, Ioannina, Greece
** chlekka @cc.uoi.gr*

Titanium dioxide (TiO_2) is one of the most important transition metal oxides due to its potential in technological applications like in catalysis and gas sensing. The fabrication of nanoscaled TiO_2 is of considerable interest and recently carbon nanotubes have been used as support to anatase coating. In this work we present Density Functional Theory calculations on Ti and TiO_2 deposition on zig-zag (n,0) Single Wall Nanotubes (SWNTs) (n<10). In particular, we study the early stage adsorption mechanisms and the nature of bonding between the Ti-SWNT and TiO_2-SWNT, as well as its influence on the electronic distribution. We found that the chelation sites depend on the SWNTs diameter, while the system's electronic density of states are also affected by the metallic or semi-metallic nature of the (n,0) SWNTs. For n < 4 nanotubes the Ti adatom binds through d-p hybridization with the two C atoms along the tube axis, while for n > 8 even four C atoms can be bound together. In addition, Ti introduces new energy states at the Fermi level, while this electronic enhancement is due to Ti(d)-C(p) orbital hybridization and depends on the size of the SWNT. The oxygen addition complicates the Ti adsorption introducing anti-bonding hybridizations with the SWNT, while the deposition of a TiO_2 octahedral nanocluster exhibits different electronic properties than those of anatase and rutile. These findings could shed light on the interaction mechanisms and the early growth stages of metallic carbides on SWNT.

References

1. D. Eder, Ian.A.Kinloch, A.H.Windle, Chem.Commun.1448-1450 (2006)
2. X,B,Yan, B.K.Tay, Y.Yang, J.Phys.Chem.B 110, 25844 (2006)

Poster B37

Lithium Ion Induced Nanophase Ordering and Ion Mobility in Ionic Block Copolymers

E. F. Ioannou[1], G. Mountrichas[1], S. Pispas[1], E. I. Kamitsos[1] and G. Floudas[2]
[1]*Theoretical and Physical Chemistry Institute, National Hellenic Research Foundation 48 Vass. Constantinou Ave., 116 35 Athens, Greece*
[2]*Department of Physics and Foundation for Research and Technology-Hellas, Biomedical Research Institute (FORTH-BRI), University of Ioannina, P.O. Box 1186, 45110 Ioannina, Greece*

In recent years interest has been focused on solid-state materials that exhibit enhanced ion transport properties. Among them, polymer solid electrolytes constitute a class of materials of high promise for technological applications including batteries, fuel cells and other electrochemical devices.[1,2] A class of these materials derives from block copolymers.[3] When a lithium-salt-solvating polymer is chosen as one of the block components, continuous, nanoscopic ion-conducting pathways can form. One suitable polymer with ionic groups forming complexes with metal ions is poly(methacrylic acid) (PMAA), the complexation ability of which has been investigated under different experimental conditions.[4,5]

In the present study, diblock copolymers of poly(styrene-*b*-methacrylic acid) (PS-PMAA) of various compositions have been prepared by anionic polymerization and were employed as templates for the development of polymer electrolyte systems. Lithium ions were introduced as the effective component that alters the phase state and contributes to ionic conductivity of the resulted block polyelectrolytes.[6] The local structure, microdomain morphology and ion dynamics of the pure block copolymers and of the block polyelectrolytes were investigated by infrared spectroscopy (IR), small-angle X-ray scattering (SAXS), differential scanning calorimetry (DSC) and dielectric spectroscopy (DS).

Structural aspects at the molecular level were studied by IR as shown in Figure 1, which depicts the infrared spectra of a diblock copolymer acid (SMAA2, M_w=34500, f_{PMAA}=0.23) and of the block polyelectrolytes prepared by neutralizing the acids. Local bonding in the PMAA phase is probed by characteristic stretching vibrations of carboxylic group (1300-1800 cm^{-1})[4,7] because oxygen atoms of this group form the coordination environment of Li^+ cations. Absorption in this region changes progressively as Li^+ ions are introduced in the ionic domains, with most pronounced the decrease of the relative intensity at ca. 1700 cm^{-1}, attributed to ν(C=O) when the carboxylic acid forms hydrogen-bonded dimers, while new bands develop at ca. 1660 and 1548 cm^{-1} as the Li-carboxylate content increases. These bands are attributed to the $\nu_{as}(CO_2^-)$ when carboxylate anions are in two different coordination states with lithium ions, the chelating bidentate (1548 cm^{-1}) and the bridging bidentate (1660 cm^{-1}).[4] Thus, complexation of lithium ions with the carboxylate units involves few ions at low Li-PMAA contents, and aggregates of many ions at higher Li-PMAA contents.

The effect of Li^+ ions on the block polyelectrolyte microdomain morphology was investigated by SAXS as shown in Figure 3. The scattering pattern of diblock SMAA1 (f_{PMAA}=0.13) (Fig. 3a) suggests a spherical structure in the absence of long-range order. Complexation of PMAA with Li^+ ions in SMAA1Li results in chain stretching and hexagonally packed cylinders with long-range order. For SMAA2, which is in disordered phase, complexation with Li^+ leads to the formation of lamellar microdomain morphology with long-range order. Contrary to SMAA1 and SMAA2, complexation of SMAA3 with Li^+ ions does not change appreciably the morphology from disordered phase (Fig. 3c), but chain stretching is observed.

Investigation of dynamics revealed a new dielectrically active process, associated with a local relaxation of Li^+ ions coupled to the PMAA segments. The ionic conductivity of the block polyelectrolytes increased by about three orders of magnitude relative to the corresponding acidic form. It was found that ion motion is bound to PMAA segments and several inter-segmental Li^+ ion hopping events in the channels of the PMAA phase are necessary to explore the whole ionic domain.

The above results show complexation of lithium ions with the carboxylate units of the PMAA phase in two types of coordination (chelating vs. bringing), that alters the phase state of

the copolymers and results in a change from the weak- to the strong-segregation limit. The investigation of dynamics revealed a new dielectrically active process, associated with a local relaxation of lithium ions coupled to the PMAA segments via the two types of coordination. The ionic conductivity of the block polyelectrolytes was found enhanced by about three orders of magnitude relative to that of the parent copolymers. These results contribute to a better understanding of the changes in microdomain morphology, as well as of the ion dynamics in systems resulting from the association of lithium ions with the charged PMAA block.

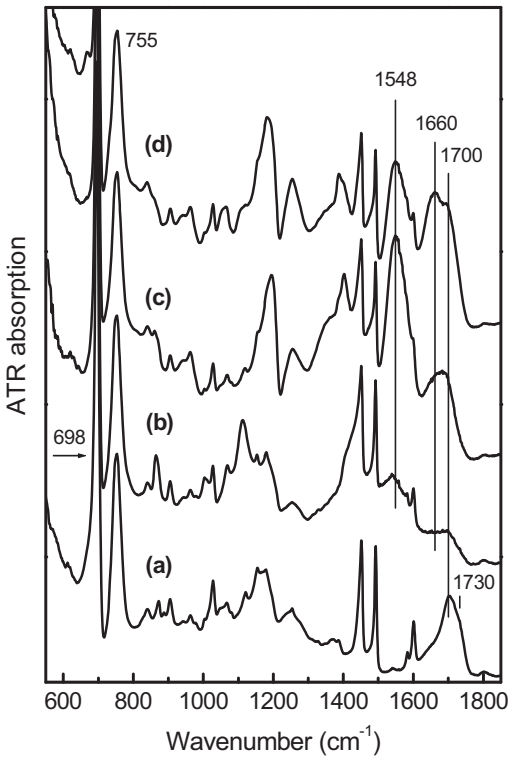

Figure 1

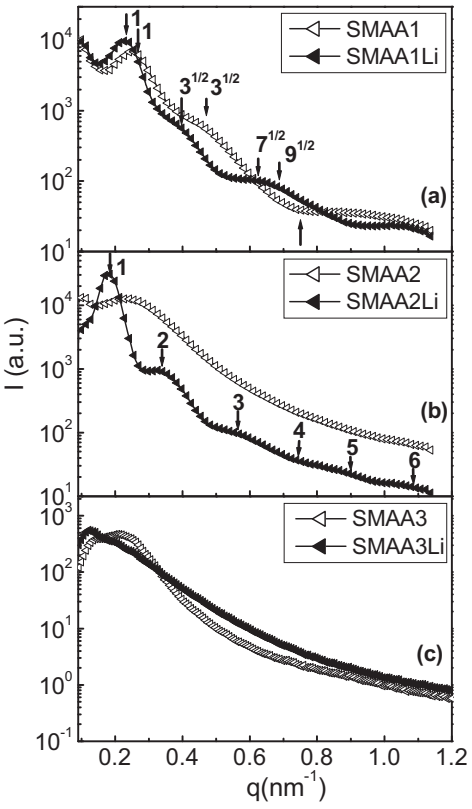

Figure 2

Figure 1. ATR absorption spectrum of the diblock copolymer SMAA2 (M_w=34500, f_{PMAALi} =0.23) (a), and of the block polyelectrolytes resulted from the introduction of Li^+ ions in the PMAA phase; (b) SMAA1Li (M_w=45500, f_{PMAALi}=0.14); (c) SMAA2Li (M_w=35400, f_{PMAALi}=0.25); (d) SMAA3Li (M_w=30300, f_{PMAALi}=0.37). All spectra are scaled on the 698 cm^{-1} band and offset to facilitate comparison.

Figure 2. SAXS curves from the diblock copolymers and the resulted block polyelectrolytes; (a) SMAA1 (f_{PMAA}=0.13): arrow indicates peak at positions $1:3^{1/2}$ relative to the main peak, SMAA1Li (f_{PMAALi} =0.14): arrows indicate peaks at positions $1:3^{1/2}:7^{1/2}:9^{1/2}$ relative to the main peak (the up arrow in the Figure gives the form factor minimum); (b) SMAA2 (f_{PMAA}=0.23): in disordered phase, SMAA2Li (f_{PMAALi}=0.25): arrows indicate peaks at positions 1:2:3:4:5:6 relative to the main peak; (c) SMAA3 (f_{PMAALi}=0.35): in disordered phase, SMAA3Li (f_{PMAALi}=0.37): in disordered phase.

References

1. Chandrasekhar, V. *Adv. Polym. Sci.* **1998**, 135, 139-205.
2. Tarascon, J. M.; Armand, M. *Nature* **2001**, 414, 359-367.
3. Soo, P. P.;Huang, Y. I.; Olugebefola, S.; Chiang, Y. M.; Sadoway, D. R.; Mayes, A. M. *J. Electrochem. Soc.* **1999**, 146(1), 32-37.
4. Konradi, R.; Rühe, M. *Macromolecules* **2004**, 37, 6954-6961.
5. Walters, R. M.; Sohn, K. E.; Winey, K. I.; Composto, R. J. *J. Polym. Sci. Part B: Polym. Phys.* **2002**, 41, 2833-2841.
6. Ioannou, E. F.; Mountrichas, G., Pispas, S.; Kamitsos, E. I.; Floudas, G. *Macromolecules*, submitted.
7. Painter, P. C.; Brozoski, B. A.; Coleman, M. *J. Polym. Sci.: Polym. Phys. Ed.* **1982**, 20, 1069-1080.

Poster B38

Reversible self-assembled nanostructures from block polyampholytes

Christos Mantzaridis, Stergios Pispas
Theoretical and Physical Chemistry Institute, National Hellenic Research Foundation, 48 Vass. Constantinou Ave., 11635 Athens, Greece

Polyampholytes are a family of polymers that not only contain a charge per monomeric unit like simple polyelectrolytes, but additionally bear opposite charges within their chains. This feature affects and dictates the physical behavior of polyampholytes significantly. The field of polyampholytes research has drawn considerable attention[1,2,3,4] due to their behavioral similarities with biological macromolecules (e.g. proteins). Apart from their academic interest polyampholytes are used in a variety of applications, from petroleum extraction to additives in industry [2]. Lately, research has been focused in the development of block polyampholytes, where each block of the copolymer bears different charges, due to the large variety of self-assembled nanostructures that can be obtained in solutions of such macromolecules.

In this work we report on the synthesis and the solution self-assembly properties of novel diblock polyampholytes based on poly(2-vinylpyridine), P2VP, and poly(sulfamate-carboxylate-isoprene), SCPI. The precursor block copolymers for the polyampholytes, are PI-b-P2VP diblock copolymers, which were prepared by living anionic polymerization high vacuum techniques, utilizing a sequential addition scheme for isoprene and 2 vinylopyridine polymerization. After the polymerization a two step reaction was utilized in order to produce the polyampholytes, involving the reaction of the PI block with chlorosulfonylisocyanate, followed by alkaline hydrolysis (Scheme 1).

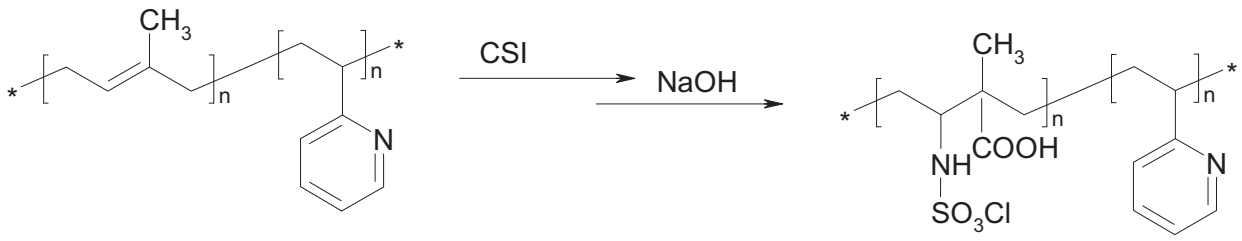

Scheme 1: Functionalization reaction for the formation of SCPI-P2VP block polyampholyte.

The behavior of the resulting polyampholytes was investigated in aqueous solutions at varying pH values. The experiments proved that the self-assembly of the new polyampholytes is pH dependent. Characteristic results from light scattering experiments are depicted in figure 2. In figure 2a the light scattering intensity is monitored with respect to solution pH. A decreasing trend is observed as the pH is becoming alkaline, denoting a decrease in the mass of the aggregates. On the contrary in figure 2b an increasing trend for the hydrodynamic radius, R_h, of the aggregates is observed. This behavior can explained with the hypothesis that at lower pH values, where P2VP is protonated, complexes are formed in the solution of the polyampholytes, due to electrostatic attraction between the oppositely charged blocks. As the solution pH shifts to higher values, these complexes seem to disassociate and the polymeric chains adopt a core-shell micellar structure with a P2VP uncharged (hydrophobic) core and a CSI-PI charged corona. The nanostructures were found to be reversible to changes in pH.

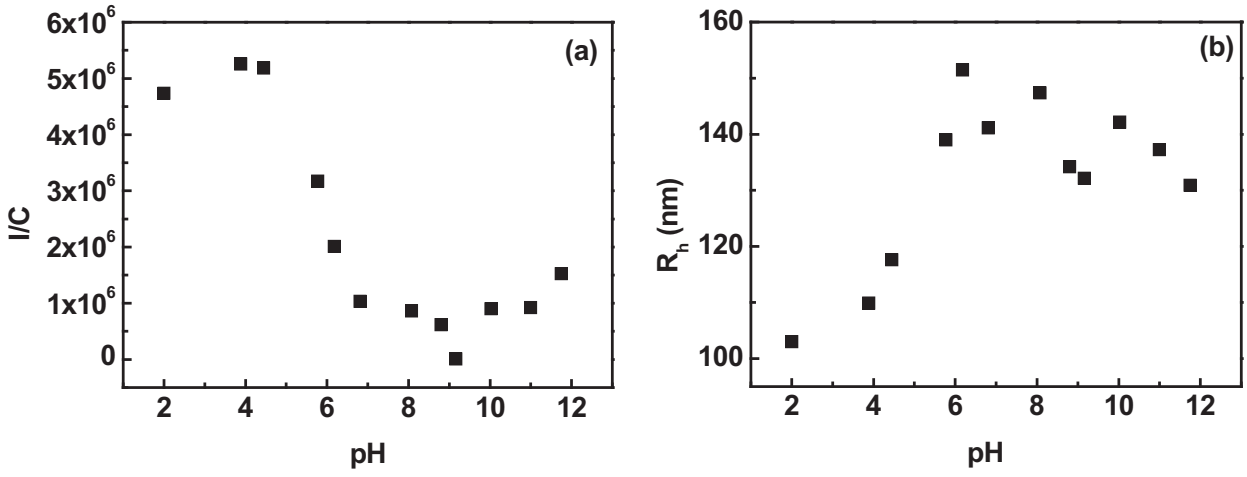

Figure 2: (a) Light scattering intensity vs pH and (b) R_h vs pH for sample SCPI-P2VP-1.

Additional experiments including fluorescence spectroscopy and atomic force microscopy support this hypothesis and give additional information regarding the structure and the microenvironment of the self-assembled nanostructures.

References
1. J. Bohrish, C. D. Eisenbach, W. Jaeger, H. Mori, A. H. E. Muller,M. Rehahn, C. Schaller, S. Traser, P. Wittmeyer Adv. Polym. Sci. (2004), 165, 1.
2. A. V. Dobrynin, R. H. Colby, M. Rubinstein, J. Polym. Sci. Part B (2004), 42, 3513.
3. A. Ciferri, S. Kudaibergenov, Macromol Rapid. Commun. (2007), 28, 1953.
4. A. Ciferri, S. Kudaibergenov, Macromol Rapid. Commun. (2007), 28, 1969.
5. R. G. Ezell, C. L. Macormick, J. Appl. Polym. Sci. (2007), 104, 2812.

Poster B39

Self-assembly in mixed amphiphilic diblock copolymers-zwitterionic surfactants aqueous solutions

K. Dimitroulopoulos, S. Pispas
Theoretical and Physical Chemistry Institute, National Hellenic Research Foundation, 48 Vass. Constantinou Ave., 11635 Athens, Greece

Amphiphilic block copolymers have been the focus of much interest during the last 30 years because of their ability to self assemble in aqueous media, leading to a creation of nanoscale micellar structures, as a result of the microphase separation between the two blocks of the copolymer.[1] The size, shape and morphology of these structures depend on the molecular weight of the two different blocks, and also on the chemical identity and the composition of the comonomers. Predicting the characteristic sizes and morphologies of these nanostructures has been an intense topic of investigation from both the theoretical and experimental points of view.

Addition of secondary species such as surfactants in the system of a diblock copolymer leads to copolymer-surfactant mixed aggregates. Mixed systems of amphiphilic copolymers and surfactants have been studied throughout the years giving interesting results concerning the aggregation behavior of block copolymer mixed assemblies. [1,2]

In the current study we discuss the interactions between an amphiphilic poly(isoprene-b-ethylene oxide) diblock copolymer (PI-b-PEO) and two zwitterionic surfactants that take place in aqueous media. The PI-b-PEO diblock copolymer used in this study was synthesized by anionic polymerization high vacuum techniques and has well defined molecular characteristics and a narrow molecular distribution. The characterization of the copolymer was realized by size excluding chromatography (SEC), ^{1}H NMR spectroscopy and light scattering techniques. The zwitterionic surfactants used in the mixed system are dimethyldodecylammoniopropane sulfonate ($DC_{12}APS$) and N,N-Dimethyl-N-dodecylglycine betaine (EMPIGEN®), whose micellar properties are known.[3]

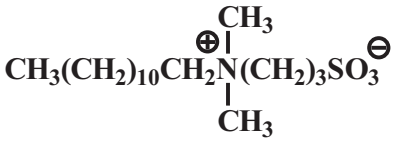

$DC_{12}APS$

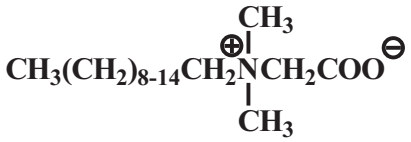

EMPIGEN

Figure 1. Chemical structures of the surfactants utilized in this study.

A series of mixed polymer/surfactant aqueous solutions were prepared and investigated utilizing static and dynamic light scattering. In one of the series of mixed solutions the concentration of the polymer was kept constant, while the concentration of the surfactant gradually increased, within a region of concentrations below and above the surfactant's critical micelle concentration. In the second series the surfactant concentration was kept constant and the polymer concentration was varied.

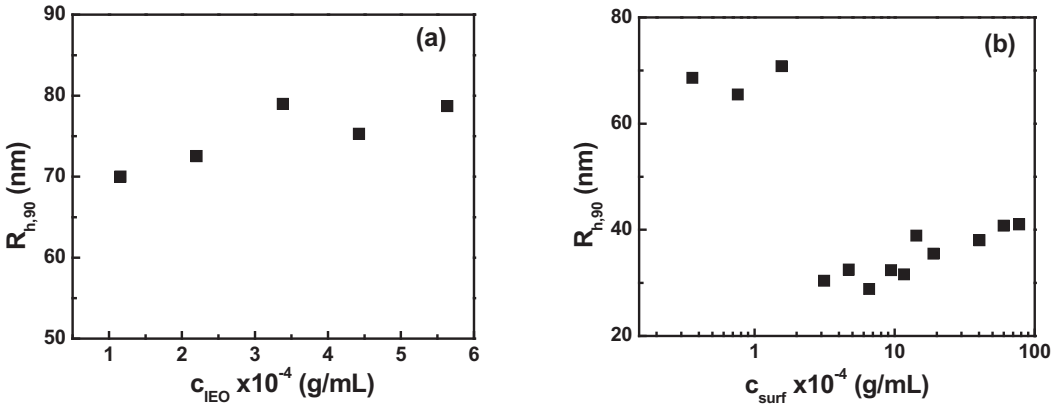

Figure 2. a) Hydrodynamic radii versus copolymer concentration, and b) hydrodynamic radii versus surfactant concentration for PI-b-PEO/DC_{12}APS mixed solutions.

Representative results from DLS measurements are shown in Figure 2, showing that substantial interaction occurs between the block copolymer micelles and the surfactant as indicated by the change in size, and probably in the morphology, of the nanoassemblies.

Zeta potential measurements of the same series of mixed solutions show the existence of negative charges on the surface of the complexes for low concentrations of the zwitterionic surfactant (DC_{12}APS) and practically no charge at higher concentrations. Further investigations are in progress in order to elucidate the effects of temperature, ionic strength, pH and molecular weight and composition of the block copolymer on the characteristics of the self-assembled structures in the mixed solutions.

References

1. P. Alexandridis, B. Lindman, Eds *Amphiphilic Block Copolymers. Self Assembly and Applications*, Elsevier: Amsterdam, 2000.
2. N. V. Sastry, H. Hoffmann Colloids Surf. A 2004, 250, 247.
3. K. W. Herrmann, J. Colloid Interface Sci. 1966, 22, 352.

Poster B40

Self assembly core-shell PCL-co-PSu nanoparticles based on crystalline amorphous moieties for efficient controlled drug release

Sofia Papadimitriou[1], Dimitrios Bikiaris[1], Kostantinos Avgoustakis[2]

[1]*Laboratory of Organic Chemical Technology, Department of Chemistry, Aristotle University of Thessaloniki, GR- 541 24, Thessaloniki, Macedonia, Greece.*

[2]*Laboratory of Pharmaceutical Technology, Department of Pharmacy, University of Patras, Rio, 26500, Patras, Greece.*

Introduction.

During the past few decades there has been an increasing interest in the development of biodegradable nanoparticles for effective drug, peptide, protein and DNA delivery[1]. Incorporation of the drug into a particulate carrier can protect the active substance against degradation, offers possibilities of targeting, improves the therapeutic effect, prolongs the biological activity, controls the drug release rate and decreases the administration frequency[2]. Polycaprolactone is a biodegradable and biocompatible material with the advantage of being high permeable from drugs which makes it an important candidate for drug delivery applications. However polycaprolactone has a slow rate of biodegradation in human tissue due to its high degree of hydrophobicity and crystallinity. In order to overcome these problems it is essential to modify polymer properties in a way that will meet specific and desirable requirements. The most common and easy way is copolymerization. Copolymers are widely used for the preparation of drug loaded nanoparticles. New matrices of poly(ε-caprolactone)-co-(propylene succinate) were synthesized and characterized. The application of these copolymers as potential nanoparticulate drug carriers of Tibolone drug was evaluated by examining the physicochemical characteristics of nanoparticles and the in vitro drug release.

Experimental.

Synthesis of polyesters

PCL-co-PSu copolymers with various molar ratios, such as 97.5/2.5, 5/95, 10/90, 25/75 w/w, were prepared by the two-stage melt polycondensation method (esterification and polycondensation) according to the procedures described by Seretoudi et al[3].

Polymer characterization

The intrinsic viscosities [η] were calculated using the Solomon-Ciuta equation[4]. Molecular weight determinations were performed by GPC. ^{1}H-NMR and ^{13}C-NMR spectra of polyesters were obtained. Differential scanning calorimetry (DSC) as well as X-Ray Diffractrometry (XRD) was used for the identification of the thermal and physical properties of the copolyesters. Biodegradation and in vitro biocompatibility studies for copolyesters were also performed.

Preparation of PCL-co-PSu nanoparticles

Nanoparticles were prepared by o/w solvent evaporation method. Copolymer (100mg), and Tibolone (10mg) were dissolved in CH_2Cl_2. This solution was transferred to an aqueous solution of sodium cholate and probe sonicated for 1min[5].

Characterization of Nanoparticles

The morphological examination of nanoparticles were performed using transmission electron microscope (TEM) and scanning electron microscopy (SEM). The particle size distribution of nanoparticles was determined by dynamic light scattering (DLS). The nanoparticle yield, drug loading and drug entrapment efficiency were also calculated. FT-IR spectra of freeze dried nanoparticles were obtained. XRD was used for the identification of the crystal (structure and changes) of the polymers and also drug in case of nanoparticle samples. In vitro drug release studies were also performed. Dissolution Apparatous II basket method was used (37^{0}C). Drug-loaded nanoparticle suspensions were placed in a dialysis cellulose membrane bag, with a molecular weight cut-off 12.400, tied, and placed into the baskets. At predetermined time

intervals 4 mL of aqueous solution was withdrawn from the release media. The samples were filtered and the quantitation analysis was performed using HPLC method and an appropriate calibration curve.

Results and Discussion.

From copolymers characterization it was found that increasing the PPSu ratio the melting point and the crystallinity of copolymers decreases. The copolyesters shows a fast biodegradation rate also PPSu polymer as well as copolymers exhibited low toxicity against HUVEC cells The size of the nanoparticles and the nanoparticle yield are also affected from the ratio of PPSu. As the ratio of PPSu is increased the size is reduced, as was verified from DLS measurements, from 188 nm for neat PCL to 152 nm for PCL/PPSu 75/25 w/w and the yield of nanoparticle formation is increased from 58.9 for PCL to 85.91 for PCL/PPSu 75/25 w/w. SEM photographs showed that the drug-loaded nanoparticles had a discrete spherical shape with a diameter about 180 nm or less, a fact that is in agreement with the measurements of dynamic light scattering. From TEM micrographs it was found that the crystalline phase of PCL is placed at the shell of nanoparticles, while amorphous PPSu forms the core. XRD patterns, FT-ir spectra and TEM of the corresponding samples of nanoparticles verified that Tibolone appears as nanocrystals dispersed in the nanoparticles, mainly in the amorphous core. The dissolution studies revealed that increasing the PPSu ratio in copolymers, the dissolution rate of the drug decreases.

References

1. G Barratt, CMLS, Cell. Mol. Life Science, 60 (2003) 21-37
2. Patrick Couvreur, Christine Vauthier, Pharmaceutical Research, Vol 23, No 7, July 2006
3. G. Seretoudi, D. Bikiaris and C. Panayiotou, Polymer, Volume 43, Issue 20, 1 September 2002, Pages 5405-5415.
4. Solomon, O.F; Ciuta, I.Z. J Appl Polym Sci 1962, 6, 683
5. K. Avgoustakis, A. Beletsi, Z. Panagi, P. Klepetsanis, A.G. Karydas, D.S Ithakisios, Journal of Controlled Release 79 (2002) 123-135.

Poster B41

Formation of Gold Nanoparticles in the Corona of Di- and Triblock Copolymers

Meristoudi A.[1,2], Pispas S.[1], Vainos N.[1,2]

[1]*Theoretical and Physical Chemistry Institute, National Hellenic Research Foundation, 48Vass. Constantinou Ave., Athens 11635, Greece*
[2] *Materials Science Department, University of Patras, Patras 26504, Greece*

Gold nanoparticles have received great attention since they exhibit significantly different properties from those of bulk material, depending on their size, morphology or the surrounding medium.[1] These properties, such as the catalytic behavior or the optical properties,[2] make metal nanoparticles potential candidates for photonic devices, biosensors, nanoreactors and useful in biomedical applications. Gold nanoparticles can be also formed in the micelle cores of amphiphilic block copolymers. However, some of the properties that gold nanoparticles display are inhibited because they are embedded in the dense micellar core. In order to avoid this, gold nanoparticles could be fixed in the corona of polymeric micelles[3].

In this work, we utilized poly[(sodium sulfamate-carboxylate-isoprene)-b-tert-butylstyrene] (CSI-BSI) diblock copolymer and poly(methacrylic acid)-b-poly(styrene)-b-poly(methacrylic acid) (MA-S-MA) triblock copolymer, synthesized by anionic polymerization, for the synthesis of Au nanoparticles in water. For both systems, H_2O is a selective solvent for one of the blocks, leading to the formation of well-defined micelles consisting of a hydrophobic core and a hydrophilic corona. Furthermore, stoichiometric equivalents of $HAuCl_4$ were added to each solution, as the metal precursor, which were preferentially dissolved and coordinated to the corona of each micelle and subsequently reduced, by the groups of the corona block, to Au nanoparticles (fig. 1). The systems, which were of good colloidal stability, were investigated by dynamic light scattering (DLS), an in situ characterization technique, at all stages of nanoparticle synthesis in order to extract information on the structural transformations taking place in the solutions. Additional information on the structure of the hybrid systems, on polymer-inorganic material interactions and metal nanoparticle characteristics were gathered by attenuated total reflectance Fourier transform infrared spectroscopy (ATR-FTIR), UV-visible spectroscopy, and atomic force microscopy (AFM).

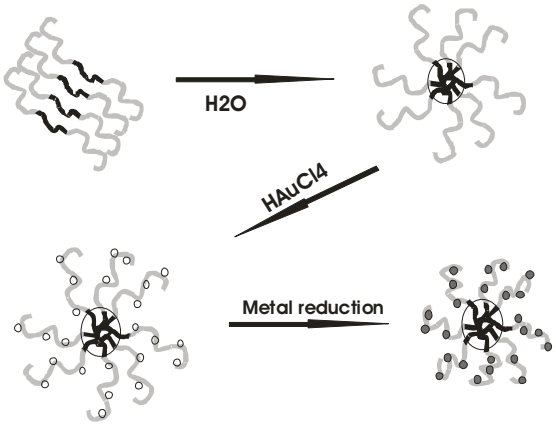

Fig. 1: Schematic showing the preparation protocol for metal nanoparticle/block copolymer hybrid assemblies for the case of MA-S-MA block copolymers in H_2O.

In figure 2a, the distribution of hydrodynamic radii for the CSI-BSI sample in H_2O is shown. Two distinct diffusing species are present. The one with a hydrodynamic radius of 73nm should be attributed to block copolymer micelles, while that with an R_h=11nm to unimers. After the addition of either 0.25 or 0.5equiv. of $HAuCl_4$, which was subsequently reduced to metallic Au, the R_h of the micelles was reduced to 47nm, while the intensity of the unimers peak was decreased. The DLS results of the MA-S-MA/Au complex system are presented in figure 2b. Accordingly, after the dissolution of MA-S-MA triblock copolymer in H_2O, a single population with an R_h= 111nm was observed. However, in the presence of gold nanoparticles a decrease in the size of the micelles was observed (R_h=67nm for the addition of 0.5equiv. of gold) and a population with

R_h=16nm was also present in this case. The peak may originate from the presence of small gold nanoparticles surrounded by single copolymer chains.

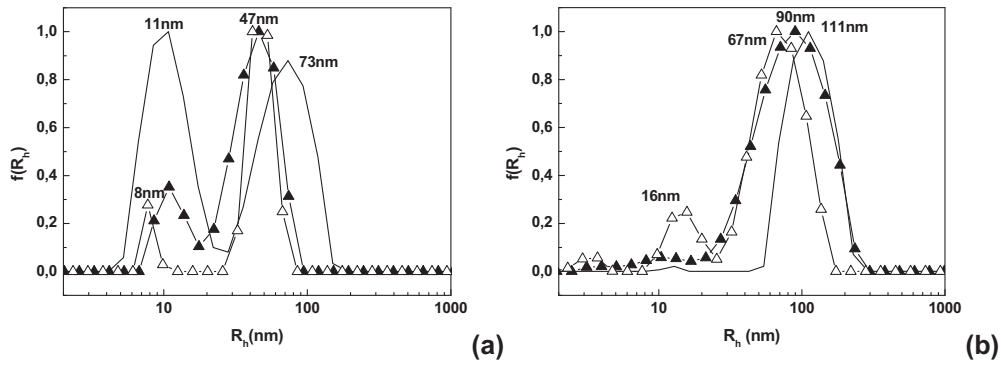

Fig. 2: Hydrodynamic radius distribution of a) CSI-BSI block copolymer before (solid line) and after addition of 0.25 or 0.5 equiv. of gold nanoparticles (closed and open triangles respectively) and b) MA-S-MA tri-block copolymer before (solid line) and after addition of 0.25 or 0.5 equiv. of gold nanoparticles (closed and open triangles respectively)

A representative UV-vis spectrum of CSI-BSI solution containing gold nanoparticles is presented in figure 3. The absorption band at ~540nm was attributed to the surface plasmon resonance of gold nanoparticles. The absence of a pronounced second peak in the region of 700nm to 1100nm indicates that the gold nanoparticles are nearly spherical[1] and their morphology is uniform. Their size should be relatively small (ca. 5 nm).[4]The pure block copolymer solutions do not show absorption peaks in this region. Altering the ratio between the CSI units and the metal precursor led to a shift of the absorption spectra. Decreasing the quantity of the metal salt, both the intensity of the absorption band and λ_{max} decreased and consequently the size of the gold nanoparticles decreased (ca.3 nm)[1,4]. Similar trends were observed in the case of MA-S-MA copolymer solutions.

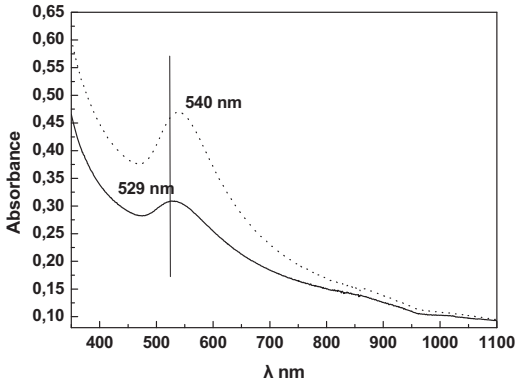

Fig. 3: UV-vis spectra of CSI-BSI/Au 4:1 (solid line) and CSI-BSI/Au 2:1 (doted line) hybrid solutions.

The systems described above, can be regarded as potential nanocarriers of different agents[3], since they display different chemistry in their core and corona.

References

1. Eustis, S.; El-Sayed, M.A. Chem. Soc. Rev. 2006, 35, 209
2. Thomas, K.G.; Kamat, P.V. Acc. Chem. Res. 2003, 36, 888
3. Chen, X.; Liu, Y.; An, Y.; Shi, L.Macrom. Rapid Commun. 2007, 28, 1350
4. Liu, J.; Raveendran, P.; Shervani, Z.; Ikushima, Y.; Hakuta, Y. Chem. Eur. J. 2005, 11, 1854

Acknowledgements The Greek General Secretariat for Research and Technology, Ministry of Development, is acknowledged for the PENED NYBRIPHOS grant (No 03EΔ888).

Poster B42

Charge Transport of Conjugated Polymer Coated Core-Shell Nanoparticles

Mpoukouvalas K.[1], Wang J.[1], Sun L.[1], Wei C.[1], Beierlein, T.[2], Muehlebach, A.[3], Bonaccurso E.[1], Butt H.-J.[1], Wegner G.[1]

[1] *Max Planck Institute for Polymer Research, Ackermannweg 10, 55128 Mainz, Germany*
[2] *CSEM - Centre Suisse d'Electronique et de Microtechnique SA, Divison Photonics - Polymer Optoelectronics, Badenerstrasse 569, CH-8048 Zurich, Switzerland*
[3] *Ciba Specialty Chemicals Inc. Group Research, K-420.3.15, Klybeckstrasse 141, CH-4002 Basel, Switzerland*

Conjugated polymer[1] coated latex particles have found intense interest since they have first been reported in 1987.[2] A conventional nonconducting core polymer renders the composite film-forming ability and the formed film transparency and flexibility, while a thin conjugated polymer shell is required to obtain particles with useful electrical features. We have synthesized redispersible polypyrrole (PPy) core-shell nanoparticles with a nonconductive polymer core and a polystyrene sulfonate (PSS) shell loaded with PPy and investigated their application as hole injection layers in PLEDs.[3] *I-V-L* plots of the PLED device reveals comparable performance with the one from the Poly(3,4-ethylenedioxythiophene) PEDOT/PSS. As such, conjugated polymer coated core-shell nanoparticles could be a promising candidate for printable electronics.

Morphology and charge transport of the PPy embedded in our core-shell nanoparticles are of paramount importance to understand and improve the performances of devices based on our core shell nanoparticles. Therefore, we characterized our newly synthesized redispersible polypyrrole core shell nanoparticles in terms of charge transport, using mainly broadband dielectric spectroscopy.[4,5] Using temperature-frequency-voltage dependent conductivity data we experimentally proved different charge transport mechanisms i.e. hopping and fluctuation-induced tunneling mechanisms[6] in the core shell nanoparticles. Furthermore, electrode and interfacial polarization processes were observed. The results were compared with data based on the corresponding bulk counterparts. Complementary experimental techniques have been used in order to study and understand the relationship between morphology and charge transport.

References

[1] Skotheim, T.A.; Elsenbaumer, R.L.; Reynolds, J. in “Handbook of Conducting Polymers” Marcel Dekker, New York, **1998**.
[2] a) Yassar, A.; Roncali, J.; Garnier, F. *Polym. Commun.* **1987**, *28*, 103; b) Armes, S. P.; Gottesfeld, S.; Beery, J.G.; Garzon, F.; Agnew, S. F., *Polymer* **1991**, *32*, 2325; c) Liu, C-F.; Maruyama, T.; Yamamoto, T. *Polym. J.*, **1993**, *25*, 363; d) Khan, M. A.; Armes, S. P. *Adv. Mater.* **2000**, *12*, 671; e) Huijs, F. M.; Vercauteren, F. F.; de Ruiter, B.; Kalicharan, D.; Hadziioannou, G. *Synth. Met.* **1999**, *102*, 1151.
[3] Wang, J.; Sun, L.; Mpoukouvalas, K. *et. al.*, submitted in *Adv. Mater.*
[4] Kremer, F.; Schönhals, A. in “Broadband Dielectric Spectroscopy”, Springer, Berlin **2002**.
[5] Barsoukov, E.; Macdonald, J. R. in “Impedance Spectroscopy”, Wiley-Interscience, **2005**.
[6] a) Mott N. F.; Davis, E. A. in “Electronic Process in Non-Crystalline Materials” Clarendon Press, Oxford, **1979**; b) Sheng, P. *Physical Review B* **1980**, *21*, 2180.

Poster B43

Microcellular Nanocomposite Polymers Prepared with Supercritical CO_2: The Role of Nanoclays on Porous Structure

Ioannis Tsivintzelis[1], Sotirios I. Marras[1,2], Ioannis Zuburtikudis[2] and Costas Panayiotou[1]
[1]*Department of Chemical Engineering, Aristotle University of Thessaloniki, 54124 Thessaloniki, Greece*
[2]*Department of Industrial Design Engineering, TEI of Western Macedonia, 50100 Kozani, Greece*

Recently, various supercritical fluid processing methods have been developed for the production of polymer-based materials such as foams, microparticles, membranes and fibers[1]. In this direction, cellular polymers can be formed through the gas foaming technique. According to this method, the polymer is saturated with a gas or supercritical fluid (usually CO_2) at constant temperature and pressure. Then, the system is quenched in a supersaturated state by reducing pressure (pressure-induced phase separation) resulting in the nucleation and growth of pores - cells inside the polymer matrix[1]. The growth of the pores continues until the polymer vitrifies or the viscosity of the polymer matrix is increased up to the point that the retractive force, which restricts cell growth, becomes unexcelled[1].

Nanostructured hybrid organic/inorganic composites have attracted considerable attention in many areas of polymer applications. Introduction of small quantities of high aspect ratio nano-sized silicate particles can significantly improve mechanical and physical properties of the polymer matrix[2].

In this study, nanocomposite Poly(L-lactic acid) ($P_{D,L}LA$) with organically modified montmorillonite, Cloisite 25A (Cl 25A), was prepared in a micro-extruder (ThermoHaake, Minilab). Mixing was preformed for 25 min, at 130 °C and in N_2 atmosphere. Microcellular nanocomposite $P_{D,L}LA$ foams were prepared with the batch foaming technique (pressure-induced phase separation). One compression-molded disc was placed inside the pressure vessel and the latter was immediately filled with CO_2 at the desired temperature and pressure. The system remained at these conditions at least for 4 hr and then it was rapidly depressurized, in less than 20 s. In all cases, structures with uniform cross sections were obtained.

Figure 1 presents the XRD patterns of pure and nanocomposite $P_{D,L}LA$. The initial (001) peak of the organomodified montmorillonite was shifted at lower 2θ values indicating that polymer chains diffused into the silicate galleries expanding the clay structure. A typical porous structure is presented in figure 2, while the effect of clay content on the average pore diameter and the pore population density (number of pores per unit volume) is presented in figures 3 and 4, respectively.

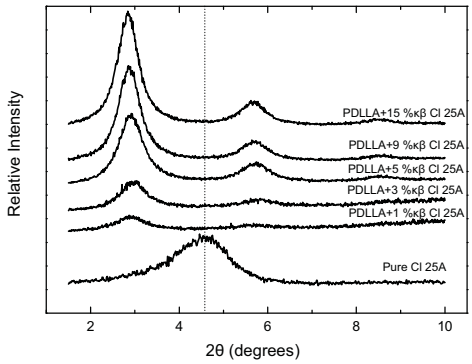

Figure 1. X-ray diffraction patterns of $P_{D,L}LA$ nanocomposites with various loadings of the organophilic clay.

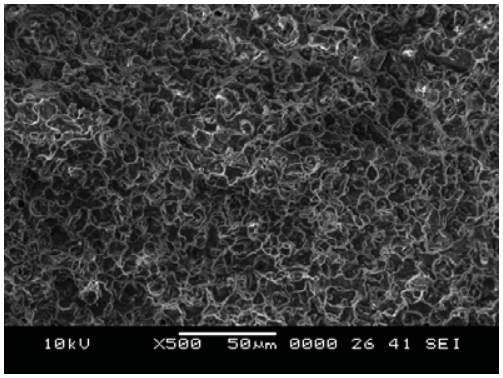

Figure 2. Porous $P_{D,L}LA$ with 5 wt. % clay content. Foaming was performed at 45 °C and 150 bar.

As presented in figures 3 and 4 the mean pore diameter decreases, while the cell population density increases with increase of clay content up to 5 wt. %. Further increment of the clay content to 15 wt. % had no major effect on the cell diameter and cell population density.

The production of porous structures is achieved through the fast depressurization of the system, which causes thermodynamic instability and results in the nucleation and growth of gas bubbles into the polymer matrix. According to the nucleation theory, the energy barrier for nucleation is related to the pressure drop and the interfacial tension between the newly formed gas bubble and its surrounding material[1]. The lower interfacial tension results in the decrease of the nucleation energy barrier and to the formation of more gas nuclei that finally are converted in more pores[1].

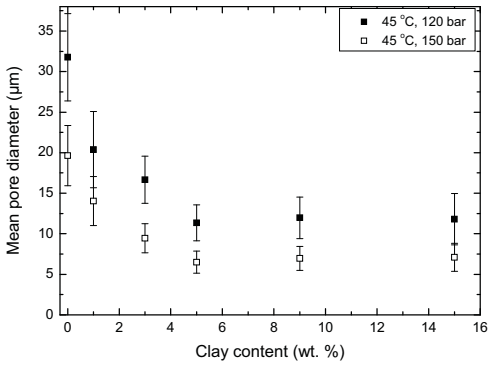

Figure 3. Effect of the clay content on the average pore size

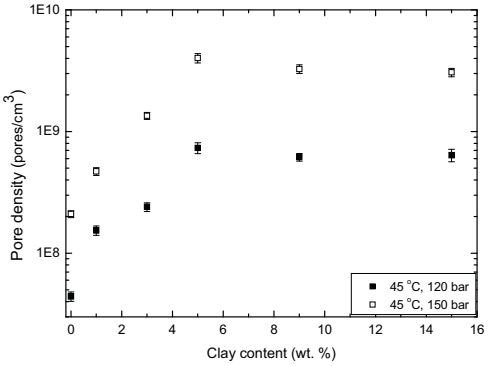

Figure 4. Effect of the clay content on the pore population density

The results indicate that the introduction of the dispersed clays into the polymer matrix favored the heterogeneous nucleation. In other words, nucleation on the surface of the clays was favored compared to the nucleation into the locally homogeneous polymer counterpart. Consequently, the higher nucleation efficiency resulted in the production of porous structures with higher cell population density at least up to 5 wt. %, as indicated in figure 4.

The final cell size is affected by the number of the initial nuclei that are formed in the system during the depressurization, their growth rate and the coalescence of neighboring cells. The introduction of the clay reduces the energy barrier for nucleation and favors the formation of more nuclei in the system. In addition, it results in a significant viscosity increment of the polymer matrix, which hinters the growth of pores as well as the coalescence of neighboring cells. These phenomena favor the formation of smaller cells. On the other hand, the introduction of clay reduces the diffusivity of the gaseous foaming agent through the polymer matrix. The latter delays the growth of pores but also hinters the diffusion of CO_2 outside of the polymeric material. As indicated by the results, the net effect of all these factors is a decrease in the average pore size with increase of the clay content, at least up to 5 wt. %.

Finally, as indicated by figures 3 and 4, increase of the clay content from 5 to 15 wt. % does not affect the cell size and the cell population density. According to Lee et al., in the foaming of polymer nonocomposite materials the observed cell density is much lower than the potential nucleant density, implying that either nucleants are not energetically effective or that their effect has been compromised due to poor dispersion[3]. The dispersion of filler platelets becomes more difficult as the clay content increases and lower ratio of exfoliated to intercalated clay platelets is observed into the polymer matrix[2,3]. This results in the existence of fewer effective sites for heterogeneous nucleation and a plateau in the cell population density and pore diameter is finally observed into the produced porous structure.

References

1. Tsivintzelis I., Angelopoulou A., Panayiotou C., *Polymer*, 2007, 48, 5928-5939.
2. Marras S.I., Zuburtikudis I., Panayiotou C., *Eur. Polym. J.*, 2007, 43, 2191–2206.
3. Lee H., Wang K.H., Park C.B., Sain M., *J. Appl. Polym. Sci.*, 2007, 103, 2129–2134.

Poster B44

Poly(ethylene succinate) Nanocomposites with a Multifunctional Nanofiller: Mechanical Properties and Biodegradability.

Alexandros A. Vassiliou, Dimitrios N. Bikiaris
Laboratory of Organic Chemical Technology, Department of Chemistry, Aristotle University of Thessaloniki, 541 24, Thessaloniki, Greece.
e-mail: alexandv@chem.auth.gr

Introduction

Ecological problems due to waste plastics has evoked an urgent need for the development of "green polymeric materials" that do not involve the use of toxic or noxious components in their manufacturing and that could compost to naturally occurring degradation products. Poly(ethylene succinate) is a typical two component aliphatic polyester, considered to be one of the most accessible biodegradable polymers in terms of synthetic easiness, but with poor properties, which hinders its use in many applications. The formation of a biodegradable nanocomposite system could lead to significant improvements, opening the possibility of a wide range of applications, without impeding its biodegradation characteristics. Nanocomposites of poly(ethylene succinate) with fumed silica nanoparticles (Aerosil® 200) were prepared using the in situ method. The dispersion degree of the silica nanoparticles in the polymeric matrix was evaluated through SEM observation. Measurements of tensile properties were carried out. Furthermore, enzymatic hydrolysis of the prepared materials using a lipase originated from *Pseudomonas cepacia* was also studied.

Experimental

Succinic acid (Su), 1,4-ethanediol (Et), titanium(IV) butoxide (TBT) and triphenyl phosphate (TPP), all of purum grade, were obtained from Fluka. Fumed silica (SiO_2) nanoparticles under the trade name AEROSIL® 200 were obtained from Degussa AG (Hanau, Germany) and had an average primary particle size of 12 nm. Nanocomposites of poly(ethylene succinate) (PESu) were prepared in situ by the two-stage melt polycondensation of Su and Et in a glass batch reactor at a mol ratio of 1:1.3 Su:Et. Appropriate amount of filler was dispersed in Et by ultrasonic vibration (50 W) and intense stirring with a magnetic stirrer (300 rpm) for 10 min, prior to polymerization. The mixture was heated under a nitrogen atmosphere for 3 h at 200 °C, with water removed as the reaction by-product of esterification. Then, 0.3 wt% of TPP as heat stabilizer and 1.0×10^{-3} mol per mole of succinic acid of TBT as polycondensation catalyst were added. Reaction was continued under high vacuum (5.0 Pa) at 220 and 240 °C for 1h intervals, respectively. The intrinsic viscosities [η] measured at 25 °C in chloroform and calculated using the Solomon-Ciuta equation of the prepared materials are presented in Figure 1a.

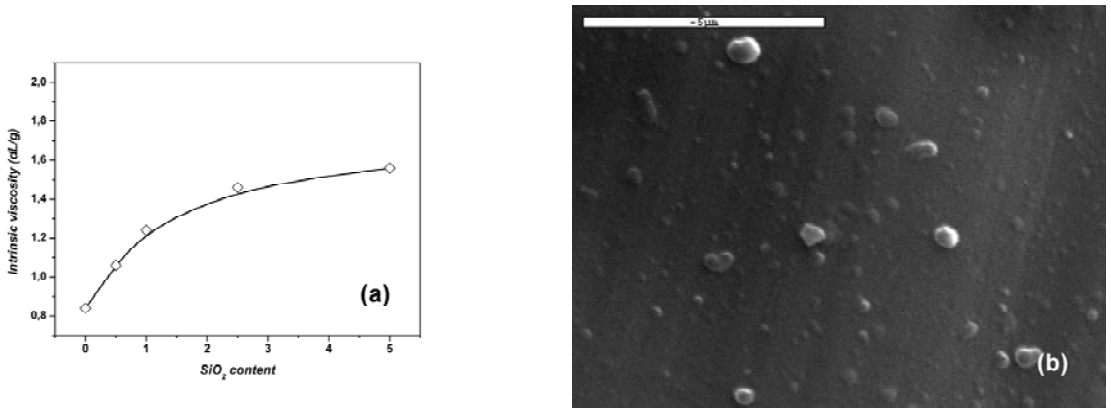

Figure 1. (a) Intrinsic viscosity of the prepared materials and (b) SEM photograph of sample PESu containing 5 wt% fumed silica.

SEM micrographs were obtained using a JEOL JMS-840A performed on film samples coated with carbon black. Tensile mechanical properties of compression moulded samples at 130 ± 5 °C and 500 ± 50 μm thickness were measured in accordance with ASTM D638 on an Instron 1122 dynamometer using a crosshead speed of 50 mm/min. Enzymatic hydrolysis was carried out on compression moulded films (10×20×0.5 mm^3), placed in an ampoule and dipped in 10 ml of a lipase solution (1,24 $mg \cdot ml^{-1}$, 0.1 M KH_2PO_4/KOH aq., pH 6.0). The ampoule was sealed and kept at 50 °C for a predetermined time. The samples were removed, washed with distilled water and ethanol and dried under vacuum at RT. As a control, the experiment was carried out without the lipase added under the same conditions.

Results and Discussion

Observation of the filler's dispersion degree by SEM revealed that the nanoparticles were finely dispersed in the polymeric matrix (Figure 1b). Some agglomeration did occur, which is almost inevitable for this type of filler, leading to aggregates ≤ 500 nm in size. The surface silanol groups of fumed silica participated in an esterification reaction with the hydroxyl end groups of PESu (determined by NMR), thus acting as a multifunctional chain extender, resulting in branching or cross-linking, depended on the extend of the reaction (Figure 1a). The prepared samples were readily hydrolyzed by the action of the lipase (Figure 2b). The presence of the filler resulted in a decrease of the observed biodegradation rate. However the biodegradability of the material was not hindered or compromised to a great extent. The reduction could be attributed to the decreased area available for biodegradation, considering the large surface area of the inorganic filler (200 m^2/g), the cross-linking, which is known to decrease biodegradation rates, the increased molecular weight and the small increase of crystallinity, since fumed silica has been shown to act as a nucleating agent.

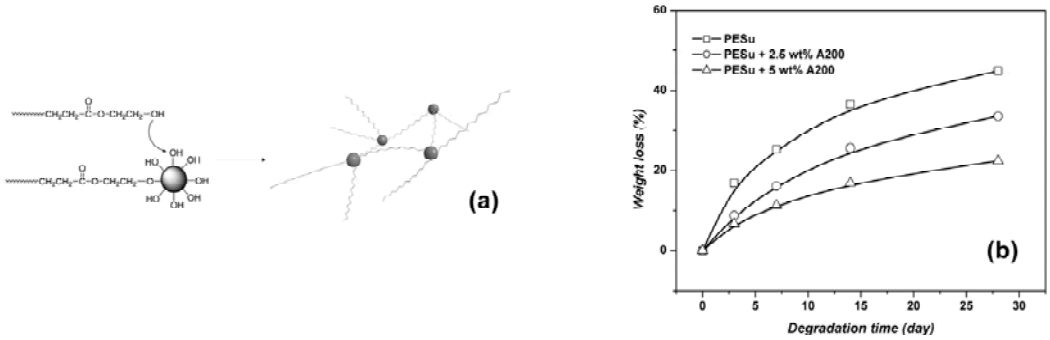

Figure 2. (a) Crosslinking reaction eith the filler and (b) weight loss caused by enzymatic degradation.

Mechanical properties were dramatically improved due to the presence of the filler, the cross-linking reaction and the increased molecular weight. Tensile strength at the break point and Young's modulus (Figure 3) increased with increasing amounts of filler by as much as 113% and 133%, respectively.

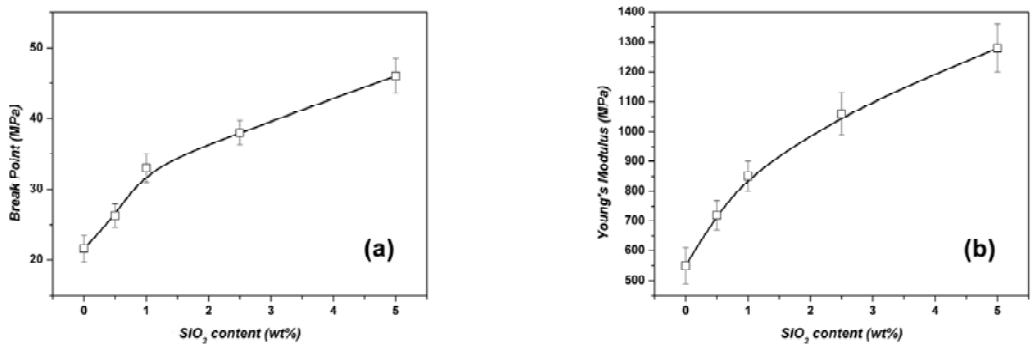

Figure 3. (a) Tensile strength at break point and (b) Young's modulus of the prepared materials.

Poster B45

A new approach of segmental orientation in amorphous epoxy resin/carbon black nanocomposites

C. A. Stergiou [a], Th. V. Kosmidou [b] and C. G. Delides [b]
[a] Department of Electrical and Computer Engineering, Aristotle University, Thessaloniki, Greece, mail: chstergi@auth.gr
[b] Technological Education Institute (TEI) of Western Macedonia, Laboratories of Physics and Materials Technology, Kozani, Greece. mail: kdelidis@yahoo.com

Carbon black (CB) is widely used as a reinforcing agent in epoxy resin products to improve the mechanical and electrical properties; addition of CB can increase hardness, tensile strength, modulus and conductivity[1,2]. Carbon Black is also used in composites to provide UV resistance, as CB can absorb the UV radiation. Due to their excellent properties, CB/epoxy nanocomposites are broadly employed in the manufacture of a variety of products. Despite the extensive research already performed on epoxy composites, concerning their properties and behaviour, there are still some points open to question.

In this work, besides the study of the CB particle-particle network formation and the effect of nanoparticles content on the thermomechanical properties, we focus our attention on the formation and structural characterization of the segmental orientation of the matrix. An epoxy resin, based on diglycidyl ether of bisphenol A (DGEBA), cured with triethylenetetramine (TETA) and filled with high conductivity carbon black (CB) were used. The recipe of preparation was already presented in details elsewhere[2]. The high level of filler dispersion was achieved by a combination of mechanical stirring and ultrasonics and checked by Scanning Electron Microscopy (SEM). Some segmental orientation of the matrix, observed for the first time, has been demonstrated and studied, using Wide Angle X-ray Diffraction (WAXRD) measurements.

Epoxy resin composites are amorphous systems. The X-ray patterns, for these particular composites presented in Fig. 1, show a broad peak corresponding to 2θ of about 19^o. Usually the XRD diagrams of polymers show reflections with relatively acute peaks that overlay on one or more wide peaks, characterized as amorphous halos. The presence of these wide peaks over the general background is possibly due to some loose segmental orientation of the macromolecules and can be characterized as «pseudocrystallinity».

The full width at half maximum (FWHM) of this amorphous peak can be correlated with the degree of orientation of polymeric chains. Thus, the size of the orientation regions L can be calculated by the Scherrer's formula[3]:

$$L=0.9\lambda/(\cos\theta\cdot FWHM)$$

where: λ is the wavelength in Å, θ is the Bragg angle of the peak and FWHM is in radians. According to Scherrer's formula, for large or small values of FWHM, we have respectively small or large values of L.

As it is known[3-5] the sum of integrated intensities of crystalline reflections, owed to the diffraction of X-rays, are directly proportional to the crystalline mass of the polymer. Likewise, the integrated intensities of pseudocrystalline halos will be analogous to amorphous mass of polymer consisted of the clusters with the segmental orientation. For this reason, the experimental curve of intensities, obtained from a polymeric sample, can be analyzed in individual curves (pseudo-Voigt shape function) corresponding to crystalline and pseudocrystalline regions, the number of which depends on the peaks of X-ray spectrum. The area under these curves (after the removal of background) is analogous to the crystalline and pseudocrystalline mass, respectively. After some basic calculations, θ, I_{max} and FWHM for each peak can be easily estimated. The process of this method is realized semi-automatically by the CRYSTWIN program, written for this aim by A. C. Stergiou[5].

By using this program the experimental data have been successfully analyzed. The results for the sample with 1% CB are shown in Fig. 2. From this analysis it can be concluded that the broad X-ray patterns can be mainly constructed by the accumulation of three peaks,

one larger corresponding to 2θ=18.857° and two smaller ones (2θ=30.367° and 2θ=42.546°). The amount of the oriented part of the matrix is approximately 2.3%.

Using Scherrer's formula, the size of the small clusters with the segmental orientation of the matrix was calculated to be about 8 Å. The formation of these clusters is possibly due to the effect of shear forces developed during the preparation procedure, helping that way the close alignment of the epoxy elements of the matrix which occurs when the bisphenol groups are able to close pack. The size of these clusters with the oriented elements is not affected by the filler content. This is tentatively attributed to the poor interface interaction between carbon black particles and matrix in the nanocomposite and therefore, they have no significant contribution to the segmental orientation[2].

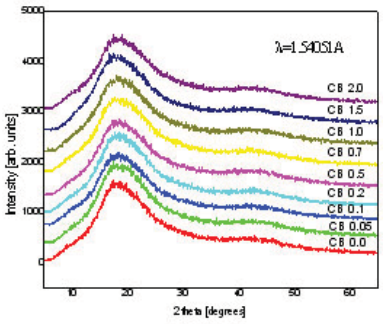

Fig. 1: X-ray diffraction patterns.

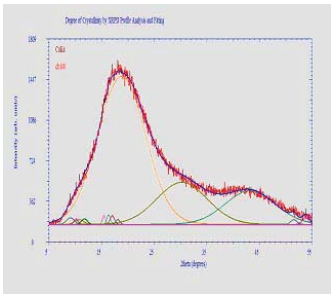

Fig. 2: Spectral analysis of 1% CB content.

Acknowledgements.

This work has partially been funded by the project "Archimedes II". Acknowledgements are expressed to Professor R.A. Pethrick for the stimulating discussions during this work and to student Vangelis Varsamidis for his contribution to sample preparation.

References

1. W. Zhang, R. S. Blackburn, A. A. Dehghani-Sanij. *Effect of carbon black concentration on electrical conductivity of epoxy-carbon black-silica nanocomposites.* J. Mater.Sci.42, 7861-7865 (2007).
2. Th. V. Kosmidou, A. S. Vatalis, C. G. Delides, E. Logakis, P. Pissis, G. C. Papanicolaou. *Structural, mechanical and electrical characterization of epoxy-amine/carbon black nanonocomposites.* Express Polymer Letters 5(2), 364-372 (2008**)**.
3. A. Guinier. *X-ray Diffraction in Crystals, Imperfect Crystals and Amorphous Bodies.* Editor: W. H. Freeman and Company, San Francisco USA (1963).
4. M. Kakudo and N. Kasai. X-ray Diffraction by Polymers, Elsevier Publishing Company (1972).
5. A. C. Stergiou. *"CRYSTWIN ver. 3", Program for determination of crystallinity, by deconvolution-fitting of XRD profile.* Department of Physics. Aristotle University of Thessaloniki, Thessaloniki, (2006).

Poster B46

End-grafted Polymer Chains onto Inorganic Nanoparticles

D. S. Achilleos, D. Moatsou and M. Vamvakaki
Institute of Electronic Structure and Laser, Foundation for Research and Technology - Hellas, 711 10 Heraklion, Crete, Greece and
Department of Materials Science and Technology, University of Crete, 710 03 Heraklion, Crete, Greece

During the last decade, polymer/nanoparticle hybrids have attracted great interest due to the combination of both the properties of the inorganic nanoparticles (thermal stability, mechanical strength) with those of the polymer (solubility, flexibility).[1] The organic polymer shell determines the external chemical properties of such materials and their interactions with their environment whereas their physical properties are governed by both the size and the shape of the inorganic core and the surrounding organic layer.[2] Surface-initiated Atom Transfer Radical Polymerization (Si-ATRP) has attracted great attention, as one of the most effective methods for tailoring the surface properties of various surfaces.[3,4] ATRP allows the controlled synthesis of uniform polymer layers with well-defined film thickness and grafting density covalently bound to the surface.[5]

In the present study, we report the synthesis of end-grafted polymer chains from curved inorganic surfaces, by ATRP. Colloidal multifunctional initiators were first prepared by the surface functionalization of TiO_2 (d_{50} = 25 nm), ZnO (d_{50} ~ 100 nm) and SiO_2 (d_{50} ~ 23 nm) nanoparticles with 2-bromoisobutyrate groups. Subsequently, ATRP was carried out from the nanoparticles surface to obtain the polymer-modified nanohybrids. The hydrophilic monomers used were oligo(ethylene glycol) methacrylate (OEGMA) (neutral, water soluble, biocompatible) and 2-(dimethylamino)ethyl methacrylate (DMAEMA) (ionizable, water soluble), while methyl methacrylate (MMA) was employed as the hydrophobic monomer (see Figure 1).

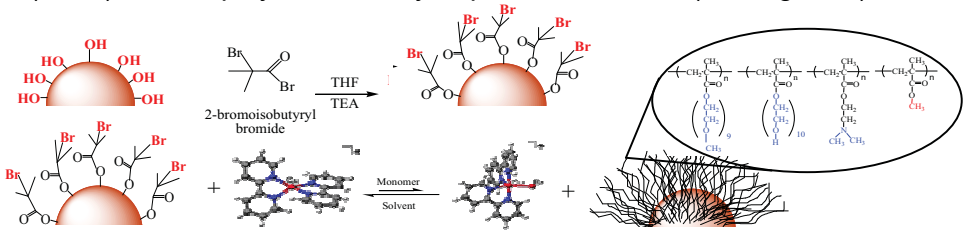

Figure 1. Synthetic procedure followed for the preparation of the end-grafted polymer chains

The successful synthesis of the organic/inorganic hybrids was confirmed by attenuated total reflectance-FTIR spectroscopy, while thermogravimetric analysis was used to determine the weight fraction of the polymer. Dynamic light scattering measurements were performed to assess the hydrodynamic radius, R_h, of the polymer modified colloidal particles and the size of the polymeric shell. The polymer grafting density was calculated from the molecular weight of the end-grafted polymer chains as a function of reaction time. Transmission and scanning electron microscopy were employed to determine the degree of dispersion and the morphology of the polymer-modified nanospheres, respectively. The responsive behavior of the PDMAEMA functionalized nanoparticles in aqueous media as a function of the solution pH and temperature was investigated.

Results and Discussion

Figure 2 shows the ATR-FTIR spectra of the bare, the PMMA-coated (Figure 2a) and the PDMAEMA-coated (Figure 2b) SiO_2 nanoparticles. The bare SiO_2 nanoparticles exhibit two peaks at 1046 cm^{-1} and 792 cm^{-1} attributed to the Si-O-Si asymmetric stretching and the Si-O-Si bending vibration, respectively. For the hybrid samples, the characteristic carbonyl ester peak at 1728 cm^{-1}, the peaks at 2991 and 2950 cm^{-1} assigned to the C-H stretching modes of the CH_2 and the CH_3 groups and the 1233 cm^{-1} peak due to the single carbon-oxygen bond of the O=C-O group, verify the presence of the grafted polymer onto the surface of the inorganic nanoparticles.

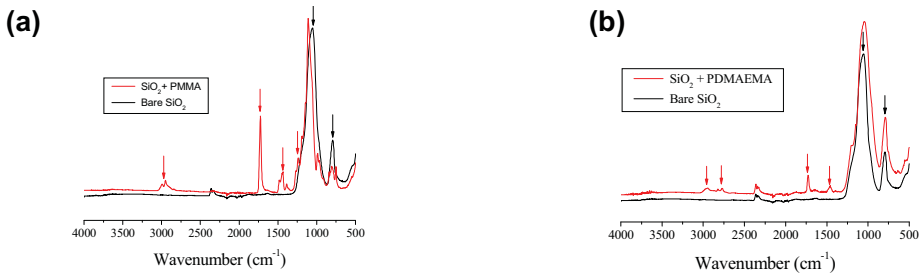

Figure 2. ATR-FTIR spectra of the bare and the PMMA-coated (a) and the bare and the PDMAEMA-coated (b) SiO_2 nanoparticles

Table 1 summarizes the weight losses measured by TGA for TiO_2, ZnO and SiO_2 nanohybrids over the temperature range from 200 to 600 °C and the calculated polymer volume fraction ($\Phi_{polymer}$). A 2 - 63 wt% loss was obtained attributed to the decomposition of the polymeric component of the hybrid materials.The highest volume fraction was observed for the SiO_2 nanoparticles due to the absence of aggregation which results in a complete and uniform surface coverage of the particles by the polymer. A dependence of the polymer content of the hybrid on the solvent medium used for the polymerization was found. The highest polymer fraction was observed for the PHOEGMA-coated TiO_2 nanohybrid synthesized in water while lower polymer contents were obtained for nanohybrids synthesized in organic or mixed aqueous media. In the latter solvents the polymerization rate reduces substantially leading to a more controlled growth of the polymer brushes compared to that in aqueous media.[6]

Table 1. Weight loss and polymer volume fraction of the hybrid materials

Sample name	Solvent (v/v)	Weight loss (%)	$\Phi_{polymer}$
TiO_2 – PHOEGMA	H_2O	21	0.47
TiO_2 – PDMAEMA	Xylene	6	0.20
ZnO – PDMAEMA	MeOH/H_2O 4/1	9	0.31
SiO_2-PMMA	Xylene	63	0.65

Figures 3a and **3b** show the SEM images of the bare and the PMMA-coated silica nanoparticles, respectively. A uniform dispersion of the inorganic colloids within the polymer film is observed for the hybrid material. The average diameter of the initiator-functionalized particles as estimated by SEM was similar to that found for the bare particles (d~30 nm) (Figure 3a). However, after the grafting of the PMMA chains from the nanoparticles surface the nanoparticle diameter increased significantly to ~100 nm (Figure 3b).

Figure 3. SEM images of the bare (a) and the PMMA-coated silica nanoparticles (b).

References

1. Zhang, K.; et al. *J. Mater. Sci. Lett.* **2007**, *61*, 949
2. Advincula, R. C. *J. Dispersion Sci. Technol.* **2003,** *24,* 343
3. Edmondson, S.; Osborne, V. L.; Huck, W. T. S. *Chem. Soc. Rev.* **2004**, *33,* 14
4. Pyun, J.; Matyjaszewski, K. *Chem. Mater.* **2001,** *13,* 3436
5. Kim, D. J.; et al. *Macromol. Chem. Phys.* **2005**, *206*, 1941
6. Tsarevsky, V. N.; Pintauer, T.; Matyjaszewski, K. *Macromolecules* **2004,** *37,* 9768

Poster B47

Adsorption of oligomers and polymers in nanoporous alumina

Sotiria Karagiovanaki, Alexandros G. Koutsioubas, Nikolaos Spiliopoulos and Chris Toprakcioglu

Department of Physics, University of Patras, Greece 26500

ABSTRACT

We have studied the adsorption of end-functionalised oligomers and polymers in nanoporous alumina by means of FTIR spectroscopy. Under suitable anodisation conditions using electrolyte solutions of sulphuric or oxalic acid, thin films (ca. 10 μm - 100 μm) of aluminium can be oxidized electrochemically to produce nanoporous Al_2O_3 with nearly monodisperse regular, hexagonally packed arrays of parallel pores with diameters typically in the range ca. 10 nm - 50 nm. The adsorption of oligomers and polymers on the walls of such pores was investigated with FTIR spectroscopy. It is found that polymers whose radius of gyration is greater than or comparable to the pore diameter adsorb negligibly, as they are entropically hindered from entering the pores, while smaller chains or oligomers readily adsorb and populate the pore walls. Our results demonstrate the size-related selectivity of such well-defined nanoporous media and point to potential applications in size-exclusion processes and nanofluidics.

Poster B48

Fluorinated methacrylic homopolymers: Polymerization, characterization, surface properties and effectiveness for the protection of stone

S.K. Papadopoulou[1], C. Michailof [1], I. Karapanagiotis[2], A. Tsakalof[3], I. Zuburtikudis[4] and C. Panayiotou[1]

[1] *Department of Chemical Engineering, Aristotle University of Thessaloniki, 54124, Thessaloniki, Greece*
[2] *"Ormylia" Art Diagnosis Centre, Ormylia, Chalkidiki, 63071, Greece*
[3] *Department of Medicine, University of Thessaly, 41222 Larisa, Greece*
[4] *Department of Industrial Design Engineering, TEI of Western Macedonia, Kozani, 50100, Greece*

The use of fluorinated methacrylic polymers for the protection of stone surfaces has attracted the attention of current research. Apart from their low surface energy, these polymers, exhibit good adhesion and film- forming properties as well as stability towards degradation [1,2]. The above mentioned properties render this category of polymers suitable for the conservation of stone-made monuments.

Considering these points, the goal of this work was to synthesize, characterize and study the surface properties of four fluorinated methacrylic homopolymers. The polymers studied were poly(2,2,2-trifluoroethyl methacrylate) (PTFEMA), poly(1,1,1,3,3,3 hexafluoroisopropyl methacrylate) (PHFIMA), poly(2,2,3,3,3 pentafluoropropyl methacrylate) (PPFPMA) and poly(2,2,3,3,4,4,4 heptafluorobutyl methacrylate) (PHFBMA). All polymers were prepared by free radical polymerization of the monomers using 0,3 wt % 2,2'-Azobisisobutyronitrile (AIBN) as initiator in dry, over molecular sieves, tetrahydrofuran (THF) at 65±1^{o}C [1,3,4]. In order to substitute commonly used harmful organic solvents supercritical carbon dioxide was also employed as an alternative, "green" polymerization solvent [5].

The characterization techniques employed for all polymer samples were: Fourier Transform Infrared Spectroscopy (FTIR), Size Exclusion Chromatography (SEC), Differential Scanning Calorimetry (DSC), Thermo-Gravimetric Analysis (TGA) and Refractometry. Polymers' surface energy was studied with Inverse Gas Chromatography (IGC) in conjunction with the Contact Angle Method. The dispersive component of the surface energy with a series of five alkanes, the activity coefficient and the Flory-Huggins interaction parameters with a series of thirteen solvents were calculated at a pre-defined range of temperatures using IGC. The hydrophobicity of the polymers was investigated with contact angle measurements, while their surface energy (dispersive and polar components) was determined with the Contact Angle Method using both apolar and polar solvents. Moreover, the efficacy of the polymers for marble protection was investigated by means of capillary water absorption, permeability to water vapor and color alterations. Measurements were performed before and after artificial ageing to reveal the stability of the fluorinated polymers against degradation processes.

The results of the aforementioned studies will be combined to elucidate the effect of the fluorine group on the surface properties of the polymers.

Acknowledgements
This work was supported by the Greek Ministry of Development – GSRT (25%) and the European Union – European Social Fund (75%) through the research grant PENED 2003 with MIS 03EΔ 91

1. Signori, F. Lazzari, M. Castelvetro, V. Chiantore, O. Macromolecules 2006, 39, 1749-1758.
2. Vicini, S. Princi, E. Pedemonte, E. Lazzari, M. Chiantore, O. Journal of Applied Polymer Science 2004, 91, 3202-3213.
3. Huang, H. L. Goh, S. H. Wee, A. T. S. Polymer 2002, 43, 2861-2867.
4. Liu, W. H. Tang, K. Guo, Y. Z. Koike, Y. Okamoto, Y. Journal of Fluorine Chemistry 2003, 123, 147-151.
5. Kwon, S. Bae, W. Kim, H. Korean Journal of Chemical Engineering 2004, 21, 910-914.

Poster B49

Fabrication and Thermal Characterization of a Thin Poly($_L$-lactic acid) Film with the Layer-by-Layer Spin Coating Process and the Use of Thickness Shear Mode Resonators

A. Kakalis, C. Panayiotou*
Department of Chemical Engineering, University of Thessaloniki, 54124 Thessaloniki
e-mail:cpanayio@auth.gr

Abstract

Thin polymer films from biodegradable polymers, namely the poly(α-hydroxy ester) family, have been studied extensively in terms of mechanical properties for their implementation as temporary substrates for culture of living human cells[1].

Among biodegradable polymers, poly($_L$-lactic acid) (PLLA) stands as one of the most promising polymeric materials for both biological and industrial applications[2] ,as its mechanical properties can be readily enhanced.

In the light of previous studies of thin biodegradable polymer films as substrates-scaffolds for cell culture purposes, the present contribution is focused on the preparation of thin poly($_L$-lactic acid) films with the use of layer-by-layer spin coating process and the characterization of their mechanical properties with the implementation of the so-called Thickness Shear Mode Resonators at a nominal frequency of 5,2 MHz.

The polymer film thickness during the subsequent coating steps was monitored with the use of TSM quartz crystal sensors and High-Frequency Impedance Spectroscopy (HF-IS) in terms of changes in the series resonant frequency (f_s) and the electrical resistance at series resonance (R) and the results are in good agreement with previous efforts[3] (figs. 1 and 2). The final thickness of the coating was equal to 5.36 μm.

The electrical response of the PLLA film-coated TSM sensor was then recorded in three subsequent measurements for the temperatures between 30-115 ^oC and modeled with the electrical equivalent circuit modeling approach. The variation with temperature of characteristic measurement values such as the series resonance frequency (f_s), the electrical resistance at series resonance (R), the quality factor (Q) and the half-height-full-width frequency width (Δf_{hhfw}) (figs. 3, 4, 5 and 6) shows excellent qualitative agreement in comparison with respective numerical simulations[4] for the general response of TSM quartz crystal sensors coated with thin polymer films.

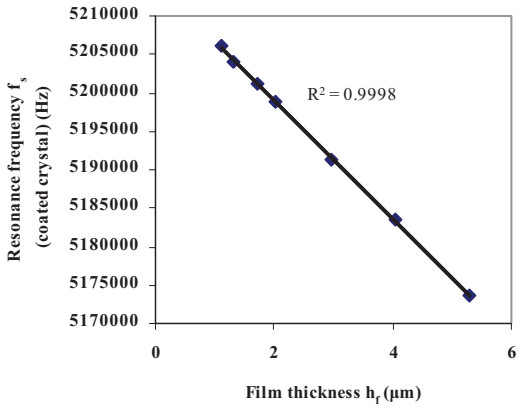

Fig. 1: Resonant frequency f_s with film thickness.

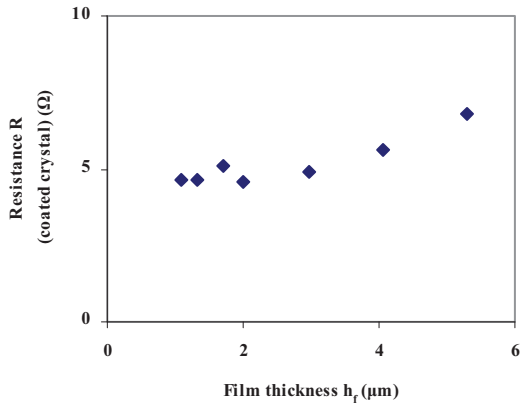

Fig. 2: Resonant resistance R with film thickness.

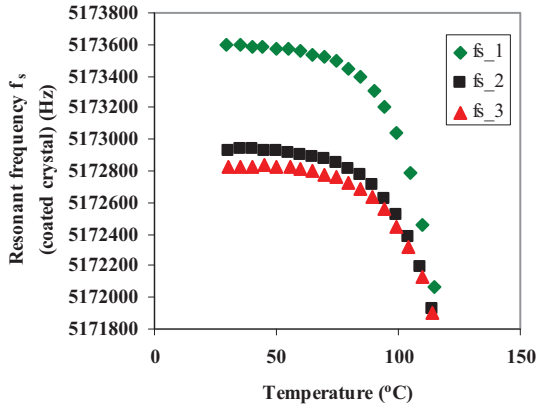

Fig. 3: Resonant frequency f_s with temperature.

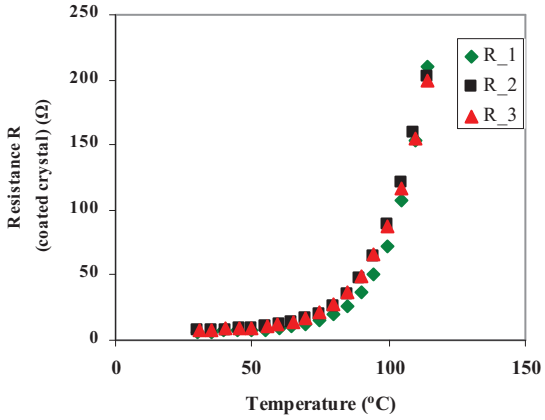

Fig. 4: Resonant resistance R with temperature.

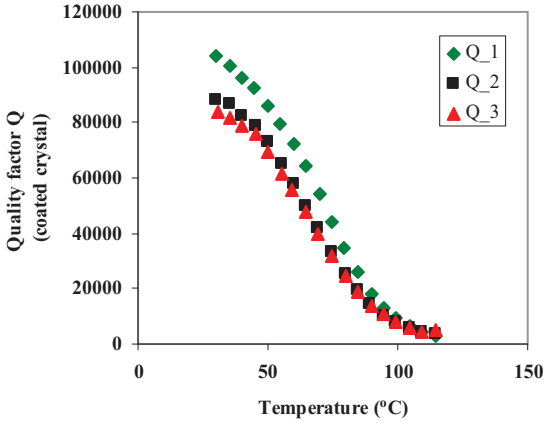

Fig. 5: Quality factor Q with temperature.

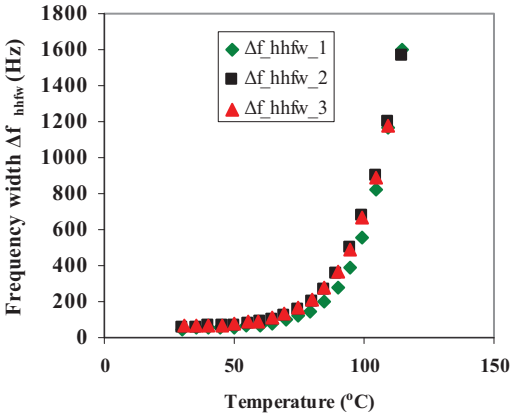

Fig. 6: Frequency width Δf_{hhfw} with temperature.

References

1. Thomson, R.C., Giordano, G.G., Collier, J.H., Ishaug, S.L., Mikos, A.G., Lahiri-Munir, D., Garcia, C.A., "*Manufacture and Characterization of Poly(a-hydroxy ester) Thin Films as Temporary Substrates for Retinal Pigment Epithelium Cells*", Biomaterials **17** (1996) 321-327.
2. Ray, S.S., Okamoto, M., "*Polymer/Layered Silicate Nanocomposites: A Review from Preparation to Processing*", Prog. Polym. Sci **28** (2003) 1539-1641.
3. Morray, B., Li, S., Hossenlopp, J., Cernosek, R., Josse, F., "*PMMA Polymer Film Characterization Using Thickness-Shear Mode (TSM) Quartz Resonator*", 2002 IEEE Int. Freq. Contr. Symp. PDA Exhib., 2002, pp. 294-300.
4. Kakalis, A., "*Thin Poly($_L$-lactic acid) Films Characterization with the Use of Thickness Shear Mode Quartz Crystal Resonators and High-Frequency Impedance Spectroscopy*", M.Sc. Thesis, Department of Chemical Engineering, Aristotle University of Thessaloniki, Thessaloniki, Greece, (2006), Ch. 7.

Poster B50

COLLOIDAL MICROGEL PARTICLES CARRYING ACIDIC OR BASIC MOIETIES

K. E. Christodoulakis and M. Vamvakaki

Institute of Electronic Structure and Laser, Foundation for Research and Technology,Hellas, P.O. Box 1527, 711 10 Heraklion Crete, Greece
Department of Materials Science and Technology, University of Crete, 710 03 Heraklion Crete, Greece

The aim of this study is the synthesis and the characterization of pH responsive microgel particles. A microgel is a chemically cross-linked network in the form of a colloidal particle stabilized in a continuous medium. The size of the particle is below 1 μm and usually varies from 100 to 700 nm. Responsive polymers are materials that can change their physical and chemical properties, such as size, charge, solubility, density, softness, etc, under certain external stimuli, such as temperature, magnetic-electric field, pH, pressure, etc. pH responsive microgel particles can become highly swollen in response to pH changes. Both thermo-responsive and pH-responsive microgels have been reported in the literature.[1,2] pH responsive microgels usually consist of either acidic or basic monomer units and in some cases hydrophobic co-monomers are incorporated. Until now the fraction of pH-responsive moieties within the gel phase was limited to a few percent and as a result the microgel particles exhibit a weak pH-responsive behavior. There are only very few examples for the preparation of pH-responsive microgels based solely on pH-sensitive monomers.[3-5]

In the present work, we have synthesized microgel particles based on 2-(diethylamino)ethyl methacrylate (DEA) or methacrylic acid (MAA) using emulsion polymerization.[6] *tert*-Butyl methacrylate (*t*-BuMA) was used as the protected form of MAA. After the synthesis the *t*-BuMA based microgels were hydrolyzed to convert the *t*-BuMA segments into MAA. The pH-responsive character of the microgel particles was examined by dynamic light scattering as a function of the degree of ionization of the monomer units (Figure 1). The effect of the microgel cross-link density on its degree of swelling was also investigated (Figure 2).

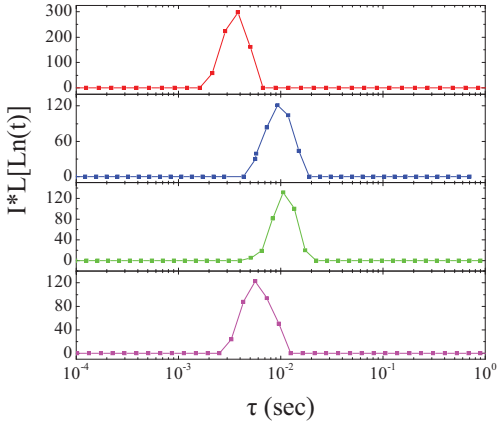

Figure 1: Distribution of relaxation times obtained from the Inverse Laplace transform of the experimental intensity autocorrelation functions for a dilute aqueous solution of MAA microgel particles at 60° scattering angle and degrees of ionization 0.0, 0.5, 0.7 and 1.0.

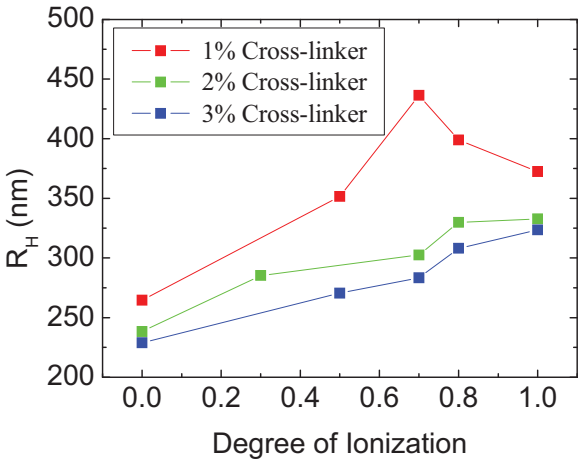

Figure 2: Hydrodynamic radius as a function of the degree of ionization for DEA based microgel particles of different cross-link densities.

The degree of swelling of the microgels first increased and thus the particle size also increased with the degree of ionization, then it decreased at high degrees of ionization due to the increase of the ionic strength of the solution which caused the screening of the electrostatic repulsions between the charged monomer units an led to a decrease of the particles size (Figure 1). Moreover, as the degree of cross-linking of the microgel particles increases the volumetric

swelling factor ($V_{max}/V_{collapsed}$) decreases due to the higher cross-link density which prevents the extensive microgel swelling (Figure 2).

Finally, we synthesized mixed microgel particles based on both DEA and MAA units randomly distributed in the particle. We examined the dependence of the size of the mixed microgel particles on the degree of ionization of the monomer units. Figure 3 shows the hydrodynamic radius of the mixed microgel particles as a function of the microgel net charge. The left part corresponds to the ionization of MAA units at high pH and thus to negative microgel net charge while the right part represents the protonation of the DEA units at low pH where the microgels have a positive net charge. Net charge is zero at the isoelectric point. The microgels swell at both high and low pH when the particle net charge is different than zero while collapsed microgel particles are found at the isoelectric point at zero net charge, where the hydrophobic interactions dominate.

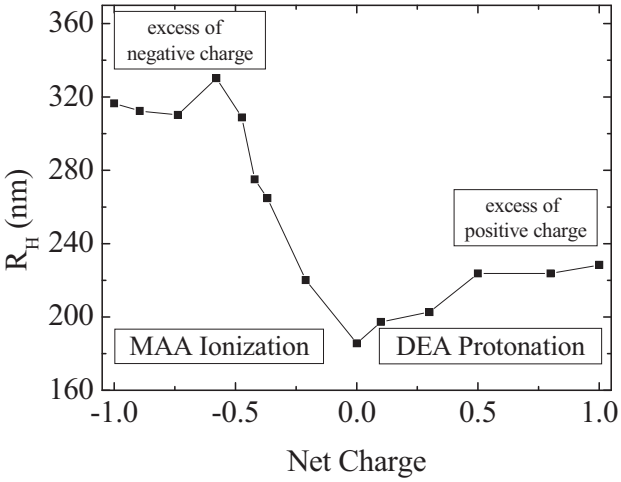

Figure 3: Hydrodynamic radius of the mixed microgel particles as a function of the microgel net charge.

The latter are very interesting materials carrying dual functionalities that will be advantageous in numerous applications such as drug-delivery, gene therapy, chemical separations, etc.

References

1. S. Nayak, D. Gan, M. J. Serpe and L. A. Lyon, *Small* **2005**, *4,* 416.
2. X.C. Xiao, L. Y. Chu, W. M. Chen, S. Wang and R. Xie, *Langmuir* **2004**, *20,* 5247.
3. A. Loxley and B. Vincent, *Colloid Polym. Sci.* **1997**, *275,* 1108.
4. B. R. Saunders, H. M. Crowther and B. Vincent, *Macromolecules* **1997**, *30,* 482.
5. Amalvy J. I.., Wanless E. J., Li Y., Michailidou V. and Armes S. P. *Langmuir* **2004**, *20,* 8992.
6. D. Palioura, S. P. Armes, S. H. Anastasiadis and M. Vamvakaki, *Langmuir* **2007**, *23,* 5761.

Poster B51

Cu^{2+}-induced gelation in aqueous solutions of maleic acid-containing polyelectrolytes

Eudokia K. Oikonomou,[1,2] Georgios Bokias [1] and Joannis K. Kallitsis[1,2]

[1]*Department of Chemistry, University of Patras, GR-26504 Patras, Greece*
[2]*Foundation of Research and Technology Hellas, Institute of Chemical Engineering and High-Temperature Chemical Processes (ICE/HT FORTH), P.O. Box 1414, GR-26504 Patras, Greece*

In recent years, the interest in metal containing polymers is continuously increasing because of the numerous applications of such hybrid materials in several fields, like pollution control, catalytic reactions or in medicine and biochemistry.[1]

The metal ions may be bound to the polymer either through electrostatic attractions, being simply the counterions of a strong polyanion, like poly(styrene sulfonate), or through coordination with adequate ligands attached to the polymer backbone, for instance carboxylate groups, forming the so-called polymer-metal complexes. Polymer-metal complexation often leads to phase separation.[2] However, especially when higher valence metal ions are used the formation of hydrogels is also reported.[3]

The introduction of Cu^{2+} ions to polymers containing such groups can be achieved either through neutralization of the acid form of the polymers with $Cu(OH)_2$ or through mixing of the sodium salt form of the polymers with $CuSO_4$.

In the present work, the two different processes of introduction of copper ions to the polymers were compared, while the influence of the nature of the interacting groups as well as the nature of the neighboring comonomers (competition for Cu^{2+} uptake, hydrophilic/hydrophobic balance) was investigated. The main binding group used in the present work is maleic acid containing 2 carboxylic units. Thus, the polymers used were copolymers of maleic acid, MAc, with either hydrophobic comonomers like vinyl acetate, VAc, or ethylene, Eth, or with hydrophilic comonomers like sodium styrene sulfonate, SSNa. For reasons of comparison, the homopolymer poly (sodium styrene sulfonate), PSSNa, was also used.

Copper ions were introduced either through neutralization of $Cu(OH)_2$ with the acid form of the (co)polymers, PSSH, P(SSH-co-MAc),P(VAc-co-MAc), P(Eth-co-MAc) or through ion exchange between $CuSO_4$ and the sodium salt form of the polymers, PSSNa, P(VAc-co-MANa) and P(SSNa-co-MaNa). The two processes were studied mainly in dilute aqueous solution through turbidimetry, viscometry, potentiometry and UV-Vis spectrometry.[4]

In general, when Cu^{2+} ions are incorporated in the aforementioned polyelectrolytes in aqueous solution, the solution remains transparent (homogeneous) for low Cu^{2+} concentrations. However, at higher Cu^{2+} concentrations phase separation is often observed, as the stoichiometry is approached. When the neutralization process is applied, the insoluble matter is the excessive $Cu(OH)_2$, as it is also indicated by the potentiometric results. However, depending on the hydrophobicity of the comonomers and when coordination is the main binding mechanism, the hydrophobic polymer-Cu^{2+} complex formed through coordination may consist the water-insoluble phase for both processes.

UV-Vis spectrophotometry in the one phase region is proved a very sensitive tool to monitor the polymer-Cu^{2+} association and to distinguish between electrostatic binding and coordination. Some characteristic results are compiled in Figure 1, where the position of the absorption band of Cu^{2+} in the visible region is plotted as a function of the mixing ratio r, defined as $r = C_{Cu}{}^{2+} / C_{active}$ where $C_{Cu}{}^{2+}$ and C_{active} is the molar concentration of Cu^{2+} ions and active groups of the polymer respectively.

As shown in Figure 1, when electrostastic attraction is the only binding mechanism, the absorption band is located at ~800 nm, as in the case of pure aqueous $CuSO_4$ solutions. On the other hand, when coordination is the predominant binding mechanism, a significant shifting of the absorption band to lower wavelengths is observed. Interestingly, when both binding units (sulfuric and carboxylic groups) are present, the electrostatic binding of Cu^{2+} by the suffocate groups, in fact, competes with coordination of Cu^{2+} with the carboxyl ate groups of MAc or Manna and a gradual shift of the absorption band is observed.

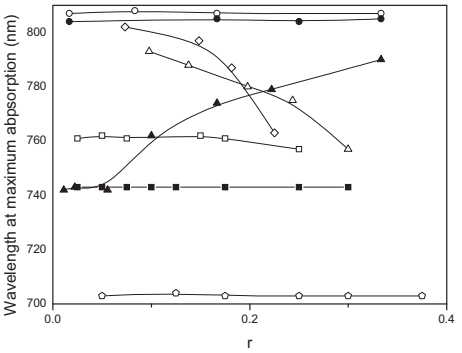

***Figure 1**: Wavelength of the maximum absorption of UV-Vis spectra of aqueous solutions of $CuSO_4$ with P(VAc-co-MANa) (■), P(SSNa-co-MaNa) (▲) , PSSNa (●) or of $Cu(OH)_2$ with P(VAc-co-MAc) (□), PSSH (○), P(SSH-co-MAc) (Δ) and P(Eth-co-MAc)(⌂).The corresponding results for the neutralization of an equimolar mixture of PSSH and P(VAc-co-MAc) with $Cu(OH)_2$ (◊) are also plotted.*

The interaction of Cu^{2+} ions with the copolymers studied is also evidenced from the isometric behavior in dilute solution, as shown in Figure 2. For reasons of comparison the ratio $r_{\eta red}$ is used, defined as $r_{\eta red} = \eta_{red} / (\eta_{red})_0$ where η_{red} and $(\eta_{red})_0$ is the reduced viscosity of each polymer in the presence and in the absence of Cu^{2+} ions, respectively. It is observed that, contrary to PSSH, for the MAc-containing copolymers $r_{\eta red}$ values larger than unity are found, indicating that interchange association may take place under these conditions, possibly leading to the formation of weak gel-like structures.

This is more evident when the copolymer P (Eth-co-MAc) is used at more concentrated solutions. In fact, under suitable conditions, the formation of stiff gels is observed (inset of Figure 3). A more detailed investigation revealed that the viscoelastic properties of these systems depend on several experimental conditions, such as polymer concentration and mixing ratio, as well as other external parameters like temperature of mixing or the time passed after mixing. Typical results concerning the storage modulus G' are reported in Figure 3.

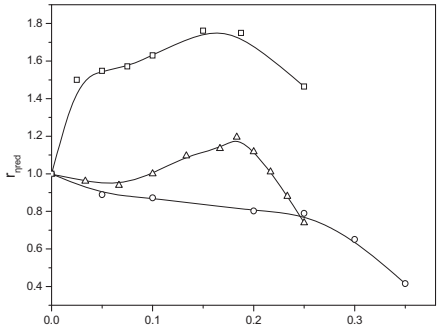

Figure 2: Variation of $r_{\eta red}$ with the mixing ratio r of aqueous solutions of $Cu(OH)_2$ with PSSH (○), P(SSH-co-MAc) (Δ) and P(VAc-co-MAc) (□)

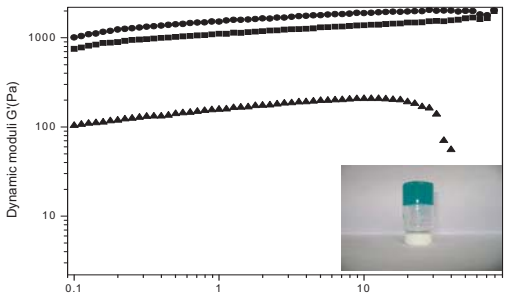

Figure 3: Frequency-dependence of the storage modulus G' of hydrogels of 40mM P(Eth-co-MAc) with 16mM Cu^{+2} ions (▲), or 100mm P(Eth-co-MAc) with 33 mM (■) or 35 mM (●) Cu^{+2}ions.

References

1. Rivas B.L., Pereira E. D., Moreno-Villoslada I. Prog Polym Sci **2003**, 28, 173
2. Mun G.A., Nurkeeva Z. S., Khutoryanskiy V. V., Sarybayeva G. S., Dubolazov A. V. Eur. Polym. J. **2003**, 39, 1687
3. Axelos M.A.V., Mestdagh M.M., Francois J. Macromolecules **1994**, 27, 6594
4. Oikonomou E.K., Bokias G., Kallitsis J. J Polym Sci: Part B: Polym Phys **2008** , 46, 1149

Acknowledgments Financial support through the program PENED 2003, 03ED825, 'Design and Development of new paints with controlled release of biocides for submarine applications' co-financed by E.U.- European Social Fund (75%) and General Secretariat for Research and Technology (GSRT), Greece, is greatly acknowledged. Partial support from Chrotex S.A., Greece, is also acknowledged.

Poster B52

Hydration Properties of Nanostructrured Hydrogels Based on Poly(2-hydroxyethyl acrylate) and Poly(2-hydroxyethyl-co-ethyl acrylate)

Ch. Pandis[1], A. Stathopoulos[1], P. Klonos[1], A Spanoudaki[1], A. Kyritsis[1], P. Pissis[1], M. Monleón Pradas[2], J. C. Rodríguez Hernández[2], J. L. Gómez Ribelles[2]

[1]*Department of Physics, National Technical University of Athens, 15780, Athens, Greece.*
[2]*Center for Biomaterials, Polytechnic University of Valencia, E-46022, Valencia, Spain.*

Corresponding author's email: pandis@mail.ntua.gr

Hydrogels are three-dimensional, hydrophilic polymeric networks capable of absorbing large amounts of water. They give exceptional promises in biomedicine and pharmacy since they are biocompatible materials. Hydrogels, among other applications, are currently used as scaffolds in tissue engineering and in contact lenses. For many of these applications, mechanical stability must be improved. This is normally achieved by addition of a second component in order to form composites, copolymers, blends and interpenetrating polymer networks (IPNs). For the present study, nanostructured hydrogels based on Poly(2-hydroxyethyl acrylate) were prepared. In order to improve mechanical stability of PHEA matrix, inorganic nanofiller, such as silica nanoparticles, has been added. Furthermore, a second hydrophobic polymer such as Poly(ethyl acrylate) (PEA) has been introduced to form copolymer with PHEA, in the presence of silica nanoparticles.

PHEA/silica and P(HEA-co-EA)/silica nanocomposites with silica content varying from 5 to 30 wt.% have been prepared by the simultaneous polymerization of the organic and the silica phases in a sol–gel process with the silica precursor tetraethyl orthosilicate (TEOS). The obtained nanocomposites retain the transparency of pure hydrogels. At concentrations above 15% wt, a silica network is expected to form, restricting the swelling of the matrix and altering the water uptake ability, mechanical and thermal properties[1].

Sorption/desorption measurements at different water activities as well as experiments of immersion in water are performed in order to study the hydration properties of hydrogels. In Fig. 1 water content w (defined as the mass of sorbed water in equilibrium divided by the mass of dry sample) is plotted against water activity α_w, for PHEA, PHEA/5%silica and PHEA/25%silica, at room temperature. An initial linear region for water activity up to 0.6 is observed. The subsequent deviation from linear behaviour for α_w >0.6, which is typical for hydrogels, is explained in terms of clustering of water molecules. Analysis of the equilibrium water sorption isotherms provides information on water clusters formed around hydrophilic sites[2]. Furthermore, no hysteresis is observed between sorption and desorption.

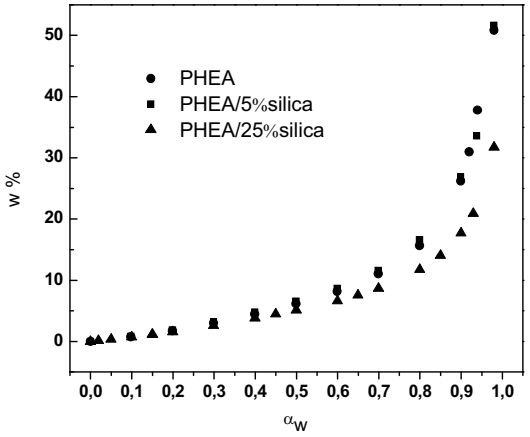

Fig. 1: Equilibrium sorption isotherms of pure PHEA and PHEA/silica nanocomposites measured at room temperature.

In Fig. 2 the water content w (%) is plotted against silica concentration for the PHEA/silica nanocomposites. The results show that water uptake is decreasing as silica content increases up to 15% by weight. Above 15 wt%, water uptake is independent of silica content. For pure PHEA, the hydrogel has the ability to swell freely, leading to high water uptake value. The addition of silica particles into PHEA matrix affects the water uptake properties of the hybrid material, by partially prohibiting the swelling of PHEA. At 15 wt% of silica content, a network of silica is formed. The above network imposes restrictions on swelling of PHEA and thus the water uptake ability of hybrid materials when immersed into water, is depressed.

Diffusion coefficient D is estimated by the continuous weighting of the samples during sorption giving valuable information about the kinetics of water molecules in the hybrid materials under study. In Fig. 3 the diffusion coefficient as a function of water content, is presented. In the hybrids under study, the clustering of water coincides with a maximum in the diffusion coefficient indicating that clustering could reduce the effective mobility of water. Furthermore, it is shown that the diffusion process is influenced by the amount of silica incorporated in the hydrogel nanocomposites. It appears that the D values corresponding to each water activity are similar for PHEA and PHEA/5%silica while lower values are obtained for PHEA/25% silica. For silica content above 15 wt%, the obtained D values indicate that the diffusion process is retarded by the presence of the silica network.

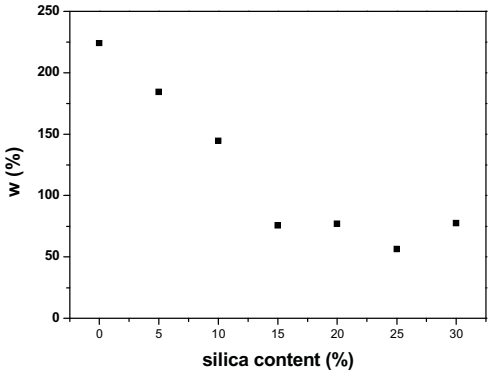

Fig 2. Water uptake against silica content for PHEA/silica nanocomposites obtained from immersion measuements at room temperature

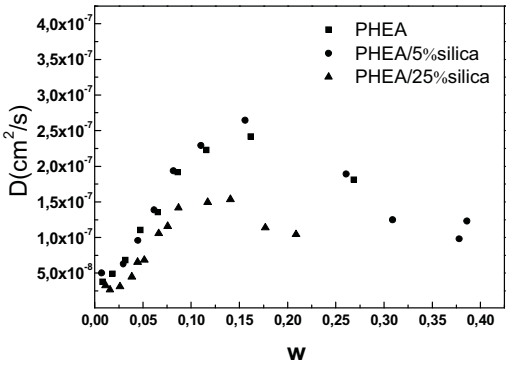

Fig 3. Diffusion coefficient against water content for PHEA, PHEA/5%silica and PHEA/25%silica

References

1. J. C. Rodríguez Hernández, M. Salmerón Sánchez, J. L. Gómez Ribelles, M. Monleón Pradas, European Polymer Journal 43, 2775-2783, 2007
2. G. L. Brown, Clustering of water in polymers, in: Water in Polymers, edited by S. P, Rowland, ACS Symposium Series 127, American Chemical Society, Washington DC, 441-450, 1980

Acknowledgments

This work has been funded by the project PENED 2003. The project is co-financed 75% of public expenditure through EC - European Social Fund, 25% of public expenditure through Ministry of Development - General Secretariat of Research and Technology and through private sector, under measure 8.3 of OPERATIONAL PROGRAMME "COMPETITIVENESS" in the 3rd Community Support Programme."

Poster B53

Molecularly Imprinted Polymers (MIPs) as Selective Sorbents in Trichromatic Dye Mixtures

George Z. Kyzas, Dimitrios N. Bikiaris, Nikolaos K. Lazaridis*

Division of Chemical Technology, School of Chemistry, Aristotle University of Thessaloniki, GR- 541 24, Thessaloniki, Greece

The novelty of this study is the preparation of MIPs for the selective removal of dye molecules from trichromatic dye aqueous solutions. Two azo-dyes, a reactive and a basic, were used as templates. The rebinding properties and the sorption capacity were demonstrated by equilibrium/rebinding batch experiments. The selectivity/specificity of the obtained materials was elucidated by performing sorption experiments in trichromatic dye solutions. Moreover, the regeneration possibility of the dye-loaded polymers was evaluated, offering additional impetus for improved process economics.

For the preparation of Red Reactive dye-MIP (RR-MIP) (Figure 1a), 2mmol AAm, 10 mmol MBA, 1 mmol Reactive Red dye (RR) and 0.185 mmol KPS were dissolved in 50 mL of water into a glass flask, while for Basic Red dye-MIP (BR-MIP) (Figure 1b) 2mmol of MAA, 10 mmol EGDMA, 1.6 mmol Basic Red dye (BR) and 0.05 g AIBN were dissolved in 50 mL of the organic solvent DMF. In both methods, the mixture of reagents was stirred for 2 h, followed by nitrogen sparging (~5 min) to remove oxygen. After then, the flask was immediately sealed and stirring was continued at 75 °C for 12 h. The flask was then smashed and the monolithic polymers obtained, were ground in a laboratory mortar and pestle. Next, the obtained particles were washed with acetone and hot water followed by extraction in a Soxhlet apparatus using methanol, in order to remove residuals of the monomers and template molecules. Non-imprinted polymers (NIPs) were prepared with the same procedure just in the absence of the template molecules, denoted hereafter as R-NIPs and B-NIPs, respectively.

The experimental observations are summarized below:

The BR-MIP was prepared in organic medium while RR-MIP in aqueous. Both of them presented relatively low swelling percentage (63-86%).

1. The proposed rebinding mechanism (hydrogen bonding – electrostatic interactions) is affirmed by the shift of the carbonyl peak from NIPs to MIPs.
2. The optimum condition for sorption experiments was found to be pH=2 for BR-MIP while pH=10 for RR-MIP (Figure 2c). Effective diffusion coefficients were found to be at the order $5x10^{-13}$ m^2/s. Desorption of loaded BR-MIP (91%) succeeded at pH 2, while for the respective RR-MIP (88%) at pH 10 (Figure 2d).
3. Equilibrium data were successfully fitted to the Freundlich isotherm (Figure 2b). The maximum sorption loading, under the studied experimental conditions, found to be about 12 mg/g for both MIPs. Affinity distribution analysis revealed an increase of affinity sites in MIPs versus NIPs (50 times for low and 20 times for high affinity sites).
4. MIPs were applied in four sequential cycles of sorption-desorption with a limited loss of sorption capacity, only 6% (Figure 2a).
5. Selectivity studies showed that MIPs were selective to their template molecules presenting high distribution coefficients (650-1100 mL/g) and high separation factors (40-75).

Acknowledgements

The authors are grateful for this study to the Greek Ministry of Development through the Greek – German Bilateral Corporation for the financial support (project No. GSRT 107-c).

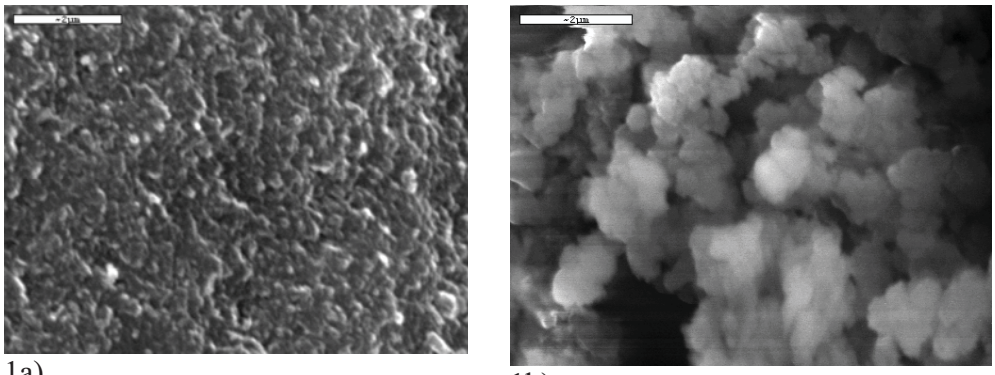

1a) 1b)

Figure 1. SEM micrographs of MIPs after template extraction: (a) RR-MIP; (b) BR-MIP.

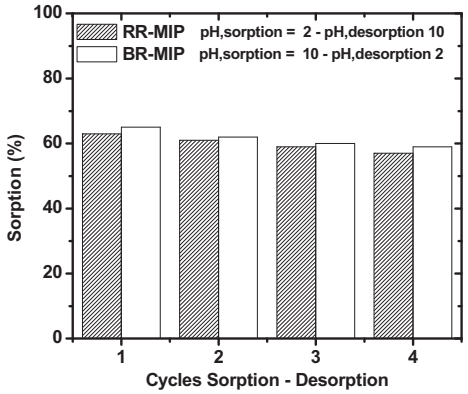

2a)

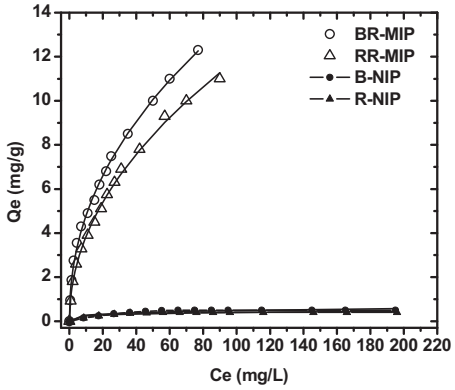

2b)

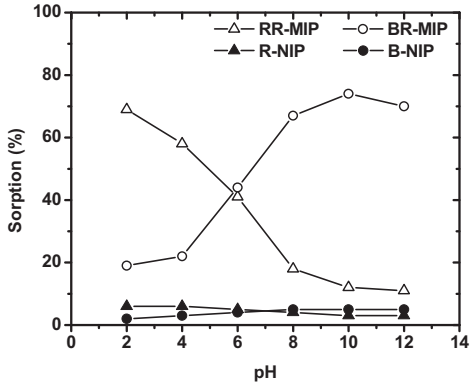

2c)

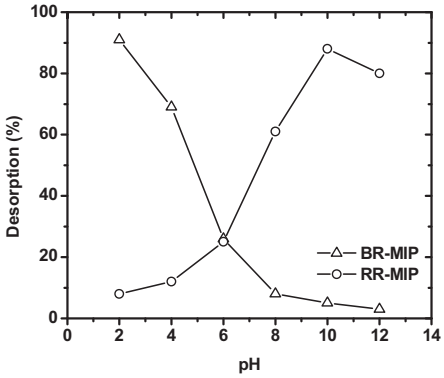

2d)

Figure 2a, Sorption – Desorption cycles for BR-MIP and RR-MIP.
Figure 2b, Sorption/Binding isotherms, fitted to the Freundlich model, for BR-MIP and RR-MIP (initial concentartion = 10 - 120 mg/L; volume = 0.05 L; sorbent (MIPs) = 0.5 g; contact time = 24 h; agitation speed 160 rpm; temperature = 25 °C).
Figure 2c, Effect of pH on the sorption of RR and BR onto RR-MIP and BR-MIP, respectively. 2d, Effect of pH on desorption of RR and BR from RR-MIP and BR-MIP, respectively (initial concentartion = 100 mg/L; volume = 0.05 L; sorbent (MIPs, NIPs) = 0.5 g; contact time = 24 h; agitation speed 160 rpm; temperature = 25 °C).

Poster B54

pH-controlled Quenching of the Fluorescence of Hydrophobic Probes solubilized in Ternary Poly(acrylic acid)-Surfactant-Cu^{2+} Complexes in Aqueous solution

Zacharoula Iatridi and Georgios Bokias
Department of Chemistry, University of Patras, GR-26504 Patras, Greece

Poly(acrylic acid), PAA, is probably the most known water-soluble synthetic polymer bearing carboxylic groups along the macromolecular chain. When PAA (usually under the neutralized form), is mixed in aqueous solution with multivalent metal ions like Cu^{2+}, the coordination of the carboxylate anions with the metal ion leads to the formation of a PAA-Cu^{2+} complex.[1-4] Alternatively, when neutralized PAA is mixed in aqueous solution with a cationic surfactant, like N,N.N,N-dodecyltrimethylammonium chloride, DTAC, mixed polymer-surfactant aggregates (the so-called PAA-DTAC complex) are formed, at a critical surfactant concentration, cac, as a result of electrostatic attractions in cooperation with hydrophobic interactions.[5-7] The aim of the present work was to study the formation of ternary PAA-DTAC-Cu^{2+} complexes, exploiting the multifunctional characteristics of PAA, namely its ability to form both coordination complexes with Cu^{2+} ions and polymer-surfactant complexes with oppositely charged surfactants, like DTAC, in aqueous solution. From techniques, like turbidimetry, viscometry and fluorescence probing, it was confirmed that such ternary complexes with a compact structure are indeed formed, followed by phase separation when the net charge of the complex becomes negligible.

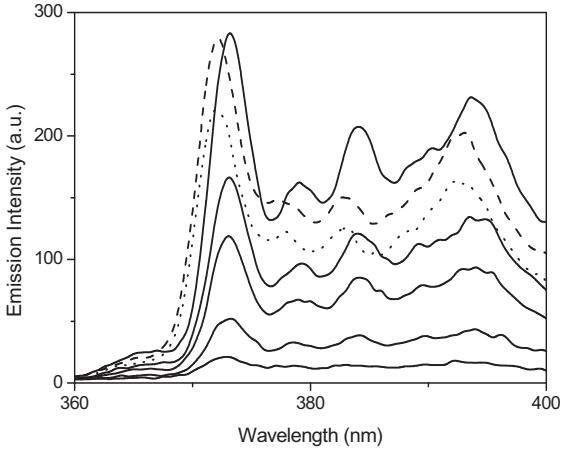

Figure 1. Emission spectra of 8 10^{-7} M pyrene in aqueous solutions of PAA 2.7mM at pH=7.6 with DTAC 0.05mM, in the absence (----) or in the presence of 0.2mM Cu^{2+} ions (····). With the solid lines, the emission spectra of pyrene in the sane polymer solution containing DTAC 1mM upon addition of Cu^{2+} ions. From top to bottom, the concentration of Cu^{2+} ions increase form 0 up to 0.4 mM.

For the fluorescence probing studies, pyrene and Nile Red were used as probes of the hydrophobic microdomains. Interestingly, in these studies, a strong quenching of the fluorescence of the probes was observed under certain conditions. For example, in **Figure 1**, the emission spectra of pyrene in aqueous PAA solutions with DTAC, in the absence or the presence of Cu^{2+} ions, are shown. As it is seen, when the concentration of DTAC is high enough, addition of Cu^{2+} ions to this PAA-DTAC solution, leads to a substantial decrease of the emission of pyrene. Nevertheless, this significant quenching ability of Cu^{2+} ions is related to the formation of polymer-surfactant aggregates, as the level of the emission of pyrene decreases just slightly at a lower DTAC concentration. From such detailed investigations under various experimental conditions, it was evidenced that the fluorescence quenching from Cu^{2+} ions strongly depends on the relative positions of the probe and the quencher.

As a result of the weak acidic character of PAA, both the polymer-surfactant and the polymer-metal ion complexation are controlled from the pH of the solution. This pH-sensitivity (combined with the high quenching ability of complexed Cu^{2+} ions) was exploited to demonstrate, in principle, that the formation-deformation of ternary PAA-DTAC-Cu^{2+} complexes may act as a pH-controlled 'ON-OFF' switch of the fluorescence of pyrene in aqueous solution. In **Figure 2** the variation with pH of the intensity of the first vibronic band of the emission of pyrene in PAA-surfactant mixtures, in the absence as well as in the presence of 0.2 mM Cu^{2+}

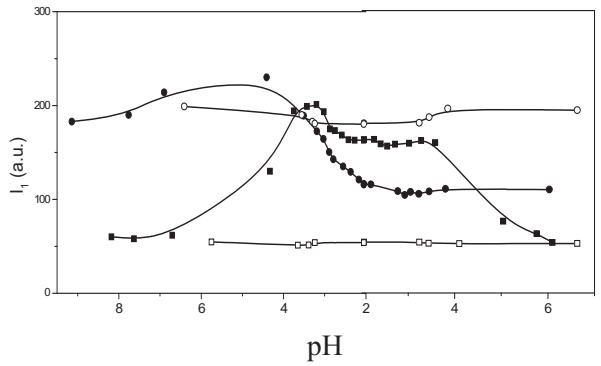

Figure 2. Variation with pH of the intensity I_1 of the first emission peak of 8 10^{-7} M pyrene in aqueous solutions containing 1 mM DTAC and PAA 2.7 mM or PSSNa 2.7 mM, in the absence (●, ○) or in the presence of 0.2 mM Cu^{2+} ions (■, □). Full symbols refer to PAA solutions, while open symbols refer to PSSNa solutions.

ions is shown. As seen, the emission of pyrene in the aqueous PAA-DTAC-Cu^{2+} mixture depends strongly on the pH of the solution: at high pH the emission of pyrene is low, while an almost fourfold increase is observed upon decreasing pH. This behavior may be considered, at a first glance, reversible, as pyrene returns to its initial state when pH increases again to higher values. In addition, the role of the weak polyacid PAA is crucial, as no pH dependence is observed when a strong polyelectrolyte, namely poly(sodium styrene sulfonate), PSSNa, is used. In the latter case, regardless of pH, a constant emission of pyrene is found, either strong or weak, in the absence or presence of Cu^{2+} ions, respectively.

The whole behavior is schematically illustrated in **Scheme I**. At high pH, the polymer chain is negatively charged and complexation of PAA with both Cu^{2+} and DTAC occurs. As a consequence, under these conditions, pyrene is solubilized in the hydrophobic PAA-DTAC complexes, in close proximity with the Cu^{2+} ions, complexed also with the carboxylate groups of the polymer. Quenching of the emission of pyrene by the Cu^{2+} ions is, therefore, favored, resulting in the weak emission intensity recorded at pH>4. On the contrary, at low pH the polymer is practically uncharged and no complexation of PAA with either Cu^{2+} ions or DTAC takes place. As a result, both Cu^{2+} ions and pyrene are free in the aqueous solution and quenching is now less significant, so that a high emission of pyrene is recorded at pH<4.

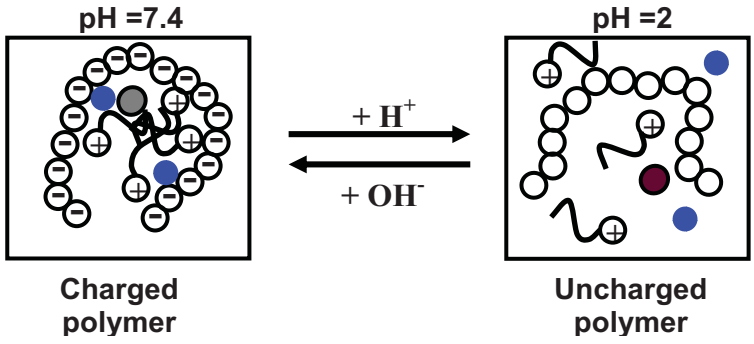

Scheme I. Schematic explanation of the pH-controlled "ON-OFF" switching properties of the fluorescence of pyrene in aqueous ternary PAA/DTAC/Cu^{2+} solutions.

Acknowledgments.
Financial support through the program PENED 2003, 03ED825, 'Design and Development of new paints with controlled release of biocides for submarine applications' co-financed by E.U.- European Social Fund (75%) and General Secretariat for Research and Technology (GSRT), Greece, is greatly acknowledged. Partial support from Chrotex S.A., Greece, is also acknowledged.

References

(1) Francois, J.; Heitz, C.; Mestdagh, M.M. *Polymer* **1997**, *38*, 5321-5332.
(2) Ikeda, Y.; Beer, M.; Schmidt, M.; Huber, K. *Macromolecules* **1998**, *31*, 728-733.
(3) Mun, G. A.; Nurkeeva, Z. S.; Khutoryanskiy, V. V.; Sarybayeva, G. S.; Dubolazov, A. V. *Eur. Polym. J.* **2003**, *39*, 1687-1691.
(4) Iatridi Z.; Bokias G.; Kallitsis. J.K. *J. Appl. Polym. Sci.*, **2008**, 108, 769.
(5) Hayakawa, K.; Santerre, J. P.; Kwak, J. C. T. *Macromolecules* **1983**, *16*, 1642-1645.
(6) Thalberg, K.; Lindman, B.; Bergfeldt, K. *Langmuir* **1991**, *7*, 2893-2898.
(7) Wang, C.; Tam, K. C. *Langmuir* **2002**, *18*, 6484-6490.

Poster B55

Development of New Semiconducting Polymer Functionalized Carbon Nanotubes

A.A. Stefopoulos[1,2], C.L. Chochos[1], K. Papagelis[3] and J.K. Kallitsis[1]

[1]*Department of Chemistry, University of Patras, Patras 26500 Greece*
[2]*Foundation for Research and Technology Hellas, Institute of Chemical Engineering and High Temperature Processes (FORTH-ICEHT), P.O. Box 1414, Patras 26500, Greece*
[3]*Department of Materials Science, University of Patras, 26504 Rio, Patras, Greece*

Carbon nanotubes are the most promising materials for applications in nanoelectronics devices, sensors, and high-strength materials due to their unusual properties[1-3]. Multiwall carbon nanotubes have the highest tensile strength of any material yet measured and desirable electrical properties. Moreover in this field is found that metallic nanotubes can have an electrical current density more than 1000 times greater than metals such as silver and copper[4]. The initial disadvantage of poor solubility has been overcome by various functionalization techniques using either the covalent attachment of different organic groups through reactions onto the π-conjugated backbone of the CNTs or the non-covalent adsorption or wrapping of various functional moieties.

Our effort in this direction is the semiconducting polymer modification of Single-Wall Carbon Nanotubes (SWCNTs), in order to develop new composite materials that combine the electron donor or acceptor properties of the covalently attached polymers with those of the nanotubes. The final products were fully characterized with all the conventional methods employed for CNTs such as TGA, UV-Vis/NIR, Raman, FTIR, Photoluminescence spectroscopies.

Using the “grafting from” method, two different carbon nanotubes modification procedures were used, resulting in amino- or hydroxyl-functionalized CNTs, which were finally converted to active ATRP initiators. Polymerization of the vinylquinoline monomer resulted in highly soluble oligoquinoline-modified SWCNTs (Figure 1). The emission spectrum of SWNT-OQuin1 exhibits different optical behavior in contrast to the respective homopolymer PDPQ upon protonation. The excimer formation of polyquinolines is inhibited as was demonstrated in this work due to the immobilization of the quinoline units on to the nanotube surface.

Second, using the method “grafting to”, we successfully functionalize SWCNTs with one-end functionalized rrP3OT (Figure 2), having phenol or alkyl halide (ATRP Initiator) as terminal group. In the first attempt decoration of the hydroxyl functionalized SWCNTs[6] with one-end phenol functionalized rrP3OT was accomplished by an ether bond formation (Mitsunobu type reaction). And the second attempt to covalently attach polymer chain on to SWCNTs was by employing similar reaction conditions with ATRP between alkyl halide one end functionalized rrP3OT and SWNT. Depending on the reaction conditions and the system used, various degree of attachment of the polymeric materials on to the carbon nanotubes was achieved. The obtained materials were easily soluble in common solvents and in some cases film forming properties exhibit. Moreover in the case of regioregular P3OT functionalized nanotubes, an efficient electron transfer from the regioregular poly(3-octylthiophene) to the nanotube is demonstrated, based on the results obtained from the study of their optical properties.

Such hybrid materials in general provide a way to combine the electronic properties of the SWCNTs with those of the attached polymers, which in the first case is the electron-accepting or the strong emission ability of the quinoline groups and the second for electron-donating ability of the regioregular polythiophene, leading to multifunctional materials that are of high interest in the field of optoelectronic devices.

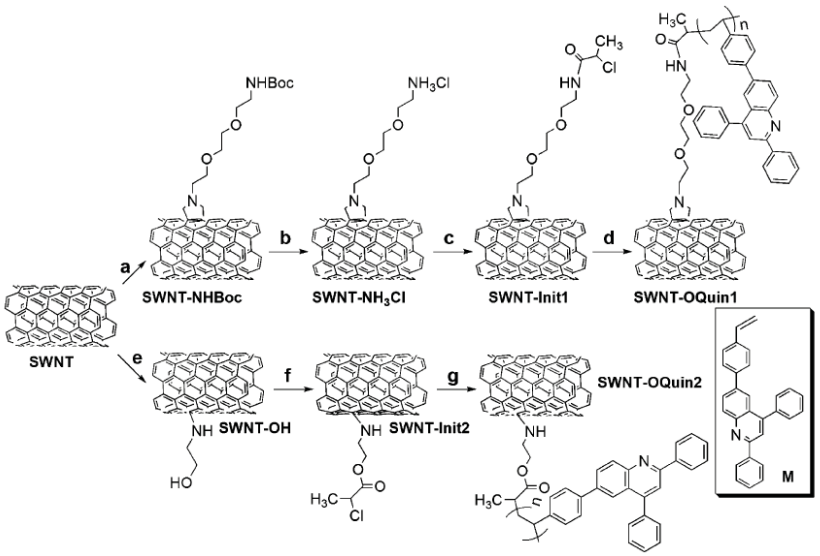

Fig. 1. Synthetic routes toward the preparation of Oligoquinoline Modified SWCNTs[5]

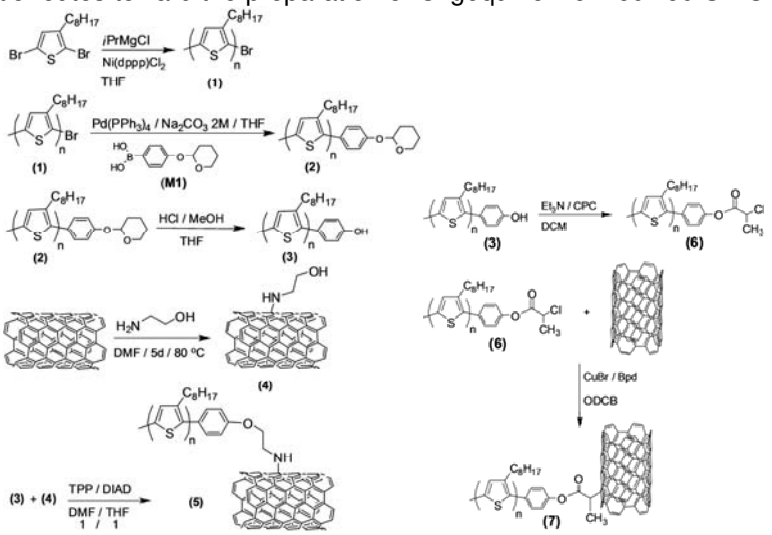

Fig. 2. Synthetic routes toward the preparation of rrP3OT Modified SWCNTs[6]

References

1. M. S. Dresselhaus, G. Dresselhaus, P. Avouris, Carbon Nanotubes: Synthesis Structure, Properties, and Applications 2001, Springer, Berlin
2. P. M. Ajayan, Chem. Rev. 1999, 99, 1787–1799
3. R. Saito, G. Dresselhaus, M. S. Dresselhaus, Physical Properties of Carbon Nanotubes 1998, Imperial College Press, London
4. P. Avouris and J Appenzeller, Electronics and Optoelectronics with Carbon Nanotubes, The Industrial Physicist, JUNE/JULY 2004, American Institute of Physics
5. Chochos, C. L.; Stefopoulos, A. A.; Campidelli, S.; Prato, M.; Gregoriou, V. G.; Kallitsis, J. K., Macromolecules; (Article); 2008; 41(5); 1825-1830
6. Andreas A. Stefopoulos, Christos L. Chochos, Maurizio Prato, George Pistolis, Kostas Papagelis, Foteini Petraki, Stella Kennou and Joannis K. Kallitsis, Chem. Eur. J. Accepted.